Effect of the Position of Geminal Di-Substitution of γ Amino Acid Residues on Their Conformational Preferences

A Dissertation Submitted to the

Indian Institute of Technology Guwahati

As Partial Fulfilment for the Award of Degree of

Doctor of Philosophy

In Chemistry

Submitted by

Swapna Debnath

Roll No. 166122021

Supervisor

Dr. Sunanda Chatterjee

Associate Professor

Dept. of Chemistry

Co-Supervisor

Dr. Priyadarshi Satpati

Associate Professor

Dept. of Biosciences and Bioengineering

Department of Chemistry

Indian Institute of Technology Guwahati

Guwahati 781039

June 2023

TH-3141_166122021

Dedicated To

My parents and My family

TH-3141_166122021

Declaration

I do hereby declare that the matter embodied in this thesis entitled ***''Effect of the Position of Geminal Di-Substitution of Gamma Amino Acid Residues on their Conformational Preferences''*** has been carried out by me under the supervision of Dr. Sunanda Chatterjee, Associate Professor, during the period July 2016 to June 2023, at Department of Chemistry, Indian Institute of Technology Guwahati (IITG), India. The work presented here has not been submitted for the award of any other degree or diploma at any other institution.

In keeping with the general practice of reporting scientific observations, due acknowledgements have been made whenever the work described is based on the findings of the other investigators.

IIT Guwahati
June 2023

Swapna Debnath
166122021

TH-3141_166122021

Certificate by the Supervisor(s)

This is to certify that the thesis entitled "***Effect of the Position of Geminal Di-Substitution of Gamma Amino Acid Residues on their Conformational Preferences***" submitted by Ms. Swapna Debnath (Roll number: 166122021) for the award of Ph.D. degree to IIT Guwahati is absolutely based on his own research work under my supervision. This thesis or any part of it has not been submitted for any degree/ diploma or any academic award anywhere before.

Dr. Sunanda Chatterjee
Associate Professor
Dept. of Chemistry
Indian Institute of Technology Guwahati
Contact: +91 361 258 3310
Email: sunanda.c@iitg.ac.in

Dr. Priyadarshi Satpati
Associate Professor
Dept. of BSBE
Indian Institute of Technology Guwahati
Contact: +91 361 258 3205
Email: psatpati@iitg.ac.in

TH-3141_166122021

Acknowledgement

To begin with, I would like to express my heartfelt gratitude and respect to my supervisor ***Dr. Sunanda Chatterjee***, Associate Professor, Dept. of Chemistry, IIT Guwahati, for her endless guidance, enthusiasm, persistent encouragement, and generous support. I would be grateful to her for providing me with a favorable ambience with the greatest research facilities and freedom for working throughout my research work in the lab. It has been an immense pleasure to learn many things while working under her supervision. Her suggestions and advice carried me through all the stages of writing my papers and thesis. I would not have completed this challenging journey without her help.

Besides my supervisor, I would like to convey my sincere regards to my Co-Supervisor, ***Dr. Priyadarshi Satpati***, Associate Professor, Dept. of Biosciences and Bioengineering, IIT Guwahati, for his continuous guidance, motivation, and support throughout my research work. A heartfelt thanks to him and his group members for performing insilico studies for my research work. I will not forget those enriching discussions with him and my supervisor at each stage of my research work, which always turned out to be several hours long and helped me complete all my research projects. It has been an amazing experience working with two research groups across different departments.

It is my privilege to extend my sincere thanks to my Doctoral Committee members, Chairperson ***Prof. Subhas Chandra Pan***, Professor, Department of Chemistry, IIT Guwahati, ***Dr. Pavan Kumar Kancharla***, Associate Professor, Department of Chemistry, IIT Guwahati, and ***Dr. Dipankar Srimani***, Associate Professor, Department of Chemistry, IIT Guwahati for their valuable comments, suggestions, constant support and encouragement throughout my research work and positive evaluation during my all annual progress seminar.

TH-3141_166122021

I would like to express my sincere thanks to the new Doctoral Committee members, Chairperson ***Prof. Subhas Chandra Pan***, Professor, Department of Chemistry, IIT Guwahati, ***Prof. Debapratim Das***, Professor, Dept. of Chemistry, IIT Guwahati, and ***Dr. Rajkumar P. Thummer,*** Assistant Professor, Dept. of Biosciences and Bioengineering, IIT Guwahati for evaluating my PhD Viva-Voce examination.

I would like to thank my thesis examiners (both Indian and Foreign) for evaluating my thesis.

I owe my profound thanks to our collaborator, ***Dr. Prema G Vasudev***, CSIR-Central Institute of Medicinal and Aromatic Plants (CIMAP), Lucknow, and her student Dinesh Kumar for her support by solving the crystal structure and help in analyzing the data of my research.

I would like to thank ***Dr. Dipankar Srimani and his group*** for providing me with the facility of -80^{o}C instrument to perform one of my reactions for amino acid synthesis.

I would like to express my sincere obligations to ***Prof. Debapratim Das***, Professor, Dept. of Chemistry, IIT Guwahati, and my supervisor ***Dr. Sunanda Chatterjee*** for conducting the group meeting every week for oral presentations and scientific discussions. It enhanced my scientific knowledge and confidence level while presenting scientific work.

I take this opportunity to thank ***Prof. S. Raghothama***, Professor, NMR Research Centre, IISc, and ***Prof. N. Suryaprakash***, Professor, NMR Research Centre, IISc, for their precious suggestions on the NMR experiments which helped me to improve the quality of NMR data.

I would like to pay my sincere thanks to ***Dr. Sudipta Kishore Goswami***, Application Scientist, Bruker BioSpin, for his enormous help and support in learning various NMR experimental techniques.

I am also grateful to ***Mr. Chandan Borgohain***, Technical Officer, Grade-I (CIF, IIT Guwahati), and ***Mr. Deep Manoram Baruah***, Junior Technical Superintendent (CIF, IIT

Guwahati), for their immeasurable support during troubleshooting in NMR and for allowing me to perform my time- taking NMR experiments adequately.

My special thanks to ***Dr. Babulal Das***, Technical officer Grade-I, Dept. of Chemistry, IIT Guwahati, for helping me with his time to diffract and initial refinement of the crystals reported in this thesis.

I am also thankful to ***Mr. Imdadul Islam***, Technical Superintendent, Dept. of Chemistry, IIT Guwahati, for helping me to perform the VT NMR experiment.

I wish to thank **Dr. *Suvankar Ghosh*** and ***Vignesh S. R.*** (Dept. of Biosciences and Bioengineering) for performing insilico studies.

I am grateful and fortunate enough to get constant encouragement and support from my seniors, friends, and juniors. (special mentions, ***Rajatsubhra Giri, Suresh Bhaiya, Kalicharan Das, Angshuman Mahapatra, Sandip Mondal, Bitan Sardar, Jityendra, Abhay***).

I would like to acknowledge the Department of Chemistry, IIT Guwahati, for providing all the instrumentation facilities for carrying out my research work. I would also like to thank the staff members of the Department of Chemistry for being there when needed.

I would also like to show my great thanks to the Central Instruments Facility (CIF), IIT Guwahati for providing facilities like 600 MHz NMR, FESEM, PXRD, MALDI, XRD and FETEM instruments.

Words fail when I want to thank my lab mates (**Dr. *Gopal Pandit,* Dr. *Karabi Roy, Monikha Chetia, and Maitery Yadav***). You all have been with me through all my ups and downs. My heartiest thanks and love to all of you for providing a friendly lab environment and supporting me with your help in completing my research work. I am also thankful to all project students for helping me in my research.

TH-3141_166122021

I gratefully acknowledge Indian Institute of Technology Guwahati for providing me with all the facilities and financial assistantship for carrying out my work smoothly.

Finally, my heartfelt thanks go to ***my parents and my family members*** for their affection and encouragement in all my academic endeavors.

My heartfelt thanks to almighty.

June 2023 **Swapna Debnath**

TH-3141_166122021

Abstract

Use of Unnatural amino acid residues have been very powerful tool employed in the area of peptidomimetics to generate peptides with natural peptide like folding abilities and improved resistance towards proteolytic degradation. Backbone homologated amino acid residues like β and γ are known to be able to give rise to several novel well-folded secondary structures. Geminally backbone di-substituted amino acid residues have restricted backbones, with the flanking torsion angles about the point of di-substitution adopting gauche conformations. This property of the geminally di-substituted amino acid residues have led to them being used in the design of helical structures in short synthetic peptides. There are reports of geminally di-substituted γ amino acid residues in the literature, which mostly give rise to C_9 and C_{14} helical conformation in homomers and C_{12}/C_{13} helical conformations in hybrid αγ/βγ heteromers respectively. There are also examples of these amino acid residues to be accommodated in mixed helices of different ring sizes (12/10 helices or 15/17 helices) or helices containing opposite directionality hydrogen bonds (12/10 helix). In a rare example, geminally di-substituted γ amino acid residue Gpn also was accommodated in the (i+2) position of a non-helical β-turn.

As γ amino acid residues contain three methylene carbons in the backbone, three different geminally di-substituted γ amino acid residues are possible. There are: $\gamma^{2,2}$, $\gamma^{3,3}$ and $\gamma^{4,4}$ amino acid residues. Though there are studies on individual amino acid residues there have never been a comparative study of their conformational preferences or abilities. In these three differently di-substituted γ amino acid residues, three different sets of backbone torsion angles are restricted. In this thesis we wanted to investigate if this difference generated any effect on the conformational preference of these geminally di-substituted γ amino acid residues. For this, we have selected different model peptides which are known to have a strong propensity towards

certain secondary structures and incorporated the different γ amino acid residues one at a time, to generate different groups of peptides. Next we studied the conformation of these peptides containing different γ amino acid residues in solid, solution states and in *silico* to compare their conformational propensities.

In **Chapter 2**, we have looked at the conformation and assembly of simple Fmoc derivatives of $\gamma^{x,x}$ (x,x = 2,2/3,3/4,4, **21-23**) residues in solid and solution states. Crystal structure of $\gamma^{2,2}$ and $\gamma^{4,4}$ derivatives showed distinct conformations (open/close for $\gamma^{2,2}$/$\gamma^{4,4}$) that differed in torsion angles, hydrogen-bonding and most importantly the π-π Fmoc-stacking interactions (relatively favourable for $\gamma^{4,4}$-close). Fmoc derivatives existed in an equilibrium between major-monomeric (low energy, non-hydrogen bonded) and minor-dimeric (high energy, hydrogen bonded) populations in solution. Rate of major/minor population exchange was dependent on the position of substitution, highest being for $\gamma^{4,4}$ derivative. In solution, assembly of Fmoc derivatives was solvent dependent, but it was independent of the position of geminal substitution. Crystallization was primarily governed by the stabilization of high-energy dimer by favourable π-π stacking involving Fmoc moieties. High free-energy of the dimers ($\gamma^{2,2}$-close, $\gamma^{3,3}$-open/close) offset favourable stacking interactions and hindered crystallization.

In **Chapter 3**, we have investigated the relative ease of $\gamma^{x,x}$ (x,x = 2,2/3,3/4,4) residues to be accommodated into all α amino acid containing helical scaffolds. This chapter is devided into two parts. In the first part we have incorporated the different γ amino acid residues in tripeptide (Boc-U$\gamma^{x,x}$U-OMe where U=Aib, x,x = 2,2/3,3/4,4) and hexa peptide (Boc-U$\gamma^{x,x}$ULUV-OMe where U=Aib, x,x = 2,2/3,3/4,4) scaffolds. From the studies it was clear that $\gamma^{3,3}$ and $\gamma^{4,4}$ residues have an enhanced propensity of being accommodated in the C_{12} helical conformation in comparison to the $\gamma^{2,2}$ amino acid residue. We also concluded that while $\gamma^{2,2}$ and $\gamma^{3,3}$ residues

TH-3141_166122021

can be accommodated in left handed and right handed helical conformations, $\gamma^{4,4}$ always gets accommodated only in right handed helical conformation.

Chirality is an omnipresent feature in nature's architecture starting from simple molecules like amino acids to complex higher order structures viz. proteins, DNA and RNA. The L configuration of proteinogenic amino acids give rise to right-handed helices. Ambidexterity is as rare in organisms as in molecules. There are only a few reports of ambidexterity in single peptide molecules composed of either mixed L and D or achiral residues. Here, we report for the first time, the ambidextrous and left-handed helical conformations in the chiral αγ nonapeptides (**31-33)-Nona** (Boc-LUVU$\gamma^{x,x}$ULUV-OMe where U=Aib, x,x = 2,2/3,3/4,4), containing chiral L alpha amino acid residues, in addition to the usually observed right-handed helical conformation in crystals and in solution state. The centrally located achiral γ residue, capable of adopting both left and right-handed helical conformations, induce its handedness on the neighbouring chiral and achiral residues, leading to the observation of both left and right-handed helices in **32-Nona** and **33-Nona**. Presence of a single water molecule proximal to the γ residue induces reversal of helix handedness by forming distinct and stable water mediated hydrogen bonds. This gives rise to ambidextrous helices as major conformer in **31-Nona** and **32-Nona**. Absence of the observation of ambidexterity in **33-Nona**, might be due to the inability of $\gamma^{4,4}$ in the recruitment of water molecule. Populants observed in the solution were mapped to the conformations observed in the solid state and the structures obtained from *in silico* methods. Calculation of the relative energies of the various conformations, helped to understand the population distribution in the solution state. Experiments (NMR and X-ray) and DFT calculations suggested that the position of geminal di-substitution is crucial for determining the population of the amenable helical conformations (ambidextrous, left and right-handed) in these chiral αγ peptides.

In **Chapter 4** we have attempted the construction of isolated αγ non-helical C_{12} β-turn mimics in small tetrapeptides by the incorporation of $\gamma^{x,x}$ (x,x = 2,2/3,3/4,4) at the (i+2) position of the turn. Solution conformation was probed in detail using NMR spectroscopy. Irrespective of the solvent polarity, **41** containing $\gamma^{2,2}$ amino acid residues failed to form the isolated tight β-turn mimetic while peptides **42** and **43** containing $\gamma^{3,3}$ and $\gamma^{4,4}$ residues successfully adopted isolated non-helical C_{12} β-turn mimic structure. Conformations in the solution state were established from the observation of characteristic long range NOEs while hydrogen bonds were established from the DMSO-d_6 titration experiment. DFT optimized structures corroborated the conformations observed in the solution. Since the tetrapeptides **41-43** were identical in every other way, such stark difference in the stereochemical ability of these di-substituted amino acid residues could be attributed to the difference in the position of the di-substitution along the backbone of the residue.

The effect of insertion of $\gamma^{x,x}$ (x,x = 2,2/3,3/4,4) at the (i+2) position of a two residue αγ C_{12} turn segment, in a model octapeptide sequence Leu-Phe-Val-Aib-Xxx-Leu-Phe-Val (where Xxx = γ amino acid residues) has been investigated in **Chapter 5**. Solution conformational studies (NMR, CD and IR) and DFT calculations indicated that $\gamma^{3,3}$ and $\gamma^{4,4}$ residues were well accommodated in the β-hairpin nucleating αγ C_{12} turns, which gave rise to well registered hairpins, in contrast to $\gamma^{2,2}$ which was unable to form a tight C_{12} β-hairpin nucleating turn and promote a well registered β-hairpin. Geminal di-substitution at the C^{α} carbon in $\gamma^{2,2}$ led to unfavorable steric contacts, disabling its accommodation in αγ C_{12} hairpin nucleating turn unlike the $\gamma^{3,3}$ and $\gamma^{4,4}$ residues. Geminal di-substitutions at different carbons along the backbone, constrained backbone torsion angles for the three γ amino acid residues differently, generating diverse conformational preferences in them. Folded hairpins were energetically

stabler (~8-9 kcal/mol) than the unfolded peptides. Conformational preference of the peptides was independent of N-terminal protecting group.

TH-3141_166122021

Contents

TH-3141_166122021

TH-3141_166122021

TH-3141_166122021

TH-3141_166122021

TH-3141_166122021

TH-3141_166122021

TH-3141_166122021

TH-3141_166122021

TH-3141_166122021

Abbreviations

L-Amino Acid with Abbreviations and Single Letter Codes

Amino Acid	Abbreviation	One letter code
Alanine	Ala	A
Valine	Val	V
Isoleucine	Ile	I
Leucine	Leu	L
Methionine	Met	M
Phenylalanine	Phe	F
Tyrosine	Tyr	Y
Tryptophan	Trp	W
Threonine	Thr	T
Serine	Ser	S
Asparagine	Asn	N
Glutamine	Gln	Q
Cysteine	Cys	C
Glycine	Gly	G
Proline	Pro	P
Arginine	Arg	R
Lysine	Lys	K
Histidine	His	H
Aspartic acid	Asp	D
Glutamic acid	Glu	E

TH-3141_166122021

Unnatural Amino Acids with Abbreviations

Amino Acid	Abbreviations
$\gamma^{2,2}$	4-amino-2,2-dimethylbutanoic acid
$\gamma^{3,3}$(Abd)	4-amino-3,3-dimethylbutanoic acid
$\gamma^{4,4}$(Aic)	4-amino-4,4-dimethylbutanoic acid
Aic	4-aminoisocaproic acid
Abd	4-amino-3,3-dimethylbutanoicacid
Aib	α- Amino isobutyric acid
ACC	2-aminocyclopropanecarboxylic acid
ACPC	2-aminocyclopentanecarboxylic acid
ACHC	2-aminocyclohexanecarboxylic acid
Gpn	Gabapentin
Amb	3-amino-5-bromo-2-methoxy benzoic acid
L-pGlu	L-pyroglutamic acid
5-F-Trp	5-fluoro tryptophane
L-Dip	L-diphenylalanine
L-Phg	L-Phenylglycine
Homo-Phe	Homo-phenyl-alanine
H- β^3hXaa-OH	β^3-homo-amino acids
H- β^2hXaa-OH	β^2-homo-amino acids
H- γ^4hhXaa-OH	γ^4-bis(homo-aminoacids)
H- γ^3hhXaa-OH	γ^3-bis(homo-aminoacids)
H- γ^2hhXaa-OH	γ^2-bis(homo-aminoacids)
$\beta^{3,3}$	3-amino-3-methyl butanoic acid
$\beta^{2,2}$	3-amino-2,2- dimethyl propanoic acid
$\beta^{2,2}$ Ac_3c	1-aminomethylcyclopropane
$\gamma^{4,4}$	4-amino-4-methyl pentanoic acid
$\gamma^{3,3}$	4-amino-3,3-dimethyl butanoic acid
$\gamma^{2,2}$	4-amino-2,2-dimethyl butanoic acid
$\beta^{3,3}$ Ac_6c	2-(1-aminocyclohexyl) acetic acid

TH-3141_166122021

$\beta^{2,2}$ Ac_6c	1-aminomethylcyclohexane carboxylicacid
Gpn	1-aminomethylcyclohexane acetic acid
2-ACPC	2-amino-cyclopentane carboxylic acid
2-ACHC	2-aminocyclohexane carboxylic acid
3-ACPC	3-aminopentane carboxylic acid
APCH	Aminopropyl cyclohexane carboxylic acid
AMCP	Aminomethyl-pentane carboxylic acid
AMCH	Aminomethyl-hexane carboxylic acid
R-Nip	R-Nipecotic acid
S-Nip	S-Nipecotic acid
AMCH	2-(aminomethyl)-hexane carboxylic acid
dγAic	trans-α, β-unsaturated 4-aminoisocaproic acid

TH-3141_166122021

Abbreviations

AMP: Antimicrobial Peptide

UV: Ultraviolet

SCXRD: Single crystal X-ray diffraction

PXRD: Powder X-ray diffraction

MALDI: Matrix-assisted laser desorption/ionization

HRMS: Higher-resolution mass spectroscopy

FESEM: Field Emission Scanning Electron Microscopy

FETEM: Field Emission Transmission Electron Microscope

FTIR: Fourier Transform Infrared Spectroscopy

ESI-MS: Electrospray Ionization Mass Spectrometry

LC-MS: Liquid chromatography–mass spectrometry

Q-TOF: Quadrupole time-of-flight

CD: Circular Dichroism

DLS: Dynamic Light Scattering

NMR: Nuclear Magnetic Resonance

NOESY: Nuclear Overhauser Effect Spectroscopy

TOCSY: Total Correlation Spectroscopy

TPPI: Time-proportional phase incrementation

CCDC: Cambridge Structural Database accession number

TLC: Thin layer chromatography

J: Coupling constant

1D: One Dimension

2D: Two Dimension

MD: Molecular Dynamics

DFT: Density Functional Theory

PCM: Polarizable continuum model

SPPS: Solid Phase Peptide Synthesis

TH-3141_166122021

HPLC: High Performance Liquid Chromatography

Boc: Tert-butoxycarbonyl

Fmoc: Fluorenylmethyloxycarbonyl

TFA: Trifluoroacetic acid

DNA: Deoxyribonucleic acid

RT: Room Temperature

THF: Tetrahydrofuran

HOBt: Hydroxybenzotriazole

PyBOP: Benzotriazole-1-yl-oxy-tris-pyrrolidino-phosphonium hexafluorophosphate

DMAP: 4-dimethylaminopyridine

DIC: N, N′-diisopropylcarbodiimide

DIPEA: N, N-diisopropylethylamine

DCM: Dichloromethane

D_2O: Deuterium Oxide

CH_3CN: Acetonitrile

$CHCl_3$: Chloroform

TFE: Tetrafluoroethylene

DMSO: Dimethylsulfoxide

NaCl: Sodium Chloride

$CaCl_2$: Calcium Chloride

mM: Millimolar

µM: Micromolar

TH-3141_166122021

MDR: Multi-drug resistant

EtOH: Ethanol

EDC.HCl: N-(3-dimethylaminopropyl)-N′-ethylcarbodiimide hydrochloride

MeOH: Methanol

Fmoc-OSU: N-(9-Fluorenylmethoxycarbonyloxy) succinimide

ACN: Acetonitrile

EXSY: Exchange cross peaks

CAC: Critical aggregation concentration

TIPS: Triisopropylsilane

g,g: *gauche-gauche*

g,t: *gauche-trans*

$SOCl_2$: Thionyl chloride

LiOH: Lithium hydroxide

CaH_2: Calcium hydride

TPPI: Time-proportional phase incrementation

n-Buli: n-Butyl lithium

$NaBH_4$: Sodium borohydride

$NiCl_2$: Nickel chloride

H_2SO_4: Sulphuric acid

HCl: Hydrochloric acid

DBU: 1, 8-Diazabicyclo [5.4.0]undec-7-ene]

$HCOONH_4$: Ammonium formate

K_2CO_3: Potassium carbonate

$NaHCO_3$: Sodium bicarbonate

Na_2SO_4: Sodium sulphate

TH-3141_166122021

BTAC: Benzyl triethyl ammonium chloride

Pd/C: Palladium charcoal

RT: Room temperature

TH-3141_166122021

Chapter1
Introduction

TH-3141_166122021

1. Introduction

Peptides are an integral part of proteins present in all living organisms. It plays a crucial role by influencing important physiological mechanisms and controls many biological functions including, immune defense, digestion, metabolism, reproduction, respiration, etc.[1-6] Most of the polypeptides are functional upon obtaining the appropriate conformation.[7-14] Two fundamental secondary structures, α-helix, and β-sheet, predominate the structural diversity of polypeptide chains, containing genetically coded α amino acids. In the last few decades, the supramolecular assembly of peptides has drawn attention due to its efficacy in designing biomaterials and the fabrication of nano-structures with tunable physical and chemical properties. Depending on their diverse architecture, peptide-based nano-materials have been widely utilized in various fields, including drug delivery, tissue engineering, bio mineralization.[15-21] Peptides are also a potential class of molecules used for the development of therapeutics to treat various pathological conditions like chronic diseases (Type II diabetes),[22,23] neurodegenerative diseases (Alzheimer's),[24-27] microbial infections,[28-31] cancer[32-37].

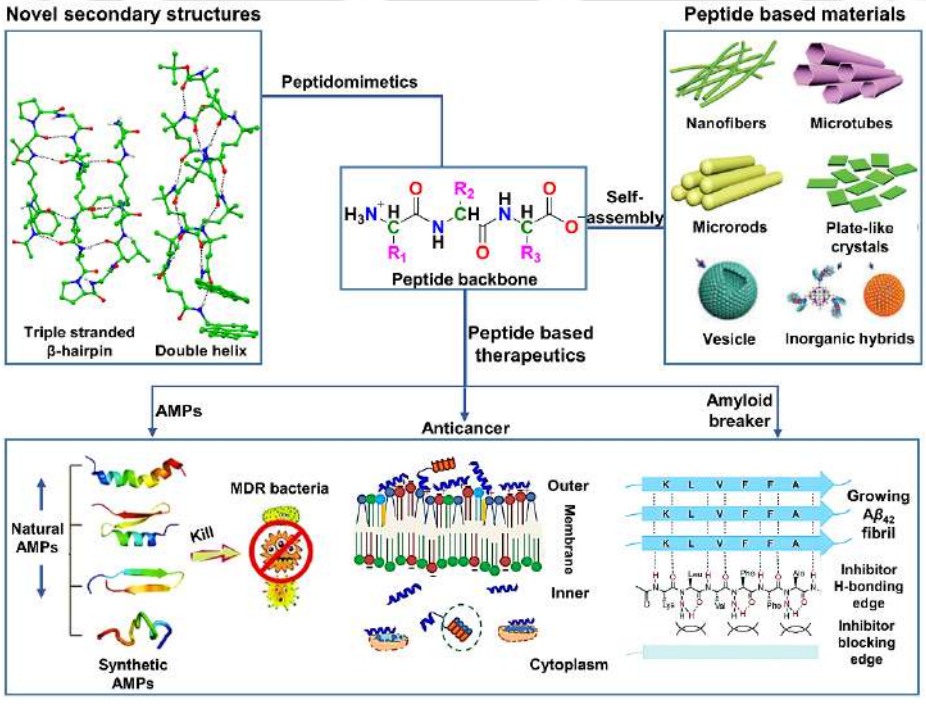

Figure 1.1. Schematic showing the significance of peptides.[38-42]

TH-3141_166122021

1.1. Peptides based therapeutics

Peptides are high potential as therapeutics, molecularly spaced in between the large proteins and the small drug molecules. Peptides are natural molecules with high immunocompatibility, that can mimic the biological ligands and can bind to several proteins, cell surfaces. with high affinity and specificity.[43-47] Peptides with their easily tunable physicochemical properties and secondary structures can be used to mimic the molecular recognition in between bio-molecules in several physiological pathways. A lot of new targets in medicinal chemistry involve peptides as receptor ligands or as enzyme substrates.[48,49] Peptides have high binding affinity and excellent target specificity, less toxicity, and higher pharmaceutical activity, making them good candidates for therapeutic approaches. Peptides can be generated in industrial scale due to their relatively easy production, making them economically viable. Bremelanotide, Leuprorelin, Afamelanotide, and Octreotide are some peptide-based synthetic drugs available in the market. Also most of the peptide-based drugs are stable molecules, easy to handle and have long shelf life. However, one of the major disadvantages of using peptide based therapeutics stems from their short systemic half-life owing to degradation by proteases.[50-55] Scientists all over the world are developing various peptidomimetic approaches to circumvent this problem.[56] Saladin *et. al.* reported that the peptide therapeutics market reached the multi-billion-dollar level in the year 2008.[57] Presently about sixty peptide-based molecules or peptide-based therapeutic agents are available commercially. Approximately 140 peptides are currently in clinical trials and more than 200 peptides are in preclinical development.[58] Insulin and vasopressin are examples of some peptide based hormones, vancomycin and daptomycin are examples of peptide based antimicrobials while bleomycin is an anticancer peptide that are commercially available.[59-62]

1.2. Why studying peptide conformations are important?

Most of the biochemical processes are mediated by protein-protein interactions, and thus its dysfunction could lead to human diseases. The molecular recognitions are governed by stereo

TH-3141_166122021

electronic requirements which are controlled to a large extent by the structure of the molecules. Helices, β-sheets and turns are the most common types of protein secondary structures which are stabilized principally by the hydrogen bond interactions. They play a significant role in molecular recognition. Epitopes derived from protein interaction sites are usually defined by secondary structures, specifically α-helices, β-sheets, β-strands, turns, and loops.[63-67] From the Protein Data Bank, it has been found that about 62% of the helical interfaces contribute to protein-protein interaction.[68-71] Thus one of the main goals in the development of peptide-based therapeutics is to develop synthetic molecules that mimic the natural peptides in their bioactive conformation. Understanding the conformations of peptides and studying them have become extremely important in the pursuit of development of peptide-based therapeutics. Several strategies, such as incorporating homologated amino acids, have been developed in peptidomimetic chemistry to rationally direct the desired secondary structures in synthetic molecules.[72-74]

1.3. Why unnatural amino acids?

In spite of several advantages of peptides that make them potential therapeutic molecules, there are some short-comings that limit their commercial application. Firstly, natural peptides are readily degraded by proteases in the digestive tract and serum, thus limiting their oral administration.[50,52,53,55] Peptides are cleared rapidly from systemic circulations which shortens their systemic half-life.[51,54] Secondly, poor absorption of peptides because of their hydrophilic nature and large structure, accompanied by lack of specific transport systems, results in reduced ability of peptides to cross physiological barriers to target intracellular targets.[75,76] The concept of peptidomimetics has been developed to address the drawbacks associated with natural peptides, and generate synthetic analogs with enhanced protease stability, good bioavailability, high receptor affinity, and specificity. Unnatural amino acid residues are used to induce protease resistance and structural constraints in the peptides. The proteases in the biological

TH-3141_166122021

system can only identify the peptide bonds in between the natural amino acids. Thus replacement of the natural peptide bonds by the unnatural peptide bonds leads to protease resistance. The construction of bioactive peptides containing unnatural amino acid units is a very widely used and valuable methodology adopted to modulate structures, protease stability, conformational preferences, and physicochemical properties of peptides.[77,78]

1.4. Unnatural amino acids

In nature, 20 amino acids are found called proteinogenic amino acids, which are the building block of all naturally occurring proteins/peptides. Unnatural amino acids are non-proteinogenic or non-coded amino acids and are generally not found in natural polypeptide chains. Some of them do occur naturally and are produced as intermediates of biosynthesis and secondary metabolites in bacteria, fungi, plants, or marine organisms.[79,80] Peptides containing unnatural amino acid residues that occur in the lower organisms are made through non-ribosomal protein synthesis pathway.[81-84] More than 800 naturally occurring non-proteinogenic amino acids are reported in the literature.[85-87] A broad range of unnatural amino acids have been synthesized in the chemical laboratory. Some unnatural amino acids are synthesized from the 20 naturally occurring proteinogenic amino acids but altered using chemical modifications. Based on the modifications various classes of unnatural amino acids are discussed in the next section.

1.4.1. Unnatural amino acids with side chain variation

The side chains of the α amino acid residues can be modified by substitution with different functional groups. E.g., the substitution of the aromatic side chains with heterocycles, larger aromatic groups[88-92] and other functional groups (such as halogen, nitro, hydroxide groups, etc.).[86,91-95] Side chains can also be modified by the addition/removal of extra methylene (CH_2) group from the side chain of amino acids.[92] Basic and acidic amino acids are modified by

TH-3141_166122021

substituting their side chain moiety with different isosteres.[92,96,97] Figure 1.2 demonstrates the examples of side chain variant amino acid residues.

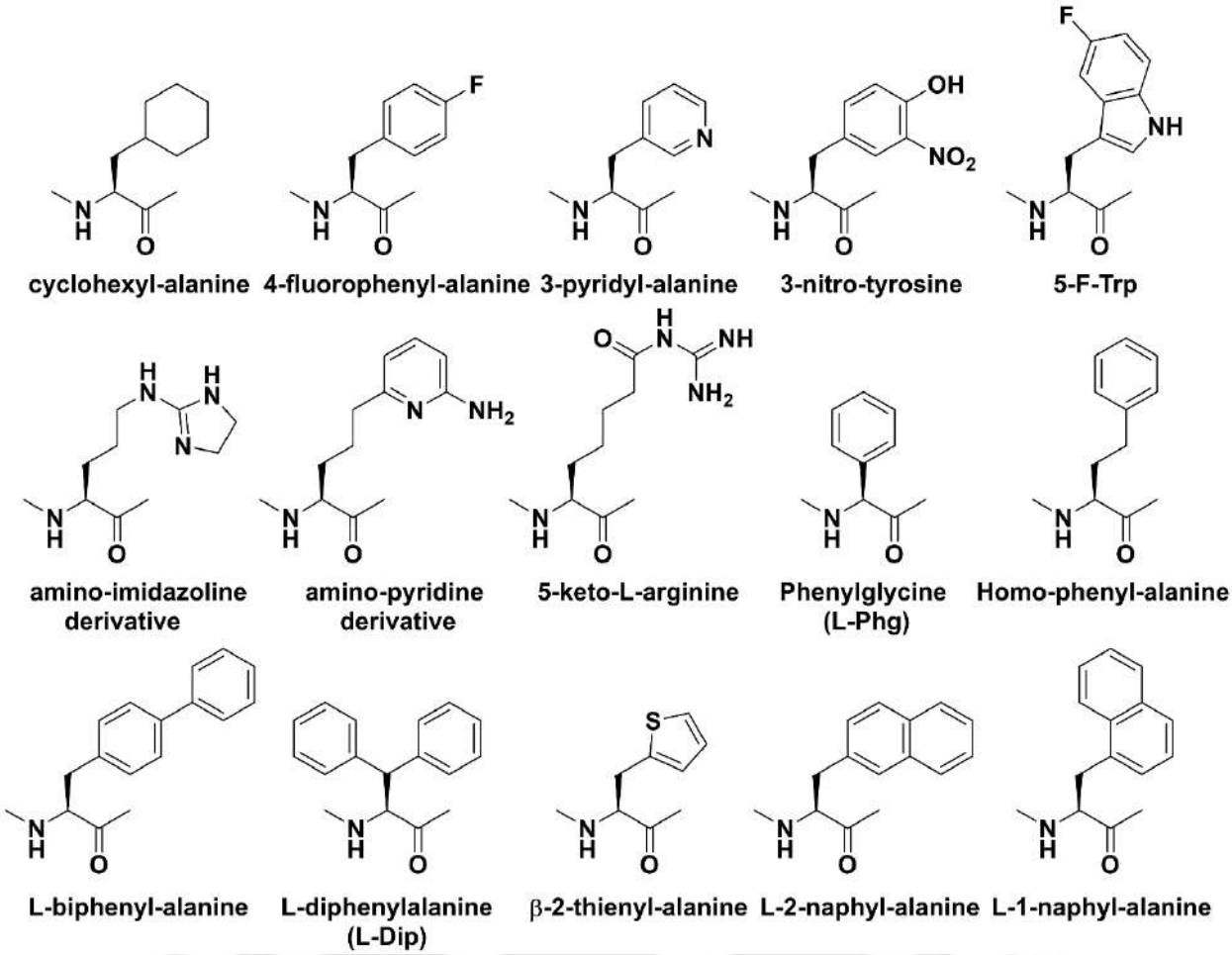

Figure 1.2. Examples of side chain modified α amino acid residues.[92,96]

1.4.2. N-alkyl amino acid residues

When an alkyl group is attached to the nitrogen of the amino group of an α amino acid residue, it is known as N-alkylated amino acid residue[98,99] (Figure 1.3). These are highly valuable as chiral building blocks for synthesizing pharmaceutically active compounds, biodegradable polymers, ligands for asymmetric catalysis, and peptidomimetics especially anti-microbial peptides and cell-penetrating peptides.[100-103]

TH-3141_166122021

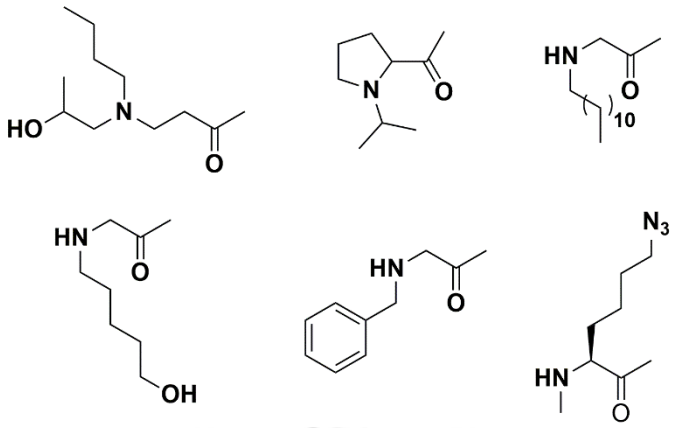

Figure 1.3. Examples of N-alkylated α amino acid residues.[98,99]

1.4.3. Modification of the α-carbon

This can be achieved by modifications of the α-carbon, including inversion of configuration at an α-carbon, replacement of the α-hydrogen by the alkyl or other group, and isoelectronic replacement of the α-carbon atom by a heteroatom (mostly nitrogen). Modified residues with the α-carbon replaced by the N atom are called aza amino acid residues (Figure 1.4). These common operations on the α-carbon of peptides result in novel peptidic compounds with different secondary structures and new pharmacological properties.[104-107]

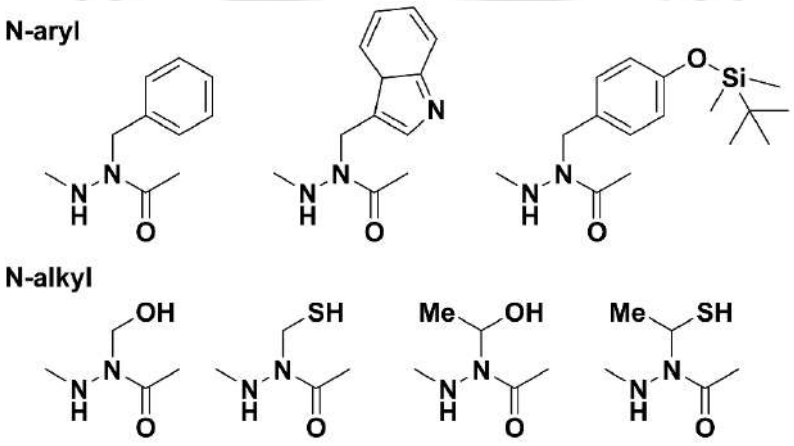

Figure 1.4. Examples of aza amino acid residues.[104,105]

TH-3141_166122021

1.4.4. Backbone extended higher homologues of α amino acid residues: ω amino acid residues

Residues in which additional carbon atoms $(C)_n$ are inserted in between the terminal amino and carboxylic acid group of the α amino acid residue are called homologated amino acid residues. When n=1, it is called β residue; n=2, it is called γ residue, and so on. All the homologated amino acid residues are called omega (ω) amino acid residues in general (Figure 1.5). α amino acid residue backbone can be defined by three torsional variables namely ϕ (N-C^{α} bond), ψ (C^{α}-C bond) and ω (CO-NH- bond). As the peptides bonds are planer moieties with trans stereochemistry (except proline), ω is usually 180°. Insertion of additional carbon atoms into the backbone of the ω amino acid residues increases the number of degrees of torsional freedom and subsequently the number of torsional variables in them. These additional torsional variables are called θ_n, where n is a positive integer that represents the number of additional carbon atoms that have been inserted into the backbone of the α amino acid residues. θ_n is numbered from the N-terminus to the C-terminus of the residue. Thus, β amino acid residues, where one carbon is inserted into the backbone of the α amino acid residues *i.e.* n = 1, has three torsional angles ϕ, θ and ψ, while γ amino acid residue with two carbons inserted in the backbone (*i.e.* n = 2), has four ϕ, θ_1, θ_2, and ψ torsional variables (Figure 1.5). Peptides composed of all α amino acid residues are known as α peptides, while peptides containing all homologated residues are termed as ω peptides. Peptides containing α and ω amino acid residues are called hybrid peptides.[108]

TH-3141_166122021

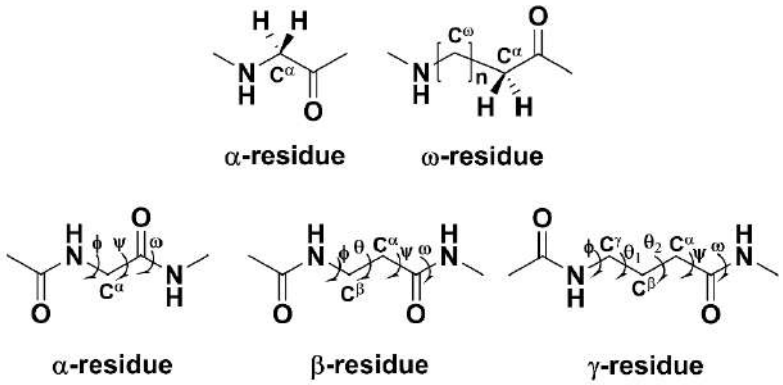

Figure 1.5. Chemical structures of α and ω amino acid residues (top) and definition of backbone torsion angles of α, β, and γ residues (bottom). The number of torsional variables is also indicated.[108]

1.4.4.1. Importance of ω amino acids in peptides

There are many different advantages of incorporating homologated amino acids in peptides,

i. As homologated amino acid residues have additional carbon in between amino and carboxylic acid groups, there is a chance for the expansion of energetically accessible conformational space.

ii. Due to the backbone's expansion, ω amino acid residues can form novel intramolecular H-bonds that are backbone expanded analogs of the canonical H-bonds found in all α amino acid residue containing peptides.

iii. In spite of their increased degrees of freedom, ω amino acid residues are accommodated into well-folded secondary structures with great facility.

iv. Several novel foldamers have been designed by the use of ω amino acids.

v. Lastly, peptides composed of ω amino acid residues are generally protease resistant, which may lead to the rational design of proteolytically stable analogues of medicinally important peptides.

TH-3141_166122021

1.5. β- and γ-amino acid residues

Probably the most common, and perhaps the most important naturally occurring β- and γ-amino acids are HβhGly-OH, or β-alanine and γAbu, respectively. Due to their conformational flexibility, they can be accommodated into helices, turns, and random coils with equal ease. The simple backbone of these two ω amino acid residues can be modified in various ways to generate different classes of ω amino acid residues that have been discussed below.

1.5.1. Mono-substitution with proteinogenic and non-proteinogenic side chain

Homologated β and γ-amino acids can be synthesized from proteinogenic α amino acids and by other reaction method, which generate mono-substituted β and γ-amino acids.[109-126]. All the amino acid residues with proteinogenic side chain have L-configuration in Fischer nomenclature. Figure 1.6 shows chemical structures of some exemplary mono-substituted β and γ amino acid residues. The one-letter nomenclature of amino acid residues have been adopted from the literature.[111] In the case of β-residue, substitutions at C2 and C3 are possible. The stereochemistry for C3 mono-substituted β^3-amino acid is retained (except β^3hVal, β^3hIle, β^3hCys) similar to the α-residue ('S'-configuration),[111] but in the case of C2 mono-substituted β^2-residue, the stereochemistry becomes reversed ('R'-configuration) (except β^2hCys, β^2hSer, β^2hThr).[111] In the case of γ-residue, three substitutions at C2, C3, and C4 are possible. The stereochemistry at the substituent carbons are 'R' (at C4, except γ^4hhAla), 'S' (at C3), and 'S' (at C2, except γ^2hhAla and γ^2hhCys), respectively.[111]

TH-3141_166122021

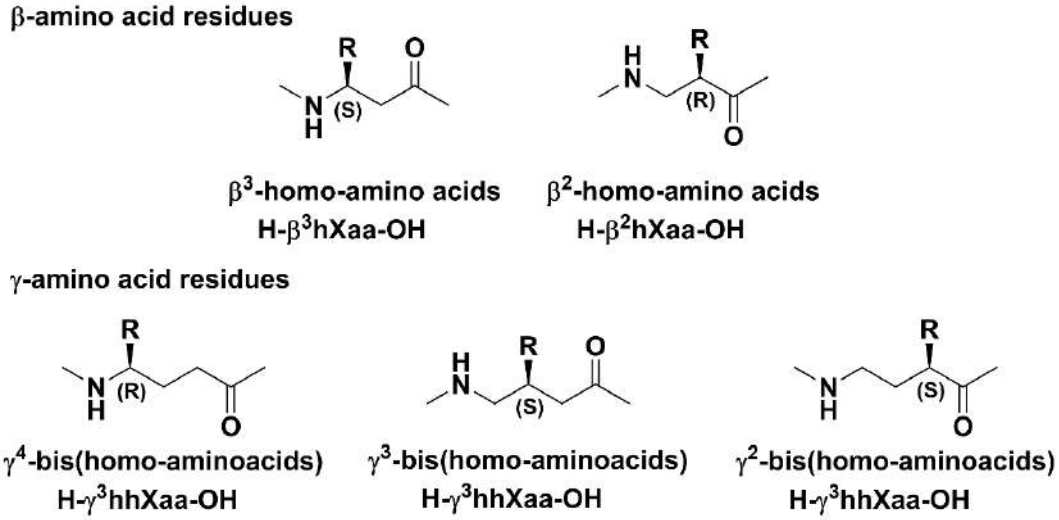

Figure 1.6. Examples of mono-substituted β and γ-amino acid residues. R= proteinogenic side chain of α-residues.[111]

1.5.2. Geminal di-substitutions (non-cyclized and cyclized)

When di-substitution is present at the same carbon atom, it is called geminal di-substitution. Di- substituted β- and γ-residues are designated as $\beta^{2,2}/\beta^{3,3}$ and $\gamma^{2,2}/\gamma^{3,3}/\gamma^{4,4}$ respectively, depending on the location of di-substitution. Some examples of such classes of ω amino acid residues are given in Figure 1.7.[127-135]

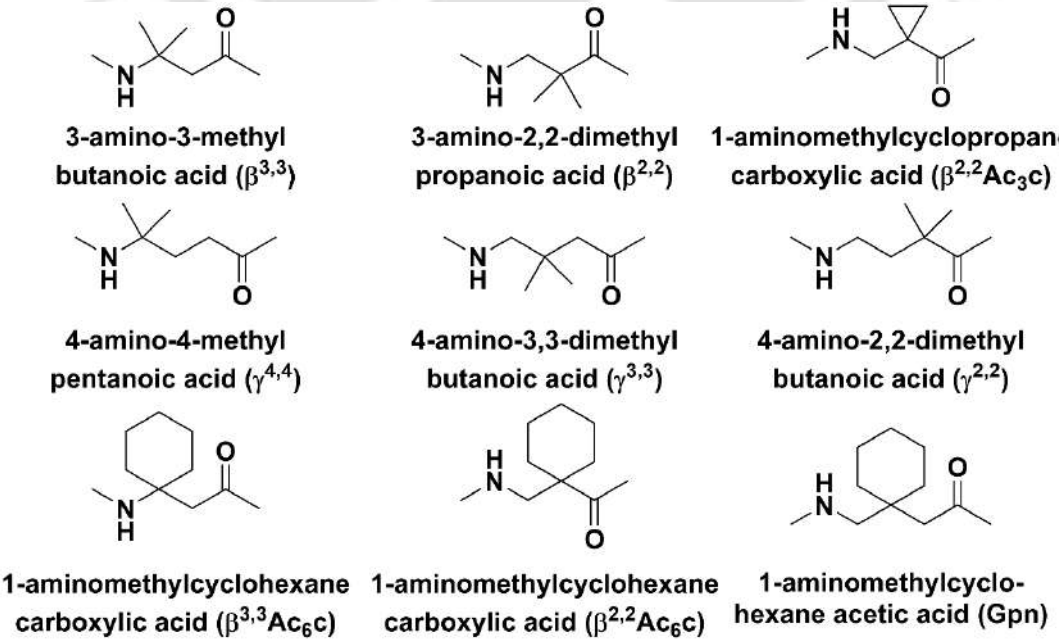

Figure 1.7. Examples of some geminally di-substituted β and γ-amino acid residues.[127-135]

TH-3141_166122021

1.5.3. Vicinal di-substitutions (non-cyclized and cyclized)

When di-substitution is present at the neighboring backbone carbon atoms, it is known as vicinal di-substitution. Two types of vicinally di-substituted ω amino acid residues are possible: (a) non-cyclized and (b) cyclized. In the case of a non-cyclized di-substitution, β-residue has two possible isomers. In the similar situation, γ-residue has six possible isomers, depending on the substitution position and its stereochemistry.[113,120,121,136-150] In the case of cyclized one, the side chain of the amino acid backbone is cyclized. For β-residue, the cyclization is in between C^{α} and C^{β} substituents, while for γ-residue, it can either be between C^{α}-C^{β} or C^{β}-C^{γ} substituents. There is another type of cyclized β-residue, where the amine group is cyclized with the side-chain. Many studies have used vicinal di-substituted β and γ-amino acid residues (Figure 1.8) to induce secondary structure in synthetic peptides.[149,151-165]

TH-3141_166122021

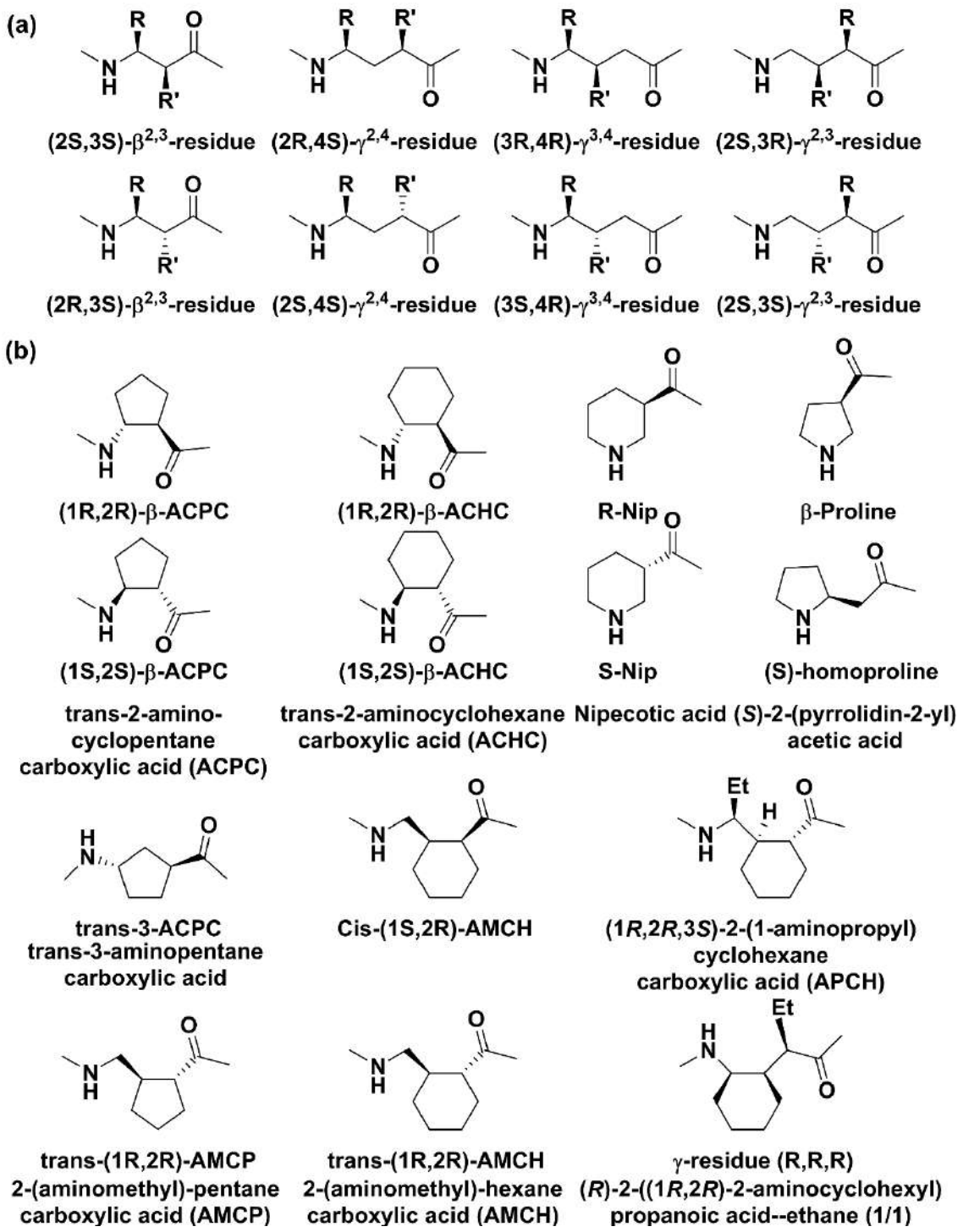

Figure 1.8. Example of various vicinally di-substituted β and γ-residues (a) Non-cyclized residues, where R= proteinogenic side chain of α-residues and (b) Cyclized residues.

TH-3141_166122021

1.5.4. Backbone unsaturated ω amino acid residues

γ-residues are mainly studied in this particular class of ω amino acid residues, where unsaturation is placed at the C^{α}-C^{β} bond. These amino acid residues are known as vinylogous-γ-amino acid residues. Depending on the geometry of the double bond, it can either be cis (Z) or trans (E). There are studies where vinylogous-γ-amino acid residues have been incorporated to generate secondary structures like C_{12} helix,[166,167] double-helix,[168,169] parallel sheets,[169,170] anti-parallel sheets,[170] anti-parallel strands of β-hairpin,[170,171] and non-helical isolated β-turns.[172] Some examples of this class of ω amino acid residues are shown in Figure 1.9.

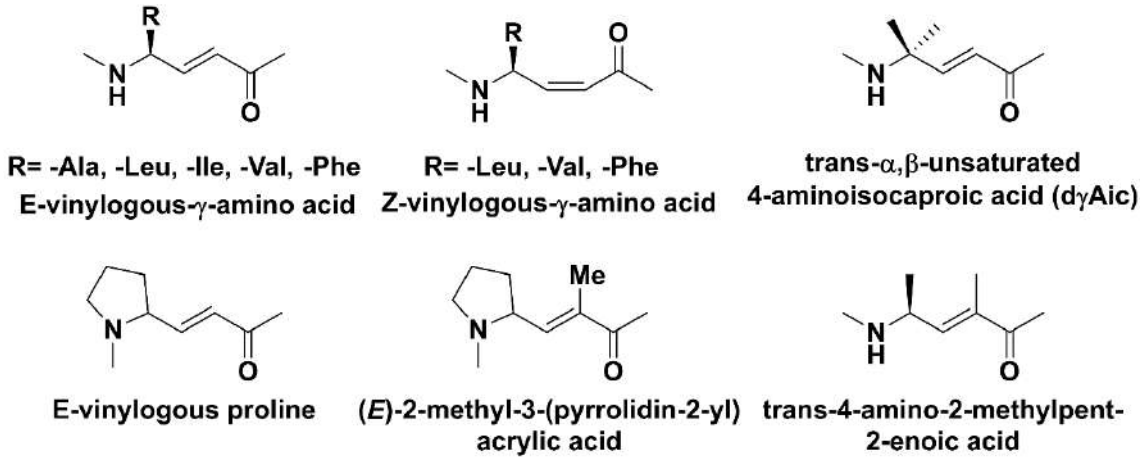

Figure 1.9. Examples of various E or Z-vinylogous-γ-amino acid residues reported in the literature.[167-174]

1.5.5. Mono and di-substitution (geminal and vicinal) with furanoid sugar moiety

These amino acids containing different furanoside side chains, such as D-lyxo, D-xylo, D-ribo etc., are called C-linked carbo-X-amino acids (where X=β, γ) or furanoid sugar amino acids.[175-183] Both mono (substitution only at C3 and C4 carbon for β and γ residue, respectively)[175-183] and di-substituted (both geminal and vicinal cyclized β-residues)[184-187] furanoid sugar amino acids have been reported in the literature. Figure 1.10 illustrates various examples of mono and di-substituted sugar amino acid residues.

TH-3141_166122021

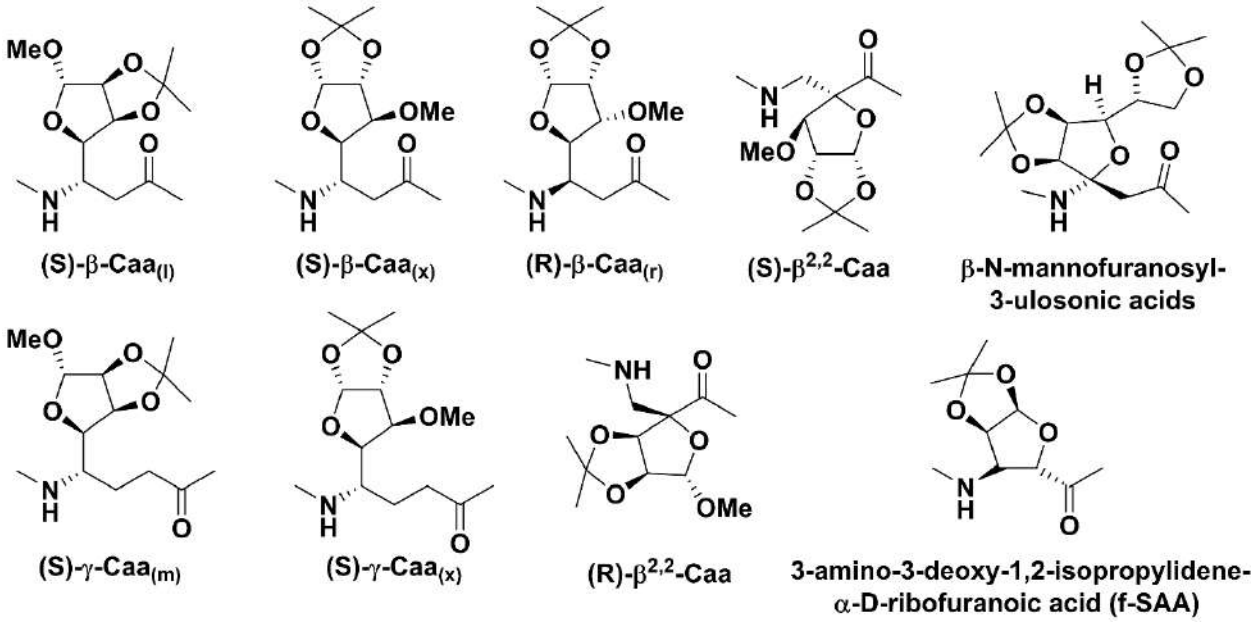

Figure 1.10. Examples of mono and di-substituted furanoid sugar amino acid residues.[170-182]

1.5.6. Aromatic ω amino acid residues

In this class of ω amino acid residues, aromatic moieties are placed in the backbone of the β and γ-amino acid residues. Figure 1.11 represents examples of aromatic ω amino acid residues.[188-192]

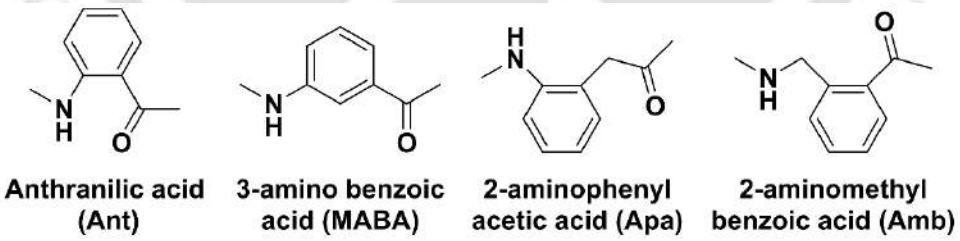

Figure 1.11. Examples of aromatic ω amino acid residues.[189-191]

TH-3141_166122021

1.6. Torsional variables of α-amino acid residues and Ramachandran map

Torsion angles of the α amino acid residues in polypeptides and proteins define rotations about N-C^{α} (ϕ) and C^{α}-C (ψ) bonds. The values of torsion angles, ϕ and ψ range from -180° to +180°. The third torsion angle ω of the α polypeptide chain is about the peptide bond and hence restricted to mostly 180°(trans) and 0° (cis, in the case of proline). The allowed conformational space of amino acid residues in a protein/polypeptide structures (ϕ and ψ) is conveniently represented in a 2D map of ϕ and ψ, known as the Ramachandran plot (Figure 1.12).[193-195] Each secondary structure adopted by the polypeptides has characteristic range of torsion angles (ϕ and ψ). Conformations that adopt non-allowed torsion angles are energetically unfavorable and hence do not exist. Right-handed helices have torsional angles ϕ = -57°, ψ = -47°, which lies in the lower left quadrant in the Ramachandran map. The β-sheet, which has extended structure, adopts a value of ϕ ≈ -120° to 140°, ψ ≈ 113° to 135°, and appears in the upper left coordinate, while the left-handed α helices occur in the upper right quadrant (ϕ = +57°, ψ = +47°).[196,197]

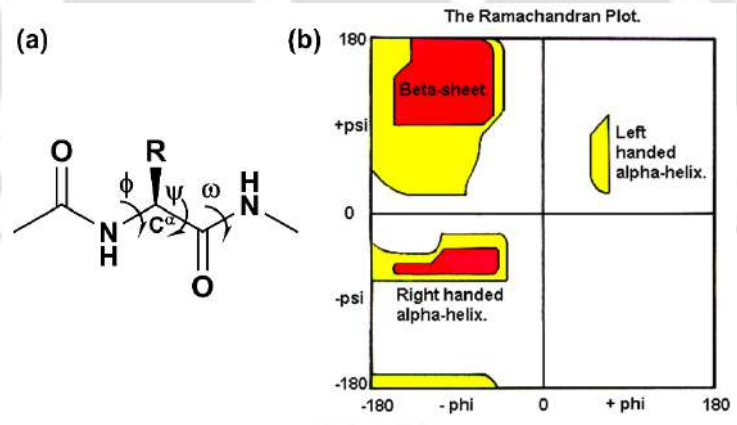

Figure 1.12. (a) Chemical structure of α-peptide backbone and its torsion angles (b) Sterically allowed conformational space of the α polypeptide backbone in Ramachandran map.[193]

Each α amino acid residue adopts certain torsion angles depending on its side chain. Among 20 proteinogenic amino acids, Gly is the simplest amino acid residue as it has no side chain. Due to its flexibility, it can adopt any values of ϕ, and ψ. Thus, it can access larger

TH-3141_166122021

conformational space (Figure 1.13a).[198-200] The available space reduces significantly when one methyl substitution is added to the C^{α} proton, i.e., for Ala residue (Figure 1.13b). Alanine shows considerably higher propensity for helices, but can adopt other conformations as well.[193-195,197] Aib, a known non-standard amino acid residue (primarily found in the lower organisms), becomes rigid when the second methyl substitution is added to Ala. The torsion angles flanking the di-substituted C^{α} carbon atom, adopt gauche conformations. The conformational space available to this amino acid residue is extremely reduced due to this. As the torsion angles that the residue can adopt matches to that of the helices, this residue has a high propensity to be accommodated in the helices. Thus, geminal di-substitution can constrain the flanking torsion angles about the point of di-substitution to gauche values.[201-203] (Figure 1.13c)

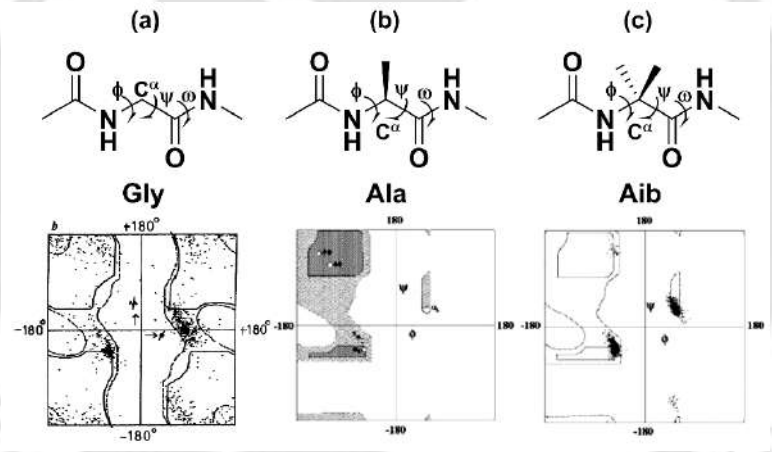

Figure 1.13. Ramachandran plot for a) Glycine,[198] b) Alanine[197] and c) 2-amino isobutyric acid (Aib).[197]

Proline (Figure 1.14a) is the only residue among all α amino acid residues in which side-chain cyclizes with the backbone. Due to this, the torsional freedom about the torsion angle ϕ is restricted (Figure 1.14b) to ~ -60° to -80°.[197,204] Non-helical β turns help the polypeptide chain to reverse its directionality. Proline can be accommodated at the (i+2) position of the Type I' and Type II' beta turn. On the other hand due to its conformational rigidity, Proline produces

TH-3141_166122021

a kink in the helix or the β-sheet. Thus backbone cyclization can constrain the torsion angles which are part of the cycle.

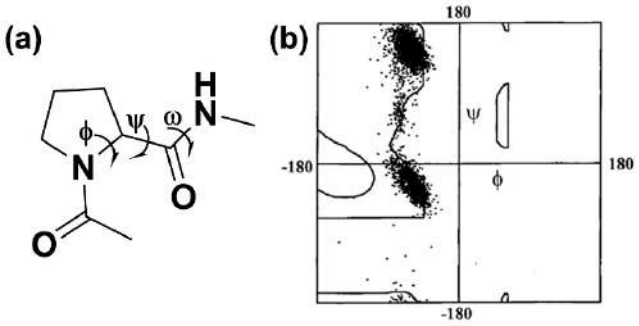

Figure 1.14. (a) Chemical structure, (b) Ramachandran map for Proline residue.[197]

1.7. Conformationally constrained amino acid residues

Directing secondary structure in short peptides:

Adoption of α helical structure in short all proteinogenic α amino acid residues containing peptides is difficult. Protein folding is an entropy driven process. Longer the chain of the peptide, larger the entropic gain achieved upon folding of the peptide chain by releasing larger number of caged water molecules. Hence it's difficult to fold shorter chains. Rational design of secondary structures in short peptides is a challenging task. However, this has been achieved in peptidomimetics by the use of constrained amino acid residues, whose torsion angle values match to the typical torsion angle of the desired secondary structure. This is one of the major advantages of using conformationally constrained amino acid residues. Inspired by the constraining of torsion angles in the α amino acid residues, similar strategies have been adopted for the ω amino acid residues. Constrain in the amino acid backbone can be incorporated in the following ways.

1.7.1. Geminal di-substitution

Several geminally di-substituted amino acid residues have been used in the synthetic peptides (Figure 1.15). The geminal substituents might be both acyclic or cyclic in nature. In all of these,

TH-3141_166122021

torsional variables flanking the point of di-substitution adopts *gauche* conformations, which are ideal for generating folded helical conformations. Geminal di-substituted α amino acid, Ac_6c is known to adopt 3_{10} helical conformations just like Aib and can also be accommodated at the i+2 position of the Type II' β-turns.[205-209] (Figure 1.15) The introduction of geminally di-substituted β (di-substitution at C2 and C3 carbon with different cycloalkyl group)[127,128,210] and γ-amino acid residues (β,β'-di-substituted, Gpn)[211-219] into the synthetic peptides has been started by the group of Seebach and Balaram, respectively. For α,α' and β,β'-di-substituted β-amino acid residues like $\beta^{2,2}$-Ac_3c/$\beta^{2,2}$-Ac_6c and $\beta^{3,3}$-Ac_6c, the dialkyl substitution present at C^{α} and C^{β} carbons respectively, restricts the torsion angles (θ, ψ) and (ϕ, θ) primarily to the *gauche* conformations.[128,210] Similarly, for the β,β'-disubstituted γ-amino acid residue, Gpn, di-substitution at the C^{β} carbon restricts the torsion angles θ_1 and θ_2 to *gauche* values.[217-219] Due to their restricted conformational behavior, peptides constructed with these amino acid residues could embrace various novel folded structures both in homo as well as in hetero-oligomers.[206-214] Peptides containing di-methyl substituted γ amino acid residues, 4-amino-4-methylpentanoic acid (Aic or $\gamma^{4,4}$)[135] and 4-amino-3,3-dimethylbutanoic acid (Adb or $\gamma^{3,3}$)[133] have been reported for the first time by Gopi and co-workers and mainly shown to promote various helical conformations (both for Aic, and Adb containing αγ-hybrid peptide) like 12-helix,[220,221] mixed 12/10-helix,[220] 15/17-helix,[221] ambidextrous helix,[133] ε-helix[222] in addition to extended structures for homo-oligomers composed of Aic.[135]

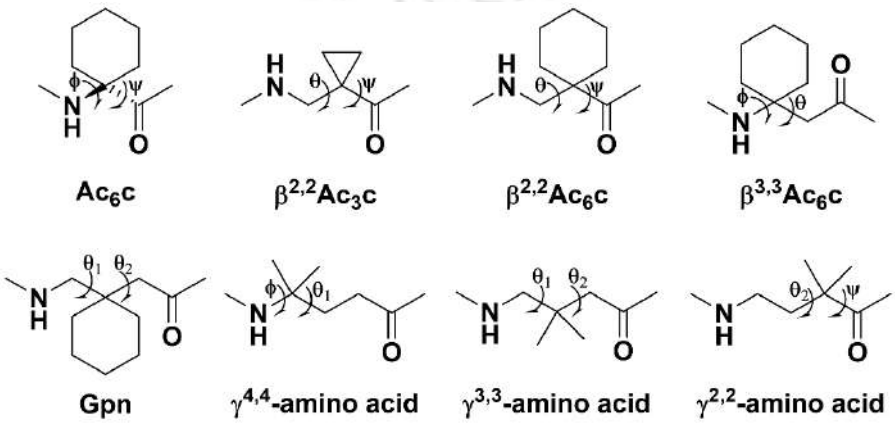

TH-3141_166122021

Figure 1.15. Geminally di-substituted β and γ amino acid residues and their corresponding constrained torsion angels (marked by the black arrow).

1.7.2. Vicinal di-substitution with cyclization

Homo-oligomers composed of side chain cyclized β-amino acids trans-2-ACPC and trans-2-ACHC have been characterized crystallographically for the first time by Gellman and co-workers, which were found to form helical conformations.[151-154] Side chain cyclization restricted the torsion angle θ to adopt *gauche* conformation, leading to helix formation. Backbone cyclized β-amino acids, Nipecotic acids (R-Nip and S-Nip) were used to nucleate β-hairpin turn as both of them have constrained dihedral angles ϕ and θ through cyclization.[155,156] Leah *et. al*. reported PPII-like helical conformations of β-proline hexamer with the opposite handedness than α-proline.[164] Here, the conformational preference was controlled by the constrained torsion angle ϕ. Gellman and co-workers also studied peptide conformations by using several ring-constrained γ amino acid residues.[152-158] The conformations adopted by these residues were mostly helices, and very few promoted extended conformations. The structural analysis was done both with the homo-oligomeric sequences as well as different alternating hybrid peptide sequences like αγ, βγ and αβγ etc. The structural differences depended on the main three factors, such as stereochemistry of the stereogenic centers, ring size as well as the placement of the ring. For example, residue trans-3-ACPC, where a five-member ring was placed in between C^{α} and C^{γ}, adopted a parallel sheet secondary structure. For the tri-substituted γ residue EtACHA, where the constraint was present in between the C^{β}-C^{γ} bond (θ_1 torsion angle), displayed *gauche-gauche* conformations at the θ_1 and θ_2 which supported them to promote helical structures in γ (14-helix),[160] αγ (12-helix),[157] βγ (13-helix)[158] and αβγ-peptides (12-helix).[223] Similar results were observed by Guo *et. al*. for the cis-AMCH residue, where the cyclohexyl ring linked the C^{α} and C^{β} carbon.[161] Giuliano *et. al*. have examined the conformation of αγ peptide composed of a tri-substituted γ amino acid residue, APCH, in which

TH-3141_166122021

θ_1 and θ_2 torsion angles were constrained, due to the presence of a six-membered cyclohexyl ring across C^{α}-C^{β} bond. The αγ-peptides adopted 12/10-helix with alternating H-bond directionality.[163] Despite of having cyclopentyl ring constraining the backbone of trans-AMPC residue, it was found to have less propensity to adopt any specific secondary structures of αγ-hybrid peptides.[162] Gellman and co-workers showed that residue trans-AMCH in adopted *trans-gauche* conformation for torsion angles θ_1 and θ_2 respectively, in a αγ dipeptide, which was predicted to form 15/17-helix but never established experimentally.[161,224] Figure 1.16 shows the chemical structures of backbone cyclized constrained ω amino acid residues.

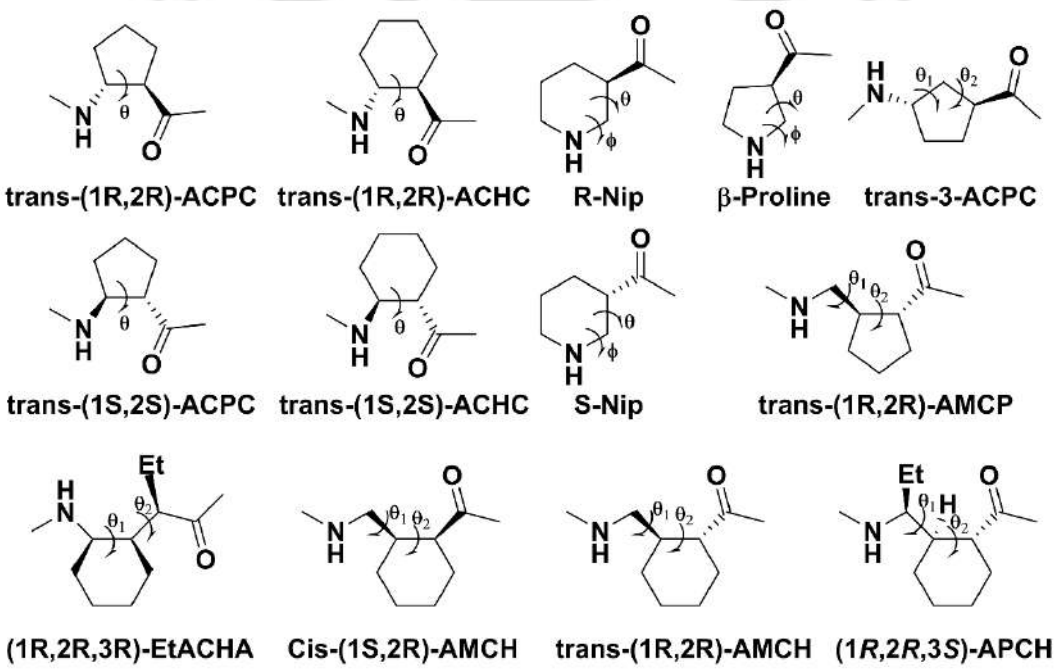

Figure 1.16. Examples of β and γ amino acid residues in which torsional freedom has been restricted using side chain-backbone cyclization. Black arrows mark the constrained torsion angles.

1.7.3. Backbone unsaturation

The conformational space of the γ amino acid residues can also be restricted by the insertion of unsaturation in the backbone (Figure 1.17). Unsaturation provided *cis* and *trans* geometry

TH-3141_166122021

at the peptide backbone. While *trans* geometry mainly preserved the planarity of the peptide bond, cis geometry could twist the backbone a little. Oligomers composed of α, β or β, γ-unsaturated (θ_2 and θ_1 constrained respectively) γ amino acid residues are called vinylogous peptides.[161-169] Substitution at C^{α} along with unsaturation restricted the torsion angles θ_2 and ψ.[170,172,174] Di-substitution at C^{γ} limited the torsional freedom for ϕ, θ_1 and θ_2 respectively.[168,169] So far, several groups have explored the conformations of their homo-oligomers as well as hetero-oligomers. Based on the geometry and substitution pattern present at the C^{α} and C^{γ} carbon atom of the amino acid residues, it could adopt various secondary structures like extended parallel[169,170] and anti-parallel sheets,[170] β-hairpin nucleating turns,[172] double helix,[168,169] 12-helix[166,167] etc.

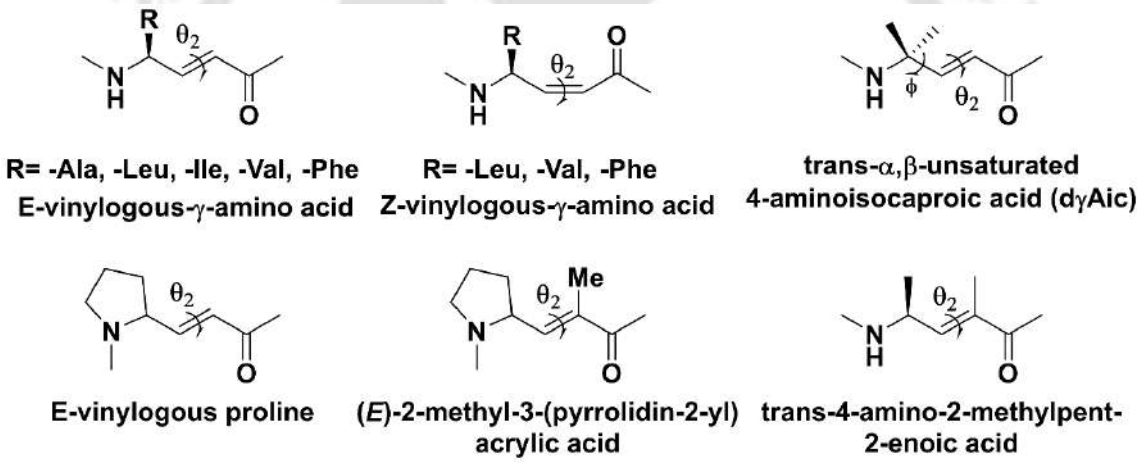

Figure 1.17. Examples of vinylogous-γ amino acid residues. Torsional freedom has been restricted by introducing double bond in the backbone. The constrained torsion angles are marked by black arrows.

1.7.4. Aromatic ω amino acid residues

β and γ amino acid residues with aromatic backbone have been frequently used in the literature (Figure 1.18).[183-187] 2-amino benzoic acid or anthranilic acid (Ant),[188,189,191] 3-amino benzoic acid (MABA),[190] 2-aminomethyl benzoic acid (Amb), 2-aminophenylacetic acid (Apa)[191] are

TH-3141_166122021

some constrained aromatic amino acids. In the case of Ant, which is a β-residue, the constrained torsion angle is θ while for MABA, θ_1 and θ_2 are constrained. For Apa and Amb, the restricted torsion angles are θ_1 and θ_2, respectively. They have been used to understand the influence of steric constraints on conformational behavior.

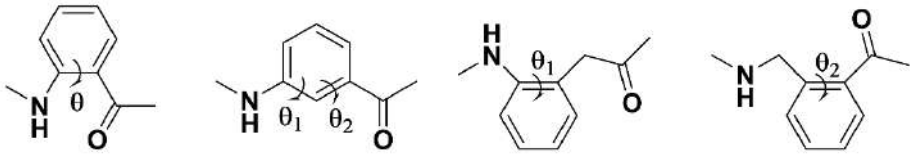

Figure 1.18. Examples of aromatic β and γ amino acid residues with aromatic ring induced torsional constraint. Black arrows mark the constrained torsion angles.

1.8. Directionality of H-bonds

H-bonds stabilize the secondary structures s of peptides. These H-bonds have been divided into two categories depending on their directionality as normal and reverse.

1.8.1. Normal Directionality: CO (i)……. NH (i+n)

In the normal directionality of H-bonds, the H-bond acceptor group CO lies towards the N-terminus, and the H-bond donor, i.e., NH, lies towards the C-terminus. The H-bond formed between the CO of the i^{th} residue with the NH of the $(i+n)^{th}$ residue. The schematic representation is shown in Figure 1.19. In nature, there are several examples of the normal directionality of H-bonds. For example, C_{10} hydrogen bond stabilizes 3_{10} helix (CO(i)….NH(i+3)),[225-228] C_{13} H-bond (CO(i)….NH(i+4)) stabilizes the α helix,[229,230] and the C_{16} bond (CO(i)….NH(i+5)) stabilizes the π-helix.[227,231-233]

TH-3141_166122021

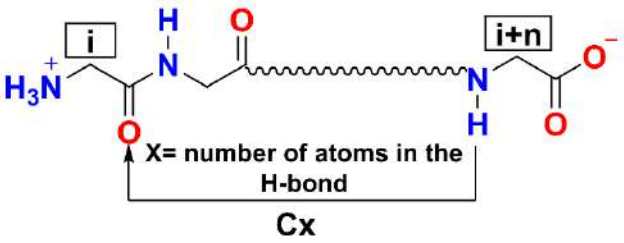

Figure 1.19. Schematic representation of the normal directionality of H-bonds.

1.8.2. Reverse Directionality: NH (i)…….CO (i+n)

For reverse directionality H-bond, the H-bond donor (NH) lies towards the N-terminus, and the acceptor (CO) lies towards the C-terminus. The H-bond formed between the NH of the i^{th} residue with the CO of the $(i+n)^{th}$ residue (Figure 1.20). This class of hydrogen bonds is rarely seen in nature.[234] However, in peptidomimetic studies, they have been characterized where homologated amino acid residues are incorporated.[151,222,235,236]

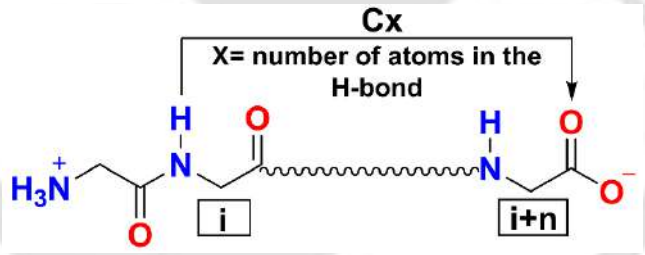

Figure 1.20. Schematic representation of the reverse directionality of H-bonds.

1.9. Expanded H-bonded turns

ω amino acid residues have additional carbon atoms in their backbones, so when these residues form H-bonds, they increase the hydrogen bonded ring size compared to their all α amino acid analog.[108] Hydrogen bonds are named as Cx, where x stands for the number of atoms in the hydrogen bonded ring.

TH-3141_166122021

1.9.1. One residue H-bonds

Examples of one residue H-bonded turn both in the normal (3→1) and reverse (1→1) direction are shown in Figure 1.21. In the normal direction, a one residue H-bonded ring of α-amino acid residue would be C_7, stabilized by a 3→1 hydrogen bond between CO (i)…..NH (i+2).[237] The C_7 H-bonded ring of α peptides expanded to a C_8[205] and C_9[212,238] H-bonded turn when a β amino acid residue and a γ amino acid residue was used respectively. Similarly, in the reverse direction, the size of the ring for α amino acid was C_5[239,240] which expanded to C_6[128,241,242] and C_7[212,243] for β and γ amino acid residues, respectively.

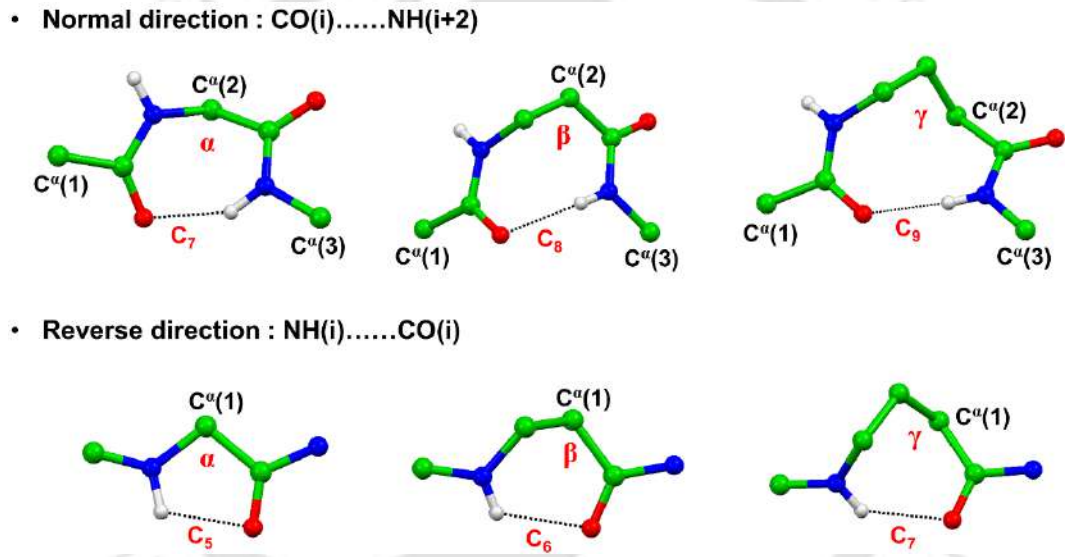

Figure 1.21. Crystallographically characterized examples of one residue H-bonded turns in normal (3→1)[210,212,237] and reverse (1→1)[239,242,243] directions.

1.9.2. Two residue H-bonds

Both homo and hetero dipeptide segments can form two residue H-bonded rings. For the α peptides in the normal direction (4→1), the turn is C_{10} turn which is known as β-turn. There are different classes of β-turns which are classified on the basis of their backbone torsion angles. Those β-turns which upon repetition gives rise to helices are called helical turns while

TH-3141_166122021

those which do not give rise to helices rather bring about a reversal in the direction of the polypeptide chain are known as the non-helical β-turns.[108] The C_{10} αα[244] β-turn is expanded to a C_{11} in the case of an αβ unit,[245-248] C_{12} for αγ[157,161,212,214,215,220,221,249] and ββ segments,[151,152,154,250] a C_{13}-turn in the case of a βγ unit[158] and C_{14} for γγ unit.[251,252] The C_{13} βγ turn is equal in size to a C_{13} ααα three residue turn in all α-peptides. Similarly, in the reverse direction (1→2), C_8 turn is formed in the case of αα unit, which gets expanded to a C_9 turn in the case of αβ or βα,[241] or to a C_{10} turn in the case of a ββ segment.[210] Figure 1.22 illustrates the crystallographically characterized examples of 4→1 and 1→2, two residue H-bonded turns.

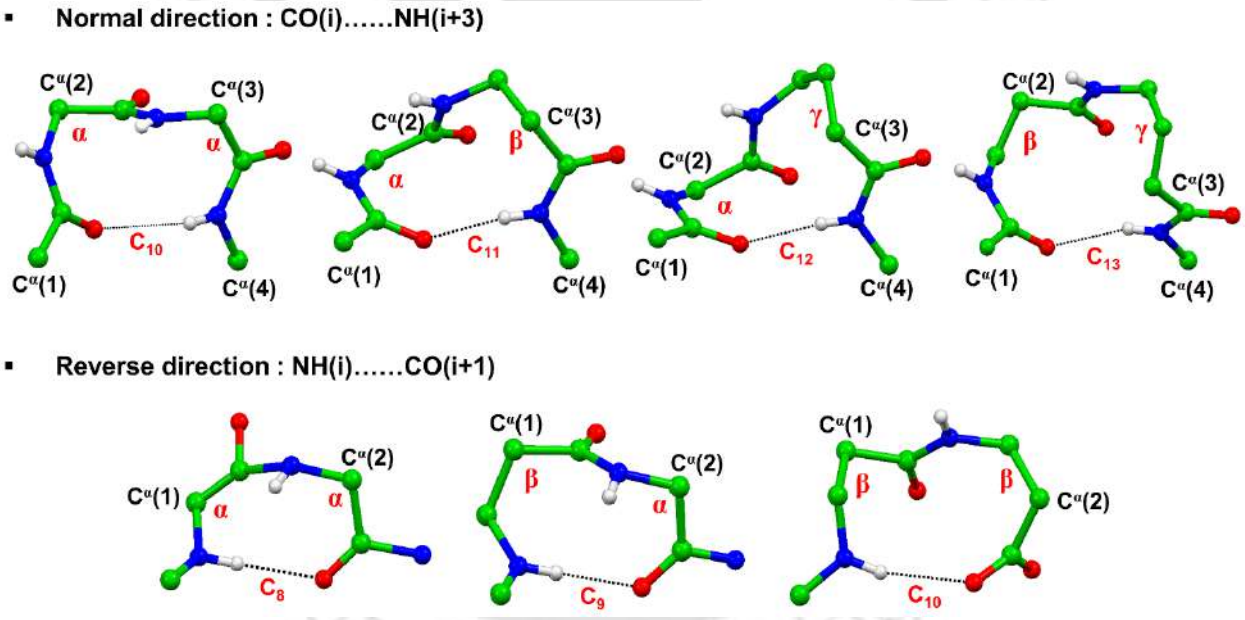

Figure 1.22. Crystallographically characterized examples of two residue H-bonded turns in normal (4→1)[212,215,244,245] and reverse (1→2) directions.[210,241]

1.9.3. Three residue H-bonds

In the case of normal direction three residue turn, the C_{13} turn (across the ααα segment) of α-peptides, stabilized by CO (i)….NH (i+4), 5→1 H-bonds along the backbone gets expanded to a C_{14} (ααβ),[214] C_{15} (αββ)[253] and C_{17} (γαγ)[221,243]H-bonded turn upon incorporation of ω amino

TH-3141_166122021

acid residues. All of these turns can be repeated and generates continuous helices. In the case of reverse direction three residue turns (1→3), a C_{14} turn was characterized in all $(\beta)_n$ sequences.[151] (Figure 1.23)

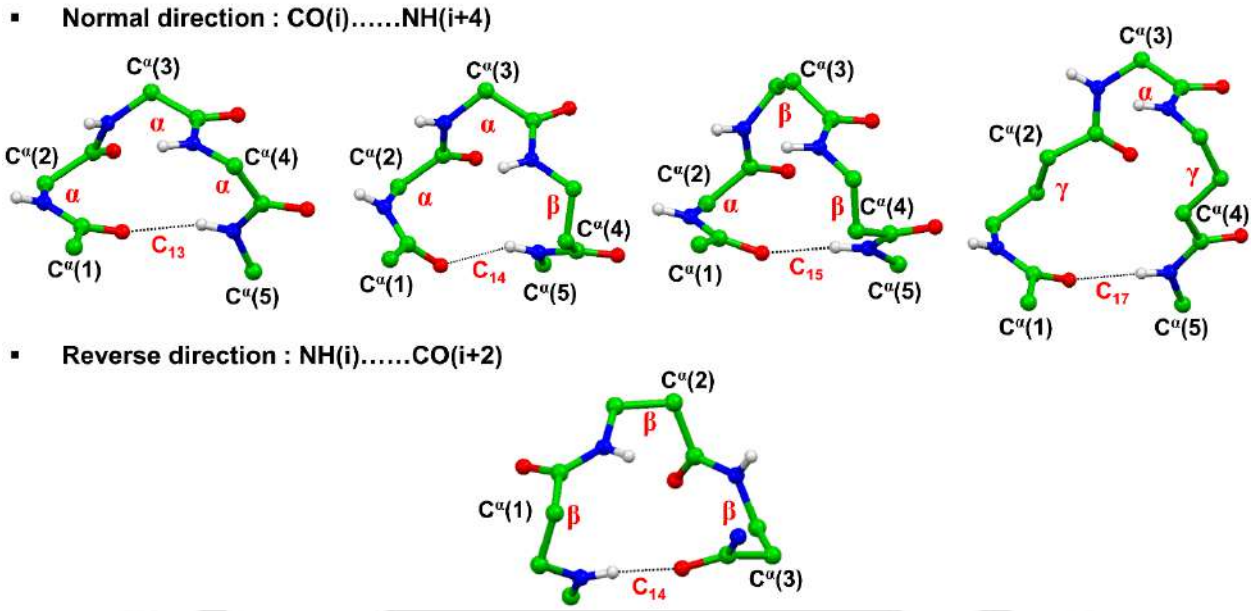

Figure 1.23. Crystallographically characterized examples of three residue H-bonded turns in normal (5→1)[214,221,253] and reverse (1→3) directions.[151]

1.10. ω amino acid residues in secondary structures

ω amino acid residues have additional torsional variables owing to the homologated backbone. This imparts greater flexibility to them. Studies on the peptides containing ω amino acid residues have been enhanced in the last few decades owing to the fact, that ω amino acid residues can very well be accommodated into well folded secondary structures.[108,111,150,217,254-259] Most of these structures are backbone expanded analogs of the canonical all α amino acid residue containing peptide structures. The secondary structures of the peptides containing ω amino acid residues are stabilized by the expanded hydrogen bonds that have been discussed in the earlier section. The introduction of ω amino acids into the field of peptidomimetics has

TH-3141_166122021

made by Seebach and co-workers by the incorporation of backbone homologated β-amino acid residues,[111] synthesized from the proteinogenic α amino acid residues.[111] Gellman and co-workers have studied peptide conformations by incorporating cyclic β and γ amino acid residues.[157-163,254,255] The introduction of geminally di-substituted γ amino acid, Gabapentin (Gpn) into the synthetic peptides was achieved by Balaram and co-workers.[206-214] There are several reports where ω residues have been accommodated into helices, extended structures, and non-helical turns characterized experimentally in solids and solutions. In the section below, we have described examples of various secondary structures adopted by ω amino acid residues.

1.10.1. Helices

Helices are protein's most common secondary structural elements and constitute about 30-40% of its polypeptide chain. They are stabilized by intramolecular H-bonding interactions and can be classified based on the number of residues present in one turn or the number of atoms in the hydrogen bonded ring. Most of the helices (around 90%) in globular proteins consist of the alpha helix or 3.6_{13}-helix (3.6 residue per turn and 13 membered H-bond), while the other 10%, are constituted of the 3_{10}-helix and rarely by the π-helix (4.4_{16} helix). There are several reports in the literature where peptides containing all, alternating or a few ω amino acids have adopted helical conformations in solid and solution states, described in detail in the next section.

1.10.1.1. Helices stabilized by one residue H-bonds

In homooligomeric peptides containing ω amino acid residues, ribbon-like structures are generated by repetitive one residue H-bonds both in normal as well as in the reverse directions respectively.

1.10.1.1.1. X-ray studies:

- **Normal Direction (3→1)**

Figure 1.24 illustrates the crystallographically characterized examples of peptides containing one residue H-bonded turns. A boat-type structure was established in the homomeric β

TH-3141_166122021

tripeptide Boc-(1-(aminomethyl)cyclopropanecarboxylic acid)$_3$-OMe, that was stabilized by C_8 H-bonded turns.[210] In another example gabapentin (Gpn) favors C_9 conformation in a dipeptide and tetrapeptide sequence, Boc-(Gpn)n-NHMe (n = 2, 4).[238] The repetition of these helical turns would generate 8 and 9-helix, respectively, which are alternately known as ribbon structures.

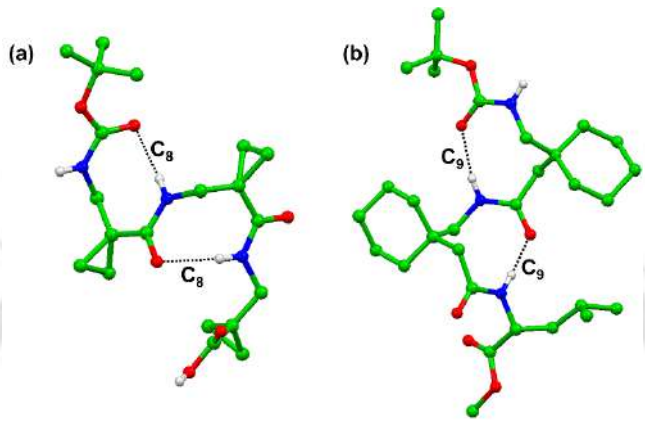

Figure 1.24. One residue 3→1 hydrogen-bonded structures (a) C_8 conformation in crystal of a tripeptide Boc-$\beta^{2,2}$Ac$_3$c-$\beta^{2,2}$Ac$_3$c-$\beta^{2,2}$Ac$_3$c-OH[210] (b) C_9 conformation of a dipeptide Boc-Gpn-Gpn-NHMe in crystal.[238]

- **Reverse direction (1→1)**

A 6-helix (C_6) is observed in an oligo 2,3-disubstituted β-peptide, stabilized by one residue H-bond in the reverse direction (Figure 1.25).[260] This type of helix is rarely characterized in crystals.

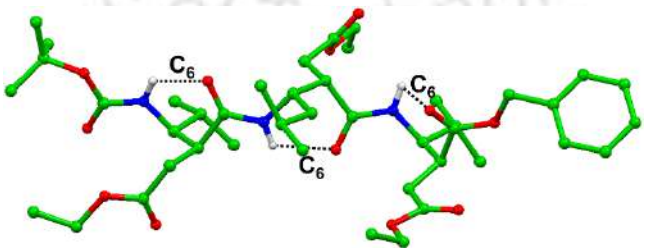

Figure 1.25. One residue 1→1 hydrogen-bonded structures. C_6-helical conformation in a crystal of a homomeric tripeptide containing $\beta^{2,3}$ noncyclic amino acid residues.[260]

TH-3141_166122021

1.10.1.1.2. NMR

There are several studies where one residue stabilized helical structures were characterized in solution by NMR experiments.

- **Normal Direction**

Sharma and co-workers reported 8 and 9-helical conformations in the tetramer of $\beta^{2,3}$-furanoid sugar amino acid and both in the tetramer/hexamer of alternating α C-linked carbo-γ^4-amino acid and γ-aminobutyric acid respectively in $CDCl_3$ solution.[178,261] These structures were stabilized by normal directionality one residue H-bonds. In all of them, all NHs were engaged in H-bonds except NH (1).

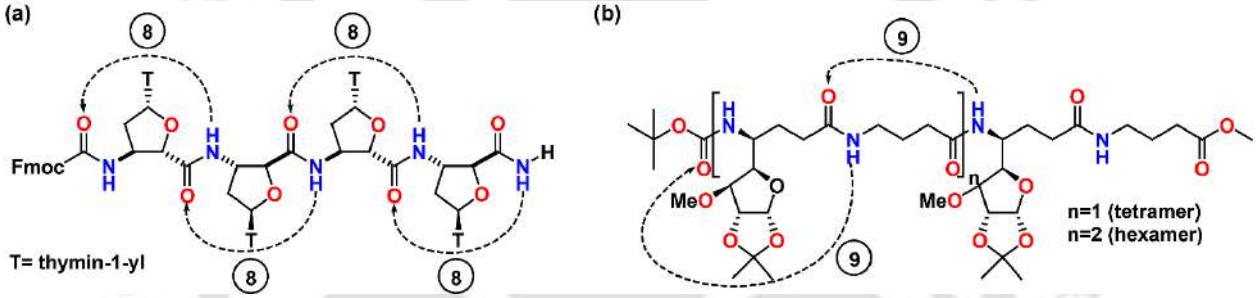

Figure 1.26. (a) 8-helix in a tetrapeptide[261] (b) 9-helix of tetra/hexapeptide.[178] The corresponding H-bonds are shown in broken black arrows.

- **Reverse direction**

6 and 7-helices were observed for homooligomers of β-(C-linked carbo-$\beta^{2,2}$-amino acids)[262] and homochiral γ-peptides[263] constitute of 2,3-trans-dioxolane-constrained γ-amino acid derivative in solution (Figure 1.27). There are other studies where heterochiral γ-peptide also adopted C_7-helix.[212,243]

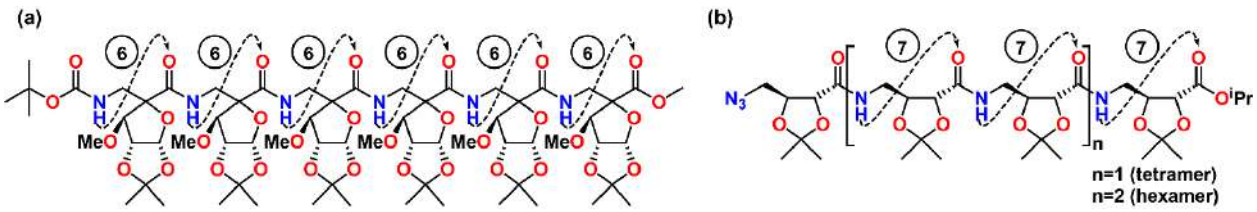

TH-3141_166122021

Figure 1.27. (a) C_6-helix in hexamer of β-(C-linked carbo-$\beta^{2,2}$-amino acids)[262] (b) C_7-helix in homochiral tetra/hexamer of 2,3-trans-dioxolane-constrained γ-amino acid derivative[263](ref258) The corresponding H-bonds are shown in broken black arrows.

1.10.1.2. Helices stabilized by two residue H-bonds

Helical structures stabilized by two residue H-bonds are the expanded analogs of 3_{10}-helical structures. These type of helices have been observed in oligo β and γ-peptides and also in hybrid peptides containing α, β, and γ residues and characterized both in solid (crystallographically) and solution (NMR).

1.10.1.2.1. X-ray

Figure 1.28 represents two residue normal direction H-bonded helical structures in synthetic $(\alpha\beta)_n$, $(\beta)_n$, $(\alpha\gamma)_n$, $(\beta\gamma)_n$, and $(\gamma)_n$ sequences which are examined experimentally by X-ray diffraction.

- **Normal Direction (4→1)**

11-helix was observed in the case of αβ sequence Boc-Aib-ACPC-Aib-ACPC-Aib-ACPC-Aib-ACPC-OBn[245] (Figure 1.28a). Balaram and co-workers reported 12-helix for an octapeptide in alternating $(\alpha\gamma)_n$ sequence Boc-(Gpn-Aib)$_4$-OMe[215] (Figure 1.28b). There is another report where 12-helix was formed for oligo β-peptide, Boc-$(ACPC)_6$-OBn.[153] A 13-helix is formed in the case of βγ hybrid peptide Boc-ACPC-EtACHA-ACPC-EtACHA-ACPC-OBn.[158] (Figure 1.28c) Another isolated C_{13} helical turn was observed across a βγ sequence in a tripeptide, Boc-βLeu-Gpn-Val-OMe[212]. Seebach and colleagues established a right-handed 14-helical conformation in a hexapeptide H-(γ^4-hhVal-γ^4hhAla-γ^4hhLeu)$_2$-OH[264] containing mono-sunstituted γ^4 amino acid resodie and a tetrapeptide containing (R,R,R)-trisubstituted $\gamma^{2,3,4}$-residue[251] (Figure 1.28d). Gellman and co-workers have also been reported a C_{14} helix of homo-oligomer of cyclic γ-amino acid (EtACHA).[155]

TH-3141_166122021

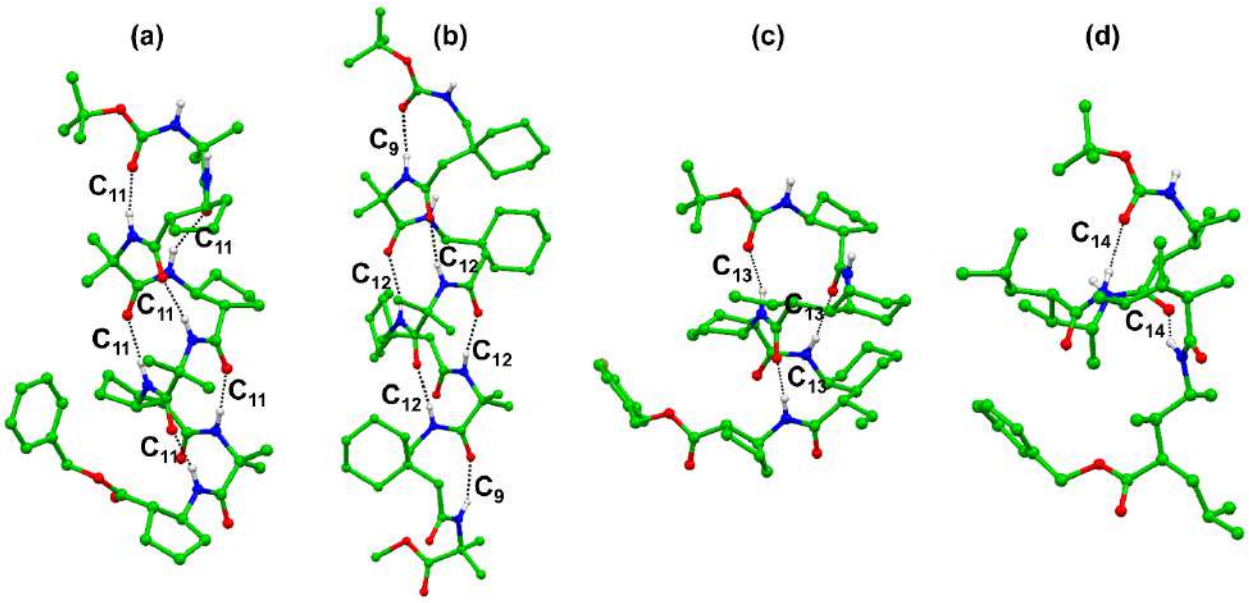

Figure 1.28. Helices stabilized by 4→1 H-bonded turns in β, γ and hybrid peptides. (a) 11-helix formed by αβ-hybrid peptide, Boc-Aib-ACPC-Aib-ACPC-Aib-ACPC-Aib-ACPC-OBn,[245] (b) αγ 12-helix, formed in Boc-Gpn-Aib-Gpn-Aib-Gpn-Aib-Gpn-Aib-OMe,[215] (c) C_{13}-helix formed in the case of βγ-hybrid peptide, Boc-ACPC-EtACHA-ACPC-EtACHA-ACPC-OBn,[158] (d) γ-peptide, C_{14}-helix formed in Boc-(4-amino-2,3,4-trimethylbutanoyl-4-amino-3,4-dimethyl-2(2-methyl-1-propyl) butanoyl)$_2$-OBn.[251]

- **Reverse direction (1→2)**

For the reverse H-bond directionality, two residue H-bonded turns can give rise to 9-helix for an αβ-hybrid peptide and a 10-helix for a β-peptide. Figure 1.29 illustrates the examples of C_9 and C_{10} hydrogen bonded turns formed by a αβ tetrapeptide (alternating Pro and Ant residues)[265] and a β tripeptide ($\beta^{2,2}Ac_6c$).[128] These kinds of repetitive H-bonded helical structures are rarely observed.

TH-3141_166122021

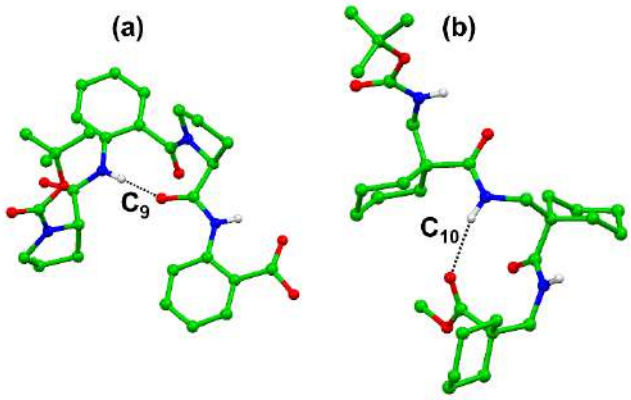

Figure 1.29. Helical structures by 1→2 H-bonded turns in β and hybrid αβ-peptides. (a) C_9 turn formed in a αβ-hybrid peptide, Boc-Pro-Ant-Pro-Ant-COOH,[265] (b) β-peptide, C_{10} turn formed in Boc-$\beta^{2,2}Ac_6c$-$\beta^{2,2}Ac_6c$-$\beta^{2,2}Ac_6c$-OMe.[123]

- **Mixed direction**

Apart from this, ω amino acid residues were reported to be accommodated into well folded structures which were stabilized by the H-bonds of opposite directionality. In such helices a normal direction H bond is repeated by a reversed direction H-bond. Such helices were identified for β-peptides and hybrid peptides such as $(\alpha\beta)_n$, $(\alpha\gamma)_n$, and $(\beta\gamma)_n$.

The crystal structure of a αβα tripeptide, iodobenzoyl-Ala-α,α-dimethyl-D-β-homoalanine-Phe-OMe containing the di-substituted β-residue, adopted two consecutive turns of two types, C_{11} across the αβ segment (4→1, normal direction) and C_9 across the βα segment (1→2, reverse direction) (Figure 1.30a). The repetitive C_{11}/C_9 turns could generate a 11/9-helix. Similarly, an alternate C_{12} (4→1)/C_{10} (1→2) turn was formed for a αγ (γ= APCH) hybrid tetrapeptide, where repetition of such turns generated a 12/10-helix.[163]In a separate study, 12/10 H-bonded structure was reported in a αγ-tetrapeptide, Boc-Leu-Gpn-Leu-Aib-OMe[213] (Figure 1.30b). These hydrogen bonds were helical and were theoretically repeated to give rise to a well registered helix stabilized by alternating 12/10 hydrogen bonds.[213]

TH-3141_166122021

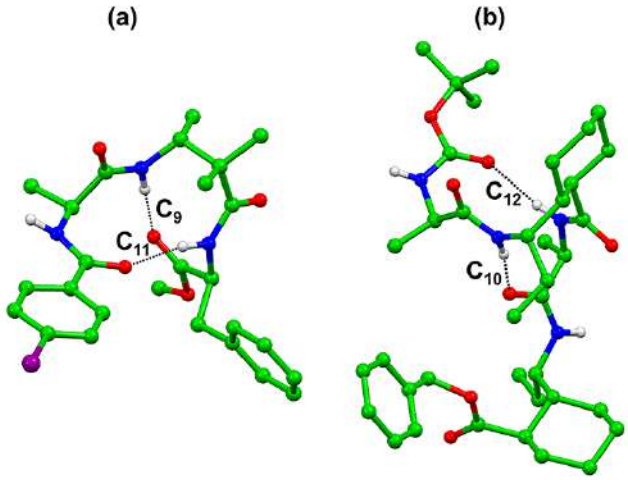

Figure 1.30. Structures with alternate H-bond bond directionality (a) C_{11}/C_9 conformations adopted by a αβ-tripeptide, iodobenzoyl-Ala- α-dimethyl-D-β-homoalanine-Phe-OMe,[241] (b) A αγ hybrid tetra peptide, Boc-^{D}Ala-APCH-^{D}Ala-APCH-OBn formed a C_{12}/C_{10} conformations in crystal.[213]

1.10.1.2.2. NMR

In several studies helical structures stabilized by two residue H-bonded turns, were reported in ω amino acid containing peptides in solution using NMR experimental techniques (Figure 1.31).

- **Normal Direction**

Figure 1.31 represents the examples of 12, 13, and 14-helical conformations adopted by heterogeneous (αγ and βγ-hybrid) and homogeneous (oligomer of γ) peptides in solution. Sonti *et. al.* reported a C_{12} helical conformation of a αγ-peptide (γ amino acid residue = unconstrained, mono-substituted with proteinogenic side chains) in $CDCl_3$ solution (Figure 1.30a).[266] Gellman and co-workers investigated the C_{12} helical conformational stability of two αγ-peptides in polar protic solvents methanol and water.[267] The first peptide contained a noncyclic (R)γ^4-residue with a proteinogenic side chain, and the second one contained a cyclic γ-residue. The acyclic residue could adopt the structure only in methanol, but the cyclic residue stabilized the C_{12} helix in both solvents.[267] Two residue H-bonded, C_{13}-helical structures were

TH-3141_166122021

mainly generated by βγ-hybrid peptides. There were very few examples in the literature where βγ peptide adopted 13-helix. Atkins and co-workers reported a 13-helix in $CDCl_3$, formed by βγ peptide containing alternating trans-aminocyclobutanecarboxylic acid (tACBC) and singly substituted (R)γ^4-residue (Figure 1.31c).[268] Hanessian *et. al.* synthesized a tetrapeptide containing (R, R) $\gamma^{2,4}$-residue, which adopted right-handed 14-helical conformation in pyridine-d_5 solution, while (S, R) $\gamma^{2,4}$-residue which adopted opposite configuration could not adopt helical conformation (Figure 1.31b).[147] Balaram and co-workers have reported 14-helical conformation of short homo-oligomer sequences containing mono-substituted γ^4 amino acid residues (γ^4Leu, γ^4Ile and γ^4Val).[269]

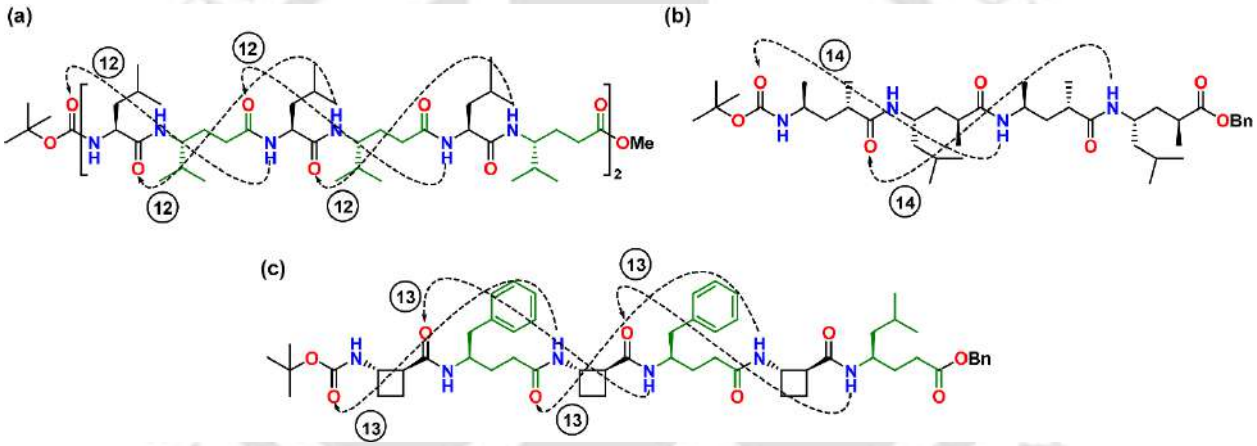

Figure 1.31. Helices stabilized by 4→1 H-bonds in solution. (a) αγ sequence, 12-helix adopted by a 12 residue peptide, Boc-[Leu-γ^4(R)Val-Leu-γ^4(R)Val-Leu-γ^4(R)Val]$_2$-OMe,[267] (b) 14-helix adopted by a γ-peptide, Boc-[α-methyl-γ^4h(S)Ala-α-methyl-γ^4h(R)Leu]$_2$-OBn,[147] (c) βγ sequence hexapeptide Boc-tACBC-γ^4Phe-tACBC-γ^4Phe-tACBC-γ^4Leu-OBn adopted C_{13}-helical conformation.[268]

- **Reverse direction**

Helices stabilized by two residue H-bond in the reverse direction are extremely infrequent in peptidimimetic studies. Toniolo, Balaram, and colleagues reported 11-membered H-bond turns or ε-turns in a comprehensive literature of protein and peptide structures.[270] Recently, Misra *et.*

TH-3141_166122021

al. reported the ε-helical conformation of βγ-hybrid tetrapeptides composed of chiral β^3-residue along with achiral $\gamma^{3,3}/\gamma^{4,4}$-amino acid residue.[222] The NMR-derived structures confirmed the formation of ε-helices.

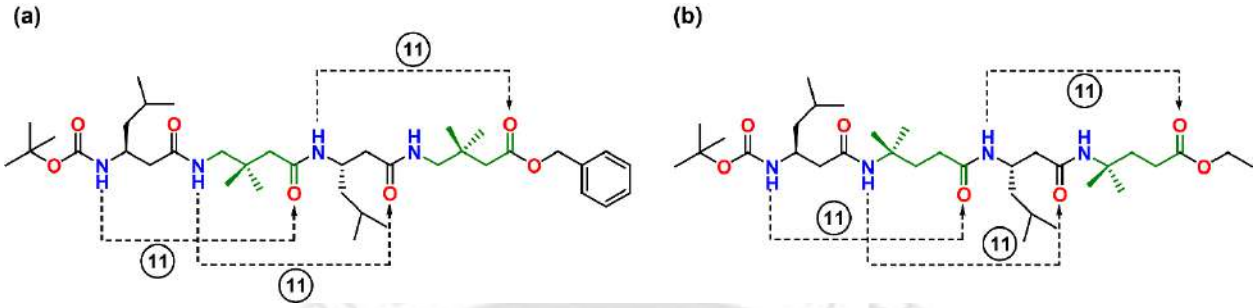

Figure 1.32. ε-helical structures stabilized by 1→2 H-bonds in βγ peptides. (a) Boc-[β^3hLeu-$\gamma^{3,3}$]$_2$-OBn,[222] (b) Boc-[β^3hLeu-$\gamma^{4,4}$]$_2$-OEt.[222]

- **Mixed direction**

Mixed directionality helices were rarely characterized in crystals. However, many studies showed that longer peptide sequences adopted helices with alternate H-bond directionality in solution.[175-177,179,184,220,271-273] Different possible helices were stabilized by alternate hydrogen bonds like: C_{11} (4→1)/C_9 (1→2) (in case of αβ sequence),[176,271] C_{12} (normal direction)/C_{10} (reverse direction) (observed for both β and αγ-hybrid peptides),[175,177,179,184,220,272,273] and C_{11} (1→2)/C13 (4→1 (for βγ peptide) H-bonds.[179] 11/9-helix was observed in an αβ (β = β^3hVal) peptide (Figure 1.33a).[271] Sharma and co-workers reported 11/9-helix for a αβ peptide composed of L-ala and C-linked carbo-β-amino acid residue.[176] Cyclic β (furanoid side chain)[184](Figure 1.33c) and γ-residue (AMCP)[272](Figure 1.33b) were accommodated into the mixed 12/10-helical conformations. Several other studies were reported where 12/10-mixed helices were characterized in solution.[175,177,179,220,273] A 11/13-helix was observed in βγ peptide containing alternating mono-substituted C-linked carbo-β and γ-amino acid residues (Figure 1.33d).[179]

TH-3141_166122021

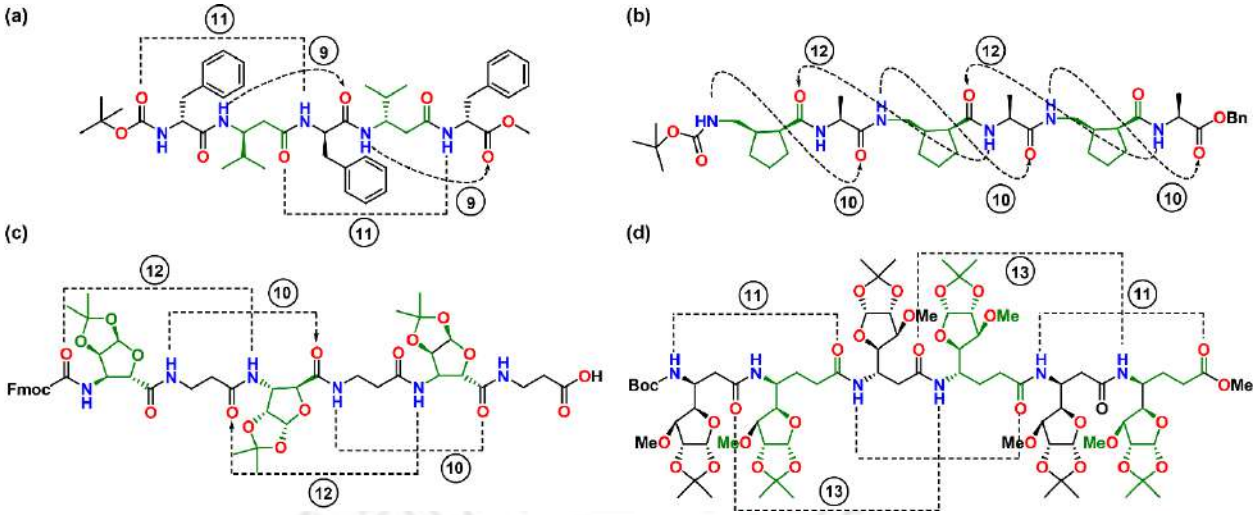

Figure 1.33. Mixed directionality helices stabilized by alternate H-bond directionality. (a) 11/9-helix in αβ peptide Boc-^{D}Phe-β^{3}hVal-^{D}Phe-β^{3}hVal-^{D}Phe-OMe,[271] (b) 12/10-helix in αγ peptide Boc-AMCP-Ala-AMCP-Ala-AMCP-Ala-OMe,[272] (c) 12/10-helix in βγ sequence Fmoc-[β^{2,3}(sugar)-βhGly]$_3$-OH,[184] (d) 11/13-helix in βγ peptide Boc-[β^{3}Caa-γ^{4}Caa]$_3$-OMe.[179]

1.10.1.3. Stabilized by three residue H-bonds

In all α-peptide, the repetitive three residue H-bonded turns (5→1) stabilize α-helix. So, when one or more α-residues in the hydrogen bonded turn is replaced by ω-residue(s), it generates expanded analogs of α-helix.

1.10.1.3.1. X-ray

- **Normal Direction**

Figure 1.34 illustrates conformations in crystals of ω amino acid containing hybrid peptides that are stabilized by three residue H-bonds. For αβ peptide, Boc-Ala-ACPC-Aib-ACPC-Aib-ACPC-Aib-ACPC-Aib-OBn (ACPC = trans-2-aminocyclopentanecarboxylic acid), 14/15-helix was observed which was stabilized by repetitive C14 and C15 H-bonds.[274,275] Expanded alternating H-bonds, C14 and C15 were formed across αβα and βαβ segments. There are some other studies where isolated 14 (across Aib-βPhe-Leu segment) and 15 (across Aib-βVal-βPhe segment) membered H-bonds have been formed in octa and undecapeptides, Boc-Leu-Phe-

TH-3141_166122021

Val-Aib-βPhe-Leu-Phe-Val-OMe[214] and Boc-Val-Ala-Phe-Aib-βVal-βPhe-Aib-Val-Ala-Phe-Aib-OMe,[253] characterized in crystals. Recently, Gopi and co-workers have reported a 15/17-helix in αγ peptide composed of alternating Aib and $\gamma^{4,4}$-residues.[221] The expanded 15 and 17 turns are observed towards the C-terminus across the αγα and γαγ segments, respectively.

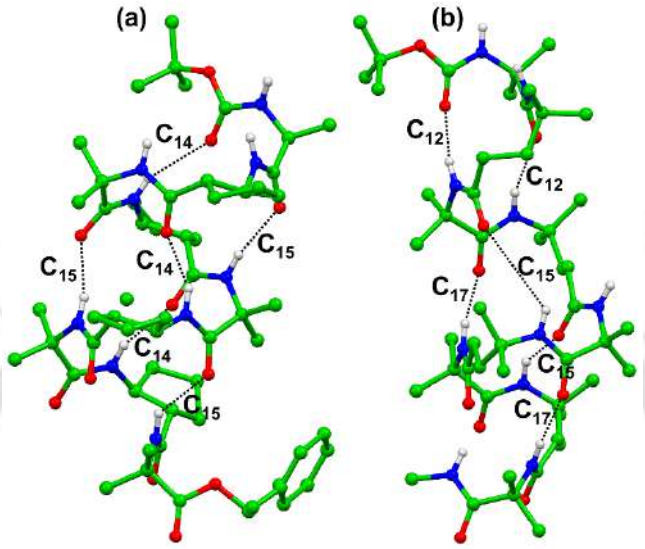

Figure 1.34. Three residue H-bond stabilized helical structures in the normal direction. (a) 14/15-helix observed in αβ peptide, Boc-Ala-ACPC-Aib-ACPC-Aib-ACPC-Aib-ACPC-Aib-OBn,[275] (b) 15/17-helix formed in αγ peptide, Boc-[Aib-$\gamma^{4,4}$-Aib-$\gamma^{4,4}$-Aib-$\gamma^{4,4}$]$_2$-Aib-NHMe.[221]

- **Reverse direction**

Helices stabilized with three residue reverse directionality H-bonds are very much limited. There is only one study where a 14-helix was characterized in crystal for β-peptide composed of cyclicβ-residue ACHC, represented in Figure 1.35.[146]

TH-3141_166122021

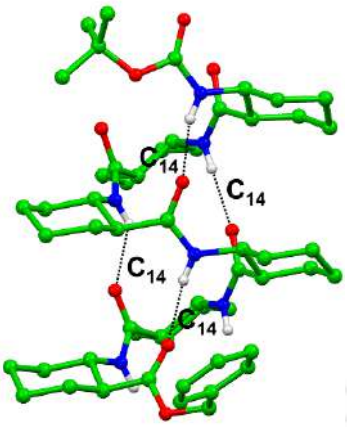

Figure 1.35. 14-helical conformation in β-peptide, Boc-$(ACHC)_6$-OBn,[151] stabilized by three residue reverse directionality H-bonds.

1.10.1.3.2. NMR

- **Normal Direction**

Expanded three residue H-bonded turns were also characterized in solution for αβ-hybrid peptides. Two different β-residues (ACPC and β^3Caa) have been utilized to generate these kinds of expanded helical turns.[181,276] Figure 1.36 illustrates the examples of three residue hybrid turns in αβ-peptides.

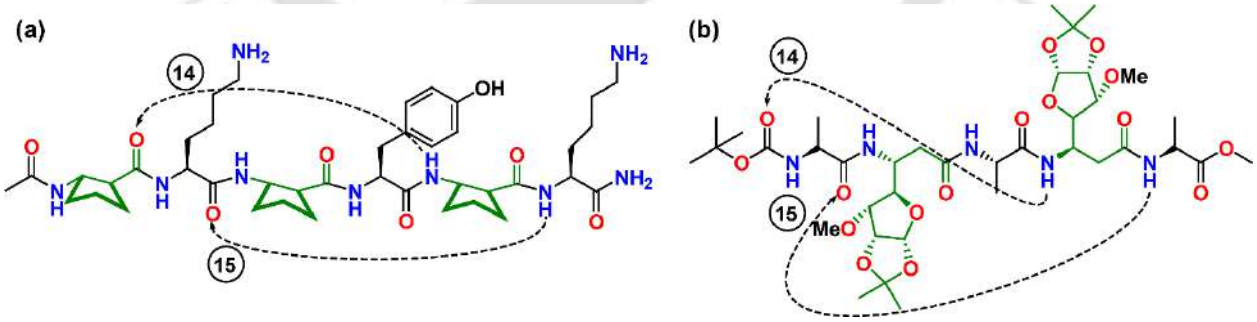

Figure 1.36. Helices stabilized by three residue H-bonded turns in solution. (a) 14/15-helix observed in βα-hybrid peptide, Ac-ACPC-Lys-ACPC-Tyr-ACPC-Lys-$CONH_2$,[276] (b) 14/15-helix adopted by αβ-peptide, Boc-Ala-β^3Caa-Ala-β^3Caa-Ala-OMe.[181]

TH-3141_166122021

- **Reverse direction**

Seebach and co-workers have first reported a 14-helix, stabilized by reverse H-bond directionality. It has been observed in the solution of β-peptide containing acyclic mono-substituted β^3-residue with a proteinogenic side chain (Figure 1.37).[277] Similar results were also observed for the β-peptides containing mono-substituted β^2-residue. However, the previous structure is more stable compared to the later one.

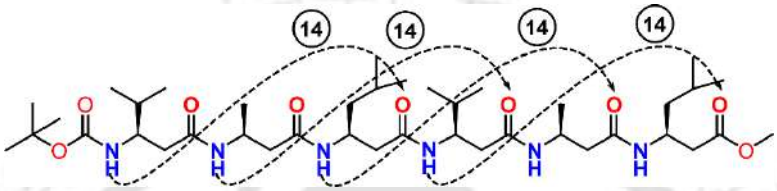

Figure 1.37. 14-helical structure characterized in solution for β-peptide Boc-β^3hVal-β^3hAla-β^3hLeu-β^3hVal-β^3hAla-β^3hLeu-OMe.[277]

1.10.2. Double helical structures

ω amino acid residues have also been reported to give rise to double helical structures where two peptide molecules intertwine with each other and have intermolecular amide H-bonds across the strands. The name is derived from the double-helical DNA structures, with analogical structures. The first double helical structure of γ-peptide composed of E-vinylogous-γ-residue have been characterized in crystal by Gopi and co-workers (Figure 1.38a).[168,169] In another study, γ-peptide containing achiral di-substituted $\gamma^{4,4}$-residue assembled into a double helical type of arrangement in crystal (Figure 1.38b).[135]

TH-3141_166122021

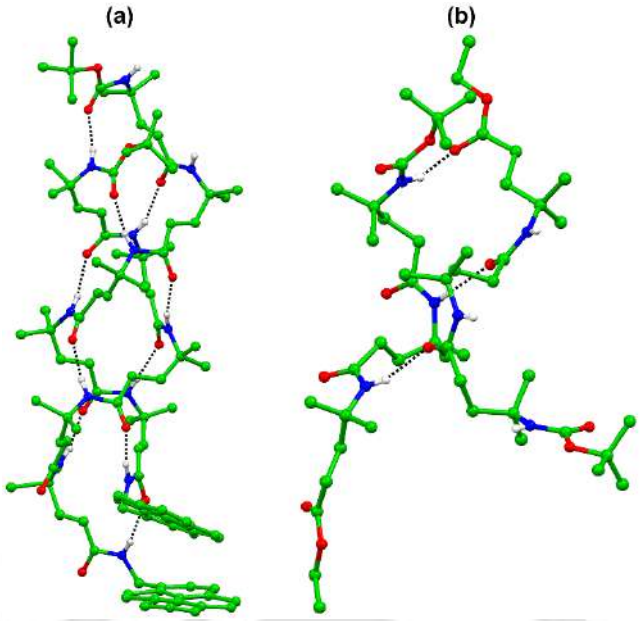

Figure 1.38. Double-helical structure characterized in crystals for β-peptides (a) Boc-(dγAic)$_5$-NH-Py[168] and (b) Boc-($\gamma^{4,4}$)$_4$-OEt.[135]

1.10.3. β-sheets

β-Sheets are another major secondary structure element in proteins which consists of β-strands (a polypeptide chain composed of 3 to 10 amino acids) connected by intermolecular hydrogen bonds. In β-sheet, the amide bonds are almost coplanar, and the side chains are oriented alternatively above or below the plane. Strands are classified as parallel or antiparallel based on the directionality of the two termini.

1.10.3.1. Parallel Sheets

In the parallel arrangement, the consecutive strands are oriented in the same direction. ω amino acid residues are known to be accommodated into extended structures like parallel sheets and are mainly characterized crystallographically using X-ray diffraction.

TH-3141_166122021

1.9.3.1.1. X-ray

The oligomer of $\beta^{2,3}$-amino acid residues in a tripeptide was expected to adopt plated parallel sheets.[278] There are other examples where E-vinylogous-γ^4-amino acid residues were also accommodated into the extended parallel sheets for small di and tetrapeptides.[169] In another study, cyclic trans-3-ACPC residue showed a higher propensity for parallel sheet secondary structures in amide-linked stand sequences.[159] Smith and colleagues have studied tripeptide conformations containing cyclopropane γ-amino acid residue which shown to adopts parallel sheet structure in crystal and stabilized by the formation of bifurcated hydrogen-bond between the CO of one strand with the NH and one CH of the cyclopropane ring.[279]

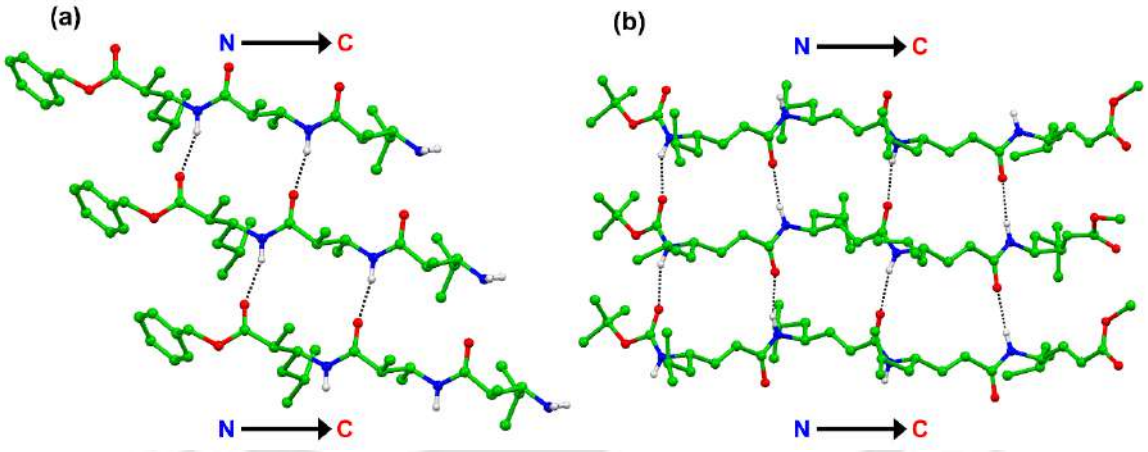

Figure 1.39. Parallel sheet secondary structures identified in crystals for (a) tripeptide containing $\beta^{2,3}$ amino acids, $CF_3COOH.NH_2$-α-methyl-$\beta^{2,3}$hVal-α-methyl-$\beta^{2,3}$hAla- α-methyl-$\beta^{2,3}$hLeu-OBn[278] and (b) tetrapeptide composed of E-vinylogous-γ^4Leu-residue.[169]

1.10.3.2. Anti-parallel Strands

In the anti-parallel arrangement, consecutive strands run in antiparallel direction. β-hairpin comprises of a turn region and anti-parallel strand region. ω amino acid residues have been accommodated into the anti-parallel strands of a β- hairpin and characterized experimentally both in solid and solution.

TH-3141_166122021

1.10.3.2.1. X-ray

Figure 1.40 represents the example of β-hairpin, in which βPhe and E-vinylogous-γ-residues were accommodated in the anti-parallel strands.[171,280] There are other studies where vinylogous and di-substituted γ residue were incorporated in the anti-parallel strands of β-turns.[170,281] Gellman and co-workers reported anti-parallel sheet formation by a tetrapeptide which contained α,β di-substituted β-residue.[281]

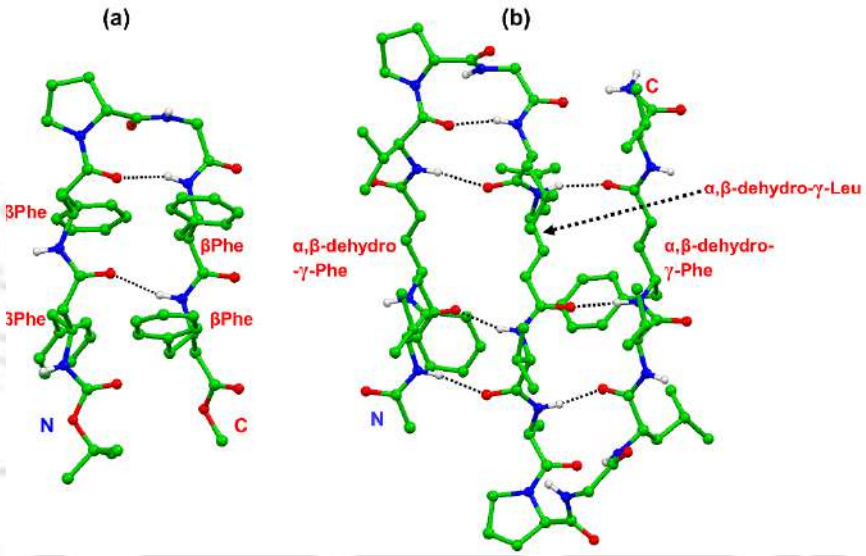

Figure 1.40. ω amino acid residues in the anti-parallel strands of β-hairpin observed in crystals (a) βPhe residues present at the anti-parallel strand of a hexapeptide, Boc-βPhe-βPhe-^{D}Pro-Gly-βPhe-βPhe-OMe,[280] (b) E-vinylogous-γ^4-Phe and E-vinylogous-γ^4-Leu accommodated at the anti-parallel strand of a triple stranded β-hairpin of a 15-residue peptide Boc-Val-dgF-Val-^{D}Pro-Gly-Leu-dgL-Val-Ala-^{D}Pro-Gly-Leu-Val- dgF-Val-$CONH_2$.[171]

1.10.3.2.2. NMR

Roy *et. al*. established formation of a β-hairpin conformation in solution, where βGly and γAbu residues were incorporated at the anti-parallel strands of 10-residue peptides (Figure 1.41).[282]

TH-3141_166122021

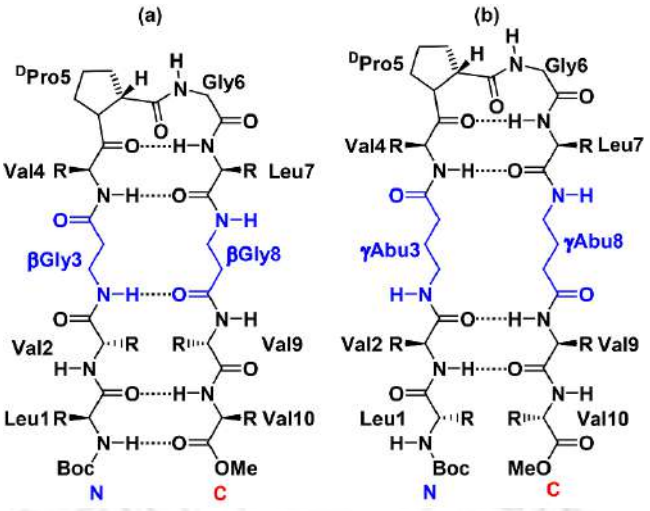

Figure 1.41. ω amino acid residues in the anti-parallel strands of β-hairpin in solution (a) βGly[282] and (b) γAbu[282] residues incorporated at the anti-parallel strands of a 10-residue model peptide, Boc-Leu-Val-Xxx-Val-^{D}Pro-Gly-Leu-Xxx-Val-Val-OMe, where Xxx = βGly, γAbu .

1.10.4. Non-helical β-turns

β-turns are irregular secondary structures in protein that causes the change in the directionality of the polypeptide chains and possesses non-repetitive dihedral angles of their backbone. It is composed of four residues and stabilized by a 4→1 10-membered H-bonds between the CO (i) and NH (i+3). They mainly occur in the loop region of the proteins and play a vital role in molecular recognition. In nature, the most common β-turn inducing segment is ^{D}Pro-Gly. Replacement of amino acid at i+1 and/or i+2 position with a suitable ω amino acid residue can induce and mimic the β-turn. α-aminoisobutyric acid Aib (at the i+1 position), Ac_6c and various ω residues (at the i+2 position) are some frequently used turn-inducing elements.

1.10.4.1. Isolated β-turns

1.10.4.1.1. X-ray

The nucleation of non-helical isolated β-turns has been achieved using β-amino acid residues. A β-peptide formed expanded C_{12} β-turn where the turn-inducing residues were both β-residue

TH-3141_166122021

(R and S-Nipcotic acid) (Figure 1.42a).[155] In another study, a small protected dipeptide adopted an expanded C_{11} non-helical β-turn, which was characterized in crystals (Figure 1.42b).[242]

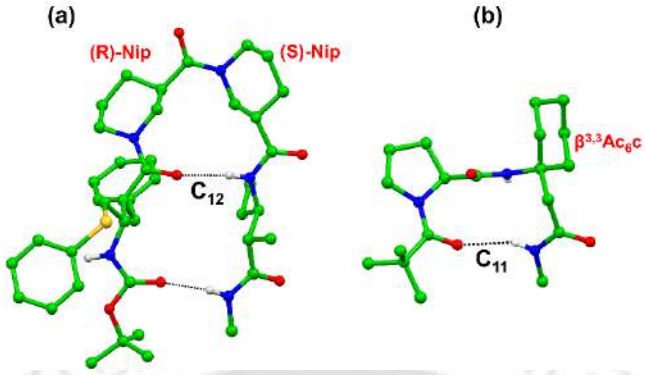

Figure 1.42. ω amino acid residues in isolated β-tur mimics identified in crystals. (a) Cyclic β-residues, (R)-nipecotic acid and (S)-nipecotic acid residues at turn segment of a β-peptide,[155] (b) Expanded C_{11} turn where $\beta^{3,3}Ac_6c$-residue is placed at the i+2 position of a dipeptide, Boc-^{D}Pro-$\beta^{3,3}Ac_6c$-NHMe.[242]

1.10.4.1.2. NMR

β^3hLys-β^2hTrp have been used as a turn segment to nucleate isolated non-helical β-turn mimics where both residues are non-cyclic mono-substituted β-residues (Figure 1.43a).[283] This segment generates an expanded turn which forms H-bonds in the reverse direction. E-vinylogous-γ-residue has also been accommodated at the turn region to generate expanded C_{12} turn (Figure 1.43b).[172]

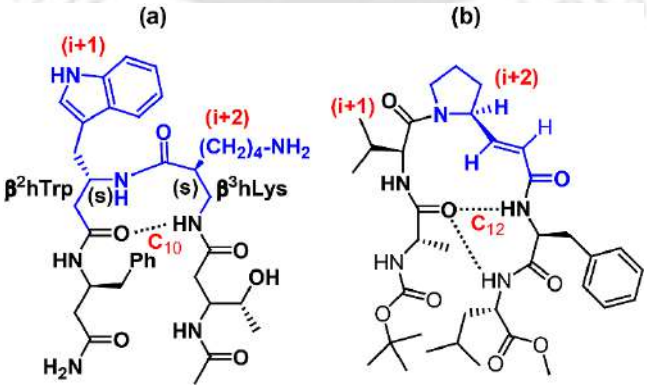

Figure 1.43. ω amino acid residues in isolated β-turn mimics characterized in solution. (a) Acyclic β-residues, β^2hTrp and β^3hLys residues at turn segment of a β-peptide, stabilized by

TH-3141_166122021

reverse H-bond directionality,[283] (b) Expanded C_{12} turn mimic, where E-vinylogous-γ-residue is placed at the (i+2) position of a pentapeptide.[172]

1.10.4.2. β-Hairpin

When β-turns are extended on either side by antiparallel β-strands, which are well registered through inter-strand hydrogen bonds, a β-hairpin is generated. Thus β-turns can nucleate β-hairpin conformation. Dipeptide segments, such as ^{D}Pro/^{L}Pro and ^{D}Pro/^{L}Gly are the most common motifs used in turns to stabilize a β-hairpin by allowing the strand registry and th formation of inter-strand hydrogen bonds. There are several studies reported in the literature, where ω residues have been accommodated at the i+2 position of the turns of β-hairpins. The incorporation of homologated amino acid residues expanded the H-bonded ring size.

1.10.4.2.1. X-ray

Figure 1.44 illustrates the crystallographically characterized examples of β-hairpin conformations where, Gpn[215] and δAva[209] have been placed at the i+2 position of turn segment to generate expanded C_{12} and C_{13} turns in an octapeptide, respectively.

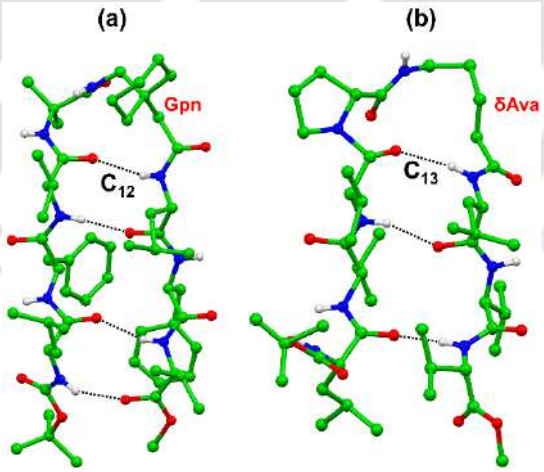

Figure 1.44. ω amino acid residues at the turn region (i+2 position) of β-hairpin identified in crystals. (a) γ amino acid residue Gpn placed at the turn segment of Boc-Leu-Phe-Val-Aib-Gpn-Leu-Phe-Val-OMe.[215] (b) Expanded C_{13} turn induced by ^{D}Pro-δAva segment in an octapeptide, Boc-Leu-Val-Val-^{D}Pro-δAva-Leu-Val-Val-OMe.[209]

TH-3141_166122021

1.10.4.2.2. NMR

Balaram and co-workers have studied the β-hairpin conformation of octapeptides with ^{D}Pro-Xxx (Xxx= $\beta^{3,3}Ac_6c$, Gpn) segments in solution (Figure 1.45).[209]

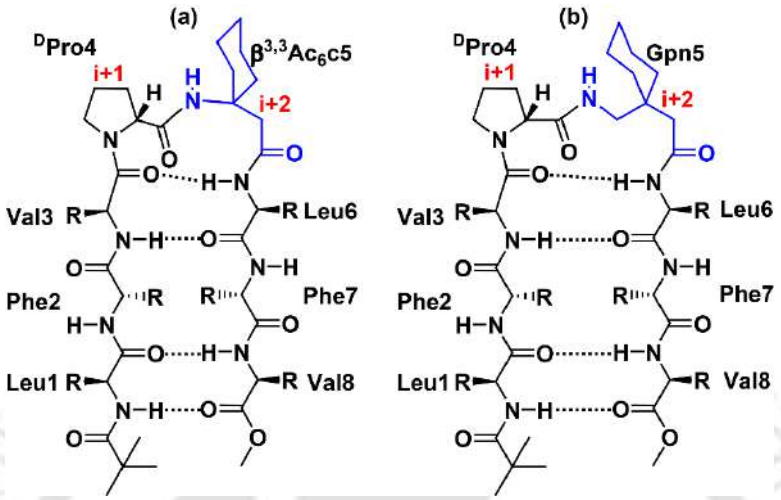

Figure 1.45. ω amino acid residues at the turn region (i+2 position) of β-hairpin identified in solution (a) ^{D}Pro-Gpn segment form expanded C_{12} turn in Boc-Leu-Val-Val-^{D}Pro-Gpn-Leu-Val-Val-OMe,[209] (b) expanded C_{11} turn induced by ^{D}Pro-$\beta^{3,3}Ac_6c$ segment in an octapeptide, Boc-Leu-Phe-Val-^{D}Pro-$\beta^{3,3}Ac_6c$-Leu-Phe-Val-OMe.[209]

1.11. Geminally di-substituted γ-amino acid residues

Several geminally di-substituted amino acid residues (α and ω) have been used to induce secondary structures in short peptides.[133,202,210,217,220-222,256,284,285] Geminal di-substitution restricts the flanking torsion angles to gauche values and hence are used to nucleate helical structures mostly. However, there are examples of these amino acid residues of being accommodated into non-helical turn segments.[210] As our thesis entails use of this class of γ amino acid residues, we have described the earlier attempts of using di-substituted γ amino acid residues in details in the following section.

TH-3141_166122021

1.11.1. Gabapentin (Gpn)

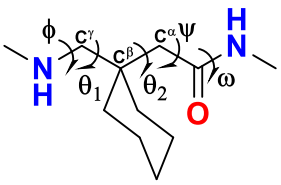

Figure 1.46. Chemical structure and torsional variables for β, β'-disubstituted γ amino acid residue, Gabapentin [1-(aminomethyl) cyclohexaneacetic acid].

Balaram and co-workers studied conformations of small synthetic peptides containing geminally di-substituted γ amino acid, gabapentin (Gpn)(Figure 1.46). In Gpn, the torsion angles θ_1 and θ_2, mostly adopt gauche conformation.[217] Due to this, structures of most of the peptides that contain Gpn are helical. For example, homooligomeric peptide, Boc-$(Gpn)_n$-NHMe (n =2, 4) adopted ribbon-like conformation in crystals.[238] C_{12} helix was formed for an octapeptide, Boc-$(Gpn\text{-}Aib)_4$-OMe, characterized by X-ray and NMR.[215] C_{13} helical turn was observed in crystal for a βγ small tripeptide, Boc-βLeu-Gpn-Val-OMe.[212] A C_{13} model helix was built using the C_{13} H-bond. Gpn could be accommodated in a C_{12}/C_{10} motif containing hydrogen bonds of reverse directions in the tetrapeptide, Boc-Leu-Gpn-Leu-Aib-OMe.[213] A model 12/10-mixed helix was built based on the experimentally realized mixed directionality C_{12}/C_{10} H-bond. In a rare example, Gpn was incorporated into the i+2 position of a non-helical turn that nucleated a β-hairpin in an octapeptide, Boc-Leu-Phe-Val-Aib-Gpn-Leu-Phe-Val-OMe.[215] All the helices, characterized in crystals and the modeled helical structures, are shown in Figure 1.47.

TH-3141_166122021

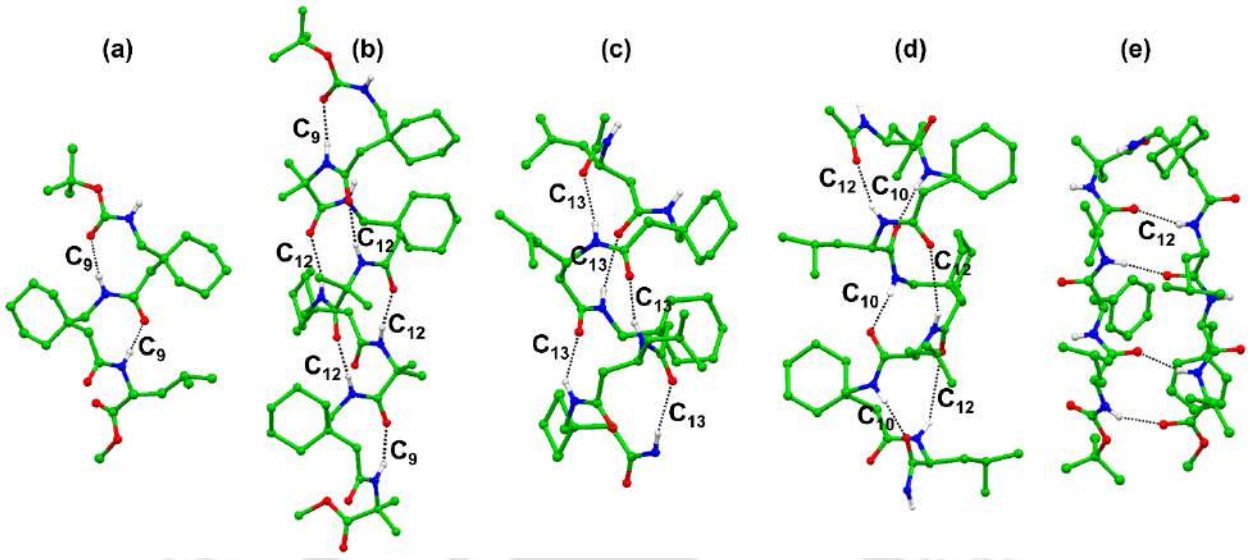

Figure 1.47. Secondary structures of synthetic γ and hybrid peptides composed of Gpn. (a) C_9-ribbon structure observed in crystal of a dipeptide, Boc-$(Gpn)_2$-OMe,[238] (b) C_{12}-helix is formed in a αγ-hybrid peptide, Boc-$(Gpn\text{-}Aib)_4$-OMe, characterized in crystal,[215] (c) Modelled βγ C_{13} helix, built by using the parameters from the C_{13} helical turn of a tripeptide,[217] (d) a modelled αγ C_{12}/C_{10}-mixed helix, generated by using the parameters obtained from crystal structure of a tetrapetide.[217]

Torsion angles Phi (ϕ) and Psi (ψ) for the γ amino acid residue (Gpn) in peptides, obtained from crystallographically characterized secondary structures were plotted in the Ramachandran map, assuming the θ_1 and θ_2 to be a constant of gauche-gauche values for helical conformations and gauche-trans values for non-helical β-turn respectively (Figure 1.48). Different regions of this map are represented in Figure 1.47, which have specific phi and psi values for different kinds of secondary structures. The various circles are the areas where different kinds of secondary structures (helical or non-helical) were characterized for the Gpn residue.

TH-3141_166122021

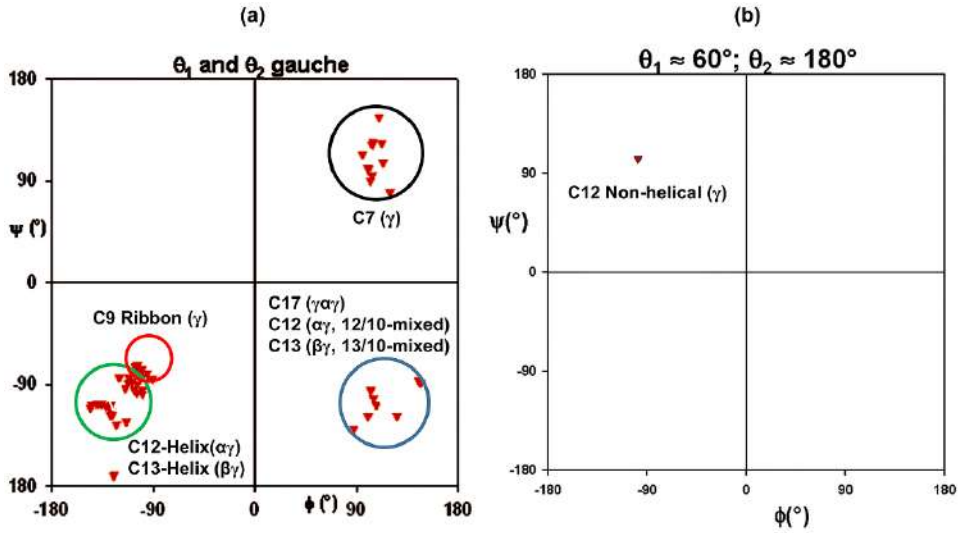

Figure 1.48. Scatter plot for the experimentally observed conformations of Gpn residue for (a) ribbon and helical conformations in γ and hybrid peptides ($\theta_1 \approx \theta_2 \approx 60°$). The regions marked with different colored circles denote various secondary structures adopted by Gpn,[108] (b) non-helical turn adopted by Gpn where θ_1 and θ_2 are in *gt* conformation.[217]

1.11.2. $\gamma^{3,3}$ (Adb) and $\gamma^{4,4}$ (Aic)-gamma amino acid residues

Gopi and co-workers have explored geminally dimethyl substituted $\gamma^{3,3}$ and $\gamma^{4,4}$ amino acid residues (Figure 1.49). In these residues, the flanking torsion angles have been restricted (θ_1, θ_2 for $\gamma^{3,3}$ and ϕ, θ_1 for $\gamma^{4,4}$ respectively) at the point of di-substitutions to *gg* conformation. Both of these residues mostly go into helical conformation. 12-helix and 15/17-mixed helix were observed in a crystal of an $\alpha\gamma^{4,4}$-hybrid peptide, stabilized by conventional normal directionality two residue and three residue H-bonds respectively.[221] A 12/10-mixed helix was realized in solution for $\alpha\gamma^{4,4}$ peptide with alternate H-bond directionality in the hybrid peptide .[220] Achiral $\alpha\gamma^{3,3}$-hybrid peptide adopted ambidextrous helical conformation in crystals.[133] In another study, a very rare ε-helix was formed for $(\beta^3\gamma^{3,3})_n$ peptide in solution with reverse H-bond directionality.[222] In a rare example, $\gamma^{4,4}$ amino acid residue was shown to be accommodated in extended parallel sheet-like conformation in a $\gamma^{4,4}$-oligomeric peptide.[130]

TH-3141_166122021

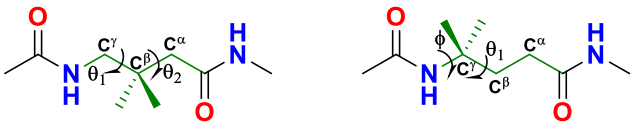

$\gamma^{3,3}$-amino acid residue

θ_1 and θ_2

$\gamma^{4,4}$-amino acid residue

ϕ and θ_1

Figure 1.49. Chemical structures and constrained torsional variables for $\gamma^{3,3}$ (Adb, 4-amino-3,3-dimethylbutanoic acid) and $\gamma^{4,4}$ (Aic, 4-amino-4-methylpentanoic acid)-amino acid residues.

1.12. Knowledge gap

Though several studies are there on the secondary structure of peptides containing geminally di-substituted γ amino acid residues, there are still certain areas which needs to be delved into deeper. Its established that in the geminally di-substituted γ amino acid residues (similar to the α or β amino acid case), the flanking torsion angles about the point of di-substitution adopt gauche conformation which helps them to be accommodated into the folded structures like the helix. There are reports where studies on conformations of different peptides composed of various individual geminally di-substituted residues have been conducted. However, there is no literature available where the conformational preference of the differently di-substituted γ amino acid residues, that are di-substituted at different carbon atoms has been compared . In a γ amino acid residue, there are three backbone carbon atoms (α, β and γ). Di-substitution at these different carbon atoms leads to three different γ amino acid residues namely $\gamma^{2,2}$, $\gamma^{3,3}$ and $\gamma^{4,4}$. Differential position of di-substitution leads to constraining of different sets of torsion angles in these residues. For example, in the α di-substituted γ amino acid residue, θ_2 and ψ are constrained, while in the β and γ amino acid residues, θ_1/θ_2 and ϕ/θ_1 are constrained respectively (Figure 1.50). There is no literature available where the effect of constraining different sets of backbone torsion angles of the γ amino acid residues, on the secondary structure of the peptides containing them has been investigated.

TH-3141_166122021

1.13. Our study: Main objective

The main objective of this thesis was to study the effect of the differential position of geminal di-substitution of the γ amino acid residues on the conformation of the peptides that they constitute. We wanted to compare the conformational propensity of the three γ amino acid residues ($\gamma^{2,2}$, $\gamma^{3,3}$ and $\gamma^{4,4}$). Thus we chose different model peptides which are well-known to generate different kinds of secondary structures like helix, isolated non-helical β-turn mimic, β-hairpin etc. Then in each model peptide, one different geminally di-substituted γ amino acid residue ($\gamma^{x,x}$ x,x = 2,2/3,3/4,4) was incorporated one at a time, to give rise to a group of peptides. These peptides were exactly similar to each other except the kind of γ amino acid residue they contained. Thereafter, the conformations of the peptides within a group were studied in solid and solution states. We have also studied their conformations in *silico* using DFT.

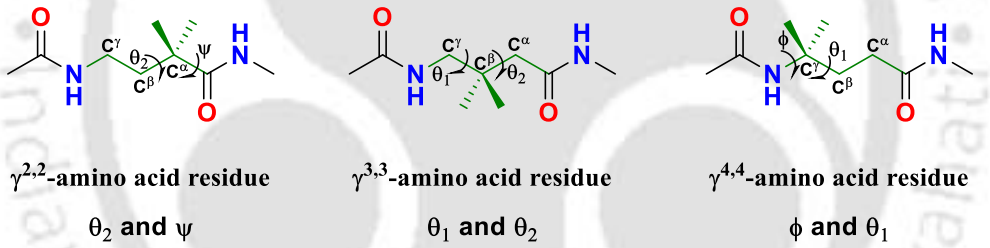

Figure 1.50. Chemical structures of $\gamma^{2,2}$, $\gamma^{3,3}$ and $\gamma^{4,4}$ amino acid residues and their constrained sets of torsion angles are shown.

TH-3141_166122021

1.14. Methodology

This section describes the methodology that has been adopted to achieve our objective. Thewhole methodology can broadly be divided into the following parts.

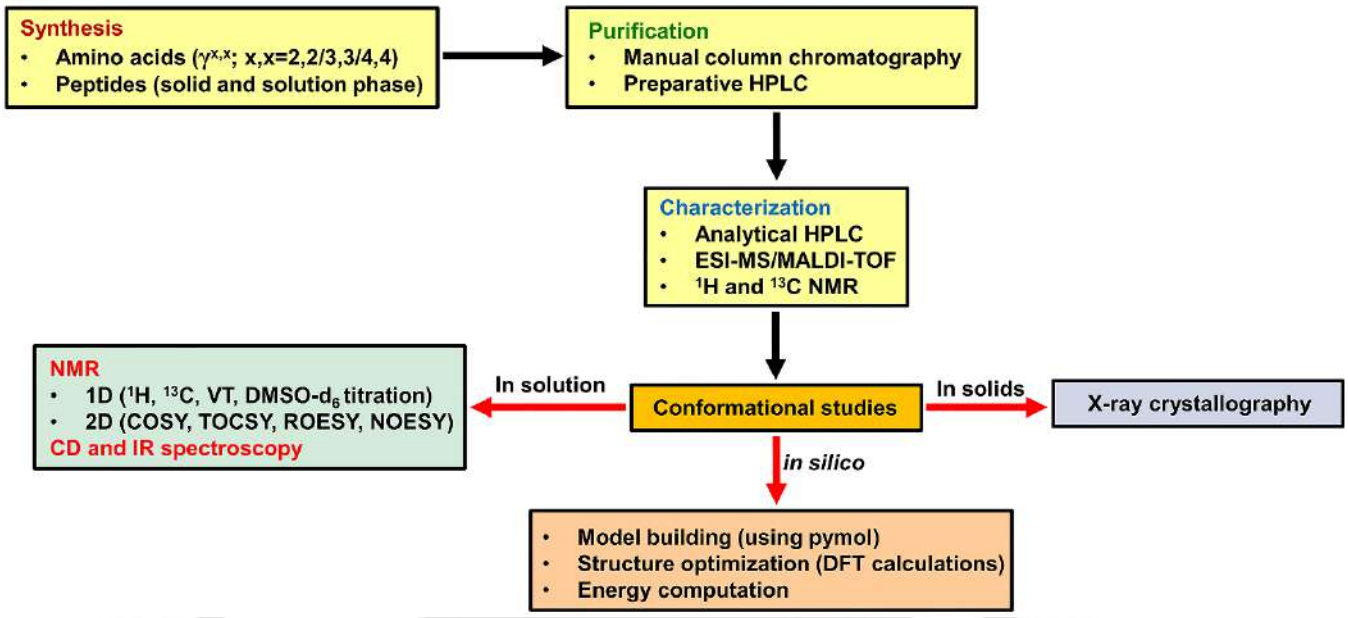

Figure 1.51. A schematic representation of the methodology adopted in the course of this thesis work.

1.14.1. Synthesis

All the dimethyl-substituted $\gamma^{x,x}$ (x,x = 2,2/3,3/4,4) residues were synthesized in the laboratory for this project by using the existing protocols in the literature with some modification to increase the percentage of yield. Peptides were synthesized using both solid and solution phase peptide synthesis strategies.

1.14.1.1. Synthesis of γ Amino Acids ($\gamma^{2,2}$, $\gamma^{3,3}$, and $\gamma^{4,4}$)

$\gamma^{2,2}$, $\gamma^{3,3}$, and $\gamma^{4,4}$ were synthesized using solution-based organic synthesis.[131,286-290] The syntheses of the amino acid residues have been described below. Amino acids were derivatized

TH-3141_166122021

using Fmoc-OSu in basic conditions. Column purified Fmoc protected γ amino acids were used for the manual solid phase synthesis of the peptides.

1.14.1.1.1. Synthesis of 4-Amino-2,2-dimethylbutanoic Acid ($\gamma^{2,2}$)

Alkylation of ester **1** with bromoacetonitrile at -78°C with LDA (*in situ* generation by the reaction of nBuLi and diisopropylethylamine) as a base in THF afforded β-cyanoalkanoate ester **1a** in yields 45%.[131] The $NaBH_4$ reduction of nitriles **1a** in THF/water (2:1, v/v) at 0°C in the presence of $NiCl_2.H_2O$, after 48 hr of stirring at room temperature, resulted in the concomitant cyclization of the intermediate amino ester to form lactam **1b** in good yield (68%).[131] The desired amino acid **1c** was obtained after the cleavage of the lactam **1b** in presence of 6N HCl under reflux for 12 hr (Scheme3).[286]

The compound has also been synthesized by other methods in the literature.[130]

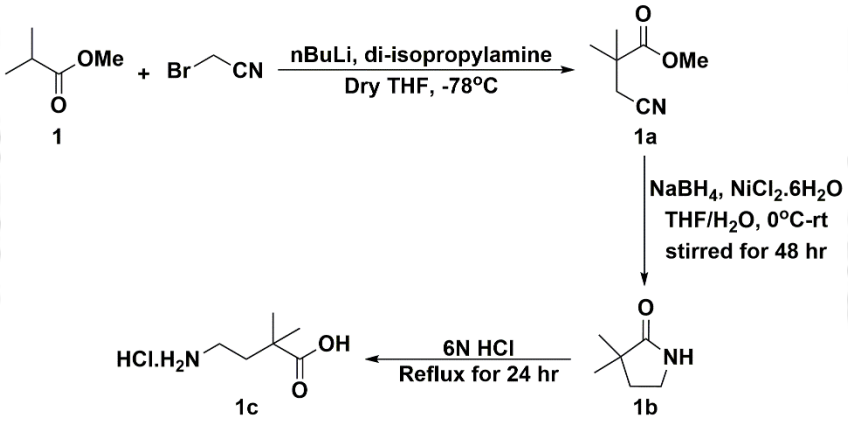

Scheme 1.1. Synthesis of 4-amino-2,2-dimethylbutanoic acid ($\gamma^{2,2}$).

1.14.1.1.2. Synthesis of 4-Amino-3,3-dimethylbutanoic Acid ($\gamma^{3,3}$)

The compounds methyl 3-methylbut-2-enoate, **2a**, and methyl 3,3-dimethyl-4-nitrobutanoate, **2b**, were synthesized as described in the literature with sufficient yields.[287-289] Finally, the reduction of the nitro group of **2c** was carried out by transfer hydrogenation using ammonium formate in the presence of 10% Pd/C (Scheme 1.2).[290]

TH-3141_166122021

A total of 10.5 g of methyl 3,3-dimethyl-4-nitrobutanoate, **2b** (60 mmol), was dissolved in 25 mL of EtOH to which $LiOH \cdot H_2O$ (6.29 g, 150 mmol) in 130 mL of H_2O was added. The reaction mixture was refluxed in an oil bath at 95 °C temperature for 12 hr. After evaporation of ethanol, water was added to the residue. The aqueous layer was washed with ethyl acetate to remove unreacted nitro methyl ester, cooled in an icebath, acidified with 1N HCl to pH 2, and was extracted with EtOAc (3 × 150 mL). The combined organic layer was washed with brine, dried over Na_2SO_4, and evaporated in *vacuo*. A gelatinous yellowish residue was obtained, which was purified using column chromatography over silica gel (50% EtOAc in hexane) to give pure **2c** (7.7 g, 80%) as a colorless semisolid material.The reduction of the nitro group of **2c** (4.02 g, 25 mmol) was carried out by transfer hydrogenation using ammonium formate (11.03 g, 175 mmol) in the presence of 10% Pd/C (1.5 g) in dry methanol (150 mL) under a reflux condition (oil bath) for 3 hr. The reaction mixture was cooled to room temperature, filtered through a Celite pad, and washed with methanol (3 × 50 mL). The filtrate was concentrated in *vacuo* and precipitated by cold Et_2O to give the white crystalline solid **2d** (2.45 g, 75%). **2d** has also been synthesized in the literature by other methods.[132]

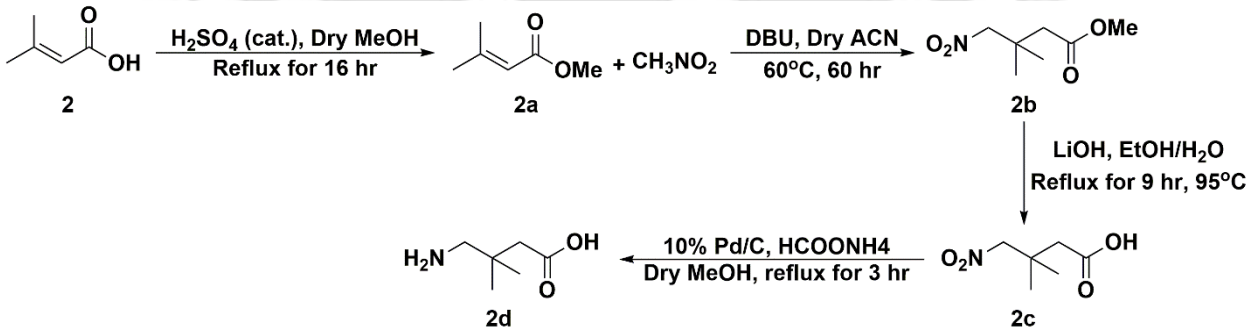

Scheme 1.2. Synthesis of 4-amino-3,3-dimethylbutanoic acid ($\gamma^{3,3}$).

1.14.1.1.3. Synthesis of 4-Amino-4-methylpentanoic Acid ($\gamma^{4,4}$)

The compound benzyl 4-methyl-4-nitropentanoate, **3a**, was synthesized by following the protocol reported in the literature.[134] Simultaneous hydrogenolysis and reduction of the nitro

TH-3141_166122021

group of **3a** were carried out using ammonium formate in the presence of 10% Pd/C. That was the easiest way of synthesizing **3b** without using hydrogen gas (Scheme 1.3).[290]

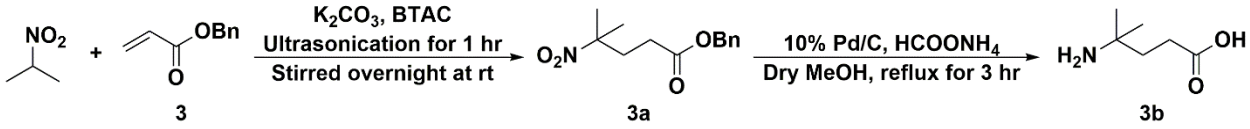

Scheme 1.3. Synthesis of 4-amino-4-methylpentanoic acid ($\gamma^{4,4}$)

1.14.1.2. Synthesis of Fmoc Protected Amino Acids

General Procedure: The amino acid (10 mmol, 1 equiv) was dissolved in water, and $NaHCO_3$ (20 mmol, 2 equiv) was added with stirring. The resulting solution was cooled to 5 °C, and Fmoc-OSU (11 mmol, 1.1 equiv) was added slowly as a solution in dioxane. The resulting mixture was stirred at 0 °C for 1 hr and allowed to attain rt overnight. Water was added, and the aqueous layer was extracted 2 times with EtOAc. The organic layer was back-extracted twice with a saturated solution of $NaHCO_3$. The combined aqueous layer was acidified to a pH of 1 with 10% HCl and then extracted 3 times with EtOAc. The combined organic layers were dried (Na_2SO_4) and concentrated in *vacuo* to give Fmoc-$\gamma^{2,2}$-OH (white solid, 2.61 g, 74%),[291] Fmoc-$\gamma^{4,4}$-OH (white solid, 2.47 g, 70%),[292] and Fmoc-$\gamma^{3,3}$-OH (semisolid, 2.54 g, yield 72%).

1.14.1.3. General Procedures of Peptide Synthesis

1.14.1.3.1. Solid phase (Fmoc Chemistry)

Peptides were synthesized by manual solid-phase synthesis using Fmoc chemistry on a Rink amide resin (0.1 mmol, 1 equiv). For coupling at each step, Fmoc amino acids (0.25 mmol, 2.5 equiv.), HBTU (0.25 mmol, 2.5 equiv.), HOBt (0.25 mmol, 2.5 equiv.), and DIPEA (0.5 mmol, 5 equiv.) were used. For an incomplete reaction, coupling cycles were repeated, followed by capping with 7:2:1 DMF, acetic anhydride, and pyridine. Fmoc deprotection prior to each step of coupling was done using 20% piperidine in DMF. The N terminal protected peptide amides

TH-3141_166122021

were cleaved off from the resin using a cleavage cocktail of 96% TFA, 2.5% TIPS, and 1.5% water for 3 hr. The crude peptide amide was precipitated by cold diethyl ether followed by centrifugation to obtain the crude peptide in the solid form.

1.14.1.3.2. Solution phase (Boc Chemistry)

Peptides were synthesized through conventional solution phase chemistry using a fragment condensation strategy. Tert-Butyloxycarbonyl (Boc) was used for N-terminus protection, and the C-terminus was protected as a methyl ester (in some cases the C-terminal was protected as an N-methyl amide). Deprotection of Boc group was achieved by TFA in DCM (1:1), and the methyl group was removed by saponification using LiOH in mixture of methanol and water (2:1). Peptide coupling was mediated by EDC.HCl and HOBt in dry DCM. The reaction mixture was allowed to attain room temperature and stirred for 2-4 days (depending upon the length of peptide sequence). DCM was evaporated and residue was taken in ethyl acetate and washed with water. The organic layer was washed successively with 0.5 M Citric acid (3 × 30 ml), 1M Sodium bicarbonate (3× 30 ml) and brine (3 × 30 ml). This layer was dried over anhydrous sodium sulphate and evaporated in vacuo to yield crude peptide.

1.14.2. Purification

1.14.2.1. γ-Amino acids and Fmoc-derivatives purification

Purification of intermediates during the synthesis of amino acid residues was performed by various techniques like fractional distillation, Kugelrohr distillation, trituration, and column chromatography. Trituration was performed using a methanol/ether and acetone/chloroform solvent mixture. Column chromatography was done using silica gel (60−120 mesh size) as the stationary phase and hexane/ethyl acetate (3:2) as the eluent. All of the amino acids were purified using trituration techniques (using methanol/diethyl ether/acetone) while the Fmoc

TH-3141_166122021

amino acids were purified by silica gel column chromatography using 50% EtOAc in a hexane solvent system.

1.14.2.2. Peptide purification

The fragments of peptides in solution phase were purified by manual column chromatography using silica gel (60−120 mesh size) as the stationary phase and hexane/ethyl acetate (50-70%) as the eluent. Crude peptides were purified by reverse-phase HPLC using a binary CH_3OH−H_2O/ACN-H_2O solvent system at a flow rate of 10 mL/min using dual UV detection at 214 and 256 nm. To check the purity, analytical HPLC was performed with a flow rate of 1 mL/min and a linear gradient using CH_3OH−H_2O/ACN-H_2O solvent. All purified peptides were white amorphous solids in nature.

1.14.3. Characterization

All Fmoc-derivatives and peptides were characterized using analytical HPLC, ESI-MS/HRMS/MALDI-TOF, 1D ^{1}H NMR, and ^{13}C NMR.

1.14.4. Conformational studies

1.14.4.1. In solid: Single crystal X-ray diffraction

1.14.4.1.1. Fmoc-derivatives: Single crystals of Fmoc-$\gamma^{2,2}$-OH and Fmoc-$\gamma^{4,4}$-OH were grown by slow evaporation from ethyl acetate/hexane solvent mixture. The X-ray data for Fmoc-derivatives were collected at room temperature on Oxford Supernova E, CCD diffractometer using Mo X-ray source (λ = 0.71073 Å). Data was processed using the CrysAlispro software. The structures were obtained by direct methods using SHELXS[293] and were refined against F2 with full-matrix least squares method using SHELXL-2014.[294] All the non-hydrogen atoms were anisotropically refined. All the hydrogen atoms in Fmoc-$\gamma^{4,4}$-OH and the hydrogen atoms attached to the amide NH and carboxylic OH in Fmoc-$\gamma^{2,2}$-OH were located from difference electron density and were refined isotropically. All the other hydrogen atoms were geometrically fixed in idealized positions and were refined as riding over the atoms to which

TH-3141_166122021

they are bonded. The final R factors obtained for Fmoc-$\gamma^{2,2}$-OH and Fmoc-$\gamma^{4,4}$-OH were 7.44% and 4.07% respectively.

1.14.4.1.2. Peptides: Single crystals of the peptides were grown mostly from ACN/H_2O and in some cases from mixture of solvents ACN/MeOH/H_2O. Data was collected at temperatures 105 K, 176 K and 297 K, respectively. Intensity data was collected with Mo-Kα radiation (λ = 0.71073 Å) by a Bruker (D8 Quest) diffractometer. Data was processed using the Bruker SAINT package. All the structures were solved by direct methods using either SHELXS[293] or SHELXD[295] and were refined using the Least-squares method in SHELXL-14.[294] All hydrogen atoms were fixed in ideal geometries and were refined as riding against the atoms to which they are bonded. The crystal structures have been deposited at the Cambridge Crystallographic Data Centre (CCDC) with deposition numbers 2206582-2206586.

1.14.4.2. In solution

Conformations of all peptides was studied in solution state extensively using NMR (1D ^{1}H NMR, variable temperature (VT) 1D NMR, 2D NMR ROESY, NOESY, solvent titration etc.). CD and IR spectroscopy was also performed in the case of some of the peptides. Solution conformation and assembly of Fmoc-derivatives of amino acid residues was studied by NMR (1D ^{1}H NMR, variable temperature (VT) 1D NMR, 2D NMR NOESY, solvent titration etc.), IR, and Fluorescence spectroscopy. Morphology of Fmoc-derivatives were analyzed by using FESEM and FETEM.

1.14.4.2.1. NMR

All NMR experiments (both 1D and 2D) were carried out on a Bruker Ascend Aeon 600 and 400 MHz spectrometer respectively. All spectra were recorded in either $CDCl_3$ or CD_3OH at room temperature. Coupling constant (*J*) was measured in Hertz. The chemical shift values were reported in ppm downfield from tetramethylsilane, using $CDCl_3$ (δ = 7.26 ppm for ^{1}H and 77.2 ppm for ^{13}C NMR) and residual methanol, using CD_3OH (δ = 3.33 ppm for ^{1}H and 49.0

TH-3141_166122021

ppm for ^{13}C NMR) respectively. All spectra were recorded at 10-12 mM and 5-7 mM concentrations for the Fmoc-derivatives and peptides respectively. Water suppression was done using the excitation sculpting scheme (in case of CD_3OH solvent system). The chemical shift values and coupling constants were measured from 1D NMR spectra. Variable temperature 1D NMR experiments were carried out in between 263 K-323 K. Concentration dependent NMR experiments were performed within the concentration range of 0.1mM to 10 mM. Solvent titration experiment was done using polar MeOH and DMSO-d_6 respectively. Proton assignments of the Fmoc derivatives were done by COSY and NOESY experiments. Complete resonance assignments of the protons of all peptides were done by TOCSY and ROESY experiments. All the 2D experiments (except COSY) were done in phase sensitive mode by using time-proportional phase incrementation (TPPI) method. For all peptides TOCSY spectra was recorded with a mixing time of 80 ms but for ROESY/NOESY spectra different mixing times (400 ms for NOESY and 150-300 ms for ROESY) were used respectively. The spectral width was 6009.6 or 12019.2 Hz in both dimensions. The total number of scans were fixed to 32/16 for TOCSY and ROESY, respectively. Data points were set to 2048 and 300 in f2 and f1 dimensions, respectively for both TOCSY and ROESY spectra. Zero filling was done to finally yield a data set of 4K x 2K. All NMR spectra were processed using Topspin 3.6 and Mestre Nova software.

1.14.4.2.2. CD Spectroscopy

The CD spectra were recorded using a 200 μL quartz cuvette of 1 mm path length with a Jasco J-1500 spectropolarimeter at room temperature. The CD studies were performed in methanol at 500 μM concentrations. Spectra were collected at a scan rate of 100 nm·min^{-1} and 2 nm bandwidth from 200 nm to 260 nm or 200−330 nm (for Fmoc protected peptides) with five scans for averaging. Before running the sample, methanol was run to correct the baseline.

TH-3141_166122021

1.14.4.2.3. IR Spectroscopy

The solution IR of all Fmoc-derivatives and peptides were carried out by using PerkinElmer Spectrum Two spectrometer. All FT-IR spectra were recorded in the region of 400−4000 cm^{-1}. Spectra were recorded in two solvents $CDCl_3$ and MeOH at different concentrations (10 mM and 1 mM for Fmoc-derivatives and peptides respectively).

1.14.4.2.4. Fluorescence Spectroscopy

To gain an insight into the self-assembly behaviour of Fmoc-derivatives, fluorescence experiments were performed by monitoring the fluorescence emission of the Fmoc moiety on a Fluoromax-4 spectrophotometer. Samples of different concentrations were prepared in 70% MeOH/H_2O and their fluorescence emission was monitored keeping the fluorescence excitation wavelength fixed at 301 nm.

1.14.4.2.4. Field Emission Scanning Electron Microscopy (FESEM)

FESEM images of the reported Fmoc-derivatives were obtained on a FESEM Sigma Zeiss Sigma microscope. For FESEM study two sets of solvent systems (70% MeOH/H_2O and bicarbonate buffer pH 10) were used. For the first system, a drop of the solution of the molecules in 70% MeOH/H_2O was casted on a silicon wafer and was allowed to dry for a few hours under vacuum before imaging. For the second system, the molecules were heated slightly (for 2-3 min) due to the poor solubility of Fmoc-derivatives in aqueous medium before casting.

1.14.4.2.5. Field Emission Transmission Electron Microscopy (FETEM)

FETEM studies were performed on JEOL JEM (model 2100F) at an operating voltage of 200 kV by casting 1 μL of 150 μM 70% MeOH-H_2O solution of the Fmoc-$\gamma^{2,2}$-OH on carbon-coated copper grids (300 mesh). Solvent was removed by slow evaporation, and the grid was allowed to dry under vacuum at room temperature for 3 days.

TH-3141_166122021

1.14.4.3. *in silico*

1.14.4.3.1. Model building: Fmoc-derivatives and peptides

We modelled Fmoc-derivatives Fmoc-$\gamma^{x,x}$-OH for the different geminal substitutions (x,x = 2,2/3,3/4,4) using Avogadro v1.2.0 software.[296] For peptides used in the construction of isolated non-helical β-turn mimics, we took the crystal structure of the C13 β-turn mimic formed across the D-Pro-δAva in a model octapeptide as our starting structure.[209] We modified our model by deleting one of the backbone CH_2's (γ) of the δAva residue, modified the geminal substitutions and used it as a template for structure optimization. (Cambridge Crystallographic Data Centre, CCDC number: 608845). The β-hairpin structure of octapeptide was taken from the Cambridge Structural Database (accession number CCDC 711306) and used as a template to model.[215] For helical conformation, we modelled helical peptides using the experimental data (both solid and solution) as input. All the peptides were modelled using PyMOL software.[297]

1.14.4.3.2. Structure optimization and energy optimization: DFT studies

The structures of the monomers and the dimers of Fmoc-derivatives and all peptides were subjected to geometry optimization and normal mode frequency calculations using Gaussian16 software[298] employing density functional theory (B3LYP/6-31+G* and B3LYP/6-311++G* level).[299-303] Calculations were performed on peptides (**41-43**) in vacuum as well as embedded in two different implicit solvent models (chloroform and methanol). Solvation was considered by employing polarizable continuum model (PCM)[304] in which the solvent was modeled as a continuum dielectric. The peptides were accommodated into a cavity surrounded by implicit solvent dielectric. The cavity was created by inter locking the atomic radii of the atoms of the peptide. The dipole in the solute induces a dipole in the dielectric. The system was stabilized by the dipole-induced dipole interaction. **41-43** were optimized in the gas phase, and then, the gas phase optimized coordinates were subjected to re-optimization considering polarizable

TH-3141_166122021

continuum models. In case of β-hairpin peptides, polarizable continuum model[305,306] was employed to include methanol as the continuum dielectric and implicitly consider the solvent effects toward the energetics. The polarity of the peptides induced a dipole in the dielectric medium, and a dipole-induced dipole interaction led to stabilization. Geometry optimization and normal model frequency calculations were performed for all peptides in the implicit toluene solvent. All the reported structures were true minima in the potential energy hypersurface, supported by the positive normal model frequencies. Gibbs free energy of the optimized structures were used to estimate the free energy differences.

TH-3141_166122021

Chapter 2

Effect of Differential Backbone Di-substitution of γ Amino Acid Residues on the Conformation and Assembly of Their Fmoc Derivatives in Solid and Solution States

TH-3141_166122021

2.1. Introduction

In this Chapter we have studied the conformation and assembly of the Fmoc derivatives of three differentially substituted $\gamma^{x,x}$ (x,x = 2,2/3,3/4,4) amino acid residues in solid and solution states. We wanted to study the effect of variable position of di-substitution along the backbone of these γ amino acid residues on their conformation and assembling behavior. With an intention of avoiding the effect that the sequence may have on the conformation of the peptides, we decided to work with the simple N-terminal protected Fmoc derivatives of $\gamma^{2,2}$, $\gamma^{3,3}$ and $\gamma^{4,4}$ amino acid residues (Figure 2.1). In this study we have employed various experimental techniques like X-ray, NMR, IR, fluorescence, FETEM and FESEM. We have also performed *ab initio* structure calculation and compared the stabilities of the monomeric and dimeric units in various conformations that were observed in the crystals of Fmoc derivatives.

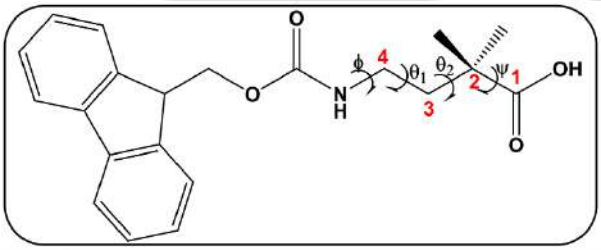

	Position of di-substitution		
Gamma amino acids	$\gamma^{2,2}$	$\gamma^{3,3}$	$\gamma^{4,4}$
Name of the molecules	Fmoc-$\gamma^{2,2}$-OH 21	Fmoc-$\gamma^{3,3}$-OH 22	Fmoc-$\gamma^{4,4}$-OH 23

Figure 2.1. Chemical structure of the Fmoc-$\gamma^{2,2}$-OH and definition of the backbone torsion angles. List of derivatives studied in this Chapter.

TH-3141_166122021

2.2. Experimental Section

2.2.1. Synthesis, Purification and Characterization of Fmoc derivatives

N-terminal protection of all γ amino acids was done using Fmoc-OSu under basic conditions. ($NaHCO_3$, pH 7). Purification was done by column chromatography. General synthetic protocols and purification of all Fmoc derivatives have been detailed in sections 1.14.1.2 and 1.14.2.1, respectively. The purified Fmoc-derivatives were characterized by analytical HPLC (Appendix, Figures A2-A4x), Electrospray Ionization Mass Spectrometry (ESI-MS) (Appendix, Figures A5-A7x), and 600 MHz ^1H (Appendix, Figures A8-A10) and ^{13}C (Appendix, Figures A11-A13) NMR spectra in $CDCl_3$.

Fmoc-$\gamma^{2,2}$-OH: Two sets of lines were present with the ratio of 2:1 in the ^1H NMR spectrum.

Major Populant: ^1H NMR (600 MHz, Chloroform-*d*) δ 7.76 (d, *J* = 7.5 Hz), 7.58 (t, *J* = 7.1 Hz), 7.39 (t, *J* = 7.5 Hz), 7.31 (td, *J* = 7.5, 1.1 Hz), 4.87 (t, *J* = 5.9 Hz), 4.37 (d, *J* = 7.0 Hz), 4.20 (t, *J* = 7.0 Hz), 3.27 – 3.21 (m), 1.82 – 1.76 (m), 1.23 (s).

Minor Populant: ^1H NMR (600 MHz, Chloroform-*d*) δ 7.76 (d, *J* = 7.5 Hz), 7.58 (t, *J* = 7.1 Hz), 7.39 (t, *J* = 7.5 Hz), 7.31 (td, *J* = 7.5, 1.1 Hz), 6.06 (broad), 4.47 (d, *J* = 6.4 Hz), 4.25 (t, *J* = 6.6 Hz), 3.13 (m), 1.65 (t, *J* = 6.2 Hz), 1.14 (s).

^{13}C {1H} NMR (150 MHz, Chloroform-d): δ 182.8, 156.4, 144.1, 141.4, 127.8, 127.2, 125.2, 125.1, 120.1, 67.3, 66.8, 47.4, 40.9, 40.2, 40.0, 38.2, 37.7, 25.3.

Fmoc-$\gamma^{3,3}$-OH: Two sets of lines were present with the ratio of 5:1 in the ^1H NMR spectrum.

Major Populant: ^1H NMR (600 MHz, Chloroform-*d*) δ 7.77 (d, *J* = 7.5 Hz), 7.60 (d, *J* = 7.6 Hz), 7.41 (t, *J* = 7.4 Hz), 7.36 – 7.30 (m), 5.14 (t, *J* = 6.8 Hz), 4.49 (d, *J* = 6.6 Hz), 4.22 (t, *J* = 6.6 Hz), 3.13 (d, *J* = 6.8 Hz), 2.20 (s), 1.01 (s).

TH-3141_166122021

Minor Populant: ^{1}H NMR (600 MHz, Chloroform-*d*) δ 7.77 (d, *J* = 7.5 Hz), 7.60 (d, *J* = 7.6 Hz), 7.41 (t, *J* = 7.4 Hz), 7.36 – 7.30 (m), 5.75 (broad), 4.49 (d, *J* = 6.6 Hz), 4.22 (t, *J* = 6.6 Hz), 2.98 (d, *J* = 6.6 Hz), 2.15 (s), 0.87 (s).

^{13}C NMR {1H} (150 MHz, Chloroform-d): δ 176.6, 157.4, 143.9, 141.5, 127.8, 127.2, 125.1, 124.9, 120.1, 67.3, 66.9, 50.4, 47.5, 47.3, 43.9, 43.5, 35.1, 25.6, 25.4.

Fmoc-γ^{4,4}-OH: only one set of line was present in the ^{1}H NMR spectrum.

^{1}H NMR (600 MHz, Chloroform-*d*) δ 7.78 (d, *J* = 7.5 Hz), 7.61 (d, *J* = 7.5 Hz), 7.42 (t, *J* = 7.5 Hz), 7.37 – 7.31 (m), 4.72 (s), 4.48 – 4.36 (m), 4.21 (t, *J* = 6.6 Hz), 2.35 (broad), 2.06 (broad), 1.31 (s).

^{13}C {1H} NMR (150 MHz, DMSO-d_6): δ 175.2, 154.9, 144.5, 141.2, 128.1, 127.5, 125.8, 120.6, 65.3, 51.9, 47.3, 34.9, 29.5, 27.1.

2.2.2. NMR Spectroscopy

All NMR experiments (both 1D and 2D) of the Fmoc derivatives were recorded at 10-12 mM concentration in $CDCl_3$ at room temperature. Variable temperature 1D NMR experiments was carried out between 263-323 K. Concentration-dependent NMR experiments were performed within the concentration range of 0.1 mM to 10 mM. ^{1}H NMR spectra were also recorded in polar solvent DMSO-d_6 and 70% CD_3OD/D_2O, respectively, to prove the presence of both monomeric and dimeric species in solution. Proton assignments of the Fmoc derivatives were done by COSY (scan 4) and NOESY (scan 4 and mixing time 400 ms) experiments. All information regarding 2D NMR has been discussed in Section 1.14.4.2.1.

TH-3141_166122021

2.2.3. FT-IR Spectroscopy

FT-IR spectra of all Fmoc derivatives were carried out in solid and solution states. A solution study was done in $CDCl_3$ at 10 mM concentrations at 298 K.

2.2.4. Single crystal X-ray diffraction

Single crystals of Fmoc-$\gamma^{2,2}$-OH and Fmoc-$\gamma^{4,4}$-OH for X-ray data collection were grown by slow evaporation from ethyl acetate/hexane mixture. Unfortunately, we were unable to crystallize the Fmoc-$\gamma^{3,3}$-OH. The X-ray data were collected at room temperature on Oxford Supernova E, CCD diffractometer using Mo X-ray source (λ = 0.71073 Å). Data processing and refinement were explained adequately in section 1.14.4.1.2.

Crystallographic information of Fmoc-$\gamma^{2,2}$-OH: Space group : *P*bca, Unit Cell: a = 14.619 (1) Å; b = 9.883 (1) Å; c = 26.233 (2) Å; $\alpha = \beta = \gamma = 90°$, V = 3789.8 (5) $Å^3$Orthorhombic, chemical formula $C_{21}H_{23}NO_4$, F (000) = 1504; Measured reflections = 10629; unique reflections = 4340; observed reflections ($|F| > 4\sigma$ (F)) = 1840; number of parameters = 244; , R-factor = 7.44 %; wR2 = 19.75 %; S = 0.970.

Crystallographic information of Fmoc-$\gamma^{4,4}$-OH: Space group : P-1, Unit Cell: a = 6.887 (1) Å; b = 10.517 (2) Å; c = 14.047 (2) Å; α = 69,14 (1)°; β = 80.60 (2)°; γ = 77.40 (1)°, V = 923.7 (2), triclinic, Z = 2 for chemical formula $C_{21}H_{23}NO_4$; F (000) = 376; Measured reflections = 24398; unique reflections = 3851; observed reflections ($|F| > 4\sigma$ (F)) = 2820; number of parameters = 327; R-factor = 4.07 %; wR2 = 11.21 %; S = 1.035.

TH-3141_166122021

2.2.5. Quantum Chemical Calculations

Crystal structures of $\gamma^{2,2}$ and $\gamma^{4,4}$ were considered as a template to model the monomer and dimer of the Fmoc derivatives of $\gamma^{2,2}$, $\gamma^{3,3}$ and $\gamma^{4,4}$. The dimers in the X-ray structures ($\gamma^{2,2}$ and $\gamma^{4,4}$) were distinctly different in terms of the intermolecular interaction and the orientation of the Fmoc group relative to the axis of intermolecular hydrogen bonding. We defined Fmoc-$\gamma^{2,2}$-OH and Fmoc-$\gamma^{4,4}$-OH backbone conformations as "open" and "close" structures respectively. Next, we modelled "open" and "closed" structures for the monomers: $M^{x,x}$ (open/Close) as well as the dimers $D^{x,x}$ (open/Close) for the different geminal substitutions (x,x = 2,2/3,3/4,4) using Avogadro v1.2.0 software.[296] The structures of the monomers and the dimers were subjected to geometry optimization and normal mode frequency calculations using Gaussian16 software[298] employing density functional theory (B3LYP/6-31+G* level).[299-301] All the reported structures were true minima in the potential energy hypersurface, supported by the positive normal model frequencies. Gibbs free energy of the optimized structures were used to estimate the free energy differences.

2.2.6. Field Emission Scanning Electron Microscopy (FESEM)

Morphology of the Fmoc derivatives in 70% MeOH/H_2O and bicarbonate buffer pH 10 were analyzed by FESEM. The method of sample preparation is described in section 1.14.4.2.4.

2.2.7. Field Emission Transmission Electron Microscopy (FETEM)

FETEM studies were performed to check the nature of spherical morphology obtained from FESEM and analyzed at 150 μM concentration in 70% MeOH/H_2O solution of the Fmoc-$\gamma^{2,2}$-OH The detail of sample preparation is mentioned in section 1.14.4.2.5.

TH-3141_166122021

2.2.8. Fluorescence Spectroscopy

Concentration dependent fluorescence experiments were performed to gain an insight into the self-assembly behavior and determine the CAC of Fmoc-derivatives in 70% MeOH/H_2O by monitoring the fluorescence of the Fmoc moiety. The excitation wavelength for this experiment was fixed to 301 nm.

2.3. Results and Discussion

Fmoc derivatives of the three γ amino acid residues (Figure 2.1) were synthesized in solution phase, purified using column chromatography and characterized using analytical HPLC (Appendix, Figures A2-A4), ESI-MS (Appendix, Figures A5-A7), ^{1}H (Appendix, Figures A8-A10) and ^{13}C NMR (Appendix, Figures A11-A13).

2.3.1. Structure in solution

2.3.1.1. NMR studies

2.3.1.1.1. Solution population (in $CDCl_3$): ^{1}H NMR

Figure 2.2 shows the stacked partial ^{1}H NMR spectrum of Fmoc-$\gamma^{2,2}$-OH, Fmoc-$\gamma^{3,3}$-OH and Fmoc-$\gamma^{4,4}$-OH in $CDCl_3$ at room temperature. In the ^{1}H NMR spectrum of Fmoc-$\gamma^{2,2}$-OH and Fmoc-$\gamma^{3,3}$-OH, two distinct sets of NMR lines were seen at room temperature. Though only one set of lines were observed in the NMR spectrum of Fmoc-$\gamma^{4,4}$-OH at room temperature, the line widths of the signals were broadened. All the NMR lines were assigned using 2D COSY (Appendix, Figures A14-A16) and NOESY (Appendix, Figures A17-A19) NMR techniques. As we had established earlier using analytical HPLC (Appendix, Figures Ax), that all the Fmoc derivatives were pure, presence of two sets of lines in the NMR at room temperature most probably indicated presence of mixed populations of two distinct species like conformers[213, 307,308] or oligomers[309,310] in solution. From the intensity of the two sets of lines

TH-3141_166122021

seen in the NMR spectra, the ratio of the two populations were determined to be monomer:dimer = 2:1 and 5:1 in the case of Fmoc-$\gamma^{2,2}$-OH and Fmoc-$\gamma^{3,3}$-OH respectively. Fmoc-$\gamma^{4,4}$-OH, contained only one set of broad lines suggesting presence of either only one species or a very rapid rate of exchange (with respect to the NMR time scale) at room temperature in between the different species populating the solution.

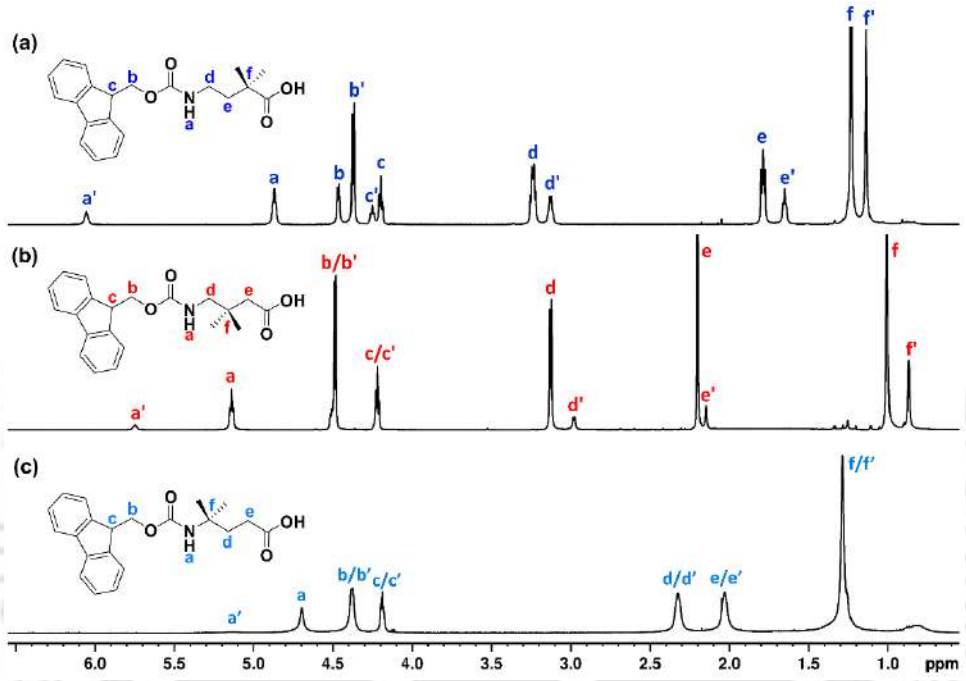

Figure 2.2. 600 MHz partial stacked 1D ^{1}H NMR spectra of (a) Fmoc-$\gamma^{2,2}$-OH, (b) Fmoc-$\gamma^{3,3}$-OH and (c) Fmoc-$\gamma^{4,4}$-OH in $CDCl_3$ at 298 K at 10 mM concentration. Fmoc-$\gamma^{2,2}$-OH and Fmoc-$\gamma^{3,3}$-OH contain two sets of lines while Fmoc-$\gamma^{4,4}$-OH contains one set of broadened lines.

2.3.1.1.2. Variable temperature 1D ^{1}H NMR

To investigate the nature of the two species present in solution further, 1D ^{1}H NMR for all the three Fmoc derivatives of the γ amino acid residues were recorded over a temperature range of 263-323 K (Figure 2.3). In the case of Fmoc-$\gamma^{2,2}$-OH and Fmoc-$\gamma^{3,3}$-OH, upon increasing the

TH-3141_166122021

temperature, the NMR signals from the two sets of lines started coming closer until they coalesced into a single signal. Upon increase in the temperature of the system, the rate of exchange in between the two species that populated the solution increased, until at a certain point, when this rate became faster than the NMR time scale two lines coalesced into one single signal. This is a characteristic temperature dependent feature observed for exchange phenomenon in between the conformations or various oligomeric states[311] and proved beyond doubt that the two populating species in solution were either conformations or different oligomeric states of the same molecule. It was note-worthy, that upon cooling down to a temperature of ~ 263 K, two sets of lines were also observed in the case of Fmoc-$\gamma^{4,4}$-OH (Figure 2.3c). This established the presence of two species in the solution of Fmoc-$\gamma^{4,4}$-OH that were not clearly seen due to very fast rate of exchange in between them at room temperature. For Fmoc-$\gamma^{2,2}$-OH, the major populant contained NH signal at ~ 5.00 δ ppm while the minor populant contained the NH signal at ~ 6.0 δ ppm. Upon increasing the temperature of the $CDCl_3$ solution, the NH peak at 6.0 δ ppm showed an upfield shift while the signal at 5.00 δ ppm remained unchanged (Figure 2.3a). This suggested that the NH in the minor populant was hydrogen bonded, which got disrupted upon enhancement of temperature leading to the shielding of the NH signal, while the NH in the major populant being non-hydrogen bonded did not show any shift in the position of NH signal. Similar observations were also encountered upon performing variable temperature NMR for Fmoc-$\gamma^{3,3}$-OH (Figure 2.3b). Upon increasing temperature, the lines sharpened in the case of Fmoc-$\gamma^{4,4}$-OH, while they broadened upon cooling and eventually gave rise to two sets of lines at 263 K (Figure 2.3c).

TH-3141_166122021

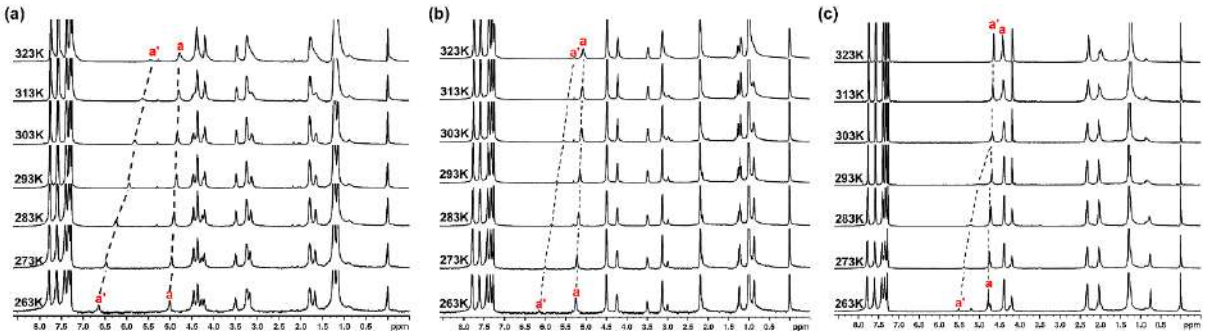

Figure 2.3. Stacked 500 MHz 1D ^{1}H NMR spectra of (a) Fmoc-$\gamma^{2,2}$-OH (b) Fmoc-$\gamma^{3,3}$-OH and (c) Fmoc-$\gamma^{4,4}$-OH over the temperature range of 263-323 K in $CDCl_3$ at 10 mM concentration.

2.3.1.1.3. Observation of exchange cross peaks (NOESY NMR)

Figures 2.4 and 2.5 represent the partial NOESY spectra of Fmoc-$\gamma^{2,2}$-OH and Fmoc-$\gamma^{3,3}$-OH respectively. Both positive (solid circles, Figures 2.4, 2.5) and negative (broken rectangles, Figures 2.4, 2.5) exchange cross peaks (EXSY peaks), were obtained in between the same protons or different protons respectively of the two populants. EXSY peaks arose from the slow exchange in between the two populants, which has been earlier reported in the literature.[213,307-312] In the case of Fmoc-$\gamma^{4,4}$-OH, though only one set of lines were observed at room temperature (Figure 2.2), presence of EXSY peaks (Figure 2.6) confirmed the presence of two species in solution. This conclusively proved that the two species in solution for all the Fmoc derivatives were in an equilibrium with each other. The rate of exchange in between these populants was dependent on the activation barriers in the exchange pathway, and determined whether one set or two sets of lines would be observed in the NMR spectra at a particular temperature.

TH-3141_166122021

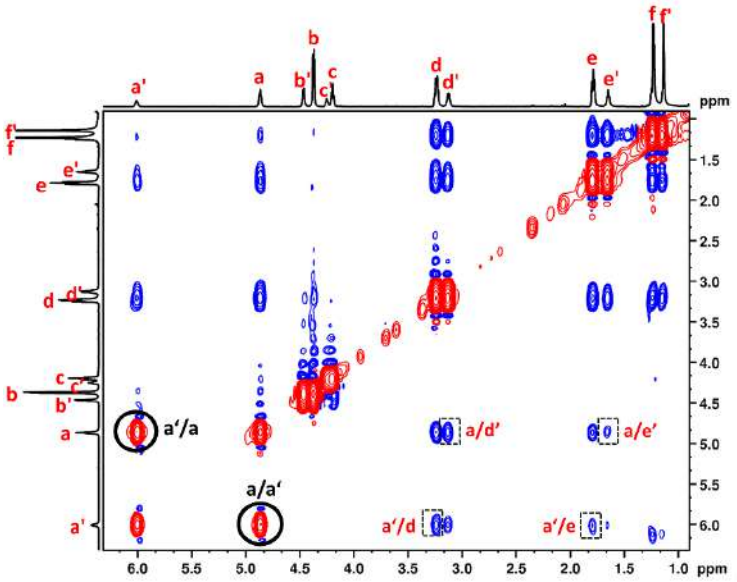

Figure 2.4. 600 MHz Partial NOESY spectra of Fmoc-$\gamma^{2,2}$-OH in $CDCl_3$ at 10 mM concentration and at 298 K representing aliphatic region. Black circles and broken rectangles indicate positive and negative EXSY peaks respectively.

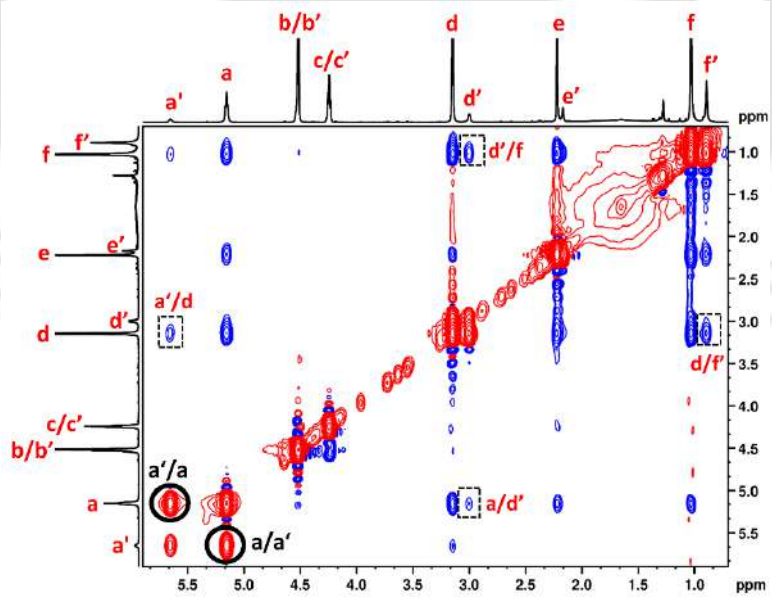

Figure 2.5. 600 MHz Partial NOESY spectra of Fmoc-$\gamma^{3,3}$-OH in $CDCl_3$ at 10 mM concentration and at 298 K representing aliphatic region. Black circles and broken rectangles indicate positive and negative EXSY peaks respectively.

TH-3141_166122021

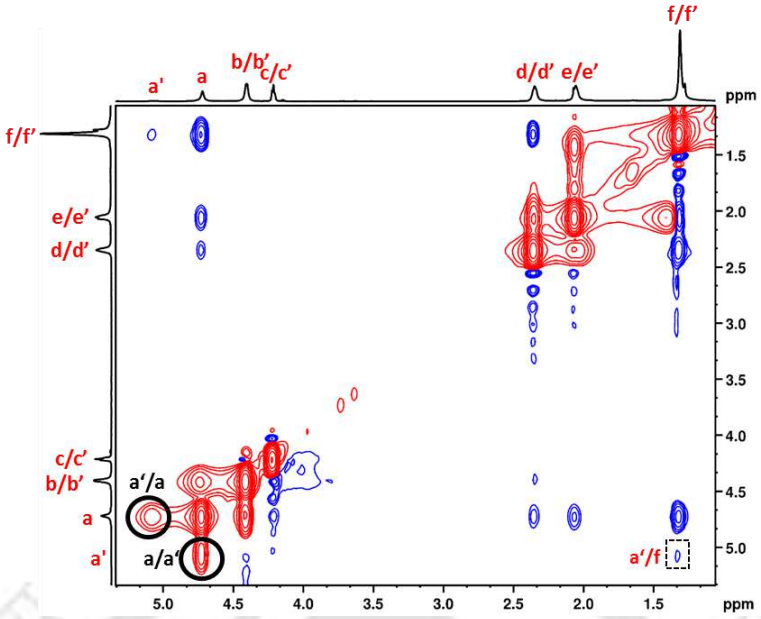

Figure 2.6. 600 MHz Partial NOESY spectra of Fmoc-$\gamma^{4,4}$-OH in $CDCl_3$ at 10 mM concentration and at 298 K representing aliphatic region. Black circles and broken rectangles indicate positive and negative EXSY peaks respectively.

2.3.1.1.4. Determination of nature of hydrogen bonding: Methanol titration

Next, in order to further look at the hydrogen bonded state of the amide NH's of the two species populating the solution, we performed ^{1}H NMR of the Fmoc derivatives in the presence of increasing concentrations of polar protic MeOH (Figures 2.7 and 2.8). Addition of 10% MeOH to the $CDCl_3$ solution of Fmoc-$\gamma^{2,2}$-OH, resulted in the downfield shift ($\Delta\delta \sim 0.6$ ppm) of the NH signal at ~ 5.00 δ ppm of the major populant, suggesting its participation in hydrogen bond formation with MeOH (Figure 2.7). This proved that the major populant contained non-hydrogen bonded NH. The signal at ~ 6.0 δ ppm from the minor populant showed a shielding ($\Delta\delta \sim 0.5$ ppm) upon addition of MeOH, suggesting that it was hydrogen bonded. This slight shielding probably was due to the breakdown of the intermolecular hydrogen bonds in between the Fmoc-$\gamma^{2,2}$-OH molecules and the formation of new hydrogen bonds between Fmoc-$\gamma^{2,2}$-OH and MeOH molecules. Similar trends were observed upon titrating Fmoc-$\gamma^{3,3}$-OH with MeOH

TH-3141_166122021

(Figure 2.8a). Addition of MeOH also led to the downfield shift of the averaged NH signal in Fmoc-$\gamma^{4,4}$-OH (Figure 2.8b).

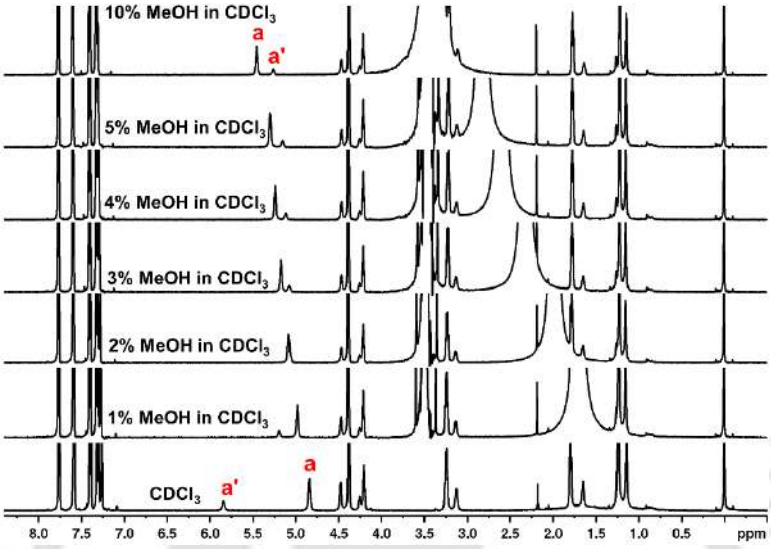

Figure 2.7. Stacked 600 MHz 1D ^{1}H NMR spectra with increasing percentages of MeOH added to the $CDCl_3$ solution of Fmoc-$\gamma^{2,2}$-OH at 298 K at 10 mM concentration. NH peaks from the major and the minor conformer have been denoted as a and a' respectively.

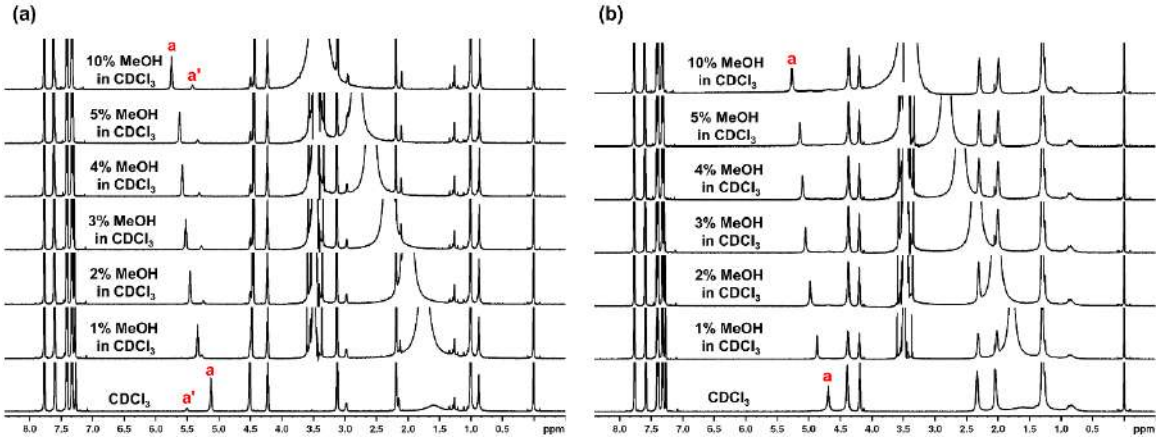

Figure 2.8. Stacked 600 MHz 1D ^{1}H NMR spectra with increasing percentages of MeOH added to the $CDCl_3$ solution at 298 K of (a) Fmoc-$\gamma^{3,3}$-OH and (b) Fmoc-$\gamma^{4,4}$-OH. NH peaks from the major and the minor conformer have been denoted as a and a' respectively.

TH-3141_166122021

2.3.1.1.5. Determination of nature of hydrogen bonding: Concentration Dependent NMR

Further to look at the effect of concentration on the NMR lines, we performed a concentration dependent ^{1}H NMR over a range of 0.1-10 mM in $CDCl_3$ at 298 K. Figure 2.9 shows the stacked plots of the partial ^{1}H NMR spectra of Fmoc-$\gamma^{2,2}$-OH at different concentrations. At a very low concentration, signals from only the major populant was observed. However, upon increasing the concentration of Fmoc-$\gamma^{2,2}$-OH, signals from the minor populant started appearing. Notably, upon the build-up of the minor populant with the increase in the concentration, its NH signal showed a systematic downfield shift. This proved that the minor species in solution could only exist at higher concentrations and the NH in the minor population was hydrogen bonded. This is in lines with the earlier NMR observations. As the major populant was present in very low concentrations and had a non-hydrogen bonded NH, it might be the monomeric species of Fmoc-$\gamma^{2,2}$-OH. On the other hand, the minor populant in solution which was present only at a high concentration, might be the dimeric species.

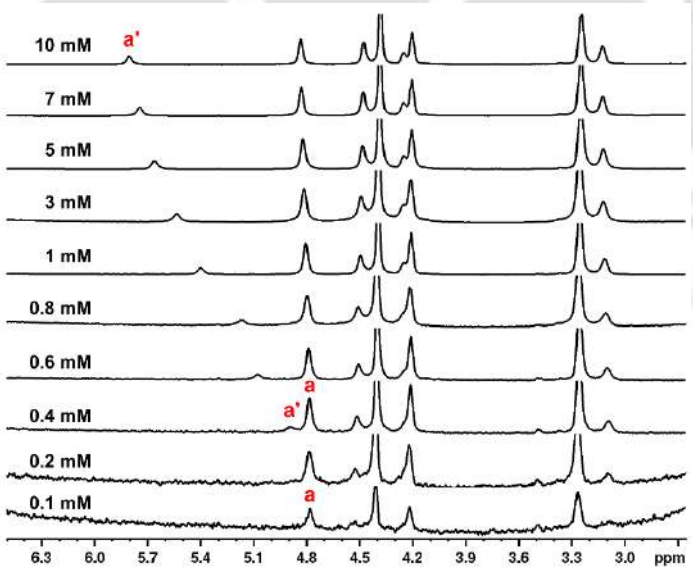

Figure 2.9. Concentration dependent 1D ^{1}H spectra of Fmoc-$\gamma^{2,2}$-OH in 600 MHz in $CDCl_3$ at 298 K.

TH-3141_166122021

2.3.1.1.6. Solution population in 70% CD_3OD/D_2O and DMSO-d_6 solvent systems

Having established the presence of both monomeric and dimeric species in $CDCl_3$ solution, we were interested to probe if such a situation existed in other solvent systems as well for the three Fmoc derivatives. Figures 2.10-2.11 shows the stacked 1D ^1H NMR spectrum of the three Fmoc derivatives in 70% CD_3OD/D_2O and DMSO-d_6 . Though in both of these solvent systems, there were presence of both the monomeric species and the dimeric species for Fmoc-$\gamma^{2,2}$-OH and Fmoc-$\gamma^{3,3}$-OH, the population of the later diminished considerably. This was due to the increase in the polarity of the solvent leading to the breakdown of the hydrogen bonds and destabilization of the dimers. It is mention-worthy that in none of these solvents were two species seen in the case of Fmoc-$\gamma^{4,4}$-OH. One set of broad lines were obtained for Fmoc-$\gamma^{4,4}$-OH in all cases suggesting the fast rate of exchange in between the monomeric and dimeric species. Thus it can be concluded that the fast rate of exchange in between the monomeric and dimeric species is an inherent property of Fmoc-$\gamma^{4,4}$-OH. As the three Fmoc derivatives were similar in every other way, difference in the rates of exchange in between their monomeric and dimeric species might attributed to the position of di-substitution along the backbone of the γ amino acid residues.

TH-3141_166122021

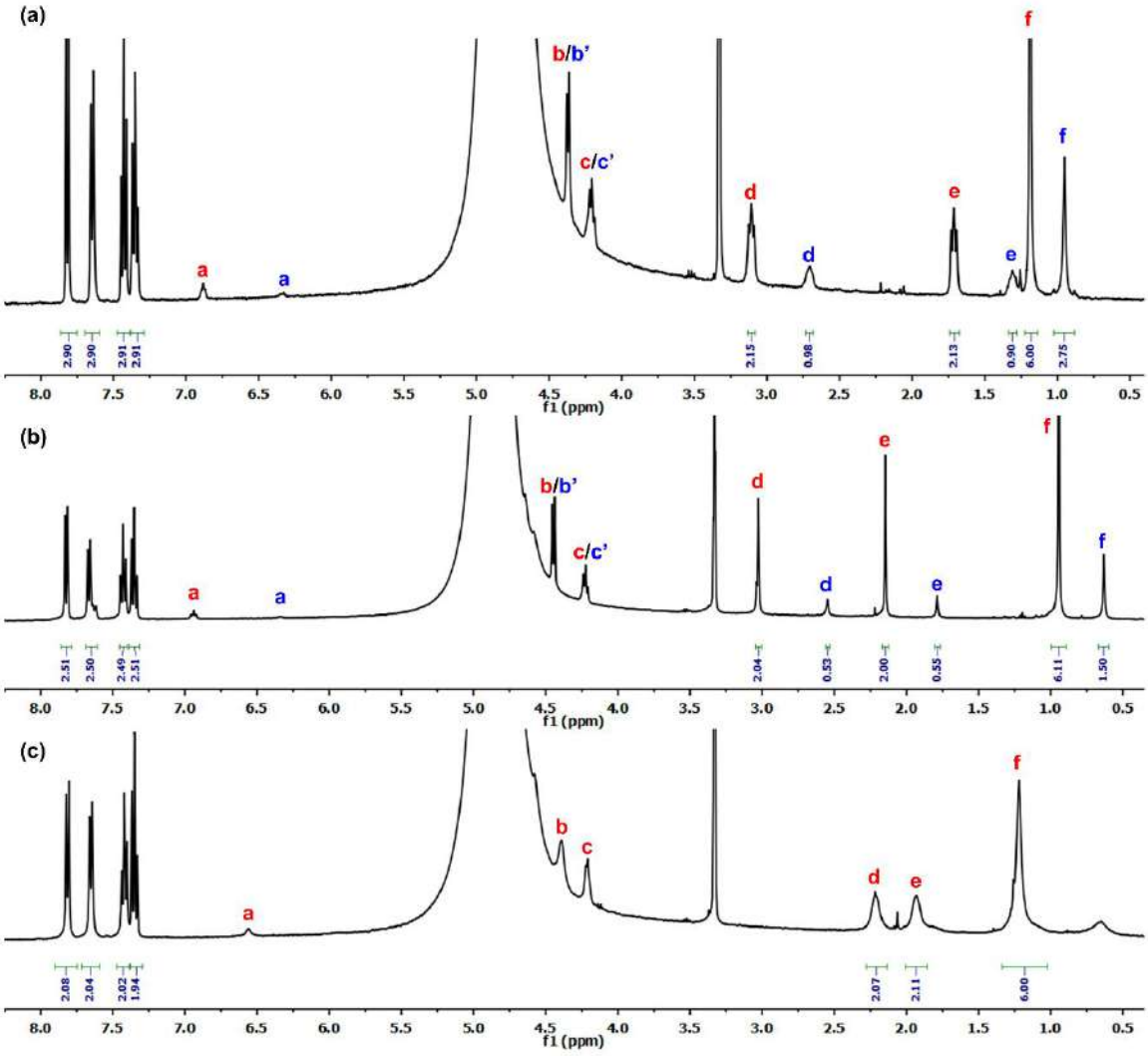

Figure 2.10. 400 MHz ^{1}H NMR spectra of (a) Fmoc-$\gamma^{2,2}$-OH (b) Fmoc-$\gamma^{3,3}$-OH (c) Fmoc-$\gamma^{4,4}$-OH in 70% CD_3OD/D_2O at 10 mM concentration at 298 K. Major and minor conformers have been marked in red and blue.

TH-3141_166122021

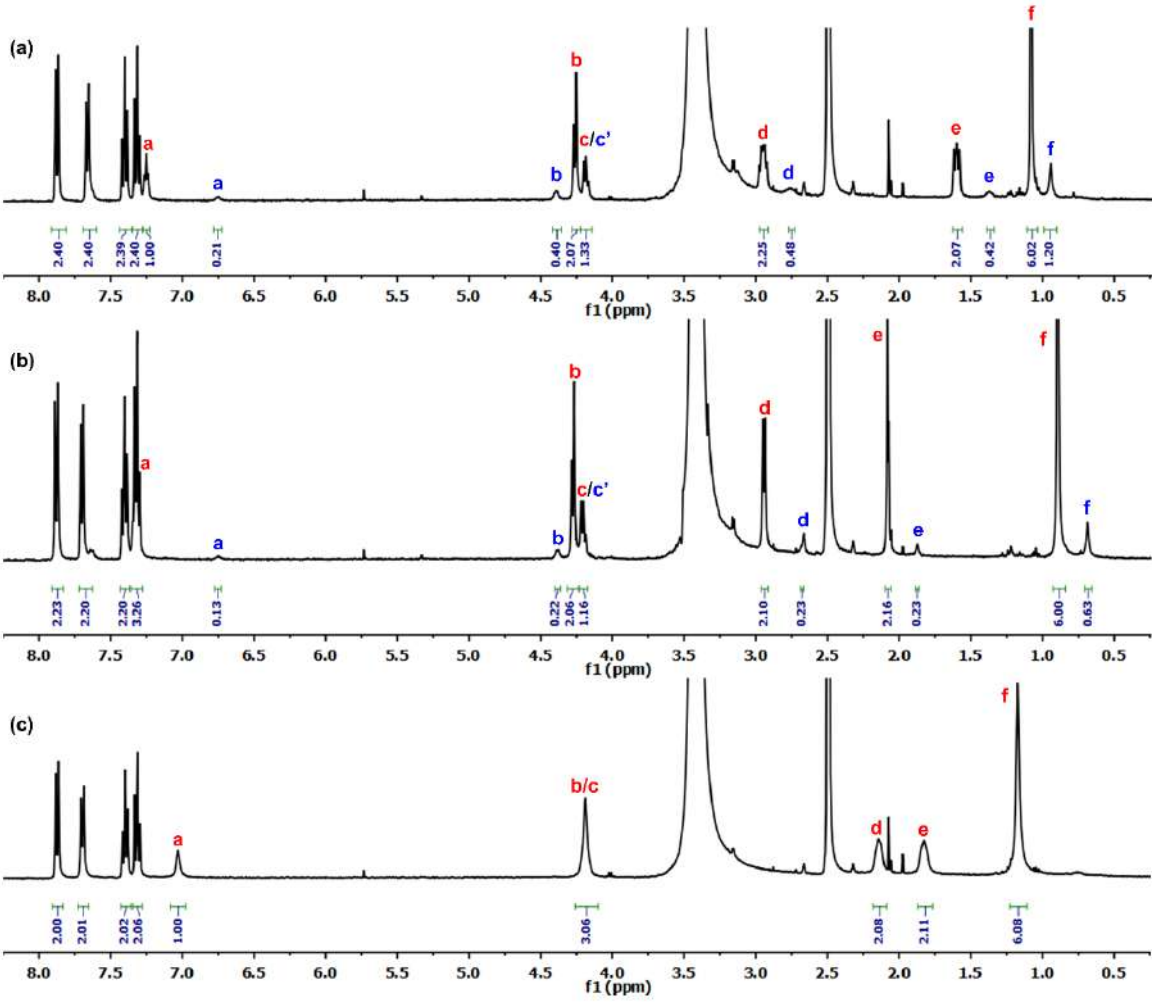

Figure 2.11. 400 MHz ^{1}H NMR spectra of (a) Fmoc- $\gamma^{2,2}$-OH (b) Fmoc- $\gamma^{3,3}$-OH (c) Fmoc- $\gamma^{4,4}$-OH in DMSO-d_6 at 10 mM concentration at 298 K.

2.3.1.1.7. Presence of dimeric species: ESI-MS

It is noteworthy to mention that in the ESI-MS both monomeric ($(M+H)^+$, $(M+Na)^+$) and dimeric species ($(2M+Na)^+$) were observed in solution which suggested the presence of both the species in solution. (Figures 2.12-2.14)

TH-3141_166122021

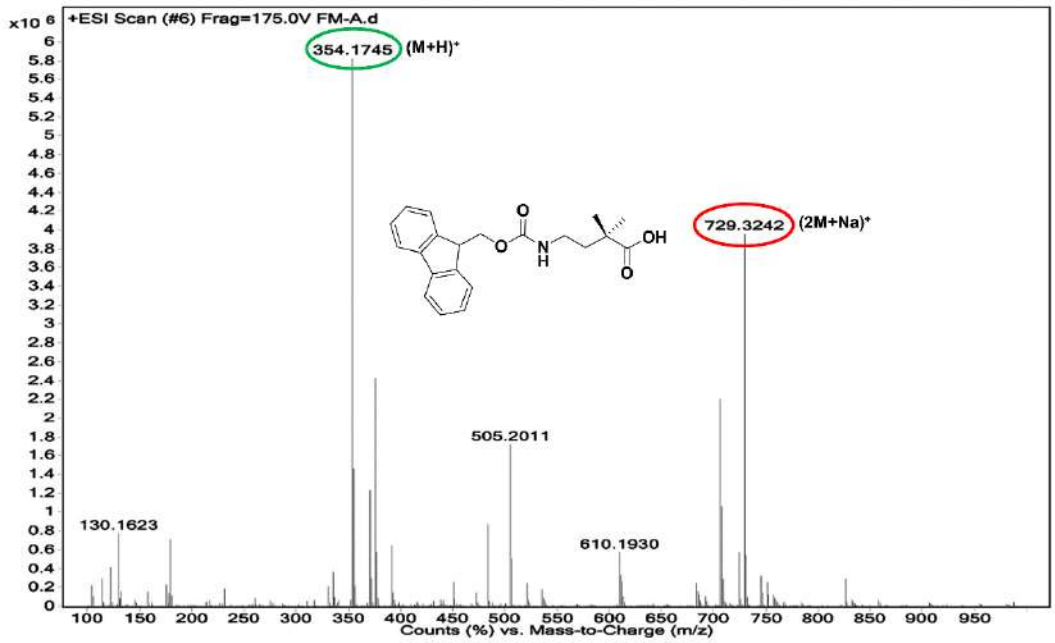

Figure 2.12. ESI-MS (m/z) of (Fmoc-$\gamma^{2,2}$-OH) Calc. $(M+H)^+$ for $C_{21}H_{23}NO_4$ = 354.4155 Da Obs. $(M+H)^+$ = 354.1745 Da, $(2M+Na)^+$ = 729.3242 Da. The monomeric and dimeric species are encircled in green and red respectively.

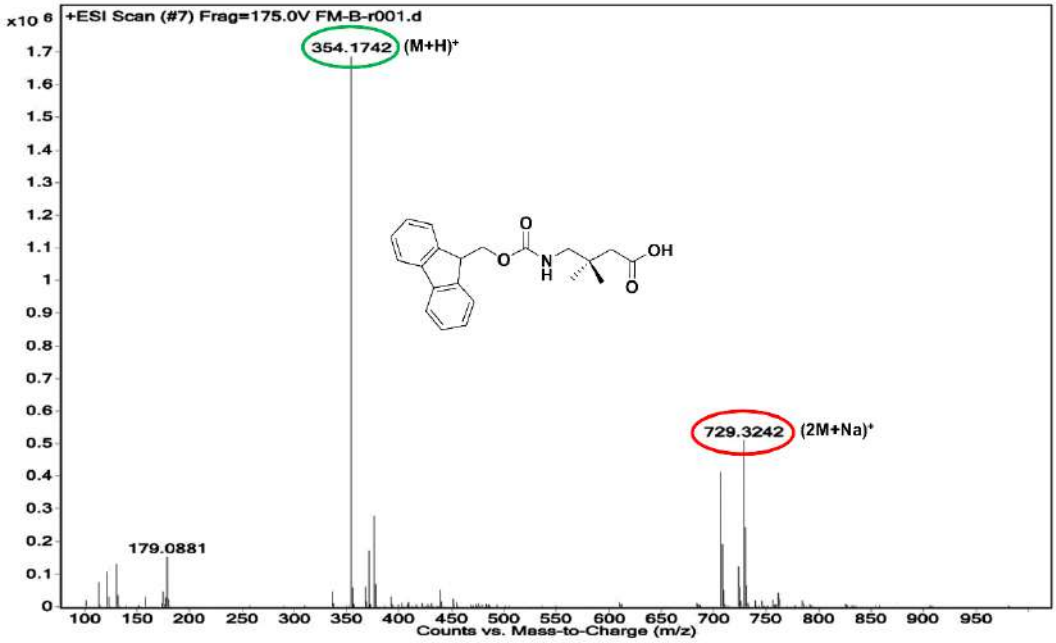

TH-3141_166122021

Figure 2.13. ESI-MS (m/z) of (Fmoc-$\gamma^{3,3}$-OH) Calc. $(M+H)^+$ for $C_{21}H_{23}NO_4$ = 354.4155 Da Obs. $(M+H)^+$ = 354.1742 Da, $(2M+Na)^+$ = 729.3242 Da. The monomeric and dimeric species are encircled in green and red respectively.

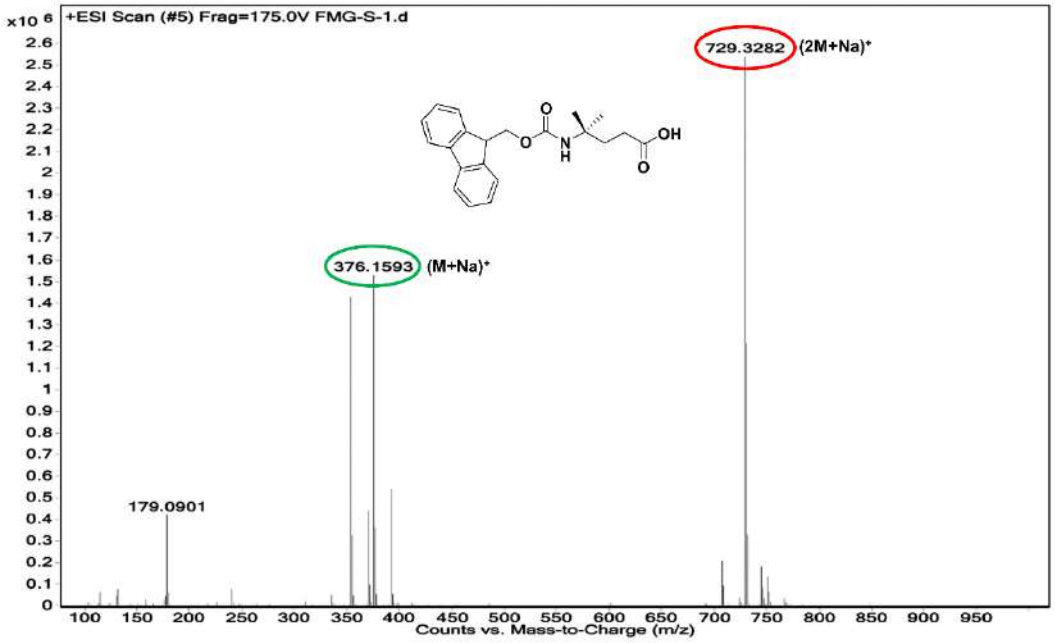

Figure 2.14. ESI-MS (m/z) of (Fmoc-$\gamma^{4,4}$-OH) Calc. $(M+H)^+$ for $C_{21}H_{23}NO_4$ = 354.4155 Da Obs. $(M+Na)^+$ = 376.1593 Da, $(2M+Na)^+$ = 729.3282 Da. The monomeric and dimeric species are encircled in green and red respectively.

2.3.1.2. Conformational studies using Infrared Spectroscopy

In order to further investigate the structures of the Fmoc derivatives in solution, we performed FT-IR experiments both in the solid (as synthesized state) and in the $CDCl_3$ solution at 298 K (Figure 2.15). For all the three Fmoc γ amino acid derivatives, a sharp peak for the non-hydrogen bonded NH was observed at ~ 3350 Å in the case of powdered sample. Two peaks, a broad one at 3335 cm^{-1} and another one at 3415 cm^{-1} were observed in solution for the hydrogen bonded and non-hydrogen bonded NH's respectively in case of all the three Fmoc

TH-3141_166122021

derivatives. Presence of the two types of NH's in the $CDCl_3$ solution confirmed the presence of both the monomeric (non-hydrogen bonded NH) and dimeric (hydrogen bonded NH) species in solution.

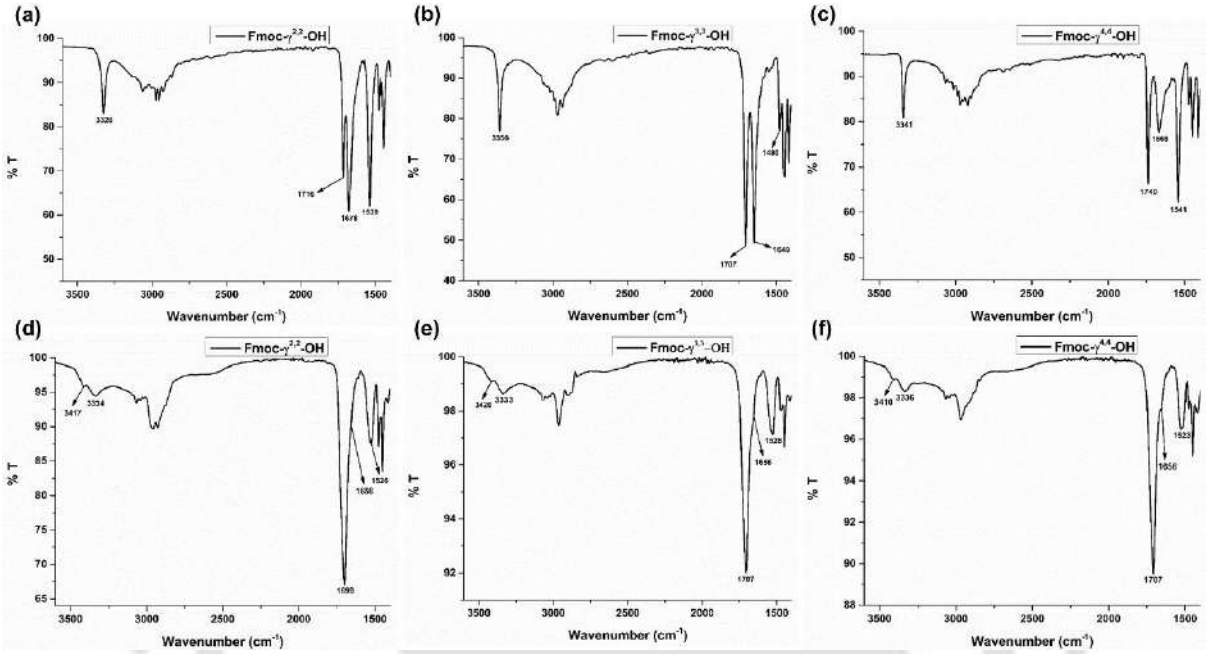

Figure 2.15. FT-IR spectra of (a, d) Fmoc-$\gamma^{2,2}$-OH (b, e) Fmoc-$\gamma^{3,3}$-OH and (c, f) Fmoc-$\gamma^{4,4}$-OH recorded in solid state and solution state (at 10 mM concentration in $CDCl_3$) at 298 K.

2.3.2. Structure in solid state: X-ray crystallographic studies

2.3.2.1. Molecular conformation

Even upon several attempts, we could only obtain crystals for Fmoc-$\gamma^{2,2}$-OH and Fmoc-$\gamma^{4,4}$-OH so far. Figure 2.16 shows the molecular conformation of γ amino acid derivatives Fmoc-$\gamma^{2,2}$-OH and Fmoc-$\gamma^{4,4}$-OH in single crystals. The backbone conformation of γ amino acid residues are defined by four torsion angles, ϕ (C0'-N1-C^{γ}-C^{β}), θ_1 (N1-C^{γ}-C^{β}-C^{α}), θ_2 (C^{γ}-C^{β}-C^{α}-C') and ψ (C^{β}-C^{α}-C'-N2). The values of the four torsion angles obtained from the crystals are listed in Table 2.1.

TH-3141_166122021

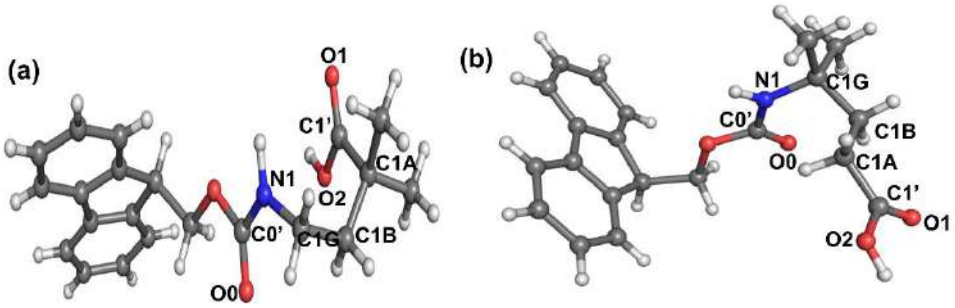

Figure 2.16. Molecular conformations of (a) Fmoc-$\gamma^{2,2}$-OH, and (b) Fmoc-$\gamma^{4,4}$-OH in crystals.

Table 2.1. Backbone dihedral angles of Fmoc-$\gamma^{2,2}$-OH and Fmoc-$\gamma^{4,4}$-OH in single crystals.

Compound	ϕ	θ_1	θ_2	ψ
Fmoc-$\gamma^{2,2}$-OH	74.82	63.36	-66.46	-51.90
Fmoc-$\gamma^{4,4}$-OH	-59.70	-68.44	166.75	177.48

It was interesting to note that, the dimethyl substitution on the backbone carbon atoms restricted the conformations about that particular backbone carbon atom largely to *gauche* conformation. For example, in Fmoc-$\gamma^{2,2}$-OH, the values of θ_2 (C^{γ}-C^{β}-C^{α}-C1') and ψ (C^{β}-C^{α}-C1'-O2) were approximately 50-70° for the C^{α}-dimethyl substituted $\gamma^{2,2}$ amino acids. Similarly, ϕ (C0'-N1-C^{γ}-C^{β}) and θ_1 (N1-C^{γ}-C^{β}-C^{α}) for Fmoc-$\gamma^{4,4}$-OH adopted *gauche* conformation (Table 2.1). All the four dihedral angles of Fmoc-$\gamma^{2,2}$-OH corresponded to *gauche* values. A semi-extended backbone conformation was observed in Fmoc-$\gamma^{4,4}$-OH in contrast to a completely folded conformation for Fmoc-$\gamma^{2,2}$-OH. No intramolecular hydrogen bonds were observed in either of the Fmoc derivatives.

TH-3141_166122021

2.3.2.2. Molecular packing/assembly

Two types of intermolecular hydrogen bonds were present in the crystals, O-H...O and N-H...O (Figure 2.17). The relevant parameters of these interactions are listed in Table 2.2.

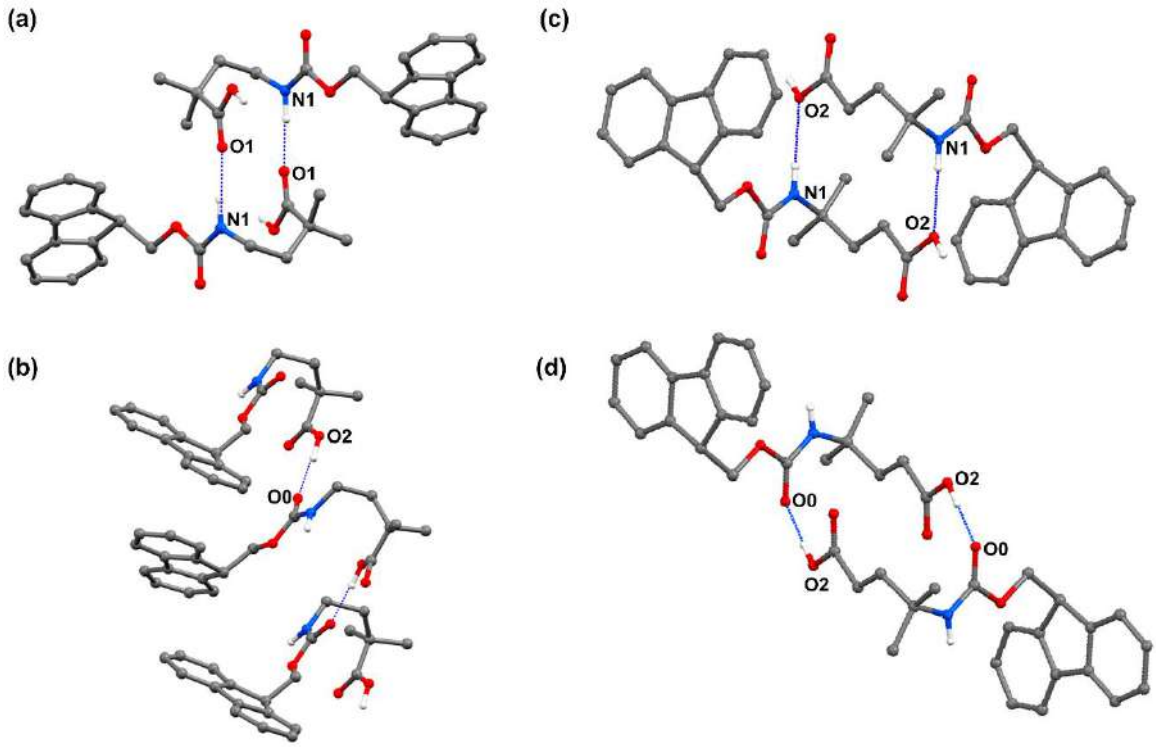

Figure 2.17. (a) C=O1…H-N intermolecular hydrogen bonds in dimer and (b) C=O0…H-O intermolecular hydrogen bonds in the crystals of Fmoc-$\gamma^{2,2}$-OH, (c) HO2…H-N intermolecular hydrogen bonds in dimer and (d) C=O0…H-O intermolecular hydrogen bonds in the crystals of Fmoc-$\gamma^{4,4}$-OH.

Table 2.2. Intermolecular hydrogen bond parameters in single crystals.

Compound	**Hydrogen bond**	**D...A (Å)**	**H...A (Å)**	**∠D-H...A (°)**
Fmoc-$\gamma^{2,2}$-OH	O0...H-O2	2.655	1.728	172.8
	O1...H-N1	2.877	1.915	165.5

TH-3141_166122021

Fmoc-$\gamma^{4,4}$-OH	O0...H-O2	2.649	1.710	171.0
	O2...H-N1	3.01	2.09	177.2

The crystal lattice of Fmoc-$\gamma^{2,2}$-OH and Fmoc-$\gamma^{4,4}$-OH (Figures 2.18a, b) show distinctly different intermolecular hydrogen bonding and Fmoc stacking interactions (Figures 2.18c, d).

In Fmoc-$\gamma^{2,2}$-OH, a centrosymmetric dimer was formed by the N-H…O1 hydrogen bonding, between the NH of one molecule to the CO of the amino acid residue of the other molecule (Figures 2.17a, 2.18c). The hydroxyl group (-OH) of the C-terminal formed hydrogen bonds with the –C=O of the Fmoc group (O0...H-O2) of the neighboring dimer (symmetry-related molecule) (Figures 2.17b, 2.18c). The OH...O hydrogen bonds connected such dimers in the crystal lattice. The same Fmoc group also formed tilted stacking interaction with the central dimer unit (Figure 2.18c).

In the case of Fmoc-$\gamma^{4,4}$-OH, the dimer units were stabilized by hydrogen bonds between the NH group of the amino acid of one molecule to the C-terminal OH group (N1-H...O2) of another molecule (Figures 2.17c, 2.18d). However, the –CO1 of the amino acid residue lacked a hydrogen-bonding partner. Moreover, the -OH group of the central C-terminal dimer formed hydrogen bonding with the -CO of the Fmoc group of another monomer that was not involved in stacking with the central dimer (Figures 2.17d, 2.18d). The Fmoc group from the neighboring dimer formed excellent parallel-displaced stacking in the Fmoc-$\gamma^{4,4}$-OH crystal (Figure 2.18d).

In the crystal lattice of Fmoc-$\gamma^{2,2}$-OH, the overall packing showed an alternating pattern of hydrophilic and hydrophobic regions along the crystallographic c-direction (Figure 2.19). The bulky aromatic Fmoc groups at the N-terminal promoted molecular assembly through π..π interactions in both Fmoc-$\gamma^{2,2}$-OH and Fmoc-$\gamma^{4,4}$-OH. While the planes of the Fmoc moieties

TH-3141_166122021

were tilted at an angle in Fmoc-$\gamma^{2,2}$-OH , they were completely parallel in Fmoc-$\gamma^{4,4}$-OH. The centroid…centroid distance between the aromatic rings of Fmoc groups were approximately 6-6.5 Å in Fmoc-$\gamma^{2,2}$-OH and 4 Å in Fmoc-$\gamma^{4,4}$-OH respectively. This established stronger π..π interactions in Fmoc-$\gamma^{4,4}$-OH compared to Fmoc-$\gamma^{2,2}$-OH (Figures 2.18c, d).

Thus, the torsion angles of the γ amino acid derivatives were completely controlled by the position of the backbone di-substitution of the γ amino acid residues. Both in the Fmoc-$\gamma^{2,2}$-OH and Fmoc-$\gamma^{4,4}$-OH, the flanking torsion angles θ_2, ψ and ϕ, θ_1 respectively adopted gauche conformations. However, though $\gamma^{2,2}$ adopted a fully folded conformation, $\gamma^{4,4}$ adopted a semi-extended conformation. Due to their distinct molecular conformations in the crystalline state, these derivatives manifested unique molecular packing in the crystals which was stabilized by distinct hydrogen bonding patterns and more importantly the π-π stacking interactions. Hence the differential position of backbone di-substitution had a direct consequence on the conformations of the γ amino acid derivatives in crystals.

TH-3141_166122021

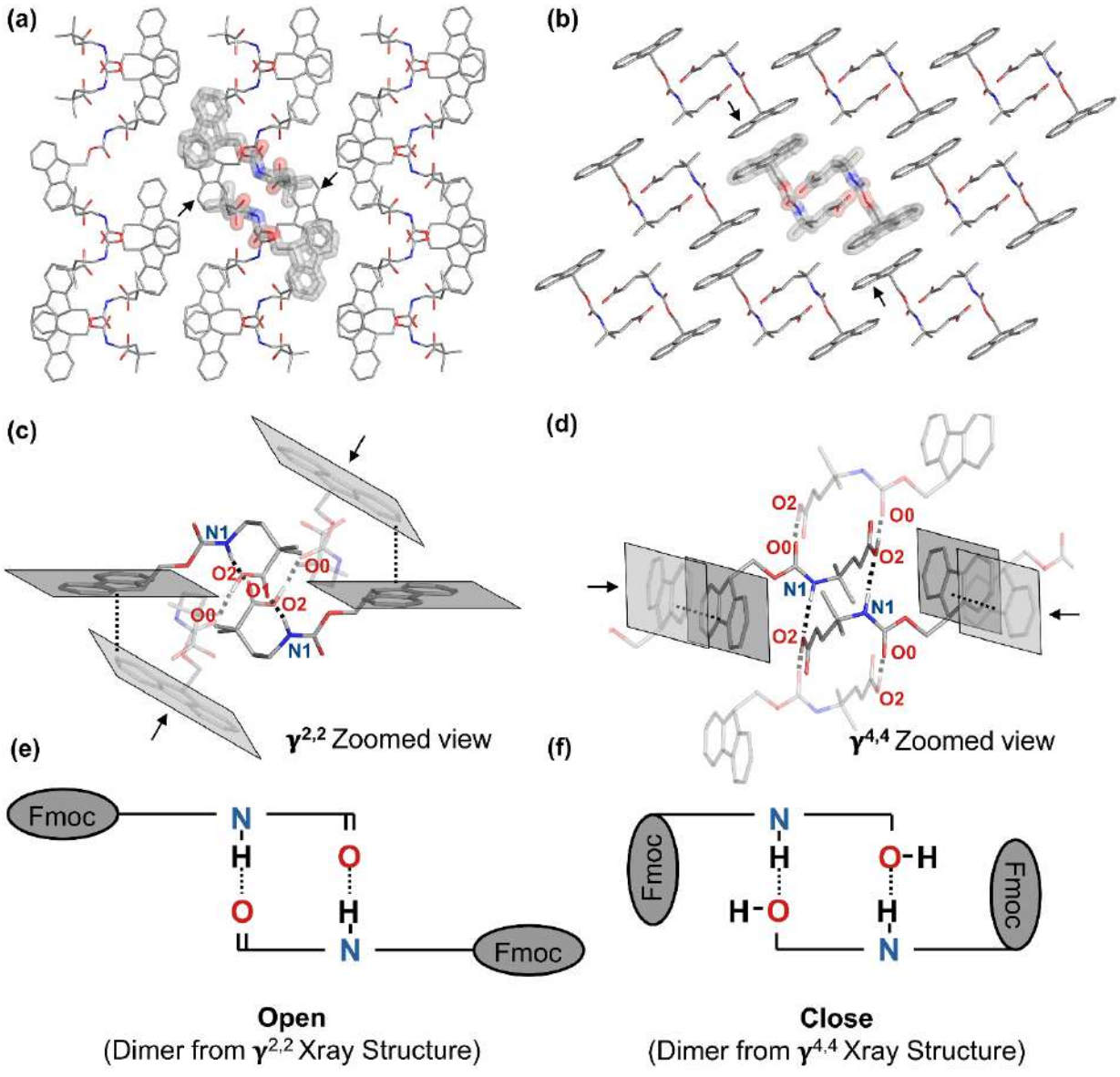

Figure 2.18. Crystal packing of a) Fmoc-$\gamma^{2,2}$-OH top view and b) Fmoc-$\gamma^{4,4}$-OH side view. A dimeric unit is highlighted with transparent sticks and the neighboring residues that form stacking interactions with the Fmoc group of the central dimeric unit are highlighted with black arrows. Zoomed-in view of the dimeric unit and its interaction with the neighboring unit observed in the X-ray structures of (c) Fmoc-$\gamma^{2,2}$-OH and (d) Fmoc-$\gamma^{4,4}$-OH. Intermolecular hydrogen bonds and Fmoc stacking are represented as broken lines. A schematic representation of the "open" and "close" states: (e) Open- Fmoc group is perpendicular to the backbone -NH, (f) Close- Fmoc group is parallel to the backbone -NH. The intermolecular hydrogen bonding

TH-3141_166122021

in the dimer is distinctly different between $\gamma^{2,2}$(open) and $\gamma^{4,4}$(Close); the former involves –C=O and the latter involves a hydroxyl group (OH) for hydrogen bonding.

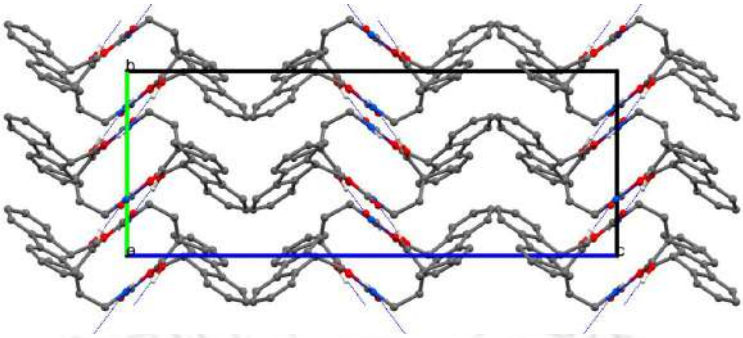

Figure 2.19. A view of the molecular packing in unit cell in Fmoc-$\gamma^{2,2}$-OH.

2.3.3. Computational studies: Structure optimization (DFT studies) and energy calculations

In order to gain insight into the energetics of the conformational preferences of the Fmoc derivatives in the solid and solution state, we performed quantum mechanical calculations.

X-ray structure of Fmoc-$\gamma^{4,4}$-OH appeared to have better stacking interactions relative to Fmoc-$\gamma^{2,2}$-OH. Based on the orientation of the Fmoc group in the X-ray structures of the central dimeric unit relative to the backbone -NH group, we defined two states: open (Fmoc perpendicular to -NH) and close (Fmoc parallel to -NH) states of the monomer/dimer ($M^{x,x}/D^{x,x}$, where x,x = 2,2 or 3,3 or 4,4) (see method in experimental section) (Figures 2.18 e, f). It can be concluded that both the open Fmoc-$\gamma^{2,2}$-OH and close Fmoc-$\gamma^{4,4}$-OH dimers were stabilized by forming two intermolecular hydrogen bonds and had distinctly different stacking interactions with their surrounding in the X-ray structures. The close state seemed to have better stacking (parallel-displaced, Figure 2.18d) relative to the open state (tilted stacking, Figure 2.18c).

TH-3141_166122021

Geometry optimization of the monomers using density functional theory (DFT) showed that the $M^{2,2}$(open) and $M^{3,3}$(open) states were more stable relative to their close conformers $M^{2,2}$(close) and $M^{3,3}$(close) respectively. However, $M^{4,4}$(close) was more stable than $M^{4,4}$(open) (Figure 2.20) conformer. Open and close conformers of the monomers of the different γ amino acid residues differed by ΔG ~ 2-3 kcal/mol. The free energy of the dimer ($D^{x,x}$) was found to be uphill (ΔG ~ 8-12 kcal/mol) relative to their most stable monomeric state (i.e. 2 molecules of $M^{x,x}$) (Figure 2.20) for all the γ amino acids. Noticeably the $D^{x,x}$(open) dimer was relatively more stable than $D^{x,x}$ (close) dimer from the most stable conformer of the monomeric residues. $D^{x,x}$(open) was most stable compared to $D^{x,x}$(closed) for Fmoc-$\gamma^{2,2}$-OH (5.4 kcal/mol), followed by Fmoc-$\gamma^{3,3}$-OH (2.3 kcal/mol) and Fmoc-$\gamma^{4,4}$-OH (0.5 kcal/mol) (Figure 2.20). The non-hydrogen bonded monomeric form was found to be more stable than the hydrogen-bonded dimer. Thus, in solution, the non-hydrogen bonded monomeric form might be expected to be preferred and populate the solution majorly, while the dimeric hydrogen-bonded form might be expected to be present in smaller populations and increase with the increase in concentration. This was exactly in lines with the observations from the various NMR experiments performed in solution (Figures 2.2-2.11). Thus to summarize, the major monomeric species was in equilibrium with the minor dimeric species in solution. As both the open and close conformation of the monomeric species were relatively lower in energy, either of them might be present in solution for all the γ amino acid residues. However, as the open conformations of the dimeric species were stabler than their respective close conformations, the dimers of the Fmoc derivatives were most probably present in their open conformations in solution.

An excellent agreement of the H-bond and the torsional angle parameters were observed in between the optimized dimers and the X-ray structure (Tables 2.3, 2.4). H-bond parameters (Table 2.3) obtained from the geometry optimized structures of the dimers of all the Fmoc

TH-3141_166122021

derivatives confirmed that the two intermolecular hydrogen bonds within the central dimer (Figures 2.18c, 2.18d) were preserved except for the $D^{2,2}$(close) dimer, where one of the hydrogen bonds was broken (Table 2.3 and Figure 2.20). The steric clash between the methyl groups of the two $\gamma^{2,2}$ residues resulted in the disruption of the hydrogen bond in the $D^{2,2}$(close) dimer (Figure 2.20), imposing the highest free energy penalty (ΔG = 13 kcal/mol). Favorable Fmoc stacking interactions seemed to be insufficient for stabilizing the high energy of $D^{2,2}$(close) dimer in the X-ray structure; a plausible explanation why $D^{2,2}$(close) dimer was not observed in the crystals. The free energy of the $D^{2,2}$(open) conformer was the lowest and it was further stabilized by forming titled stacking and hydrogen bonding with the neighboring residues, resulting it being observed in the X-ray structure. Free energy of the Fmoc-$\gamma^{4,4}$-OH dimers, $D^{4,4}$(open) and $D^{4,4}$(close) were similar, the former being marginally stable by 0.5 kcal/mol. The favorable Fmoc stacking (parallel-displaced) stabilized the $D^{4,4}$(close) dimer in the X-ray structure and explained its experimental observation. The high free energy of Fmoc-$\gamma^{3,3}$-OH dimers (ΔG (close) = 12.2 kcal/mol and ΔG (open) = 9.9 kcal/mol) most probably prevailed over the stacking stabilization and hindered the crystal formation. Though geometry optimization of a dimeric unit was certainly insufficient to address why Fmoc-$\gamma^{2,2}$-OH was observed in an open state and Fmoc-$\gamma^{4,4}$-OH was observed in a close state in crystal structures, while was Fmoc-$\gamma^{3,3}$-OH not observed in crystals so far, nevertheless, the results provided the structural and energetic aspects of dimer formation and hinted at the possible explanation for higher-order structure formation.

TH-3141_166122021

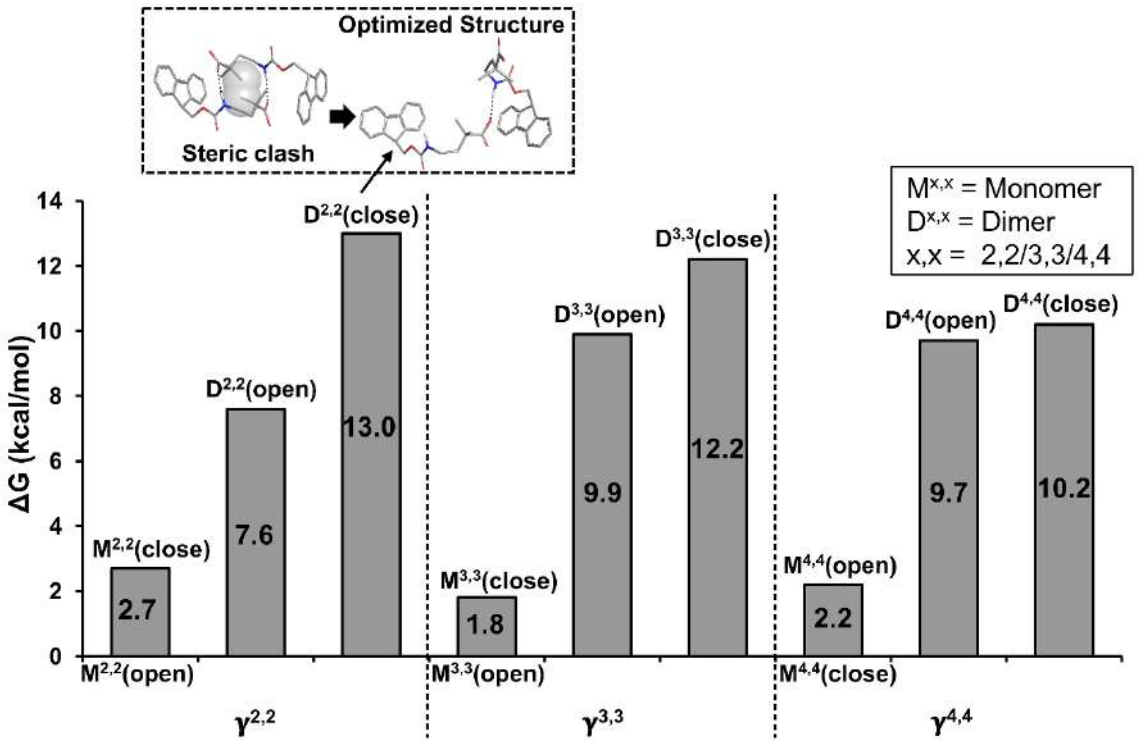

Figure 2.20. Free energy of the various monomers and dimers for the Fmoc derivatives of the three γ amino acid residues, relative to the most stable monomer ($M^{2,2}$(open)). The model of the $D^{2,2}$(open) dimer state indicates the steric clash (transparent spheres) between the methyl units. Geometry optimization results in single intermolecular hydrogen-bonded $D^{2,2}$(open) state.

TH-3141_166122021

Table 2.3. Intermolecular hydrogen-bond parameters in the optimized structures of the dimer. Parameters obtained from X-ray structures are given within the parenthesis and highlighted in bold for comparison. Distance in "Ångstrom" and angle in "degree". Two intermolecular hydrogen bonds in the dimer are HB1 and HB2 (See Figures 2.18c, d). The broken hydrogen bond is represented with a "-".

		H-Bond Parameters	$D^{2,2}$ **(X-ray)**	$D^{3,3}$	$D^{4,4}$ **(X-ray)**
Open N1-H…O1	HB1	Distance, Angle	2.05, 158.2 **(1.9, 165.0)**	2.06, 153.4	2.10, 173.1
	HB2	Distance, Angle	2.05, 158.2 **(1.9, 164.9)**	2.06, 153.5	2.10, 173.0
Close N1-H…O2	HB1	Distance, Angle	-	2.19, 165.7	2.25, 171.0 **(2.10, 177.3)**
	HB2	Distance, Angle	2.12, 165.2	2.19, 165.7	2.25, 171.1 **(2.10, 177.3)**

Table 2.4. Backbone torsion angles (in degree) of the monomeric units (residue 1, residue 2) in the optimized dimer. Torsional angles obtained from the X-ray structures are given in the parenthesis.

	Residue	ϕ [CO]-N-C^{γ}-C^{β}	θ_1	θ_2	ψ C^{β}-C^{α}-[CO]-OH
$D^{2,2}$-Open **(X-ray)**	1	-84.8 **(-74.7)**	-65.6 **(-63.7)**	68.7 **(66.8)**	54.1 **(51.7)**
	2	84.8 **(74.7)**	65.5 **(63.7)**	-68.7 **(-66.9)**	-54.0 **(-51.7)**
$D^{3,3}$-Open	1	101.5	61.5	-62.9	-69.1
	2	-101.4	-61.4	62.9	69.1
$D^{4,4}$-Open	1	-67.2	-66.3	65.5	62.1
	2	67.2	66.2	-65.5	-62.0
$D^{4,4}$-close **(X-ray)**	1	-65.9 **(-59.7)**	-56.1 **(-58.4)**	-174.7 **(-165.7)**	-175.2 **(-177.4)**
	2	65.9 **(59.7)**	56.0 **(58.4)**	174.6 **(165.7)**	175.1 **(177.5)**
$D^{2,2}$-close	1	92.0	84.0	-174.6	176.0
	2	-76.6	-67.2	-167.7	-176.7
$D^{3,3}$-close	1	-111.0	-60.9	-176.3	179.7
	2	111.1	-60.9	176.3	-179.8

TH-3141_166122021

2.3.4. Molecular assembly of Fmoc γ amino acid derivatives in solution

There are reports in the literature of Fmoc amino acid derivatives to be having high self-assembling tendency.[313-320] Additionally, packing of Fmoc-$\gamma^{2,2}$-OH and Fmoc-$\gamma^{4,4}$-OH in the crystal lattice showed the presence of π-π stacking interaction in between the Fmoc groups, more strongly in the later than the former. Thus hypothesizing that the Fmoc γ amino acid derivatives might also have strong self-assembling abilities in solution, we investigated it. We wanted to probe if the differential position of the backbone geminal di-substitution of the γ amino acid residues had any effect on their self-assembling abilities in solution.

2.3.4.1. Study of morphology: FESEM and FETEM

Self-assembly of the Fmoc γ amino acid derivatives was solvent dependent. While there was no well-formed morphology observed in the organic solvents like $CDCl_3$, DMSO-d_6, MeOH, 70% ACN/H_2O etc., all the three Fmoc derivatives formed well-formed spherical aggregates in 70% MeOH/H_2O (Figure 2.21) and nanorod composed floral nanostructures in the sodium bicarbonate buffer pH = 10 (Figure 2.21). The absence of any well-formed morphology in the organic solvents was probably due to the high solubility of the molecules in them. The highly favorable solute solvent interactions in the organic solvents, superseded the solute-solute interactions that were needed for the assembly formation.

TH-3141_166122021

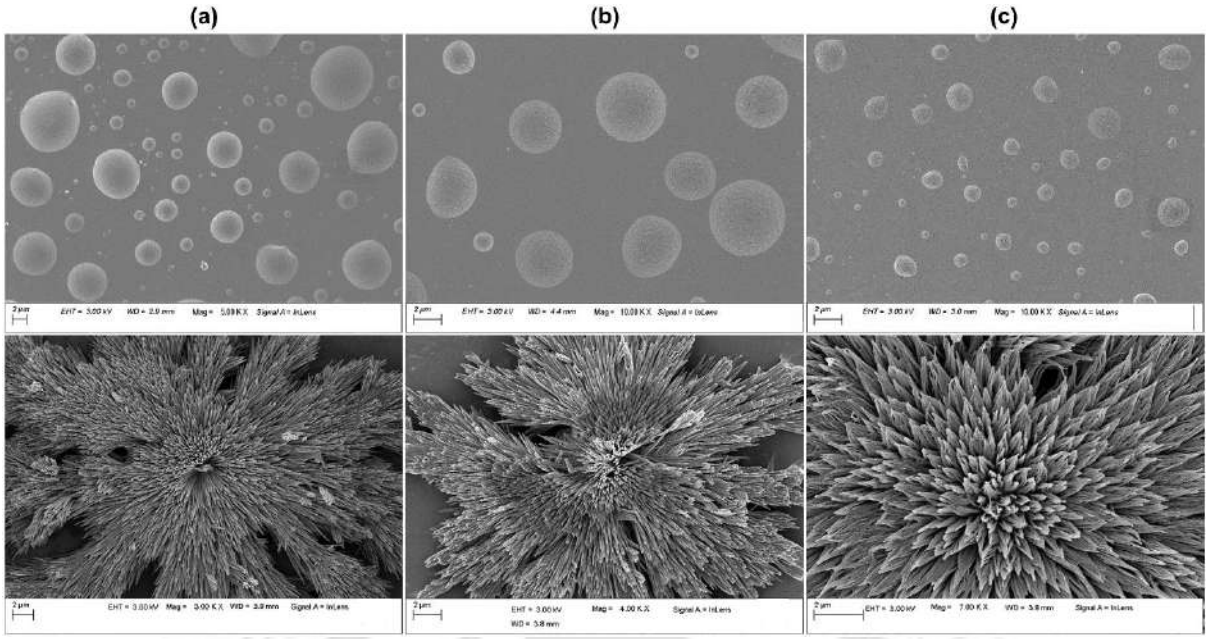

Figure 2.21. FESEM images of (a) Fmoc-$\gamma^{2,2}$-OH, (b) Fmoc-$\gamma^{3,3}$-OH and (c) Fmoc-$\gamma^{4,4}$-OH at 10 mM concentration in 70% MeOH-H_2O (upper panel) and sodium bicarbonate buffer pH = 10.00 (lower panel) respectively.

In order to probe if the morphology seen in the FESEM was present in the solution or formed during the course of drying the solvent in the sample preparation process, we further performed FESEM with samples that were freeze dried right after drop casting (Figure 2.22). We found that microsphere like morphology present in 70% MeOH/H_2O for all the derivatives, identical to that observed from the previous experiment where solvent was allowed to evaporate at room temperature while sample preparation, suggesting that microsphere morphology was indeed present in the solution and was not formed during slow evaporation of the solvent. However, in the case of bicarbonate buffer pH 10, though nanorods were present in the solution for all the Fmoc derivatives, the floral kind of arrangement seen earlier was absent. Thus we conclude that all Fmoc derivatives adopted nanorod like morphology in sodium bicarbonate buffer (pH 10) in solution which arranged into beautiful floral kind of arrangements during the solvent evaporation process involved in the sample preparation step.

TH-3141_166122021

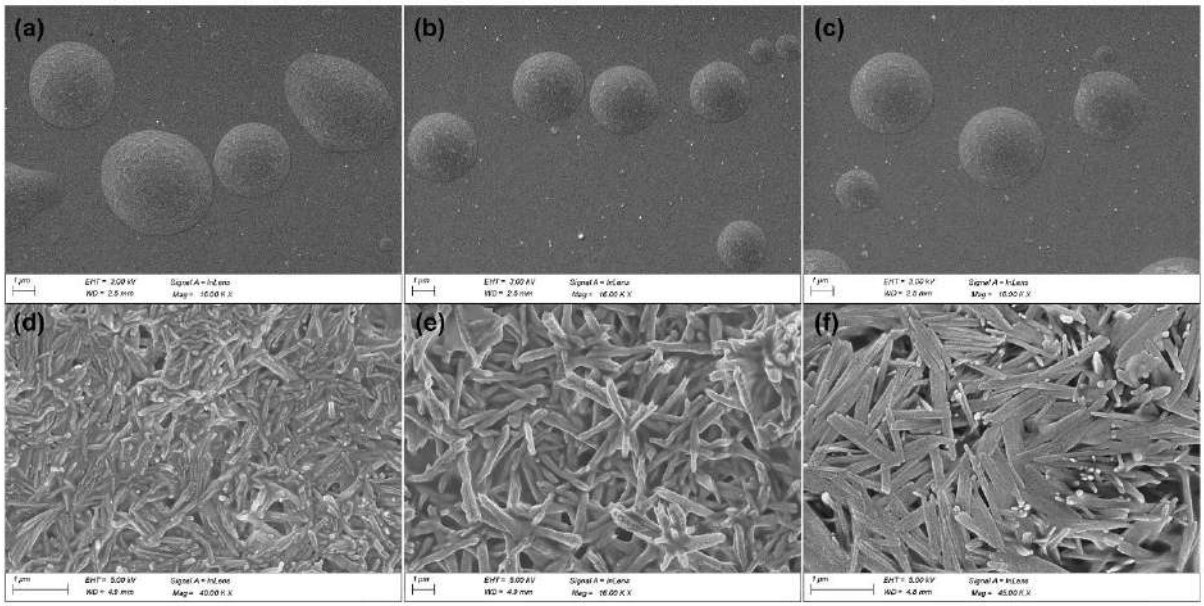

Figure 2.22. Morphology of the Fmoc derivatives of $\gamma^{2,2}$, $\gamma^{3,3}$ and $\gamma^{4,4}$ amino acid residues at 10 mM concentration respectively as present in (a-c) 70% MeOH/H_2O and (d-f) Sodium bicarbonate buffer, pH 10 solution.

Unchanged spherical morphology of the nanostructures obtained in the 10 days aged samples suggesting that the self-assembly pathway in 70% MeOH/H_2O was most probably thermodynamically governed (Figure 2.23).

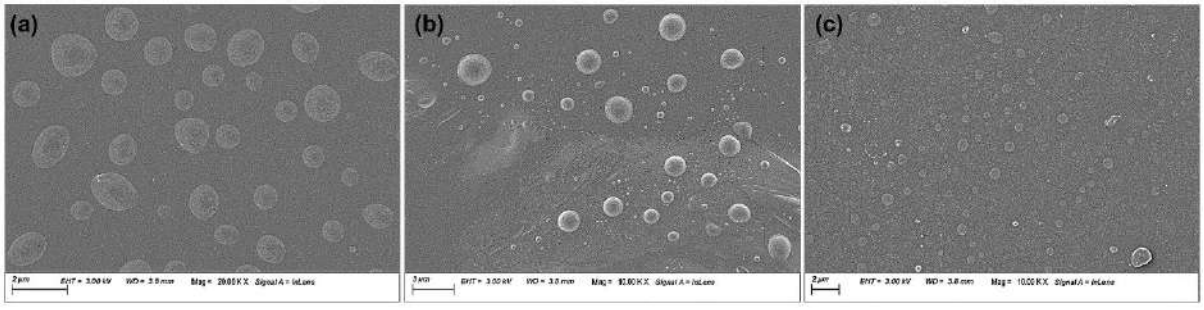

Figure 2.23. FESEM images of 10 days old sample of (a) Fmoc-$\gamma^{2,2}$-OH, (b) Fmoc-$\gamma^{3,3}$-OH and (c) Fmoc-$\gamma^{4,4}$-OH in 70% MeOH/H_2O at 10 mM concentration.

TH-3141_166122021

In order to investigate the spherical aggregate morphology further, we performed FETEM of Fmoc-$\gamma^{2,2}$-OH in 70% MeOH/H_2O at 150 μM (Figure 2.24) and found them to be solid microspheres and not hollow structures.

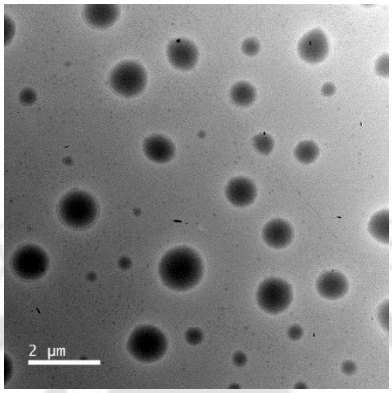

Figure 2.24. FETEM image of Fmoc-$\gamma^{2,2}$-OH at 150 μM concentration in 70% MeOH/H_2O.

2.3.4.2. CAC determination in 70% MeOH/H_2O: Fluorescence spectroscopy

The critical aggregation concentration (CAC) in the assembly process of the Fmoc derivatives was investigated by monitoring the fluorescence emission of the Fmoc moiety as a function of the Fmoc derivative concentration (Figures 2.25-2.26). Initially upon increasing the concentration of the compounds till 100 μM, the fluorescence intensity of the emission peaks increased, beyond which they decreased (Figure 2.26). The decrease in the fluorescence emission intensity was characteristic of the stacking of the aromatic rings of the Fmoc group as the result of the π-π stacking.[321,322] Such π-π stacking indicated the close approach of the monomers and the formation of self-assembly. Quenching of the fluorescence emission of the fluorophores (Trp, Fmoc) have been used in the literature regularly for determination of the CAC of the molecular self-assembly processes.[323,324] Thus from the fluorescence experiments we could conclude that the CAC of the self-assembly process in 70% MeOH-H_2O of the Fmoc derivatives of all the γ amino acid residues was about 100 μM.

TH-3141_166122021

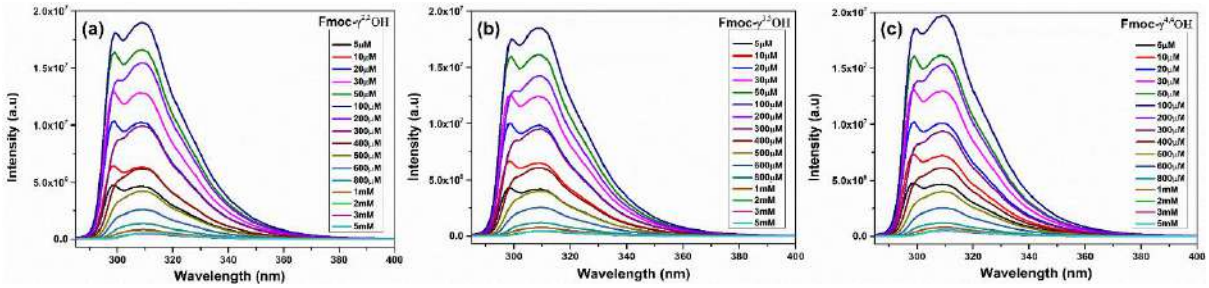

Figure 2.25. Concentration dependent fluorescence spectrum of (a) Fmoc-$\gamma^{2,2}$-OH, (b) Fmoc-$\gamma^{3,3}$-OH and (c) Fmoc-$\gamma^{4,4}$-OH in 73% MeOH/H_2O.

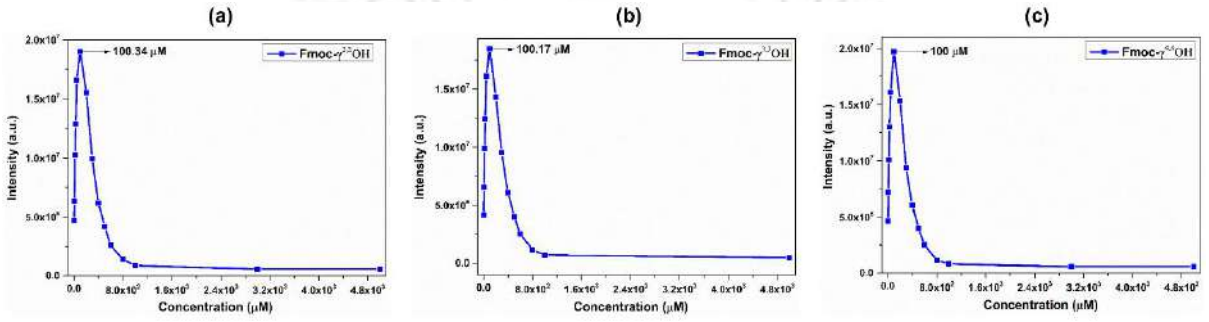

Figure 2.26. Plot of fluorescence emission max. vs concentration of (a) Fmoc-$\gamma^{2,2}$-OH, (b) Fmoc-$\gamma^{3,3}$-OH and (c) Fmoc-$\gamma^{4,4}$-OH in 73% MeOH/H_2O.

2.3.4.3. Morphology at CAC and size distribution

The assembly in 70% MeOH/H_2O was concentration dependent (Figures 2.21 and 2.27). At about 100 µM concentration, the nanospheres of about 150-190 nm in diameter, while at a higher concentration of 10 mM, larger microspheres of about 1-3 µm diameter were formed (Figures 2.21 and 2.27, 2.28).

TH-3141_166122021

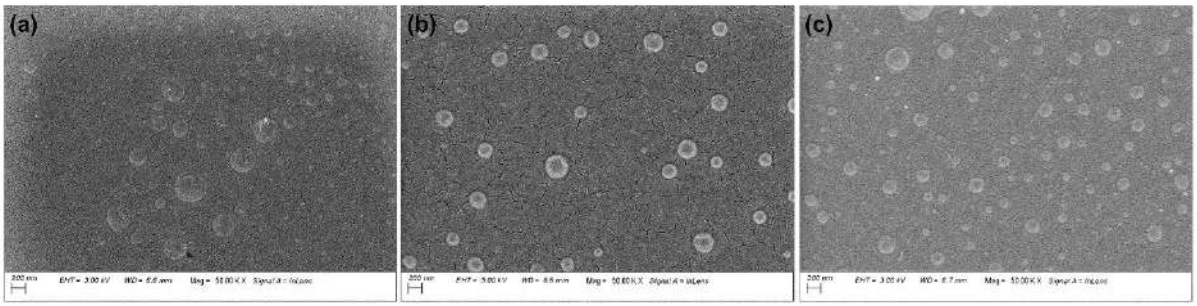

Figure 2.27. FESEM images of (a) Fmoc-$\gamma^{2,2}$-OH, (b) Fmoc-$\gamma^{3,3}$-OH and (c) Fmoc-$\gamma^{4,4}$-OH at 100 μM concentration in 70% MeOH/H_2O.

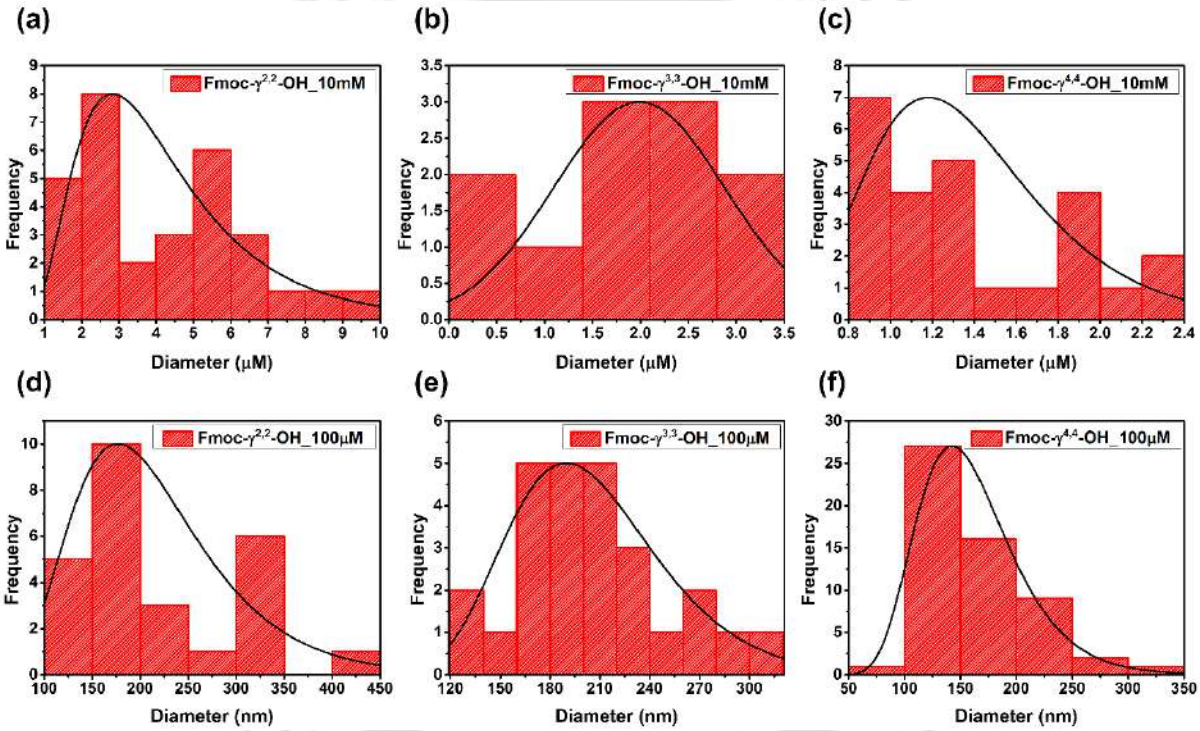

Figure 2.28. Size distribution of the micro/nanospheres formed by (a, d) Fmoc-$\gamma^{2,2}$-OH, (b, e) Fmoc-$\gamma^{3,3}$-OH and (c, f) Fmoc-$\gamma^{4,4}$-OH at 10 mM and 100 μM respectively in 70% MeOH/H_2O.

TH-3141_166122021

2.3.4.4. Effect of pH on Fmoc protection: ESI-MS analysis

In the sodium bicarbonate buffer (pH 10) a completely different morphology resembling nanorods was observed for all the three Fmoc derivatives. With an intention of solubilizing the Fmoc derivatives in water, which were insoluble at neutral pH we had increased the pH of the medium using sodium bicarbonate buffer, hypothesizing that C-terminal deprotonation would solubilize the molecules. The molecules were finally soluble at pH 10. However, as Fmoc was a base labile protecting group, analysis of the chemical identity of the molecules was confirmed by ESI-MS (Figures 2.29-2.32). The molecules were shown to retain their Fmoc moieties even at this pH, till an hour. As the sample preparation was done immediately after the dissolution of the derivatives in the buffer, it may be concluded that the nanorod morphology was indeed adopted by the Fmoc derivatives and not by the deprotected amino acid residues. In summary, all the three Fmoc derivatives of the γ amino acid residues showed identical tendency of self-assembly in any specific solvent or experimental conditions. It might therefore be concluded that the differential position of the backbone substitution in three γ amino acid residues did not have any effect on the self-assembling behavior of its Fmoc derivatives in solution.

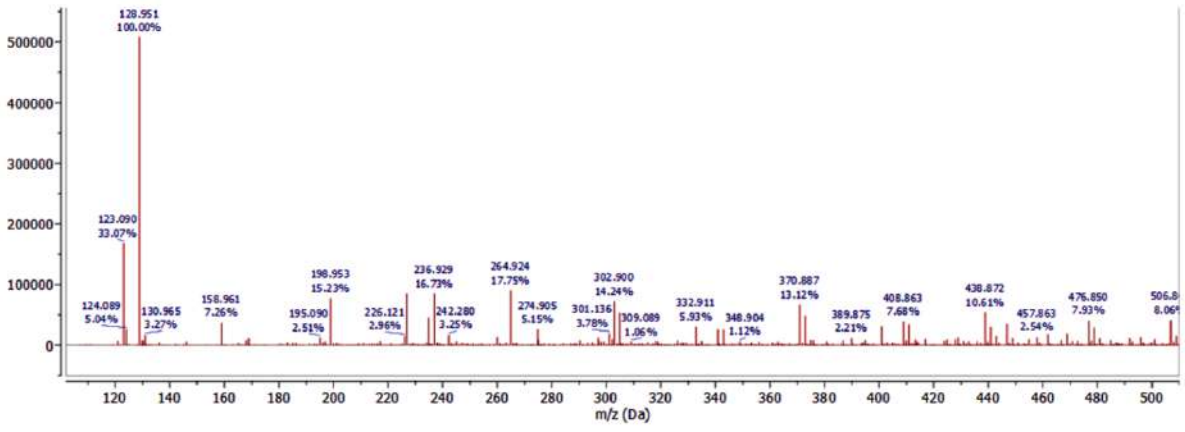

Figure 2.29. ESI-MS of bicarbonate buffer at pH 10.

TH-3141_166122021

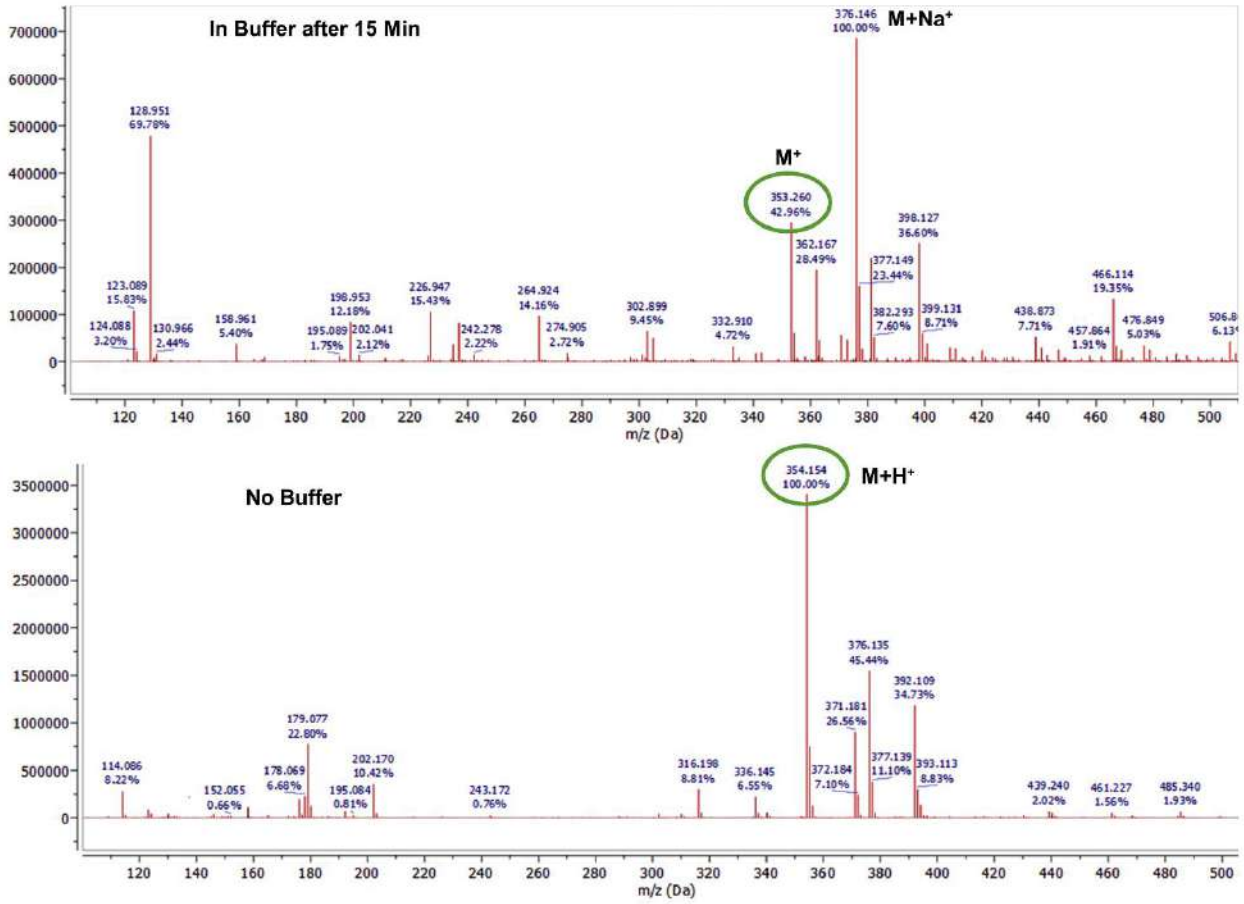

Figure 2.30. ESI-MS of Fmoc-$\gamma^{2,2}$-OH without buffer solution and in sodium bicarbonate buffer at pH 10.

TH-3141_166122021

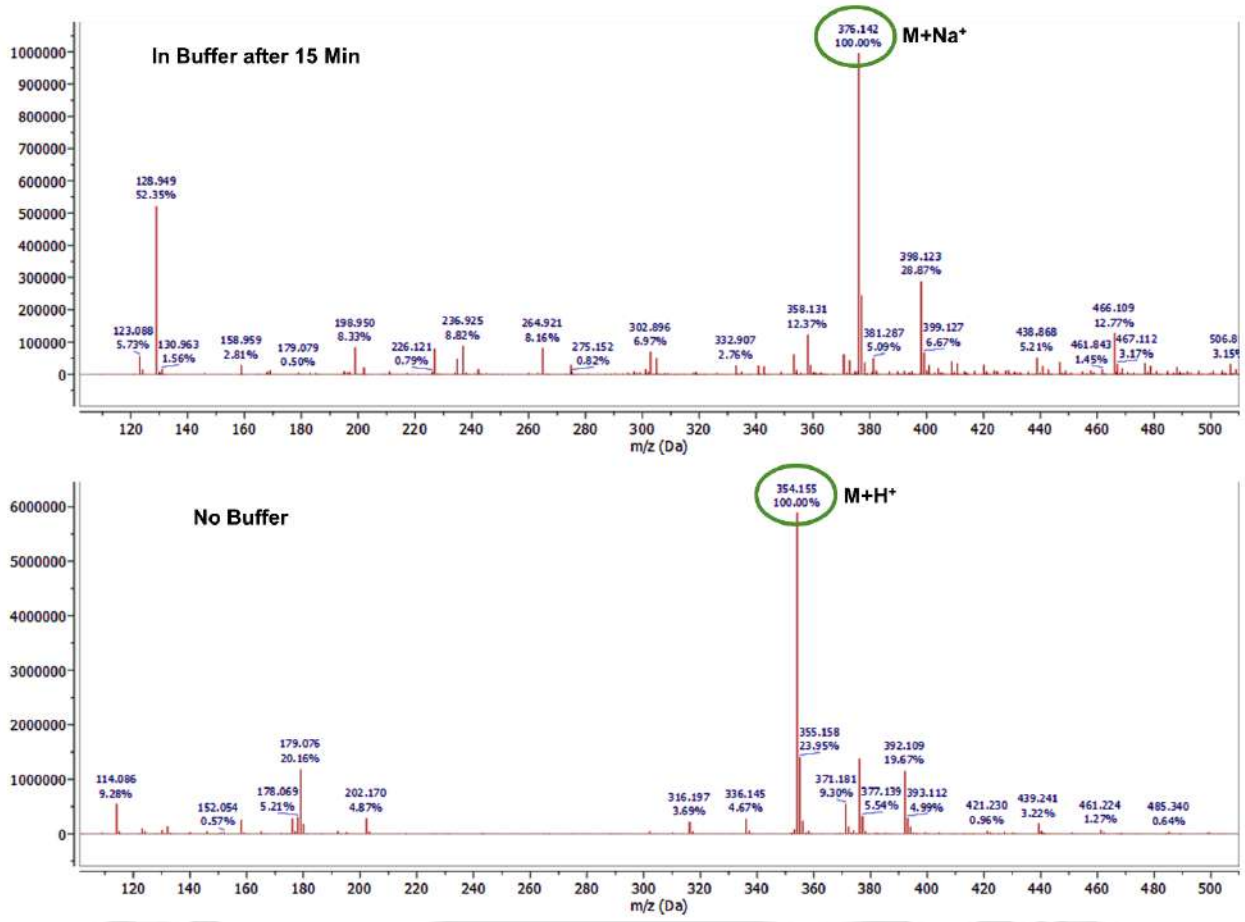

Figure 2.31. ESI-MS of Fmoc-$\gamma^{3,3}$-OH without buffer solution and in sodium bicarbonate buffer at pH 10.

TH-3141_166122021

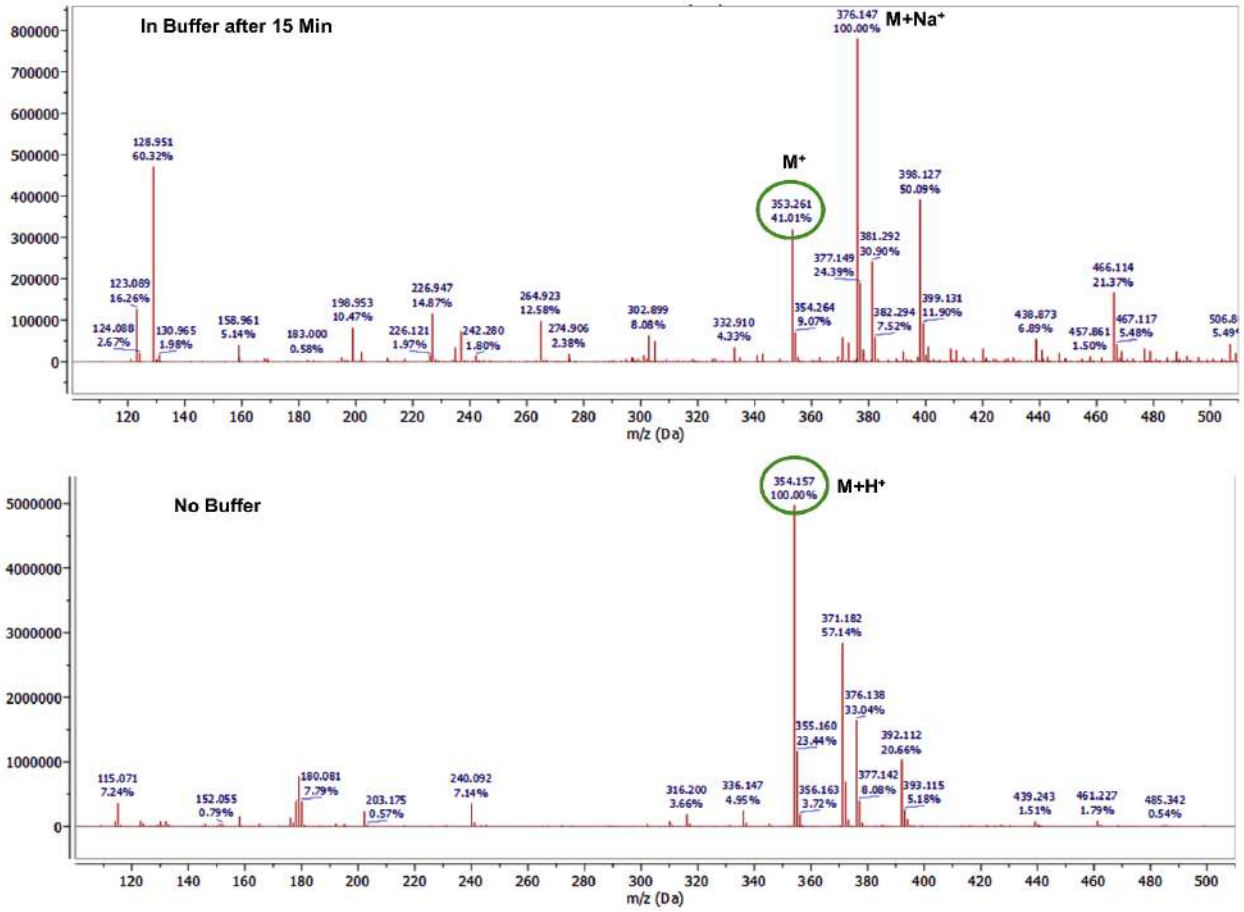

Figure 2.32. ESI-MS of Fmoc-$\gamma^{4,4}$-OH without buffer solution and in sodium bicarbonate buffer at pH 10.

TH-3141_166122021

2.4. Conclusion

We have studied the conformation of the Fmoc derivatives of three differently backbone di-substituted γ amino acid residues ($\gamma^{2,2}$, $\gamma^{3,3}$, $\gamma^{4,4}$) in solution and in single crystals. In solution, all the Fmoc derivatives of all the γ amino acids remained in equilibrium in between their low energy monomeric and high energy dimeric states. The rate of interconversion in between the monomeric and dimeric states was slow for Fmoc-$\gamma^{2,2}$-OH and Fmoc-$\gamma^{3,3}$-OH while it was the fastest for the Fmoc-$\gamma^{4,4}$-OH. In crystals, different γ amino acid residues adopted different torsion angles which was a direct consequence of their differential position of geminal di-substitution. In both $\gamma^{2,2}$ and $\gamma^{4,4}$ amino acid residues, torsion angles flanking the di-substituted carbon atom attained gauche conformation, though Fmoc-$\gamma^{2,2}$-OH adopted an open conformation while Fmoc-$\gamma^{4,4}$-OH adopted a close conformation in crystals. Fmoc-$\gamma^{2,2}$-OH and Fmoc-$\gamma^{4,4}$-OH, attained distinct conformations which gave rise to entirely different kind of crystal packing in them. Though the dimer in open conformation was lower in energy than the close conformation for all the Fmoc derivatives, exceptionally good π-π stacking interaction in between the Fmoc moieties in the Fmoc-$\gamma^{4,4}$-OH in the crystal lattice lead to the observation of close conformation in the crystals. Thus the crystal conformation of the Fmoc derivatives were clearly controlled by the variable position of backbone substitutions along their backbones, while the assembly in solid state was governed by Fmoc π-π stacking interactions. However, the self-assembly of the derivatives in solution was independent of the effect of variable geminal backbone di-substitutions. It was thermodynamically governed, solvent and concentration dependent phenomenon for all the Fmoc derivatives. Such studies are vital in developing our understanding and enabling the control over the conformational tuning of unnatural amino acid residues, which is of central importance in rational designing of peptidomimetics.

TH-3141_166122021

Chapter 3

Helices in all α Amino Acid Host Peptides Containing One Different Guest Geminally Di-substiuted γ Amino Acid Residue ($\gamma^{2,2}$, $\gamma^{3,3}$, $\gamma^{4,4}$)

TH-3141_166122021

3.1. Introduction

In the present chapter we have tried to study the relative propensity of the three differently geminally disubstituted gamma amino acid residues ($\gamma^{2,2}$, $\gamma^{3,3}$, $\gamma^{4,4}$) to be accommodated into all α helical model peptide sequences. We have chosen the peptide scaffold Boc-LUV-UXU-LUV-OMe where U = Aib and X = $\gamma^{2,2}$, $\gamma^{3,3}$, $\gamma^{4,4}$. The model peptide contains high percentages of Aib, an achiral α amino acid residue known to induce helical conformation, along with chiral α amino acid residues. As length of peptides play a major role in its ability to adopt helical structures, with longer peptides having a higher propensity of forming helical conformation, we have constructed peptides of different lengths. We have considered the central tripeptide fragment (Boc-UXU-OMe, X = $\gamma^{2,2}$, $\gamma^{3,3}$, $\gamma^{4,4}$), the hexappetide fragment (Boc-UXU-LUV-OMe, X = $\gamma^{2,2}$, $\gamma^{3,3}$, $\gamma^{4,4}$) and the nonapeptide (Boc-LUV-UXU-LUV-OMe) and studied the conformation at each level in both solid and solution states. As the whole study entails a large body of work, we have separated it into two halves. Part 3A describes the investigations carried out on the Tri and hexapeptides while Part 3B describes the study with the nonapeptides.

TH-3141_166122021

Chapter 3A

Enhanced C_{12} helical propensity of $\gamma^{3,3}$ and $\gamma^{4,4}$ amino acid residues compared to $\gamma^{2,2}$ amino acid residues

TH-3141_166122021

3A.1. Introduction

Table 3A.1 details the sequences of the peptides studied in this chapter.

Table 3A.1. Peptide sequences synthesized in the present study

Name of the Peptide	**Peptide Sequence**
31-Tri	Boc-Aib-$\gamma^{2,2}$-Aib-OMe
32-Tri	Boc-Aib-$\gamma^{3,3}$-Aib-OMe
33-Tri	Boc-Aib-$\gamma^{4,4}$-Aib-OMe
31-Hexa	Boc-Aib-$\gamma^{2,2}$-Aib-Leu-Aib-Val-OMe
32-Hexa	Boc-Aib-$\gamma^{3,3}$-Aib-Leu-Aib-Val-OMe
33-Hexa	Boc-Aib-$\gamma^{4,4}$-Aib-Leu-Aib-Val-OMe

3A.2. Experimental Section

3A.2.1. General Procedure of Peptide Synthesis (31-33)-Tri and (31-33)-Hexa

All peptides both tri and hexa were synthesized through conventional solution phase chemistry using a fragment condensation strategy, involving a 1+2 and 3+6 coupling in the final step for tri and hexapeptides respectively. Tert-Butyloxycarbonyl (Boc) was used for N-terminus protection, and the C-terminus was protected as a methyl ester. Peptide coupling was mediated by EDC.HCL and HOBt. Deprotection of Boc group was achieved by TFA in DCM (1:1), and the methyl group was removed by saponification using LiOH in mixture of methanol and water (2:1).

TH-3141_166122021

Scheme 3A.1. Synthetic flow chart of peptide **(31-33)-Tri and (31-33)-Hexa**

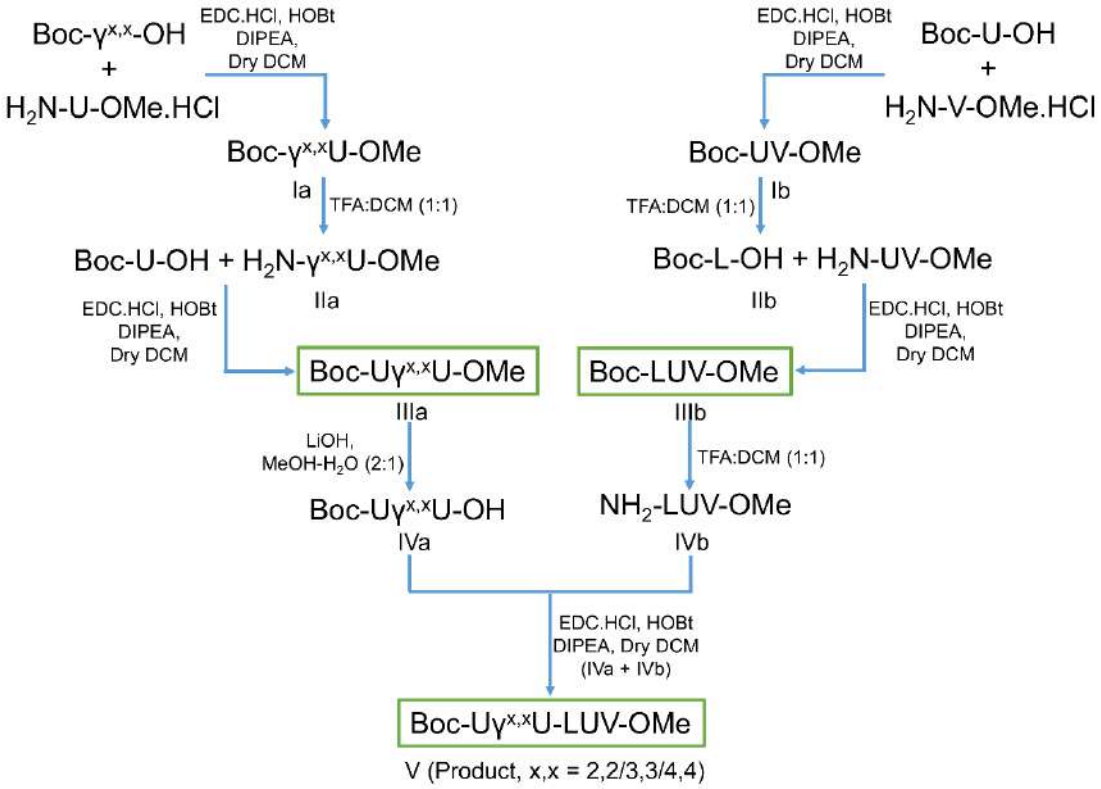

3A.2.2. Purification:

Crude peptides were purified by reverse-phase HPLC using binary acetonitrile/water (92−100%) solvent system at a flow rate of 10 mL/min using dual UV detection at 214 and 220 nm. To check the purity, analytical HPLC was performed with a flow rate of 1 mL/min and a linear gradient of 50−100% in acetonitrile/water system.

3A.2.3. Characterization

3A.2.3.1. Characterization of Boc-$\gamma^{x,x}$-OH

Boc-$\gamma^{2,2}$-OH

ESI-MS (m/z) of **Boc-$\gamma^{2,2}$-OH**: Calc. for $(M+H)^+$ $C_{11}H_{21}NO_4$ = 232.1504 Da; Obs. = 232.1570 Da, $(M+Na)^+$ = 254.1389, $(2M+H)^+$ = 463.6031 (Appendix, Figure A21). ^{1}H NMR (600 MHz, Chloroform-*d*) (Appendix, Figure A24): δ 6.41 (t, *J* = 6.0 Hz, 1H), 4.68 (b, 1H), 3.17 (b, *J* =

TH-3141_166122021

6.6 Hz, 3H), 1.78 (q, *J* = 7.8, 6.6 Hz, 3H), 1.51-1.40 (m, 15H), 1.48 (s, 6H), 1.27-1.19 (m, 10H). ^{13}C NMR (150 MHz, Chloroform-*d*) (Appendix, Figure A27): δ 183.0, 155.9, 79.3, 40.9, 40.4, 39.9, 38.1, 37.1, 28.4, 25.1, 24.9.

Boc-γ^{3,3}-OH

ESI-MS (m/z) of **Boc-γ^{3,3}-OH**: Calc. for $(M+H)^+$ $C_{11}H_{21}NO_4$ = 232.1504 Da; Obs. = 232.1619 Da, $(M+Na)^+$ = 254.1425, $(2M+H)^+$ = 463.3123 (Appendix, Figure A22). ^{1}H NMR (600 MHz, Chloroform-*d*) (Appendix, FigureA25): δ 5.00 (t, *J* = 7.0 Hz, 1H), 3.08 (d, *J* = 6.9 Hz, 2H), 2.26 (s, 2H), 1.47 (s, 11H), 1.03 (s, 7H). ^{13}C NMR (150 MHz, Chloroform-*d*) (Appendix, Figure A28): δ 174.5, 157.6, 80.5, 49.7, 44.1, 34.9, 28.3, 25.7.

Boc-γ^{4,4}-OH

ESI-MS (m/z) of **Boc-γ^{4,4}-OH**: Calc. for $(M+H)^+$ $C_{11}H_{21}NO_4$ = 232.1504 Da; Obs. = 232.1604 Da, $(2M+H)^+$ = 463.3129 (Appendix, Figure A23). ^{1}H NMR (600 MHz, Chloroform-*d*) (Appendix, Figure A27): δ 5.68 (b), 4.49 (b, 1H) (m, 1H), 2.50 – 2.24 (m, 3H), 2.04 (s, 3H), 1.44 (s, 12H), 1.28 (s, 9H). ^{13}C NMR (150 MHz, Chloroform-*d*) (Appendix, Figure A29): δ 178.9, 51.9, 34.7, 34.7, 29.4, 28.4, 27.3.

3A.2.3.2. Characterization of peptides

Boc-Aib-γ^{2,2}-Aib-OMe (31-Tri)

Analytical HPLC retention time: 3.96 min (Appendix Figure A30). ESI-MS (m/z) of **31-Tri**: Calc. for $(M+H)^+$ $C_{20}H_{37}N_3O_6$ = 416.2716 Da; Obs. = 416.2773 Da (Appendix, Figure A33). ^{1}H NMR (600 MHz, Chloroform-*d*) (Appendix, Figure A36): δ 6.70 (b, 1H), 6.63 (s, 1H), 5.00 (b, 1H), 3.73 (s, 3H), 3.28 – 3.20 (m, 2H), 1.75 – 1.71 (m, 2H), 1.54 (s, 6H), 1.47 (s, 6H), 1.44

TH-3141_166122021

(s, 9H), 1.19 (s, 6H). ^{13}C {1H} NMR (150 MHz, Chloroform-*d*) (Appendix, Figure A39): δ 176.7, 175.2, 174.9, 154.7, 56.6, 56.3, 52.5, 41.2, 39.3, 36.5, 28.3, 25.9, 24.9.

Boc-Aib-γ^{3,3}-Aib-OMe (32-Tri)

Analytical HPLC retention time: 4.43 min (Appendix Figure A31). ESI-MS (m/z) of **31-Tri**: Calc. for $(M+H)^+$ $C_{20}H_{37}N_3O_6$ = 416.2716 Da; Obs. = 416.2823 Da, $(2M+Na)^+$ = 853.5355 (Appendix, Figure A34). ^{1}H NMR (600 MHz, Chloroform-*d*) (Appendix, Figure A37): δ 7.47 (s, 1H), 6.99 (s, 1H), 4.96 (s, 1H), 3.71 (s, 3H), 3.20 (d, *J* = 6.7 Hz, 2H), 2.04 (s, 2H), 1.53 (s, 6H), 1.50 (s, 6H), 1.44 (s, 9H), 0.99 (s, 6H). ^{13}C {1H} NMR (150 MHz, Chloroform-*d*) (Appendix, Figure A40): δ 175.2, 170.7, 154.7, 56.9, 55.9, 52.3, 48.3, 45.2, 35.2, 28.3, 26.4, 25.0.

Boc-Aib-γ^{4,4}-Aib-OMe (33-Tri)

Analytical HPLC retention time: 4.31 min (Appendix Figure A32). ESI-MS (m/z) of **31-Tri**: Calc. for $(M+H)^+$ $C_{20}H_{37}N_3O_6$ = 416.2716 Da; Obs. = 416.2813 Da, $(2M+Na)^+$ = 853.5323 (Appendix, Figure A35). ^{1}H NMR (600 MHz, Chloroform-*d*) (Appendix, Figure A38): δ 6.52 (b, 1H), 6.43 (s, 1H), 4.98 (s, 1H), 3.72 (s, 3H), 2.21 – 2.14 (m, 2H), 2.06 (dd, *J* = 9.2, 6.3 Hz, 2H), 1.51 (s, 6H), 1.46 (s, 6H), 1.45 (s, 9H), 1.29 (s, 6H). ^{13}C {1H} NMR (150 MHz, Chloroform-d) (Appendix, Figure A41): δ 173.98, 173.10, 77.24, 57.0, 56.1, 53.2, 52.5, 35.3, 31.6, 28.3, 27.0, 24.9.

Boc-Aib-γ^{2,2}-Aib-Leu-Aib-Val-OMe (31-Hexa)

Analytical HPLC retention time: 6.71 min (Appendix Figure A42). ESI-MS (m/z) of **31-H**exa: Calc. for $(M+H)^+$ $C_{35}H_{64}N_6O_9$ = 713.4768 Da; Obs. = 713.4899 Da, $(2M+Na)^+$ = 1447.9489 Da (Appendix, Figure A45). ^{1}H NMR (600 MHz, Chloroform-*d*) (Appendix, Figure A48): δ 7.43 (s, 1H), 7.37 (b, 1H), 7.26 (b, J = 5.76 Hz, 1H), 6.85 (t, *J* = 6.2 Hz, 1H), 6.65 (s, 1H), 4.94

TH-3141_166122021

(s, 1H), 4.43 (dd, *J* = 8.5, 5.7 Hz, 1H), 4.24-4.19 (m, 1H), 3.70 (s, 3H), 3.25 – 3.19 (m, 1H), 3.15 – 3.09 (m, 1H), 2.22 – 2.15 (m, 1H), 1.85 - 1.71 (m, 5H), 1.57 (s, 3H), 1.55 (s, 3H), 1.52 (s, 3H) 1.51 (s, 3H), 1.46 (s, 3H), 1.44 (b, 12H), 1.17 (s, 3H), 1.15 (s, 3H), 1.00 – 0.85 (m, 12H). ^{13}C {^{1}H} NMR (150 MHz, Chloroform-*d*) (Appendix, Figure A51): δ 177.5, 175.5, 175.1, 174.9, 172.5, 172.2, 154.7, 80.4, 57.7, 57.5, 56.9, 56.6, 52.9, 51.8, 41.7, 40.1, 39.1, 36.9, 30.9, 28.3, 26.2, 26.1, 25.9, 25.6, 25.6, 25.1, 24.3, 23.4, 21.1, 19.1, 18.1, 15.3.

Boc-Aib-γ^{3,3}-Aib-Leu-Aib-Val-OMe (32-Hexa)

Analytical HPLC retention time: 8.84 min (Appendix Figure A43). ESI-MS (m/z) of **32-H**exa: Calc. for $(M+H)^+$ $C_{35}H_{64}N_6O_9$ = 713.4768 Da; Obs. = 713.4924 Da, $(2M+Na)^+$ = 1447.5938 Da (Appendix, Figure A46). ^{1}H NMR (600 MHz, Chloroform-*d*) (Appendix, Figure A49): δ 8.28 (b, 1H), 7.71 (s, 1H), 7.40 (d, *J* = 8.6 Hz, 1H), 7.32 (s, 1H), 6.56 (dd, *J* = 8.8, 4.5 Hz, 1H), 5.18 (s, 1H), 4.42 (dd, *J* = 8.6, 6.3 Hz, 1H), 4.19 – 4.13 (m, 1H), 3.70 (s, 3H), 3.47 – 3.37 (m, 1H), 2.86 (d, *J* = 13.9 Hz, 1H), 2.22 (h, *J* = 6.7 Hz, 1H), 2.15 (d, *J* = 13.9 Hz, 1H), 1.96 (d, *J* = 13.9 Hz, 1H), 1.82 – 1.77 (m, 3H), 1.57 (s, 6H), 1.51 – 1.44 (m, 15H), 1.43 (s, 3H), 1.42 (s, 3H), 1.15 (s, 3H), 1.06 – 0.83 (m, 15H). ^{13}C {^{1}H} NMR (150 MHz, Chloroform-*d*) (Appendix, Figure A52): δ 175.6, 174.6, 172.5, 172.3, 171.7, 57.9, 57.4, 56.8, 56.7, 53.8, 51.7, 47.3, 43.5, 39.1, 35.5, 30.8, 28.4, 27.6, 26.6, 26.3, 26.1, 25.5, 25.1, 24.3, 24.2, 23.4, 20.9, 19.2, 18.3.

Boc-Aib-γ^{4,4}-Aib-Leu-Aib-Val-OMe (33-Hexa)

Analytical HPLC retention time: 7.24 min (Appendix Figure A44). ESI-MS (m/z) of **33-H**exa: Calc. for $(M+H)^+$ $C_{35}H_{64}N_6O_9$ = 713.4768 Da; Obs. = 713.4911 Da, $(2M+NH_4)^+$ = 1442.9949 Da (Appendix, Figure A47). ^{1}H NMR (600 MHz, Chloroform-*d*) (Appendix, Figure A50): δ 7.57 (s, 1H), 7.43 (s, 1H), 7.28 (b, 2H), 5.96 (s, 1H), 4.97 (s, 1H), 4.45 (dd, *J* = 8.7, 5.9 Hz, 1H), 4.26 – 4.21 (m, 1H), 3.70 (s, 3H), 2.50 (b, 1H), 2.23 – 2.19 (m, 1H), 2.17 – 2.11 (p, *J* =

TH-3141_166122021

8.8 Hz, 2H), 1.99 (dt, *J* = 14.0, 8.4 Hz, 1H), 1.86 – 1.74 (m, 3H), 1.57 (s, 6H), 1.53 (s, 3H), 1.47 (s, 9H), 1.45 (s, 3H), 1.43 (s, 3H), 1.39 (s, 3H), 1.26 (s, 3H), 1.14 (s, 3H), 0.99 – 0.88 (m, 12H). ^{13}C {^{1}H} NMR (150 MHz, Chloroform-*d*) (Appendix, Figure A53): δ 175.3, 175.2, 174.7, 173.9, 172.3, 154.9, 81.2, 57.7, 57.5, 57.1, 56.6, 53.7, 53.3, 51.8, 39.3, 34.3, 30.9, 29.9, 28.3, 27.7, 27.6, 26.9, 26.4, 26.2, 25.2, 25.0, 24.0, 23.9, 23.4, 20.9, 19.2, 18.1.

3A.2.4. Single crystal X-ray diffraction:

Crystallization of all the tri and hexapeptides were carried out in the ethylacetate/hexane and methanol/H_2O system respectively. Data was collected at room temperature. Table Sx and Sx provides the crystal and refinement parameters for all the peptide structures. Intensity data was collected with Mo-Kα radiation (λ = 0.71073 Å) by a Bruker (D8 Quest) diffractometer. Data was processed using the Bruker SAINT package. All the structures were solved by direct methods using either SHELXS or SHELXD[293,295] and were refined using the Least-squares method in SHELXL-14.[294] All hydrogen atoms were fixed in ideal geometries and were refined as riding against the atoms to which they are bonded. The crystal structures have been deposited at the Cambridge Crystallographic Data Centre (CCDC) with deposition numbers 2237860-2237865.

Table 3A.2. Crystal and refinement parameters of **(31-33)-Tri.**

Parameters	**31-Tri**	**32-Tri**	**33-Tri**
Empirical formula	$C_{20}H_{37}O_6N_3$	$C_{20}H_{37}O_6N_3$	$C_{20}H_{37}O_6N_3$
Formula weight	415.52	415.52	415.52
Crystal system	Monoclinic	Triclinic	Monoclinic
Space group	$P2_1/n$	*P*-1	$P2_1/n$
Unit cell dimensions			
a (Å)	14.0484 (9)	10.2997 (13)	10.465(3)
b (Å)	9.8787 (7)	15.4367 (19)	17.206(4)
c (Å)	18.3495 (12)	16.044 (2)	13.542(3)
α (°)	90	102.376 (3)	90
β (°)	110.671 (2)	94.203 (3)	98.160 (8)
γ (°)	90	101.538 (3)	90

TH-3141_166122021

V (Å)	2382.6 (3)	2423.2 (5)	2413.7 (10)
Z	4	4	4
Temperature (K)	297 (2)	300 (2)	296 (2)
Radiation	MoKα (λ = 0.71073Å)	MoKα (λ = 0.71073 Å)	MoKα (λ = 0.71073 Å)
2θMax (°)	23.555	24.972	28.290
F (000)	904	904	904
Measured reflection	46608	28014	388342
R_{int}	0.0924	0.0453	0.0817
Unique reflection	3407	8070	5955
Observed reflection $\|F\| > 4\sigma$ (F)	2350	5709	3819
R-factor	0.0679	0.0628	0.0534
wR_2	0.1549	0.1286	0.1315
Goodness-of-fit S	1.119	1.107	1.023
$\Delta\rho_{max}$ (e $Å^{-3}$)	0.235	0.193	0.213
$\Delta\rho_{min.}$ (e $Å^{-3}$)	-0.239	-0.182	-0.246
Shift/esd (max)	0.000	0.000	0.000
No. of restrains/parameter	0/262	0/524	0/262
Data to parameter ratio	8.969:1	10.895:1	14.576:1

TH-3141_166122021

Table 3A.3. Crystal and refinement parameters of **(31-33)-Hexa**.

Parameters	**31-Hexa**	**32-Hexa**	**33-Hexa**
Empirical formula	$C_{35}H_{66}O_{10}N_6$	$C_{35}H_{64}O_9N_6 + 2H_2O$	$C_{35}H_{64}O_{11}N_6$
Formula weight	744.94	728.92	744.92
Crystal system	Monoclinic	Monoclinic	Orthorhombic
Space group	$P2_1$	$P2_1$	$P2_12_12_1$
Unit cell dimension			
a (Å)	13.131(3)	12.5230 (7)	9.1840(18)
b (Å)	12.770 (3)	26.0249 (15)	21.456(5)
c (Å)	25.871 (6)	13.4521 (8)	22.782(5)
β(°)	91.185(6)	91.030 (2)	90
V (Å)	4337.2(16)	4383.5 (4)	4492.0(17)
Z	4	4	4
Temperature (k)	110(2)	298 (2)	293(2)
Radiation	MoKα (λ = 0.71073Å)	MoKα (λ = 0.71073 Å)	MoKα (λ = 0.71073 Å)
2θ Max (°)	24.703	20.803	24.711
F (000)	1620	1584	1616
Measured reflection	121868	72060	114511
R_{int}	0.0422	0.0840	0.1975
Unique reflection	14740	9124	7650
Observed reflection |F| > 4σ (F)	13562	5584	3663
R factor	0.0387	0.0878	0.0743
wR_2	0.0975	0.1923	0.1676
Goodness-of-fit S	0.984	1.145	1.101
$\Delta\rho_{max}$ (e Å^{-3})	0.357	0.286	0.278
$\Delta\rho_{min.}$ (e Å^{-3})	-0.275	-0.206	-0.275
Shift/esd (max)	0.000	0.042	0.002
No. of restrains/parameter	1/934	1/920	1/651
Data to parameter ratio	15.78	6.06	11.75

TH-3141_166122021

3A.2.5. NMR Spectroscopy:

All NMR experiments were carried out on a Bruker Ascend Aeon 400 and 600 MHz spectrometer respectively. The peptide concentrations were in the range of 5-7 mM in $CDCl_3$ for both 1D and 2D NMR experiments. The chemical shift values and coupling constants were measured from 1D NMR spectra. Variable temperature 1D NMR experiments were carried out in between 273-323 K. Complete resonance assignments of the protons of (**31-33)-Hexa** were done by TOCSY and ROESY experiments. All the 2D experiments were done in phase sensitive mode by using time-proportional phase incrementation (TPPI) method. For all peptides TOCSY spectra was recorded with a mixing time of 80 ms but for ROESY spectra mixing times of 300 ms were used respectively. The spectral width was 6009.6 Hz in both dimensions. The total number of scans were fixed to 32 for TOCSY and ROESY, respectively. Data points was set to 2048 and 300 in f2 and f1 dimensions, respectively for both TOCSY and ROESY spectra. Zero filling was done to finally yield a data set of 4K x 2K. All NMR spectra were processed using Topspin 3.6 software.

3A.2.6. CD Spectroscopy:

The CD spectra were recorded for **(31-33)-Hexa** using a 200 μL quartz cuvette of 1 mm path length with a Jasco J-1500 spectropolarimeter at room temperature. The CD studies were performed in acetonitrile at 600 μM concentrations for all peptides. Spectra were collected at a scan rate of 100 $nm \cdot min^{-1}$ and 2 nm bandwidth from 190 nm to 260 nm with five scans for averaging. Before running the sample, acetonitrile was run to correct the baseline.

TH-3141_166122021

3A.2.7. FT-IR Spectroscopy:

Conformation of the hexapeptides **(31-33)-Hexa** was studied using solution FT-IR. The experiment was performed using the protocol detailed in section 1.14.4.2.3 earlier.

3A.3. Results and Discussion:

Peptides **(31-33)-Tri** and **(31-33)-Hexa** were synthesized using conventional solution phase synthesis strategy using Boc Chemistry. Peptides/fragments were purified using column chromatography and the final purification was done using Preparative HPLC. Purified peptides were characterized using Analytical HPLC (Appendix, Figures A42-A44), ESI-MS (Appendix, Figures A45-A47), ^{1}H (Appendix, Figures A48-A50) and ^{13}C NMR (Appendix, Figures A51-A53).

3A.3.1. Molecular conformations in crystals

The molecular conformation of the tripeptides **(31-33)-Tri** and hexapeptides **(31-33)-Hexa** are shown in Figures 3A.1-3A.3. The values of the backbone torsion angles are listed in Table 3A.4 and the hydrogen bond parameters are listed in Table 3A.5. The backbone conformation of γ amino acid residues are defined by four torsion angles, ϕ (C0'-N1-C^{γ}-C^{β}), θ_1 (N1-C^{γ}-C^{β}-C^{α}), θ_2 (C^{γ}-C^{β}-C^{α}-C') and ψ (C^{β}-C^{α}-C'-N2).

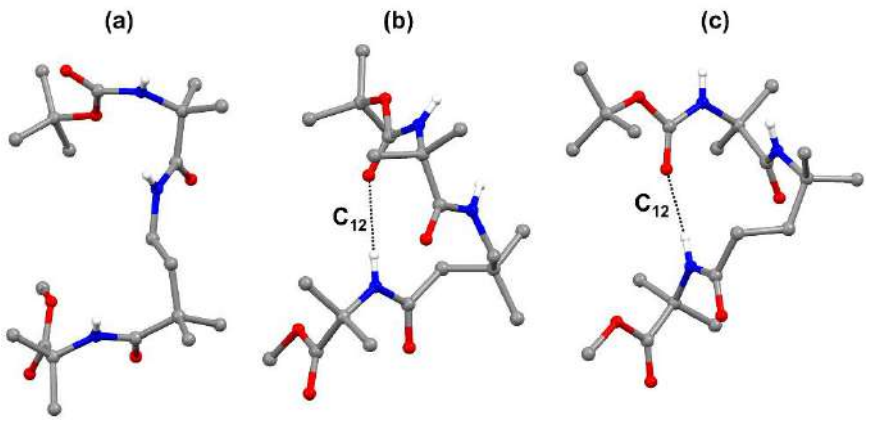

Figure 3A.1. Molecular Conformations of tripeptides in crystals. (a) Boc-Aib-$\gamma^{2,2}$-Aib-OMe (**31-Tri**), (b) Boc-Aib-$\gamma^{3,3}$-Aib-OMe (**32-Tri**) and (c) Boc-Aib-$\gamma^{4,4}$-Aib-OMe (**33-Tri**).

TH-3141_166122021

Table 3A.4. Backbone dihedral angles of (31-33)-Tri

Peptide	Amino Acid Residue	ϕ (°)	θ_1 (°)	θ_2 (°)	ψ (°)
31-Tri	Aib (1)	-59.4			-42.9
	$\gamma^{2,2}$ (2)	128.2	-164.9	-48.9	-61.2
	Aib (3)	-45.6			-47
32-Tri	**MOL-1**				
	Aib (1)	61.9			34.9
	$\gamma^{3,3}$ (2)	132.6	-57.2	-60.8	103.9
	Aib (3)	-52.6			-47.1
	MOL-2				
	Aib (1)	59.8			36.9
	$\gamma^{3,3}$ (2)	129.5	-57.2	-59.6	108.4
	Aib (3)	-51.6			-45.4
33-Tri	Aib (1)	-57.3			39.5
	$\gamma^{4,4}$ (2)	-54.9	-56.7	146.8	-96.4
	Aib (3)	52.41			46.7

Table 3A.5. Intramolecular and intermolecular hydrogen bond parameters of (31-33)-Tri

Peptide	H-Bonds	D.....A (Å)	H...A (Å)	∠D-H...A (°)
	MOL-1			
32-Tri	N3—H3....O0	3.0	2.23	167.8
	MOL-2			
	N3—H3....O0	3.0	2.15	169.4
33-Tri	N3—H3....O0	2.8	2.03	163.7

3A.3.1.1. Molecular conformation of (31-33)-Tri

In all the three tripeptides **(31-33)-Tri**, Aib adopted helical conformations. A reversal of the handedness was observed for the C-terminal Aib residue in the peptides **32-Tri** and **33-Tri**. The γ amino acids adopted different backbone conformation in the three peptides. The alpha-di-substituted residue, $\gamma^{2,2}$ in **31-Tri** adopted semi-extended conformation for the dihedral angle ϕ (128.3°) and *gauche* conformation for the dihedral angle ψ (-61.3°). The dihedral angles θ_1

TH-3141_166122021

and θ_2 adopted trans (165.0°) and *gauche* (-48.8°) conformations, respectively. In contrast, the $\gamma^{3,3}$ residue showed *gauche* conformation for both θ_1 and θ_2, and semi-extended conformations for both ϕ and ψ. In **33-Tri**, the $\gamma^{4,4}$ residue adopts *gauche* conformation for the torsional angles ϕ and θ_1, while semi-extended conformation was observed for θ_2 and ψ. The combination of sign (+/-) for the four torsional angles (ϕ, θ_1, θ_2, ψ) in the three cases were also different. In the $\gamma^{2,2}$ residue, the four dihedral angles show (+,-,-,-) combination, while it is (+,-,-+) in the $\gamma^{3,3}$, and (-, -, +, -) in the $\gamma^{4,4}$ residue. The hydrogen bond parameters listed in Table 3A.5 indicate that an intramolecular, $\alpha\gamma$ C_{12} hydrogen bond is present in both **32-Tri** and **33-Tri**, while the semi-extended conformation in **31-Tri** is not stabilized by any intramolecular hydrogen bonds.

3A.3. 1.2. Packing in tripeptide crystals: Table 3A.5 provides intermolecular hydrogen bonding parameters and Figure 3A.2 provide their illustrations. The amide NH groups of second and third amino acid residues form hydrogen bond interactions with the carbonyl O atoms (O2 and O1) of a molecule related by the 2_1-screw axis. The NH group of the Aib (1) residue is not involved in hydrogen bonding. In **32-Tri** and **33-Tri**, the N3 atom of the Aib (3) is involved in intramolecular hydrogen bonding. The remaining amino groups (N1 and N2) of **32-Tri** are involved in intermolecular hydrogen bonds as depicted in Figures 3A.2b and 3A.2c. In **33-Tri**, hydrogen bonding interaction from N1 is observed, while that from the N2 atom has a longer H…O distance (N…O = 3.35 Å, H…O = 2.72 Å). In both **32-Tri** and **33-Tri**, the head-to-tail intermolecular hydrogen bonding pattern results in a supramolecular helical column, which is a common packing motif observed for helical peptides in crystals.

TH-3141_166122021

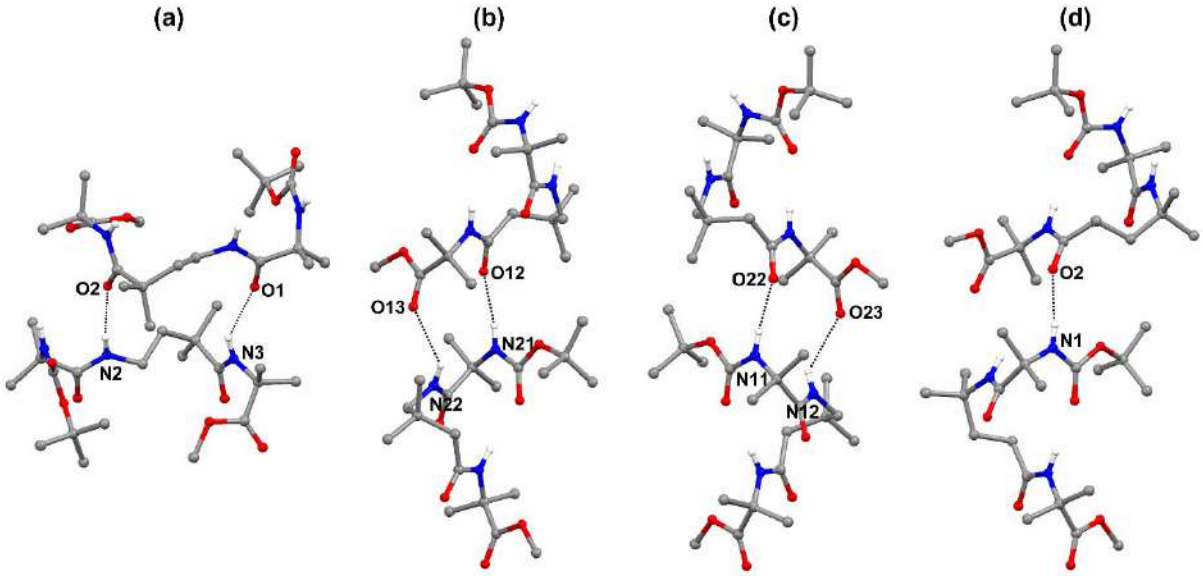

Figure 3A.2. Packing of tripeptides **(31-33)-Tri** in crystals showing intermolecular hydrogen bonds.

3A.3.1.3. Molecular conformations in (31-33)-Hexa:

All the hexapeptides adopted helical conformations. The dimethyl substitution at the C^{α}, C^{β} and C^{γ} atoms promotes *gauche* conformation about the flanking single bonds in the α/β/γ-di-substituted γ amino acid residues, as evidenced from Table 3A.6. The remaining two dihedral angles show torsion angle values close to 90° or 180°. However, the combination of sign for the four torsion angles are different in the three amino acid residues. The flanking Aib residues on either side of the γ amino acid residues shows dihedral angles in the helical region of the Ramachandran map.

TH-3141_166122021

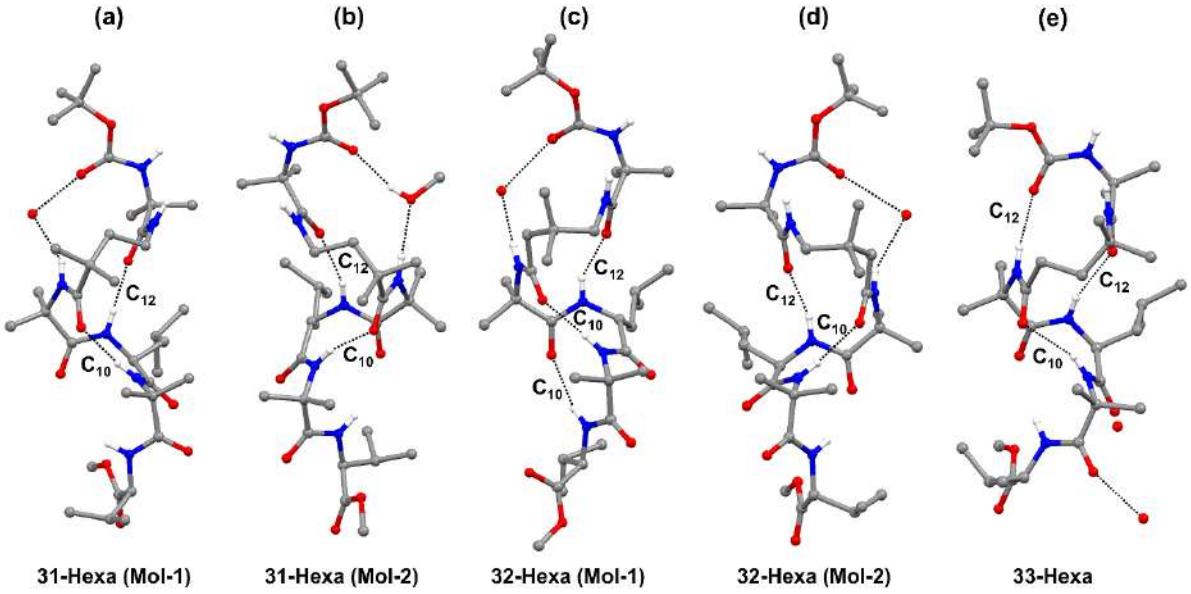

Figure 3A.3. Conformations in crystals of hexapeptides **(31-33)-Hexa**. Two molecules were present in the asymmetric unit of **(33-32)-Hexa**. Right handed and left handed helices of (a,b) **31-Hexa**, (c,d) **32-Hexa** respectively. (e) Right handed helix of **33-Hexa**.

Table 3A.6. Backbone dihedral angles of (31-33)-Hexa

Peptide	Amino Acid Residue	ϕ (°)	θ_1 (°)	θ_2 (°)	ψ (°)
31-Hexa	**MOL-1**				
	Aib (1)	-58.8 (4)			-45.6(3)
	$\gamma^{2,2}$ (2)	-89.7(3)	153.8(3)	-66.0(4)	-44.1(4)
	Aib (3)	-51.1(4)			-40.2(4)
	Leu (4)	-84.3(3)			4.5(4)
	Aib (5)	-46.9(4)			-55.0(3)
	Val (6)	-118.6(3)			-4.5(4)
	MOL-2				
	Aib (1)	56.3(4)			48.9(3)
	$\gamma^{2,2}$ (2)	85.2(4)	-160.4(3)	60.6(3)	60.7(3)
	Aib (3)	55.1(4)			40.8(4)
	Leu (4)	60.6(3)			19.7(4)
	Aib (5)	49.8(4)			41.4(4)
	Val (6)	-61.0(4)			-31.8(4)
32-Hexa	**MOL-1**				
	Aib (1)	-69(2)			-29(2)
	$\gamma^{3,3}$ (2)	-103.6(17)	63.9(18)	59.5(19)	-154.9(13)
	Aib (3)	-55.6(19)			-29(2)
	Leu (4)	-57.3(19)			-21.0(19)
	Aib (5)	-51.4(19)			-39(2)
	Val (6)	80(2)			-154(2)

TH-3141_166122021

	MOL-2				
	Aib (1)	65 (2)			33 (2)
	$\gamma^{3,3}$ (2)	99.8 (18)	-57.8 (18)	-62.4(18)	154.9 (13)
	Aib (3)	53.6(19)			35(2)
	Leu (4)	82.6(17)			-3(2)
	Aib (5)	52.1(19)			45(2)
	Val (6)	114(2)			12(3)
33-Hexa	Aib (1)	-61.3 (9)			-42.4 (8)
	$\gamma^{4,4}$ (2)	-49.9(10)	-50.6(9)	143.3(7)	-118.5(7)
	Aib (3)	-55.5(8)			-34.5(8)
	Leu (4)	-76.0(8)			-20.4(9)
	Aib (5)	-63.2(10)			-33.0(11)
	Val (6)	-131.4(10)			-16.7(15)

Table 3A.7. Intramolecular and intermolecular hydrogen bond parameters of (31-33)-Hexa

Peptide	H-Bonds	D.....A (Å)	H...A (Å)	∠D-H...A (°)
31-Hexa	**MOL1**			
	N11—H11....O42[a]	2.803(3)	2.31	115.3
	N12—H12….O42[a]	3.173(3)	2.31	166.6
	N13—H13… O2W	2.909(3)	2.12	149.5
	N14—H14….O11	2.860(3)	2.04	153.6
	N15—H15…. O21	2.887(3)	2.03	165.5
	N16—H16…O1W[b]	2.904(3)	2.04	167.7
	MOL 2			
	N12 —H12…O41[c]	2.780(3)	2.01	146.1
	N22—H22….O51[c]	3.010(3)	2.29	139.5
	N32—H32…O1S	3.006(4)	2.13	170.6
	N42—H42….O12	2.867(3)	2.05	153.9
	N52— H52….O22	2.940(3)	2.09	161.3
	N62— H62…O32	3.400(3)	2.59	152.7
32-Hexa	**MOL1**			
	N11— H11…O24[a]	2.790 (19)	1.99	153.5
	N13—H13…O2w	2.998 (17)	2.14	176.5
	N14—H14…O11	2.787 (17)	2.04	145.3
	N15— H15…O12	2.940 (17)	2.09	167.4
	N16—H16…O13	3.38 (2)	2.55	163.3
	O01…O2w	2.803	-	-
	MOL2			
	N21 —H21…O14[b]	2.754 (17)	1.99	147.2
	N23 —H23…O1w	3.18 (2)	2.38	154.1
	N24—H24…O21	2.820 (17)	2.00	158.8
	N25— H25…O22	2.904 (16)	2.07	164.1
	O02…O1w	2.832	-	-
33-Hexa	N1—H1….O4[f]	2.933(8)	2.08	174.1
	N2 —H2…O1W[f]	2.950(9)	2.18	148.1

TH-3141_166122021

	N3—H3….O0	2.935(8)	2.08	172.0
	N4—H4… O1	3.105(8)	2.27	162.6
	N5— H5….O2	3.070(8)	2.26	157.3

For 31-Hexa and 33-Hexa: [a] (x,y,z); [b] (-x, y+1/2, -z+2); [c] (x+1, y-1, z); [d] (-x+2, y-1/2, -z+1); [e](-x+1, y+1/2, -z+2); [f] (-x+1, y+1/2, -z)
For 32-Hexa: [a](-x, y+1/2, -z+1); [b](-x+1, y-1/2, -z); [c](x-1, y,z)

In case of **31-Hexa** and **32-Hexa**, helices with different handedness are present (Figure 3A.3). There are two molecules in the asymmetric unit of **31-Hexa** and **32-Hexa**. In **31-Hexa**, MOL-1 adopt negative values of ϕ and ψ for all the α amino acid residues, as expected for a right-handed helical conformation. However, the sign of torsion angles is reversed in MOL-2, except for the C-terminal Val residue. For 32-Hexa, in the right handed helix (MOL1), the C-terminal Val (6) residue shows a fraying, while in the left handed helix (MOL 2) all the residues adopt positive ϕ,ψ values. The molecular conformation of the hexapeptide **31-Hexa** is stabilized by two hydrogen bonds; a γα C_{12} hydrogen bond followed by a αα C_{10} hydrogen bond. A prospective αγ hydrogen bond between the CO of the Boc and the NH of the $\gamma^{2,2}$ (3) residue was interrupted by the insertion of solvent molecule. Interestingly in the crystal structures of the hexapeptide **31-Hexa** the last NH hydrogen of Val (6) is non hydrogen bonded in both the right and left handed helices. The molecular conformation in **32-Hexa** is stabilized by three consecutive hydrogen bonds, a γα C_{12} hydrogen bond followed by two αα C_{10} hydrogen bonds in Mol-1 (right-handed helix), while Mol-2 (left-handed helix) is stabilized by one γα C_{12} hydrogen bond and a αα C_{10} hydrogen bond (Table 3A.5). The N...O distance of the last intramolecular C_{10} hydrogen bond in MOL-2 (N6H...O3) is above the ideal values to be considered as hydrogen bond in both **31-Hexa** and **32-Hexa**. However, the **33-Hexa** adopted an ideal 12/10 mixed right-handed helical conformation.[213] In the right handed helix of **33-Hexa**, NH6 is also non-hydrogen bonded. In all right-handed helices of **(31-33)-Hexa**, NH6 remains non-hydrogen bonded. (Table 3A.7)

TH-3141_166122021

3A.3.2. Conformation in solution:

The conformation of the hexa-peptides in solution were probed using NMR, CD and FT-IR.

3A.3.2.1. Conformation in solution at different temperatures: variable temperature NMR

Figure 3A.4a shows the stacked plots of the NH region of the 1D ^{1}H NMR spectra of **(31-33)-Hexa** in $CDCl_3$ at 298 K. Only one set of sharp and well dispersed NMR lines were observed for all the three hexapeptides **(31-33)-Hexa**. This suggested that the peptides adopted a well folded secondary structure in solution. In order to investigate whether there was only one conformation populating the solution, or there was a mixture of more than one populants exchanging at a very fast rate at 298 K, thus generating only one set of lines, we recorded ^{1}H NMR at a lower temperature of 263 K(-10°C) **(**Figure 3A.4b). Even at the lower temperature only one set of sharp lines were observed which suggested that the peptides existed only in one conformation in solution. Interestingly, there was no noticeable change in the chemical shifts of the NH's even at lower temperatures, which excludes the possibility of intermolecular associations in between peptide molecules.

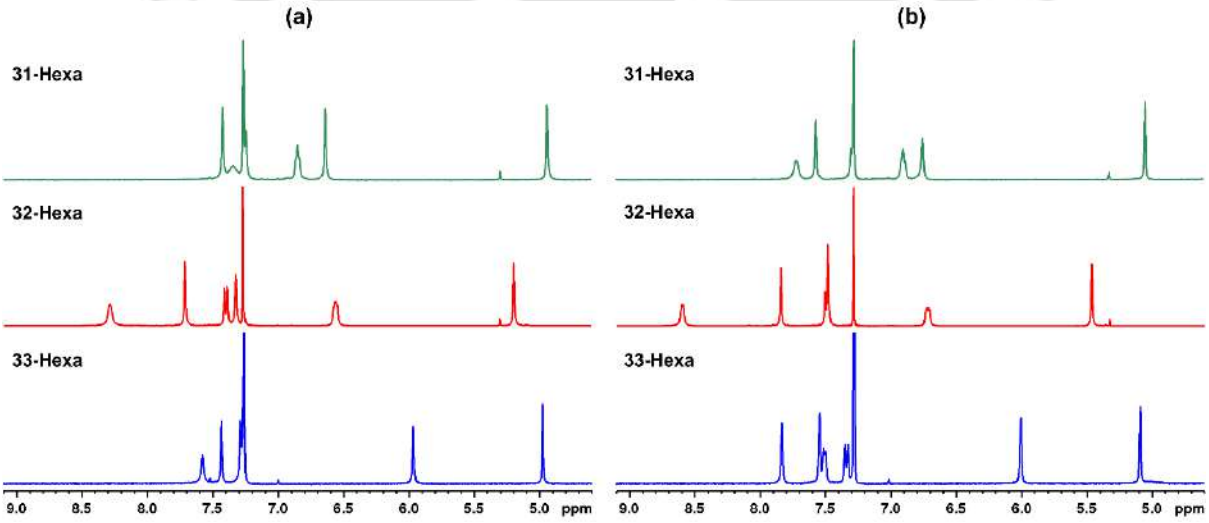

Figure 3A.4. Partial 1D ^{1}H NMR spectra representing the amide proton resonances of **(31-33)-hexa in** $CDCl_3$ at (a) room temperature and (b) at 263 K.

TH-3141_166122021

3A.3.2.2. ROESY:

Figure 3A.5 and 3A.6 represents the NH-NH region and the NH-$C^{\alpha}H$ region respectively of the ROESY spectrum of **(31-33)-Hexa**. All the sequential d_{NN} NOEs except that between NH $\gamma^{2,2}$(2) and NH Aib (3) were observed in the spectra of **31-Hexa**. In the case of **32-Hexa** and **33-Hexa** all the sequential d_{NN} NOEs are observed. The intensity of the d_{NN} NOE across the $\gamma^{x,x}$ (x,x = 3,3/4,4) residue were weaker compared to those across the α residues. This suggested that the peptides adopted helical conformation in solution as well. The difference in the intensity of the d_{NN} NOEs (weak and strong for αγ and αα segment respectively) across α and γ amino acid residues reported earlier in the literature,[215,220,221] suggested the presence of C_{12} helical conformation at the γ residue and C_{10} helical conformation at the α amino acid residues. However, unlike the crystals where helices of opposite handedness were observed for **31-Hexa** and **32-Hexa** peptides, there was to be only one conformation present for all the three peptides in solution.

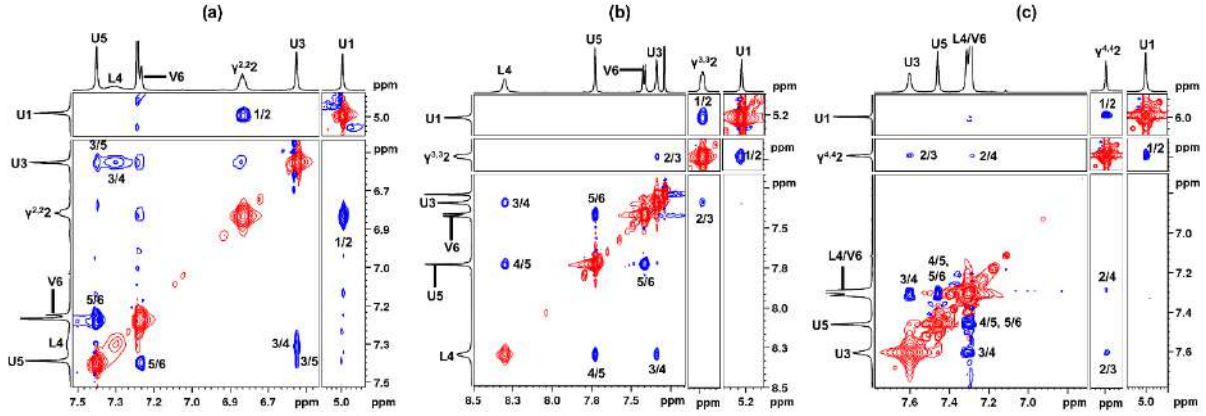

Figure 3A.5. Partial 600 MHz ROESY spectra of (a) **31-Hexa**, (b) **32-Hexa** and (c) **33-Hexa** representing d_{NN} NOEs in $CDCl_3$ at 298 K.

TH-3141_166122021

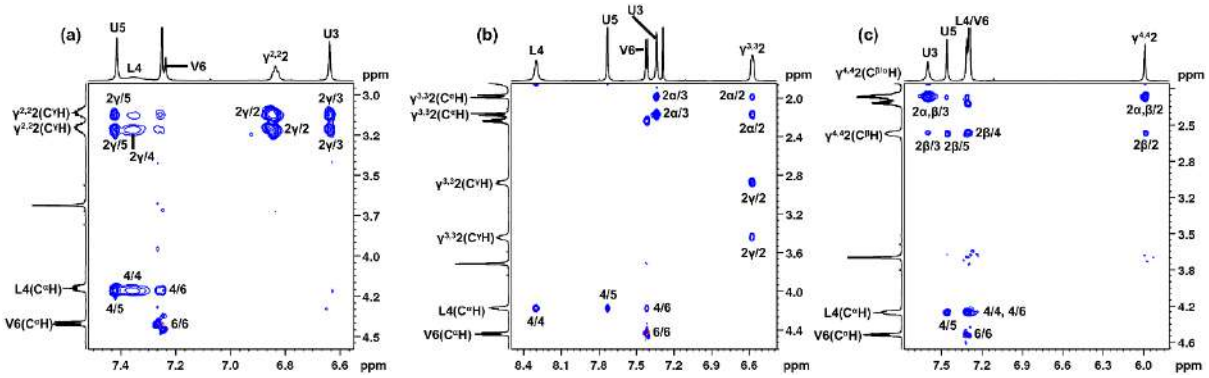

Figure S3A.6. 600 MHz partial ROESY spectra of (a) **31-Hexa**, (b) **32-Hexa** and (c) **33-Hexa** representing NOEs between NH↔C$^{\alpha}$H protons in $CDCl_3$ at 298 K.

3A.3.2.3. Intramolecular hydrogen bonds in the solution conformation: DMSO-d_6 solvent titration:

In order to probe the hydrogen bonding pattern in the three hexa peptides in solution, DMSO-d_6 titration experiment was performed. Upon addition of the polar solvent DMSO-d_6 to the solution of peptides in non-polar $CDCl_3$, the non-intramolecularly hydrogen bonded NH's form hydrogen bonds with DMSO-d_6 and show a downfield movement of their chemical shifts. The intramolecularly hydrogen bonded NH's show no change in the chemical shift values. Figures 3A.7 and 3A.8 show the change of chemical shift values ($\Delta\delta$ ppm) of the NH protons of (**31-33)-Hexa** upon addition of 40% DMSO-d_6 to the $CDCl_3$ solution of the peptides. A large magnitude of the $\Delta\delta$ ppm (>0.5 ppm) indicates solvent exposure or non-hydrogen bonded status of the NH's while a small value of $\Delta\delta$ ppm (<0.5 ppm) suggests intramolecular H-bond formation. In the case of **32-Hexa** and **33-Hexa**, all the NH's other than the first two N-terminal NH's had low values of $\Delta\delta$, suggesting them to be hydrogen bonded. It further suggested that these peptides adopted helical conformation which was stabilized by two residue hydrogen bonds. From earlier reports in the literature they can be concluded to have adopted a 10/12 helical conformation.[215,221] Earlier, in the crystals of **32-Hexa**, $\gamma^{3,3}$ (3) NH-Boc(0) CO hydrogen bond was intercepted by the presence of solvent molecules. However, in the solution this

TH-3141_166122021

hydrogen bond seemed to have formed. Also, presence of hydrogen bonding for Val (6) NH in the solution indicateed that **32-Hexa** must have adopted right handed helical conformation in solution. NH(6) of 33-Hexa which was non hydrogen bonded in the crystals, was observed to be hydrogen bonded in the solution. Thus the solution seems to promote helical conformation in 32 and 33-Hexa by the formation of hydrogen bonds.

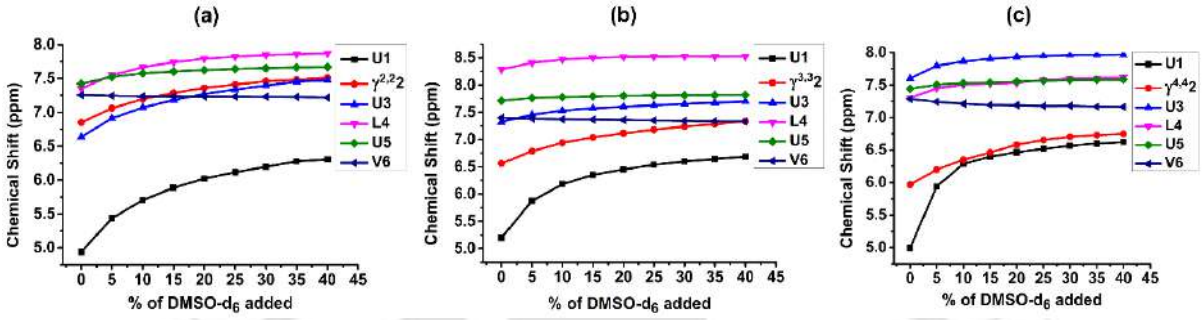

Figure 3A.7. Solvent dependence of NH chemical shifts of the peptides: (a) **31-Hexa**, (b) **32-Hexa** and (c) **33-Hexa**.

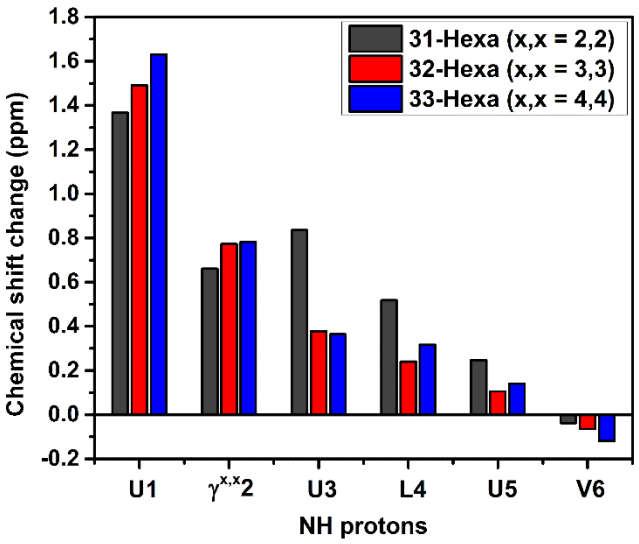

Figure 3A.8. Plot of the change of NH chemical shift value of the residues of **(31-33)-Hexa** in $CDCl_3$ with increasing concentration of DMSO-d_6 (0-40 %).

TH-3141_166122021

In the case of **31-Hexa**, the first three NH's (Aib (1), $\gamma^{2,2}$ (2) and Aib (3)) from the N-terminal were non-hydrogen bonded (similar to the situation in crystals), while the Leu (4) NH seemed to have a weak hydrogen bond. This observation proved absence of $\alpha\gamma^{2,2}$ C_{12} hydrogen bond and presence of a weak $\gamma^{2,2}\alpha$ hydrogen bond in **31-Hexa**. This in turn suggested the weaker ability of $\gamma^{2,2}$ residue to adopt C_{12} helical conformation. However, unlike in crystals, NH6 was hydrogen bonded in solution. This suggested presence of an additional hydrogen bond in the solution conformation. However, it was difficult to conclude about the handedness of the helix present in solution from the solvent titration experiment.

3A.3.2.4 CD Spectroscopy:

To ascertain the handedness of the helical conformation present in solution for the three peptides **(31-33)-Hexa**, CD experiment was performed (Figure 3A.9) in acetonitrile. **31-Hexa** and **32-Hexa** formed helices of either handedness in crystals while **33-Hexa** adopted only right handed helical conformation. In all the peptides, a strong negative cotton effect peak is observed around 202 nm with a slight shoulder peak at 220 nm. CD spectra of the right handed 3_{10} helix is characterized by a strong negative cotton effect peak at ~ 202 nm and a negative shoulder at ~ 222 nm.[325] Thus it can be concluded that all the peptides adopted a right-handed helical conformation in solution. This further establishes the conclusion from NMR, that the one set of lines observed in the NMR spectra indeed originated from a single right-handed helical conformation and not a mixture of two helical conformations in fast exchange with each other at room temperature. The weakest intensity of the negative cotton effect peak at 202 nm for **31-Hexa** among all the three peptides, suggested least helicity for this peptide. This was most probably owing to the least number of hydrogen bonds stabilizing it in comparison to **32-Hexa** and **33-Hexa**. This is most probably due to the fact that $\gamma^{2,2}$ in **31-hexa** was least prone to adopt C_{12} helical conformation in solution, thus leading to a shorter helix.

TH-3141_166122021

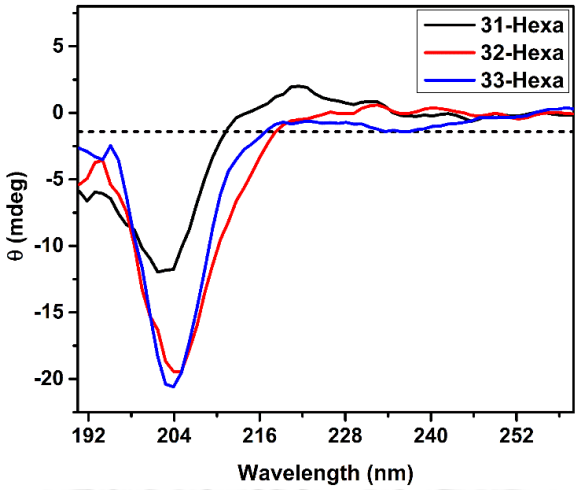

Figure 3A.9. CD spectra of **(31-33)-Hexa** in ACN at 600 μM. All the hexapeptides adopt right handed helical conformation in solution. The helical content of the hexapeptides are in the order **32-Hexa~33-Hexa** > **31-Hexa**.

3A.3.2.5. FT-IR Spectroscopy:

Figure 3A.10 demonstrates the stacked plots of the solution FT-IR for (**31-33)-Hexa** in $CDCl_3$ (1 mM) at room temperature. The characteristic peak ~1650 cm^{-1} in the spectra of all the peptides (**31-33)-Hexa**, indicated that all of them adopted helical conformation.[326,327]

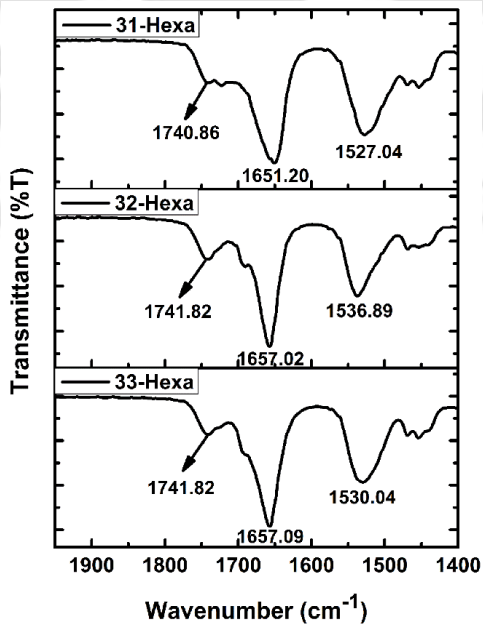

TH-3141_166122021

Figure 3A.10. FT-IR spectra of **(31-33)-Hexa** at 1 mM concentration in $CDCl_3$ at room temperature.

3A.4. Conclusion:

Among the three geminally di-substituted γ amino acid residues, the facility for adopting C_{12} helical conformation decreases in the order $\gamma^{4,4} > \gamma^{3,3} > \gamma^{2,2}$. Even in the tripeptide state, $\gamma^{2,2}$ does not participate in C_{12} helical conformation (**31-Tri**) unlike for $\gamma^{3,3}$ and $\gamma^{4,4}$. It is also noteworthy that peptides **31-Hexa** and **32-Hexa** can adopt either handedness of the helical conformation in crystals. In solution, both of these two peptides adopt right-handed helical conformation. **33-Hexa** however only adopts right-handed conformation both in the solid and in the solution states. It should also be noted that the ability to adopt C_{12} helical conformation is enhanced in solution state. As all the three peptides are similar to each other, except for a single γ amino acid residue, the ability to adopt either handedness might be related to the difference in the γ amino acid residues in question. Thus $\gamma^{2,2}$ and $\gamma^{3,3}$ amino acid residues can be accommodated in both handed helices while $\gamma^{4,4}$ amino acids can only give rise to right-handed helices.

TH-3141_166122021

Chapter 3B

Ambidexterity and Left Handedness Induced by Single Geminally Dimethyl Substituted γ Amino Acid Residues in all Alpha Chiral Helical Peptides

TH-3141_166122021

3B.1. Introduction

Figure 3b.1 illustrates the peptides studied in this Chapter.

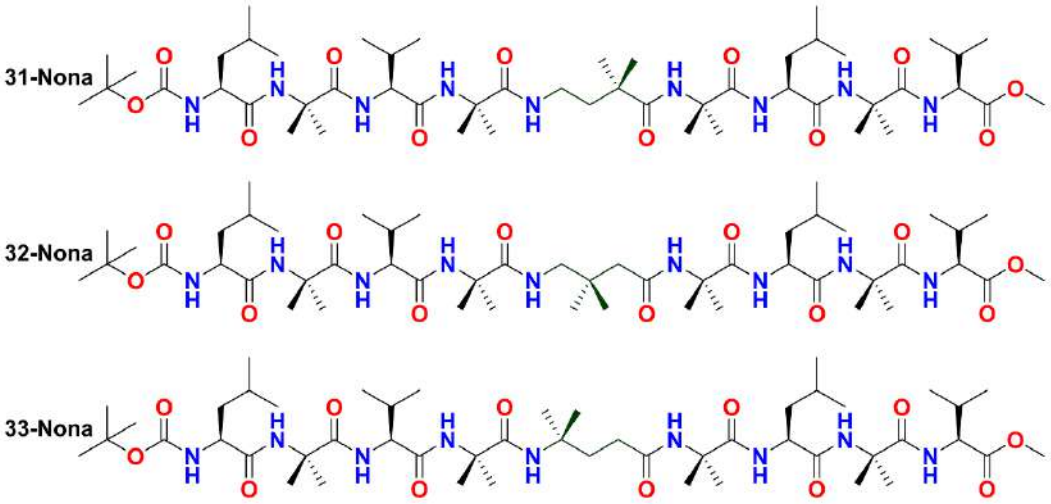

Figure 3B.1. Chemical structures of the peptides (**31-33)-Nona**.

3B.2. Experimental Section

3B.2.1. General Procedure of Peptide Synthesis (31-33)-Nona

All peptides (**31-33**)**-Nona** were synthesized through conventional solution phase chemistry using a fragment condensation strategy, involving a 3+6 coupling in the final step. (Scheme 3B.1) The general protocol is described in section 10.1.3.2.

TH-3141_166122021

Scheme 3B.1. Synthetic flow chart of peptide **(31-33)-Nona**

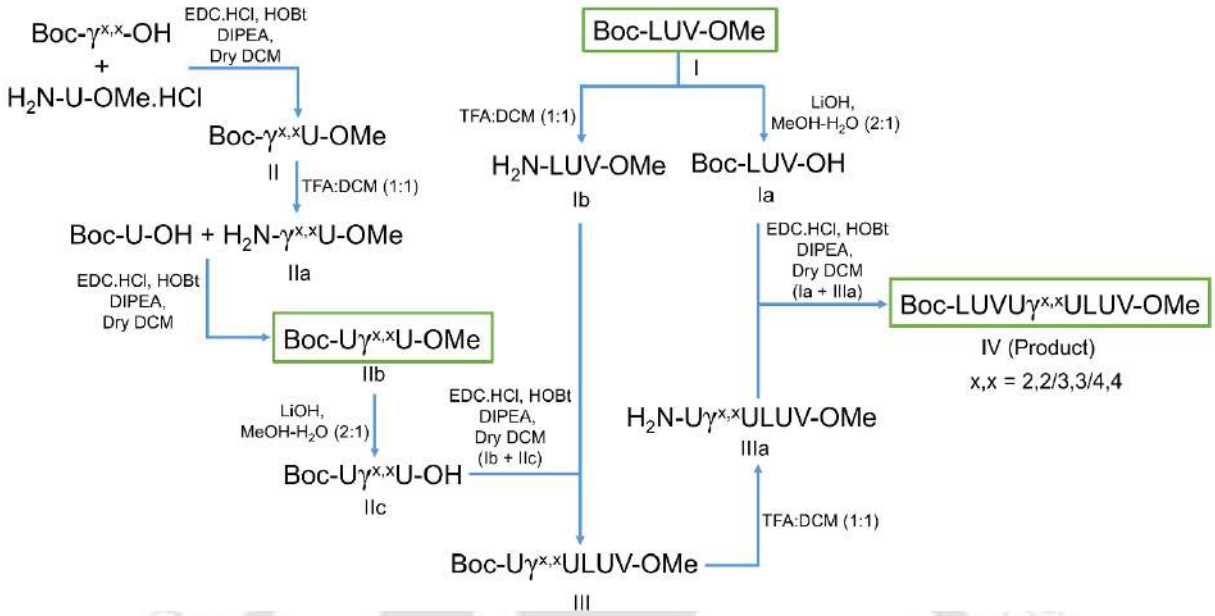

3B.2.2. Purification

Crude peptides were purified by reverse-phase HPLC using binary methanol/water (92−100%) solvent system at a flow rate of 10 mL/min using dual UV detection at 214 and 220 nm. To check the purity, analytical HPLC was performed with a flow rate of 1 mL/min and a linear gradient of 50−100% in acetonitrile/water system.

3B.2.3. Characterization of peptides

All peptides (**31-33)-Nona** were characterized using MALDI-TOF (Appendix, Figures A60-A62), ^{1}H NMR (Appendix, Figures A63-A65), and ^{13}C NMR (Appendix, Figures A66-A68) spectroscopy.

Boc-Leu-Aib-Val-Aib-γ^{2,2}-Aib-Leu-Aib-Val-OMe (31-Nona)

^{1}H NMR (600 MHz, Chloroform-*d*) (Appendix, Figure A63): δ 7.92 (d, *J* = 6.3 Hz), 7.72 (s), 7.58 (s), 7.53 (s), 7.38 (s), 7.33 (d, *J* = 8.2 Hz), 7.26 (br) 7.24-7.20 (br), 7.19 (s), 7.12 (d, *J* = 6.0 Hz), 7.06 (s), 6.96 (s), 6.77 (s), 6.67 (s), 5.16 (s), 5.11 (s), 4.43 – 4.39 (m), 4.27 (ddd, *J* = 10.4, 6.5, 2.8 Hz), 4.00 – 3.95 (m), 3.90 (t, *J* = 5.9 Hz), 3.87 – 3.81 (m), 3.78 (t, *J* = 6.1 Hz),

TH-3141_166122021

3.70-3.69 (br), 3.28 – 3.22 (m), 3.21 – 3.13 (m), 3.08-2.97 (m), 2.22 (dh, *J* = 19.4, 6.7 Hz), 1.86 – 1.71 (m), 1.66 – 1.57 (m), 1.56 – 1.43 (m), 1.17 (br, *J* = 8.8 Hz), 1.11 (br), 1.01 – 0.90 (m). ^{13}C {^{1}H} NMR (150 MHz, Chloroform-*d*) (Appendix, Figure A66): δ 177.9, 175.6, 175.5, 175.3, 172.6, 172.5, 172.0, 170.7, 156.3 (d, *J* = 86.7 Hz), 80.9, 65.8, 61.7, 61.6, 58.2, 57.9, 57.3, 57.2, 56.9, 56.8, 56.7, 56.7, 55.3, 53.8, 53.4, 53.1, 51.8, 51.7, 42.0, 41.7, 40.2, 40.1, 39.6, 39.4, 38.9, 38.6, 37.0, 36.9, 30.7, 30.6, 29.3, 29.1, 28.3, 28.2, 27.7, 27.6, 27.3, 27.2, 27.1, 27.1, 26.4, 26.1, 25.9, 25.4, 25.2, 25.0, 24.9, 24.9, 24.9, 24.8, 24.8, 24.6, 23.9, 23.5, 23.4, 23.4, 23.3, 23.2, 23.0, 22.7, 21.8, 21.7, 21.1, 21.0, 19.3, 19.1, 19.1, 19.1, 18.7, 18.4, 18.3, 18.2. MALDI-TOF of **31-Nona**, analytical HPLC peak at (a) 9.7 min [Calc. $(M+Na+2H)^+$ for $C_{50}H_{91}N_9O_{12}$= 1034.6841 Da Obs. = 1034.093 Da] and (b) 10.3 min [Calc. $(M+K)^+$ for $C_{50}H_{91}N_9O_{12}$= 1048.6424 Da Obs. = 1049.186 Da] (Appendix, Figures A60).

Boc-Leu-Aib-Val-Aib-γ^{3,3}-Aib-Leu-Aib-Val-OMe (32-Nona)

^{1}H NMR (600 MHz, Chloroform-*d*) (Appendix, Figure A64): δ 8.36 (d, *J* = 5.0 Hz), 8.17 (s), 7.86-7.78 (br), 7.75 (s), 7.67 (s), 7.58 (s), 7.51 (s), 7.44 (d, *J* = 8.8 Hz), 7.42 (d, *J*= 8.8), 7.00 (d, *J* = 6.5), 6.96 (s), 6.86 (d, *J* = 10.4 Hz), 6.77 (d, *J* = 8.4 Hz), 6.70 (s), 6.65 (s), 5.20 (s), 5.11 (s), 4.41 (dt, *J* = 8.1, 6.0 Hz), 4.18 (q, *J* = 6.4 Hz), 40.3-3.96 (m), 3.88 (t, *J* = 6.0 Hz), 3.86-3.81 (m), 3.75-3.71 (br), 3.71 (s), 3.68 (s), 3.54 (t, *J* = 11.6 Hz), 2.74 (d, *J* = 13.7 Hz), 2.54 (d, J= 13.7), 2.34 – 2.29 (m), 2.27 – 2.19 (m), 1.96 (d, *J* = 13.7 Hz), 1.94-1.87 (m), 1.86 – 1.77 (m), 1.75 – 1.62 (m), 1.58 (s), 1.57 – 1.43 (m), 1.20 (s), 1.13 (br), 1.02 – 0.91 (m). ^{13}C {^{1}H} NMR (150 MHz, Chloroform-*d*) (Appendix, Figure A67): δ 175.6, 175.3, 174.8, 172.5, 172.5, 172.2, 171.8, 171.3, 156.3 (d, *J* = 95.9 Hz), 81.0, 65.8, 61.2, 58.3, 58.0, 57.4, 57.2, 57.0, 56.9, 56.8, 56.7, 56.6, 54.1, 53.8, 53.4, 51.8, 51.6, 48.3, 43.6, 40.3, 39.3, 38.2, 35.2, 30.6, 30.6, 29.7, 29.2, 28.3, 28.2, 27.9, 27.8, 27.7, 27.5, 27.3, 27.2, 26.7, 26.6, 26.6, 25.4, 25.0, 24.9, 24.8, 24.6, 24.2, 23.6, 23.5, 23.2, 23.2, 23.0, 22.9, 22.6, 21.9, 21.7, 21.0, 20.8, 19.3, 19.2, 19.1, 18.4, 18.3, 18.2, 17.9, 15.2. MALDI-TOF of **32-Nona**, analytical HPLC peak at (a) 11.3 min [Calc.

TH-3141_166122021

$(M+Na+H)^+$ for $C_{50}H_{91}N_9O_{12}$= 1033.6763 Da Obs. = 1033.411 Da] and (b) 12.7 min [Calc. $(M+Na+H)^+$ for $C_{50}H_{91}N_9O_{12}$= 1033.6763 Da Obs. = 1033.299 Da] (Appendix, Figures A61).

Boc-Leu-Aib-Val-Aib-γ^{4,4}-Aib-Leu-Aib-Val-OMe (33-Nona)

^{1}H NMR (600 MHz, Chloroform-*d*) (Appendix, Figure A62): δ 8.18 (s), 8.02 (s), 7.58 (s), 7.55 (s), 7.54-7.51 (br), 7.46 (d, *J* = 6.7 Hz), 7.39 (s), 7.29 (d, *J* = 8.4 Hz), 7.25 (d, *J*= 8.3), 7.12 (d, *J* = 5.4 Hz), 6.79 (s), 6.72 (s), 6.58 (s), 6.48 (s), 5.39 (s), 5.22 (s), 4.41 (ddd, *J* = 8.2, 6.2, 3.5 Hz), 4.25 – 4.19 (m), 4.12 (ddd, *J* = 11.2, 7.1, 4.4 Hz), 3.90 – 3.83 (m), 3.82-3.76 (m), 3.71 (s), 3.69 (s), 2.70 – 2.62 (m), 2.48 (dd, *J* = 15.5, 7.3 Hz), 2.28-2.16 (m), 1.90 – 1.77 (m), 1.69-1.60 (m), 1.59 – 1.56 (m), 1.54 – 1.48 (m), 1.48-1.43 (m), 1.33 (s), 1.31 (s), 1.20 (s), 1.16 (s), 1.03-0.95 (m), 0.93 – 0.89 (m). ^{13}C {^{1}H} NMR (150 MHz, Chloroform-*d*) (Appendix, Figure A68): δ 175.8, 175.6, 175.5, 172.6, 172.5, 172.0, 156.1, 80.8, 65.8, 61.9, 61.7, 58.2, 58.1, 57.3, 57.2, 57.1, 57.0, 56.9, 56.6, 56.5, 56.4, 55.5, 53.8, 53.7, 53.6, 53.2, 51.8, 51.7, 40.3, 39.4, 38.6, 34.7, 34.6, 31.0, 30.7, 30.7, 30.2, 29.6, 29.2, 28.3, 28.2, 27.9, 27.8, 27.6, 27.4, 27.4, 27.3, 27.2, 27.0, 26.8, 26.7, 25.6, 25.3, 25.0, 24.9, 24.8, 24.6, 24.6, 23.5, 23.5, 23.4, 23.4, 23.3, 23.2, 23.0, 22.6, 22.5, 21.9, 21.6, 21.1, 20.8, 19.3, 19.2, 19.1, 19.0, 18.8, 18.3, 18.3, 15.2. MALDI-TOF of **33-Nona**, analytical HPLC peak at (a) 10.9 min [Calc. $(M+Na+H)^+$ for $C_{50}H_{91}N_9O_{12}$= 1033.6763 Da Obs. = 1033.171 Da] and (b) 12.4 min [Calc. $(M+Na+H)^+$ for $C_{50}H_{91}N_9O_{12}$= 1033.6763 Da Obs. = 1033.145 Da.] (Appendix, Figures A62).

TH-3141_166122021

3B.2.4. Single crystal X-ray diffraction

Crystallization of all the peptide conformers was carried out primarily in the acetonitrile/H_2O system either from mixtures of conformations or HPLC separated fractions. For **31-Nona**, crystals were grown from a mixture of conformers in ACN/H_2O solvent system. More than one crystals could be grown for **32-Nona** and **33-Nona**. In case of **32-Nona** distinct crystals could be grown from the mixture of conformations in ACN/H_2O and ACN/MeOH/H_2O solvent systems. The third crystal for **32-Nona** was grown from the separated minor conformer fraction from ACN/H_2O solvent system. In case of **33-Nona** distinct crystals were grown from the mixture of conformers and minor conformer in ACN/H_2O solvent system. Data was collected at temperatures 105 K, 176 K and 297 K, respectively. One of the crystal structures of **32-Nona** (grown from a mixture in ACN/H_2O) could not be refined well. Table 3B.1 and 3B.2 provides the crystal and refinement parameters for all the peptide structures. Intensity data was collected with Mo-Kα radiation (λ = 0.71073 Å) by a Bruker (D8 Quest) diffractometer. Data processing and refinements were discussed in section 10.4.1.2. The crystal structures have been deposited at the Cambridge Crystallographic Data Centre (CCDC) with deposition numbers 2206582-2206586.

TH-3141_166122021

Table 3B.1. Crystal and refinement parameters of **31-Nona** and **32-Nona**.

Parameters	**31-Nona (Grown from mixture in ACN/H_2O)**	**32-Nona (Grown from mixture in ACN/MeOH/H_2O)**	**32-Nona (Grown from purified minor populant fraction in ACN/H_2O)**
Empirical formula	$C_{50}H_{91}N_9O_{12}.(0.3)H_2O$	$C_{50}H_{91}N_9O_{12}.H_2O$	$C_{50}H_{91}N_9O_{12}.2H_2O$
Formula weight	1015.7(1010.3 + 5.4)	1028.3(1010.3+18)	1046.3(1010.3+36)
Crystal system	Monoclinic	Orthorhombic	Monoclinic
Space group	$P2_1$	$P2_12_12_1$	$P2_1$
Unit cell dimension			
a (Å)	9.3367(19)	11.641(2)	9.8579(9)
b (Å)	16.196(3)	14.012(3)	28.342(3)
c (Å)	19.410(4)	38.099(7)	11.3098(11)
β(°)	102.916(6)	90	93.664(3)
V (Å)	2861.0(10)	6214(2)	3153.4(5)
Z	2	4	2
Temperature (K)	105(2)	297(2)	176(2)
Radiation	MoKα (λ = 0.71073Å)	MoKα (λ = 0.71073 Å)	MoKα (λ = 0.71073 Å)
2θ Max (°)	23.256	21.870	21.990
F (000)	1105	2232	1132
Measured reflection	64953	49926	54712
R_{int}	0.0700	0.0525	0.0752
Unique reflection	8194	7472	7610
Observed reflection |F| > 4σ (F)	6727	5096	6001
R factor	0.0860	0.0663	0.0910
wR_2	0.2170	0.1705	0.1528
Goodness-of-fit S	1.082	1.075	1.210
$\Delta\rho_{max}$ (e $Å^{-3}$)	0.388	0.652	0.254
$\Delta\rho_{min.}$ (e $Å^{-3}$)	-0.378	-0.190	-0.256
Shift/esd (max)	0.000	0.015	0.000
No. of restrains/parameter	1/650	0/649	1/658
Data to parameter ratio	10.33	7.85	9.12
Flack (x) value	-0.4 (5)	-0.4 (5)	-0.6 (5)

TH-3141_166122021

Table 3B.2. Crystal and refinement parameters of **33-Nona**.

Parameters	**33-Nona (Grown from mixture in ACN/H_2O)**	**33-Nona (Grown from purified second fraction in ACN/H_2O)**
Empirical formula	$C_{50}H_{91}N_9O_{12}.H_2O$	C_{50} $H_{91}N_9O_{12}$
Formula weight	1026.3(1010.3+ 18)	1010.3
Crystal system	Orthorhombic	Orthorhombic
Space group	$P2_12_12_1$	$P2_12_12_1$
Unit cell dimension		
a (Å)	9.122(2)	9.069 (1)
b (Å)	17.215(4)	17.630 (1)
c (Å)	38.990(9)	39.241(2)
β(°)	90	90
V (Å)	6123(2)	6273.7(7)
Z	4	4
Temperature (K)	105(2)	295(2)
Radiation	MoKα (λ = 0.71073 Å)	MoKα (λ = 0.71073Å)
2θ Max (°)	21.036	26.390
F (000)	2232	2200
Measured reflection	131184	200329
R_{int}	0.0604	0.0505
Unique reflection	6610	12824
Observed reflection |F| > 4σ (F)	6065	8590
R factor	0.0631	0.0491
wR_2	0.1764	0.1292
Goodness-of-fit S	1.033	1.106
$\Delta\rho_{max}$ (e $Å^{-3}$)	0.770	0.255
$\Delta\rho_{min.}$ (e $Å^{-3}$)	-0.399	-0.161
Shift/esd (max)	0.369	0.001
No. of restrains/parameter	1/651	1/ 641
Data to parameter ratio	9.31	13.40
Flack (x) value	0.1 (3)	-0.2 (2)

TH-3141_166122021

3B.2.5. NMR Spectroscopy

All NMR experiments were carried out on a Bruker Ascend Aeon 600 and 400 MHz spectrometer respectively. The peptide concentrations were in the range of 5-7 mM in $CDCl_3$ for both 1D and 2D NMR experiments. The chemical shift values and coupling constants were measured from 1D NMR spectra. Variable temperature 1D NMR experiments were carried out in between 273-323 K. Complete resonance assignments of the protons of (**31-33)-Nona** were done by TOCSY and ROESY experiments. All the 2D experiments were done in phase sensitive mode by using time-proportional phase incrementation (TPPI) method. For all peptides TOCSY spectra was recorded with a mixing time of 80 ms but for ROESY spectra three different mixing times of 150 (for **31-Nona)**, 250 (for **32-Nona)** and 300 ms (for **33-Nona)** were used respectively. The spectral width was 6009.6 Hz in both dimensions. The total number of scans were fixed to 32 for TOCSY and ROESY, respectively. Data points was set to 2048 and 300 in f2 and f1 dimensions, respectively for both TOCSY and ROESY spectra. Zero filling was done to finally yield a data set of 4K x 2K. All NMR spectra were processed using Topspin 3.6 software.

3B.2.6. FT-IR Spectroscopy

FT-IR spectra of all peptides (**31-33)-None** were recorded in $CDCl_3$ solution at 1 mM concentration. Experimental detail is given in section 10.4.2.3.

TH-3141_166122021

3B.2.7. Electronic Structure Calculations

2D NMR experiments confirmed that the peptides (**31-33**)-Nona are helical and have two distinct conformations. DMSO-d_6 titration experiments also highlighted the backbone NH's that are solvent-exposed. However, the structure of the one conformer could not be crystalized. To gain insight into the structures we performed computational modelling. Using the experimental data as input, we modelled helical peptides in PyMOL software[297] and subjected those models to geometry optimization using Gaussian 16 program[298] employing density functional theory (B3LYP/6-311++G* level).[299,300,313] Calculations also included normal mode frequency calculations to identify the nature of the structures in the energy hypersurface.

3B.3. Results and Discussion

Peptides (**31-33)-Nona** (Figure 3B.1) were synthesized using the standard solution phase synthesis strategy (Scheme 3B.1), purified using HPLC and characterized using analytical HPLC (Figure 3B.2), MALDI-TOF (Appendix, Figures A60-A62), ^{1}H NMR (600 MHz) and ^{13}C (600 MHz) (Appendix, Figures A63-A68). It should be noted that all the ^{1}H NMR spectra of (**31-33)** showed the presence of water peaks (Appendix, Figures A63-A65), indicating its presence in solution.

3B.3.1. Analytical HPLC

Upon performing analytical HPLC using ACN/H_2O solvent system, all the peptides (**31-33)-Nona** gave rise to two peaks each, in their respective chromatograms (Figure 3B.2). Table 3B.3 summarizes the retention time of the peaks that appeared in the chromatogram. MALDI-MS, performed to ascertain the chemical identity of the eluents, indicated identical molecular mass of the components obtained from the two peaks for all of the peptides (Appendix, Figures A60-A62, Table 3B.1, 3B.2). This ruled out the possibility of the presence of impurities and suggested that the peaks were either conformers or diastereomers of (**31-33)-Nona**. The area

TH-3141_166122021

under the peaks for the peptides **31-Nona**, **32-Nona** and **33-Nona** were in the ratios of ~ 6:4, 7:3 and 1:1 respectively.

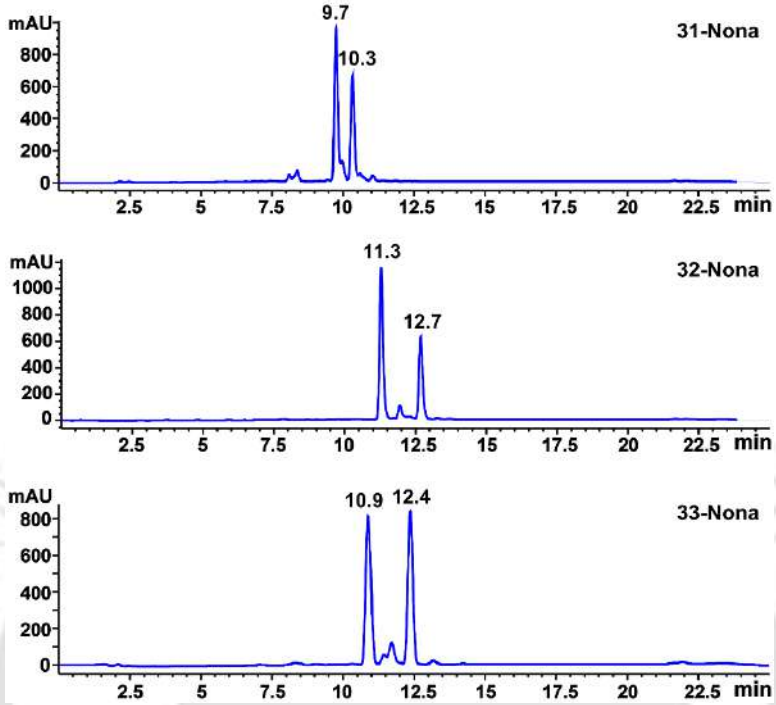

Figure 3B.2. Analytical HPLC trace of (**31-33)-Nona** showing the presence of two populants in solution. The populants of (**31-33)-Nona** are present in the ratios of ~ 60:40, 70:30, and 50:50 respectively.

Table 3B.3. Retention times of the peaks obtained in Analytical HPLC for (**31-33)-Nona**.

Peptides	**Retention time (s)**		**Ratio of the peak area**
	Peak 1	**Peak 2**	
31-Nona	9.7	10.3	60:40
32-Nona	11.3	12.7	70:30
33-Nona	10.9	12.4	50:50

TH-3141_166122021

3B.3.2. Confirmation of the presence of multiple conformations in solution for (31-33)-Nona

3B.3.2.1. 1D ^{1}H NMR

Figure 3B.3 shows the stacked plots of the NH region of 600 MHz ^{1}H NMR spectra of the peptides (**31-33)-Nona**. Surprisingly for all of the peptides, two sets of lines were clearly visible in the spectrum. Complete annotation of the NMR signals was performed using 2D NMR techniques like TOCSY (Appendix, Figures A69-A71) and ROESY (Appendix, Figures A72-A74). Chemical shifts of all the signals from the two sets of lines have been tabulated (Tables 3B.4-3B.9). The ratios of the line intensities for the two sets of lines were 6:4, 7:3 and ~1:1 for **31-Nona**, **32-Nona** and **33-Nona** respectively, which were similar to the ratios of the area under the peaks obtained in analytical HPLC earlier. This suggested that the purified peptides were a mixture of two distinct species in solution which could either be diastereomers or conformers. Both sets of lines in the spectra were completely well dispersed for each peptide (**31-33)-Nona**, which indicated a well folded structure for the peptides.

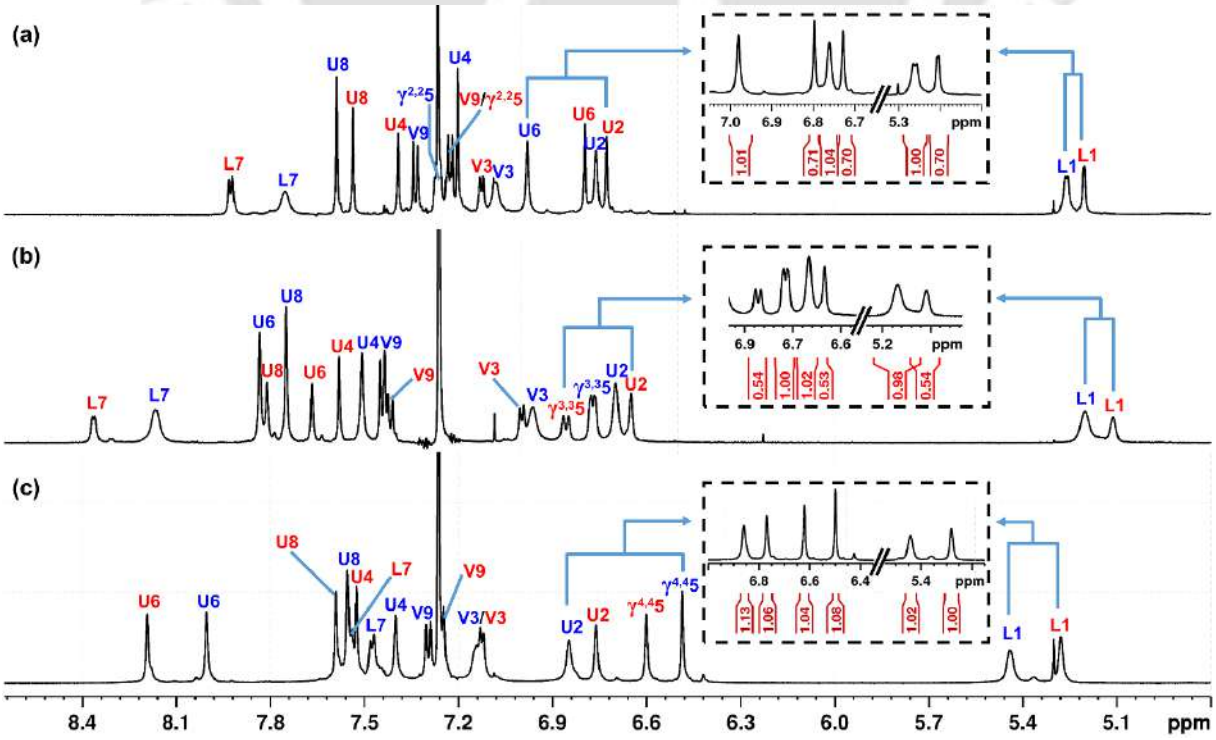

TH-3141_166122021

Figure 3B.3. Partial 1D ^{1}H NMR spectra representing the amide proton resonances of (a) **31-Nona**, (b) **32-Nona**, and (c) **33-Nona** in $CDCl_3$. Two distinct sets of lines (labelled in red and blue) are present in all the three peptides. The integration of the NH signals corresponding to the ratio of the two conformers are highlighted in the dotted box. The intensities for the two sets of lines for (**31-33)-Nona** are in the ratio of ~ 60:40, 70:30 and 50:50 respectively.

Table 3B.4. Characteristic ^{1}H parameters for the major conformer of **31-Nona** in $CDCl_3$.

Residues	Chemical Shift (ppm)					
	NH	$C^{\alpha}H$	$C^{\beta}H$	$C^{\gamma}H$	$C^{\delta}H$	$^{3}J_{NH\text{-}C^{\alpha}H}$ (Hz)
Leu (1)	5.28	3.83	1.64	1.65	0.99	5.0
Aib (2)	6.79	-	1.52	-	-	-
Val (3)	7.09	3.78	2.3	1.02	-	5.7
Aib (4)	7.21	-	1.47	-	-	-
$\gamma^{2,2}$ (5)	7.26	-	1.81	3.19, 3.07	-	-
Aib (6)	6.98	-	1.53	-	-	-
Leu (7)	7.76	3.96	1.78	1.79	0.94	5.7
Aib (8)	7.59	-	1.58	-	-	-
Val (9)	7.33	4.39	2.2	0.96	-	8.2

Table 3B.5. Characteristic ^{1}H parameters for the minor conformer of **31-Nona** in $CDCl_3$.

Residues	Chemical Shift (ppm)					
	NH	$C^{\alpha}H$	$C^{\beta}H$	$C^{\gamma}H$	$C^{\delta}H$	$^{3}J_{NH\text{-}C^{\alpha}H}$ (Hz)
Leu (1)	5.23	3.83	1.67	1.67	0.99	-
Aib (2)	6.75	-	1.47	-	-	-
Val (3)	7.12	3.90	2.2	1.04	-	6.0
Aib (4)	7.40	-	1.43	-	-	-
$\gamma^{2,2}$ (5)	7.23	-	1.88, 1.78	3.25, 3.02	-	-
Aib (6)	6.80	-	1.54	-	-	-
Leu (7)	7.92	4.27	1.61	1.61	0.91	6.3
Aib (8)	7.54	-	1.58	-	-	-
Val (9)	7.23	4.40	2.2	0.96	-	8.5

TH-3141_166122021

Table 3B.6. Characteristic ^{1}H parameters for the major conformer of **32-Nona** in $CDCl_3$.

Residues	Chemical Shift (ppm)					
	NH	$C^{\alpha}H$	$C^{\beta}H$	$C^{\gamma}H$	$C^{\delta}H$	$^{3}J_{NH\text{-}C\alpha H}$ (Hz)
Leu (1)	5.22	3.84	1.66	1.48	0.99	-
Aib (2)	6.75	-	1.51	-	-	-
Val (3)	5.97	3.88	2.31	1.03	-	5.8
Aib (4)	7.51	-	1.51	-	-	-
$\gamma^{3,3}$ (5)	6.77	2.26, 1.96	-	3.54, 2.74	-	-
Aib (6)	7.84	-	1.49	-	-	-
Leu (7)	8.17	3.99	1.89, 1.85	1.71	0.99	5.2
Aib (8)	7.75	-	1.58	-	-	-
Val (9)	7.44	4.40	2.22	1.01	-	8.7

Table 3B.7. Characteristic ^{1}H parameters for the minor conformer of **32-Nona** in $CDCl_3$.

Residues	Chemical Shift (ppm)					
	NH	$C^{\alpha}H$	$C^{\beta}H$	$C^{\gamma}H$	$C^{\delta}H$	$^{3}J_{NH\text{-}C\alpha H}$ (Hz)
Leu (1)	5.21	3.88	1.65, 1.75	1.53	1.01	-
Aib (2)	6.71	-	1.46, 1.53	-	-	-
Val (3)	7.04	4.02	2.29	1.05	-	6.5
Aib (4)	7.62	-	1.47, 1.55	-	-	-
$\gamma^{3,3}$ (5)	6.93	1.95, 2.34	-	2.56, 3.76	-	-
Aib (6)	7.72	-	1.47, 1.52	-	-	-
Leu (7)	8.36	4.21	1.82, 1.95	1.82	0.94	5.0
Aib (8)	7.84	-	1.50, 1.60	-	-	-
Val (9)	7.42	4.43	2.27	0.99	-	8.8

TH-3141_166122021

Table 3B.8. Characteristic ^{1}H parameters for the 1st conformer of **33-Nona** in $CDCl_3$.

Residues	Chemical Shift (ppm)					
	NH	$C^{\alpha}H$	$C^{\beta}H$	$C^{\gamma}H$	$C^{\delta}H$	$^{3}J_{NH\text{-}C\alpha H}$ (Hz)
Leu (1)	5.22	3.86	1.65, 1.52,	1.52	0.99	5.4
Aib (2)	6.72	-	1.44	-	-	-
Val (3)	7.12	3.90	2.21	1.02	-	5.4
Aib (4)	7.39	-	1.48	-	-	-
$\gamma^{4,4}$ (5)	6.48	2.26	2.48, 2.26	-	-	-
Aib (6)	8.02	-	1.50	-	-	-
Leu (7)	7.46	4.12	1.83	1.68	0.93	6.7
Aib (8)	7.55	-	1.56	-	-	-
Val (9)	7.29	4.41	2.24	0.98	-	8.4

Table 3B.9. Characteristic ^{1}H parameters for the 2nd conformer of **33-Nona** in $CDCl_3$.

Residues	Chemical Shift (ppm)					
	NH	$C^{\alpha}H$	$C^{\beta}H$	$C^{\gamma}H$	$C^{\delta}H$	$^{3}J_{NH\text{-}C\alpha H}$ (Hz)
Leu (1)	5.39	5.41	1.67	1.67	0.99	--
Aib (2)	6.79	-	1.49	-	-	-
Val (3)	7.12	3.81	2.20	1.02	-	5.4
Aib (4)	7.52	-	1.44, 1.53	-	-	-
$\gamma^{4,4}$ (5)	6.58	-	2.69, 2.25	2.25	-	-
Aib (6)	8.18	-	1.46, 1.56	-	-	-
Leu (7)	7.53	4.23	1.85	1.85	0.92	7.1
Aib (8)	7.58	-	1.48, 1.58	-	-	-
Val (9)	7.25	4.41	2.24	0.99	-	8.3

3B.3.3.2. Variable temperature NMR

In order to determine the effect of temperature on the population of the species observed for (**31-33)-Nona** in solution, we performed variable temperature NMR experiments. Upon heating/cooling the rate of interconversion of the conformers become faster/slower, thereby altering the appearance of the signals.[311] Figures 3B.4-3B.6 show the NH region of the ^{1}H NMR spectra recorded at variable temperatures in the range of 273-323 K for (**31-33)-Nona** respectively. For all the three peptides, both the chemical shifts of the signals and the

TH-3141_166122021

appearance of the spectral lines changed upon varying the temperature. There was a general upfield shift of the NH resonances, owing to the breakdown in the hydrogen bonds, upon increasing in the temperature suggesting a well-formed secondary structure of the peptides in solution. Interestingly, few of the NMR peaks from the same protons in the two populants came closer and finally merged at higher temperatures. In **31-Nona** (Figure 3B.4), a clear merging of the Aib (2) and Aib (8) NH resonances were seen upon increasing the temperature. In the case of **33-Nona**, some of the lines came closer [set of $\gamma^{4,4}$ (5) lines], broadened [set of Aib (2) lines] and eventually coalesced [set of Val (3) lines] (Figure 3B.6, marked protons) upon increasing the temperature. Such change in the line widths, and coalescing of the NH signals of two different populants suggested that the populants must be in exchange with each other. Observation of two sets of lines at room temperature indicated that the rate of interconversion in between the different conformers was slow at room temperature compared to the NMR timescale. This slow interconversion in turn indicated that the conformations were separated by a large activation barrier in the energy landscape. Hence it might be concluded from the above experiment that each of the peptides (**31-33)-Nona** existed as two distinct conformers at room temperature, as reported earlier in related studies.[213] The populations of the two conformers of **31-Nona**, **32-Nona** and **33-Nona** were 60:40, 70:30 and 53:47 respectively (Figure 3B.3) in solution. As everything else in (**31-33)-Nona** were identical except the constituent γ amino acid residue in question, the differential population of the conformers of (**31-33)** in solution seemed to be controlled by the variable position of the backbone di-substitution in the γ amino acid residues.

TH-3141_166122021

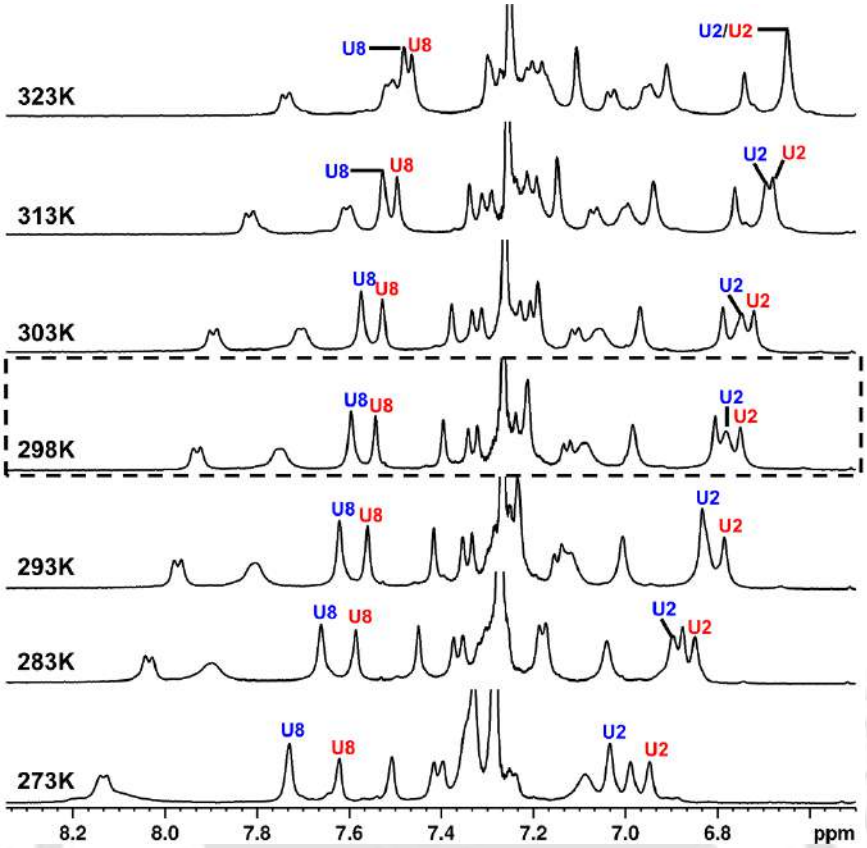

Figure 3B.4. Temperature dependence of NH resonances of **31-Nona** in $CDCl_3$. The NH signals marked as blue & red approach closer/eventually merge together with increasing temperature.

TH-3141_166122021

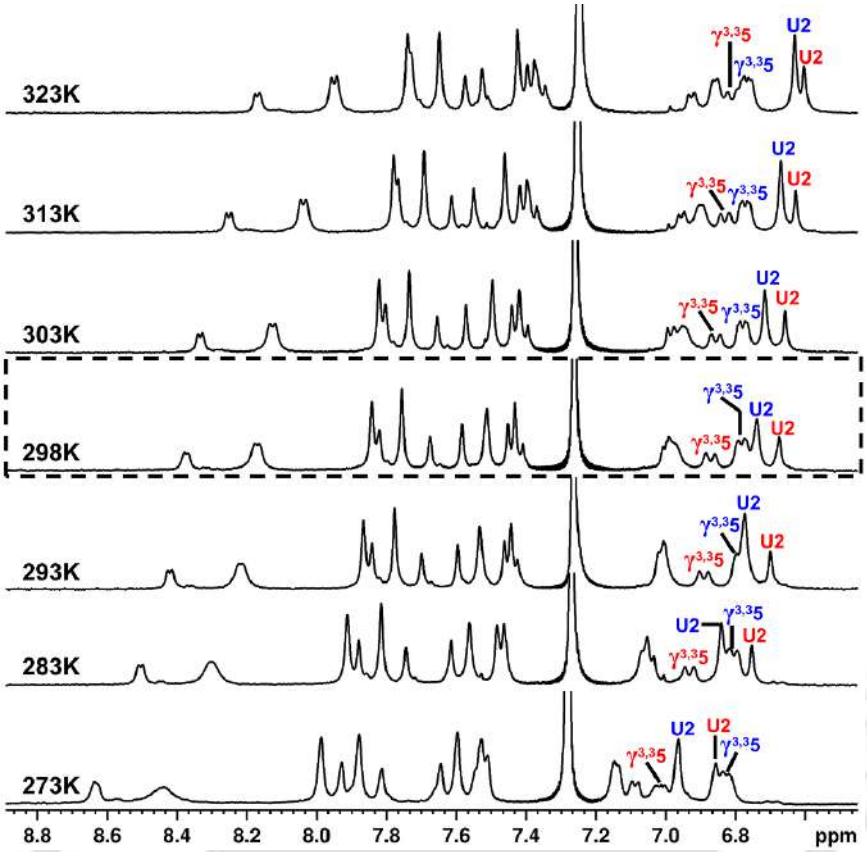

Figure 3B.5. Temperature dependence of NH resonances of **32-Nona** in $CDCl_3$. The NH signals marked as blue & red approach closer with increasing temperature.

TH-3141_166122021

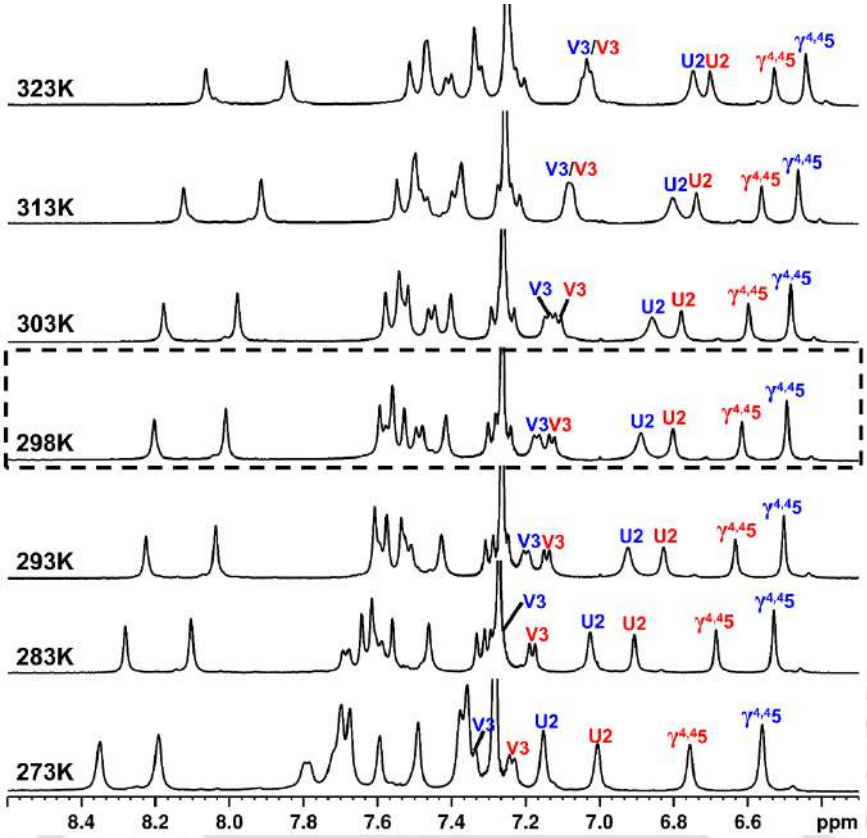

Figure 3B.6. Temperature dependence of NH resonances of **33-Nona** in $CDCl_3$. The NH signals marked as blue & red approach closer with increasing temperature.

3B.3.3. Molecular conformations of (31-33)-Nona in crystals

The molecular conformation of the nonapeptides (**31-33)-Nona** are shown in Figure 3B.7. The values of the backbone torsion angles are listed in Table 3B.10 and the hydrogen bond parameters are listed in Table 3B.11. Peptides **32-Nona** and **33-Nona** generated multiple polymorphic crystals depending on the process of crystallization, which had different conformations.

All the peptides adopted helical conformations. The backbone conformation of γ amino acid residues are defined by four torsion angles, ϕ (C0'-N1-C^{γ}-C^{β}), θ_1 (N1-C^{γ}-C^{β}-C^{α}), θ_2 (C^{γ}-C^{β}-C^{α}-C') and ψ (C^{β}-C^{α}-C'-N2). The dimethyl substitution at the C^{α}, C^{β} and C^{γ} atoms promoted

TH-3141_166122021

gauche conformation about the flanking single bonds in the α/β/γ-di-substituted γ amino acid residues ($\gamma^{2,2}$, $\gamma^{3,3}$, $\gamma^{4,4}$), as evidenced from Table 3B.10. The remaining two dihedral angles showed torsion angle values close to 90° or 180°.

31-Nona crystals were obtained from a mixture of the two conformers in ACN/H_2O solvent system. **31-Nona** adopted an ambidextrous helical conformation, stabilized by five 10-atom hydrogen bonds (C_{10}) (Figure 3B.7a). A reversal of the handedness of the helix was observed at the middle of the helix, near the $\gamma^{2,2}$ residue. Inspection of the ϕ, ψ values in Table 3B.10 showed that amino acid residues 1-4 and 5-9 adopted positive and negative values of ϕ/ψ respectively, suggesting that **31-Nona** adopted left-handedness at the N-terminus and right-handedness at the C-terminus. The $\gamma^{2,2}$ amino acid residue showed a folded conformation with both ϕ and ψ adopting negative values (right-handed helical conformation), while θ_1 and θ_2 corresponded to *gauche* + (*g*+) conformation. The combination of signs of the torsion angles of $\gamma^{2,2}$ was similar to that previously reported for the C_9 and C_{12} helical turns in Gpn/$\gamma^{3,3}$ amino acid containing peptides.[133,215] However, the $\gamma^{2,2}$ amino acid residue formed neither C_9 or C_{12} hydrogen bonds in **31-Nona**. The reversal of handedness in the peptide helix was induced by the insertion of a water molecule near the $\gamma^{2,2}$ residue that formed hydrogen bonds to Aib (4) CO and Leu (7) NH, which otherwise might have formed a γα C_{12} hydrogen bond. It is mention-worthy that this is the first report of accommodation of $\gamma^{2,2}$ amino acid residues in an overall helical conformation. Aib (6) NH forms an intermolecular hydrogen bond to Val (3) CO of a neighboring molecule in the crystal lattice (Table 3B.11).

32-Nona, containing $\gamma^{3,3}$ showed three different conformations in its polymorphic crystals. (a) **32-Nona** crystallized from the mixture of the two conformers in ACN/MeOH/H_2O led to orthorhombic crystals, wherein it adopted a left-handed helical conformation, with reversal of handedness of the terminal amino acid residues [Leu (1) and Val (9)], as compared to the rest

TH-3141_166122021

of the helix (Figure 3B.7b). The peptide was stabilized by six two residue hydrogen bonds: four C_{10} hydrogen bonds (two each at N- and C-termini) and two C_{12} hydrogen bonds in the centre (Figure 3B.7b). The first hydrogen bond in between the Val (3) NH and Boc (0) CO was obliterated by the N-terminal reversal in handedness.

(b) The monoclinic **32-Nona** polymorph grown from the minor peak isolated from the preparative HPLC in ACN/H_2O, adopted a right-handed 13/12/10 helix. It was stabilized by six intramolecular N-H...O hydrogen bonds: two C_{13}'s at the N-terminus, two central $\alpha\gamma/\gamma\alpha$ C_{12}'s and two C_{10}'s at the C-terminal (Figure 3B.7c). The combination of ϕ, θ_1, θ_2 and ψ for the $\gamma^{3,3}$-amino acid residue was -++-, with θ_1 and θ_2 adopting *g*+ conformations. Both ϕ and ψ adopted values around ~ -120° which was earlier reported for C_{12} helical conformations of $\gamma^{3,3}$/Gpn.[5, 22] (Table 3B.10). However, no reversal of handedness is observed in this case.

(c) **32-Nona** was also crystallized from the mixture of two conformers in ACN/H_2O. However, due to weak X-ray diffraction from this crystal, a well-refined structure could not be obtained. Preliminary structure calculation from this data showed that **32-Nona** in this case, adopted an ambidextrous helical (Figure 3B.8) structure similar to that observed for **31-Nona** (Figure 3B.7a) with small differences like: (i) The $\gamma^{3,3}$ amino acid residue adopted left-handed helical conformation in **32-Nona** unlike right-handed conformation adopted by $\gamma^{2,2}$ residue in **31-Nona**. (ii) An isolated one residue C_9 hydrogen bond was formed in between Aib (4) CO and Aib (6) NH across the central $\gamma^{3,3}$ amino acid residue, unlike **31-Nona**. The combination of the signs of torsion angles of $\gamma^{3,3}$ amino acid residue was (+--+), which was exactly a opposite (being left-handed helical) to that observed for Gpn in right handed C_9 helical conformation.[215]

33-Nona adopted both left and right-handed 10/12 helical conformations stabilized by a continuous stretch of two residue backbone N-H…O hydrogen bonds in two different crystals. (a) In the crystal grown from the mixture of two conformers in ACN/H_2O, the peptide formed

TH-3141_166122021

left-handed helix as evidenced from the sign of backbone torsion angles listed in Table 3B.10. In this case, the C-terminal L-Val (9) residue showed a reversal in handedness and adopted a right-handed helical conformation (Figure 3B.7d). Leu (1) at the N-terminus remained in left-handed helical conformation, due to an intermolecular hydrogen bond in between Leu (1) NH of one molecule to the Aib (8) CO of another molecule (Table 3B.11). The structure was stabilized by seven intramolecular hydrogen bonds: Five C_{10} hydrogen bonds (N- and C-termini) and two central C_{12} hydrogen bonds across the αγ/γα segments. (b) In the other crystal for **33-Nona**, grown from the later eluting HPLC fraction (retention time 12.4 min), the peptide adopted a right-handed 10/12 helical conformation, with no reversal of handedness at the helix termini. This structure was also stabilized by a total of seven hydrogen bonds, 5 C_{10}'s and two C_{12}'s. The backbone dihedral angles of the $\gamma^{4,4}$ amino acid residue adopted an usual (++-+) and (--+-) combination in the left and right handed C_{12} helical conformations respectively, as was earlier reported by Gopi and co-workers.[221] Both the structures obtained for **33-Nona** were enantiomeric to each other (in the middle stretch), except at the C-terminal Val (9) residue.

TH-3141_166122021

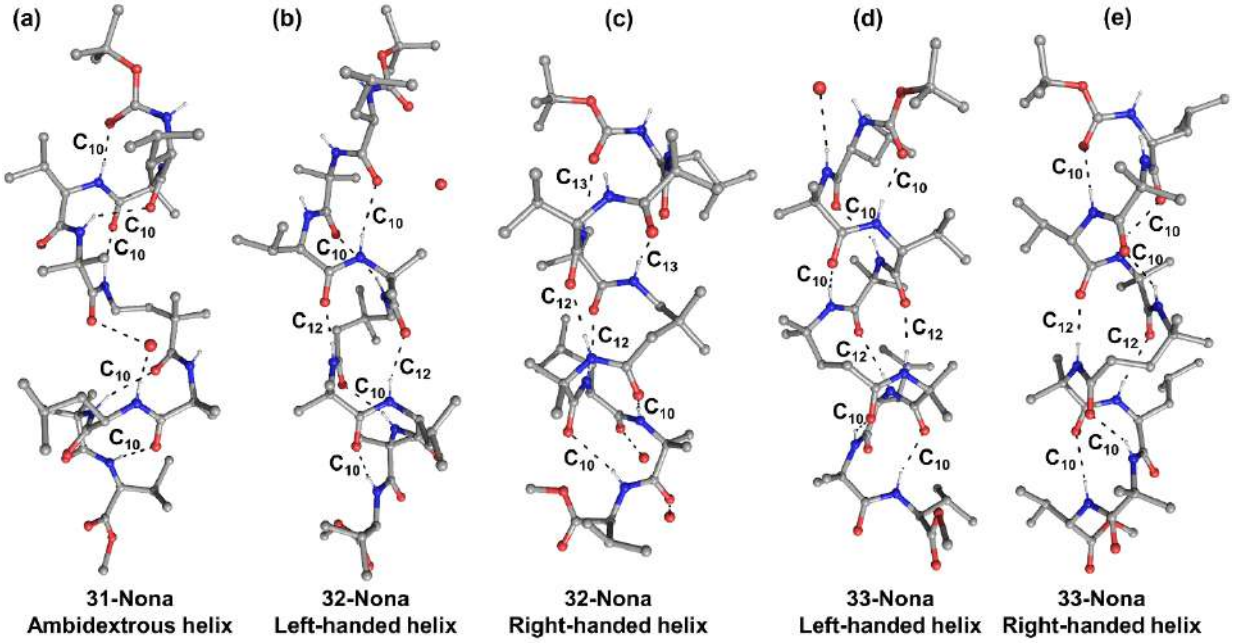

Figure 3B.7. Conformations in crystals of (a) **31-Nona**, (b, c) **32-Nona** and (d, e) **33**-Nona (a) **31-Nona** forms an ambidextrous helix with left handedness in the N-terminal (Res 1-4) and right-handedness at the C-terminal (Res 5-9). A centrally recruited water molecule (red sphere) mediated intramolecular hydrogen bond involving Leu (7) NH and Aib (4) CO, induces the reversal of handedness. It is stabilized by C_{10} hydrogen bonds. **32-Nona** forms both (b) left-handed 10/12 helix and (c) right-handed 13/12/10 helix. **33-Nona** also forms both (d) left-handed and (e) right-handed 10/12 helix. The water molecules shown in b, c and d, do not participate in intramolecular hydrogen bonds.

TH-3141_166122021

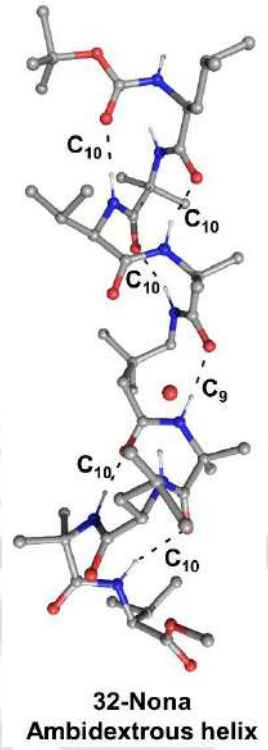

Figure 3B.8. Molecular conformation of **32-Nona** in crystals grown from a mixture in ACN/H_2O.

Table 3B.10. Backbone dihedral angles of the various conformations for peptides (**31-33)-Nona** obtained in crystals and from DFT calculations (in parentheses). AH: Ambidextrous Helix, LHH: Left- handed Helix, RHH: Right-handed Helix.

Peptide	Amino Acid Residue	ϕ (°)	θ_1 (°)	θ_2 (°)	ψ (°)
31-Nona (AH)	Leu (1)	66.8 (67.3)			27.1 (25.7)
	Aib (2)	49.3 (55.1)			37.9 (29.7)
	Val (3)	54.6 (61.2)			39.6 (25.1)
	Aib (4)	69.6 (59.7)			4.8 (24.4)
	$\gamma^{2,2}$ (5)	-117.2 (-125.9)	75.0 (93.0)	61.5 (72.0)	-166.6 (-135.5)
	Aib (6)	-58.3 (-56.1)			-36.9 (-39.2)
	Leu (7)	-61.4 (-70.8)			-26.1 (-5.0)
	Aib (8)	-59.9 (-58.0)			-31.8 (-27.7)
	Val (9)	-78.2 (-117.4)			170.4 (163.9)
31-Nona (RHH)	Leu (1)	(-73.2)			(-19.7)
	Aib (2)	(-55.0)			(-28.2)
	Val (3)	(-60.5)			(-26.7)
	Aib (4)	(-58.0)			(-27.9)

TH-3141_166122021

	$\gamma^{2,2}$ (5)	(-84.0)	(161.3)	(-62.1)	(-54.6)
	Aib (6)	(-56.3)			(-37.7)
	Leu (7)	(-61.0)			(-22.1)
	Aib (8)	(-66.9)			(-23.3)
	Val (9)	(-103.3)			(2.2)
32-Nona (AH)	Leu (1)	60.7 (68.1)			27.8 (22.0)
	Aib (2)	50.8 (54.4)			27.1 (29.8)
	Val (3)	67.3 (68.0)			10.7 (9.0)
	Aib (4)	53.0 (52.6)			29.4 (40.9)
	$\gamma^{3,3}$ (5)	99.3 (107.3)	-64.1 (-59.3)	-79.3 (-81.5)	85.0 (75.9)
	Aib (6)	-56.1 (-54.1)			-35.6 (-35.6)
	Leu (7)	-66.9 (-76.2)			-11.8 (-3.9)
	Aib (8)	-54.4 (-66.7)			-35.3 (-24.8)
	Val (9)	-127.2 (-105.4)			15.4 (-1.7)
32-Nona (LHH)	Leu (1)	-74.4 (-105.7)			-34.6 (-0.9)
	Aib (2)	58.3 (61.5)			41.7 (28.0)
	Val (3)	62.7 (72.0)			14.4 (6.4)
	Aib (4)	52.2 (56.7)			40.8 (34.9)
	$\gamma^{3,3}$ (5)	135.5 (125.1)	-57.4 (-54.3)	-54.6 (-58.0)	112.7 (124.6)
	Aib (6)	53.2 (57.7)			40.6 (33.9)
	Leu (7)	63.2 (59.4)			11.1 (19.8)
	Aib (8)	46.9 (60.0)			39.9 (26.9)
	Val (9)	-57.8 (-69.5)			-38.7 (-24.2)
32-Nona (RHH)	Leu (1)	-59.8 (-66.0)			-38.6 (-33.4)
	Aib (2)	-51.2 (-57.8)			-37.8 (-31.9)
	Val (3)	-92.3 (-93.3)			-46.0 (-42.4)
	Aib (4)	-57.1 (-57.8)			-37.4 (-39.1)
	$\gamma^{3,3}$ (5)	-124.8 (-121.3)	55.0 (54.4)	56.5 (59.2)	-117.0 (-123.9)
	Aib (6)	-51.2 (-56.8)			-43.7 (-35.3)
	Leu (7)	-74.9 (-73.4)			-7.5 (-3.4)
	Aib (8)	-59.7 (-63.9)			-31.8 (-27.1)
	Val9	-127.2 (-106.8)			-14.8 (0.0)
33-Nona (LHH)	Leu (1)	63.9 (66.7)			19.3 (27.0)
	Aib (2)	48.9 (55.1)			35.0 (28.4)
	Val (3)	60.9 (62.9)			29.3 (21.9)
	Aib (4)	56.4 (56.3)			38.0 (34.8)
	$\gamma^{4,4}$ (5)	55.4 (52.4)	53.0 (51.9)	-142.0 (-138.5)	110.1 (115.3)
	Aib (6)	51.1 (56.8)			33.2 (30.3)
	Leu (7)	56.6 (58.0)			32.0 (24.3)
	Aib (8)	68.9 (62.7)			11.1 (25.7)
	Val (9)	-84.5 (-101.3)			-51.1 (-44.5)
33-Nona (RHH)	Leu (1)	-62.8 (-72.9)			-20.7 (-20.3)
	Aib (2)	-48.6 (-54.7)			-34.7 (-28.4)
	Val (3)	-61.9 (-62.5)			-27.0 (-23.6)

	Aib (4)	-54.5 (-57.5)			-39.7 (-34.3)
	$\gamma^{4,4}$ (5)	-54.7 (-54.4)	-51.6 (-54.3)	142.8 (143.5)	-103.6 (-109.8)
	Aib (6)	-53.8 (-57.0)			-34.7 (-32.4)
	Leu (7)	-65.6 (-70.9)			-16.9 (-8.8)
	Aib (8)	-62.3 (-63.8)			-22.2 (-22.5)
	Val (9)	-58.2 (-93.7)			133.7 (-50.2)

Table 3B.11. Intramolecular and intermolecular hydrogen bond parameters from various conformations of (**31-33)-Nona** obtained in crystals and DFT studies (mentioned in parentheses). AH: Ambidextrous Helix, LHH: Left Handed Helix, RHH: Right-handed Helix.

Peptide	H-bonded ring size	H-Bonds	D....A (Å)	H....A (Å)	∠ D-H....A (°)
31-Nona (AH)	Intermolecular				
		N1—H1….O7[a]	2.85	1.98	170.3
		N2—H2….O8[a]	3.24	2.51	140.3
		N6—H6….O3[b]	3.12	2.29	157.4
		N7—H7….O1W	2.92 (3.0)	2.14 (2.0)	148.3 (167.3)
		O6….O1W	3.23		
		O4….O1W	(2.7)	(1.7)	(177.1)
	Intramolecular				
	C_{10}	N3—H3….O0	3.03 (3.3)	2.21 (2.3)	155.7 (173.1)
	C_{10}	N4—H4….O1	3.03 (3.2)	2.31 (2.2)	138.6 (168.0)
	C_{10}	N5—H5….O2	3.01 (3.1)	2.16 (2.1)	162.1 (162.6)
	C_{10}	N8—H8….O5	3.21 (3.2)	2.38 (2.2)	157.1 (165.7)
	C_{10}	N9—H9….O6	3.24 (3.2)	2.36 (2.2)	173.3 (167.4)
31-Nona (RHH)	C_{10}	N3—H3….O0	(3.4)	(2.4)	(172.8)
	C_{10}	N4—H4….O1	(3.1)	(2.1)	(167.2)
	C_{10}	N5—H5….O2	(3.1)	(2.1)	(163.9)
	C_{12}	N7—H7….O4	(2.9)	(2.0)	(159.3)
	C_{10}	N8—H8….O5	(3.3)	(2.3)	(166.7)
	C_{10}	N9—H9….O6	(3.3)	(2.3)	(170.1)
32-Nona (AH)	C_{10}	N3—H3….O0	2.94 (3.4)	1.96 (2.4)	173.9 (177.8)
	C_{10}	N4—H4….O1	2.92 (3.1)	1.96 (2.1)	164.6 (169.8)
	C_{10}	N5—H5….O2	2.98 (3.3)	2.02 (2.3)	164.5 (165.1)
		O3….O1W	4.05 (3.0)	4.11 (2.1)	79.7 (150.9)
		O4….O1W	2.96 (3.0)	2.61 (2.1)	101.2 (154.2)
		N7….O1W	2.99 (3.1)	2.03 (2.1)	165.0 (166.9)
	C_9	N6—H6….O4	2.82 (3.0)	1.85 (2.0)	169.8 (171.9)
	C_{10}	N8—H8….O5	2.87 (3.2)	1.92 (2.2)	161.7 (166.2)
	C_{10}	N9—H9….O6	3.22 (3.5)	2.28 (2.5)	157.6 (168.2)
32-Nona (LHH)	Intermolecular				
		N1—H1….O7[c]	3.14	2.31	164.2
		N2— H2….O8[c]	3.03	2.19	167.4

TH-3141_166122021

	Intramolecular				
	C_{10}	N4—H4….O1	3.13 (3.1)	2.28 (2.1)	168.9 (168.0)
	C_{10}	N5—H5….O2	3.43 (3.7)	2.60 (2.7)	163.3 (167.1)
	C_{12}	N6—H6….O3	2.88 (3.1)	2.02 (2.1)	173.0 (169.1)
	C_{12}	N7—H7….O4	2.94 (3.0)	2.12 (2.0)	158.4 (159.5)
	C_{10}	N8—H8….O5	2.99 (3.2)	2.16 (2.2)	160.7 (169.3)
	C_{10}	N9—H9….O6	3.09 (3.2)	2.25 (2.2)	165.1 (173.4)
32-Nona (RHH)	Intermolecular				
		N1—H1….O2W[d]	3.24	2.37	169.6
		N2—H2….O1W[d]	2.97	2.21	144.5
		N3—H3….O0	3.16 (3.18)	2.45 (2.23)	139.0 (156.8)
	Intramolecular				
	C_{13}	N4—H4….O0	2.94 (3.3)	2.07 (2.3)	171.6 (170.8)
	C_{13}	N5—H5….O1	3.00 (3.3)	2.14 (2.3)	162.4 (164.7)
	C_{12}	N6—H6….O3	2.92 (3.1)	2.04 (2.1)	173.6 (171.0)
	C_{12}	N7— H7….O4	2.90 (3.0)	2.05 (2.1)	162.0 (166.8)
	C_{10}	N8—H8….O5	3.05 (3.1)	2.21 (2.2)	159.9 (166.8)
	C_{10}	N9—H9….O6	3.35 (3.4)	2.49 (2.4)	166.4 (169.1)
33-Nona (LHH)	Intermolecular				
		N1—H1….O8[e]	2.82	1.97	160.9
		N2—H2….O1w	3.28	2.40	171.9
	Intramolecular				
	C_{10}	N3—H3….O0	2.95 (3.3)	2.09 (2.3)	167.8 (172.9)
	C_{10}	N4— H4….O1	2.93 (3.1)	2.14 (2.1)	149.3 (168.1)
	C_{10}	N5— H5….O2	3.15 (3.3)	2.39 (2.3)	145.5 (162.8)
	C_{12}	N6—H6 ….O3	2.87 (3.1)	2.01 (2.0)	165.6 (171.9)
	C_{12}	N7—H7….O4	2.97 (3.2)	2.16 (2.2)	152.5 (156.3)
	C_{10}	N8—H8….O5	3.01 (3.2)	2.21 (2.2)	150.5 (168.6)
	C_{10}	N9—H9….O6	2.96 (3.2)	2.10 (2.2)	163.8 (167.6)
33-Nona (RHH)	Intermolecular				
		N1—H1….O8[f]	2.86	2.00	172.5
		N2—H2….O9[f]	3.08	2.31	148.6
	Intramolecular				
	C_{10}	N3—H3….O0	3.05 (3.4)	2.21 (2.4)	164.8 (172.4)
	C_{10}	N4—H4….O1	2.90 (3.1)	2.11 (2.1)	151.8 (167.3)
	C_{10}	N5—H5….O2	3.19 (3.3)	2.43 (2.4)	147.2 (162.3)
	C_{12}	N6—H6….O3	2.91 (3.0)	2.05 (2.0)	170.9 (173.6)
	C_{12}	N7—H7….O4	3.19 (3.6)	2.35 (2.7)	164.2 (163.8)
	C_{10}	N8—H8….O5	3.00 (3.1)	2.19 (2.2)	155.9 (167.6)
	C_{10}	N9—H9….O6	3.11 (3.3)	2.27 (2.3)	164.2 (165.4)

[a](x, y+1, z); [b](x-1, y, z); [c](-x+2, y+1/2, -z); [d](x+1, y+1, z); [e](-x+1/2, -y+2, z+1/2); [f](-x+1/2, -y, z-1/2)

3B.3.4. Solution conformational studies

TH-3141_166122021

3B.3.4.1. NMR spectroscopy:

Chemical shift index for the peptides (**31-33)-Nona** were calculated by comparing the $C^{\alpha}H$ chemical shifts observed in $CDCl_3$ with the random coil shifts obtained from the Bio Mag Res Bank (BMRB)[328] and the original report of Wishart, Sykes and Richards[329] (Figure 3B.9). Upfield shifts in the $C^{\alpha}H$ resonances (negative chemical shift index), of the residues 1, 3 and 7 in both the conformers of (**31-33)-Nona** indicated helical conformations in them. It should be noted here that the positive chemical shift index observed for the C-terminal residue Val (9), might have resulted in local deviation in the secondary structure due to C-terminal fraying.

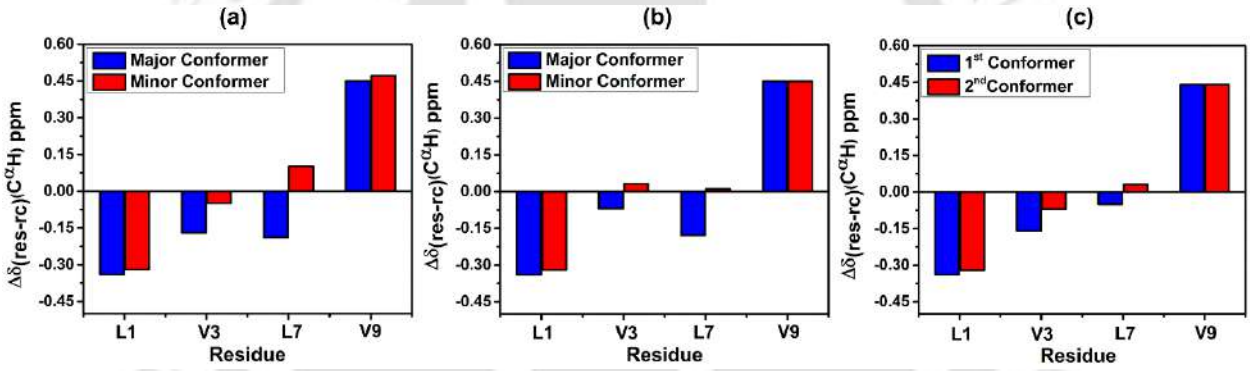

Figure 3B.9. Plot of the differences in $C^{\alpha}H$ chemical shift value of the residues with respect to random coil chemical shifts in (**31-33)-Nona**.

The helical conformation of (**31-33)-Nona** was further confirmed by low values (~5-7 Hz) of $^{3}J_{NH\text{-}C^{\alpha}H}$ coupling constants for all chiral L amino acid residues [Leu (1), Val (3), Leu (7), Val (9)] (Tables 3B.4-3B.9).

3B.3.4.1.1. ROESY:

In an attempt to further understand the secondary structure of the two conformations of (**31-33)-Nona** in detail, we performed ROESY experiment. Figures 3B.10a-b and 3B.11 represent

TH-3141_166122021

the partial NH-$C^{\alpha}H/C^{\gamma}H$ and NH-NH regions respectively of the ROESY spectrum of **31-Nona**. Most of the sequential d_{NN} NOEs were present for both the conformers. However, both in the major and the minor conformers, the 5/6 d_{NN} NOE was not observed. The NOEs observed for both the conformers were more or less similar with some exceptions. For example, NOEs $\gamma^{2,2}$ (5) $C^{\gamma}H\leftrightarrow$ Leu (7) NH and $\gamma^{2,2}$ (5) $C^{\gamma}H\leftrightarrow$ Aib (8) NH were weak and medium for the major conformer while they were both strong in intensity for the minor conformer. Leu (1) $C^{\alpha}H\leftrightarrow$ Aib (2) NH NOE was stronger and Leu (7) $C^{\alpha}H\leftrightarrow$ Leu (7) NH NOE was weaker in intensity for the major conformer with respect to the minor. Careful examination of the inter-proton distances in the conformation of **31-Nona** obtained from crystals (Figure 3B.7a) and comparison with the intensities of the observed NOEs, matched it to the major conformation obtained in solution (Figures 3B.10, 3B.11). A large inter-proton distance of 5.6 Å in between the $\gamma^{2,2}$ (5) NH and Aib (6) NH in the major conformer (Figure 3B.10c), explained the absence of the NOE in between them. Thus, the major conformer of **31-Nona** present in solution was the ambidextrous helix, while the minor conformer was still unknown. In case of **32-Nona** (Figure 3B.12), all the sequential d_{NN} NOEs were present in both the conformers. However, the intensity of the 5/6 d_{NN} NOE across the $\gamma^{3,3}$ residue was weaker compared to all the other sequential d_{NN} NOEs across the α amino acid residues (Figure 3B.12b). This could be explained by the shorter inter-proton d_{NN} distances across the α residues (~ 2.4-2.8 Å) in contrast to longer inter-proton d_{NN} distances across the γ residues (~ 3.6-4.2 Å) in the helical conformations obtained in crystals (Figures 3B.7c and 3B.7d). Alternating strong and weak NOEs across α and γ amino acid residues in helical conformation of $\alpha\gamma$ peptides, have been reported earlier in the literature.[215] Moreover, long-range NOEs like 2/4 d_{NN} NOE and 1/4 $C^{\alpha}H\leftrightarrow$NH NOE were observed for the minor conformer, while 7/9 long range $C^{\alpha}H\leftrightarrow$NH NOE was observed for both of them (Figures 3B.12a, b). These observations accompanied by stronger intra residue $C^{\alpha}H_{(i)}\leftrightarrow NH_{(i)}$ NOEs over inter residue $C^{\alpha}H_{(i)}\leftrightarrow NH_{(i+1)}$ NOE intensities,

TH-3141_166122021

suggested that both the conformers were helical. Careful analysis of the differences in the NOE intensities of the two conformers correlated to the inter-proton distances observed in the conformations obtained in crystals, confirmed that the major and the minor conformers for **32-Nona** in solution were the ambidextrous helix and right-handed mixed 13/12/10 helix respectively (Figure 3B.12). A crucial NOE that helped in the identification of the conformers was the 5/7 $C^{\gamma}H\leftrightarrow NH$ NOE which was present in the minor conformer (inter-proton distance of 2.7 Å) and absent for the major conformer (inter-proton distance of 5.0 Å). In the case of **33-Nona**, all the characteristic NOE features (presence of sequential d_{NN} NOEs, weaker d_{NN} NOE intensities across $\gamma^{4,4}$ residue in comparison to the α residues, stronger intra residue $C^{\alpha}H\leftrightarrow NH$ NOEs) complying with the helical conformation were observed (Figure 3B.13). The NOEs (both sequential and non-sequential long-range NOEs) for both the conformers were identical and matched well with the 10/12 helical conformation observed in crystals (Figure 3B.13). Thus it can be concluded that the two conformers for **33-Nona** were the left and right-handed 10/12 helix. The observation of two distinct sets of lines (with nearly equal intensities) in NMR for these two almost enantiomeric (in the middle stretch of the helix) helices might be justified by minor deviation in the conformation at the helix termini (Val (9) residue), giving rise to diastereomeric helices.

TH-3141_166122021

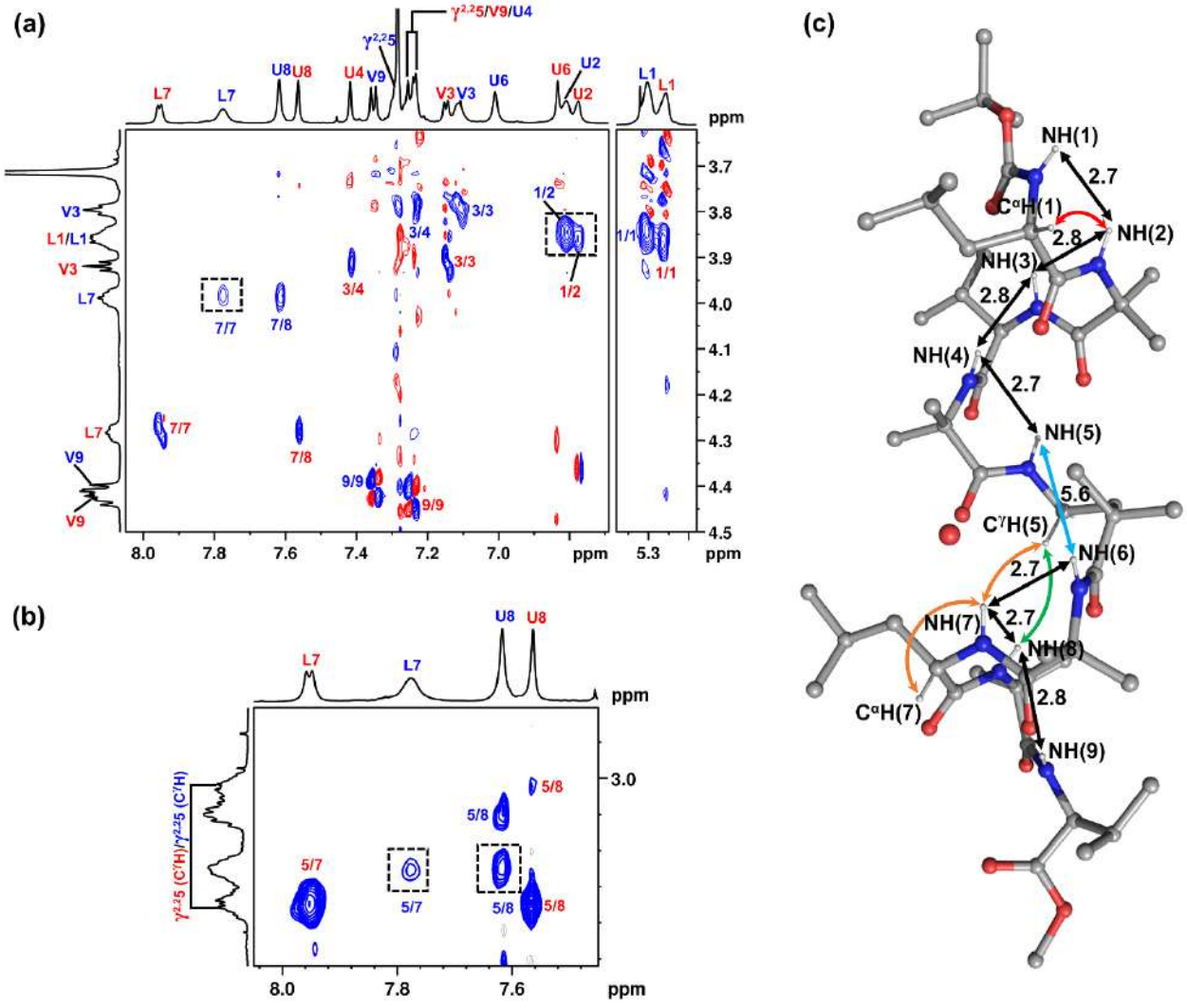

Figure 3B.10. Partial 600 MHz ROESY spectra of **31-Nona** representing (a) NOEs between NH↔C$^{\alpha}$H and (b) NH↔C$^{\gamma}$H ($\gamma^{2,2}$ residue) protons in $CDCl_3$ at 298 K. (c) Crystal structure of ambidextrous helical **31**-Nona showing the notable NOEs [red (strong), green (medium) and orange (weak) arrows] observed for the major conformer in solution. The d_{NN} distance across the α residues and $\gamma^{2,2}$ (5)-Aib (6) segment are shown by black and cyan blue arrows respectively.

TH-3141_166122021

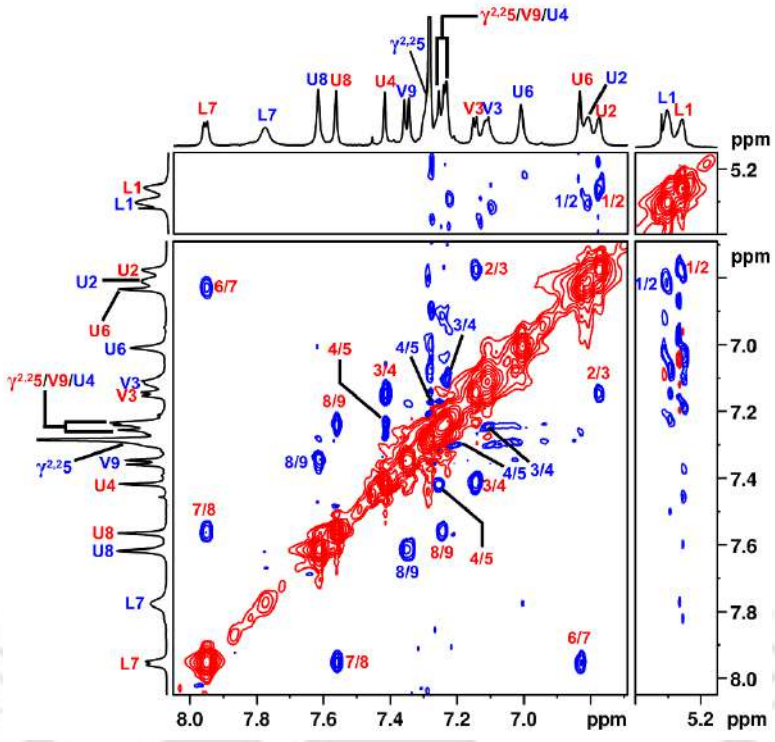

Figure 3B.11. Partial 600 MHz ROESY spectra of **31-Nona** representing d_{NN} NOEs in $CDCl_3$ at 298 K.

TH-3141_166122021

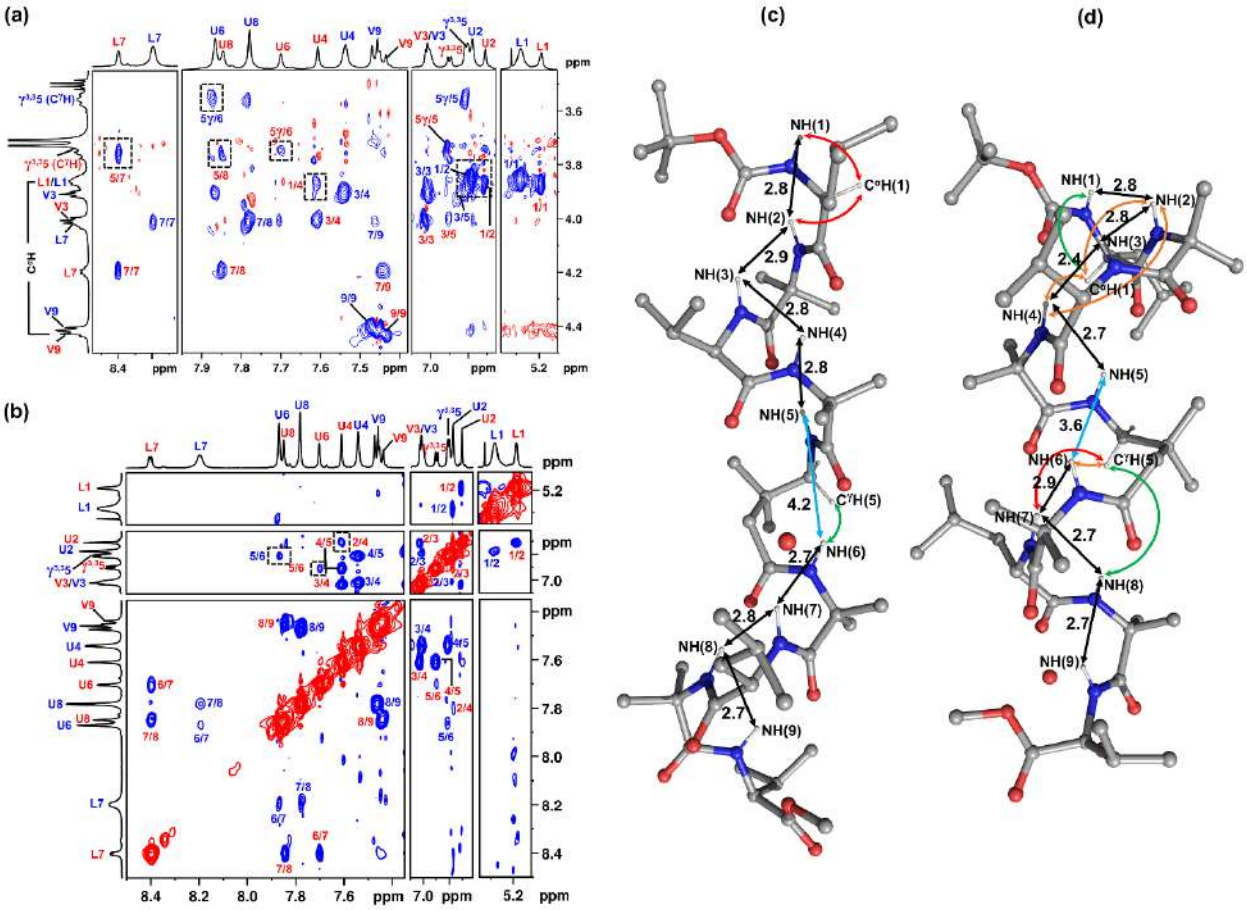

Figure 3B.12. Partial 600 MHz ROESY spectra of **32-Nona** representing (a) NOEs between NH↔$C^{\alpha}H/C^{\gamma}H$ ($\gamma^{3,3}$ residue) (b) NH↔NH protons in $CDCl_3$ at 298 K. (c) Crystal structure (low resolution) of **32-Nona** (grown from a mixture in ACN/H_2O) showing notable NOEs observed for the major conformer. (d) Crystal structure of **32-Nona** (Grown from purified minor populant fraction in ACN/H_2O) showing notable NOEs observed for the minor conformer. Strong, medium and weak NOEs are represented as red, green and orange arrows respectively. The d_{NN} distance across the α residues and $\gamma^{2,2}$ (5)-Aib (6) segment are shown by black and cyan blue arrows respectively.

TH-3141_166122021

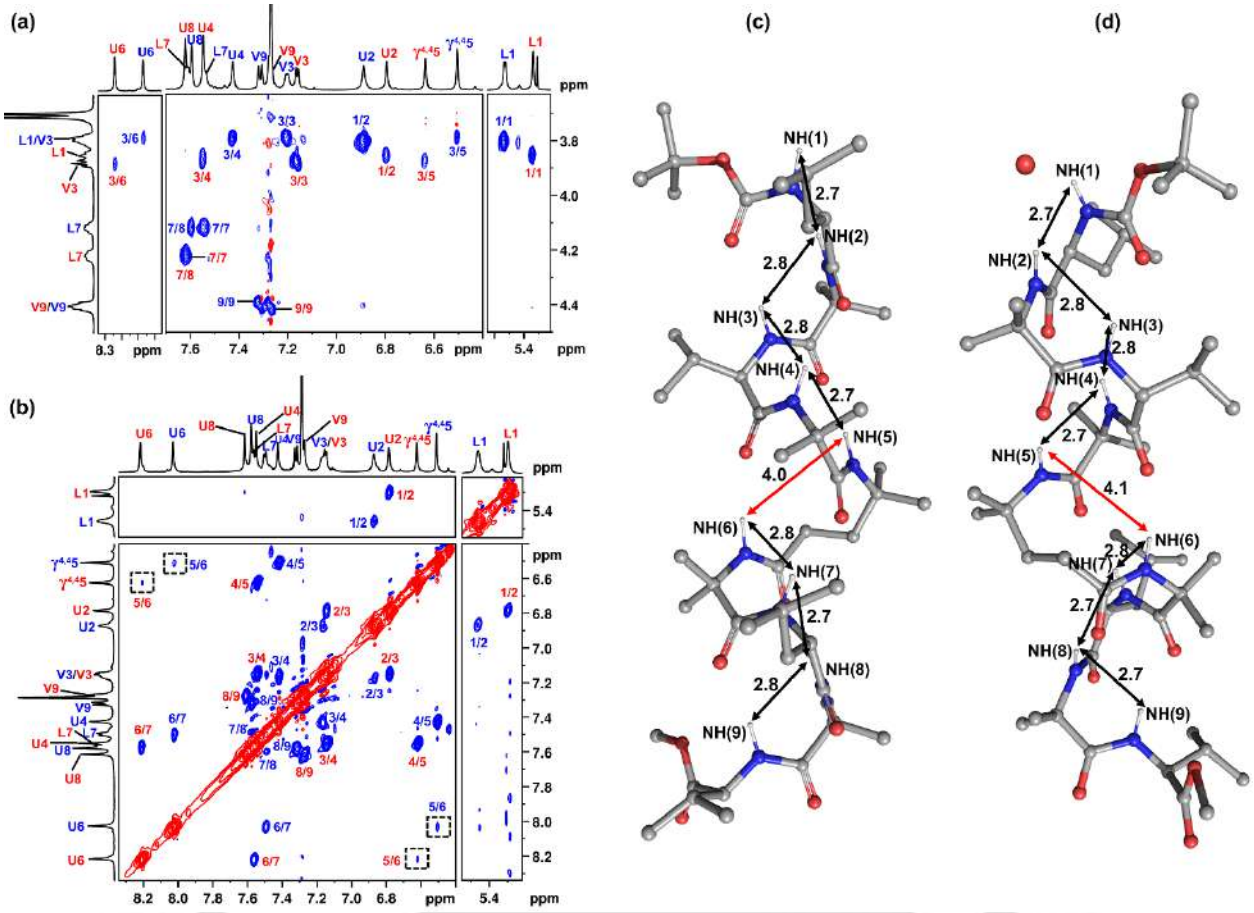

Figure 3B.13. Partial 600 MHz ROESY spectra of **33-Nona** representing (a) NOEs between NH↔C$^{\alpha}$H (b) NH↔NH protons in $CDCl_3$ at 298 K. Inter-proton distances in between subsequent NH protons (d_{NN}) marked on the conformations of **33-Nona** in crystals (c) grown from a mixture in ACN/H_2O and (d) grown from the purified second fraction in ACN/H_2O. d_{NN} distances across α amino acid residues are shorter and across γ residue is larger in 10/12 helical conformation denoted by black and red double-headed arrows respectively.

3B.3.4.1.2. DMSO-d_6 titration:

For further confirming the secondary structures of the conformers of (**31-33)-Nona** from their hydrogen bonding pattern, DMSO-d_6 solvent titration was performed and its results compared with the crystal structures. Upon addition of polar DMSO-d_6 to the solution of peptides in non-polar $CDCl_3$, solvent accessible non-hydrogen bonded NH's form H-bonds with DMSO-d_6 and

TH-3141_166122021

move downfield. The intra-molecularly H-bonded NH's on the other hand are solvent inaccessible and do not move. Figures 3B.14-3B.15 and Table 3B.12 show the change in the chemical shift values of the NH resonances of the conformers of (**31-33)-Nona** upon addition of 40% DMSO-d_6 to their $CDCl_3$ solution (~5-7 mM). In **31-Nona**, both the major and the minor conformers have completely solvent exposed Leu (1) and Aib (2) NH's ($\Delta\delta > 1.3$ ppm) and partially solvent exposed Aib (6) NH ($\Delta\delta \sim 0.6$ ppm) (Figure 3B.14a). Earlier, from the NOE studies, **31** major conformer was determined to be an ambidextrous helix as observed in the crystals (Figure 3B.7a). In the crystal structure, all of Leu (1), Aib (2) and Aib (6) NH's were non-hydrogen bonded intramolecularly, and hence expected to be solvent exposed showing similar shifts ($\Delta\delta$ ppm) in the DMSO-d_6 titration. The lesser shift for Aib (6) observed could be attributed to its crowded hydrophobic environment limiting the approach of the DMSO-d_6 molecules, in contrast to the terminal NH protons. In case of the minor conformer of **31-Nona**, Leu (1), Aib (2) and Aib (6) were non-hydrogen bonded, suggesting a helical structure with six intramolecular hydrogen bonds. In **32-Nona**, Leu (1) and Aib (2) NH's were completely solvent exposed in both the conformers, while all the other NH's seemed solvent shielded. Earlier NOE studies suggested the ambidextrous helix and right-handed 13/10/12 helix to be the major and minor conformer of **32-Nona** in solution. Leu (7) NH though non-hydrogen bonded intra-molecularly in the ambidextrous helical conformation observed in crystals (Figure 3B.8), appeared as a hydrogen bonded NH in the major conformer of **32-Nona** in the solvent titration experiment (Figure 3B.14b) owing to the hydrogen bonding of Leu (7) NH to a water molecule. Though, Val (3) NH was non-hydrogen bonded in the mixed 13/12/10 helical conformation observed in crystals due to the formation of the N-terminal three residue C_{13} hydrogen bond (Figure 3B.7c), it seemed hydrogen bonded in the minor conformer of **32-Nona** from the titration experiment. This discrepancy might be due to the non-accessibility of DMSO-d_6 molecules in the hydrophobic pocket of Val (3). In **33-Nona**, Leu (1) and Aib (2)

TH-3141_166122021

NH's were completely solvent exposed or non-hydrogen bonded in both the conformers, while all the other NH's were solvent shielded or hydrogen bonded (Figure 3B.14c). This observation corroborated exactly with the hydrogen bonding pattern observed in the 10/12 helices witnessed in the crystals (Figures 3B.7d, e).

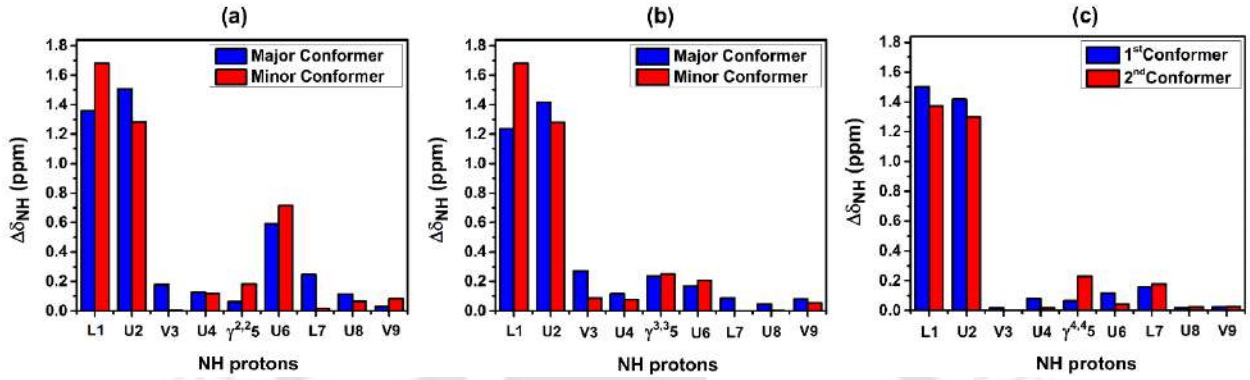

Figure 3B.14. Plot of the change of NH chemical shift value of the residues with increasing concentration of DMSO-d_6 (0-40 %) in (a) **31-Nona**, (b) **32-Nona** and (c) **33-Nona**.

TH-3141_166122021

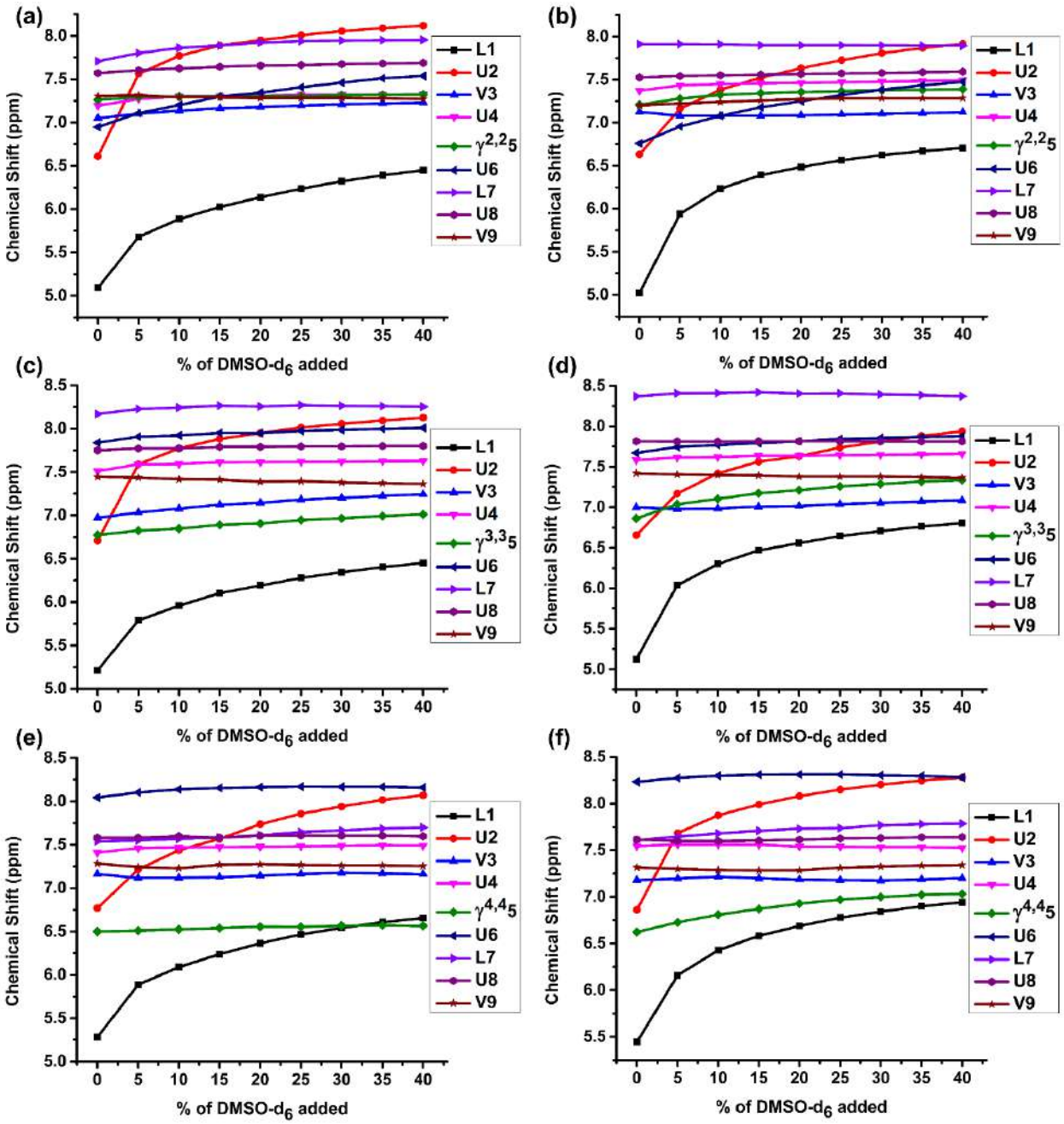

Figure 3B.15. Solvent dependence of NH chemical shifts of the peptide: **31-Nona** (a, b) Major and minor Conformer, **32-Nona** (c, d) Major and minor conformer, **33-Nona** (e, f) 1st Conformer and 2nd Conformer, at varying concentrations of DMSO-d_6.

TH-3141_166122021

Table 3B.12. NH Chemical shift differences of peptide (**31-33-Nona)** in $CDCl_3$ with increasing % of DMSO-d_6 at 298 K.

	Δδ (ppm) = [(Chemical Shift in $CDCl_3$+40% DMSO-d_6)-(Chemical Shift in $CDCl_3$)]					
	31-Nona		**32-Nona**		**33-Nona**	
	Major Conformer	Minor Conformer	Major Conformer	Minor Conformer	1st Conformer	2nd Conformer
NH (1)	1.358	1.681	1.235	1.68	1.5	1.373
NH (2)	1.507	1.284	1.418	1.28	1.418	1.3
NH (3)	0.179	0.003	0.272	0.087	0.019	0
NH (4)	0.129	0.118	0.116	0.077	0.078	0.018
NH (5)	0.061	0.181	0.237	0.250	0.064	0.230
NH (6)	0.59	0.715	0.17	0.207	0.115	0.046
NH (7)	0.247	0.018	0.086	0.001	0.159	0.177
NH (8)	0.115	0.066	0.049	0.002	0.018	0.026
NH (9)	0.033	0.084	0.08	0.055	0.026	0.028

3B.3.4.2. Infrared Spectroscopy:

Figure 3B.16 demonstrates the stacked plots of the solution FT-IR for (**31-33)-Nona** in $CDCl_3$ (1 mM) at room temperature. The characteristic peak ~1650 cm^{-1} in the spectra of all the peptides (**31-33)-Nona**, indicated that all of them adopted helical conformation.[326,327]

TH-3141_166122021

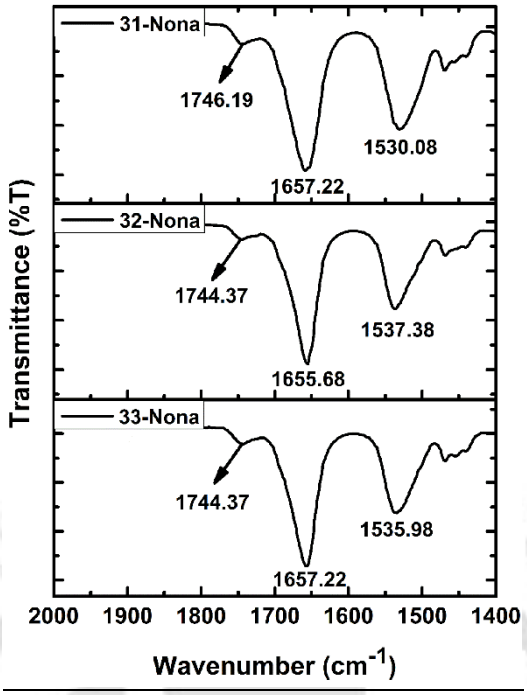

Figure 3B.16. Solution IR spectra of (**31-33)-Nona** at 1 mM concentration in $CDCl_3$ at room temperature.

3B.3.5. DFT optimized structures and energetics:

In order to gain insight into the structure of the minor conformation of **31-Nona** (observed in solution but not in crystals) and to understand the energetic origin of the population distribution of the various conformations in solution, we performed DFT calculations. As no crystals were obtained for the minor conformer of **31-Nona**, the DFT calculations in this case was performed on a **31-Nona** model having right-handed 10/12 helical conformation (decided primarily considering the ROESY, solvent titration studies and the observation of 10/12 right-handed helical conformation in case of **32-Nona** and **33-Nona**). Figures 3B.17 and 3B.18 show the optimized structures of (**31-33)-Nona**. The torsion angle values and the hydrogen bond parameters in the optimized structures were in close agreement with the crystal structure parameters (Tables 3B.10, 3.B.11). All the optimized structures were found to be a true minima in the potential energy hypersurface (supported by all positive frequencies obtained from

TH-3141_166122021

normal mode analysis). The optimized structure of **31-Nona** minor conformer (Figure 3B.17a) was helical and stabilized by a series of six two membered hydrogen bonds. There were three N-terminal C_{10} hydrogen bonds, followed by one $\gamma\alpha$ C_{12} hydrogen bond and two C-terminal C_{10} hydrogen bonds. One of the C_{12} hydrogen bonds across the Aib (4)-$\gamma^{2,2}$ (5) segment was absent resulting in the solvent exposure of the Aib (6) NH, that was seen earlier in the DMSO-d_6 titration experiments (Figure 3B.14a). The $\gamma^{2,2}$ residue adopted a folded conformation about the di-substituted C^{α} carbon atom (θ_2 = -62.1°, ψ = -54.6°) and a (-+--) combination of signs of the torsion angles. Right-handed 10/12 helices formed by the $\gamma^{3,3}$ and $\gamma^{4,4}$ amino acid residues (Figure 3B.7c,e), were seen to form two C_{12} hydrogen bonds each, unlike the $\gamma^{2,2}$ residue (Figure 3B.16a). This might be an indication that the $\gamma^{2,2}$ residue was less prone to adopt C_{12} helical conformation in comparison to the $\gamma^{3,3}$ and $\gamma^{4,4}$ residues. The computed structure for the major conformer of **32-Nona** (Figure 3B.17b) had torsion angles and hydrogen bond parameters in good agreement (Table 3B.11) to that obtained from the crystal structure (low resolution structure, Figure 3B.8). Placement of the hydrogen atoms of the co-crystalized water molecule in the computed structure, enabled the observation of three intermolecular hydrogen bonds in between **32-Nona** [Leu (7) NH, Val (3) CO and Aib (4) CO] and the water molecule. These three intermolecular hydrogen bonds seemed to have induced reversal of helix handedness in **32-Nona**, unlike two such hydrogen bonds in case of **31-Nona**.

TH-3141_166122021

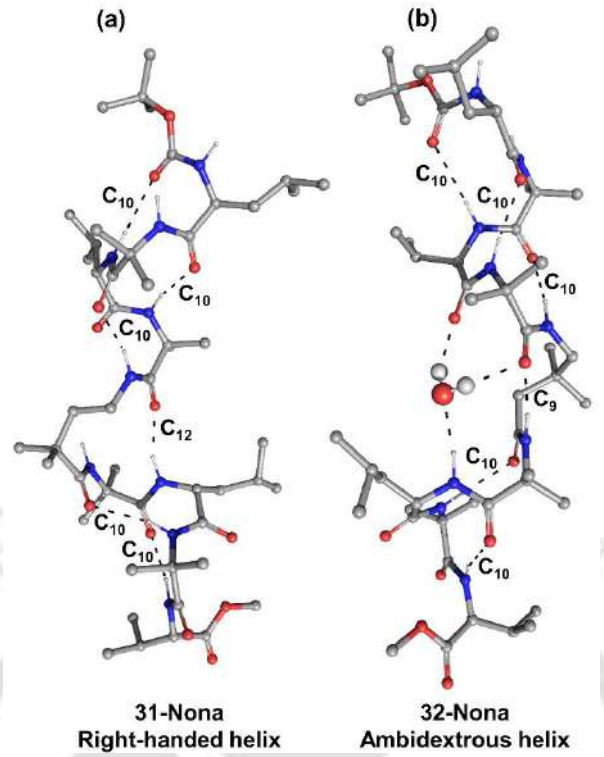

Figure 3B.17. Optimized structures of (a) Minor conformer of **31-Nona** (Right-handed 10/12 helix) and (b) Major conformer of **32-Nona** (Ambidextrous helix) from DFT calculations.

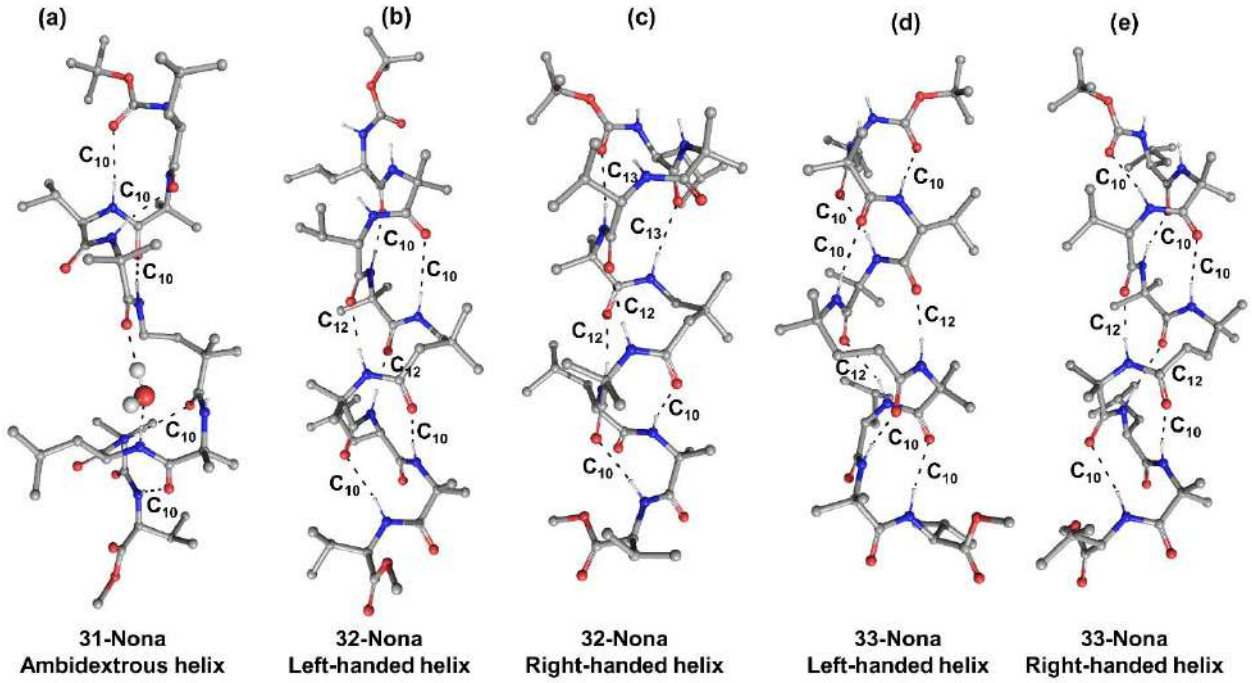

TH-3141_166122021

Figure 3B.18. Optimized structures of peptide (**31-33)-Nona** from Gaussian calculations. (a) **31-Nona** majorconformer (Ambidextrous helix), (b) Left-handed 10/12 helix for **32-Nona**, (c) **32-Nona** minor conformer (right-handed 13/12/10 helix), (d) Left-handed 10/12 helix for **33-Nona** and (e) Right-handed 10/12 helix for **33-Nona**.

Figure 3B.19 shows the relative energies of all the conformations of (**31-33)-Nona** realized in solution and crystals. Several interesting observations were made from the energy calculations: (a) Ambidextrous helices were the most stable conformers for **31/32-Nona** (which explained them being the major conformers in solution), (b) The ambidextrous helical conformation for **32-Nona** was relatively more stable than that of **31-Nona**, owing to one more water mediated hydrogen bond in the former (Figures 3B.7a, 3B.8 and 3.17b), (c) The energy difference between the major and minor conformers (~ 8, 11 and 2 kcal/mol for **31-Nona**, **32-Nona** and **33-Nona** resp.) were proportional to their relative populations (60:40, 70:30 and 53:47 for **31-Nona**, **32-Nona** and **33-Nona** resp.) in solution. The greater stability of the ambidextrous helices over the right-handed 10/12 helices of **31-Nona**, **32-Nona** might be owing to the greater number of hydrogen bonds in the former (7, 8 for **31-Nona**, **32-Nona**) with respect to the later (6, 6 for **31-Nona**, **32-Nona**) (Figures 3B.7a-c and 3B.17, Table 3B.11). A greater difference in the number of hydrogen bonds between the major and the minor conformers in case of **32-Nona** relative to **31-Nona**, led to a greater energy difference that consequently resulted in the higher population difference in **32-Nona** (70:30) with respect to **31-Nona** (60:40). High energy of the right-handed helical conformation of **31-Nona** (minor conformer in solution) might have limited its realization in the crystal state. The left and the right-handed helices of **32-Nona** and **33-Nona** have similar energies (0.5 and 2 kcal/mol) being almost enantiomeric (throughout the middle part of the helix with small differences at the termini) (Figure 3B.7b-e). The small

TH-3141_166122021

energy difference between the left and right-handed helical conformation in **33-Nona** (Figure 3B.18) led to similar populations of the two being observed in solution (Figures 3B.2, 3B.3).

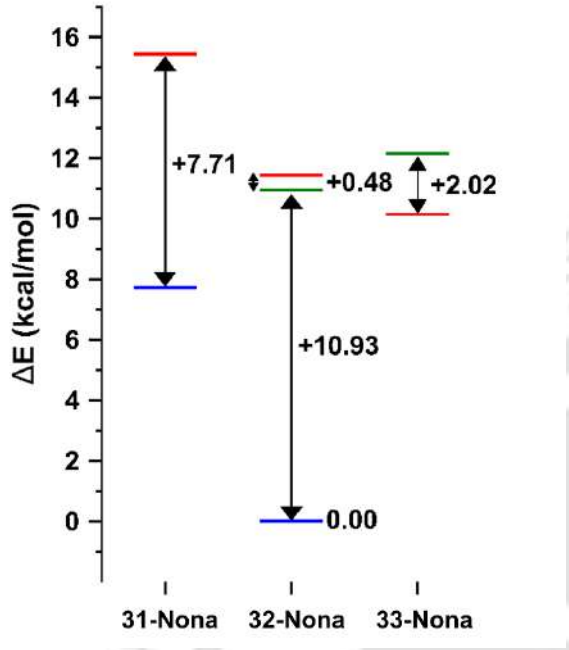

Figure 3B.19. Relative energy diagram of the different conformations adopted by (**31-33)-Nona** in solid and solution states: Ambidextrous helices of **31-Nona** and **32-Nona** (Blue line), right-handed 10/12 helix of (**31-33)-Nona** (Red line) and left-handed 10/12 helix of **32-Nona** and **33-Nona** (Green line). Ambidextrous helices of **31-Nona** and **32-Nona** are lower in energy and form major conformers in solution. Left and right-handed 10/12 helices (enantiomeric except at the termini) have close energies and are equi-populated in case of **33-Nona**.

3B.3.6. Observation of novel conformations in (31-33)-Nona: a discussion

The experimental and computational studies represented above established multiple distinct conformations adopted by (**31-33)-Nona**. (**31-33)-Nona** were composed of alpha amino acid residues of two types, the achiral Aib and the chiral L amino acid residues, Leu and Val, with a single centrally located achiral γ amino acid residue $\gamma^{x,x}$ (x = 2, 3, 4), thus making it overall chiral. As L amino acid residues are known to give rise to right-handed helical structures, (**31-33)-Nona** would have been expected to generate right-handed conformations as well.

TH-3141_166122021

However, in addition to the usually encountered right-handed 10/12 helical conformation of the chiral L alpha amino acids containing αγ peptides, (**31-33)-Nona** adopted other striking and unprecedented conformations like:

1. Ambidextrous helical conformation (containing both right and left-handedness)
2. Left-handed 10/12 helical conformation

Figure 3B.20 represents a conformational diagram which permits the understanding of the conformations of (**31-33)-Nona** with different handedness. Peptides **31-Nona** and **32-Nona** adopted ambidextrous helical conformation. Though ambidextrous helices have been reported in $(\alpha\gamma^{3,3})_n$ hybrid peptides by Gopi and co-workers,[133] they were achiral in nature. This, to the best of our knowledge, is the first report of the observation of ambidexterity in chiral αγ peptides containing L amino acid residues. A closer look at the crystal structures revealed that the ambidextrous helical conformation was induced by the presence of a water molecule at the central part of the helix (close to the γ residue) in **31-Nona** and **32-Nona**. Both the peptides had right-handedness at the C-terminus and left-handedness at the N-terminus. The change in the handedness from right to left occurred at the Aib (4) residue (*i.e.* after the $\gamma^{2,2}$ residue) in **31-Nona** while it occurred at the $\gamma^{3,3}$ residue for **32-Nona**. A water molecule formed two hydrogen bonds with the Leu (7) NH and left- handed Aib (4) CO in **31-Nona** and three hydrogen bonds with Leu (7) NH and left-handed Aib (4) CO and Val (3) CO in **32-Nona** respectively, inducing the change in handedness. This change in handedness obliterated the usual C_{12} hydrogen bonds across the Aib (4)-$\gamma^{x,x}$ (5) and $\gamma^{x,x}$ (5)–Aib (6) segments (x = 2, 3). The inability to accommodate water molecule in the central region of **33-Nona** (even in the presence of water in the crystallization solvent) might have led to the absence of the ambidextrous helix in this case. The position of di-substitution in $\gamma^{4,4}$ amino acid residue, might

TH-3141_166122021

be responsible for this preferential inability in the recruitment of the water molecule in **33-Nona**.

Achiral amino acid residues can adopt both left and right-handed conformations with equal ease. The centrally located achiral γ amino acid residues $\gamma^{3,3}$ and $\gamma^{4,4}$ could thus adopt either right or left-handedness and could induce this on its neighbouring amino acid residues, irrespective of their chirality. However, this effect of induction of handedness on the neighbouring residues (by the γ amino acid residue) seemed to be prominent only up to three amino acid residues, that resulted in the observation of diastereomers in the left and right-handed helices of **32-Nona** and **33-Nona** (differing in stereochemistry at the 4^{th} amino acid residues from γ).

In the left-handed 10/12 helices of **32-Nona** and **33-Nona**, the L amino acid residues [Val (3) and Leu (7)] in the close proximity of the central achiral γ amino acid residues, adopted left-handedness. However, residues Leu (1) and Val (9) which were further away from the central γ amino acid residue reverted back to their usual right-handed conformation in **32-Nona** (Figure 3B.7b, Table 3B.10). In case of **33-Nona**, though the Val (9) changed back to its usual right-handed conformation, the terminal Leu (1) still retained its left-handed conformation in the crystals. Thus the observation of the left-handedness in **32-Nona** and **33-Nona** was a direct consequence of the centrally located achiral γ amino acid residue. No left-handed helices were experimentally realized either in solution or crystal for **31-Nona**. Thus, similar abilities for the $\gamma^{2,2}$ remains inconclusive.

TH-3141_166122021

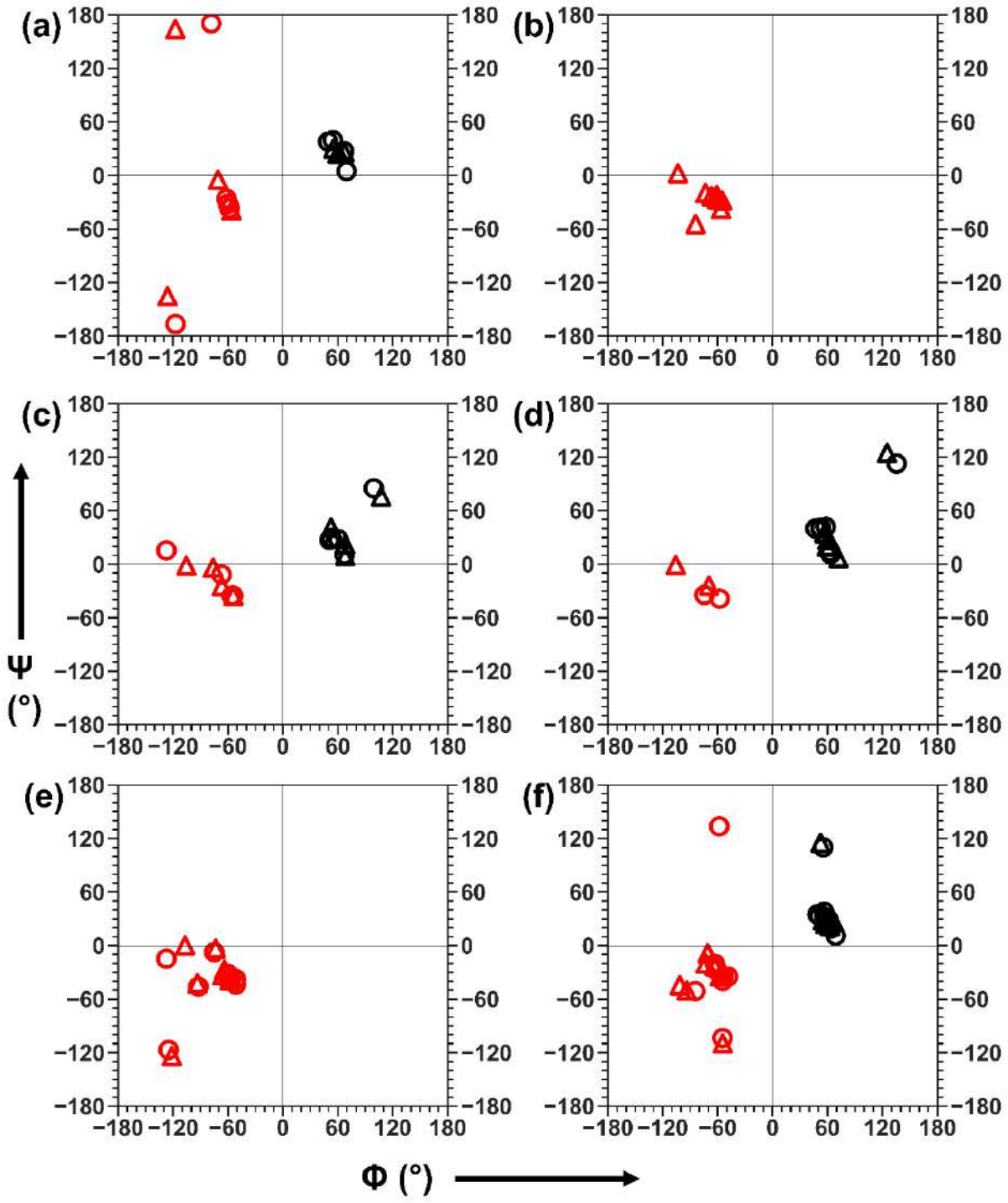

Figure 3B.20. Ramachandran plot showing the ϕ, ψ values for the torsion angles of the alpha amino acid residues of the different conformations of (**31-33)_Nona** in the crystals and the DFT computed structures. Red icons represent right-handedness while black icons represent left handedness. Open circles and triangles represent torsion angle values from crystal structures and DFT structures respectively. Population distribution of the various

TH-3141_166122021

conformations in solution are denoted in parentheses in each case. (a) **31-Nona** ambidextrous helix (major conformer), (b) **31-Nona** right-handed mixed 10/12 (minor conformer), (c) **32-Nona** ambidextrous helix (major conformer), (d) **32-Nona** left-handed 10/12 helix, (e) **32-Nona** right-handed mixed 13/10/12 helix (minor conformer) and (f) **33-Nona** left and right-handed mixed 10/12 helices (almost equi-populated conformers).

3B.4. Conclusion

Chiral peptides (**31-33)-Nona**, containing L amino acid residues, were established to be adopting a rare ambidextrous helical conformation and left-handed 10/12 helical conformation, in addition to the regular right-handed 10/12 helical conformation. Ambidexterity needing the reversal of handedness around the central part of the helix, was induced by hydrogen bonds to a centrally positioned water molecule. The differential position of di-substitution of the γ amino acid residue backbone in $\gamma^{4,4}$ of **33-Nona** might have prevented the recruitment of water in the structure, thus preventing the formation of the ambidextrous helix in **33-Nona**. The central achiral γ amino acid residues adopted either handedness and induced it on the flanking α amino acid residues irrespective of their configuration, thus generating left and right-handed 10/12 helical conformations. This ability of induction of handedness of the central γ amino acid residues on the neighbouring alpha amino acid residues (L or achiral) wore off with distance beyond three amino acid residues. The difference in stabilities in between the different conformations of (**31-33)-Nona** determined their populations in solution. Among the three differentially di-substituted γ amino acid residues, $\gamma^{4,4}$ was most prone to adopting 10/12 helical structure followed by $\gamma^{3,3}$. $\gamma^{2,2}$ seemed to be least prone to adopting the 10/12 helical structure among all the three. The present study opens up different possibilities of design of hybrid peptide architectures with mixed handedness through rational design of peptides using appropriately di-substituted γ amino acid residues.

TH-3141_166122021

Chapter 4

Position of Geminal Substitution of γ Amino Acid Residues Modulates Their Ability to Form Isolated Non-Helical C_{12} β-turn Mimics

TH-3141_166122021

4.1. Introduction

In this chapter, we wanted to investigate the ability of $\gamma^{2,2}$, $\gamma^{3,3}$ and $\gamma^{4,4}$ amino acid residues to give rise to an isolated $\alpha\gamma$ non-helical C_{12} β-turn mimic. It should be noted that in hairpins while the tight turn ensures strand registry, the inter-strand hydrogen bonds stabilize the tight turn. However, formation of the isolated turn in a small tetrapeptide entirely depends on the stereochemical preference of the turn residues. In this study, we have employed ^{D}Pro as the (i+1) residue and each of the three differentially dimethyl substituted γ amino acid residues ($\gamma^{x,x}$; x,x = 2,2/3,3/4,4) as the (i+2) residue in the tetrapeptides **41-43** (Figures 4.1). We have studied the conformations of these peptides in two different solvents (aprotic $CDCl_3$ and polar protic CD_3OH) using NMR and CD spectroscopy. The conformations adopted in solution were corroborated with DFT calculations.

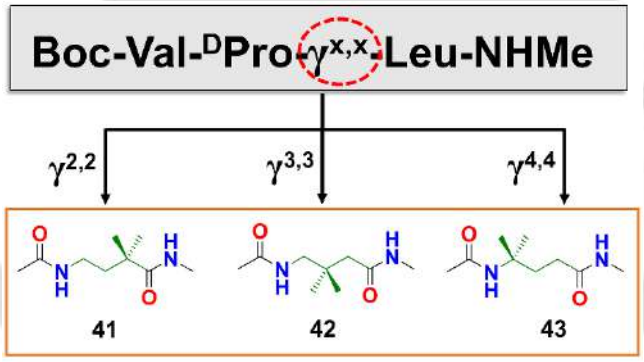

Figure 4.1. Schematic representation of synthesized peptides **41-43** containing $\gamma^{x,x}$ (x,x = 2,2/3,3/4,4) amino acid residues. Chemical structures of the γ amino acid residues incorporated into various peptides are shown in orange box.

TH-3141_166122021

4.2. Experimental Section

4.2.1. Synthetic procedure of peptide 41-43

All peptides were synthesized by conventional solution phase chemistry, using a fragment condensation strategy involving a 2 + 2 coupling in the final step. Tert-butyloxycarbonyl (Boc) was used for N-terminal protection, and the C-terminal was protected as an N-methyl amide. Peptide coupling was mediated by EDC.HCl and HOBt. TFA achieved deprotection of the Boc group in DCM (1:1), and the methyl group was removed by using LiOH in a mixture of methanol and water (2:1) (Scheme 4.1).

Scheme 4.1. Synthetic flow chart of peptides **41-43**

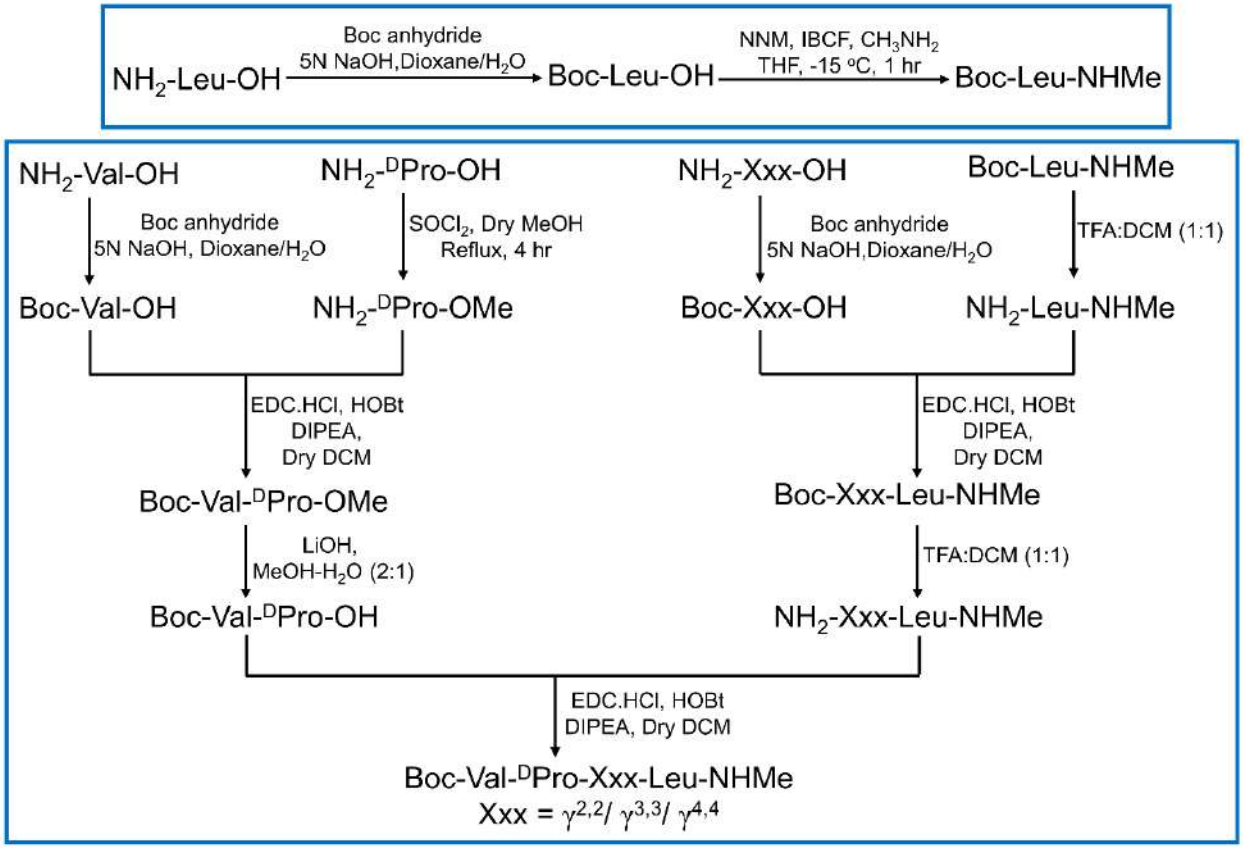

TH-3141_166122021

4.2.2. Purification

Purification of peptides **41-43** was done by reversed-phase HPLC using MeOH/H_2O (60-100%) as the solvent system at a flow rate of 10 mL/min using dual UV detection at 214 and 220 nm. To check the purity, analytical HPLC was performed with a flow rate of 1 mL/min and a linear gradient of 60−100% in the MeOH/H_2O system (Appendix, Figures A76-A78).

4.2.3. Characterization

4.2.3.1 Characterization of Boc-$\gamma^{x,x}$-OH (x,x = 2,2/3,3/4,4)

Characterization of all Boc protected γ amino acids has been mentioned in Chapter 3 (Section 3A.2.3.1)

4.2.3.2. Characterization of peptides 41-43 both in $CDCl_3$ and CD_3OH

Boc-Val-^{D}Pro-$\gamma^{2,2}$-Leu-NHMe (41)

Analytical HPLC retention time: 12.79 min (Appendix, Figure A76). ESI-MS (m/z) of **41** Calc. for $(M+H)^+$ $C_{28}H_{51}N_5O_6$ = 554.3878 Da, Obs. = 554.4045 Da, $(2M+Na)^+$ = 1129.7800 Da (Appendix, Figure A79). ^{1}H NMR (600 MHz, Chloroform-*d*) (Appendix, Figure A82): δ 7.28 (b, 1H), 6.81 (b, 1H), 6.59 (d, *J* = 7.8 Hz, 1H), 5.36 (d, *J* = 7.1 Hz, 1H), 4.56 (d, *J* = 6.8 Hz, 1H), 4.51 – 4.39 (m, 1H), 4.10 (t, *J* = 7.6 Hz, 1H), 3.87 (b, 1H), 3.53 (q, *J* = 8.5 Hz, 1H), 3.20 – 3.06 (m, 2H), 2.78 (d, *J* = 4.8 Hz, 3H), 2.33 (b, 1H), 2.05 – 1.89 (m, 4H), 1.65-1.55 (m, 2H), 1.44 (s, 9H), 1.16 (s, 6H), 1.03 – 0.88 (m, 12H). ^{13}C {^{1}H} NMR (150 MHz, Chloroform-*d*) (Appendix, Figure A88): δ 177.2, 172.9, 171.8, 171.5, 156.4, 79.9, 60.4, 57.8, 52.0, 47.1, 41.3, 40.9, 38.9, 36.6, 30.4, 28.7, 28.3, 26.2, 25.9, 25.8, 25.0, 24.3, 22.9, 22.0, 19.5, 18.1. ^{1}H NMR (600 MHz, Methanol-d_3) (Appendix, Figure A85): δ 7.93 (b, 1H), 7.82 (b, 1H), 7.58 (d, *J* = 7.5 Hz, 1H), 6.74 (d, *J* = 7.5 Hz, 1H), 4.43-4.37 (m, 2H), 4.12 (t, *J* = 7.5 Hz, 1H), 3.92 (b, 1H), 3.66 (q, *J* = 7.9 Hz, 1H), 3.23 – 3.18 (m, 1H), 3.07 – 3.01 (m, 1H), 2.74 (d, *J* = 4.6 Hz, 3H), 2.18 – 2.12 (m, 1H), 2.05-1.97 (m, 4H), 1.84 (dq, *J* = 15.7, 4.9 Hz, 1H), 1.74 – 1.64 (m, 3H), 1.58 (b, 1H), 1.47 (s, 9H), 1.22 (s, 3H), 1.18 (s, 3H), 1.00 – 0.96 (m, 10H), 0.93-0.91 (m, 3H).

TH-3141_166122021

^{13}C {^{1}H} NMR (150 MHz, Methanol-d_3) (Appendix, Figure A91): δ 179.7, 175.73, 173.9, 173.5, 158.3, 80.5, 61.9, 59.4, 53.6, 42.3, 41.9, 40.5, 37.2, 31.5, 30.6, 28.7, 26.5, 26.2, 25.9, 25.3, 25.2, 23.4, 21.7, 19.5, 18.6.

Boc-Val-^{D}Pro-γ^{3,3}-Leu-NHMe (42)

Analytical HPLC retention time: 12.74 min (Appendix, Figure A77). ESI-MS (m/z) of **42** Calc. for $(M+H)^+$ $C_{28}H_{51}N_5O_6$ = 554.3878 Da, Obs. = 554.4133 Da, $(2M+Na)^+$ = 1129.7960 Da (Appendix, Figure A80). ^{1}H NMR (600 MHz, Chloroform-*d*) (Appendix, Figure A83): δ 7.64 (d, *J* = 7.7 Hz, 1H), 7.22 (b, 1H), 6.58 (b, 1H), 5.73 (d, *J* = 8.0 Hz, 1H), 4.57 (d, *J* = 6.5 Hz, 1H), 4.43 (q, *J* = 7.8 Hz, 1H), 4.21 (t, *J* = 8.0 Hz, 1H), 4.0 (b, 1H), 3.56 (b, 1H), 3.09 (b, 2H), 2.79 (d, *J* = 4.8 Hz, 3H), 2.31 (b, 1H), 2.13 – 1.90 (m, 6H), 1.71-1.62 (m, 2H), 1.61-1.55 (m, 1H), 1.41 (s, 9H), 1.07 – 0.80 (m, 18H). ^{13}C {^{1}H} NMR (150 MHz, Chloroform-*d*) (Appendix, Figure A89): δ 172.9, 172.5, 171.7, 156.3, 79.6, 60.8, 57.8, 51.6, 48.9, 47.5, 44.9, 40.3, 35.0, 30.5, 28.8, 28.3, 26.6, 26.1, 25.2, 24.8, 24.6, 22.8, 22.1, 19.5, 18.1. ^{1}H NMR (600 MHz, Methanol-d_3) (Appendix, Figure A86): δ 8.28 (d, *J* = 7.9 Hz, 1H), 7.99-7.90 (b, 2H), 6.78 (d, *J* = 8.4 Hz, 1H), 4.44 – 4.38 (m, 1H), 4.36 (dt, *J* = 8.9, 4.3 Hz, 1H), 4.20 (t, *J* = 7.9 Hz, 1H), 3.94 (b, 1H), 3.69 (dt, *J* = 9.7, 7.0 Hz, 1H), 3.29 (dd, *J* = 13.6, 7.1 Hz, 1H), 2.98 (dd, *J* = 13.6, 6.0 Hz, 1H), 2.74 (d, *J* = 4.5 Hz, 3H), 2.23 – 2.19 (m, 1H), 2.13 – 2.00 (m, 6H), 1.71 – 1.65 (m, 1H), 1.62-1.54 (m, 2H), 1.45 (s, 9H), 1.01 – 0.96 (m, 15H), 0.94-0.92 (m, 3H). ^{13}C {^{1}H} NMR (150 MHz, Methanol-d_3) (Appendix, Figure A92): δ 175.4, 174.6, 174.0, 173.4, 158.1, 80.5, 62.1, 59.2, 53.1, 50.0, 45.8, 42.1, 36.4, 31.7, 30.6, 28.7, 26.4, 26.1, 25.9, 25.8, 25.5, 23.3, 21.8, 19.5, 18.4.

Boc-Val-^{D}Pro-γ^{4,4}-Leu-NHMe (43)

Analytical HPLC retention time: 12.89 min (Appendix, Figure A78). ESI-MS (m/z) of **43** Calc. for $(M+H)^+$ $C_{28}H_{51}N_5O_6$ = 554.3878 Da, Obs. = 554.3892 Da, $(2M+Na)^+$ = 1129.7513 Da (Appendix, Figure A81). ^{1}H NMR (600 MHz, Chloroform-*d*) (Appendix, Figure A84): δ 7.30

TH-3141_166122021

(d, *J* = 7.5 Hz, 1H), 6.66 (s, 1H), 6.44 (s, 1H), 6.17 (d, *J* = 8.3 Hz, 1H), 4.46 – 4.36 (m, 2H), 4.19 (t, *J* = 8.6 Hz, 1H), 4.01 (b, 1H), 3.55 (td, *J* = 9.7, 6.9 Hz, 1H), 2.79 (d, *J* = 4.8 Hz, 3H), 2.33 (b, 1H), 2.19 – 2.02 (m, 4H), 2.0-1.87 (m, 4H), 1.74-1.63 (m, 2H), 1.60 – 1.54 (m, 1H), 1.41 (s, 9H), 1.30 (s, 3H), 1.20 (s, 3H), 1.09-1.0 (s, 3H), 0.99 – 0.88 (m, 9H). ^{13}C {^{1}H} NMR (150 MHz, Chloroform-*d*) (Appendix, Figure A90): δ 173.9, 173.2, 173.0, 170.0, 79.4, 61.1, 58.1, 53.5, 51.4, 47.8, 40.6, 36.5, 31.9, 30.3, 28.3, 28.0, 27.4, 26.5, 26.2, 24.7, 24.6, 22.8, 22.3, 19.4, 18.3. ^{1}H NMR (600 MHz, Methanol-d_3) (Appendix, Figure A87): δ 8.05 (d, *J* = 8.0 Hz, 1H), 7.95 (b, 1H), 7.34 (s, 1H), 6.84 (d, *J* = 9.1 Hz, 1H), 4.38 (q, *J* = 8.0 Hz, 1H), 4.29 (dd, *J* = 8.7, 3.8 Hz, 1H), 4.20 (t, *J* = 8.3 Hz, 1H), 3.87 (b, 1H), 3.70 – 3.67 (m, 1H), 2.74 (d, *J* = 4.7 Hz, 3H), 2.33 – 2.25 (m, 2H), 2.22 – 2.16 (m, 2H), 2.10 – 2.06 (m, 2H), 2.00 – 1.94 (m, 3H), 1.69 – 1.65 (m, 1H), 1.59-1.57 (m, 2H), 1.46 (s, 10H), 1.32 (s, 3H), 1.29 (s, 3H), 0.98-0.95 (m, 9H), 0.93-0.92 (s, 3H). ^{13}C {^{1}H} NMR (150 MHz, Methanol-d_3) (Appendix, Figure A93): δ 176.3, 175.3, 173.7, 80.4, 62.4, 59.1, 54.40, 53.0, 42.4, 36.5, 32.2, 31.7, 30.6, 28.7, 28.6, 27.4, 27.1, 26.4, 25.8, 25.6, 23.3, 21.9, 19.7, 18.3.

4.2.4. NMR Spectroscopy

All NMR experiments were carried out on a Bruker Ascend Aeon 600 MHz spectrometer respectively. The peptide concentrations were in the range of 7-10 mM in both $CDCl_3$ and CD_3OH for both 1D and 2D NMR experiments at 298 K temperature. Variable temperature 1D NMR experiments were carried out in between 273-323 K. Concentration dependent NMR experiments were performed within the concentration range of 1 mM to 20 mM. The chemical shift values and coupling constants were measured from 1D NMR spectra. Complete resonance assignments of the protons of **41-43** were done by TOCSY and NOESY experiments. All the 2D experiments were done in phase-sensitive mode by using the time-proportional phase incrementation (TPPI) method. For all peptides, TOCSY and NOESY spectra were recorded with a mixing time of 80 and 400 ms, respectively. The spectral width was 6009.6 Hz and

TH-3141_166122021

12019.23 in both dimensions for $CDCl_3$ and CD_3OH, respectively. The total number of scans were fixed to 16 for TOCSY and NOESY (32 scans in the case of CD_3OH), respectively. Data points was set to 2048 and 256 in f2 and f1 dimensions, respectively, for both TOCSY and NOESY spectra. Zero filling was done to finally yield a data set of 4K x 2K. All NMR spectra were processed using Topspin 3.6 software.

4.2.5. FT-IR Spectroscopy

FT-IR of all peptides **41-43** were carried out in solid state. All spectra were recorded in the region of 400−4000 cm^{-1}. (Appendix, Figures A94-A96)

4.2.6. CD Spectroscopy

The CD studies were performed in methanol at 600 μM concentrations for all peptides **41-43**. Spectra were collected at a scan rate of 100 $nm \cdot min^{-1}$ and 2 nm bandwidth from 190 nm to 260 nm with five scans for averaging.

4.2.7. Electronic Structure Calculations

For structure optimization and energy calculations, all the peptides **41-43** were modelled using PyMOL software.[297] The description of model building has been discussed in section 1.13.4.3.1. The modelled structures were subjected to geometry optimization using Gaussian 16 program[298] employing density functional theory (B3LYP/6-311++G* level).[299,300,303,304] Calculations also included normal mode frequency calculations to identify the nature of the structures in the energy hypersurface. Calculations were performed on peptides in vacuum as well as embedded in two different implicit solvent models (chloroform and methanol).

4.3. Results and Discussion

The three designed tetrapeptides (**41-43**) have been synthesized, purified and characterized using analytical HPLC (Appendix, Figures A76-A78), ESI-MS (Appendix, Figures A79-

TH-3141_166122021

A811D ^{1}H NMR (Appendix, Figures A82-A87), ^{13}C NMR (Appendix, Figures A88-A93) and FT-IR spectroscopy (Appendix, Figures A94-A96).

4.3.1. Solution conformation study (in $CDCl_3$ and CD_3OH)

4.3.1.1. NMR Spectroscopy

Solution conformation of the peptides **41-43** was studied using NMR spectroscopy. To probe the effect of solvent on the conformation of the peptides in solution, NMR studies were carried out in aprotic solvent $CDCl_3$ and polar protic solvent CD_3OH. Sequence specific assignment of the backbone and side chain protons of peptides (**41-43**) were readily achieved by using a combination of TOCSY (Appendix, Figures A97-A102) and NOESY (Appendix, Figures A103-A108) experiments.

4.3.1.1.1. 1D ^{1}H NMR

Figure 4.2 shows the stacked plot of the NH region of the 1D ^{1}H NMR spectrum of **41-43** in both $CDCl_3$ and CD_3OH. In all three peptides in both the solvents, there was one set of predominant sharp NMR lines accompanied by very small peaks in the baseline. However, the intensity of these small peaks was stronger in CD_3OH than in $CDCl_3$. There was presence of exchange cross-peaks (EXSY peaks, opposite phase to the NOESY cross-peaks) in between the intense set of lines and the small set of lines in NH-NH region of the NOESY spectra, suggesting that the small peaks were from minor conformations populating the solution (Appendix, Figures A103-A108).

TH-3141_166122021

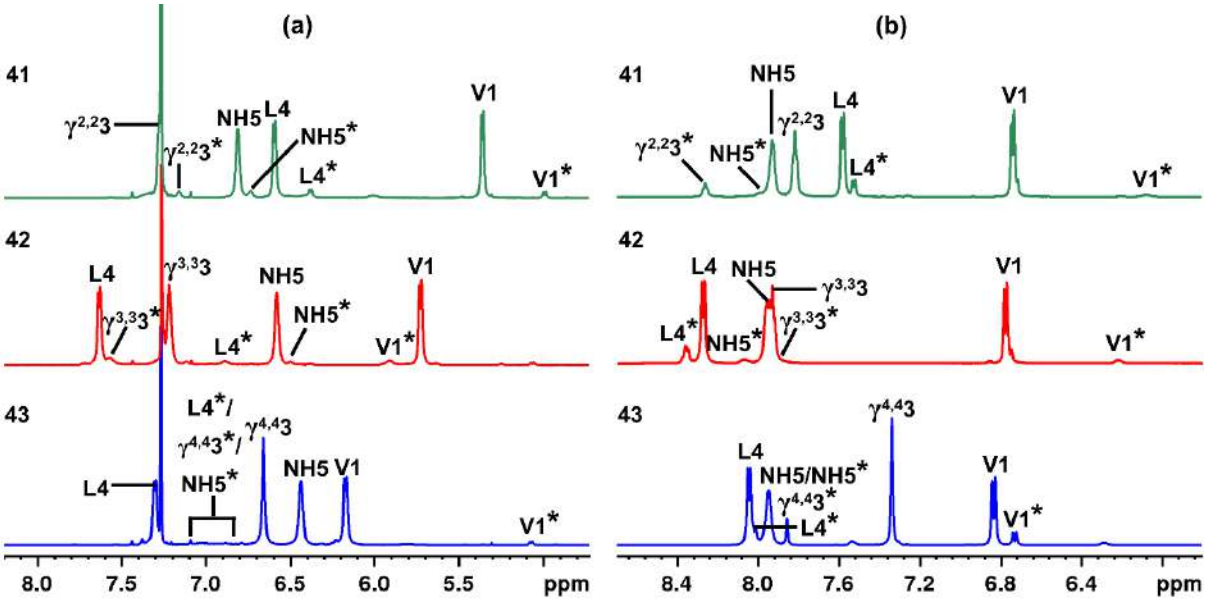

Figure 4.2. Partial 1D ^{1}H NMR spectra representing the amide proton resonances of **41-43 in** (a) $CDCl_3$ and (b) CD_3OH at 298 K. Star marks show the presence of other minor conformers.

The value of the ^{3}J constant for Val (1) and Leu (4) residues were ~7-8 Hz in both $CDCl_3$ and CD_3OH, which suggested that they adopted extended conformations (Tables 4.1-4.3). Chemical shift index for the peptides **41-43** were calculated in both the solvents as mentioned earlier in Chapter 3. Positive values of Val (1) and Leu (4) $C^{\alpha}H$'s (Figure 4.3) indicate extended conformations adopted by these residues.

TH-3141_166122021

Table 4.1. Characteristic ^{1}H Parameters of **41**.

Residues	Chemical Shift (ppm)[a]						
	NH	$C^{\alpha}H$	$C^{\beta}H$	$C^{\gamma}H$	$C^{\delta}H$	$^{3}J_{NH\text{-}C^{\alpha}H}$ (Hz)	dδ/dT (ppb/°C)
Val (1)	5.36 (6.74)	4.10 (4.12)	2.01 (1.97)	1.01-0.97 (1.0-0.97)	-	7.1 (7.5)	-10.2
^{D}Pro (2)	-	4.56 (4.40)	2.33, 1.98 (2.16, 2.05)	1.99 (2.05, 1.95)	3.87, 3.53 (3.92, 3.66)	-	-
$\gamma^{2,2}$ (3)	7.28 (7.82)	-	1.74 (1.84, 1.73)	3.17, 3.11 (3.20, 3.05)	-	-	-5.7
Leu (4)	6.59 (7.58)	4.50 (4.41)	1.74 (1.67)	1.61 (1.58)	0.96-0.90 (0.97-0.95, 0.93-0.91)	7.8 (7.5)	-10.1

[a] Chemical Shift values of proton resonances in $CDCl_3$ and CD_3OH. Values in parentheses are corresponding to CD_3OH.

Table 4.2. Characteristic ^{1}H Parameters of **42**.

Residues	Chemical Shift (ppm)[b]						
	NH	$C^{\alpha}H$	$C^{\beta}H$	$C^{\gamma}H$	$C^{\delta}H$	$^{3}J_{NH\text{-}C^{\alpha}H}$ (Hz)	dδ/dT (ppb/°C)
Val (1)	5.73 (6.78)	4.21 (4.20)	2.06 (2.03)	1.04-0.99 (1.01-0.99)	-	8.0 (8.0)	-8.0
^{D}Pro (2)	-	4.57 (4.42)	2.31, 2.10 (2.19, 2.10)	2.01 (2.05)	4.00, 3.56 (3.94, 3.69)	-	-
$\gamma^{3,3}$ (3)	6.58 (7.93)	2.08, 1.99 (2.12)	-	3.09 (3.29, 2.98)	-	-	-6.3
Leu (4)	7.64 (8.28)	4.43 (4.37)	1.70, 1.66 (1.68, 1.60)	1.59 (1.57)	0.93-0.89 (0.97-0.96, 0.94-0.92)	7.7 (8.4)	-7.1

[b] Chemical Shift values of proton resonances in $CDCl_3$ and CD_3OH. Values in parentheses are corresponding to CD_3OH.

TH-3141_166122021

Table 4.3. Characteristic ^{1}H Parameters of **43**.

Residues	Chemical Shift (ppm)[c]						
	NH	$C^{\alpha}H$	$C^{\beta}H$	$C^{\gamma}H$	$C^{\delta}H$	$^{3}J_{NH\text{-}C^{\alpha}H}$ (Hz)	dδ/dT (ppb/°C)
Val (1)	6.17 (6.84)	4.19 (4.20)	2.12 (2.05)	1.08-1.01, 0.98-0.95 (0.99-0.97)	-	8.3 (9.1)	-8.1
^{D}Pro (2)	-	4.43 (4.29)	2.33, 1.93 (2.23-2.14)	2.05 (2.11-2.05)	4.01, 3.55 (3.87, 3.68)	-	-
$\gamma^{4,4}$ (3)	6.66 (7.34)	1.96 (2.01-1.95)	2.12 (2.34-2.30)	-	-	-	-7.5
Leu (4)	7.30 (8.05)	4.41 (4.38)	1.74-1.63	1.57 (1.58)	0.95-0.90 (0.97-0.95, 0.93-0.92)	7.5 (8.0)	-7.3

[c] Chemical Shift values of proton resonances in $CDCl_3$ and CD_3OH. Values in parentheses are corresponding to CD_3OH.

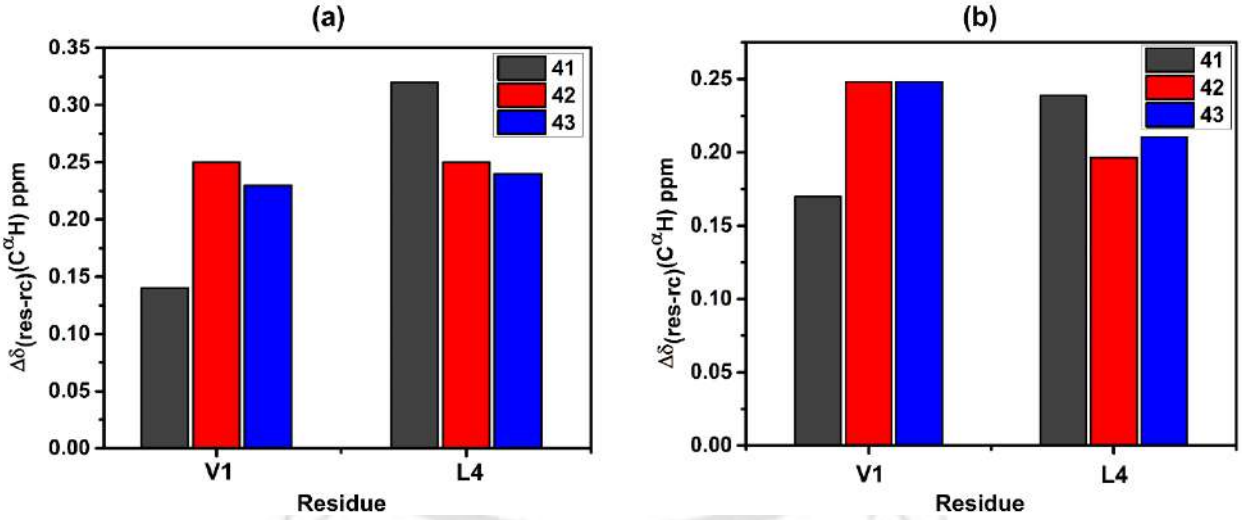

Figure 4.3. Plot of the differences in $C^{\alpha}H$ chemical shift value of the residues with respect to random coil chemical shifts of **41-43** in (a) $CDCl_3$ and (b) CD_3OH.

4.3.1.1.2. Concentration dependent NMR study

Further, to look at the effect of concentration on the aggregation of the peptides **41-43** in solution (both in $CDCl_3$ and CD_3OH), we performed a concentration dependent ^{1}H NMR in the concentration range of 1 mM to 20 mM, both in $CDCl_3$ and CD_3OH. Figures 4.4-4.6 shows

TH-3141_166122021

the stacked plots of the partial ^{1}H NMR spectra of **41-43** at three different concentrations. Very little change (Figures 4.4a-4.6a and Table 4.4) and no change (Figure 4.4b-4.6b) in chemical shift of the NH protons were observed in $CDCl_3$ and CD_3OH, respectively, upon varying the concentration from 1 mM upto 20 mM which indicated absence of aggregation in between peptides through intermolecular H-bonding. This suggested that peptide aggregation was not a significant factor in the interpretation of NMR parameters.[330,331]

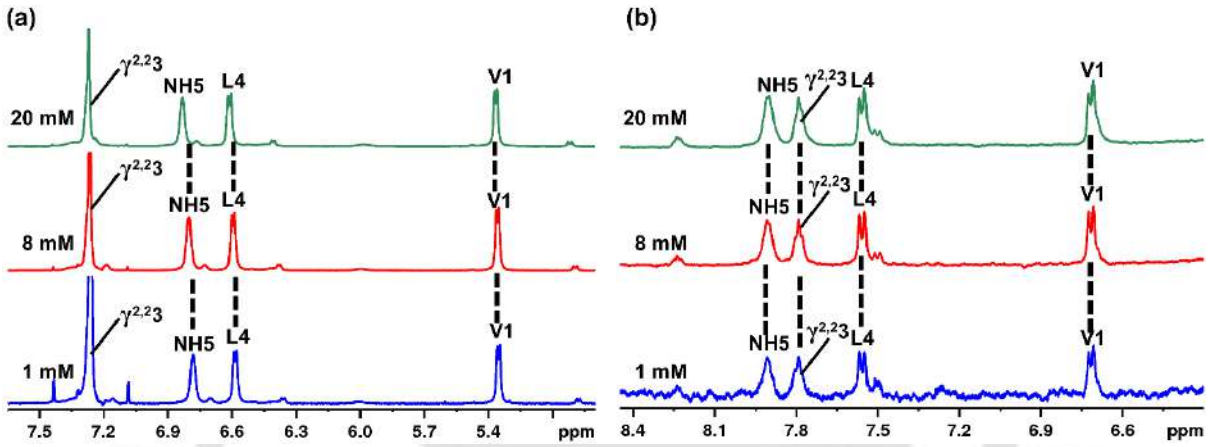

Figure 4.4. Concentration dependent 1D ^{1}H spectra of **41** in (a) $CDCl_3$ (b) CD_3OH at 298 K in 600 MHz. Dotted vertical lines are shown to represent the less movement of the NH resonances.

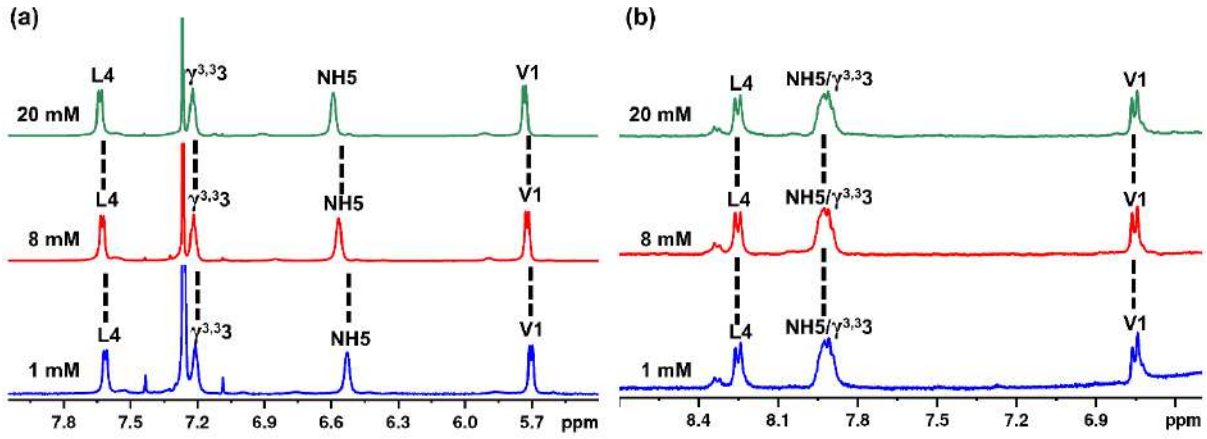

Figure 4.5. Concentration dependent 1D ^{1}H spectra of **42** in (a) $CDCl_3$ (b) CD_3OH at 298 K in 600 MHz. Dotted vertical lines are shown to represent the less movement of the NH resonances.

TH-3141_166122021

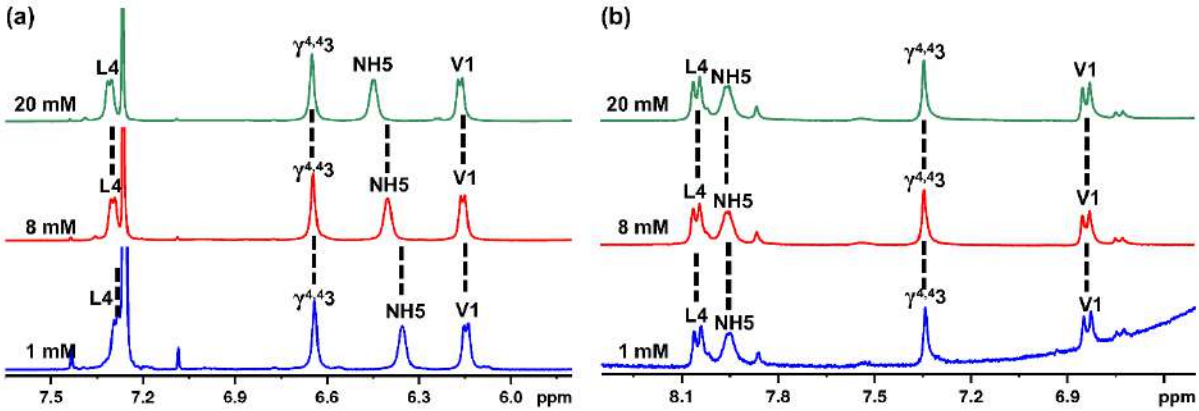

Figure 4.6. Concentration dependent 1D ^{1}H spectra of **43** in (a) $CDCl_3$ (b) CD_3OH at 298 K in 600 MHz. Dotted vertical lines are shown to represent the less movement of the NH resonances.

Table 4.4. NH Chemical shift differences of peptide **41-43** in $CDCl_3$ within the concentration range of 1 mM to 20 mM at 298 K.

NH protons	**Δδ (ppm) = [(Chemical Shift in $CDCl_3$ at 20 mM conc.)-(Chemical Shift in $CDCl_3$ at 1 mM conc.)]**		
	41	**42**	**43**
NH (1)	0.02	0.04	0.02
NH (3)	0.02	0.01	0.01
NH (4)	0.03	0.03	0.03
NH (5)	0.05	0.06	0.10

4.3.1.1.3. NOESY

Figures 4.7-4.9b and Figures 4.7-4.9c represent the partial NH-NH and NH-$C^{\alpha}H$ regions of the NOESY spectrum of **41-43** in $CDCl_3$. One noticeable feature for all the peptides, was the absence of the sequential d_{NN} NOEs. Also, inter-residue $C^{\alpha}H_i \leftrightarrow NH_{i+1}$ NOEs were more intense compared to intra-residue $NH_i \leftrightarrow C^{\alpha}H_i$ NOEs for the residues Val (1) and Leu (4). Both these features hinted to a non-helical conformation in these peptides.

TH-3141_166122021

A strong NOE between Val (1) $C^{\alpha}H \leftrightarrow {}^{D}Pro$ (2) $C^{\delta}H$ was observed for all the three peptides which confirmed the trans geometry at the Val (1)-^{D}Pro (2) peptide bond (Figures 4.10). Presence of inter-residue NOEs in peptides **41-43** in between ^{D}Pro (2) $C^{\alpha}H/C^{\delta}H \leftrightarrow \gamma^{2,2/3,3/4,4}$ (3) NH; $\gamma^{3,3/4,4}$ (3) $C^{\alpha}H/\gamma^{2,2/4,4}$ (3) $C^{\beta}H/\gamma^{2,2/3,3}$ (3) $C^{\gamma}H \leftrightarrow$Leu (4) NH, were indicative of the formation of bent stereochemistry across the ^{D}Pro (2)-$\gamma^{2,2/3,3/4,4}$ (3) segment (Figures 4.7-4.9c).

Presence of a long-range d_{NN} NOEs of medium intensity in between Val (1) NH$\leftrightarrow$ Leu (4) NH in **42** and **43**, established the formation of two residue $\alpha\gamma$ tight turn across ^{D}Pro (2)-$\gamma^{3,3/4,4}$ (3) segment. However, absence of this NOE in **41**, suggested that in this peptide, no tight turn was formed across the ^{D}Pro (2)-$\gamma^{2,2}$ (3) segment. Additional long range NOEs between Boc (0) methyl protons $\leftrightarrow$ NH (5)(w)/Terminal methyl (NH-Me)(m) were observed (Figures 4.8d, 4.9d) clearly in **42** and **43** which further conclusively established the formation of tight turn across the ^{D}Pro (2)-$\gamma^{3,3/4,4}$ (3) segment. These long-range NOEs were absent in **41** corroborating the absence of tight $\alpha\gamma$ turn in the peptide. In short, all the above data, suggested that both **42** and **43** formed well-structured isolated β-turn mimic across the $\alpha\gamma$ segment which was the expanded analog (C_{12} non-helical turn) of the β-turn formed across the $\alpha\alpha$ segment (C_{10} non-helical). Though in the case of **41**, there was presence of a bent structure across the ^{D}Pro (2)-$\gamma^{2,2}$ (3) segment, as evidenced from presence of some inter-residue NOEs mentioned above, it failed to form a tight β-turn mimic as present in **42** and **43**.

TH-3141_166122021

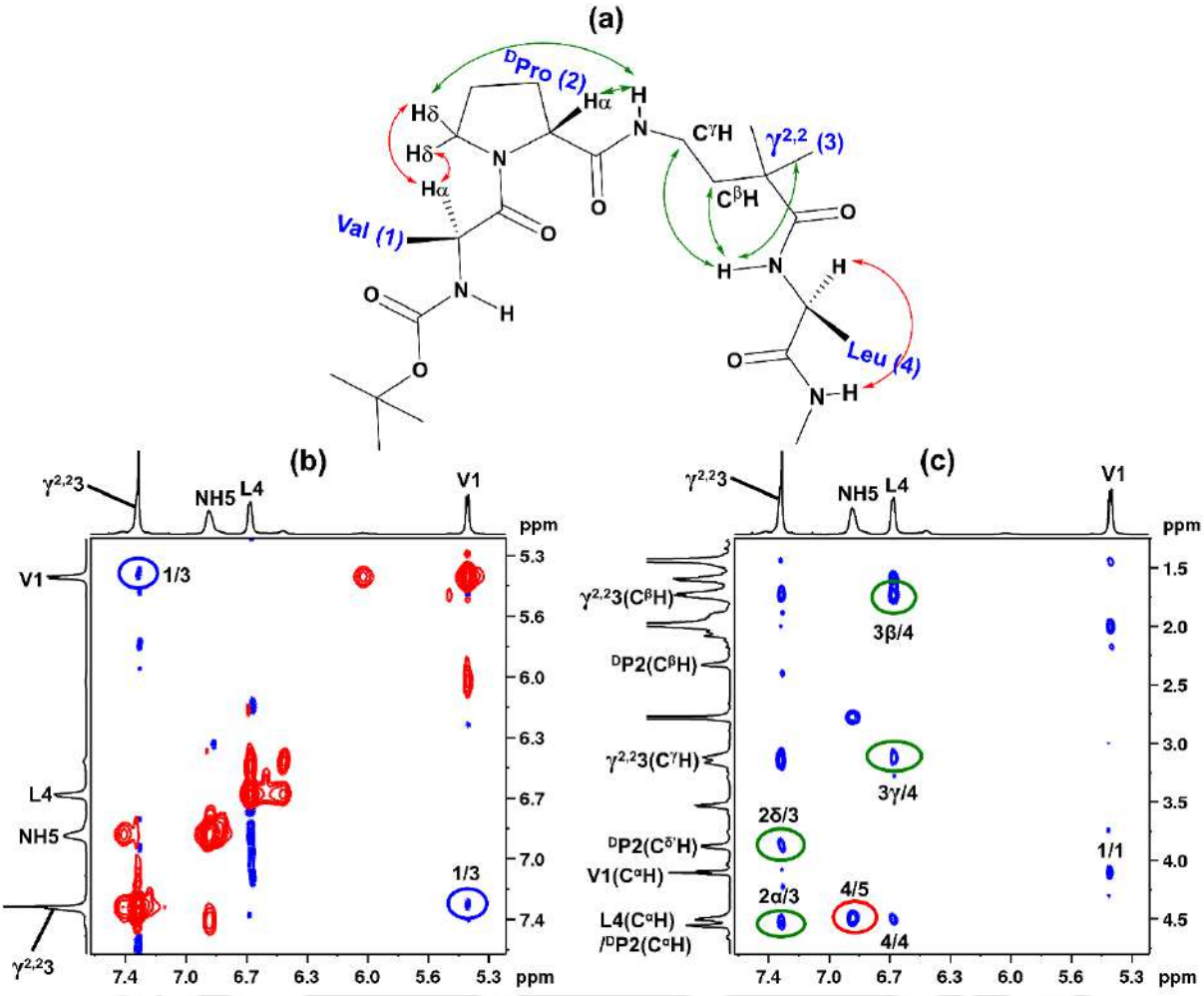

Figure 4.7. (a) Schematic representation of observed NOEs for **41** in $CDCl_3$. Partial 600 MHz NOESY spectrum at 298 K representing (b) NH-NH and (c) NH-$C^{\alpha-\delta}H$ region of **41**. Color codes have been used to map the NOEs marked in the schematic (a) and those observed in the NOESY spectrum (b, c), except Val (1) $C^{\alpha}H \leftrightarrow {}^{D}$Pro (2) $C^{\delta}H$ NOE, which is shown in Figure

TH-3141_166122021

4.10a.

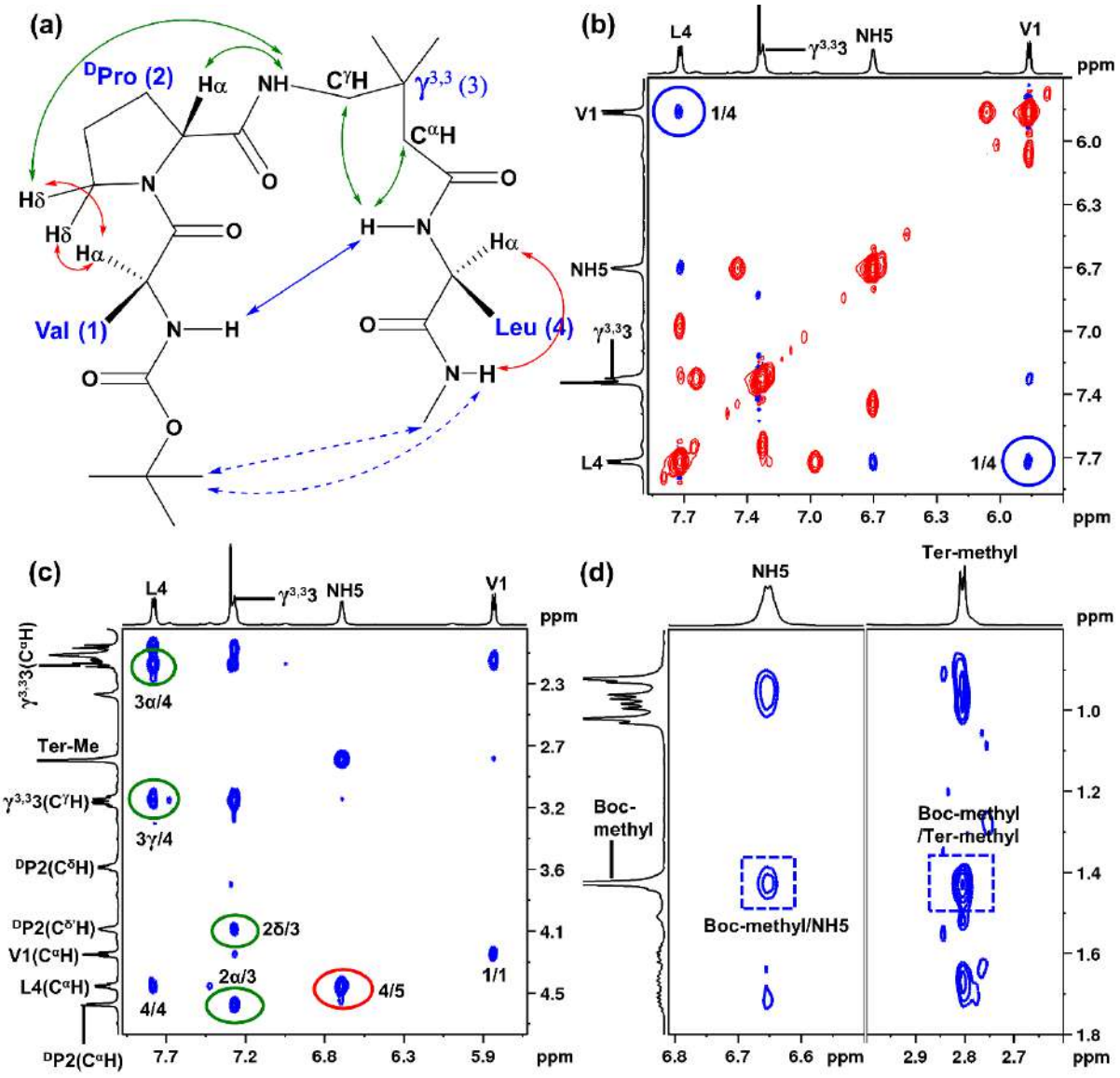

Figure 4.8. (a) Schematic representation of observed NOEs for **42** in $CDCl_3$. The long-range NOEs compatible with the β-turn conformation are marked in blue. Partial 600 MHz NOESY spectrum at 298 K representing (b) NH-NH, (c) NH-$C^{\alpha\text{-}\delta}H$ region and (d) other long-range NOEs of **42**. Color codes have been used to map the NOEs marked in the schematic (a) and those observed in the NOESY spectrum (b, c, d), except Val (1) $C^{\alpha}H \leftrightarrow {}^{D}Pro$ (2) $C^{\delta}H$ NOE, which is shown in Figure 4.10b.

TH-3141_166122021

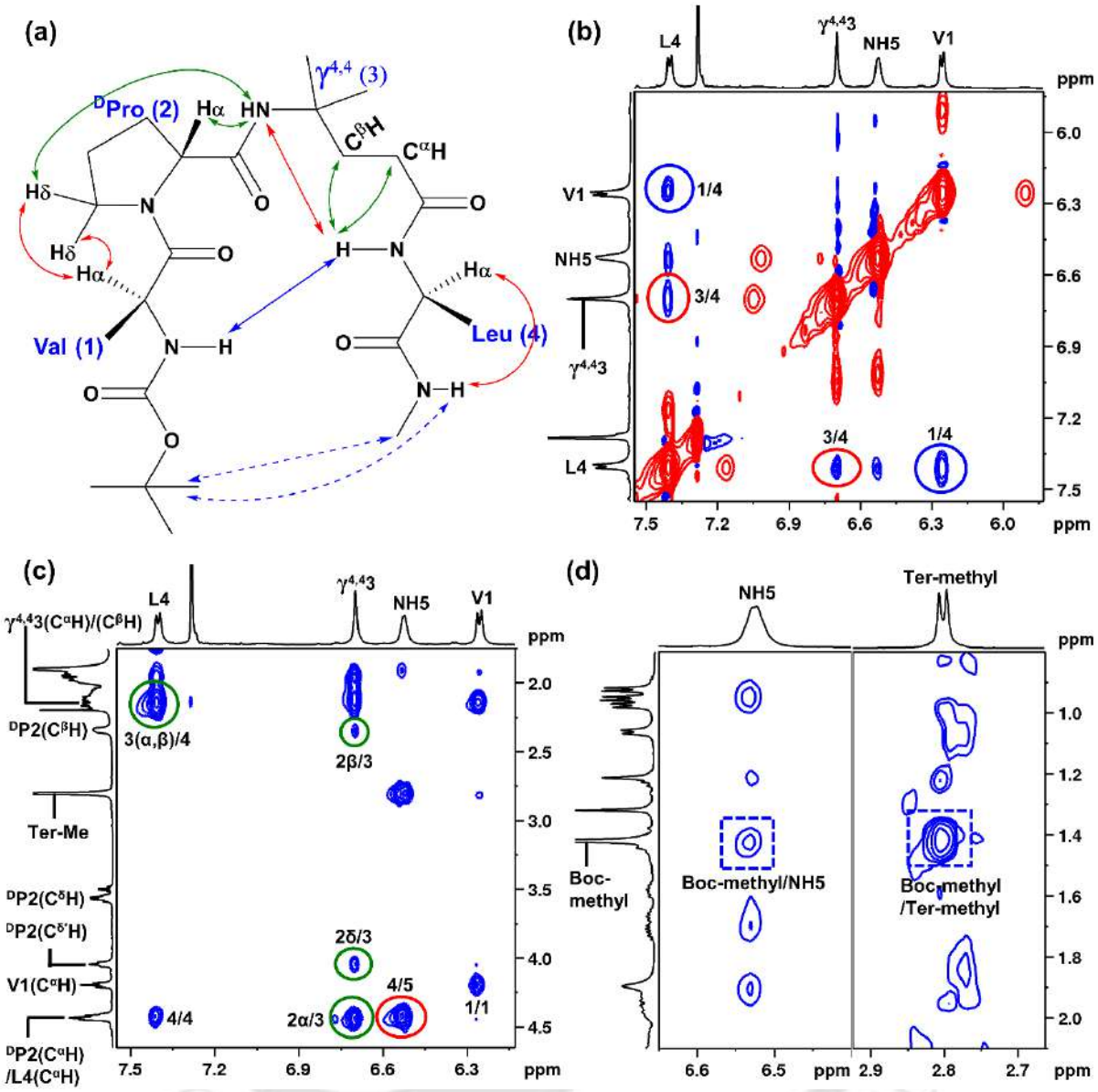

Figure 4.9. (a) Schematic representation of observed NOEs for **43** in $CDCl_3$. The long-range NOEs compatible with the β-turn conformation are marked in blue. Partial 600 MHz NOESY spectrum at 298 K representing (b) NH-NH, (c) NH-$C^{\alpha-\delta}H$ region and (d) other long-range NOEs of **43**. Color codes have been used to map the NOEs marked in the schematic (a) and those observed in the NOESY spectrum (b, c, d), except Val (1) $C^{\alpha}H \leftrightarrow {}^{D}$Pro (2) $C^{\delta}H$ NOE, which is shown in Figure 4.10c.

TH-3141_166122021

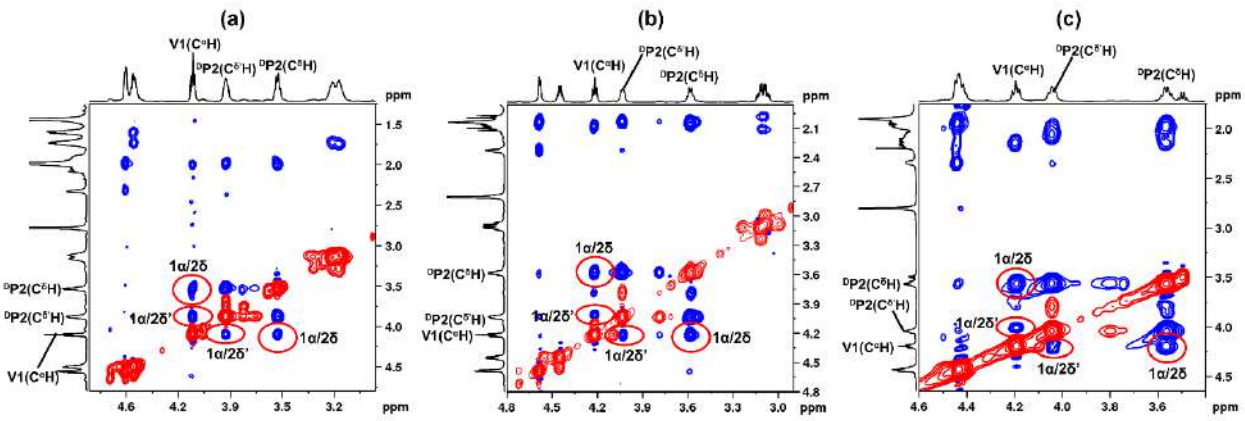

Figure 4.10. Partial 600 MHz NOESY spectrum displaying $C^{\alpha}H \leftrightarrow C^{\delta}H$ NOEs of (a) **41, (b) 42 and (c) 43** in $CDCl_3$ at 298 K.

Polar protic solvent CD_3OH is known in the literature to promote non-helical conformations like β-hairpins and turns due to the formation of solute-solvent hydrogen bonds.[215,332-334] Thus, in order to probe the solvent susceptibility of the conformation of the tetrapeptides in solution, we performed NMR in CD_3OH (Figures 4.2b, 4.11-4.13 and 4.14). NOEs observed for all the peptides **41-43**, were almost similar to that obtained in $CDCl_3$. In case of **42** and **43**, the observation of long-range NOEs like Val(1) NH↔Leu (4) NH and Boc (0) methyl protons ↔ Terminal methyl (NH-Me) (Figures 4.12-4.13d) established the formation of the tight isolated β-turn mimic (C_{12} non-helical) across the $\alpha\gamma^{x,x}$ segment (x,x = 3,3/4,4). In the case of **41**, absence of these long-range NOEs suggested the absence of the C_{12} hydrogen bonded turn, though the presence of other NOEs (^{D}Pro (2) $C^{\alpha}H/C^{\delta}H \leftrightarrow \gamma^{2,2}$ (3) NH; $\gamma^{2,2}$ (3) $C^{\beta}H/ C^{\gamma}H/$ Methyl ↔Leu (4) NH) proved the presence of a bent stereochemistry across the $\alpha\gamma^{2,2}$ segment. Thus it can be concluded that the conformations adopted by the tetrapeptides **41-43** were independent of the solvent effect. While $\gamma^{3,3}$ and $\gamma^{4,4}$ could be accommodated in the (i+2) position of the C_{12} β-turn mimic, $\gamma^{2,2}$ was unable to do so.

We performed variable temperature NMR for all the peptides **41-43** to understand the effect of temperature on the isolated turn conformations. The values of dδ/dT have been tabulated in

TH-3141_166122021

Table 4.1-4.3. In the β-turns/mimics formed in peptides/rigid peptidomimetic units, the H-bonded and the exposed NHs have distinct dδ/dT values of <4.5 (ppb/ ºC) and >4.5 (ppb/ºC) respectively.[330,331,335-338] In **41-43**, the dδ/dT values for most of the NHs lied in the above mentioned ranges, that corroborated the earlier established secondary structures. However, a few H-bonded NHs adopted borderline dδ/dT values. There are earlier examples in literature where H-bonded NH's were reported to adopt borderline dδ/dT values in peptides which formed β-hairpins in solution.[209,339,340] It was thus concluded from the above experiment that peptides **42** and **43** adopted a tight turn geometry that was destabilized by increasing the temperature.

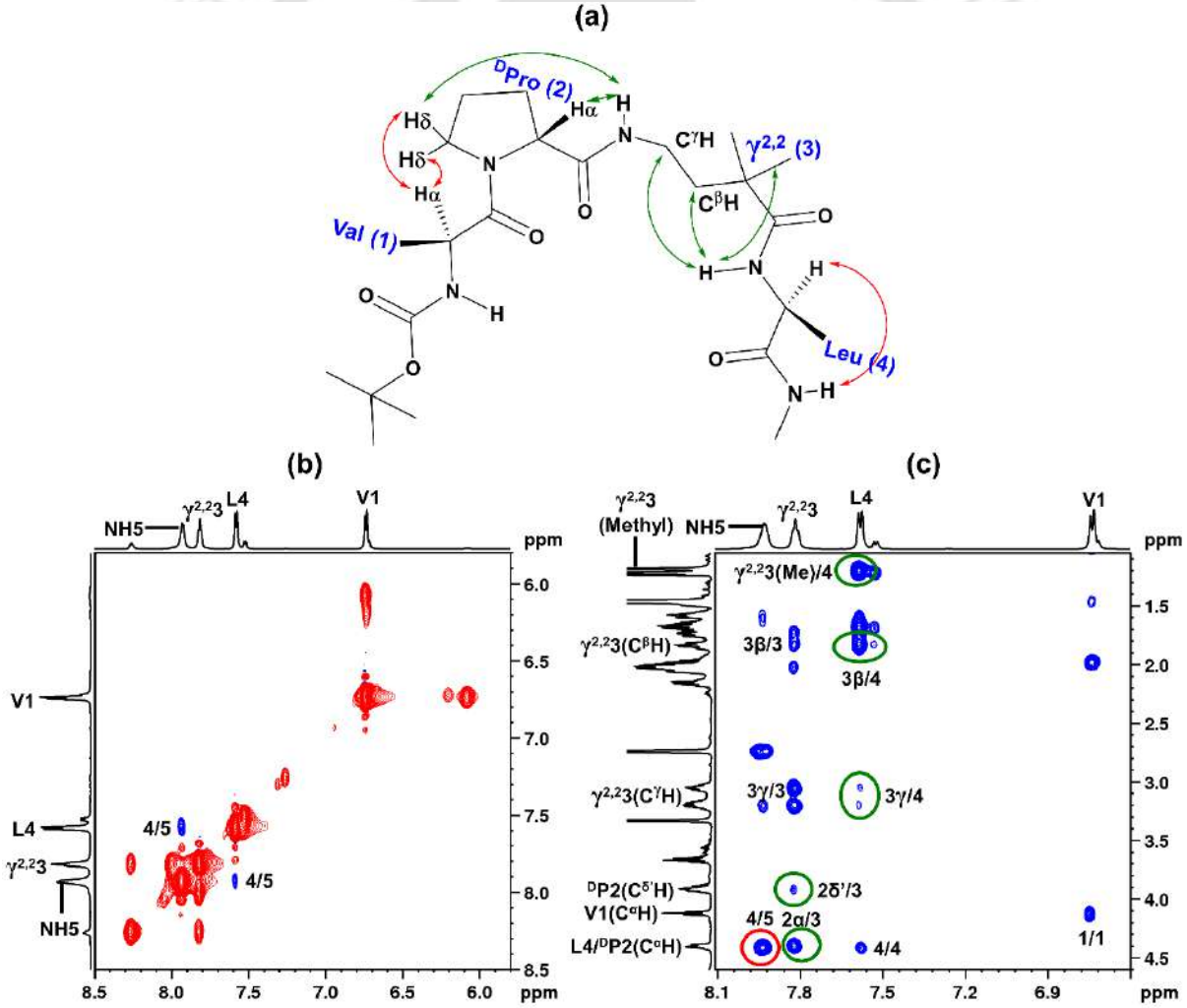

TH-3141_166122021

Figure 4.11. (a) Schematic representation of observed NOEs for **41** in CD_3OH. Partial 600 MHz NOESY spectrum at 298 K representing (b) NH-NH and (c) NH-$C^{\alpha-\delta}H$ region of **41**. Color codes have been used to map the NOEs marked in the schematic (a) and those observed in the NOESY spectrum (b, c), except Val (1) $C^{\alpha}H \leftrightarrow {}^{D}Pro$ (2) $C^{\delta}H$ NOE, which is shown in Figure 4.14a.

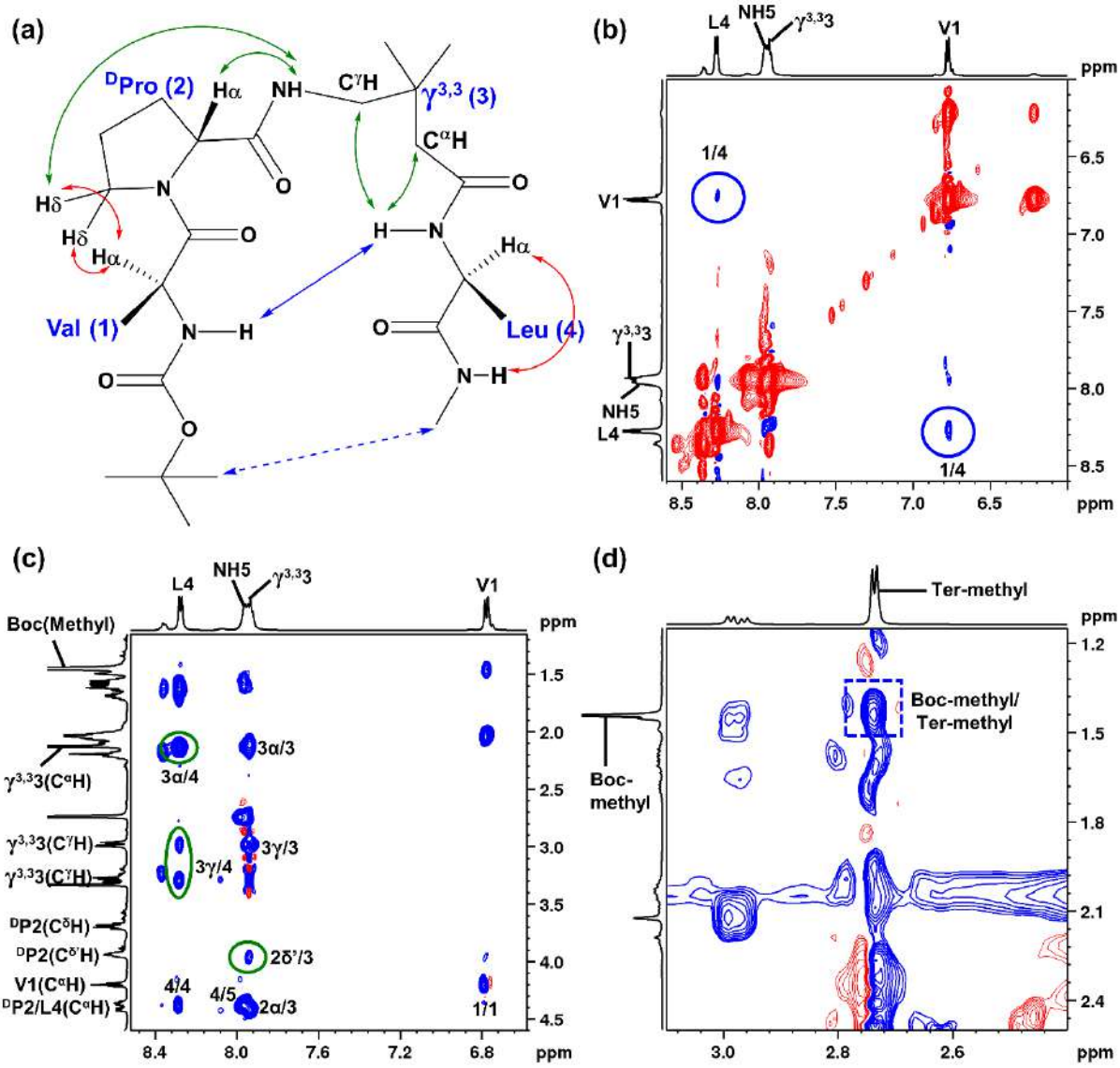

Figure 4.12. (a) Schematic representation of observed NOEs for **42** in CD_3OH. The long-range NOEs compatible with the β-turn conformation are marked in blue. Partial 600 MHz NOESY spectrum at 298 K representing (b) NH-NH, (c) NH-$C^{\alpha-\delta}H$ region and (d) other long-range NOEs of **42**. Color codes have been used to map the NOEs marked in the schematic (a) and

TH-3141_166122021

those observed in the NOESY spectrum (b, c, d), except Val (1) $C^{\alpha}H \leftrightarrow {}^{D}Pro$ (2) $C^{\delta}H$ NOE, which is shown in Figure 4.14b.

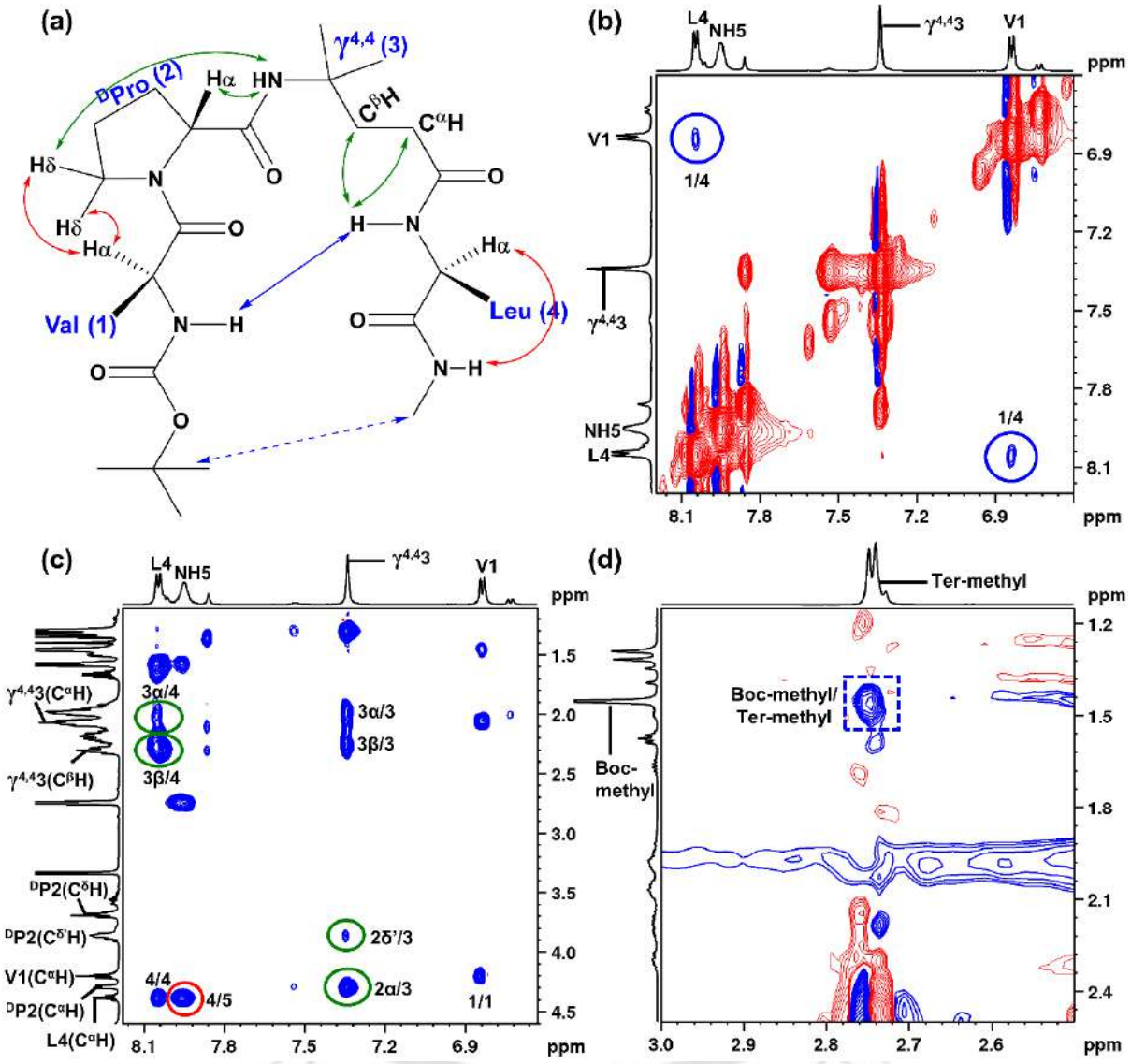

Figure 4.13. (a) Schematic representation of observed NOEs for **43** in CD_3OH. The long-range NOEs compatible with the β-turn conformation are marked in blue. Partial 600 MHz NOESY spectrum at 298 K representing (b) NH-NH, (c) NH-$C^{\alpha\text{-}\delta}H$ region and (d) other long-range NOEs of **43**. Color codes have been used to map the NOEs marked in the schematic (a) and those observed in the NOESY spectrum (b, c, d), except Val (1) $C^{\alpha}H \leftrightarrow {}^{D}Pro$ (2) $C^{\delta}H$ NOE, which is shown in Figure 4.14c.

TH-3141_166122021

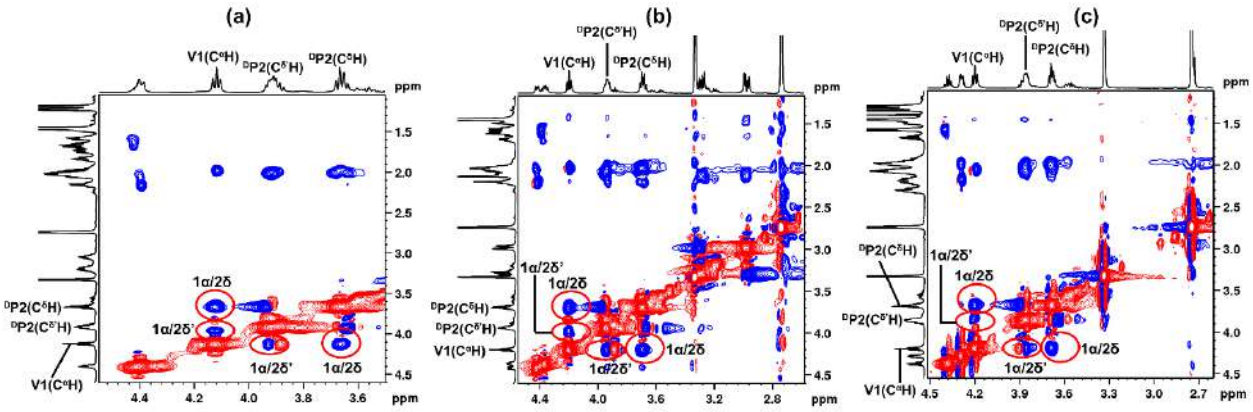

Figure 4.14. Partial 600 MHz NOESY spectrum displaying $C^{\alpha}H \leftrightarrow C^{\delta}H$ NOEs of (a) **41, (b) 42** and **(c) 43** in CD_3OH at 298 K.

4.3.1.1.4. DMSO-d_6 titration: In order to establish the hydrogen bond pattern in the solution conformation of **41-43** in $CDCl_3$, we performed DMSO-d_6 titration experiment. Figures 4.15 and 4.16 show the plots of the change in the chemical shift values ($\Delta\delta$ ppm, Table 4.5) of the NH protons upon addition of DMSO-d_6 to the $CDCl_3$ solution of **41-43**. Upon addition of polar DMSO-d_6 to the peptide solution in non-polar $CDCl_3$, non-hydrogen bonded (solvent exposed) NHs formed hydrogen bond with DMSO-d_6, and show a downfield movement of the chemical shift values, while the already intra-molecularly hydrogen bonded NHs or solvent shielded NHs show no movement. In case of **41**, all the NHs other than NH (3) showed considerable downfield shifting of the NH protons (Table 4.5), suggesting them to be non-hydrogen bonded. NH (3) with a $\Delta\delta$ value of 0.23 might be solvent shielded or intra-molecularly hydrogen bonded. As the hydrogen bonds in between Val (1) NH $\leftrightarrow$ Leu (4) CO and Leu (4) NH $\leftrightarrow$ Val (1) CO are essential for stabilizing the tight turn across $\alpha\gamma^{2,2}$ segment, the absence of formation of hydrogen bonds by Val (1) NH and Leu (4) NH as seen from the solvent titration experiment, suggested the absence of tight turn across the $\alpha\gamma^{2,2}$ segment, thus supporting the conclusions from the NOE experiment described earlier. In the case of **43**, Val (1) NH and Leu (4) NH show low $\Delta\delta$ values suggesting them to be hydrogen bonded, while NH (5) ($\Delta\delta$ ~1.2) was

TH-3141_166122021

completely solvent exposed suggesting it to be non-hydrogen bonded. This observation was in line with the formation of tight turn across the $\alpha\gamma^{4,4}$ segment in **43** stabilized by a C_{12} hydrogen bond in between Val (1) CO ↔ Leu (4) NH and a second hydrogen bond in between Val (1) NH ↔ Leu (4) CO. In **42**, while Leu (4) NH was completely hydrogen bonded ($\Delta\delta$ ~ 0.25), Val (1) NH was partially solvent exposed ($\Delta\delta$ ~ 0.50), suggesting a weaker hydrogen bond in between Val (1) NH and Leu (4) CO in comparison to that between Val (1) CO ↔ Leu (4) NH. NH (5) remained non-hydrogen bonded while NH (3) was solvent shielded in **42**. It should be noted that NH (3) in the tight $\alpha\gamma$ C_{12} turns should remain non-hydrogen bonded, as reported earlier in the literature.[215,221] The counterintuitive small change in the chemical shift value of this NH, observed in all the peptides might be owing to the inaccessibility of DMSO-d_6 to this proton, due to its crowded environment.

Thus in short, solvent titration experiments confirmed the formation of C_{12} tight turn in **42** and **43** (across $\alpha\gamma^{3,3}$ and $\alpha\gamma^{4,4}$ segments respectively), but not in **41** (across $\alpha\gamma^{2,2}$ segment).

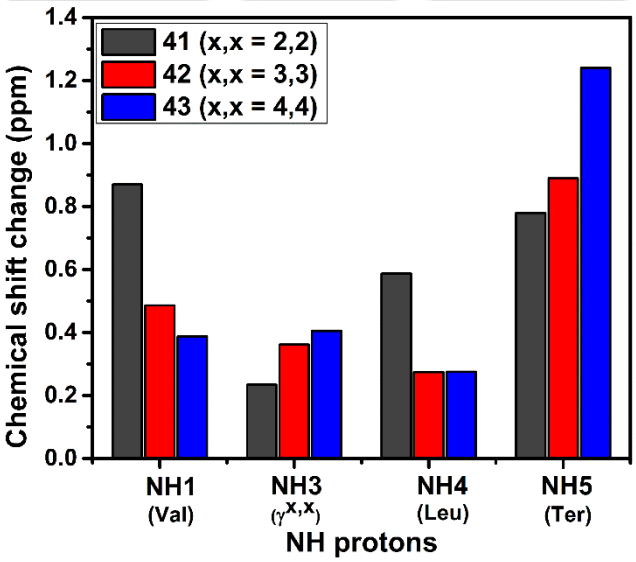

Figure 4.15. Plot of the change of NH chemical shift value of the residues of **41-43** in $CDCl_3$ with increasing concentration of DMSO-d_6 (0-40 %) at 298 K.

TH-3141_166122021

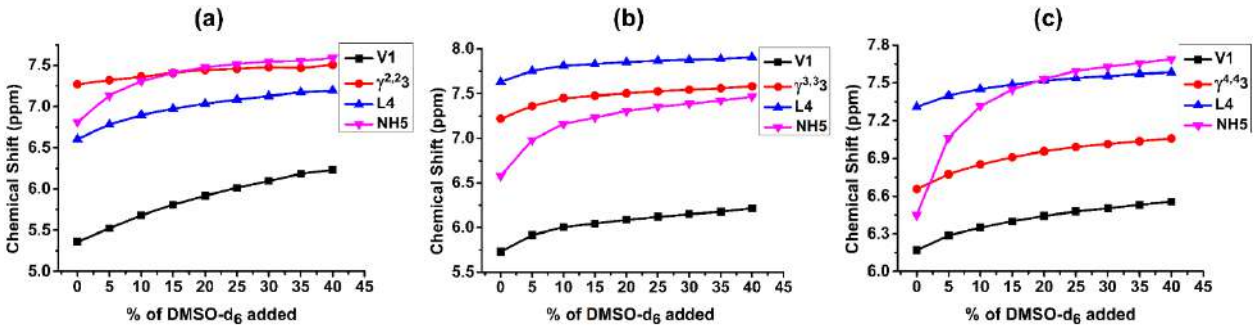

Figure 4.16. Solvent dependence of NH chemical shifts of the peptide, (a) **41**, (b) **42**, and (c) **43** at varying concentrations of DMSO-d_6 in $CDCl_3$ at 298 K.

Table 4.5. NH Chemical shift differences of peptide **41-43** in $CDCl_3$ with increasing % of DMSO-d_6 at 298 K.

	Δδ (ppm) = [(Chemical Shift in $CDCl_3$+40% DMSO-d_6)-(Chemical Shift in $CDCl_3$)]		
	41	**42**	**43**
NH (1)	0.9	0.5	0.4
NH (3)	0.23	0.3	0.4
NH (4)	0.6	0.25	0.24
NH (5)	0.8	0.9	1.2

4.3.1.2. CD Spectroscopy

Far-UV circular dichroism spectra of **41**−**43** were recorded in methanol for understanding their secondary structure (Figure 4.17). **41**−**43** exhibited a positive band at ~207 nm. A negative band appeared at ~226 nm (for **41**), ~233 nm (for **42**) and ~236 nm (for **43**) respectively. β-turns predominantly one have strong $\pi \rightarrow \pi*$ positive band at 200–210 nm, negative band at 180–190 nm and a weak negative $n \rightarrow \pi*$ band at 220–230 nm.[325] The intensities of the bands at 207 and ~233 nm for **42** and **43** established well-formed β-turns in both of them. However, in the case of **41** the positive band at 207 nm had diminished intensity and the negative band was red-shifted to 226 nm, suggesting absence of the β-turn conformation. Thus, the CD data supported the formation of isolated non-helical β-turn in **42** and **43**, While **41** failed to accommodate at the i+2 position of a β-turn mimic as observed from NMR studies.

TH-3141_166122021

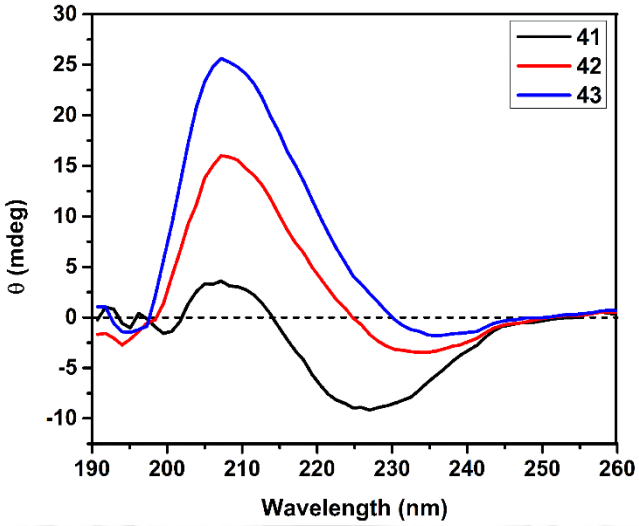

Figure 4.17. Far-UV circular dichroism spectra of peptides **41**−**43** recorded in methanol at concentrations of 600 μM.

4.3.2. DFT optimized structures of 41-43

Unfortunately, despite several attempts, crystals of **41-43** could not be grown. In order to gain better insight into the solution conformation of **41-43**, we computed their structures using DFT calculations (Figure 4.18, Tables 4.6 and 4.7). The optimized structures corroborated with the observations from the solution NMR studies. **41** formed a bent structure due to the presence of ^{D}Pro residue but was unable to form the C_{12} expanded tight β-turn analog across the ^{D}Pro-$\gamma^{2,2}$ segment. $\gamma^{2,2}$ (3) NH was most probably involved in a C_7 hydrogen bond with Val (1) CO across the ^{D}Pro (2) residue as seen from the energy optimized structure of **41** (Figure 4.18a, Table 4.7), thus explaining the very less change in the chemical shift of the $\gamma^{2,2}$ (3) NH as observed in the solvent titration experiment earlier (Figures 4.15, 4.16). The long NH (1) ↔ NH (4) inter proton distance of 9.0 Å (Figure 4.18a) observed in the optimized structure explained the absence of the observation of NOE in between them (Figures 4.7b and 4.11b). Thus it might be concluded that irrespective of whichever amino acid residue is placed at the (i+1) position, $\gamma^{2,2}$ cannot be accommodated at the (i+2) position of the non-helical C_{12} turn. On the contrary,

TH-3141_166122021

both **42** and **43**, gave rise to isolated C_{12} non-helical turns (Figures 4.18b, c) in the optimized structures which corroborated with the NMR observations. The short NH (1) ↔ NH (4) inter-proton distances of 3.1 and 3.2 Å in **42** and **43** respectively, validated the observation of long-range NOEs in between these protons and the evidence of tight turn stereochemistry. $\gamma^{3,3}$ (3) NH and $\gamma^{4,4}$ (3) NH in **42** and **43** respectively were not engaged in C_7 hydrogen bonds as seen from the optimized structures. The relatively low movement of their chemical shifts as seen from the solvent titration experiment (Figure 4.15, 4.16) earlier could thus be attributed to their crowded environment leading to limited solvent accessibility. High energy of **41** peptide (ΔE ~ 8 kcal/mol, Figure 4.18d) relative to the most stable **42** peptide could be attributed to the loss of intra molecular hydrogen bonds (Figure 4.18a). Energy of the **43** and **42** peptides differ by only ~ 0.5 kcal/mol (Figure 4.18d) due to similar hydrogen bonding interactions (Table 4.6). The structural parameters (Table 4.6, Table 4.7) and the energetics (Figure 4.18d) were found to be similar in the absence (vacuum) and presence of solvents (chloroform and methanol).

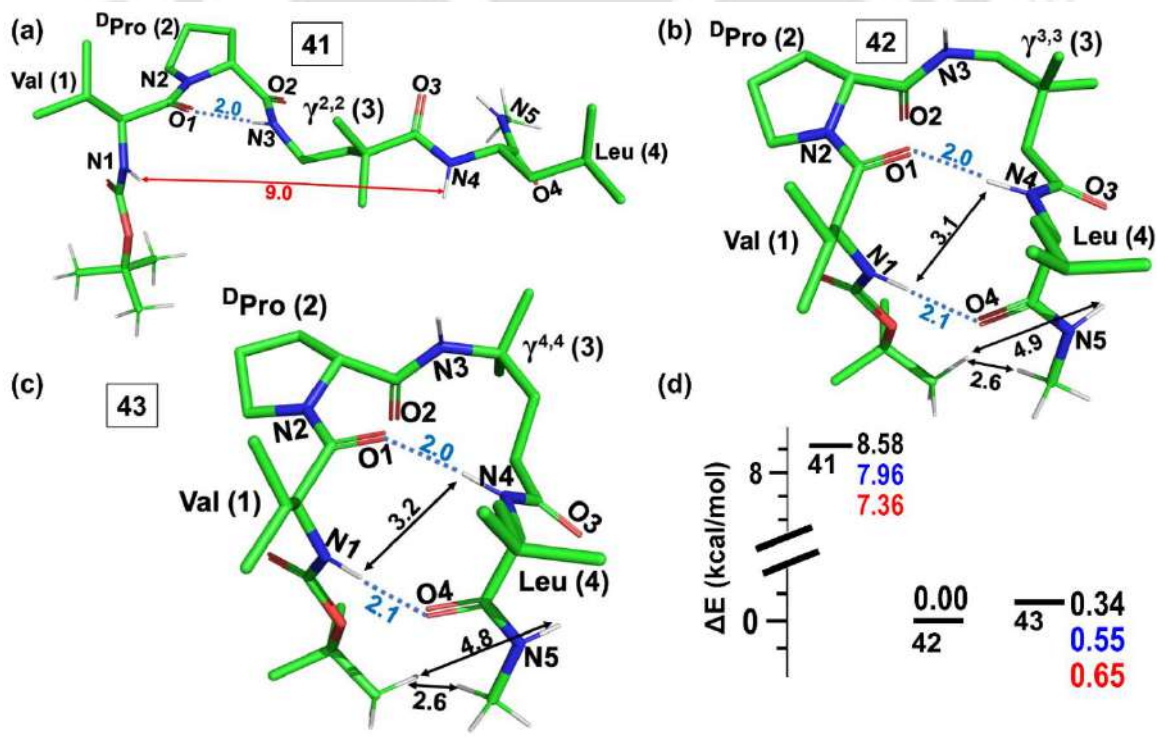

TH-3141_166122021

Figure 4.18. (a-c) Energy optimized structures for **41-43** from DFT calculations. Solid black and red double-headed arrows indicate the distances (in Å) in between protons where long range NOEs were (**42**, **43**) or were not (**41**) observed respectively. Broken blue lines indicate the hydrogen bonds present in the structures with the hydrogen bond distances in Å (H…A) mentioned alongside. Hydrogens are only shown for the peptide backbone and the terminal capping for clarity. (d) Energies of the optimized structures relative to the most stable **42** peptide in vacuum (black), methanol (blue) and chloroform (red). Y-axis was broken for clarity.

TH-3141_166122021

Table 4.6. Backbone dihedral angles (in degree) of peptides **41-43** obtained from DFT optimized structures in vacuum (black) and implicit solvent models (methanol: blue, chloroform: red).

	41				
	ϕ	θ_1	θ_2	ψ	ω
Val (1)	-111.0 -112.9 -112.9	-	-	121.3 122.4 122.3	171.1 174.1 172.9
^{D}Pro (2)	80.9 81.5 81.2	-	-	-75.2 -73.7 -74.8	177.3 177.2 177.3
$\gamma^{2,2}$ (3)	**92.3** **87.6** **89.8**	**81.7** **83.1** **83.0**	**-172.1** **-171.1** **-171.5**	**-118.1** **-118.4** **-117.8**	**176.7** **176.9** **176.7**
Leu (4)	-84.1 -86.0 -85.2	-	-	79.8 79.3 79.9	-178.2 176.9 -177.6
	42				
Val (1)	-93.2 -100.3 -99.3	-	-	112.7 123.0 121.4	178.7 178.0 178.0
^{D}Pro (2)	60.6 59.4 60.3	-	-	-130.6 136.0 -134.2	-177.9 -178.9 -179.1
$\gamma^{3,3}$ (3)	**-100.9** **-100.8** **-101.4**	**64.6** **65.7** **65.7**	**-160.8** **-161.9** **-161.9**	**99.5** **111.0** **110.0**	**177.1** **177.5** **176.9**
Leu (4)	-84.5 -107.2 -105.6	-	-	93.8 123.4 120.0	173.1 179.1 178.7
	43				
Val (1)	-93.0 -99.4 -98.5	-	-	112.5 123.6 120.3	178.8 177.8 177.8
^{D}Pro (2)	56.9 58.6 57.8	-	-	-133.8 -138.0 -136.9	-177.6 -179.1 -178.5
$\gamma^{4,4}$ (3)	**-84.1** **-86.8** **-85.9**	**70.0** **66.7** **67.7**	**-160.6** **-164.2** **-163.9**	**77.3** **100.6** **96.9**	**177.8** **176.2** **176.5**
Leu (4)	-82.9 -108.4 -103.2	-	-	90.9 122.1 117.3	176.8 -177.8 -179.1

TH-3141_166122021

Table 4.7. Hydrogen bond parameters of **41-43** obtained from DFT optimized structures in vacuum (black) and implicit solvent models (methanol: blue, chloroform: red). Hydrogen bonds essential for the formation of the isolated tight turn across the $\alpha\gamma^{x,x}$ segment are marked in bold and observed in **42** and **43**.

	41		**42**		**43**	
	Heavy atom distance (Å)	Angle (°)	Heavy atom distance (Å)	Angle (°)	Heavy atom distance (Å)	Angle (°)
N4-H4…O1 (C_{12} turn)	-	-	**3.0** **3.0** **3.0**	**172.3** **170.8** **170.4**	**3.0** **3.0** **3.0**	**176.3** **171.7** **172.4**
N1-H1…O4	-	-	**3.2** **3.0** **3.0**	**168.8** **171.4** **170.6**	**3.1** **3.0** **3.0**	**167.3** **172.0** **171.0**
N3-H3…O1	2.8 2.9 2.9	143.7 144.2 143.7	-	-	-	-
N5-H5…O3	3.0 3.0 3.0	140.8 139.7 139.9	-	-	-	-

4.3.3. Differential position of di-substitution along the γ amino acid backbone and its stereochemical implication

Longer β-hairpin peptides contain two distinct parts: (a) the β-turn and (b) the strands. While the turn promotes the stand registry, the hydrogen bonds in between the strands stabilize the β-turn in return. Formation of isolated tight turns in smaller peptides however is completely dependent on the conformational attributes of the turn residues, and hence are challenging.

From our present study, it could be conclusively proved that model tetrapeptides with $\gamma^{3,3}$ and $\gamma^{4,4}$ methyl di-substituted γ amino acid residues (**42** and **43**), adopted a tight turn conformation across ^{D}Pro (2)-$\gamma^{x,x}$ (3) segment in solution, while the peptide **41** with $\gamma^{2,2}$ methyl di-substituted amino acid residue could not form the stable isolated tight turn. The canonical β-turn in all α peptides across the αα dipeptide segment is stabilized by 10 membered hydrogen bond. In the

TH-3141_166122021

peptides **42** and **43**, the turn is formed across the αγ segment and hence should be stabilized by a 12 membered hydrogen bond which is the higher homologue of the canonical β-turn. DMSO-d_6 solvent titration studies established the formation of the C_{12} hydrogen bond (in between Leu (4) NH and Val (1) CO) in peptides **42** and **43**. The isolated turns formed in the solution by **42** and **43** were insensitive to the polarity of the solvent indicating their robustness. Thus both $\gamma^{3,3}$ and $\gamma^{4,4}$ methyl di-substituted gamma amino acid residues could be incorporated at the (i+2) position of a non-helical C_{12} αγ turn, with different α amino acid residues like Aib or ^{D}Pro positioned at (i+1) location of the turn. Similar to our earlier studies, where $\gamma^{2,2}$ failed to nucleate a β-hairpin, it also failed to nucleate an isolated C_{12} non-helical turn in our present studies. All the model tetrapeptides were identical to each other in all other aspects, except the gamma amino acid residue used. Thus this difference in the ability of the peptides **41-43** to form isolated expanded β-turn mimics may be attributed to their only difference, that is the stereochemical preference of the three differentially di-substituted γ amino acid residues, which in turn is a direct consequence of the variable position of di-substitution along their backbone.

TH-3141_166122021

4.4. Conclusion

We have successfully constructed isolated β-turn mimics in small tetrapeptides **42** and **43,** which are stabilized by C_{12} hydrogen bond across the central $\alpha\gamma^{x,x}$ (x,x = 3,3 and 4,4) segment. While $\gamma^{3,3}$ and $\gamma^{4,4}$ could easily be incorporated at the (i+2) position of the β-turn, $\gamma^{2,2}$ could not be incorporated at the same location. We have also proved that the conformation adopted by the peptides were robust and independent of the solvent polarity. This distinct difference in the stereochemical behavior of the three gamma amino acid residues ($\gamma^{2,2}$, $\gamma^{3,3}$, $\gamma^{4,4}$) was attributed to the difference in the position of di-substitution along the backbone of these residues. Thus the correct choice of the position of backbone di-substitution might be used in advantage to generate myriad structures.

TH-3141_166122021

Chapter 5

Effect of Differential Geminal Substitution of γ Amino Acid Residues Incorporatedat the (i+2) Position of αγ Turn Segments on the Conformation of Template β-Hairpin Peptides

TH-3141_166122021

5.1. Introduction

In this chapter, we wanted to investigate the effect of the variable backbone constraint of the dimethyl substituted γ amino acids ($\gamma^{2,2}$, $\gamma^{3,3}$, and $\gamma^{4,4}$) on their conformational preferences in being able (a) to be accommodated into the (i+2) position of the αγ C_{12} expanded type II′ β-turn and (b) to nucleate the β-hairpin conformation in a model octapeptide (Figure 5.1). For studying the role of N-terminal substitution on the peptide conformation, two sets of peptides with acetyl (**51**−**53**) and Fmoc (**54**−**56**) N-protecting groups were synthesized (Figure 5.1, Table 5.1). Solution conformation of the peptides was studied in detail using spectroscopic techniques like NMR, CD, and IR. Attempts to grow single crystals of the peptides have been futile so far. *ab initio*-optimized structures of the peptides were obtained from density functional theory (DFT) calculations. The final structures obtained from the experimental and theoretical approaches were in good agreement with each other and gave a detailed picture of the conformations adopted by the peptides in solution.

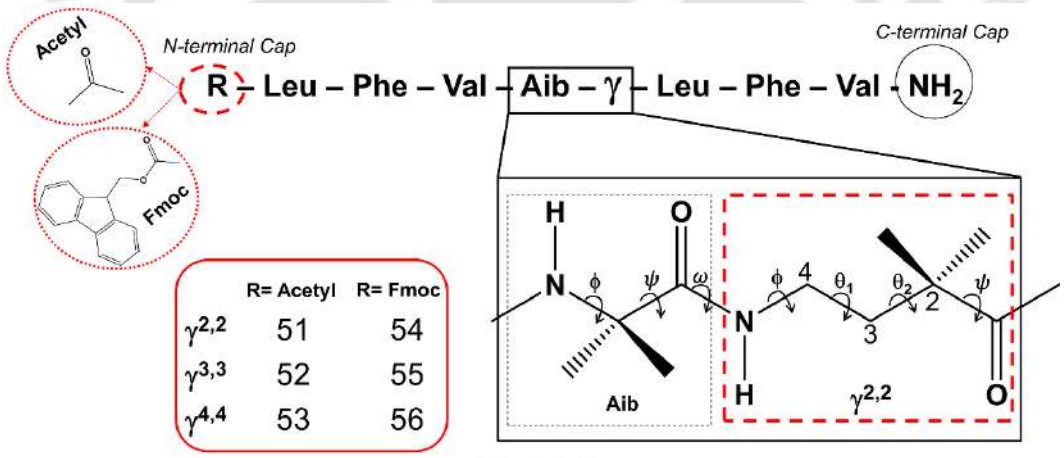

Figure 5.1. Schematic of synthesized peptides **51**−**56** containing $\gamma^{2,2}$, $\gamma^{3,3}$, and $\gamma^{4,4}$ amino acid residues at the 5th position of model β-hairpin peptides (Ac/Fmoc)-LFV-U-Xxx-LFV-$CONH_2$. Chemical structure and definition of torsion angles of the Aib-$\gamma^{2,2}$ segment are demonstrated in the inset.

TH-3141_166122021

Table 5.1. Model octapeptides **51-56** synthesized in the present study

Peptide	Sequence	Mass (Da)			Retention Time (min)
		$M+H^+_{calc.}$/ $M+Na^+_{calc.}$	$M+H^+_{obs.}$	$M+Na^+_{obs.}$	
51	Ac- Leu-Phe-Val-Aib-$\gamma^{2,2}$-Leu-Phe-Val-$CONH_2$	976.6230	976.6237	---	14.66
52	Ac- Leu-Phe-Val-Aib-$\gamma^{3,3}$-Leu-Phe-Val-$CONH_2$	976.6230	976.6224	---	14.77
53	Ac- Leu-Phe-Val-Aib-$\gamma^{4,4}$-Leu-Phe- Val-$CONH_2$	976.6230	976.6239		14.78
54	Fmoc- Leu-Phe- Val-Aib-$\gamma^{2,2}$-Leu-Phe-Val-$CONH_2$	1156.6805/ 1178.6630	---	1178.6640	18.24
55	Fmoc- Leu-Phe- Val-Aib-$\gamma^{3,3}$-Leu-Phe-Val-$CONH_2$	1156.6805/ 1178.6630		1178.6638	18.31
56	Fmoc- Leu-Phe- Val-Aib-$\gamma^{4,4}$-Leu-Phe-Val-$CONH_2$	1156.6805/ 1178.6630	1156.6805	1178.6626	19.36

5.2. Experimental section

5.2.1. Synthesis of γ amino acids ($\gamma^{2,2}$, $\gamma^{3,3}$, and $\gamma^{4,4}$)

The syntheses of the γ amino acids have been described in section 1.14.1.1 of Chapter 1. Fmoc protected γ amino acids were used for the manual solid-phase synthesis of the peptides.

5.2.2. Synthesis of Fmoc protected amino acids

Amino acids were derivatized using Fmoc-OSu in basic conditions. General synthesis and purification protocols of all Fmoc derivatives have been detailed in sections 1.14.1.2 and 1.14.2.1 of Chapter 1.

TH-3141_166122021

5.2.3. Peptide Synthesis

All peptides (**51-56**) were synthesized through conventional solid phase chemistry. The general protocol is described in section 1.14.1.3.1 of Chapter 1.

5.2.4. Peptide purification

Crude peptides were purified by reverse-phase HPLC using a binary CH_3OH/H_2O (90−100%) solvent system at a flow rate of 10 mL/min using dual UV detection at 214 and 256 nm. All purified peptides (**51−56**) were white amorphous solids in nature. To check the purity, analytical HPLC was performed with a flow rate of 1 mL/min and a linear gradient of 90−100% CH_3OH/H_2O was used (Appendix, Figures A110-A115).

5.2.5. Characterization of peptides 51−56

Ac-Leu-Phe-Val-Aib-$\gamma^{2,2}$-Leu-Phe-Val-$CONH_2$ (**51**): Analytical HPLC retention time: 14.66 min (Appendix, Figure A110). HRMS (ESI) m/z: $(M + H)^+$ Calc. for $C_{52}H_{81}N_9O_9$ 976.6230; Obs. 976.6237 (Appendix, Figure A116). ^{1}H NMR (600 MHz, methanol-d_3) (Appendix, Figure A122): δ 8.21 (d, 1H, J = 7.7 Hz), 8.14 (br, 2H), 8.12 (d, 1H, J = 8.2 Hz), 8.01 (d, 1H, J = 7.0 Hz), 7.93 (d, 1H, J = 8.6 Hz), 7.67 (t, 1H, J = 5.6 Hz), 7.56 (d, 1H, J = 7.6 Hz), 7.22 (m, 11H), 7.01 (s, 1H), 4.69 (m, 2H), 4.43 (ddd, 1H, J = 10.0, 7.6, 5.1 Hz), 4.32 (q, 1H, J = 7.4 Hz), 4.16 (dd, 1H, J = 8.7, 6.7 Hz), 3.99 (t, 1H J = 7.2 Hz), 3.17 (dd, 1H, J = 14.1, 4.7 Hz), 3.06 (m, 3H), 2.95 (ddd, 2H, J = 14.1, 11.1, 8.9 Hz), 2.05 (m, 2H), 1.92 (s, 3H), 1.76 (m, 1H), 1.69 (m, 1H), 1.58 (m, 4H), 1.44 (m, 8H), 1.15 (m, 6H), 0.89 (m, 24H). ^{13}C {1H} NMR (150 MHz, metha8nol-d_3) (Appendix, Figure A128): δ 178.5, 175.4, 174.5, 173.7, 173.5, 172.6, 172.1, 171.9, 171.7, 137.1, 136.9, 129.1, 128.1, 126.4, 60.0, 58.6, 56.7, 54.7, 54.5, 52.4, 41.0, 40.5, 38.9, 37.2, 37.0, 36.2, 30.5, 30.1, 25.2, 24.6, 24.4, 24.0, 23.5, 22.0, 21.9, 21.2, 20.9, 20.7, 18.3, 17.8, 17.1.

TH-3141_166122021

Ac-Leu-Phe-Val-Aib-$\gamma^{3,3}$-Leu-Phe-Val-$CONH_2$ (**52**): Analytical HPLC retention time: 14.77 min (Appendix, Figure A111). HRMS (ESI) m/z: $(M + H)^+$ Calc. for $C_{52}H_{81}N_9O_9$ 976.6230; Obs. 976.6224 (Appendix, Figure A117). ^1H NMR (600 MHz, methanol-d_3) (Appendix Figure A123): δ 8.86 (d, 1H, J = 9.4 Hz), 8.70 (d, 1H, J = 7.9 Hz), 8.53 (s, 1H), 8.29 (br, 2H), 8.25 (d, 1H, J = 9.3 Hz), 7.93 (br, 2H), 7.26 (t, 2H, J = 7.6 Hz), 7.21 (m, 2H), 7.11 (m, 1H), 7.02 (dd, 1H, J = 8.3, 6.4 Hz), 6.97 (t, 2H, J = 7.5 Hz), 6.89 (s, 1H), 6.74 (s, 1H), 6.59 (d, 2H, J = 7.5 Hz), 5.20 (ddd, 1H, J = 10.8, 8.9, 3.6 Hz), 4.73 (m, 2H), 4.47 (br, 1H), 4.33 (m, 1H), 4.08 (dd, 1H, J = 9.4, 7.1 Hz), 3.27 (dd, 2H, J = 13.7, 8.1 Hz), 2.88 (m, 3H), 2.77 (dd, 1H, J = 13.0, 5.6 Hz), 2.71 (dd, 1H, J = 13.4, 5.3 Hz), 1.96 (m, 3H), 1.88 (s, 3H), 1.68 (b, 1H), 1.53 (m, 6H), 1.42 (d, 6H, J = 3.4 Hz), 1.05 (s, 3H), 0.90 (m, 23H), 0.77 (d, 3H, J = 6.7 Hz). ^{13}C {1H} NMR (150 MHz, methanol-d_3) (Appendix, Figure A129): δ 175.6, 173.9, 173.2, 173.1, 172.9, 172.7, 171.9, 171.7, 171.4,121 137.7, 136.0, 129.2, 129.0, 128.2, 127.7, 126.5, 126.3, 58.5, 58.1, 56.8, 54.5, 51.4, 50.7, 49.7, 47.7, 43.5, 42.3, 41.9, 37.8, 37.4, 36.0, 31.9, 30.7, 25.8, 24.9, 24.4, 24.3, 24.3, 22.6, 22.2, 21.7, 20.9, 18.4, 18.2, 18.1, 17.3.

Ac-Leu-Phe-Val-Aib-$\gamma^{4,4}$-Leu-Phe-Val-$CONH_2$ (**53**): Analytical HPLC retention time: 14.78 min (Appendix, Figure A112). HRMS (ESI) m/z: $(M + H)^+$ Calc. for $C_{52}H_{81}N_9O_9$ 976.6230; Obs. 976.6239 (Appendix, Figure A118). ^1H NMR (600 MHz, methanol-d_3) (Appendix, Figure A124): δ 8.61 (d, 1H, J = 9.0 Hz), 8.56 (d, 1H, J = 7.2 Hz), 8.38 (d, 1H, J = 8.7 Hz), 8.33 (s, 1H), 8.28 (d, 1H, J = 9.1 Hz), 8.24 (d, 1H, J = 8.7 Hz), 8.06 (d, 1H, J = 8.0 Hz), 7.20 (m, 2H, J = 7.2 Hz), 7.09 (m, 6H), 6.96 (s, 1H), 6.84 (m, 4H), 5.08 (td, 1H, J = 9.1, 5.2 Hz), 4.71 (q, 1H, J = 7.6 Hz), 4.56 (td, 1H, J = 9.0, 5.3 Hz), 4.44 (q, 1H, J = 7.7 Hz), 4.25 (t, 1H, J = 8.0 Hz), 4.14 (t, 1H, J = 7.9 Hz), 2.97 (dd, 1H, J = 13.3, 8.6 Hz), 2.84 (m, 3H), 2.34 (t, 1H, J = 12.2 Hz), 2.21 (m, 1H), 2.10 (td, 1H, J = 12.0, 6.2 Hz), 1.96 (m, 5H), 1.69 (br, 2H), 1.54 (br, 2H), 1.42 (m, 12H), 1.13 (s, 3H), 0.89 (m, 21H), 0.79 (d, 3H, J = 6.7 Hz). ^{13}C {1H} NMR (150 MHz, methanol-d_3) (Appendix, Figure A130): δ 175.3, 173.4, 172.7, 174.5, 174.2, 172.1, 171.8,

TH-3141_166122021

171.6, 137.1, 136.4, 129.1, 128.0, 126.4, 126.4, 58.4, 58.3, 56.9, 54.7, 54.3, 53.2, 51.7, 51.3, 47.7, 41.7, 41.3, 38.1, 37.3, 35.3, 32.0, 31.5, 30.6, 26.1, 26.0, 25.3, 24.4, 24.2, 23.1, 22.2, 22.0, 21.5, 20.9, 20.9, 18.4, 17.7, 17.3.

Fmoc-Leu-Phe-Val-Aib-$\gamma^{2,2}$-Leu-Phe-Val-$CONH_2$ (**54**): Analytical HPLC retention time: 18.24 min (Appendix, Figure A113). HRMS (ESI) m/z: $(M + Na)^+$ Calc. for $C_{65}H_{89}N_9O_{10}$ 1178.6630; Obs. 1178.6640 (Appendix, Figure A119). ^1H NMR (600 MHz, methanol-d_3) (Appendix, Figure A125): δ 8.10 (m, 3H), 7.96 (d, 1H, J = 7.0 Hz), 7.90 (d, 1H, J = 9.0 Hz), 7.80 (m, 2H), 7.65 (br, 3H), 7.55 (d, 1H, J = 7.6 Hz), 7.39 (t, 2H, J = 7.5 Hz), 7.34 (d, 1H, J = 7.1 Hz), 7.30 (t, 2H, J = 7.4 Hz), 7.17 (m, 10H), 7.08 (t, 1H, J = 7.2 Hz), 6.99 (s, 1H), 4.70 (b, 1H), 4.64 (q, 1H, J = 7.6 Hz), 4.43 (br, 2H), 4.27 (dd, 1H, J = 10.5, 6.8 Hz), 4.20 (t, 1H, J = 6.9 Hz), 4.12 (m, 2H), 3.94 (t, 1H, J = 7.1 Hz), 3.16 (dd, 1H, J = 14.1, 4.7 Hz), 3.05 (m, 2H), 2.94 (dd, 2H, J = 13.7, 8.5 Hz), 2.03 (hept, 2H, J = 6.8 Hz), 1.72 (m, 1H), 1.58 (m, 1H), 1.47 (s, 3H), 1.42 (m, 5H), 1.29 (s, 2H), 1.13 (br, 6H), 0.88 (m, 27H). ^{13}C {1H} NMR (150 MHz, methanol-d_3) (Appendix, Figure A131): δ 178.5, 175.1, 174.5, 174.0, 173.6, 171.8, 143.7, 141.2, 136.8 (d, J = 15.4 Hz), 129.1, 129.0, 128.1, 127.4, 126.8, 126.4, 124.9, 119.6, 78.1, 66.7, 60.1, 58.6, 56.7, 54.7, 54.4, 54.1, 52.4, 40.9, 40.6, 40.5, 38.9, 37.2, 36.2, 30.4, 30.0, 29.3, 25.3, 25.1, 24.6, 24.4, 24.0, 23.5, 22.8, 22.0, 21.9, 20.8, 20.7, 18.4, 18.3, 17.9, 17.1.

Fmoc-Leu-Phe-Val-Aib-$\gamma^{3,3}$-Leu-Phe-Val-$CONH_2$ (**55**): Analytical HPLC retention time: 18.31 min (Appendix, Figure A114). HRMS (ESI) m/z: $(M + Na)^+$ Calc. for $C_{65}H_{89}N_9O_{10}$ 1178.6630; Obs. 1178.6638 (Appendix, Figure A120). ^1H NMR (600 MHz, methanol-d_3) (Appendix, Figure A126): δ 8.72 (d, 1H, J = 7.4 Hz), 8.66 (d, 1H, J = 9.2 Hz), 8.45 (s, 1H), 8.30 (d, 1H, J = 9.1 Hz), 8.15 (d, 1H, J = 9.2 Hz), 8.08 (d, 1H, J = 9.3 Hz), 7.84 (t, 1H, J = 6.6 Hz), 7.80 (dd, 2H, J = 7.7, 3.0 Hz), 7.70 (d, 1H, J = 7.5 Hz), 7.65 (d, 1H, J = 7.5 Hz), 7.39 (br, 2H), 7.31 (br, 2H), 7.21 (t, 2H, J = 7.6 Hz), 7.14 (br, 2H), 7.09 (br, 1H), 7.00 (m, 3H), 6.75 (br, 2H), 6.60 (s, 1H), 6.13 (s, 1H), 5.24 (td, 1H, J = 9.9, 3.5 Hz), 4.64 (m, 2H), 4.53 (dd, 1H, J =

TH-3141_166122021

10.7, 6.8 Hz), 4.37 (m, 2H), 4.23 (t, 1H, J = 6.5 Hz), 4.12 (m, 2H), 3.14 (dd, 1H, J = 13.4, 7.2 Hz), 2.85 (m, 5H), 2.26 (d, 1H, J = 12.9 Hz), 2.13 (d, 1H, J = 12.8 Hz), 2.03 (m, 1H), 1.95 (m, 1H), 1.67 (m, 1H), 1.50 (m, 5H), 1.38 (m, 6H), 1.02 (s, 3H), 0.97 (s, 3H), 0.91 (m, 16H), 0.82 (dd, 6H, J = 14.5, 6.7 Hz), 0.70 (d, 3H, J = 6.8 Hz). ^{13}C {1H} NMR (150 MHz, methanol d_3) (Appendix, Figure A132): δ 174.3, 173.5, 173.1, 172.6, 172.2, 171.4, 156.9, 144.0, 143.7, 141.3, 137.2, 136.1, 129.3, 129.2, 128.1, 127.9, 127.4, 126.8, 126.5, 124.8, 119.6, 66.4, 58.2, 56.8, 54.6, 54.0, 53.7, 50.9, 49.6, 43.6, 41.9, 41.1, 38.7, 37.1, 35.8, 31.9, 30.2, 29.3, 25.6, 24.7, 24.5, 24.4, 22.7, 22.1, 22.0, 20.8, 20.7, 18.5, 18.3, 17.9, 17.0.

Fmoc-Leu-Phe-Val-Aib-$\gamma^{4,4}$-Leu-Phe-Val-$CONH_2$ (**56**): Analytical HPLC retention time: 19.36 min (Appendix, Figure A115). HRMS (ESI) m/z: $(M + Na)^+$ Calc. for $C_{65}H_{89}N_9O_{10}$ 1178.6630; Obs.1178.6626 (Appendix, Figure A121). ^{1}H NMR (600 MHz, methanol-d_3) (Appendix, Figure A127): δ 8.58 (d, 1H, J = 7.0 Hz), 8.54 (d, 1H, J = 8.9 Hz), 8.39 (d, 1H, J = 8.5 Hz), 8.30 (s, 1H), 8.18 (br, 2H), 7.79 (d, 2H, J = 7.8 Hz), 7.69 (d, 1H, J = 7.5 Hz), 7.65 (d, 1H, J = 7.5 Hz), 7.38 (m, 2H), 7.31 (m, 2H), 7.14 (q, 3H, J = 9.7, 8.6 Hz), 7.10−6.99 (m, 6H), 6.88 (d, 2H, J = 7.2 Hz), 6.85 (s, 1H), 6.73 (s, 1H), 6.49 (s, 1H), 5.11 (br, 1H), 4.66 (br, 1H), 4.55 (br, 1H), 4.49 (m, 1H), 4.36 (m, 1H), 4.27 (br, 1H), 4.22 (m, 1H), 4.16 (m, 2H), 2.94 (dd, 1H, J = 13.3, 8.4 Hz), 2.82 (m, 3H), 2.33 (t, 1H, J = 12.7 Hz), 2.20 (t, 1H, J = 11.9 Hz), 2.06 (m, 2H), 1.95 (m, 1H), 1.68 (m, 2H), 1.52 (m, 1H), 1.40 (m, 10H), 1.28 (s, 3H), 1.12 (s, 3H), 0.87 (m, 22H), 0.73 (d, 2H, J = 6.8 Hz). ^{13}C {1H} NMR (150 MHz, DMSO-d_6) (Appendix, Figure A133): δ 173.4, 172.9, 172.7, 172.6, 171.1, 156.3, 141.1, 141.1, 138.1, 138.0, 129.6, 128.4, 128.3, 128.1, 128.0, 127.5, 127.5, 126.6, 126.6, 125.7, 125.7, 120.6, 120.5, 66.0, 58.5, 57.7, 56.8, 54.1, 53.7, 53.5, 52.7, 51.1, 47.0, 41.5, 41.1, 37.7, 37.3, 35.5, 30.9, 30.7, 26.9, 26.8, 25.8, 24.9, 24.5, 24.4, 23.4, 23.4, 22.2, 21.9, 19.6, 19.6, 18.7, 18.1.

TH-3141_166122021

5.2.6. NMR Spectroscopy

All NMR experiments were carried out on a Bruker Ascend Aeon 600 MHz spectrometer. The peptide concentrations were in the range of 5−7 mM in CD_3OH for both 1D and 2D NMR experiments. The chemical shift values and coupling constants were measured from 1D NMR spectra. Variable-temperature 1D NMR experiments were carried out between 291.6 and 323 K. Complete resonance assignments of the protons of **51−56** were done by TOCSY and ROESY experiments. All of the 2D experiments were done in the phase-sensitive mode using the time-proportional phase incrementation (TPPI) method. For all peptides, TOCSY spectra were recorded with a mixing time of 80 ms, but for ROESY spectra, two different mixing times of 150 (for **51−53**) and 200 (for **54−56**) ms were used. The spectral width was 12019.2 Hz in both dimensions. Water suppression was done using the excitation sculpting scheme. The total numbers of scans were fixed at 32 and 8 for TOCSY and ROESY, respectively. Data points were set to 2048 and 300 in f2 and f1 dimensions, respectively, for both TOCSY and ROESY spectra. Zero filling was done to finally yield a data set of 4K × 2K. All NMR spectra were processed using Topspin 3.6 software.

5.2.7. CD Spectroscopy

The CD studies were performed in methanol at 500 μM concentrations of all peptides except for **56** (at 250 μM) due to its poor solubility in methanol. Experimental protocol has been discussed in section 1.14.4.2.2.

5.2.8. FT-IR Spectroscopy

FT-IR spectra of all peptides **51-56** were recorded in CD_3OH solution at 1 mM concentration. Experimental detail is given in section 1.14.4.2.3 of Chapter 1.

TH-3141_166122021

5.2.9. Quantum Chemical Calculations

The β-hairpin structure of octapeptide was taken from the Cambridge Structural Database (accession number CCDC 711306)[215] and used as a template to model **51−56**. The modeled structures (**51−56**) were subjected to ab initio geometry optimization using Gaussian16 software.[298] The B3LYP[299,300] function with the 6-31+G* basis set[301,302] was used for performing optimization, in which methanol was included as the solvent.

5.3. Results and Discussion

Peptides **51−56** were synthesized on a Rink amide resin using conventional manual solid-phase synthesis techniques, purified (Appendix, Figures A110-115) and characterized using HRMS (ESI) (Appendix, Figures A116-A121), ^{1}H NMR (Appendix, Figures A122-A127), and ^{13}C NMR (Appendix, Figures A128-A133). Table 5.1 details the sequences and the physicochemical properties of the peptides synthesized in the present study.

5.3.1 Solution Conformational Studies

5.3.1.1. NMR Spectroscopy

The 600 MHz spectrum of **51−56** revealed a completely dispersed set of sharp NH resonances in CD_3OH, as shown in Figure 5.2 (Tables 5.2 and 5.3). Observation of well-dispersed spectra was an indication of the formation of well-folded secondary structures in solution. Observation of one set of resonances accounting for all of the protons in the compounds was also an indirect proof of the presence of only one conformation in solution. Sequence-specific assignments of the backbone and side-chain proton resonances were achieved for peptides **51−56** using a combination of ^{1}H−^{1}H TOCSY (Appendix, Figures A134-A139) and ^{1}H−^{1}H ROESY experiments (Appendix, Figures A140-A145). $^{3}J_{NH-C^{\alpha}H}$ values (Tables 5.2 and 5.3) of peptides **52**, **53**, **55**, and **56** were very high ($^{3}J \geq 8.0$ Hz) for residues 1−3 and 6−8, indicating extended

TH-3141_166122021

β-strand conformations across LFV (1−3/6−8) segments. On the other hand, for peptides **51** and **54**, most of the $^{3}J_{NH-C^{\alpha}H}$ values were ≤8.0 Hz, which hinted at not so well-formed β-strand conformations.

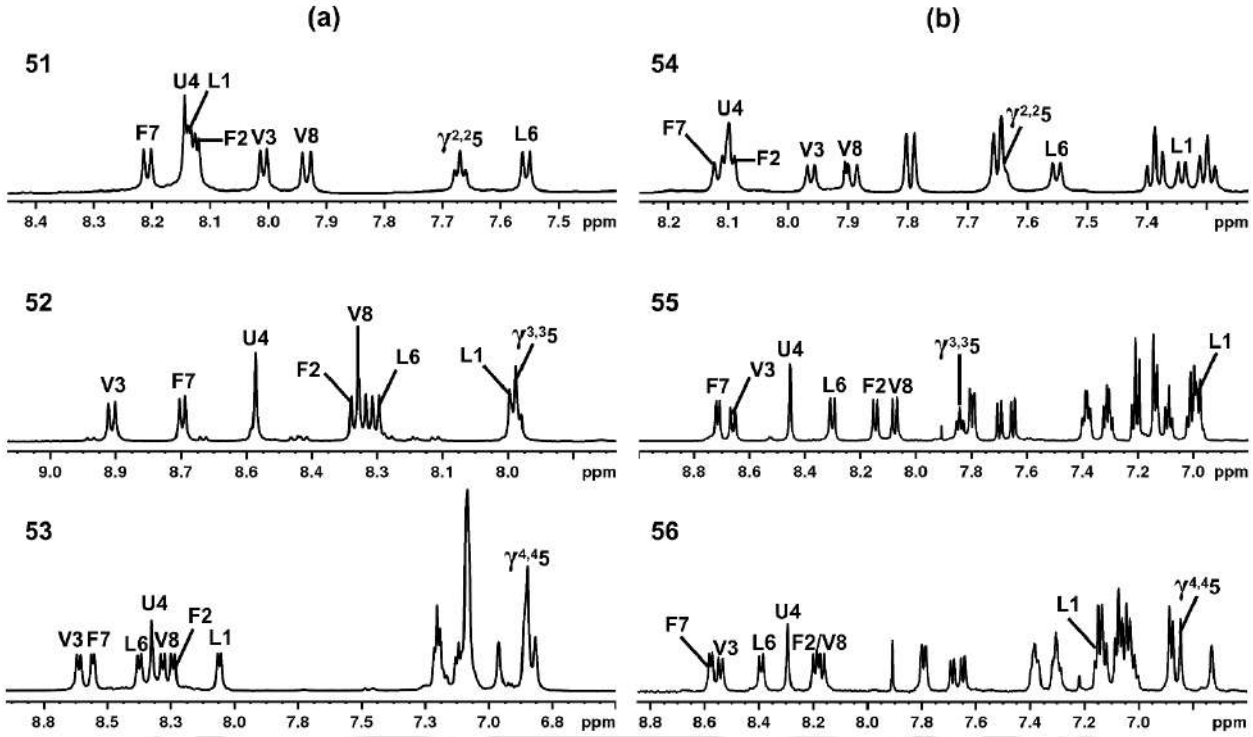

Figure 5.2. Partial 600 MHz 1D ^{1}H NMR spectra at 298K highlighting the amide proton resonances of (a) **51-53**, (b) **54-56** in CD_3OH.

Table 5.2. NH & $C^{\alpha}H$ Chemical Shifts and $^{3}J_{NH-C^{\alpha}H}$ coupling constant of peptides **51**, **52** & **53** in CD_3OH at 298 K.

Residue	Chemical Shift (ppm)						$^{3}J_{NH-C^{\alpha}H}$ (Hz)[b]		
	NH			$C^{\alpha}H$					
	51	**52**	**53**	**51**	**52**	**53**	**51**	**52**	**53**
Leu (1)	8.14	7.93	8.06	4.32	4.47	4.44	b	8.4	8.0
Phe (2)	8.12	8.29	8.24	4.70	5.20	5.08	8.2	9.3	8.7
Val (3)	8.01	8.86	8.61	3.99	4.33	4.25	7.0	9.4	9.0
Aib (4)	8.15	8.53	8.33	-	-	-	-	-	-
Xxx[a] (5)	7.67	7.93	6.85	-	-	-	5.6	5.4	-
Leu (6)	7.56	8.25	8.38	4.43	4.73	4.56	7.6	9.3	8.7
Phe (7)	8.21	8.70	8.56	4.66	4.73	4.71	7.7	7.9	7.2
Val (8)	7.93	8.29	8.28	4.16	4.08	4.14	8.6	8.8	9.1

[a] Xxx = $\gamma^{2,2}$ (**51**), $\gamma^{3,3}$ (**52**) and $\gamma^{4,4}$ (**53**); [b] Coupling constant could not be determined in some cases because of resonance overlap.

TH-3141_166122021

Table 5.3. NH & $C^{\alpha}H$ Chemical Shift and $^{3}J_{NH\text{-}C^{\alpha}H}$ coupling constant of peptides **54**, **55** & **56** in CD_3OH at 298 K.

Residue	Chemical Shift (ppm)						$^{3}J_{NH\text{-}C^{\alpha}H}$ (Hz)[b]		
	NH			$C^{\alpha}H$					
	54	**55**	**56**	**54**	**55**	**56**	**54**	**55**	**56**
Leu (1)	7.34	6.98	7.13	4.11	4.12	4.16	7.1	b	b
Phe (2)	8.10	8.15	8.19	4.70	5.24	5.11	7.8	9.2	8.8
Val (3)	7.96	8.66	8.54	3.94	4.37	4.27	7.0	9.3	8.9
Aib (4)	8.10	8.45	8.30	-	-	-	-	-	-
Xxx[a] (5)	7.65	7.84	6.85	-	-	-	5.1	6.6	-
Leu (6)	7.55	8.30	8.39	4.42	4.64	4.55	7.6	9.1	8.5
Phe (7)	8.12	8.72	8.58	4.64	4.64	4.66	7.8	7.4	7.0
Val (8)	7.90	8.08	8.17	4.13	4.11	4.16	9.0	9.3	9.4

[a] Xxx = $\gamma^{2,2}$ (**54**), $\gamma^{3,3}$ (**55**) and $\gamma^{4,4}$ (**56**); [b] Coupling constant could not be determined because of resonance overlap.

Figures 5.3a and 5.3b show the aromatic resonances of peptides **51**−**53** and **54**−**56** in CD_3OH, respectively. Aromatic protons of **52** and **53** were very well-dispersed, in contrast to those of **51**. A pair of equivalent aromatic protons was significantly upfield shifted to 6.57 ppm for **52** and 6.84 ppm for **53** (Figure 5.3a). In contrast, the aromatic proton resonances of **51** were merged and exhibited chemical shifts in the range of 7.13−7.27 ppm, with no upfield shift of aromatic protons. Similarly, Figure 5.3b shows a pair of equivalent aromatic protons upfield-shifted to 6.73 ppm for **55** and 6.88 ppm for **56**. The aromatic region of **54** was less dispersed than **55** and **56** and closely clustered around 7.06−7.23 δ. Dispersion of the aromatic resonances and the shielding (upfield shifting) of some of them were a consequence of the anisotropic effect of the Phe rings from the other facing strand. This effect can only be seen when the facing Phe rings are in close proximity to each other upon strand registry and has been reported in other studies.[341-343] Thus, it can be concluded that peptides **52**, **53**, **55**, and **56** formed well-registered β-hairpins in contrast to **51** or **54**.

TH-3141_166122021

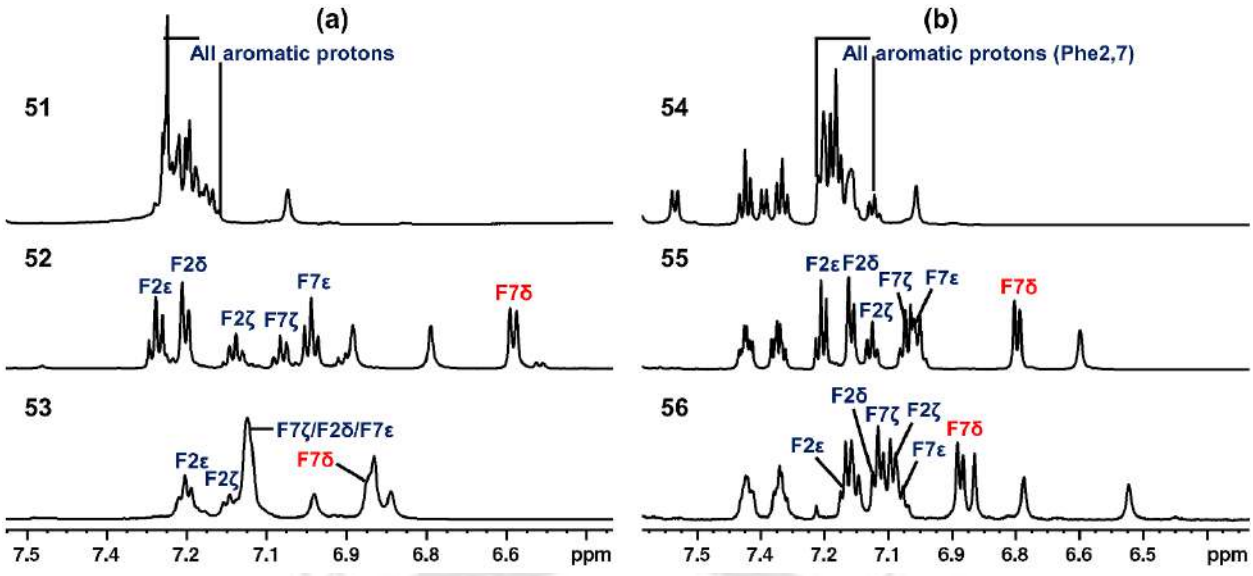

Figure 5.3. Aromatic proton resonances of (a) **51-53**, (b) **54-56**, representing the upfield shift of Phe (7) δ protons (highlighted in red). Aromatic protons are well-dispersed for peptides **52**, **53, 55 and 56** but are clustered together for peptides **51** and **54**.

Figures 5.4 and 5.5 represent the partial NH−$C^{\alpha}H$ and NH−NH regions of the ROESY spectrum of **51**−**53**. For all of the peptides, inter-residue $C^{\alpha}_{i}H \leftrightarrow N_{i+1}H$ NOEs were more intense compared to $C^{\alpha}_{i}H \leftrightarrow N_{i}H$ intra-residue NOEs for the segments Leu (1)-Aib (4) and Leu (6)-Val (8), suggesting an extended conformation in the LFV segments. This was supported by the observation of high ^{3}J values for these residues as mentioned earlier. The presence of strong inter-residue NOEs in peptides **51**−**53** between Aib (4) NH $\leftrightarrow\gamma^{2,2/3,3/4,4}$ (5) NH, Aib (4) Methyl $\leftrightarrow \gamma^{2,2/3,3/4,4}$ (5) NH (Figure 5.6) and $\gamma^{2,2/4,4}$ (5) $C^{\beta}H$/ $\gamma^{2,2/3,3}$ (5) Methyl ↔Leu (6) NH (Figure 5.6) and a weak NOE between $\gamma^{2,2}$ (5) $C^{\gamma}H$ ↔ Leu (6) NH (Figure 5.6a) was indicative of turn formation across the Aib (4)-$\gamma^{2,2/3,3/4,4}$ (5) segment. Additionally, the presence of long-range d_{NN} NOE between Val (3) NH↔ Leu (6) NH in peptides **52** and **53** established the formation of two-residue αγ tight turns across the Aib (4)-$\gamma^{3,3/4,4}$ (5) segment. However, the absence of this NOE in **51** suggested that in this peptide the αγ turn formed was not as tight as that formed in peptides **52** and **53**. The long-range d_{NN} NOE Leu (1) ↔ Val (8) was observed clearly in **53**,

TH-3141_166122021

which confirmed strand registry in β-hairpins. In **52**, Leu (1) ↔ Val (8) NOE could not be unequivocally assigned due to the overlap of the Phe (2) and Val (8) NH resonances. Interestingly, for both **52** and **53**, a weak long-range NOE between N-ter (methyl proton) ↔ C-ter NH_2 (Figures 5.6 b, c) was observed, supportive of the strand registry, even at the termini of the hairpin. In short, all of the above data suggested that both **52** and **53** formed well-structured β-hairpins with registered strands. In the case of **51**, neither of these two long-range NOEs that indicate proper strand registry in hairpins was present.

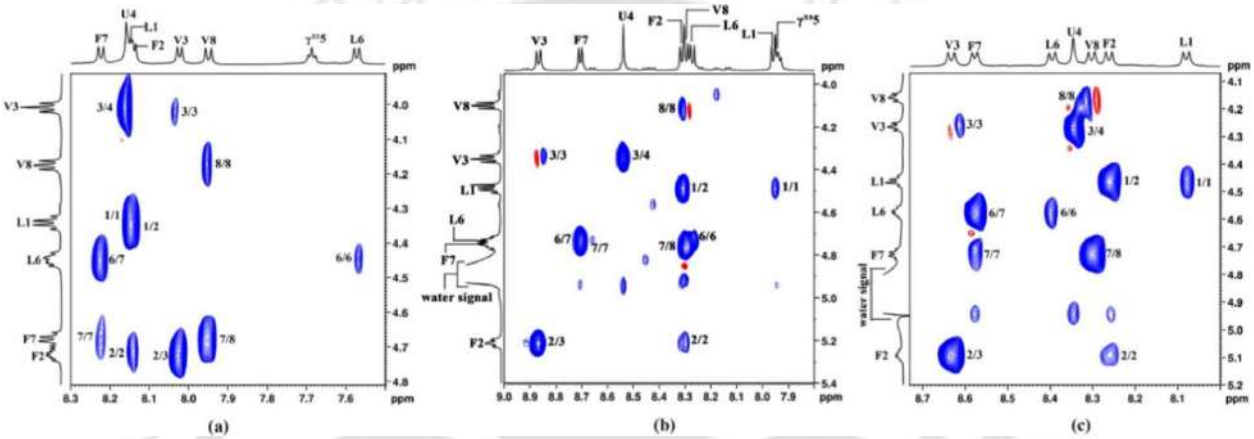

Figure 5.4. NH−$C^{\alpha}H$ region of the partial 600 MHz ROESY spectrum of (a) **51**, (b) **52**, and (c) **53** in CD_3OH at 298K.

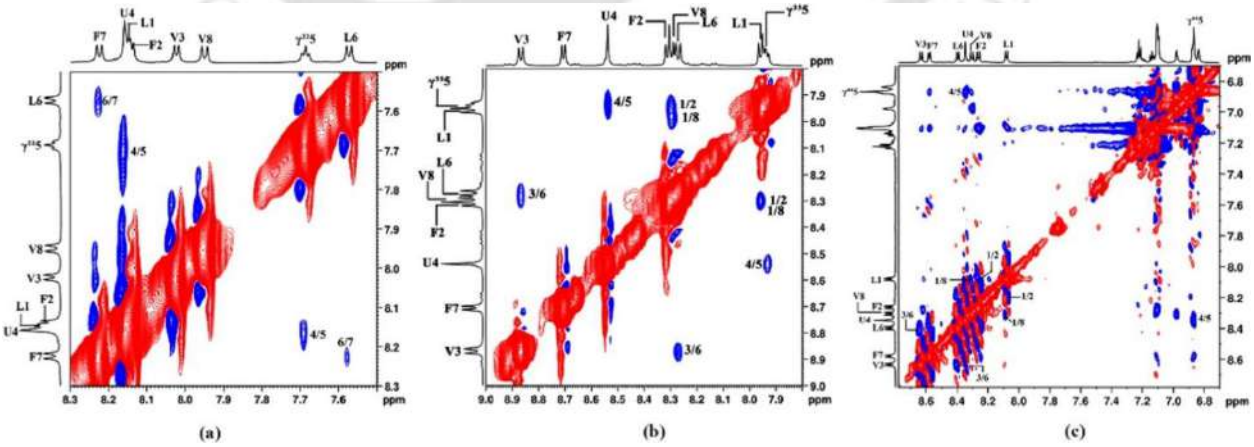

Figure 5.5. NH−NH region of the partial 600 MHz ROESY spectrum of (a) **51**, (b) **52**, and (c) **53** in CD_3OH at 298K.

TH-3141_166122021

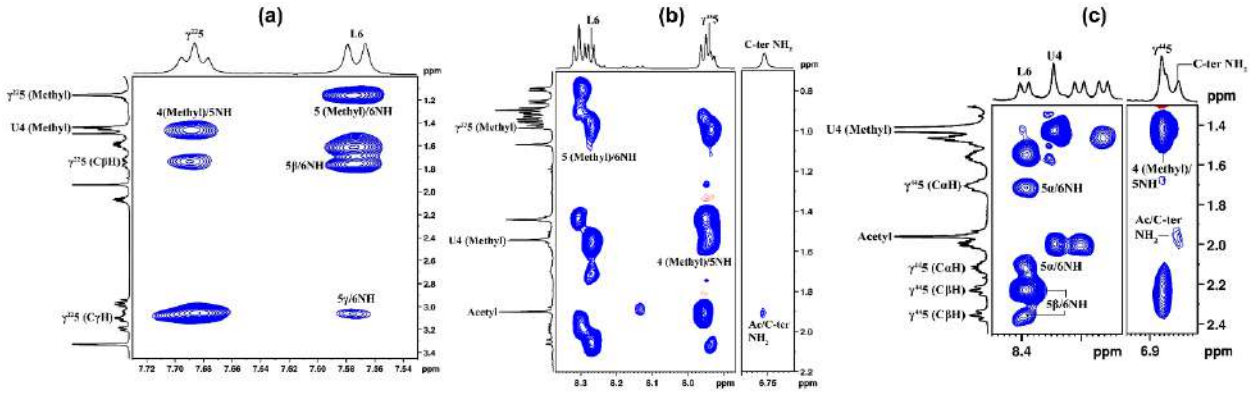

Figure 5.6. Partial 600 MHz ROESY spectra of peptide (a) Ac-Leu-Phe-Val-Aib-$\gamma^{2,2}$-Leu-Phe-Val- $CONH_2$ (**51**) representing NOEs between NH ↔ $C^{\beta}H$/ $C^{\gamma}H$ and NH ↔ Methyl protons, (b) Ac-Leu-Phe-Val-Aib-$\gamma^{3,3}$-Leu-Phe-Val- $CONH_2$ (**52**) representing NOEs between NH ↔ Methyl and Ac ↔ C-ter NH_2 protons, (c) Ac-Leu-Phe-Val-Aib-$\gamma^{4,4}$-Leu-Phe-Val- $CONH_2$ (**53**) representing NOEs between NH ↔ $C^{\alpha}H$/$C^{\beta}H$, NH ↔ Methyl and Ac ↔ C-ter NH_2 protons in CD_3OH at 298K.

In the case of peptide **54**, identical NOEs were obtained as for peptide **51**, suggesting the formation of a "loose" β-turn across the Aib (4)-$\gamma^{2,2}$ (5) segment (Figure 5.7a). Furthermore, no evidence of formation of strand registry was obtained for **54** just as in the case of **51**. For **55**, all NOEs were observed (Figures 5.9b, 5.8b, and 5.9b) as in **52** except for the Leu (1) NH ↔ Val (8) NH long-range NOE, suggesting that although the β-hairpin was formed for **55**, fraying of the strands might be present at the termini. This might be a consequence of the N capping moiety, Fmoc in **55**, instead of the acetyl group in **52**. **56** had very poor solubility in CD_3OH. Partial ROESY spectra (Figures 5.7c and 5.8c) of **56** contained similar NOEs as were observed in **53** except for the long-range NOEs characteristic for hairpin conformation. This was attributed to the poor solubility of the peptide. However, the presence of the well-dispersed aromatic proton resonances was an indirect proof of well-registered strands in the β-hairpins in both **55** and **56**. The observed NOE connectivities for peptides **51**−**53** and **54**−**56** are indicated schematically in Figures 5.10 and 5.11.

TH-3141_166122021

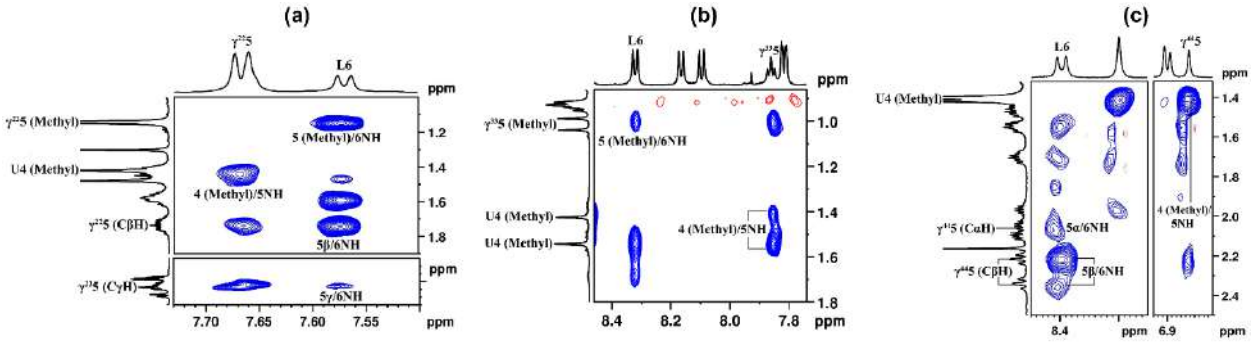

Figure 5.7. Partial 600 MHz ROESY spectra of peptide Fmoc-Leu-Phe-Val-Aib-$\gamma^{2,2}$-Leu-Phe-Val-$CONH_2$ (**54**) representing NOEs between NH ↔ $C^{\beta}H$/ $C^{\gamma}H$ and NH ↔ Methyl protons, (b) Fmoc-Leu-Phe-Val-Aib-$\gamma^{3,3}$-Leu-Phe-Val-$CONH_2$ (**55**) representing NOEs between NH ↔ Methyl protons, (c) Fmoc-Leu-Phe-Val-Aib-$\gamma^{4,4}$-Leu-Phe- Val-$CONH_2$ (**56**) representing NOEs between NH ↔ $C^{\alpha}H$/$C^{\beta}H$ and NH ↔ Methyl protons

in CD_3OH at 298 K

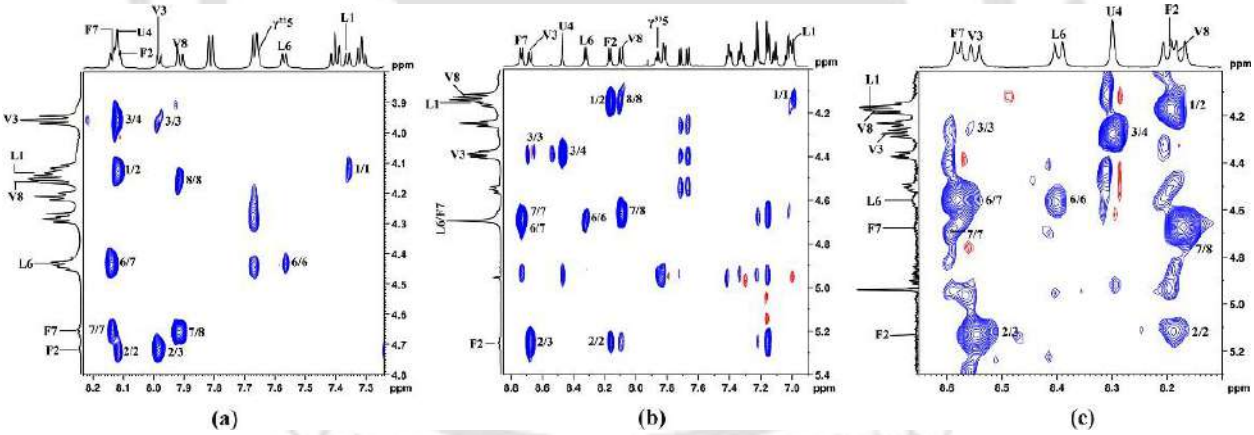

Figure 5.8. Partial 600 MHz ROESY spectra of peptide (a) Fmoc-Leu-Phe-Val-Aib-$\gamma^{2,2}$-Leu-Phe-Val-$CONH_2$ (**54**), (b) Fmoc-Leu-Phe-Val-Aib-$\gamma^{3,3}$-Leu-Phe-Val-$CONH_2$ (**55**) and (c) Fmoc-Leu-Phe-Val-Aib-$\gamma^{4,4}$-Leu-Phe-Val-$CONH_2$ (**56**) in CD_3OH at 298K representing NOEs between NH ↔ $C^{\alpha}H$ protons.

TH-3141_166122021

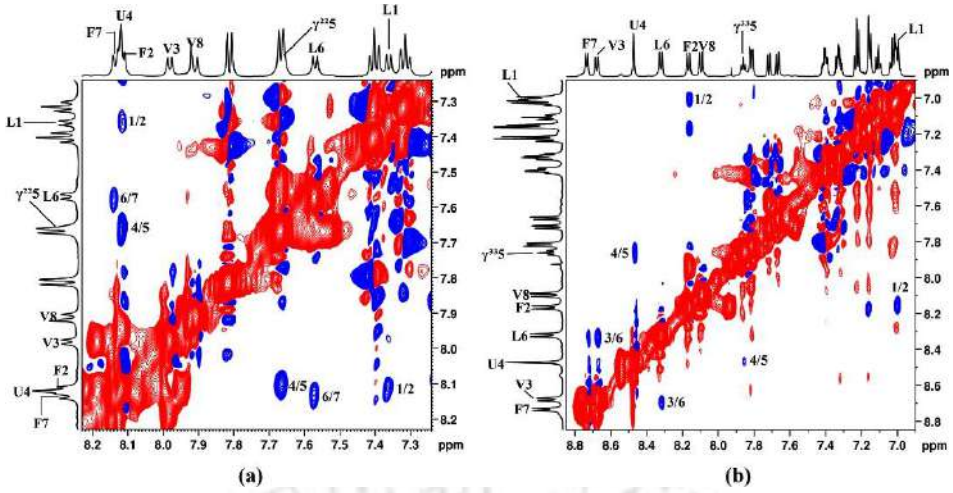

Figure 5.9. Partial 600 MHz ROESY spectra of peptide (a) Fmoc-Leu-Phe-Val-Aib-$\gamma^{2,2}$-Leu-Phe-Val-$CONH_2$ (**54**) and (b) Fmoc-Leu-Phe-Val-Aib-$\gamma^{3,3}$-Leu-Phe-Val-$CONH_2$ (**55**) in CD_3OH at 298K representing NOEs between NH ↔ NH protons.

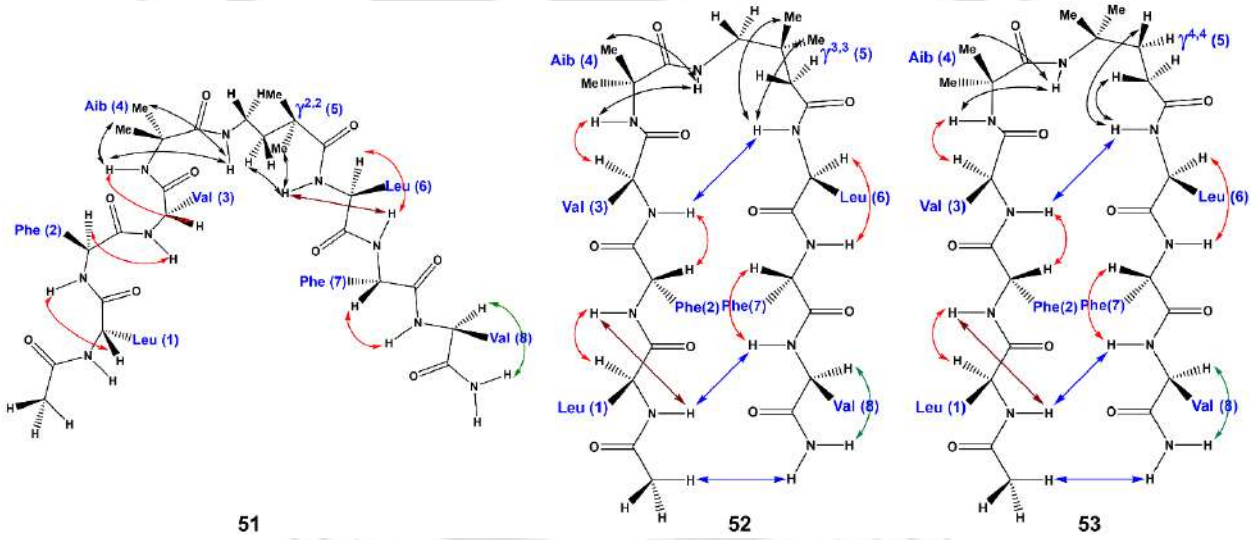

Figure 5.10. Schematic representation of observed NOEs for **51**−**53**. The long-range NOEs compatible with the hairpin conformation are marked in blue, $C^{\alpha}_{i}H \leftrightarrow N_{i+1}H$ NOEs are marked in red, NOEs suggestive of β-turn formation are marked in black, and NOEs between Ter-NH and $C^{\alpha}H$ are marked in green.

TH-3141_166122021

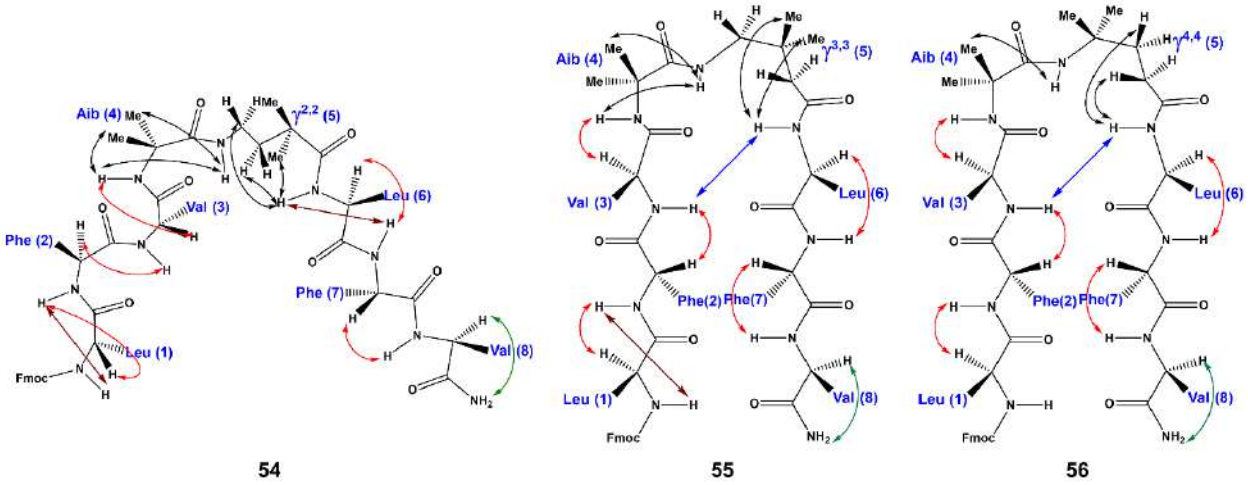

Figure 5.11. Summary of observed NOEs for peptides **54-56**. The NOEs compatible with the hairpin conformation are represented as blue (long range NOEs), red (NOEs between NH and $C^{\alpha}H$), black (NOEs suggestive for β-turn formation) and green (NOEs between Ter-NH and $C^{\alpha}H$) arrows.

A general feature observed in the spectra of all of the peptides **51**−**56** was the absence of the sequential dNN NOEs ($N_iH \leftrightarrow N_{i+1}H$) and the very weak intensity of the observed intra-residue $N_iH \leftrightarrow C^{\alpha}{}_iH$ NOEs. These rule out the presence of any helical conformations for the peptides in CD_3OH.

- **Assignment of aromatic resonances**

The assignment of the aromatic proton resonances was first achieved from the observed NOE between the Phe $C^{\beta}H$ protons and the Phe $C^{\delta,\delta'}H$ protons of peptides **52**, **53** and **55**, **56**. Subsequent assignment of the Phe $C^{\varepsilon,\varepsilon'}H$ protons of the two rings has been achieved using TOCSY (Figures 5.12b, d and Figures 5.13b, d) and strong NOEs from ROESY spectra shown in Figures 5.12a, c and Figures 5.13a, c. The nonequivalent $C^{\beta}H$ protons (for **52**, **53** and **56**) of Phe (7) were observed from 1D ^1H NMR spectra. In contrast, both $C^{\beta}H$ protons of Phe (2) showed equivalent chemical shift (for **52**, **53** and **56**). The observation of a strong NOE between the Phe (7) $C^{\beta}H$ protons and upfield shifted aromatic protons indicated the latter as the Phe (7)

TH-3141_166122021

$C^{\delta,\delta'}H$ protons (for **52**, **53**, **55** and **56**). The remaining aromatic protons $C^{\zeta}H$ of the two Phe residues were assigned from the TOCSY spectrum. Assignment of aromatic proton resonances of **51** and **54** could not be completed because of the clustering of the protons.

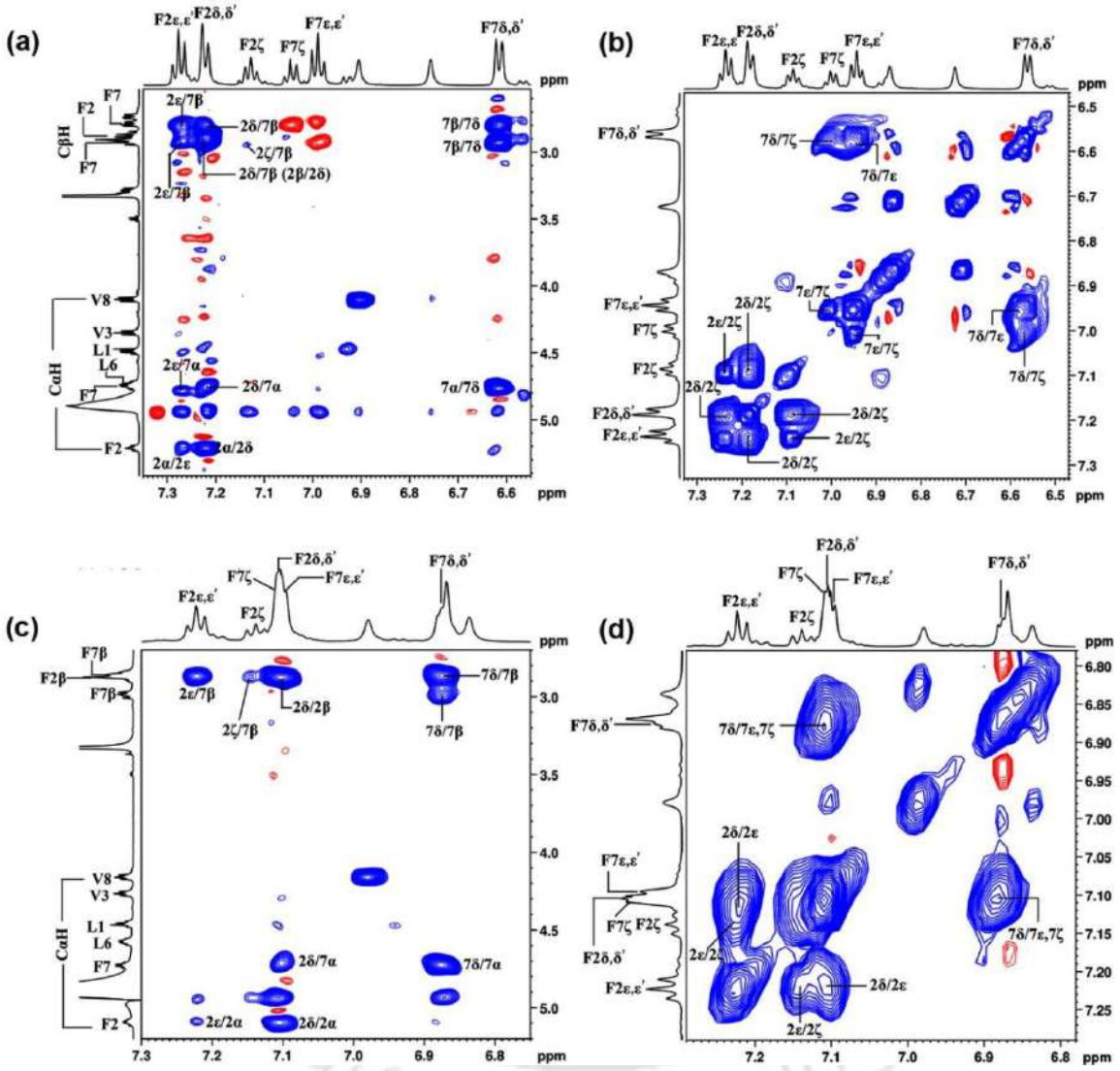

Figure 5.12. Partial 600 MHz (a), (c) ROESY and (b), (d) TOCSY spectra of **52** and **53** in CD_3OH at 298K illustrating assignment of aromatic proton resonances.

TH-3141_166122021

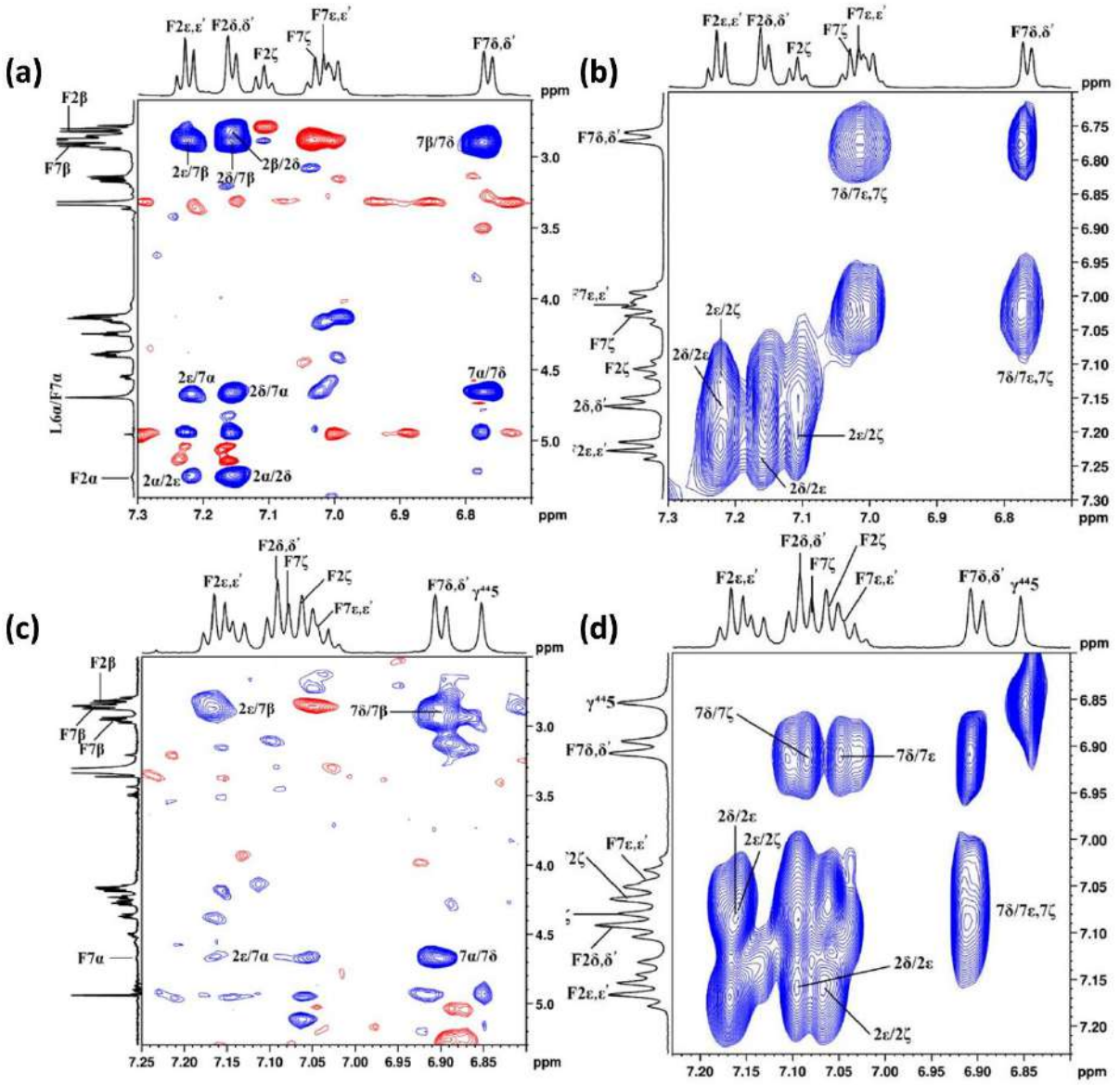

Figure 5.13. Partial 600 MHz (a), (c) ROESY and (b), (d) TOCSY spectra of **55** and **56** in CD_3OH at 298 K illustrating assignment of aromatic proton resonances.

Formation of the β-hairpin needs the strands to be in registry, which makes the phenylalanine residues from the opposite strands to be spatially proximal. As described earlier, aromatic protons of **52**, **53**, **55**, and **56** were well-dispersed in contrast to that of **51** and **54**. Dispersion of the aromatic resonances was a consequence of the anisotropic effect of the Phe from the opposite strands and an indication of the formation of a well-registered hairpin conformation. Additionally, the presence of strong NOEs between the Phe (2) and Phe (7) residues was a

TH-3141_166122021

characteristic of the β-hairpin structure in the peptides.[342,343] Figures 5.12a & 5.14 a and 5.12c & 5.14 b provide a comparison of the side-chain backbone and side-chain−side-chain NOEs involving residues Phe (2) and Phe (7) in the octapeptides **52** and **53**. NOEs like Phe (2) $C^{\delta}H$ ↔ Phe (7) $C^{\alpha}H$ (strong), Phe (2)$C^{\varepsilon}H$ ↔ Phe (7) $C^{\alpha}H$ (medium), Phe (2) $C^{\varepsilon}H$ ↔ Phe (7) $C^{\beta}H$ (strong), and Phe (2) $C^{\delta}H$/Phe (2) $C^{\varepsilon}H$ ↔ Phe (7) $C^{\delta}H$ (weak) were observed for **52** (and **55**, Figures 5.15a, b). The results presented thus far suggested that in both **52** and **55**, the phenyl rings of Phe (2) and Phe (7) were oriented in a manner similar to that observed in the crystal structure of the model octapeptide Boc-Leu-Phe-Val-^{D}Pro-^{L}Pro-Leu-Phe-Val-OMe, reported by Balaram and co-workers.[342] Upfield shifting of the aromatic $C^{\delta,\delta'}H$ atoms of Phe (7) suggested that they were placed in a shielding region of the aromatic ring of Phe (2). In solution, the rapid flipping of the Phe (7) ring about the C^{β}–C^{γ} bond rendered the $C^{\delta,\delta'}H$ and $C^{\varepsilon,\varepsilon'}H$ protons equivalent on the NMR time scale, which resulted in a significant upfield shift of the aromatic $C^{\delta,\delta'}H$ protons of Phe (7).[341-343] For **53**, Phe (2) $C^{\delta}H$ ↔ Phe (7) $C^{\alpha}H$ (strong), Phe (2) $C^{\varepsilon}H$ ↔ Phe (7) $C^{\beta}H$ (strong), and Phe (2) $C^{\varepsilon}H$ ↔ Phe (7) $C^{\delta}H$ (weak) NOEs, while for **56**, Phe (2) $C^{\varepsilon}H$ ↔ Phe (7) $C^{\alpha}H$ (weak) and Phe (2) $C^{\varepsilon}H$ ↔ Phe (7) $C^{\beta}H$ (strong) NOEs were observed (Figure 5.15c), proving spatial proximity of the two Phe residues.

TH-3141_166122021

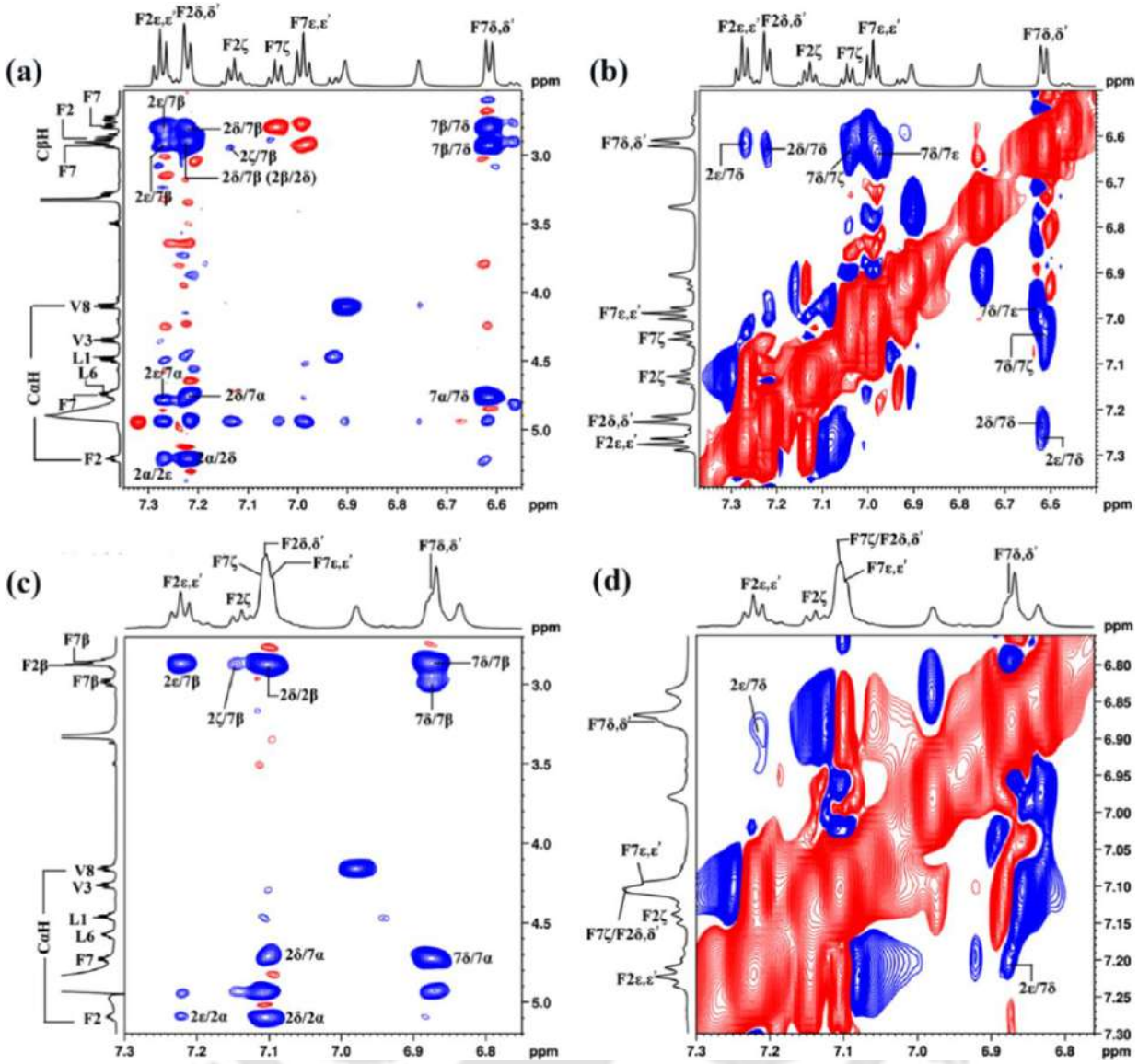

Figure 5.14. NOEs observed in the 600 MHz ROESY spectrum between Phe (2) and Phe (7) residues in **52** and **53**. NOEs between aromatic protons ↔ $C^{\alpha}H/C^{\beta}H$ NOEs in (a) **52** and (b) **53**. NOEs between aromatic protons in (c) **52** and (d) **53**.

TH-3141_166122021

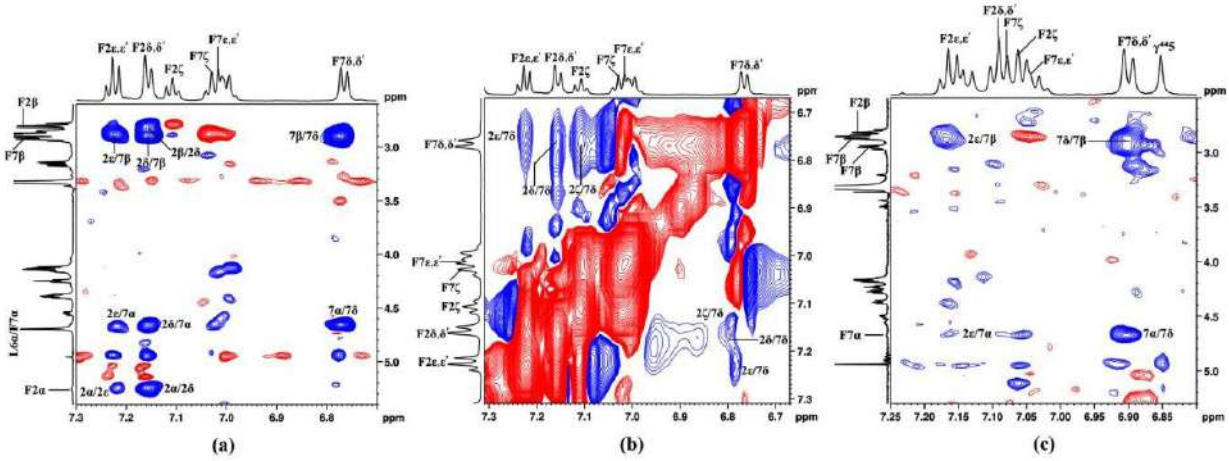

Figure 5.15. Partial 600 MHz ROESY spectra representing NOEs between aromatic protons and $C^{\alpha}H$ & $C^{\beta}H$ of Phe (2,7) of the peptide (a) **55**, (c) **56** and in between aromatic ↔ aromatic protons in (b) **55**.

Figure 5.16 illustrates the temperature dependence of the aromatic proton resonances of **51**−**53** over the temperature range of 323−291.6 K. As the temperature was gradually increased, the upfield-shifted (shielded) Phe (7) $C^{\delta,\delta'}H$ resonances moved downfield in the peptides **52** and **53**. This was attributed to the breakdown of the interstrand hydrogen bonds, destabilizing the β-hairpin conformation upon increasing the temperature. Disruption of strand registry led to moving apart of Phe (2) and Phe (7), obliterating the anisotropic effect of the rings on each other. This in turn led to the Phe protons moving back to their original chemical shift values. Upon loss of strand registry, the chemical shift dispersion in peptides **52** and **53** was lost. Temperature dependence of the aromatic protons of **52** and **53** was proof of the β-hairpin structure adopted by these peptides in solution. Aromatic protons of **51** were indifferent to the change in temperature, confirming the absence of β-hairpin conformation in them. The temperature dependence of the aromatic proton resonances in peptides **54**−**56** over the temperature range 323−291.8 K (Figure 5.17) showed exactly similar results as **51**−**53**. This suggested conformational similarity between the two sets of peptides irrespective of their N-terminal capping.

TH-3141_166122021

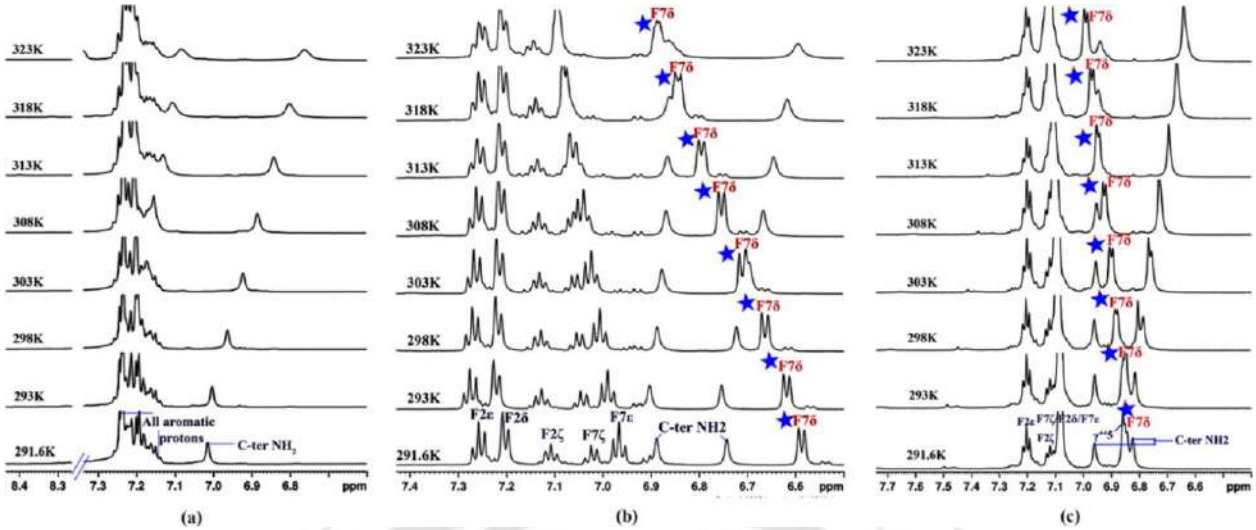

Figure 5.16. Temperature dependence of aromatic resonances of (a) **51**, (b) **52**, and (c) **53** observed in the 600 MHz ^{1}H NMR spectrum in CD_3OH. F7δ protons of **52** and **53** (marked with blue stars) move downfield upon increasing the temperature.

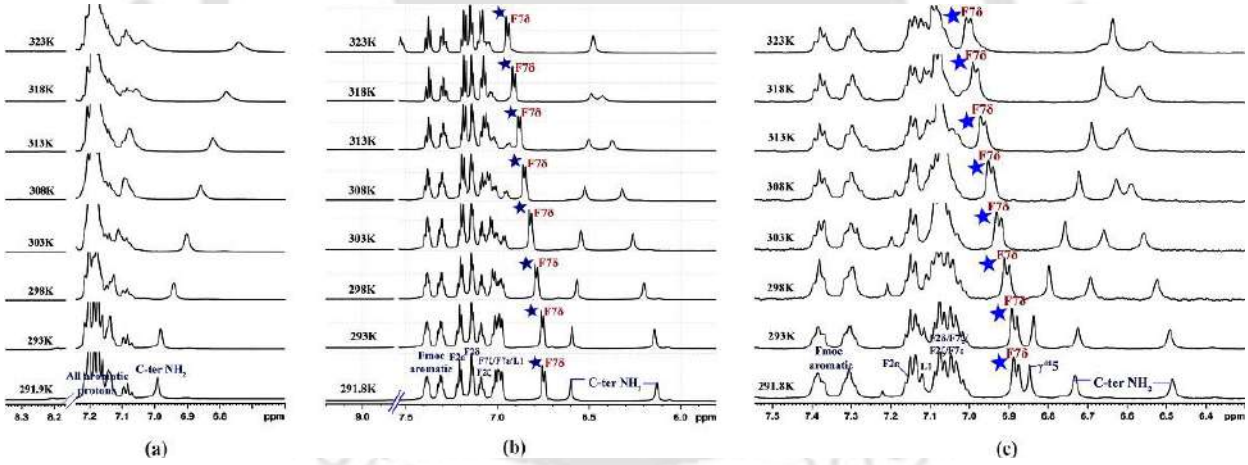

Figure 5.17. Temperature dependent 600 MHz 1D ^{1}H NMR spectra of **54-56**. Aromatic proton resonances of (a) **54** (b) **55** (c) **56** in CD_3OH showing the temperature dependence of the F7δ protons (Blue star marks).

Chemical shift indexes for peptides **51−53** were calculated by comparing the $C^{\alpha}H$ chemical shifts observed in CD_3OH with the random coil shifts obtained from the Bio Mag Res Bank (BMRB)[328] and the original report of Wishart, Sykes, and Richards[329] (Figure 5.18). Downfield

TH-3141_166122021

shifts in the $C^{\alpha}H$ resonances of the residues are considered an indication of their presence in β-strand structures. The $C^{\alpha}H$ resonances of residues 1−3, 4, and 6 of peptides **52** and **53** showed a large downfield shift, i.e., a positive chemical shift index, consistent with their β-sheet conformations in contrast to the residues from **51**. Phe (7) did not show any appreciable downfield shift of the $C^{\alpha}H$ resonances in comparison to its value in the random coil, in spite of being in the β-strand structure due to the shielding effect of the Phe (2) aromatic ring. Similar results were also obtained from the analysis of the chemical shift index of **54**−**56**.

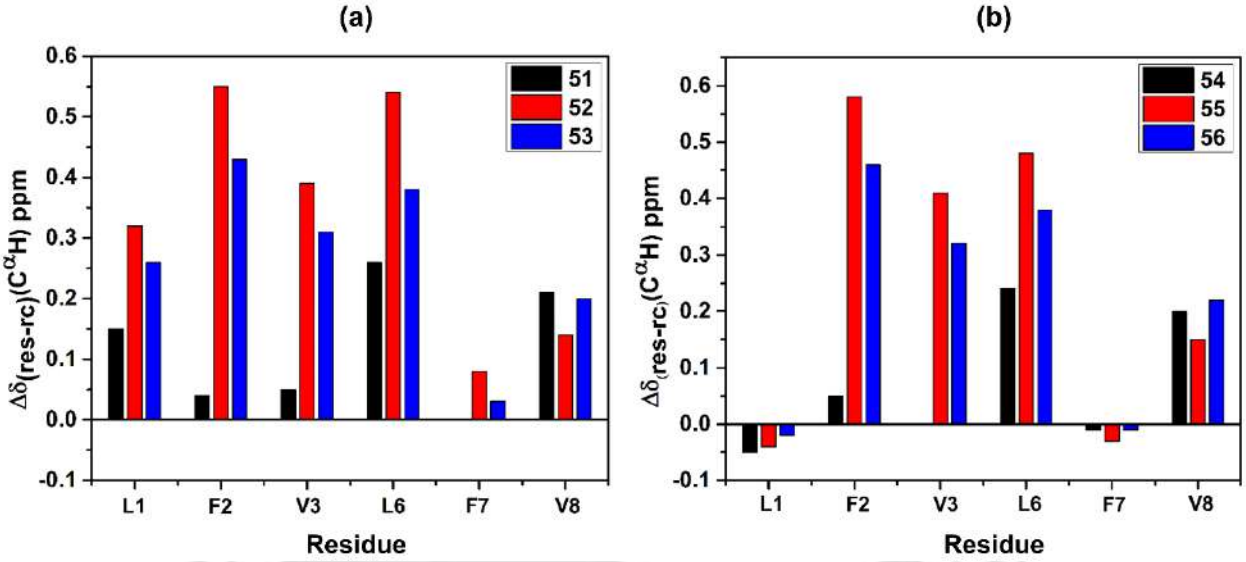

Figure 5.18. Plot of the difference in $C^{\alpha}H$ chemical shift value of the residues with respect to random coil chemical shifts in (a) **51-53**, (b) **54-56.**

Thus, from NMR, it could be conclusively proved that model octapeptides with $\gamma^{3,3}$ and $\gamma^{4,4}$ methyl di-substituted γ amino acid residues (**52**, **53**, **55**, **56**) adopted a β-hairpin conformation in solution, while those with $\gamma^{2,2}$ methyl disubstituted amino acid residue (**51** and **54**) could not form a stable hairpin. Although in the case of $\gamma^{2,2}$ containing **51** and **54** peptides, there was evidence of the formation of a turn over the Aib(4)-$\gamma^{2,2}$ (5) segment, it was not as tight a turn

TH-3141_166122021

as seen in the cases of $\gamma^{3,3}$ and $\gamma^{4,4}$ containing peptides, as suggested by the absence of the crucial Val (3) NH ↔ Leu (6) NH in the former, failing to induce proper strand registry to form the β-hairpin conformation.

5.3.1.2. Circular Dichroism

Far-UV circular dichroism spectra that originate from the n → π* and π → π* transitions of the backbone amide CO groups often give important information about the secondary structure of peptides. The ECD values of **51**−**56** were recorded in methanol for understanding their secondary structure (Figure 5.19). **51**−**53** exhibited a negative band at ~210 nm and a positive band at ~222 nm. Peptide hairpins lacking any aromatic chromophore generally exhibit a broad, negative band at ~218 nm[344] accompanied by a positive band at 195 nm characteristic of β-sheet formation. However, β-hairpins with aromatic groups such as Phe or Trp may or may not exhibit a peak at 218 nm. Instead, peaks at ~213 nm (negative) and 222 nm (positive) owing to exciton coupling of π−π* transitions, originating from the proximity of the aromatic rings in the well-registered strands of the hairpin, may be observed.[341,344-347] The intensity of the CD bands is proportional to the proximity of the aromatic moieties, and it is a good parameter to judge the structural stability of hairpins. The intensities of the bands at 209 and 222 nm in **52** and **53** were similar, indicating well-formed β-hairpins in both of them. The intensity of the bands diminished for **51**, suggesting disruption of the β-hairpin structure. **54**−**56** gave similar results as obtained for **51**−**53**.

TH-3141_166122021

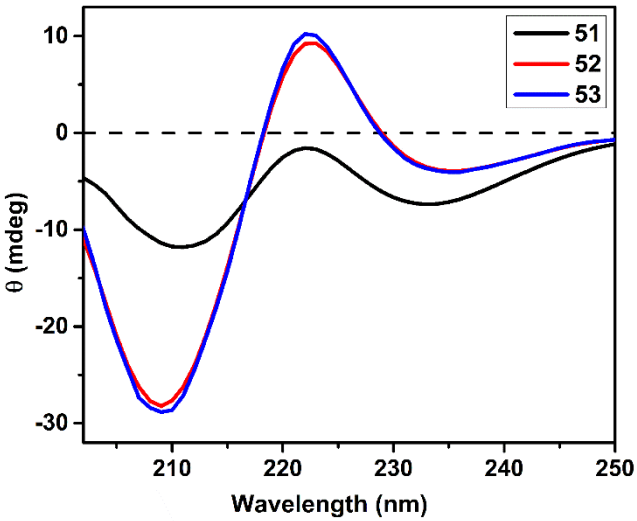

Figure 5.19. (a) Far-UV circular dichroism spectra of peptides **51**−**53** recorded in methanol at concentrations of 500 μM (in case of **51, 52**) and 250 μM (in case of **53**), respectively.

5.3.1.3. Infrared Spectroscopy

Solution conformation of peptides **51**−**56** was further probed by FT-IR spectroscopy in methanol at 1.0 mM concentration (Figure 5.20). Observation of a peak at ∼1630−1635 cm^{-1} accompanied by a hump at ∼1680 cm^{-1} is a strong feature of the antiparallel β-sheet structure in β-hairpins.[340,341] Additionally, the band at ∼1680 cm^{-1} is characteristic of β-turns. Amide I bands of **52**, **53**, **55**, and **56** appeared in the above-mentioned characteristic range, suggesting formation of both β-turn kind of structures and antiparallel β-sheets, both of which constitute the β-hairpin. Thus, the IR data corroborated formation of well-folded β-hairpins in **52**, **53**, **55**, and **56**, as seen from NMR and CD results. However, among these peptides, **53** seemed to be forming the best hairpin structure with the amide I bands at 1627 and 1685 cm^{-1}. For peptides **51** and **54**, the band at ∼1635 cm^{-1} was shifted to a longer wavenumber, accompanied by the absence of a smaller hump or shoulder at ∼1680 cm^{-1}. This suggested the absence of a β-turn kind of structure in **51** and **54**. Such a result supports the formation of a "loose turn" about the Aib (4)-$\gamma^{2,2}$ (5) segment, as concluded from the NMR studies.

TH-3141_166122021

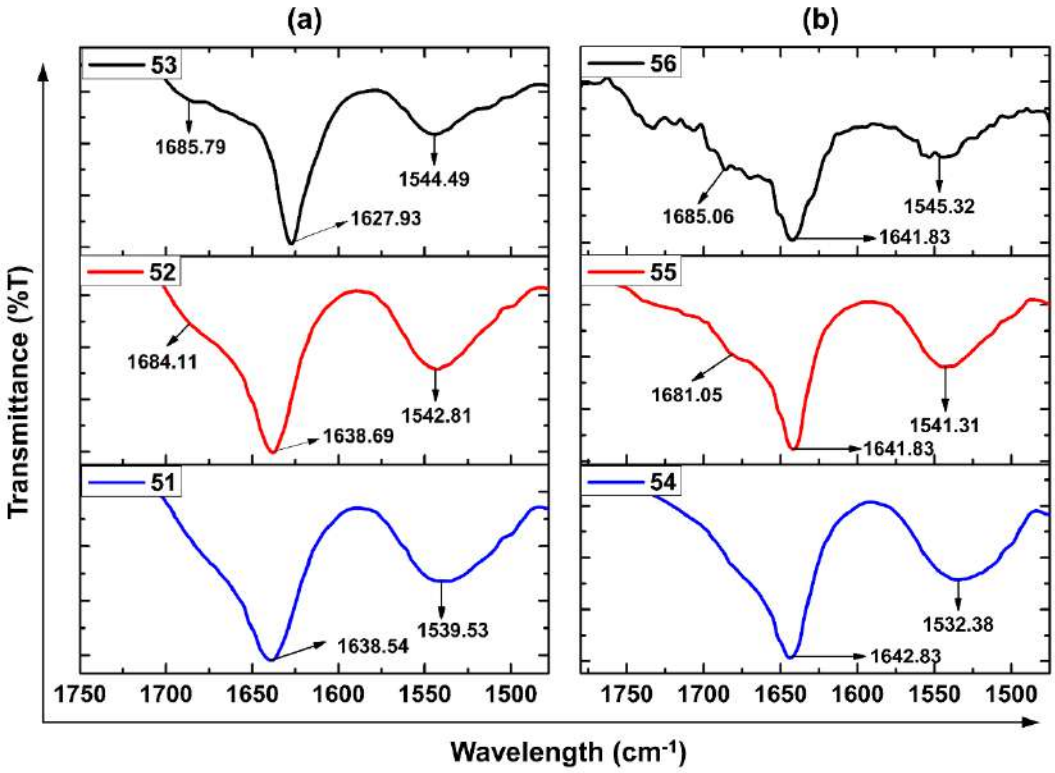

Figure 5.20. FT-IR spectra of peptides (a) 51-53 and (b) **54-56** recorded at 1.0 mM concentrations in methanol.

5.3.2. *ab initio*-Optimized Structures of Peptides

Geometry optimization in implicit MeOH dielectric suggested a stable β- hairpin geometry for the octapeptides (**52**, **53**, **55**, **56**) (Figures 5.21a, b). The β-hairpin structure was stabilized by four inter-strand backbone hydrogen bonds (between Leu-Phe-Val tripeptide segments; see Figure 5.21a and Table 5.4) with a C_{12} turn involving the two nonstandard residues Aib-$\gamma^{3,3/4,4}$. Good strand registry was found in the β-hairpin structure (**52**, **53**, **55**, and **56**). H-bond parameters (Table 5.4) suggested the terminal N1−H···O8 to be the strongest (distance 2 Å, largest hydrogen-bond angles of ∼173°, close to the ideal 180°) and the O1···H−N8 terminal to be the weakest (distance 2.2 Å, angle ∼160°) H-bond. The side chains were oriented perpendicular to the plane of the β pleated sheet, showing the proximity of Phe (2) and Phe (7) on one side, while the side chains of residues Leu (1), Val (3), Leu (6), and Val (8) lay on the

TH-3141_166122021

other side (Figure 5.21b) of the hairpin. The aromatic side chain of Phe (7) was slip-distorted and orientated at a 60^{o} angle relative to the Phe (2) aromatic side chain, thus bringing C$^{\delta}$ and C$^{\varepsilon}$ hydrogens of Phe (7) proximal to the aromatic electrons of Phe (2) (Figure 5.21b). This explained the observation of NOEs between the aromatic protons of Phe (2) and Phe (7). The N-terminal acetyl groups of **52** and **53** and the Fmoc aromatic rings of **55** and **56** were in proximity to the C-terminal amine. This explained the observation of weak NOEs between the CH_3 groups of the N-terminal acetyl group and the amide NH_2 group.

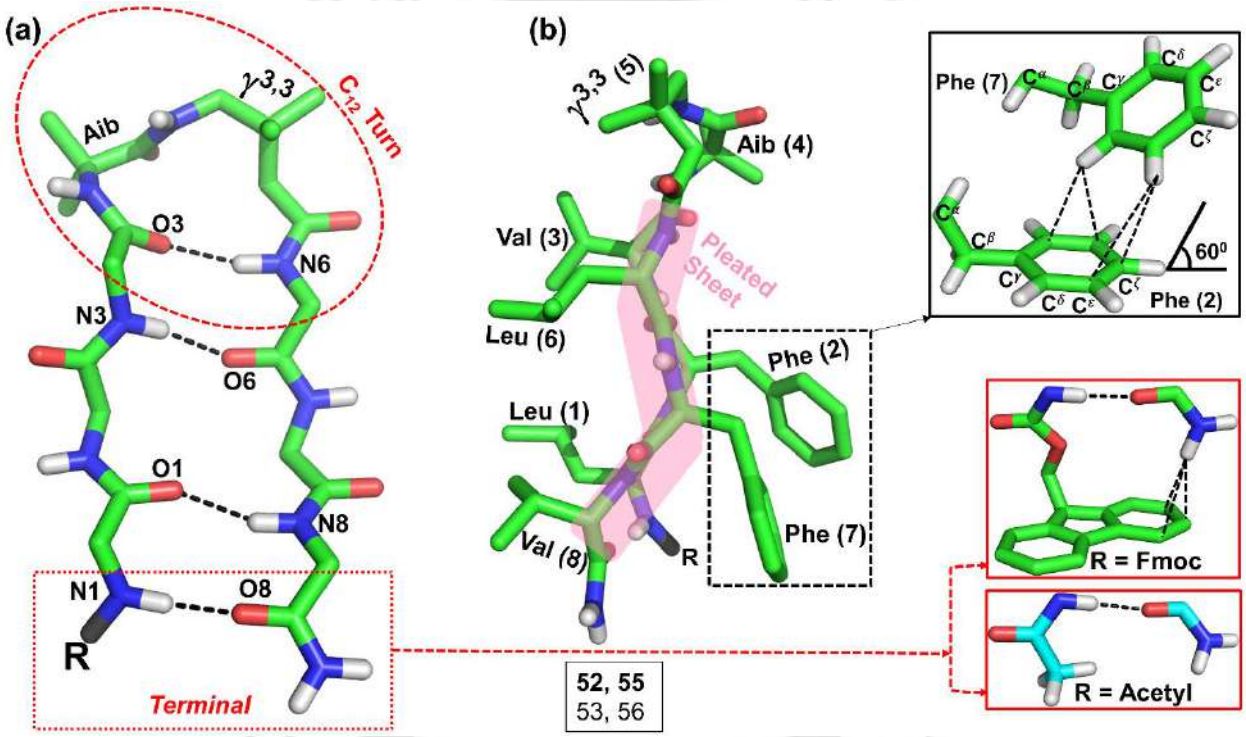

Figure 5.21. (a) Optimized β-hairpin geometry of the octapeptides **52**, **53**, **55** and **56**. Only the backbone atoms are shown for clarity. The β-hairpin is nucleated by the αγ C_{12} turn (red broken oval) and stabilized by backbone hydrogen bonds (black broken lines). The geometry of the terminal protecting groups is highlighted in the red box. (b) Side view of the β-hairpin showing the orientation of the side chains relative to the pleated sheet (formed by the backbone hydrogen

TH-3141_166122021

bonding, highlighted in pink). Zoomed-in view of the relative orientations of Phe (2)−Phe (7) aromatic side chains is shown in the black box.

Table 5.4. Intramolecular Hydrogen-Bond Parameters in **52**, **53**, **55**, and **56**[a]

H-bond parameters	51	52	53	54	55	56
N1−H···O8 (distance)	17.0	2.0	2.0	18.0	2.0	2.0
(angle)		173.9	173.7		172.8	173.5
O1···H−N8 (distance)	13.1	2.2	2.2	13.8	2.2	2.2
(angle)		160.4	160.2		159.9	160.3
N3−H···O6 (distance)	8.5	2.0	2.0	8.8	2.0	2.0
(angle)		166.3	167.3		165.6	167.1
O3···H−N6 (distance)	4.7	2.1	2.0	4.8	2.1	2.0
(angle)		162.9	162.6		163.1	162.6
energy	0.0	−8.45	−8.34	0.0	−8.9	−8.8

[a]"H···O" distances and "N−H···O angles" are in "Å" and "degree", respectively. Absence of hydrogen bonding is indicated by a large distance (>2.5 Å) for **51** and **54**. Energies (in kcal/mol) are reported relative to **51** and **54** for the sets **51**−**53** and **54**−**56**, respectively.

The backbone torsional parameters of the C_{12} turn forming residues (Aib, γ) were more or less identical in **52**, **53**, **55**, and **56** except for ϕ and ψ of $\gamma^{3,3}$ and $\gamma^{4,4}$ residues (Table 5.5). The ϕ changed from −107 to −88° and the ψ changed from +110 to +97° in response to the shift in position of disubstitution from C^{β} to C^{γ} (Figure 5.22 and Table 5.5). θ_1 and θ_2 adopted gauche and extended conformations, respectively, in both $\gamma^{3,3}$ and $\gamma^{4,4}$ residues. The Val (3) C^{α}−Leu (6) C^{α} distance of the C_{12} turn was 5.2 Å (Figures 5.22a, b), while the Val (3) NH−Leu (6) NH

TH-3141_166122021

distance was 2.8 Å in the β-hairpin structures (**52**, **53**, **55**, and **56**), justifying the observation of the strong NOEs between them.

It is interesting to note that the β-hairpin model of **51** and **54** showed steric hindrance (Figure 5.22c) of the methyl groups of the $\gamma^{2,2}$ residue with the carbonyl oxygen of Val (3) and C^{α} of Aib in the C_{12} turn. Geometry optimization led to the "loosening up" of the C_{12} turn, leading to the disruption of the hairpin structure (no pleated sheet) for **51** and **54** peptides (Figure 5.22d and Table 5.4). The "loosened" C_{12} turn had an elongated Val (3) C^{α}–Leu (6) C^{α} distance (7.7 Å for **51**, 7.9 Å for **54**) relative to **52**, **53**, **55**, and **56** (Figures 5.22a, b), explaining the absence of the d_{NN} NOE between Val (3) NH↔ Leu (6) NH. Loosening up of the turn led to the fraying away of the strands, leading to the disruption of the H-bonds and the collapse of the β-hairpin structure.

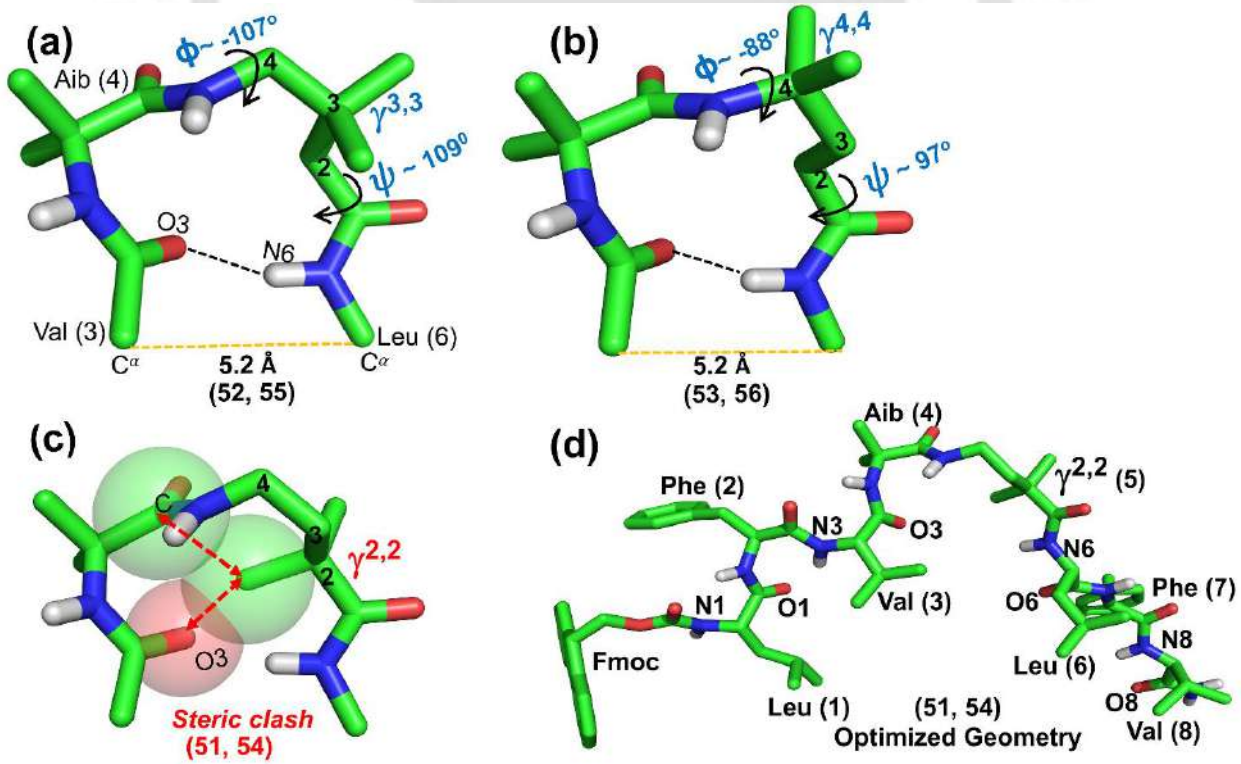

TH-3141_166122021

Figure 5.22. C_{12} turns in (a) **52**, **55** and (b) **53**, **56**. The ϕ alters significantly from −107 to −88° and the ψ changes from +109 to +97° upon change in the position of di-substitution from C^{β} to C^{γ} in $\gamma^{3,3}$ and $\gamma^{4,4}$, respectively. (c) Modeling the C_{12} turn with the $\gamma^{2,2}$ residue (**51**, **54** models) indicating the steric clash (transparent spheres). (d) Geometry optimization confirming the loss of the β-hairpin conformation in **51** and **54** (no pleated sheet accompanied by a loss of inter-strand hydrogen bonding) with an elongated Val (3) C^{α}–Leu (6) C^{α} distance of the C_{12} turn in **51** and **54**.

Table 5.5. Backbone Torsion Angles of Peptides **51**–**56**

backbone torsional parameters	51	52	53	54	55	56
ϕ	−87.2	−116.1	−116.1	−90.1	−115.6	−116.3
Leu (1) ψ	64.2	129.3	129.1	63.5	129.9	129.5
ω	−173.8	175.2	175.4	−174.7	175.0	175.0
ϕ	−88.0	−109.2	−108.9	−88.3	−111.3	−110.2
Phe (2) ψ	62.4	134.1	133.3	61.7	133.6	132.5
ω	179.3	167.2	168.4	178.6	167.4	168.5
ϕ	−89.3	−117.9	−118.4	−89.3	−118.6	−118.7
Val (3) ψ	85.0	139.5	135.7	84.7	140.1	135.6
ω	−167.4	−164.4	−165.3	−166.6	−164.1	−165.7
ϕ	−72.4	−56.6	−55.1	−72.5	−56.3	−55.2
Aib (4) ψ	−22.8	−40.0	−43.7	−23.1	−40.6	−43.5
ω	−169.0	−178.1	176.6	−167.5	−177.4	176.9
ϕ	−123.7	−107.0	−87.6	−124.1	−107.3	−87.8
γ (5) θ_1	89.7	62.9	65.7	88.9	62.1	65.0
θ_2	179.9	−163.7	−170.2	178.0	−163.1	−170.0
ψ	119.1	109.4	97.4	119.4	110.1	97.9
ω	−179.2	−175.3	−172.2	180.0	−175.4	−172.4
ϕ	−142.3	−149.1	−151.5	−141.4	−148.2	−151.3
Leu (6) ψ	132.3	143.6	142.7	127.8	142.0	141.6
ω	179.1	172.1	172.9	−179.6	172.5	173.1
ϕ	−147.2	−126.6	−127.0	−151.0	−127.8	−127.4
Phe (7) ψ	134.5	130.7	130.7	135.8	130.2	129.8
ω	176.1	176.3	176.1	175.8	175.7	175.9
ϕ	−151.4	−142.8	−143.6	−152.2	−145.5	−145.2
Val (8) ψ	153.7	146.5	147.2	154.2	144.7	145.0

TH-3141_166122021

Peptides **52**, **53** and **55**, **56** were more stable relative to **51**, **54** by ~8.5/9 kcal/mol (Table 5.4). The very small energy difference (<0.15 kcal/mol) between isomers **52** and **53** indicates that they were degenerate. The same argument holds true for **55** and **56**. This implied that (i) both $\gamma^{3,3}$ and $\gamma^{4,4}$ were equally capable of being accommodated into the (i+2) position of the C_{12} turn and nucleate equally stable β-hairpins and (ii) terminal protecting groups (Fmoc and acetyl) do not play any role in determining the stability of these model octapeptides.

Summing up the results from our studies, γ amino acid residues $\gamma^{3,3}$ and $\gamma^{4,4}$ could be successfully incorporated at the (i+2) position of the C_{12} turn, generating a well-registered β-hairpin conformation in **52**, **53**, **55**, and **56**. Observation of the strong d_{NN} NOE between Val (3) NH ↔ Leu (6) NH confirmed the formation of a tight C_{12} turn across the Aib-$\gamma^{3,3/4,4}$ segment, while that between Leu (1) NH ↔ Val (8) NH and the long-range weak NOE between N-ter (methyl proton) ↔ C-ter NH_2 suggested strand registry in **52**, **53**, **55**, and **56**. Dispersion of chemical shifts of the aromatic protons further confirmed formation of well-registered hairpins in these peptides. Structure optimization of the peptides **52**, **53**, **55**, and **56** showed the formation of four interstrand hydrogen bonds. The backbone conformations of the differently substituted γ amino acid residues, namely, $\gamma^{3,3}$ for **52** and **55** and $\gamma^{4,4}$ for **53** and **56**, were compared. For both the $\gamma^{3,3}$ and $\gamma^{4,4}$ amino acid residues, the θ_1 and θ_2 adopted gauche (+60°) and extended conformations (−180°), respectively, in spite of their different geminal di-substitution positions. While the ϕ value of $\gamma^{3,3}$ (in **52** and **55**) changed from −107 to −87° in $\gamma^{4,4}$ (in **53** and **56**), ψ of $\gamma^{3,3}$ (in **52** and **55**) changed from +110 to +97° in $\gamma^{4,4}$ (in **53** and **56**). The effect of the change in the value of ϕ was compensated by the change in the value of ψ in the residues $\gamma^{3,3}$ and $\gamma^{4,4}$, which led to both of them being accommodated at the (i+2) position of similar C_{12} turns with an identical Val (3) Cα−Leu (6) Cα distance of 5.2 Å. Thus, in spite of the different backbone di-substitution locations at C^{β} and C^{γ} for $\gamma^{3,3}$ and $\gamma^{4,4}$ residues, respectively, leading to different sets of torsion angle values, both the residues could be

TH-3141_166122021

accommodated in the hairpin nucleating αγ C_{12} turn to generate well-registered hairpins. The backbone torsion angles of the $\gamma^{2,2}$ residue were distinctly different from those of $\gamma^{3,3}$ and $\gamma^{4,4}$. The θ_1 value of $\gamma^{2,2}$ was about +89° (in **51** and **54**), in contrast to ~65° for $\gamma^{3,3}$ and $\gamma^{4,4}$, while the θ_2 value of $\gamma^{2,2}$ attained +180° instead of ~−170° for $\gamma^{3,3}$ and $\gamma^{4,4}$. ϕ and ψ adopted values of ~−120 and ~+120° in $\gamma^{2,2}$ (in **51** and **54**), respectively, which were very different from those adopted for either $\gamma^{3,3}$ or $\gamma^{4,4}$. This distinct backbone conformation of the $\gamma^{2,2}$ residue led to its inability to form a tight C_{12} turn across the Aib (4)-$\gamma^{2,2}$ (5) segment. This was witnessed in the increases of the Val (3) C^{α}−Leu (6) C^{α} distance to 7.7 and 7.9 Å in **51** and **54**, respectively, and the absence of the d_{NN} NOE between Val (3) NH ↔ Leu (6) NH. However, observation of NOEs like Aib (4) NH ↔ $\gamma^{2,2}$ (5) NH, Aib (4) Methyl ↔ $\gamma^{2,2}$ (5) NH, $\gamma^{2,2}$ (5) $C^{\beta}H/\gamma^{2,2}$ (5) Methyl ↔ Leu (6) NH, and $\gamma^{2,2}$ (5) $C^{\gamma}H$ ↔ Leu (6) NH indicated the formation of a loose turn-like conformation across the Aib (4)-$\gamma^{2,2}$ (5) segment. The steric clash between the C^{α} methyl (CH_3) groups of the $\gamma^{2,2}$ residue and the C^{α} of the Aib (4)/carbonyl oxygen of Val (3) residues (Figure 5.22c) led to the distinct backbone conformation adopted by the $\gamma^{2,2}$ residue. It is because of this steric penalty that the $\gamma^{2,2}$ residue could not be adjusted into the tight C_{12} turn unlike $\gamma^{3,3}$ and $\gamma^{4,4}$ residues. The position of the dimethyl substitution in the $\gamma^{2,2}$ residue at the C^{α} carbon atom led to the steric penalty specifically in this residue. Thus, the position of the di-substitution along the backbone has a direct implication on the conformational preferences of the residues and their role in promoting secondary structures in short peptide sequences. Investigation of the relative stability of various peptide structures using electronic structure calculations suggested that β-hairpin structures (**52**, **53** and **55**, **56**) were more stable (by ~ 9 kcal/mol) than the loose turn structures (**51** and **54**). However, stability of the β-hairpin structures was independent of the position of the substituents in $\gamma^{3,3}$ and $\gamma^{4,4}$ residues or the capping (Fmoc and acetyl) at the N-terminus.

TH-3141_166122021

$\gamma^{3,3}$ and $\gamma^{4,4}$ γ amino acid residues have earlier been studied in the literature and shown to be adopting starkly different backbone conformations.[133,135,220] While $\gamma^{3,3}$ adopted helical conformations in αγ peptides with a gauche−gauche conformation about the di-substituted C^{β} carbon,[133] $\gamma^{4,4}$ adopted semi-extended conformations (gauche−trans) in homopolymers[133] and helical conformations (gauche−gauche) in αγ hybrid peptides.[220] A similar observation like the $\gamma^{4,4}$ γ amino acid residue was reported for Gpn (a $\gamma^{3,3}$ amino acid residue), where it could adopt a more common helical gauche−gauche conformation and also an unusual gauche−trans conformation in different peptides.[215] Thus, the conformation of the γ amino acids might also depend on the nature of the other amino acid residues present in the sequence and length of the peptides, apart from their intrinsic backbone features. In our present work, we have incorporated $\gamma^{2,2}$, $\gamma^{3,3}$, and $\gamma^{4,4}$ γ amino acid residues in the 5^{th} position of the same model hairpin octapeptide sequence. $\gamma^{3,3}$ and $\gamma^{4,4}$ could be accommodated in a hairpin promoting an expanded C_{12} β-turn, where they adopted the unusual gauche−trans (g, t) conformation about the disubstituted carbon atom. However, the $\gamma^{2,2}$ amino acid residue could not be accommodated in the hairpin nucleating β-turn owing to unfavorable steric clashes, which were absent for the $\gamma^{4,4}$ and $\gamma^{3,3}$ amino acid residues.

5.4. Conclusion

In this study, we have shown that the variable backbone constraint of the three γ amino acid residues led to different conformational preferences in them, in being able to be accommodated at the (i+2) position of the β-hairpin promoting the C_{12} turn and nucleating a β-hairpin in a model octapeptide. Although $\gamma^{3,3}$ and $\gamma^{4,4}$ residues had minor differences in their torsional variables, both could be accommodated into tight C_{12} turns that nucleated well-registered β-hairpins. $\gamma^{2,2}$, on the other hand, adopted a very different backbone conformation that led to its inability to be accommodated in tight C_{12} turns and hence nucleate β-hairpins. The position of

TH-3141_166122021

the di-substitution in the $\gamma^{2,2}$ residue prevented it from adopting backbone conformations that could be accommodated in tight C_{12} turns, primarily due to steric reasons. Understanding the effect of the position of di-substitution along the backbone of the γ amino acids on their conformational preference will facilitate a directed foldamer design in the future.

भारतीय प्रौद्योगिकी संस्थान गुवाहाटी
Indian Institute of Technology Guwahati

TH-3141_166122021

Chapter 6

Conclusions and Future prospects

TH-3141_166122021

In this thesis, we have explored the relative propensities of the differently geminally di-substituted γ amino acid residues ($\gamma^{2,2}$, $\gamma^{3,3}$ and $\gamma^{4,4}$) to be accommodated in various secondary scaffolds as a consequence of their differential position of backbone substitution. For this we chose different model peptide scaffolds known to prefer different secondary structures and incorporated a single different gamma amino acid residue each time to generate different groups of peptides. Thereafter, we have studied the conformations of the peptides in details both in solid and solution states and also in silico. As the peptides within a certain group were only different in the γ amino acid residue in question, the difference in their secondary structure could directly be connected to the conformational preference of amino acid residue and in turn to the effect of the differential position of backbone di-substitution in them.

Sequence of the peptides have a role to play in determining the secondary structure of the overall peptide, which in some cases also modulate the propensity of a single amino acid residue in question. In order to avoid this effect, we started by looking at the conformation and the assembly of simple Fmoc γ amino acid residue derivatives both in solid and solution states. We established that the conformation of the derivatives was a direct consequence of the nature of the geminally-di-substituted amino acid used. However, the assembly of the derivatives in solution state was independent of the nature of the amino acids used.

In the third chapter, we studied the ability of the three γ amino acid residues to be accommodated into C_{10}/C_{12} mixed helical conformation in hybrid αγ peptides. As the length of the peptide influences the ability of helix formation, we studied peptide sequences at the tri hexa and the nonapeptide level. We concluded that unlike $\gamma^{3,3}$ and $\gamma^{4,4}$ amino acid residues, which were easily accommodable in the mixed 10/12 helix, $\gamma^{2,2}$ had the least propensity of doing so. We also established that peptides containing $\gamma^{2,2}$ and $\gamma^{3,3}$ could give rise to both the handedness of the helix unlike $\gamma^{4,4}$ residue, which could only give rise to the right handed helical

TH-3141_166122021

conformation. Hybrid peptides containing $\gamma^{2,2}$ and $\gamma^{3,3}$ were also shown to adopt a rare ambidextrous helical conformation in chiral peptides containing L amino acid residues both in crystals and in the solution. Ambidexterity in these molecules were induced by a water molecule positioned close to the gamma amino acid residue. The inability of the $\gamma^{4,4}$ amino acid residue to give rise to ambidextrous helical conformation was attributed to its ability to accommodate the water molecule in its vicinity.

In the 4th and the 5th chapter we explored the ability of the γ amino acid residues to be incorporated at the (i+2) position of the non-helical turn. In the fourth chapter we attempted to construct isolated turns while in the fifth Chapter we attempted to construct β-hairpins by using such non-helical turns. We concluded that $\gamma^{3,3}$ and $\gamma^{4,4}$ amino acid residues could successfully be accommodated in the (i+2) position of the non-helical turns, and thus give rise to both the isolated turns and β-hairpins stabilized by these turns, unlike $\gamma^{2,2}$ residue. We established that this difference in the conformational ability of the $\gamma^{2,2}$ residue was owing to the unfavourable steric contacts of the methyl substituents with the backbone CO of the previous residue. Thus the position of backbone substitution had a direct effect on the conformational preference or ability of the amino acid residues in question.

With the studies performed in this thesis we have established that not only the geminal di-substitution but also its position along the backbone can be used as a strong handle to control and design interesting secondary and super-secondary structures. Smart choice of these amino acid residues in question would open up new horizons in the field peptide materials and therapeutics.

TH-3141_166122021

References

(1) Fosgerau, K.; Hoffmann, T. Peptide therapeutics: current status and future directions. *Drug Discovery Today* **2015**, *20*, 122-128.

(2) Jones, A. T.; Sayers, E. J. Cell entry of cell penetrating peptides: tales of tails wagging dogs. *J. Controlled Release* **2012**, *161*, 582-591.

(3) Mulder, K. C.; Lima, L. A.; Miranda, V. J.; Dias, S. C.; Franco, O. L. Current scenario of peptide-based drugs: the key roles of cationic antitumor and antiviral peptides. *Front. Microbiol.* **2013**, *4*, 321-343.

(4) Ong, Z. Y.; Wiradharma, N.; Yang, Y. Y. Strategies employed in the design and optimization of synthetic antimicrobial peptide amphiphiles with enhanced therapeutic potentials. *Adv. Drug Delivery Rev.* **2014**, *78*, 28-45.

(5) Ruoslahti, E. Peptides as targeting elements and tissue penetration devices for nanoparticles. *Adv. Mater.* **2012**, *24*, 3747-3756.

(6) Kaspar, A. A.; Reichert, J. M. Future directions for peptide therapeutics development. *Drug Discovery Today* **2013**, *18*, 807-817.

(7) Bulet, P.; Hetru, C.; Dimarcq, J.-L.; Hoffmann, D. Antimicrobial peptides in insects; structure and function. *Dev. Comp. Immunol.* **1999**, *23*, 329-344.

(8) Liu, L.-N.; Chen, X.-L.; Zhang, Y.-Z.; Zhou, B.-C. Characterization, structure and function of linker polypeptides in phycobilisomes of cyanobacteria and red algae: an overview. *Biochim. Biophys. Acta, Bioenerg.* **2005**, *1708*, 133-142.

(9) Powers, J.-P. S.; Hancock, R. E. The relationship between peptide structure and antibacterial activity. *Peptides* **2003**, *24*, 1681-1691.

(10) Huang, Y.; Huang, J.; Chen, Y. Alpha-helical cationic antimicrobial peptides: relationships of structure and function. *Protein Cell* **2010**, *1*, 143-152.

TH-3141_166122021

(11) Haney, E. F.; Hunter, H. N.; Matsuzaki, K.; Vogel, H. J. Solution NMR studies of amphibian antimicrobial peptides: linking structure to function? *Biochim. Biophys. Acta* **2009**, *1788*, 1639-1655.

(12) Feng, L.; Wang, Y.; Yang, J.; Sun, Y.-f.; Li, Y.-w.; Ye, Z.-h.; Lin, H.-b.; Yang, K. Overview of the preparation method, structure and function, and application of natural peptides and polypeptides. *Biomed. Pharmacother.* **2022**, *153*, 113493-113500.

(13) Honma, T.; Shiomi, K. Peptide toxins in sea anemones: structural and functional aspects. *Mar. Biotechnol.* **2006**, *8*, 1-10.

(14) Cai, K.; Langen, R.; Hubbell, W. L.; Khorana, H. G. Structure and function in rhodopsin: topology of the C-terminal polypeptide chain in relation to the cytoplasmic loops. *Proc. Natl. Acad. Sci. U. S. A.* **1997**, *94*, 14267-14272.

(15) Fan, T.; Yu, X.; Shen, B.; Sun, L. Peptide self-assembled nanostructures for drug delivery applications. *J. Nanomater.* **2017**, *2017*, 1-16.

(16) Habibi, N.; Kamaly, N.; Memic, A.; Shafiee, H. Self-assembled peptide-based nanostructures: Smart nanomaterials toward targeted drug delivery. *Nano Today* **2016**, *11*, 41-60.

(17) Zheng, X.; Zhang, P.; Fu, Z.; Meng, S.; Dai, L.; Yang, H. Applications of nanomaterials in tissue engineering. *RSC Adv.* **2021**, *11*, 19041-19058.

(18) Wang, C.; Fu, L.; Hu, Z.; Zhong, Y. A mini-review on peptide-based self-assemblies and their biological applications. *Nanotechnology* **2021**, *33*, 1-13.

(19) Huo, Y.; Hu, J.; Yin, Y.; Liu, P.; Cai, K.; Ji, W. Self-assembling peptide-based functional biomaterials. *ChemBioChem* **2022**, *DOI: https://doi.org/10.1002/cbic.202200582*.

(20) Chen, H.; Chen, X.; Chen, X.; Lin, S.; Cheng, J.; You, L.; Xiong, C.; Cai, X.; Wang, S. New perspectives on fabrication of peptide-based nanomaterials in food industry: A review. *Trends Food Sci. Technol.* **2022**, *129*, 49-60.

TH-3141_166122021

(21) Budama-Kilinc, Y.; Ozdemir, B.; Gozutok, K.: 7-Peptide-based nanobiomaterials. In *Nanobiomaterials Science, Development and Evaluation*; Razavi, M. T., A., Eds., Ed.; Woodhead Publishing: Sawston: UK, 2017; pp 135-146.

(22) Leighton, E.; Sainsbury, C. A.; Jones, G. C. A practical review of C-peptide testing in diabetes. *Diabetes Ther.* **2017**, *8*, 475-487.

(23) Maddaloni, E.; Bolli, G. B.; Frier, B. M.; Little, R. R.; Leslie, R. D.; Pozzilli, P.; Buzzetti, R. C-peptide determination in the diagnosis of type of diabetes and its management: A clinical perspective. *Diabetes, Obes. Metab.* **2022**, *24*, 1912-1926.

(24) Baig, M. H.; Ahmad, K.; Rabbani, G.; Choi, I. Use of peptides for the management of Alzheimer's disease: diagnosis and inhibition. *Front. Aging Neurosci.* **2018**, *10*, 21-26.

(25) Ribarič, S. Peptides as potential therapeutics for Alzheimer's disease. *Molecules* **2018**, *23*, 283-313.

(26) Baig, M. H.; Ahmad, K.; Saeed, M.; Alharbi, A. M.; Barreto, G. E.; Ashraf, G. M.; Choi, I. Peptide based therapeutics and their use for the treatment of neurodegenerative and other diseases. *Biomed. Pharmacother.* **2018**, *103*, 574-581.

(27) Yadav, A.; Pandey, D.; Ashraf, G. M. Peptide Based Therapy for Neurological Disorders. *Curr. Protein Pept. Sci.* **2021**, *22*, 656-665.

(28) Lei, J.; Sun, L.; Huang, S.; Zhu, C.; Li, P.; He, J.; Mackey, V.; Coy, D. H.; He, Q. The antimicrobial peptides and their potential clinical applications. *Am. J. Transl. Res.* **2019**, *11*, 3919-3931.

(29) Mahlapuu, M.; Håkansson, J.; Ringstad, L.; Björn, C. Antimicrobial peptides: an emerging category of therapeutic agents. *Front. Cell. Infect. Microbiol.* **2016**, *6*, 194-205.

TH-3141_166122021

(30) Moretta, A.; Scieuzo, C.; Petrone, A. M.; Salvia, R.; Manniello, M. D.; Franco, A.; Lucchetti, D.; Vassallo, A.; Vogel, H.; Sgambato, A. Antimicrobial peptides: A new hope in biomedical and pharmaceutical fields. *Front. Cell. Infect. Microbiol.* **2021**, *11*, 453-478.

(31) Chen, C. H.; Lu, T. K. Development and challenges of antimicrobial peptides for therapeutic applications. *Antibiotics* **2020**, *9*, 24-43.

(32) Marqus, S.; Pirogova, E.; Piva, T. J. Evaluation of the use of therapeutic peptides for cancer treatment. *J. Biomed. Sci.* **2017**, *24*, 1-15.

(33) Boohaker, R. J.; Lee, M. W.; Vishnubhotla, P.; Perez, J. L. M.; Khaled, A. R. The use of therapeutic peptides to target and to kill cancer cells. *Curr. Med. Chem.* **2012**, *19*, 3794-3804.

(34) Xiao, Y.-F.; Jie, M.-M.; Li, B.-S.; Hu, C.-J.; Xie, R.; Tang, B.; Yang, S.-M. Peptide-based treatment: a promising cancer therapy. *J. Immunol. Res.* **2015**, *2015*, 1-13.

(35) Xie, M.; Liu, D.; Yang, Y. Anti-cancer peptides: Classification, mechanism of action, reconstruction and modification. *Open Biol.* **2020**, *10*, 200004-200013.

(36) Samec, T.; Boulos, J.; Gilmore, S.; Hazelton, A.; Alexander-Bryant, A. Peptide-based delivery of therapeutics in cancer treatment. *Mater. Today Bio* **2022**, *14*, 100248-100265.

(37) Cooper, B. M.; Iegre, J.; O'Donovan, D. H.; Halvarsson, M. Ö.; Spring, D. R. Peptides as a platform for targeted therapeutics for cancer: Peptide–drug conjugates (PDCs). *Chem. Soc. Rev.* **2021**, *50*, 1480-1494.

(38) Tao, K.; Makam, P.; Aizen, R.; Gazit, E. Self-assembling peptide semiconductors. *Science* **2017**, *358*, 9756-9762.

(39) Liu, Y.; Shi, J.; Tong, Z.; Jia, Y.; Yang, B.; Wang, Z. The revitalization of antimicrobial peptides in the resistance era. *Pharmacol. Res.* **2021**, *163*, 105276.

(40) Yan, X.; Zhu, P.; Li, J. Self-assembly and application of diphenylalanine-based nanostructures. *Chem. Soc. Rev.* **2010**, *39*, 1877-1890.

TH-3141_166122021

(41) Chiangjong, W.; Chutipongtanate, S.; Hongeng, S. Anticancer peptide: Physicochemical property, functional aspect and trend in clinical application. *Int. J. Oncol.* **2020**, *57*, 678-696.

(42) Tillett, K. C.; Del Valle, J. R. N-Amino peptide scanning reveals inhibitors of Aβ 42 aggregation. *RSC Adv.* **2020**, *10*, 14331-14336.

(43) Gruber, C. W.; Muttenthaler, M.; Freissmuth, M. Ligand-based peptide design and combinatorial peptide libraries to target G protein-coupled receptors. *Curr. Pharm. Des.* **2010**, *16*, 3071-3088.

(44) Zakeri, B.; Fierer, J. O.; Celik, E.; Chittock, E. C.; Schwarz-Linek, U.; Moy, V. T.; Howarth, M. Peptide tag forming a rapid covalent bond to a protein, through engineering a bacterial adhesin. *Proc. Natl. Acad. Sci. U. S. A.* **2012**, *109*, 690-697.

(45) Foight, G. W.; Ryan, J. A.; Gullá, S. V.; Letai, A.; Keating, A. E. Designed BH3 peptides with high affinity and specificity for targeting Mcl-1 in cells. *ACS Chem. Biol.* **2014**, *9*, 1962-1968.

(46) Li, X.; Gohain, N.; Chen, S.; Li, Y.; Zhao, X.; Li, B.; Tolbert, W. D.; He, W.; Pazgier, M.; Hu, H.; Lu, W. Design of ultrahigh-affinity and dual-specificity peptide antagonists of MDM2 and MDMX for P53 activation and tumor suppression. *Acta Pharm. Sin. B* **2021**, *11*, 2655-2669.

(47) Geng, L.; Wang, Z.; Yang, X.; Li, D.; Lian, W.; Xiang, Z.; Wang, W.; Bu, X.; Lai, W.; Hu, Z. Structure-based design of peptides with high affinity and specificity to HER2 positive tumors. *Theranostics* **2015**, *5*, 1154-1165.

(48) Giebel, L. B.; Cass, R.; Milligan, D. L.; Young, D.; Arze, R.; Johnson, C. Screening of cyclic peptide phage libraries identifies ligands that bind streptavidin with high affinities. *Biochemistry* **1995**, *34*, 15430-15435.

TH-3141_166122021

(49) Uddin, M. Z.; Li, X.; Joo, H.; Tsai, J.; Wrischnik, L.; Jasti, B. Rational Design of Peptide Ligands Based on Knob–Socket Protein Packing Model Using CD13 as a Prototype Receptor. *ACS Omega* **2019**, *4*, 5126-5136.

(50) Cavaco, M.; Andreu, D.; Castanho, M. A. The challenge of peptide proteolytic stability studies: Scarce data, difficult readability, and the need for harmonization. *Angew. Chem., Int. Ed.* **2021**, *60*, 1686-1688.

(51) Böttger, R.; Hoffmann, R.; Knappe, D. Differential stability of therapeutic peptides with different proteolytic cleavage sites in blood, plasma and serum. *PloS One* **2017**, *12*, 0178943-0178957.

(52) Starr, C. G.; Wimley, W. C. Antimicrobial peptides are degraded by the cytosolic proteases of human erythrocytes. *Biochim. Biophys. Acta, Biomembr.* **2017**, *1859*, 2319-2326.

(53) Mentlein, R. Dipeptidyl-peptidase IV (CD26)-role in the inactivation of regulatory peptides. *Regul. Pept.* **1999**, *85*, 9-24.

(54) Cavaco, M.; Valle, J.; Flores, I.; Andreu, D.; ARB Castanho, M. Estimating peptide half-life in serum from tunable, sequence-related physicochemical properties. *Clin. Transl. Sci.* **2021**, *14*, 1349-1358.

(55) Otvos Jr, L.; Wade, J. D.: Current challenges in peptide-based drug discovery. Front. Chem., 2014; Vol. 2; pp 62-65.

(56) Lai, X.; Tang, J.; ElSayed, M. E. Recent advances in proteolytic stability for peptide, protein, and antibody drug discovery. *Expert Opin. Drug Discovery* **2021**, *16*, 1467-1482.

(57) Saladin, P. M.; Zhang, B. D.; Reichert, J. M. Current trends in the clinical development of peptide therapeutics. *IDrugs* **2009**, *12*, 779-784.

TH-3141_166122021

(58) Zhang, Y.; Zhang, H.; Ghosh, D.; Williams III, R. O. Just how prevalent are peptide therapeutic products? A critical review. *Int. J. Pharm.* **2020**, *587*, 119491-119510.

(59) Craik, D. J.; Fairlie, D. P.; Liras, S.; Price, D. The future of peptide-based drugs. *Chem. Biol. Drug Des.* **2013**, *81*, 136-147.

(60) Perkins, H. R. Vancomycin and related antibiotics. *Pharmacol. Ther.* **1982**, *16*, 181-197.

(61) Steenbergen, J. N.; Alder, J.; Thorne, G. M.; Tally, F. P. Daptomycin: a lipopeptide antibiotic for the treatment of serious Gram-positive infections. *J. Antimicrob. Chemother.* **2005**, *55*, 283-288.

(62) Yu, Z.; Yan, B.; Gao, L.; Dong, C.; Zhong, J.; DOrtenzio, M.; Nguyen, B.; Seong Lee, S.; Hu, X.; Liang, F. Targeted delivery of bleomycin: a comprehensive anticancer review. *Curr. Cancer Drug Targets* **2016**, *16*, 509-521.

(63) Schreiber, G. CHAPTER 1 Protein–protein interaction interfaces and their functional implications. *In Protein-protein interaction regulators* **2020**, *The Royal society of Chemistry*, 1-24.

(64) Peng, X.; Wang, J.; Peng, W.; Wu, F.-X.; Pan, Y. Protein–protein interactions: detection, reliability assessment and applications. *Briefings Bioinf.* **2017**, *18*, 798-819.

(65) Caporale, A.; Adorinni, S.; Lamba, D.; Saviano, M. Peptide–Protein Interactions: From Drug Design to Supramolecular Biomaterials. *Molecules* **2021**, *26*, 1219-1242.

(66) Cooper, W. J.; Waters, M. L. Molecular recognition with designed peptides and proteins. *Curr. Opin. Chem. Biol.* **2005**, *9*, 627-631.

(67) Schilz, J.; Binder, U.; Friedrich, L.; Gebauer, M.; Lutz, C.; Schlapschy, M.; Schiefner, A.; Skerra, A. Molecular recognition of structurally disordered Pro/Ala-rich

TH-3141_166122021

sequences (PAS) by antibodies involves an Ala residue at the hot spot of the epitope. *J. Mol. Biol.* **2021**, *433*, 167113-167131.

(68) Bergey, C. M.; Watkins, A. M.; Arora, P. S. HippDB: a database of readily targeted helical protein–protein interactions. *Bioinformatics* **2013**, *29*, 2806-2807.

(69) Jochim, A. L.; Arora, P. S. Assessment of helical interfaces in protein–protein interactions. *Mol. BioSyst.* **2009**, *5*, 924-926.

(70) Jochim, A. L.; Arora, P. S. Systematic analysis of helical protein interfaces reveals targets for synthetic inhibitors. *ACS Chem. Biol.* **2010**, *5*, 919-923.

(71) Bullock, B. N.; Jochim, A. L.; Arora, P. S. Assessing helical protein interfaces for inhibitor design. *J. Am. Chem. Soc.* **2011**, *133*, 14220-14223.

(72) Lamers, C. Overcoming the shortcomings of peptide-based therapeutics. *Future Drug Discovery* **2022**, *4*, FDD75-FDD92.

(73) Lee, A. C.-L.; Harris, J. L.; Khanna, K. K.; Hong, J.-H. A comprehensive review on current advances in peptide drug development and design. *Int. J. Mol. Sci.* **2019**, *20*, 2383-2404.

(74) Gokhale, A. S.; Satyanarayanajois, S. Peptides and peptidomimetics as immunomodulators. *Immunotherapy* **2014**, *6*, 755-774.

(75) Naylor, M. R.; Bockus, A. T.; Blanco, M.-J.; Lokey, R. S. Cyclic peptide natural products chart the frontier of oral bioavailability in the pursuit of undruggable targets. *Curr. Opin. Chem. Biol.* **2017**, *38*, 141-147.

(76) Di, L. Strategic approaches to optimizing peptide ADME properties. *AAPS J.* **2015**, *17*, 134-143.

(77) Werle, M.; Bernkop-Schnürch, A. Strategies to improve plasma half life time of peptide and protein drugs. *Amino Acids* **2006**, *30*, 351-367.

TH-3141_166122021

(78) Li, Y.; Li, W.; Xu, Z. Improvement on Permeability of Cyclic Peptide/Peptidomimetic: Backbone N-Methylation as A Useful Tool. *Mar. Drugs* **2021**, *19*, 311-327.

(79) Fichtner, M.; Voigt, K.; Schuster, S. The tip and hidden part of the iceberg: Proteinogenic and non-proteinogenic aliphatic amino acids. *Biochim. Biophys. Acta, Gen. Subj.* **2017**, *1861*, 3258-3269.

(80) Ding, Y.; Ting, J. P.; Liu, J.; Al-Azzam, S.; Pandya, P.; Afshar, S. Impact of non-proteinogenic amino acids in the discovery and development of peptide therapeutics. *Amino Acids* **2020**, *52*, 1207-1226.

(81) Agrawal, S.; Acharya, D.; Adholeya, A.; Barrow, C. J.; Deshmukh, S. K. Nonribosomal peptides from marine microbes and their antimicrobial and anticancer potential. *Front. Pharmacol.* **2017**, *8*, 828-853.

(82) Duban, M.; Cociancich, S.; Leclère, V. Nonribosomal peptide synthesis definitely working out of the rules. *Microorganisms* **2022**, *10*, 577-595.

(83) Süssmuth, R. D.; Mainz, A. Nonribosomal peptide synthesis—principles and prospects. *Angew. Chem., Int. Ed.* **2017**, *56*, 3770-3821.

(84) Dincer, S.; Takci, H. A. M.; Ozdenefe, M. S. Nonribosomal Peptide Synthesis. *Molecular Cloning* **2022**, 108.

(85) Hartman, M. C.; Josephson, K.; Lin, C.-W.; Szostak, J. W. An expanded set of amino acid analogs for the ribosomal translation of unnatural peptides. *PloS One* **2007**, *2*, 972-986.

(86) Xue, Y.-P.; Cao, C.-H.; Zheng, Y.-G. Enzymatic asymmetric synthesis of chiral amino acids. *Chem. Soc. Rev.* **2018**, *47*, 1516-1561.

(87) Narancic, T.; Almahboub, S. A.; O'Connor, K. E. Unnatural amino acids: production and biotechnological potential. *World J. Microbiol. Biotechnol.* **2019**, *35*, 1-11.

TH-3141_166122021

(88) Faraggi, T. M.; Rouget-Virbel, C.; Rincón, J. A.; Barberis, M.; Mateos, C.; García-Cerrada, S.; Agejas, J.; De Frutos, O.; MacMillan, D. W. Synthesis of Enantiopure Unnatural Amino Acids by Metallaphotoredox Catalysis. *Org. Process Res. Dev.* **2021**, *25*, 1966-1973.

(89) Esteves, C. I.; Raposo, M. M. M.; Costa, S. P. Non-canonical amino acids bearing thiophene and bithiophene: synthesis by an Ugi multicomponent reaction and studies on ion recognition ability. *Amino Acids* **2017**, *49*, 921-930.

(90) Ferreira, R. C. M.; Raposo, M. M. M.; Costa, S. P. Heterocyclic amino acids as fluorescent reporters for transition metals: synthesis and evaluation of novel furyl-benzoxazol-5-yl-l-alanines. *New J. Chem.* **2018**, *42*, 3483-3492.

(91) Agostini, F.; Völler, J. S.; Koksch, B.; Acevedo-Rocha, C. G.; Kubyshkin, V.; Budisa, N. Biocatalysis with unnatural amino acids: enzymology meets xenobiology. *Angew. Chem., Int. Ed.* **2017**, *56*, 9680-9703.

(92) Blaskovich, M. A. Unusual amino acids in medicinal chemistry. *J. Med. Chem.* **2016**, *59*, 10807-10836.

(93) Brittain, W. D.; Lloyd, C. M.; Cobb, S. L. Synthesis of complex unnatural fluorine-containing amino acids. *J. Fluorine Chem.* **2020**, *239*, 109630-109649.

(94) Sasaki, Y.; Ambo, A. 2′, 6′-Dimethylphenylalanine: A Useful Aromatic Amino Acid Surrogate for Tyr or Phe Residue in Opioid Peptides. *Int. J. Med. Chem.* **2012**, *2012*, 498901-498912.

(95) Stevenazzi, A.; Marchini, M.; Sandrone, G.; Vergani, B.; Lattanzio, M. Amino acidic scaffolds bearing unnatural side chains: An old idea generates new and versatile tools for the life sciences. *Bioorg. Med. Chem. Lett.* **2014**, *24*, 5349-5356.

(96) Lenci, E.; Trabocchi, A. Peptidomimetic toolbox for drug discovery. *Chem. Soc. Rev.* **2020**, *49*, 3262-3277.

TH-3141_166122021

(97) Stefanic, P.; Dolenc, M. S. Aspartate and glutamate mimetic structures in biologically active compounds. *Curr. Med. Chem.* **2004**, *11*, 945-968.

(98) Kawakami, T.; Sasaki, T.; Reid, P. C.; Murakami, H. Incorporation of electrically charged N-alkyl amino acids into ribosomally synthesized peptides via post-translational conversion. *Chem. Sci.* **2014**, *5*, 887-893.

(99) Yan, T.; Feringa, B. L.; Barta, K. Direct N-alkylation of unprotected amino acids with alcohols. *Sci. Adv.* **2017**, *3*, 6494-6500.

(100) Hyslop, J. F.; Lovelock, S. L.; Watson, A. J.; Sutton, P. W.; Roiban, G.-D. N-Alkyl-α-amino acids in Nature and their biocatalytic preparation. *J. Biotechnol.* **2019**, *293*, 56-65.

(101) Perez, J. J. Designing peptidomimetics. *Curr. Trends Med. Chem.* **2018**, *18*, 566-590.

(102) Masip, I.; Perez-Paya, E.; Messeguer, A. Peptoids as source of compounds eliciting antibacterial activity. *Comb. Chem. High Throughput Screening* **2005**, *8*, 235-239.

(103) Chatterjee, J.; Rechenmacher, F.; Kessler, H. N-methylation of peptides and proteins: an important element for modulating biological functions. *Angew. Chem., Int. Ed.* **2013**, *52*, 254-269.

(104) Chingle, R.; Proulx, C.; Lubell, W. D. Azapeptide synthesis methods for expanding side-chain diversity for biomedical applications. *Acc. Chem. Res.* **2017**, *50*, 1541-1556.

(105) Avan, I.; Hall, C. D.; Katritzky, A. R. Peptidomimetics via modifications of amino acids and peptide bonds. *Chem. Soc. Rev.* **2014**, *43*, 3575-3594.

(106) Ghosh, A. K.; Osswald, H. L.; Prato, G. Recent Progress in the Development of HIV-1 Protease Inhibitors for the Treatment of HIV/AIDS. *J. Med. Chem.* **2016**, *59*, 5172-5208.

TH-3141_166122021

(107) Spiegel, J.; Mas-Moruno, C.; Kessler, H.; Lubell, W. D. Cyclic aza-peptide integrin ligand synthesis and biological activity. *J. Org. Chem.* **2012**, *77*, 5271-5278.

(108) Vasudev, P. G.; Chatterjee, S.; Shamala, N.; Balaram, P. Structural chemistry of peptides containing backbone expanded amino acid residues: conformational features of β, γ, and hybrid peptides. *Chem. Rev.* **2011**, *111*, 657-687.

(109) Lelais, G.; Seebach, D. β2-amino acids—syntheses, occurrence in natural products, and components of β-peptides1, 2. *Pept. Sci.* **2004**, *76*, 206-243.

(110) Seebach, D.; Overhand, M.; Kühnle, F. N.; Martinoni, B.; Oberer, L.; Hommel, U.; Widmer, H. β-Peptides: Synthesis by Arndt-Eistert homologation with concomitant peptide coupling. Structure determination by NMR and CD spectroscopy and by X-ray crystallography. Helical secondary structure of a β-hexapeptide in solution and its stability towards pepsin. *Helv. Chim. Acta* **1996**, *79*, 913-941.

(111) Seebach, D.; Beck, A. K.; Bierbaum, D. J. The world of β-and γ-peptides comprised of homologated proteinogenic amino acids and other components. *Chem. Biodiversity* **2004**, *1*, 1111-1239.

(112) Kimmerlin, T.; Seebach, D. '100 years of peptide synthesis': ligation methods for peptide and protein synthesis with applications to β-peptide assemblies. *J. Pept. Res.* **2005**, *65*, 229-260.

(113) Ashfaq, M.; Tabassum, R.; Ahmad, M.; Hassan, N.; Oku, H.; Rivera, G. Enantioselective Synthesis of β-amino acids: A Review. *Med. Chem.* **2015**, *5*, 295-309.

(114) Aguilar, M.-I.; Purcell, A. W.; Devi, R.; Lew, R.; Rossjohn, J.; Smith, A. I.; Perlmutter, P. β-Amino acid-containing hybrid peptides—new opportunities in peptidomimetics. *Org. Biomol. Chem.* **2007**, *5*, 2884-2890.

TH-3141_166122021

(115) Seebach, D.; Beck, A. K.; Capone, S.; Deniau, G.; Grošelj, U.; Zass, E. Enantioselective preparation of β²-amino acid derivatives for β-peptide synthesis. *Synthesis* **2009**, *2009*, 1-32.

(116) Gray, D.; Concellón, C.; Gallagher, T. Kowalski ester homologation. Application to the synthesis of β-amino esters. *J. Org. Chem.* **2004**, *69*, 4849-4851.

(117) Soloshonok, V. A.; Fokina, N. A.; Rybakova, A. V.; Shishkina, I. P.; Galushko, S. V.; Sorochinsky, A. E.; Kukhar, V. P.; Savchenko, M. V.; Švedas, V. K. Biocatalytic approach to enantiomerically pure β-amino acids. *Tetrahedron: Asymmetry* **1995**, *6*, 1601-1610.

(118) Podlech, J.; Seebach, D. Azetidin-3-ones from (S)-α-Amino Acids and Their Reactions with Nucleophiles: Preparation of some azetidine-containing amino-alcohol and amino-acid derivatives. *Helv. Chim. Acta* **1995**, *78*, 1238-1246.

(119) Podlech, J.; Seebach, D. The Arndt–Eistert reaction in peptide chemistry: A facile access to homopeptides. *Angew. Chem., Int. Ed. Engl.* **1995**, *34*, 471-472.

(120) Liljeblad, A.; Kanerva, L. T. Biocatalysis as a profound tool in the preparation of highly enantiopure?-amino acids. *Tetrahedron* **2006**, *62*, 5831-5854.

(121) Smrcina, M.; Majer, P.; Majerová, E.; Guerassina, T. A.; Eissenstat, M. A. Facile stereoselective synthesis of γ-substituted γ-amino acids from the corresponding α-amino acids. *Tetrahedron* **1997**, *53*, 12867-12874.

(122) Corvo, M.; Pereira, M. Synthesis of γ-amino acid analogues from natural α-amino acids by a radical pathway. *Amino Acids* **2007**, *32*, 243-246.

(123) Loukas, V.; Noula, C.; Kokotos, G. Efficient protocols for the synthesis of enantiopure γ-amino acids with proteinogenic side chains. *J. Pept. Sci.* **2003**, *9*, 312-319.

TH-3141_166122021

(124) Chi, Y.; Guo, L.; Kopf, N. A.; Gellman, S. H. Enantioselective organocatalytic Michael addition of aldehydes to nitroethylene: efficient access to γ2-amino acids. *J. Am. Chem. Soc.* **2008**, *130*, 5608-5609.

(125) Gil, S.; Parra, M.; Rodríguez, P. An Efficient Synthesis of γ-Aminoacids and Attempts to Drive Its Enantioselectivity. *Molecules* **2008**, *13*, 716-728.

(126) Deng, J.; Hu, X.-P.; Huang, J.-D.; Yu, S.-B.; Wang, D.-Y.; Duan, Z.-C.; Zheng, Z. Enantioselective Synthesis of β-Aryl-γ-amino Acid Derivatives via Cu-Catalyzed Asymmetric 1, 4-Reductions of γ-Phthalimido-Substituted α, β-Unsaturated Carboxylic Acid Esters. *J. Org. Chem.* **2008**, *73*, 6022-6024.

(127) Abele, S.; Seebach, D. Preparation of achiral and of enantiopure geminally disubstituted β-amino acids for β-peptide synthesis. *Eur. J. Org. Chem.* **2000**, *2000*, 1-15.

(128) Seebach, D.; Abele, S.; Sifferlen, T.; Hänggi, M.; Gruner, S.; Seiler, P. Preparation and Structure of β-Peptides Consisting of Geminally Disubstituted β2,2-and β3,3-Amino Acids: A Turn Motif for β-Peptides. *Helv. Chim. Acta* **1998**, *81*, 2218-2243.

(129) Palomo, C.; Oiarbide, M.; Bindi, S. A concise β-lactam route to short peptide segments containing β, β-disubstituted β-amino acids. *J. Org. Chem.* **1998**, *63*, 2469-2474.

(130) Royer, F.; Felpin, F.-X.; Doris, E. Synthesis of gamma-amino acids by rearrangement of alpha-cyanocyclopropanone hydrates: application to the regioselective labeling of amino acids. *J. Org. Chem.* **2001**, *66*, 6487-6489.

(131) Zhang, X. b.; Waibel, M.; Hasserodt, J. An Autoimmolative Spacer Allows First-Time Incorporation of a Unique Solid-State Fluorophore into a Detection Probe for Acyl Hydrolases. *Chem. - Eur. J.* **2010**, *16*, 792-795.

(132) Andruszkiewicz, R.; Silverman, R. B. 4-Amino-3-alkylbutanoic acids as substrates for gamma-aminobutyric acid aminotransferase. *J. Biol. Chem.* **1990**, *265*, 22288-22291.

TH-3141_166122021

(133) Misra, R.; George, G.; Saseendran, A.; Raghothama, S.; Gopi, H. N. Ambidextrous α, γ-Hybrid Peptide Foldamers. *Chem. - Asian J.* **2019**, *14*, 4408-4414.

(134) Gracia, S.; Jerpan, R.; Pellet-Rostaing, S.; Popowycz, F.; Lemaire, M. Straightforward synthesis of indolizidine alkaloid 167B. *Tetrahedron Lett.* **2010**, *51*, 6290-6293.

(135) Jadhav, S. V.; Gopi, H. N. Remarkable thermoresponsive nanofibers from γ-peptides. *Chem. Commun.* **2013**, *49*, 9179-9181.

(136) Cardillo, G.; Tomasini, C. Asymmetric synthesis of ß-amino acids and α-substituted β-amino acids. *Chem. Soc. Rev.* **1996**, *25*, 117-128.

(137) Sibi, M. P.; Prabagaran, N.; Ghorpade, S. G.; Jasperse, C. P. Enantioselective synthesis of α, β-disubstituted-β-amino acids. *J. Am. Chem. Soc.* **2003**, *125*, 11796-11797.

(138) Sewald, N. Stereoselective synthesis ofβ-amino acids via conjugate addition of nitrogen nucleophiles toα, β-unsaturated esters—Recent advances. *Amino Acids* **1996**, *11*, 397-408.

(139) Ojima, I.; Delaloge, F. Asymmetric synthesis of building-blocks for peptides and peptidomimetics by means of the β-lactam synthon method. *Chem. Soc. Rev.* **1997**, *26*, 377-386.

(140) Sewald, N. Synthetic Routes towards enantiomerically pure β-amino acids. *Angew. Chem., Int. Ed.* **2003**, *42*, 5794-5795.

(141) Zhang, J.; Kissounko, D. A.; Lee, S. E.; Gellman, S. H.; Stahl, S. S. Access to poly-β-peptides with functionalized side chains and end groups via controlled ring-opening polymerization of β-lactams. *J. Am. Chem. Soc.* **2009**, *131*, 1589-1597.

(142) Podlech, J.; Seebach, D. On the preparation of β-amino acids from α-amino acids using the Arndt-Eistert reaction: Scope, limitations and stereoselectivity. Application to

TH-3141_166122021

carbohydrate peptidation. Stereoselective α-alkylations of some β-amino acids. *Liebigs Ann.* **1995**, *1995*, 1217-1228.

(143) Liu, M.; Sibi, M. P. Recent advances in the stereoselective synthesis of β-amino acids. *Tetrahedron* **2002**, *40*, 7991-8035.

(144) Cole, D. C. Recent stereoselective synthetic approaches to β-amino acids. *Tetrahedron* **1994**, *50*, 9517-9582.

(145) DeGrado, W.; Schneider, J.; Hamuro, Y. The twists and turns of β-peptides. *J. Pept. Res.* **1999**, *54*, 206-217.

(146) Hunter, L.; Jolliffe, K. A.; Jordan, M. J.; Jensen, P.; Macquart, R. B. Synthesis and Conformational Analysis of α, β-Difluoro-γ-amino Acid Derivatives. *Chem. - Eur. J.* **2011**, *17*, 2340-2343.

(147) Hanessian, S.; Luo, X.; Schaum, R.; Michnick, S. Design of Secondary Structures in Unnatural Peptides: Stable Helical gamma-Tetra-Hexa-, and Octapeptides and Consequences of -Substitution. *J. Am. Chem. Soc.* **1998**, *120*, 8569-8570.

(148) Hanessian, S.; Schaum, R. 1, 3-Asymmetric induction in enolate alkylation reactions of N-protected γ-amino acid derivatives. *Tetrahedron Lett.* **1997**, *38*, 163-166.

(149) Ordonez, M.; Cativiela, C. Stereoselective synthesis of γ-amino acids. *Tetrahedron: Asymmetry* **2007**, *18*, 3-99.

(150) Bouillere, F.; Thétiot-Laurent, S.; Kouklovsky, C.; Alezra, V. Foldamers containing γ-amino acid residues or their analogues: structural features and applications. *Amino Acids* **2011**, *41*, 687-707.

(151) Appella, D. H.; Christianson, L. A.; Karle, I. L.; Powell, D. R.; Gellman, S. H. β-Peptide foldamers: robust helix formation in a new family of β-amino acid oligomers. *J. Am. Chem. Soc.* **1996**, *118*, 13071-13072.

TH-3141_166122021

(152) Appella, D. H.; Christianson, L. A.; Klein, D. A.; Powell, D. R.; Huang, X.; Barchi, J. J.; Gellman, S. H. Residue-based control of helix shape in β-peptide oligomers. *Nature* **1997**, *387*, 381-384.

(153) Appella, D. H.; Christianson, L. A.; Klein, D. A.; Richards, M. R.; Powell, D. R.; Gellman, S. H. Synthesis and structural characterization of helix-forming β-peptides: trans-2-aminocyclopentanecarboxylic acid oligomers. *J. Am. Chem. Soc.* **1999**, *121*, 7574-7581.

(154) Appella, D. H.; Christianson, L. A.; Karle, I. L.; Powell, D. R.; Gellman, S. H. Synthesis and characterization of trans-2-aminocyclohexanecarboxylic acid oligomers: an unnatural helical secondary structure and implications for β-peptide tertiary structure. *J. Am. Chem. Soc.* **1999**, *121*, 6206-6212.

(155) Chung, Y. J.; Christianson, L. A.; Stanger, H. E.; Powell, D. R.; Gellman, S. H. A β-peptide reverse turn that promotes hairpin formation. *J. Am. Chem. Soc.* **1998**, *120*, 10555-10556.

(156) Chung, Y. J.; Huck, B. R.; Christianson, L. A.; Stanger, H. E.; Krauthaeuser, S.; Powell, D. R.; Gellman, S. H. Stereochemical control of hairpin formation in β-peptides containing dinipecotic acid reverse turn segments. *J. Am. Chem. Soc.* **2000**, *122*, 3995-4004.

(157) Guo, L.; Chi, Y.; Almeida, A. M.; Guzei, I. A.; Parker, B. K.; Gellman, S. H. Stereospecific synthesis of conformationally constrained γ-amino acids: New foldamer building blocks that support helical secondary structure. *J. Am. Chem. Soc.* **2009**, *131*, 16018-16020.

(158) Guo, L.; Almeida, A. M.; Zhang, W.; Reidenbach, A. G.; Choi, S. H.; Guzei, I. A.; Gellman, S. H. Helix formation in preorganized β/γ-peptide foldamers: hydrogen-bond analogy to the α-helix without α-amino acid residues. *J. Am. Chem. Soc.* **2010**, *132*, 7868-7869.

(159) Woll, M. G.; Lai, J. R.; Guzei, I. A.; Taylor, S. J.; Smith, M. E.; Gellman, S. H. Parallel sheet secondary structure in γ-peptides. *J. Am. Chem. Soc.* **2001**, *123*, 11077-11078.

TH-3141_166122021

(160) Guo, L.; Zhang, W.; Reidenbach, A. G.; Giuliano, M. W.; Guzei, I. A.; Spencer, L. C.; Gellman, S. H. Characteristic Structural Parameters for the γ-Peptide 14-Helix: Importance of Subunit Preorganization. *Angew. Chem. Int. Ed.* **2011**, *123*, 5965-5968.

(161) Guo, L.; Zhang, W.; Guzei, I. A.; Spencer, L. C.; Gellman, S. H. New preorganized γ-amino acids as foldamer building blocks. *Org. Lett.* **2012**, *14*, 2582-2585.

(162) Giuliano, M. W.; Maynard, S. J.; Almeida, A. M.; Reidenbach, A. G.; Guo, L.; Ulrich, E. C.; Guzei, I. A.; Gellman, S. H. Evaluation of a cyclopentane-based γ-amino acid for the ability to promote α/γ-peptide secondary structure. *J. Org. Chem.* **2013**, *78*, 12351-12361.

(163) Giuliano, M. W.; Maynard, S. J.; Almeida, A. M.; Guo, L.; Guzei, I. A.; Spencer, L. C.; Gellman, S. H. A γ-amino acid that favors 12/10-helical secondary structure in α/γ-peptides. *J. Am. Chem. Soc.* **2014**, *136*, 15046-15053.

(164) Sandvoss, L. M.; Carlson, H. A. Conformational behavior of β-proline oligomers. *J. Am. Chem. Soc.* **2003**, *125*, 15855-15862.

(165) Abele, S.; Vögtli, K.; Seebach, D. Oligomers of β2-and of β3-homoproline: What are the secondary structures of β-peptides lacking H-bonds? *Helv. Chim. Acta* **1999**, *82*, 1539-1558.

(166) Veeresh, K.; Gopi, H. N. Design of Helical Peptide Foldamers through α, β→β, γ Double-bond Migration. *Org. Lett.* **2019**, *21*, 4500-4504.

(167) Kumar, M. G.; Thombare, V. J.; Katariya, M. M.; Veeresh, K.; Raja, K. M. P.; Gopi, H. N. Non-classical Helices with cis Carbon–Carbon Double Bonds in the Backbone: Structural Features of a, g-Hybrid Peptide Foldamers. *Angew. Chem.* **2016**, *128*, 7978-7982.

(168) Misra, R.; Dey, S.; Reja, R. M.; Gopi, H. N. Artificial β-Double Helices from Achiral γ-Peptides. *Angew. Chem.* **2018**, *130*, 1069-1073.

TH-3141_166122021

(169) Veeresh, K.; Singh, M.; Gopi, H. N. Impact of substituent effects on the design of β-sheet mimetics and β-double helices from (E)-vinylogous γ-amino acid oligomers. *Org. Biomol. Chem.* **2019**, *17*, 9226-9231.

(170) Hagihara, M.; Anthony, N. J.; Stout, T. J.; Clardy, J.; Schreiber, S. L. Vinylogous polypeptides: an alternative peptide backbone. *J. Am. Chem. Soc.* **1992**, *114*, 6568-6570.

(171) Bandyopadhyay, A.; Misra, R.; Gopi, H. N. Structural features and molecular aggregations of designed triple-stranded β-sheets in single crystals. *Chem. Commun.* **2016**, *52*, 4938-4941.

(172) Chakraborty, T. K.; Ghosh, A.; Kumar, S. K.; Kunwar, A. C. Nucleation of β-hairpin structures with cis amide bonds in E-vinylogous proline-containing peptides. *J. Org. Chem.* **2003**, *68*, 6459-6462.

(173) Mali, S. M.; Bandyopadhyay, A.; Jadhav, S. V.; Kumar, M. G.; Gopi, H. N. Synthesis of α, β-unsaturated γ-amino esters with unprecedented high (E)-stereoselectivity and their conformational analysis in peptides. *Org. Biomol. Chem.* **2011**, *9*, 6566-6574.

(174) Grison, C.; Coutrot, P.; Genève, S.; Didierjean, C.; Marraud, M. Structural investigation of "cis" and "trans" vinylogous peptides: cis-vinylog turn in folded cis-vinylogous peptides, an excellent mimic of the natural β-turn. *J. Org. Chem.* **2005**, *70*, 10753-10764.

(175) Sharma, G. V.; Reddy, K. R.; Krishna, P. R.; Sankar, A. R.; Narsimulu, K.; Kumar, S. K.; Jayaprakash, P.; Jagannadh, B.; Kunwar, A. Robust mixed 10/12 helices promoted by "alternating chirality" in a new family of C-linked carbo-β-peptides. *J. Am. Chem. Soc.* **2003**, *125*, 13670-13671.

TH-3141_166122021

(176) Sharma, G. V.; Nagendar, P.; Jayaprakash, P.; Radha Krishna, P.; Ramakrishna, K.; Kunwar, A. C. 9/11 Mixed Helices in α/β Peptides Derived from C-Linked Carbo-β-Amino Acid and l-Ala Repeats. *Angew. Chem.* **2005**, *117*, 6028-6032.

(177) Sharma, G. V.; Reddy, K. R.; Krishna, P. R.; Sankar, A. R.; Jayaprakash, P.; Jagannadh, B.; Kunwar, A. C. Left-handed Helical twists in "mixed β-peptides" derived from alternating C-linked carbo-β3-amino acids and β-hGly units. *Angew. Chem.* **2004**, *116*, 4051-4055.

(178) Sharma, G. V.; Jayaprakash, P.; Narsimulu, K.; Ravi Sankar, A.; Ravinder Reddy, K.; Radha Krishna, P.; Kunwar, A. C. A left-handed 9-helix in γ-peptides: synthesis and conformational studies of oligomers with dipeptide repeats of c-linked carbo-γ4-amino acids and γ-aminobutyric acid. *Angew. Chem. Int. Ed.* **2006**, *45*, 2944-2947.

(179) Sharma, G. V.; Jadhav, V. B.; Ramakrishna, K. V.; Jayaprakash, P.; Narsimulu, K.; Subash, V.; Kunwar, A. C. 12/10-and 11/13-mixed helices in α/γ-and β/γ-hybrid peptides containing C-linked carbo-γ-amino acids with alternating α-and β-amino acids. *J. Am. Chem. Soc.* **2006**, *128*, 14657-14668.

(180) Sharma, G. V.; Chandramouli, N.; Choudhary, M.; Nagendar, P.; Ramakrishna, K. V.; Kunwar, A. C.; Schramm, P.; Hofmann, H.-J. r. Hybrid helices: motifs for secondary structure scaffolds in foldamers. *J. Am. Chem. Soc.* **2009**, *131*, 17335-17344.

(181) Sharma, G. V.; Yadav, T. A.; Choudhary, M.; Kunwar, A. C. Design of β-Amino Acid with Backbone–Side Chain Interactions: Stabilization of 14/15-Helix in α/β-Peptides. *J. Org. Chem.* **2012**, *77*, 6834-6848.

(182) Sharma, G. V.; Thodupunuri, P.; Sirisha, K.; Basha, S. J.; Gurava Reddy, P.; Sarma, A. V. Design and synthesis of peptides with hybrid helix-turn-helix (HTH) motif and their conformational study. *J. Org. Chem.* **2014**, *79*, 8614-8628.

TH-3141_166122021

(183) Thodupunuri, P.; Katukuri, S.; Ramakrishna, K. V.; Sharma, G. V.; Kunwar, A. C.; Sarma, A. V.; Hofmann, H.-J. r. Solvent-Directed Switch of a Left-Handed 10/12-Helix into a Right-Handed 12/10-Helix in Mixed β-Peptides. *J. Org. Chem.* **2017**, *82*, 2018-2031.

(184) Gruner, S. A.; Truffault, V.; Voll, G.; Locardi, E.; Stöckle, M.; Kessler, H. Design, synthesis, and NMR structure of linear and cyclic oligomers containing novel furanoid sugar amino acids. *Chem. - Eur. J.* **2002**, *8*, 4365-4376.

(185) Andreini, M.; Taillefumier, C.; Chrétien, F.; Thery, V.; Chapleur, Y. Synthesis and solution conformation of homo-β-peptides consisting of N-mannofuranosyl-3-ulosonic acids. *J. Org. Chem.* **2009**, *74*, 7651-7659.

(186) Sharma, G. V.; Sai Reddy, P.; Chatterjee, D.; Kunwar, A. C. Synthesis and structural studies of homooligomers of geminally disubstituted β2, 2-amino acids with carbohydrate side chain. *J. Org. Chem.* **2011**, *76*, 1562-1571.

(187) Sridhar, G.; Reddy, K. R.; Sharma, G. V. Synthesis of novel β2, 2-amino acid from D-mannose and attempted synthesis of peptides from the amino acid. *J. Carbohydr. Chem.* **2018**, *37*, 94-101.

(188) Nair, R. V.; Vijayadas, K. N.; Roy, A.; Sanjayan, G. J. Heterogeneous foldamers from aliphatic–aromatic amino acid building blocks: Current trends and future prospects. *Eur. J. Org. Chem.* **2014**, *2014*, 7763-7780.

(189) Xin, D.; Burgess, K. Anthranilic acid-containing cyclic tetrapeptides: at the crossroads of conformational rigidity and synthetic accessibility. *Org. Biomol. Chem.* **2016**, *14*, 5049-5058.

(190) Srinivasulu, G.; RamanaRao, M.; KiranKumar, S.; Kunwar, A. β-Hairpin peptides containing 3-amino benzoic acid, a constrained γ-amino acid. *ARKIVOC* **2004**, *8*, 69-86.

TH-3141_166122021

(191) Ramesh, V. V.; Priya, G.; Rajamohanan, P.; Hofmann, H.-J.; Sanjayan, G. J. Expanding the structural repertoire of β/α Ant-Pro (anthranilic acid-proline) oligomers into γ/α 2-Amb-Pro (2-aminomethyl benzoic acid-proline) oligomers. *Tetrahedron* **2012**, *68*, 4399-4405.

(192) Van der Poorten, O.; Knuhtsen, A.; Sejer Pedersen, D.; Ballet, S.; Tourwe, D. Side chain cyclized aromatic amino acids: great tools as local constraints in peptide and peptidomimetic design. *J. Med. Chem.* **2016**, *59*, 10865-10890.

(193) Ramachandran, G. N.; Ramakrishnan, C.; Sasisekharan, V. Stereochemistry of polypeptide chain configurations. *J. mol. Biol.* **1963**, *7*, 95-99.

(194) Ramakrishnan, C.; Ramachandran, G. Stereochemical criteria for polypeptide and protein chain conformations: II. Allowed conformations for a pair of peptide units. *Biophys. J.* **1965**, *5*, 909-933.

(195) Ramachandran, G. N.; Sasisekharan, V. Conformation of polypeptides and proteins. *Adv. Protein Chem.* **1968**, *23*, 283-437.

(196) Hovmöller, S.; Zhou, T.; Ohlson, T. Conformations of amino acids in proteins. *Acta Crystallogr., Sect. D: Biol. Crystallogr.* **2002**, *58*, 768-776.

(197) Aravinda, S.; Shamala, N.; Roy, R. S.; Balaram, P. Non-protein amino acids in peptide design. *J. Chem. Sci.* **2003**, *115*, 373-400.

(198) Ramakrishnan, C.; Srinivasan, N. Glycyl residues in proteins and peptides: an analysis. *Curr. Sci.* **1990**, *59*, 851-862.

(199) Gunasekaran, K. Stereochemical Analysis On Protein Structures-Lessons For Design, Engineering And Prediction. Indian Institute of Science, Bangalore, 1997.

(200) Ho, B. K.; Brasseur, R. The Ramachandran plots of glycine and pre-proline. *BMC Struct. Biol.* **2005**, *5*, 1-11.

TH-3141_166122021

(201) Marshall, G. R.; Bosshard, H. E. Angiotensin. II. Studies on the biologically active conformation. *Circ. Res.* **1972**, *31*, 143-150.

(202) Venkataram, P. B.; Balaram, P.; Benedetti, E. The Stereochemistry of Peptides Containing α-Aminoisobutyric Aci. *Crit. Rev. Biochem.* **1984**, *16*, 307-348.

(203) Burgess, A. W. Designing amino acids to determine the local conformations of peptides. *Proc. Natl. Acad. Sci. U. S. A.* **1994**, *91*, 2649-2653.

(204) Bernstein, F. C.; Koetzle, T. F.; Williams, G. J.; Meyer Jr, E. F.; Brice, M. D.; Rodgers, J. R.; Kennard, O.; Shimanouchi, T.; Tasumi, M. The Protein Data Bank: a computer-based archival file for macromolecular structures. *J. Mol. Biol.* **1977**, *112*, 535-542.

(205) Tailleur, P.; Berlinguet, L. Synthesis of dipeptides containting 1-aminocycloalkylcarboxylic acids: Part II. *Can. J. Chem.* **1962**, *40*, 2214-2217.

(206) Bardi, R.; Piazzesi, A.; Toniolo, C.; Sukumar, M.; Raj, P. A.; Balaram, P. Conformations of peptides containing 1-aminocyclohexanecarboxylic acid (Acc6). Crystal structures of two model peptides. *Int. J. Pept. Protein Res.* **1985**, *25*, 628-639.

(207) Paul, P.; Sukumar, M.; Bardi, R.; Piazzesi, A.; Valle, G.; Toniolo, C.; Balaram, P. Stereochemically constrained peptides. Theoretical and experimental studies on the conformations of peptides containing 1-aminocyclohexanecarboxylic acid. *J. Am. Chem. Soc.* **1986**, *108*, 6363-6370.

(208) Harini, V. V.; Aravinda, S.; Rai, R.; Shamala, N.; Balaram, P. Molecular Conformation and Packing of Peptide β Hairpins in the Solid State: Structures of Two Synthetic Octapeptides Containing 1-Aminocycloalkane-1-Carboxylic Acid Residues at the i+ 2 Position of the β Turn. *Chem. - Eur. J.* **2005**, *11*, 3609-3620.

(209) Rai, R.; Vasudev, P. G.; Ananda, K.; Raghothama, S.; Shamala, N.; Karle, I. L.; Balaram, P. Hybrid Peptides: Expanding the β Turn in Peptide Hairpins by the Insertion of β-, γ-, and δ-Residues. *Chem. - Eur. J.* **2007**, *13*, 5917-5926.

TH-3141_166122021

(210) Abele, S.; Seiler, P.; Seebach, D. Synthesis, Crystal Structures, and Modelling of β-Oligopeptides Consisting of 1-(Aminomethyl) cyclopropanecarboxylic Acid: Ribbon-Type Arrangement of Eight-Membered H-Bonded Rings. *Helv. Chim. Acta* **1999**, *82*, 1559-1571.

(211) Ananda, K.; Aravinda, S.; Vasudev, P. G.; Raja, K. M. P.; Sivaramakrishnan, H.; Nagarajan, K.; Shamala, N.; Balaram, P. Stereochemistry of gabapentin and several derivatives: solid state conformations and solution equilibria. *Curr. Sci.* **2003**, *85*, 1002-1011.

(212) Vasudev, P. G.; Ananda, K.; Chatterjee, S.; Aravinda, S.; Shamala, N.; Balaram, P. Hybrid peptide design. Hydrogen bonded conformations in peptides containing the stereochemically constrained γ-amino acid residue, gabapentin. *J. Am. Chem. Soc.* **2007**, *129*, 4039-4048.

(213) Vasudev, P. G.; Chatterjee, S.; Ananda, K.; Shamala, N.; Balaram, P. Hybrid αγ Polypeptides: Structural Characterization of a C12/C10 Helix with Alternating Hydrogen-Bond Polarity. *Angew. Chem.* **2008**, *120*, 6530-6532.

(214) Ananda, K.; Vasudev, P. G.; Sengupta, A.; Poopathi Raja, K. M.; Shamala, N.; Balaram, P. Polypeptide helices in hybrid peptide sequences. *J. Am. Chem. Soc.* **2005**, *127*, 16668-16674.

(215) Chatterjee, S.; Vasudev, P. G.; Raghothama, S.; Ramakrishnan, C.; Shamala, N.; Balaram, P. Expanding the peptide β-turn in αγ hybrid sequences: 12 atom hydrogen bonded helical and hairpin turns. *J. Am. Chem. Soc.* **2009**, *131*, 5956-5965.

(216) Aravinda, S.; Ananda, K.; Shamala, N.; Balaram, P. α–γ Hybrid peptides that contain the conformationally constrained gabapentin residue: Characterization of mimetics of chain reversals. *Chem. - Eur. J.* **2003**, *9*, 4789-4795.

TH-3141_166122021

(217) Vasudev, P. G.; Chatterjee, S.; Shamala, N.; Balaram, P. Gabapentin: a stereochemically constrained γ amino acid residue in hybrid peptide design. *Acc. Chem. Res.* **2009**, *42*, 1628-1639.

(218) Vasudev, P. G.; Chatterjee, S.; Ramakrishnan, C.; Shamala, N.; Balaram, P. Conformational choices for the stereochemically constrained γ-amino acid residue gabapentin: Theoretical studies and correlation with experimental results. *Pept. Sci.* **2009**, *92*, 426-435.

(219) Balaram, P. Hybrid polypeptides: Gabapentin as a stereochemically constrained γ-amino acid residue. *Pept. Sci.* **2010**, *94*, 733-741.

(220) Misra, R.; Raja, K. M. P.; Hofmann, H. J.; Gopi, H. N. Modulating the Structural Properties of α, γ-Hybrid Peptides by α-Amino Acid Residues: Uniform 12-Helix Versus "Mixed" 12/10-Helix. *Chem. - Eur. J.* **2017**, *23*, 16644-16652.

(221) Misra, R.; Saseendran, A.; George, G.; Veeresh, K.; Raja, K. M. P.; Raghothama, S.; Hofmann, H. J.; Gopi, H. N. Structural Dimorphism of Achiral α, γ-Hybrid Peptide Foldamers: Coexistence of 12-and 15/17-Helices. *Chem. - Eur. J.* **2017**, *23*, 3764-3772.

(222) Misra, R.; George, G.; Reja, R. M.; Dey, S.; Raghothama, S.; Gopi, H. N. Structural insight into hybrid peptide ε-helices. *Chem. Commun.* **2020**, *56*, 2171-2173.

(223) Sawada, T.; Gellman, S. H. Structural mimicry of the α-helix in aqueous solution with an isoatomic α/β/γ-peptide backbone. *J. Am. Chem. Soc.* **2011**, *133*, 7336-7339.

(224) Baldauf, C.; Günther, R.; Hofmann, H.-J. Helix formation in α, γ-and β, γ-hybrid peptides: theoretical insights into mimicry of α-and β-peptides. *J. Org. Chem.* **2006**, *71*, 1200-1208.

(225) Huggins, M. L. The Structure of Fibrous Proteins. *Chem. Rev.* **1943**, *32*, 195-218.

(226) Bragg, W. L.; Kendrew, J. C.; Perutz, M. F. Polypeptide chain configurations in crystalline proteins. *Proc.: Math., Phys. Eng. Sci.* **1950**, *203*, 321-357.

TH-3141_166122021

(227) Donohue, J. Hydrogen bonded helical configurations of the polypeptide chain. *Proc. Natl. Acad. Sci. U. S. A.* **1953**, *39*, 470-478.

(228) Tonlolo, C.; Benedetti, E. The polypeptide 310-helix. *Trends Biochem. Sci.* **1991**, *16*, 350-353.

(229) Pauling, L.; Corey, R. B.; Branson, H. R. The structure of proteins: two hydrogen-bonded helical configurations of the polypeptide chain. *Proc. Natl. Acad. Sci. U. S. A.* **1951**, *37*, 205-211.

(230) Pauling, L.; Corey, R. B. Configurations of polypeptide chains with favored orientations around single bonds: two new pleated sheets. *Proc. Natl. Acad. Sci. U. S. A.* **1951**, *37*, 729-740.

(231) Kloosterziel, H.; Backer, H. J. The effect of the medium upon Hammett's sigma values of p-alkyl gropus and hyperconjugation. *J. Am. Chem. Soc.* **1952**, *74*, 5806-5806.

(232) Fodje, M. N.; Al-Karadaghi, S. Occurrence, conformational features and amino acid propensities for the π-helix. *Protein Eng., Des. Sel.* **2002**, *15*, 353-358.

(233) Weaver, T. M. The π-helix translates structure into function. *Protein Sci.* **2000**, *9*, 201-206.

(234) Chandrasekaran, R.; Jardetzky, T. S.; Jardetzky, O. The delta helix—a possible left-handed stable polypeptide structure in the N-terminal segment of the lac repressor. *FEBS Lett.* **1979**, *101*, 11-14.

(235) Goodman, J. L.; Petersson, E. J.; Daniels, D. S.; Qiu, J. X.; Schepartz, A. Biophysical and structural characterization of a robust octameric β-peptide bundle. *J. Am. Chem. Soc.* **2007**, *129*, 14746-14751.

(236) Pohl, G.; Beke, T.; Csizmadia, I. G.; Perczel, A. Extended apolar β-peptide foldamers: the role of axis chirality on β-peptide sheet stability. *J. Phys. Chem. B* **2010**, *114*, 9338-9348.

TH-3141_166122021

(237) Jiménez, A. I.; Ballano, G.; Cativiela, C. First observation of two consecutive γ turns in a crystalline linear dipeptide. *Angew. Chem. Int. Ed.* **2005**, *117*, 400-403.

(238) Vasudev, P. G.; Shamala, N.; Ananda, K.; Balaram, P. C9 Helices and ribbons in γ-peptides: crystal structures of gabapentin oligomers. *Angew. Chem. Int. Ed.* **2005**, *117*, 5052-5055.

(239) Benedetti, E.; Toniolo, C.; Hardy, P.; Barone, V.; Bavoso, A.; Di Blasio, B.; Grimaldi, P.; Lelj, F.; Pavone, V. Folded and extended structures of homooligopeptides from. alpha.,. alpha.-dialkylated glycines. A conformational energy computation and x-ray diffraction study. *J. Am. Chem. Soc.* **1984**, *106*, 8146-8152.

(240) Mossel, E.; Formaggio, F.; Valle, G.; Crisma, M.; Toniolo, C.; Ishida, T.; Broxterman, Q. B.; Kamphuis, J. Cα-Methyl, Cα-phenylglycine peptides: A structural study. *Lett. Pept. Sci.* **1998**, *5*, 223-225.

(241) Saavedra, C.; Hernández, R.; Boto, A.; Alvarez, E. Catalytic, One-pot synthesis of β-amino acids from α-amino acids. Preparation of α, β-peptide derivatives. *J. Org. Chem.* **2009**, *74*, 4655-4665.

(242) Vasudev, P. G.; Rai, R.; Shamala, N.; Balaram, P. Conformations of β-amino acid residues in peptides: X-ray diffraction studies of peptides containing the achiral residue 1-aminocyclohexaneacetic acid, β3, 3Ac6c. *Pept. Sci.* **2008**, *90*, 138-150.

(243) Chatterjee, S.; Vasudev, P. G.; Ananda, K.; Raghothama, S.; Shamala, N.; Balaram, P. Multiple Conformational States in Crystals and in Solution in αγ Hybrid Peptides. Fragility of the C12 Helix in Short Sequences. *J. Org. Chem.* **2008**, *73*, 6595-6606.

(244) Crisma, M.; Bisson, W.; Formaggio, F.; Broxterman, Q. B.; Toniolo, C. Factors governing 310-helix vs α-helix formation in peptides: Percentage of Cα-tetrasubstituted α-amino acid residues and sequence dependence. *Biopolymers* **2002**, *64*, 236-245.

TH-3141_166122021

(245) Schmitt, M. A.; Choi, S. H.; Guzei, I. A.; Gellman, S. H. Residue requirements for helical folding in short α/β-peptides: crystallographic characterization of the 11-helix in an optimized sequence. *J. Am. Chem. Soc.* **2005**, *127*, 13130-13131.

(246) Schmitt, M. A.; Choi, S. H.; Guzei, I. A.; Gellman, S. H. New helical foldamers: heterogeneous backbones with 1: 2 and 2: 1 α: β-amino acid residue patterns. *J. Am. Chem. Soc.* **2006**, *128*, 4538-4539.

(247) Choi, S. H.; Guzei, I. A.; Spencer, L. C.; Gellman, S. H. Crystallographic characterization of helical secondary structures in 2: 1 and 1: 2 α/β-peptides. *J. Am. Chem. Soc.* **2009**, *131*, 2917-2924.

(248) Horne, W. S.; Price, J. L.; Keck, J. L.; Gellman, S. H. Helix bundle quaternary structure from α/β-peptide foldamers. *J. Am. Chem. Soc.* **2007**, *129*, 4178-4180.

(249) Chatterjee, S.; Vasudev, P. G.; Raghothama, S.; Shamala, N.; Balaram, P. Solid state and solution conformations of a hybrid αγααγα hexapeptide. Characterization of a backbone expanded analog of the α-polypeptide 310-helix. *Pept. Sci.* **2008**, *90*, 759-771.

(250) Seebach, D.; Ciceri, P. E.; Overhand, M.; Jaun, B.; Rigo, D.; Oberer, L.; Hommel, U.; Amstutz, R.; Widmer, H. Probing the helical secondary structure of short-chain β-peptides. *Helv. Chim. Acta* **1996**, *79*, 2043-2066.

(251) Seebach, D.; Brenner, M.; Rueping, M.; Schweizer, B.; Jaun, B. Preparation and determination of X-ray-crystal and NMR-solution structures of γ2, 3, 4-peptides. *Chem. Commun.* **2001**, 207-208.

(252) Seebach, D.; Brenner, M.; Rueping, M.; Jaun, B. γ2-, γ3-, and γ2, 3, 4-Amino acids, coupling to γ-hexapeptides: CD spectra, NMR solution and X-ray crystal structures of γ-peptides. *Chem. - Eur. J.* **2002**, *8*, 573-584.

TH-3141_166122021

(253) Roy, R. S.; Karle, I. L.; Raghothama, S.; Balaram, P. α, β hybrid peptides: A polypeptide helix with a central segment containing two consecutive β-amino acid residues. *Proc. Natl. Acad. Sci. U. S. A.* **2004**, *101*, 16478-16482.

(254) Gellman, S. H. Foldamers: a manifesto. *Acc. Chem. Res.* **1998**, *31*, 173-180.

(255) Cheng, R. P.; Gellman, S. H.; DeGrado, W. F. β-Peptides: from structure to function. *Chem. Rev.* **2001**, *101*, 3219-3232.

(256) Venkatraman, J.; Shankaramma, S. C.; Balaram, P. Design of folded peptides. *Chem. Rev.* **2001**, *101*, 3131-3152.

(257) Martinek, T. A.; Fülöp, F. Peptidic foldamers: ramping up diversity. *Chem. Soc. Rev.* **2012**, *41*, 687-702.

(258) Horne, W. S.; Gellman, S. H. Foldamers with heterogeneous backbones. *Acc. Chem. Res.* **2008**, *41*, 1399-1408.

(259) Seebach, D.; Hook, D. F.; Glättli, A. Helices and other secondary structures of β-and γ-peptides. *Pept. Sci.* **2006**, *84*, 23-37.

(260) Ganesh Kumar, M.; Gopi, H. N. γ-and β-Peptide Foldamers from Common Multifaceted Building Blocks: Synthesis and Structural Characterization. *Org. Lett.* **2015**, *17*, 4738-4741.

(261) Kendrew, J. C.; Dickerson, R. E.; Strandberg, B. E.; Hart, R. G.; Davies, D. R.; Phillips, D. C.; Shore, V. C. Structure of Myoglobin: A Three-Dimensional Fourier Synthesis at 2 Å. Resolution. *Nature* **1960**, *185*, 422-427.

(262) Sharma, G. V.; Sai Reddy, P.; Chatterjee, D.; Kunwar, A. C. Synthesis and structural studies of homooligomers of geminally disubstituted $\beta^{2,2}$-amino acids with carbohydrate side chain. *J. Org. Chem.* **2011**, *76*, 1562-1571.

(263) Kothari, A.; Qureshi, M. K. N.; Beck, E. M.; Smith, M. D. Bend-ribbon forming γ-peptides. *Chem. Commun.* **2007**, 2814-2816.

TH-3141_166122021

(264) Hintermann, T.; Gademann, K.; Jaun, B.; Seebach, D. γ-Peptides Forming More Stable Secondary Structures than α-Peptides: Synthesis and helical NMR-solution structure of the γ-hexapeptide analog of H-(Val-Ala-Leu) 2-OH. *Helv. Chim. Acta* **1998**, *81*, 983-1002.

(265) Prabhakaran, P.; Kale, S. S.; Puranik, V. G.; Rajamohanan, P.; Chetina, O.; Howard, J. A.; Hofmann, H.-J. r.; Sanjayan, G. J. Sequence-specific unusual (1→ 2)-type helical turns in α/β-hybrid peptides. *J. Am. Chem. Soc.* **2008**, *130*, 17743-17754.

(266) Sonti, R.; Dinesh, B.; Basuroy, K.; Raghothama, S.; Shamala, N.; Balaram, P. C12 helices in long hybrid (αγ) n peptides composed entirely of unconstrained residues with proteinogenic side chains. *Org. Lett.* **2014**, *16*, 1656-1659.

(267) Fisher, B. F.; Gellman, S. H. Impact of γ-amino acid residue preorganization on α/γ-peptide foldamer helicity in aqueous solution. *J. Am. Chem. Soc.* **2016**, *138*, 10766-10769.

(268) Grison, C. M.; Robin, S.; Aitken, D. J. 13-Helix folding of a β/γ-peptide manifold designed from a "minimal-constraint" blueprint. *Chem. Commun.* **2016**, *52*, 7802-7805.

(269) Basuroy, K.; Dinesh, B.; Reddy, M. M.; Chandrappa, S.; Raghothama, S.; Shamala, N.; Balaram, P. Unconstrained homooligomeric γ-peptides show high propensity for C14 helix formation. *Org. Lett.* **2013**, *15*, 4866-4869.

(270) Toniolo, C.; Crisma, M.; Formaggio, F.; Alemán, C.; Ramakrishnan, C.; Kalmankar, N.; Balaram, P. Intramolecular backbone⋯ backbone hydrogen bonds in polypeptide conformations. The other way around: ε-turn. *Pept. Sci.* **2017**, *108*, 22911-22925.

(271) Srinivasulu, G.; Kumar, S. K.; Sharma, G. V.; Kunwar, A. C. 11/9-Mixed helices in the α/β-peptides derived from alternating α-and β-amino acids with proteinogenic side chains. *J. Org. Chem.* **2006**, *71*, 8395-8400.

(272) Fanelli, R.; Berta, D.; Foldes, T.; Rosta, E.; Atkinson, R. A.; Hofmann, H.-J. r.; Shankland, K.; Cobb, A. J. Organocatalytic Access to a cis-Cyclopentyl-γ-amino Acid: An

TH-3141_166122021

Intriguing Model of Selectivity and Formation of a Stable 10/12-Helix from the Corresponding γ/α-Peptide. *J. Am. Chem. Soc.* **2019**, *142*, 1382-1393.

(273) Seebach, D.; Gademann, K.; Schreiber, J. V.; Matthews, J. L.; Hintermann, T.; Jaun, B.; Oberer, L.; Hommel, U.; Widmer, H. 'Mixed'β-peptides: A unique helical secondary structure in solution. Preliminary communication. *Helv. Chim. Acta* **1997**, *80*, 2033-2038.

(274) Choi, S. H.; Guzei, I. A.; Spencer, L. C.; Gellman, S. H. Crystallographic characterization of helical secondary structures in α/β-peptides with 1: 1 residue alternation. *J. Am. Chem. Soc.* **2008**, *130*, 6544-6550.

(275) Choi, S. H.; Guzei, I. A.; Gellman, S. H. Crystallographic characterization of the α/β-peptide 14/15-helix. *J. Am. Chem. Soc.* **2007**, *129*, 13780-13781.

(276) Hayen, A.; Schmitt, M. A.; Ngassa, F. N.; Thomasson, K. A.; Gellman, S. H. Two helical conformations from a single foldamer backbone:"split personality" in short α/β-peptides. *Angew. Chem. Int. Ed.* **2004**, *43*, 505-510.

(277) Hintermann, T.; Seebach, D. Synthesis of a β-Hexapeptide from (R)-2-Aminomethyl-alkanoic Acids and Structural Investigations. *Synlett* **1997**, *1997*, 437-438.

(278) Seebach, D.; Abele, S.; Gademann, K.; Jaun, B. Pleated sheets and turns of β-peptides with proteinogenic side chains. *Angew. Chem. Int. Ed.* **1999**, *38*, 1595-1597.

(279) Qureshi, M. K. N.; Smith, M. D. Parallel sheet structure in cyclopropane γ-peptides stabilized by C–H⋯ O hydrogen bonds. *Chem. Commun.* **2006**, 5006-5008.

(280) Karle, I.; Gopi, H. N.; Balaram, P. Infinite pleated β-sheet formed by the β-hairpin Boc-β-Phe-β-Phe-d-Pro-Gly-β-Phe-β-Phe-OMe. *Proc. Natl. Acad. Sci. U. S. A.* **2002**, *99*, 5160-5164.

(281) Krauthäuser, S.; Christianson, L. A.; Powell, D. R.; Gellman, S. H. Antiparallel sheet formation in β-peptide foldamers: Effects of β-amino acid substitution on conformational preference1. *J. Am. Chem. Soc.* **1997**, *119*, 11719-11720.

TH-3141_166122021

(282) Roy, R. S.; Gopi, H. N.; Raghothama, S.; Karle, I. L.; Balaram, P. Hybrid Peptide Hairpins Containing α-and ω-Amino Acids: Conformational Analysis of Decapeptides with Unsubstituted β-, γ-, and δ-Residues at Positions 3 and 8. *Chem. - Eur. J.* **2006**, *12*, 3295-3302.

(283) Gademann, K.; Kimmerlin, T.; Hoyer, D.; Seebach, D. Peptide folding induces high and selective affinity of a linear and small β-peptide to the human somatostatin receptor 4. *J. Med. Chem.* **2001**, *44*, 2460-2468.

(284) Karle, I. L.; Balaram, P. Structural characteristics of. alpha.-helical peptide molecules containing Aib residues. *Biochemistry* **1990**, *29*, 6747-6756.

(285) Toniolo, C.; Benedetti, E. Structures of polypeptides from α-amino acids disubstituted at the α-carbon. *Macromolecules* **1991**, *24*, 4004-4009.

(286) Reddy, P. A.; Hsiang, B. C.; Latifi, T. N.; Hill, M. W.; Woodward, K. E.; Rothman, S. M.; Ferrendelli, J. A.; Covey, D. F. 3, 3-Dialkyl-and 3-alkyl-3-benzyl-substituted 2-pyrrolidinones: a new class of anticonvulsant agents. *J. Med. Chem.* **1996**, *39*, 1898-1906.

(287) Tietze, L. F.; Gericke, K. M.; Singidi, R. R.; Schuberth, I. Novel strategies for the synthesis of anthrapyran antibiotics: discovery of a new antitumor agent and total synthesis of (S)-espicufolin. *Org. Biomol. Chem.* **2007**, *5*, 1191-1200.

(288) Bunce, R. A.; Drumright, R. E. Michael Reaction of Nitromethane with β, β-Disubstituted Acrylate Esters. *Org. Prep. Proced. Int.* **1987**, *19*, 471-475.

(289) Ghosh, K.; Majumdar, A. Enantioselective sensing of lactate by pyridinium-based chiral receptor. *Tetrahedron Lett.* **2013**, *54*, 5686-5689.

(290) Das, D.; Sun, A. X.; Seidel, D. Redox-Neutral Copper (II) Carboxylate Catalyzed α-Alkynylation of Amines. *Angew. Chem.* **2013**, *125*, 3853-3857.

(291) Richardson, J. S. The anatomy and taxonomy of protein structure. *Advances in protein chemistry* **1981**, *34*, 167-339.

TH-3141_166122021

(292) RYU, Y.; SCHULTZ, P.: NAT METHODS, vol. 3, no. 4. April, 2006.

(293) Sheldrick, G. M. A short history of SHELX. *Acta Crystallogr., Sect. A: Found. Crystallogr.* **2008**, *64*, 112-122.

(294) Sheldrick, G. M. Crystal structure refinement with SHELXL. *Acta Crystallogr., Sect. C: Struct. Chem.* **2015**, *71*, 3-8.

(295) Schneider, T. R.; Sheldrick, G. M. Substructure solution with SHELXD. *Acta Crystallogr., Sect. D: Biol. Crystallogr.* **2002**, *58*, 1772-1779.

(296) Hanwell, M. D.; Curtis, D. E.; Lonie, D. C.; Vandermeersch, T.; Zurek, E.; Hutchison, G. R. Avogadro: an advanced semantic chemical editor, visualization, and analysis platform. *J. Cheminf.* **2012**, *4*, 1-17.

(297) Janson, G.; Zhang, C.; Prado, M. G.; Paiardini, A. PyMod 2.0: improvements in protein sequence-structure analysis and homology modeling within PyMOL. *Bioinformatics* **2017**, *33*, 444-446.

(298) Frisch, M. J.; Trucks, G. W.; Schlegel, H. B.; Scuseria, G. E.; Robb, M. A.; Cheeseman, J. R.; Scalmani, G.; Barone, V.; Petersson, G. A.; Nakatsuji, H.; Li, X.; Caricato, M.; Marenich, A. V.; Bloino, J.; Janesko, B. G.; Gomperts, R.; Mennucci, B.; Hratchian, H. P.; Ortiz, J. V.; Izmaylov, A. F.; Sonnenberg, J. L.; Williams; Ding, F.; Lipparini, F.; Egidi, F.; Goings, J.; Peng, B.; Petrone, A.; Henderson, T.; Ranasinghe, D.; Zakrzewski, V. G.; Gao, J.; Rega, N.; Zheng, G.; Liang, W.; Hada, M.; Ehara, M.; Toyota, K.; Fukuda, R.; Hasegawa, J.; Ishida, M.; Nakajima, T.; Honda, Y.; Kitao, O.; Nakai, H.; Vreven, T.; Throssell, K.; Montgomery Jr., J. A.; Peralta, J. E.; Ogliaro, F.; Bearpark, M. J.; Heyd, J. J.; Brothers, E. N.; Kudin, K. N.; Staroverov, V. N.; Keith, T. A.; Kobayashi, R.; Normand, J.; Raghavachari, K.; Rendell, A. P.; Burant, J. C.; Iyengar, S. S.; Tomasi, J.; Cossi, M.; Millam, J. M.; Klene, M.; Adamo, C.; Cammi, R.; Ochterski, J. W.; Martin, R. L.; Morokuma, K.; Farkas, O.; Foresman, J. B.; Fox, D. J.: Gaussian 16 Rev. C.01. Wallingford, CT, 2016.

TH-3141_166122021

(299) Becke, A. D. Density-functional exchange-energy approximation with correct asymptotic behavior. *Phys. Rev. A* **1988**, *38*, 3098-3100.

(300) Lee, C.; Yang, W.; Parr, R. G. Development of the Colle-Salvetti correlation-energy formula into a functional of the electron density. *Phys. Rev. B* **1988**, *37*, 785-789.

(301) Petersson, G.; Tensfeldt, T. G.; Montgomery Jr, J. A complete basis set model chemistry. III. The complete basis set-quadratic configuration interaction family of methods. *J. Chem. Phys.* **1991**, *94*, 6091-6101.

(302) Petersson, a.; Bennett, A.; Tensfeldt, T. G.; Al-Laham, M. A.; Shirley, W. A.; Mantzaris, J. A complete basis set model chemistry. I. The total energies of closed-shell atoms and hydrides of the first-row elements. *J. Chem. Phys.* **1988**, *89*, 2193-2218.

(303) Jensen, F. Atomic orbital basis sets. *Wiley Interdiscip. Rev.: Comput. Mol. Sci.* **2013**, *3*, 273-295.

(304) Scalmani, G.; Frisch, M. J. Continuous surface charge polarizable continuum models of solvation. I. General formalism. *J. Chem. Phys.* **2010**, *132*, 114110-114125.

(305) Barone, V.; Cossi, M. Quantum calculation of molecular energies and energy gradients in solution by a conductor solvent model. *J. Phys. Chem. A* **1998**, *102*, 1995-2001.

(306) Cossi, M.; Scalmani, G.; Rega, N.; Barone, V. New developments in the polarizable continuum model for quantum mechanical and classical calculations on molecules in solution. *J. Chem. Phys.* **2002**, *117*, 43-54.

(307) Merutka, G.; Morikis, D.; Bruschweiler, R.; Wright, P. E. NMR evidence for multiple conformations in a highly helical model peptide. *Biochemistry* **1993**, *32*, 13089-13097.

(308) Fox, R. O.; Evans, P. A.; Dobson, C. M. Multiple conformations of a protein demonstrated by magnetization transfer NMR spectroscopy. *Nature* **1986**, *320*, 192-194.

TH-3141_166122021

(309) Iadevaia, G.; Swain, J. A.; Núñez-Villanueva, D.; Bond, A. D.; Hunter, C. A. Folding and duplex formation in mixed sequence recognition-encoded m-phenylene ethynylene polymers. *Chem. Sci.* **2021**, *12*, 10218-10226.

(310) Alferov, K.; Wang, S.; Han, D.; Guan, S.; Xiao, M.; Meng, Y. 2D NMR study on chemical structure of the co-oligomers from carbon dioxide/propylene oxide/diol synthesized by a metal-free catalyst. *Polym. Test.* **2022**, *107*, 107485-107494.

(311) Gasparro, F. P.; Kolodny, N. H. NMR determination of the rotational barrier in N, N-dimethylacetamide. A physical chemistry experiment. *J. Chem. Educ.* **1977**, *54*, 258-261.

(312) Wang, L.; Coric, P.; Zhu, K.; Liu, W.-Q.; Vidal, M.; Bouaziz, S.; Broussy, S. Synthesis and characterization of water-soluble macrocyclic peptides stabilizing protein α-turn. *Org. Biomol. Chem.* **2018**, *16*, 459-471.

(313) Rajbhandary, A.; Brennessel, W. W.; Nilsson, B. L. Comparison of the self-assembly behavior of fmoc-phenylalanine and corresponding peptoid derivatives. *Cryst. Growth Des.* **2018**, *18*, 623-632.

(314) Tian, Y.; Li, J.; Zhang, X.; Wang, A.; Jian, H.; Li, Q.; Bai, S. Bioinspired self-assembled nanoparticles with stable fluorescent properties in wide visible light region. *Colloids Surf., A* **2021**, *625*, 126962-126968.

(315) Tao, K.; Yoskovitz, E.; Adler-Abramovich, L.; Gazit, E. Optical property modulation of Fmoc group by pH-dependent self-assembly. *RSC Adv.* **2015**, *5*, 73914-73918.

(316) Liu, Y.; Kim, E.; Ulijn, R. V.; Bentley, W. E.; Payne, G. F. Reversible Electroaddressing of Self-assembling Amino-Acid Conjugates. *Adv. Funct. Mater.* **2011**, *21*, 1575-1580.

(317) Quigley, E.; Johnson, J.; Liyanage, W.; Nilsson, B. L. Impact of gelation method on thixotropic properties of phenylalanine-derived supramolecular hydrogels. *Soft Matter* **2020**, *16*, 10158-10168.

(318) Xing, P.; Chu, X.; Li, S.; Ma, M.; Hao, A. Hybrid gels assembled from fmoc–amino acid and graphene oxide with controllable properties. *ChemPhysChem* **2014**, *15*, 2377-2385.

TH-3141_166122021

(319) Pizzi, A.; Lascialfari, L.; Demitri, N.; Bertolani, A.; Maiolo, D.; Carretti, E.; Metrangolo, P. Halogen bonding modulates hydrogel formation from Fmoc amino acids. *CrystEngComm* **2017**, *19*, 1870-1874.

(320) Draper, E. R.; Morris, K. L.; Little, M. A.; Raeburn, J.; Colquhoun, C.; Cross, E. R.; McDonald, T. O.; Serpell, L. C.; Adams, D. J. Hydrogels formed from Fmoc amino acids. *CrystEngComm* **2015**, *17*, 8047-8057.

(321) Pandit, G.; Roy, K.; Agarwal, U.; Chatterjee, S. Self-assembly mechanism of a peptide-based drug delivery vehicle. *ACS Omega* **2018**, *3*, 3143-3155.

(322) Roy, K.; Ghosh, S.; Chetia, M.; Satpati, P.; Chatterjee, S. Dicyclohexylurea derivatives of amino acids as dye absorbent organogels and anion sensors. *Org. Biomol. Chem.* **2019**, *17*, 3026-3039.

(323) Xu, D.; Ran, Q.; Xiang, Y.; Jiang, L.; Smith, B. M.; Bou-Abdallah, F.; Lund, R.; Li, Z.; Dong, H. Toward hemocompatible self-assembling antimicrobial nanofibers: understanding the synergistic effect of supramolecular structure and PEGylation on hemocompatibility. *RSC Adv.* **2016**, *6*, 15911-15919.

(324) Xu, D.; Samways, D. S.; Dong, H. Fabrication of self-assembling nanofibers with optimal cell uptake and therapeutic delivery efficacy. *Bioact. Mater.* **2017**, *2*, 260-268.

(325) Toniolo, C.; Formaggio, F.; Woody, R. W.: Electronic circular dichroism of peptides. Wiley, 2012; Vol. 2; pp 499-544.

(326) Krimm, S.; Bandekar, J. Vibrational spectroscopy and conformation of peptides, polypeptides, and proteins. *Adv. Protein Chem.* **1986**, *38*, 181-364.

(327) Jackson, M.; Mantsch, H. H. The use and misuse of FT-IR spectroscopy in the determination of protein structure. *Crit. Rev. Biochem. Mol. Biol.* **1995**, *30*, 95-120.

(328) Ulrich, E. L.; Akutsu, H.; Doreleijers, J. F.; Harano, Y.; Ioannidis, Y. E.; Lin, J.; Livny, M.; Mading, S.; Maziuk, D.; Miller, Z. BioMagResBank. *Nucleic Acids Res.* **2007**, *36*, 402-408.

(329) Wishart, D. S.; Sykes, B. D.; Richards, F. M. The chemical shift index: a fast and simple method for the assignment of protein secondary structure through NMR spectroscopy. *Biochemistry* **1992**, *31*, 1647-1651.

(330) Balaram, P. In *Tilte*1985; Springer.

TH-3141_166122021

(331) Iqbal, M.; Balaram, P. Aggregation of apolar peptides in organic solvents. Concentration dependence of 1H-nmr parameters for peptide NH groups in 310 helical decapeptide fragment of suzukacillin. *Biopolymers* **1982**, *21*, 1427-1433.

(332) Awasthi, S. K.; Shankaramma, S.; Raghothama, S.; Balaram, P. Solvent-induced β-hairpin to helix conformational transition in a designed peptide. *Biopolymers* **2001**, *58*, 465-476.

(333) Rajagopal, A.; Aravinda, S.; Raghothama, S.; Shamala, N.; Balaram, P. Chain length effects on helix-hairpin distribution in short peptides with Aib-DAla and Aib-Aib Segments. *Peptide Science* **2011**, *96*, 744-756.

(334) Rai, R.; Raghothama, S.; Sridharan, R.; Balaram, P. Tuning the β-turn segment in designed peptide β-hairpins: Construction of a stable type I′ β-turn nucleus and hairpin–helix transition promoting segments. *Pept. Sci.* **2007**, *88*, 350-361.

(335) Sahal, D.; Balaram, P. Peptide models of electrostatic interactions in proteins: NMR studies on two. beta.-turn tetrapeptides containing Asp-His and Asp-Lys salt bridges. *Biochemistry* **1986**, *25*, 6004-6013.

(336) Raghothama, S.; Chaddha, M.; Banumathi, S.; Ravikumar, K.; Velmurugan, D.; Balaram, P. Conformational interconversions in peptide β-turns: Discrimination between enantiomeric conformations by chiral perturbation. *Biopolymers* **1998**, *45*, 191-202.

(337) Yan, X.-S.; Luo, H.; Zou, K.-S.; Cao, J.-L.; Li, Z.; Jiang, Y.-B. Short azapeptides of folded structures in aqueous solutions. *ACS Omega* **2018**, *3*, 4786-4790.

(338) Zhang, Y.; Yan, X.; Cao, J.; Weng, P.; Miao, D.; Li, Z.; Jiang, Y.-B. Turn Conformation of β-Amino Acid-Based Short Peptides Promoted by an Amidothiourea Moiety at C-Terminus. *J. Org. Chem.* **2020**, *85*, 9844-9849.

(339) Raghothama, S.; Awasthi, S. β-Hairpin nucleation by Pro-Gly β-turns. Comparison of D-Pro-Gly and L-Pro-Gly sequences in an apolar octapeptide. *J. Chem. Soc., Perkin Trans. 2* **1998**, 137-144.

(340) Rai, R.; Raghothama, S.; Balaram, P. Design of a peptide hairpin containing a central three-residue loop. *J. Am. Chem. Soc.* **2006**, *128*, 2675-2681.

TH-3141_166122021

(341) Roy, R. S.; Gopi, H. N.; Raghothama, S.; Gilardi, R. D.; Karle, I. L.; Balaram, P. Peptide hairpins with strand segments containing α-and β-amino acid residues: Cross-strand aromatic interactions of facing Phe residues. *Pept. Sci.* **2005**, *80*, 787-799.

(342) Mahalakshmi, R.; Raghothama, S.; Balaram, P. NMR analysis of aromatic interactions in designed peptide β-hairpins. *J. Am. Chem. Soc.* **2006**, *128*, 1125-1138.

(343) Rajagopal, A.; Aravinda, S.; Raghothama, S.; Shamala, N.; Balaram, P. Aromatic interactions in model peptide β-hairpins: Ring current effects on proton chemical shifts. *Pept. Sci.* **2012**, *98*, 185-194.

(344) Du, X.; Zhou, J.; Shi, J.; Xu, B. Supramolecular hydrogelators and hydrogels: from soft matter to molecular biomaterials. *Chem. Rev.* **2015**, *115*, 13165-13307.

(345) Takekiyo, T.; Wu, L.; Yoshimura, Y.; Shimizu, A.; Keiderling, T. A. Relationship between hydrophobic interactions and secondary structure stability for trpzip β-hairpin peptides. *Biochemistry* **2009**, *48*, 1543-1552.

(346) Wu, L.; McElheny, D.; Setnicka, V.; Hilario, J.; Keiderling, T. A. Role of different β-turns in β-hairpin conformation and stability studied by optical spectroscopy. *Proteins: Struct., Funct., Bioinf.* **2012**, *80*, 44-60.

(347) Raghavender, U. S.; Aravinda, S.; Rai, R.; Shamala, N.; Balaram, P. Peptide hairpin nucleation with the obligatory Type I'β-turn Aib-D Pro segment. *Org. Biomol. Chem.* **2010**, *8*, 31.

TH-3141_166122021

APPENDIX

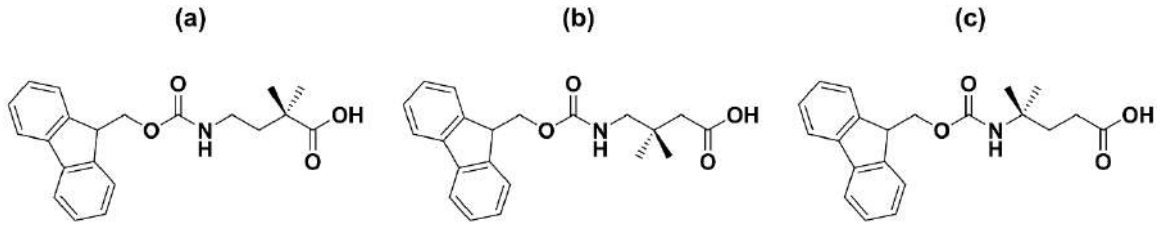

Figure A1. Chemical structures of (a) Fmoc-$\gamma^{2,2}$-OH, (b) Fmoc-$\gamma^{3,3}$-OH, and (c) Fmoc-$\gamma^{4,4}$-OH.

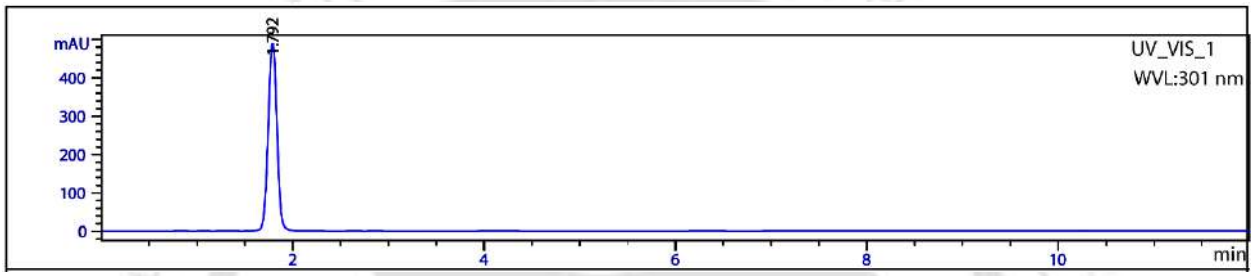

Figure A2. Analytical HPLC trace of (a) Fmoc-$\gamma^{2,2}$-OH, in ACN/ H_2O mixtures.

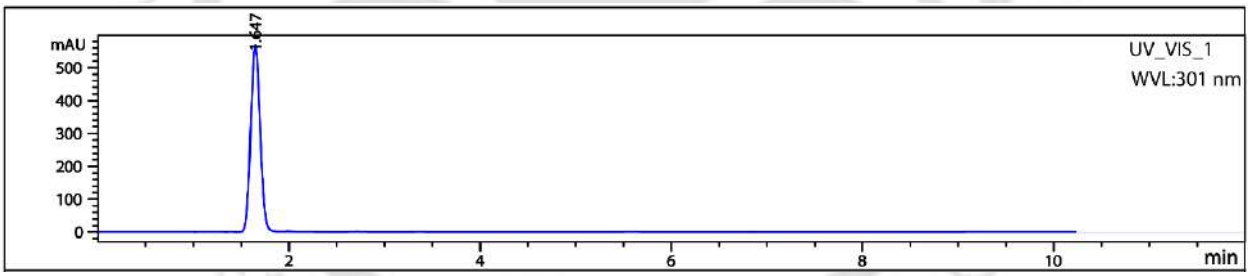

Figure A3. Analytical HPLC trace of (b) Fmoc-$\gamma^{3,3}$-OH and in ACN/ H_2O mixtures.

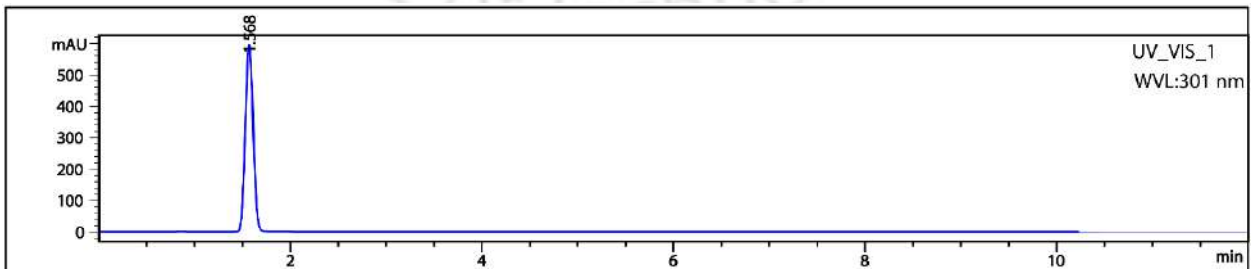

Figure A4. Analytical HPLC trace of (b) Fmoc-$\gamma^{4,4}$-OH and in ACN/ H_2O mixtures.

TH-3141_166122021

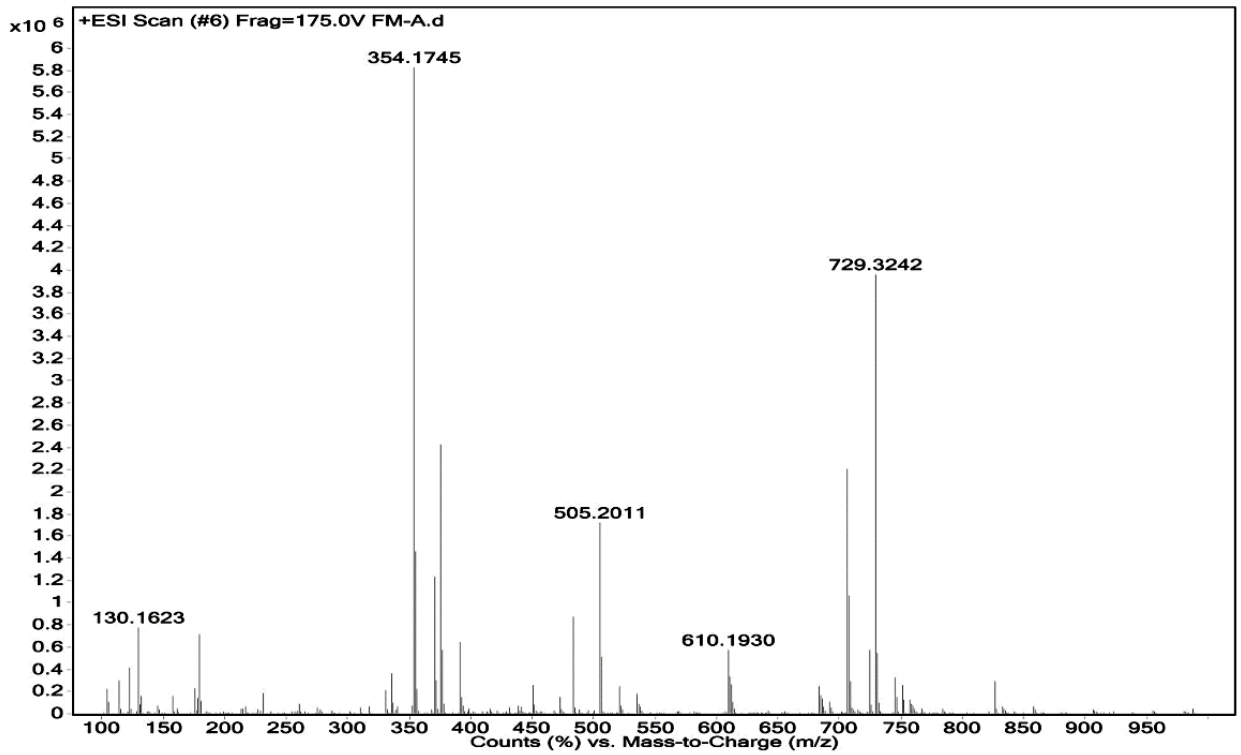

Figure A5. ESI-MS (m/z) of Fmoc-$\gamma^{2,2}$-OH. Calc. $(M+H)^+$ for $C_{21}H_{23}NO_4$ = 354.4155 Da; Obs. $(M+H)^+$ = 354.1745 Da, $(2M+Na)^+$ = 729.3242 Da.

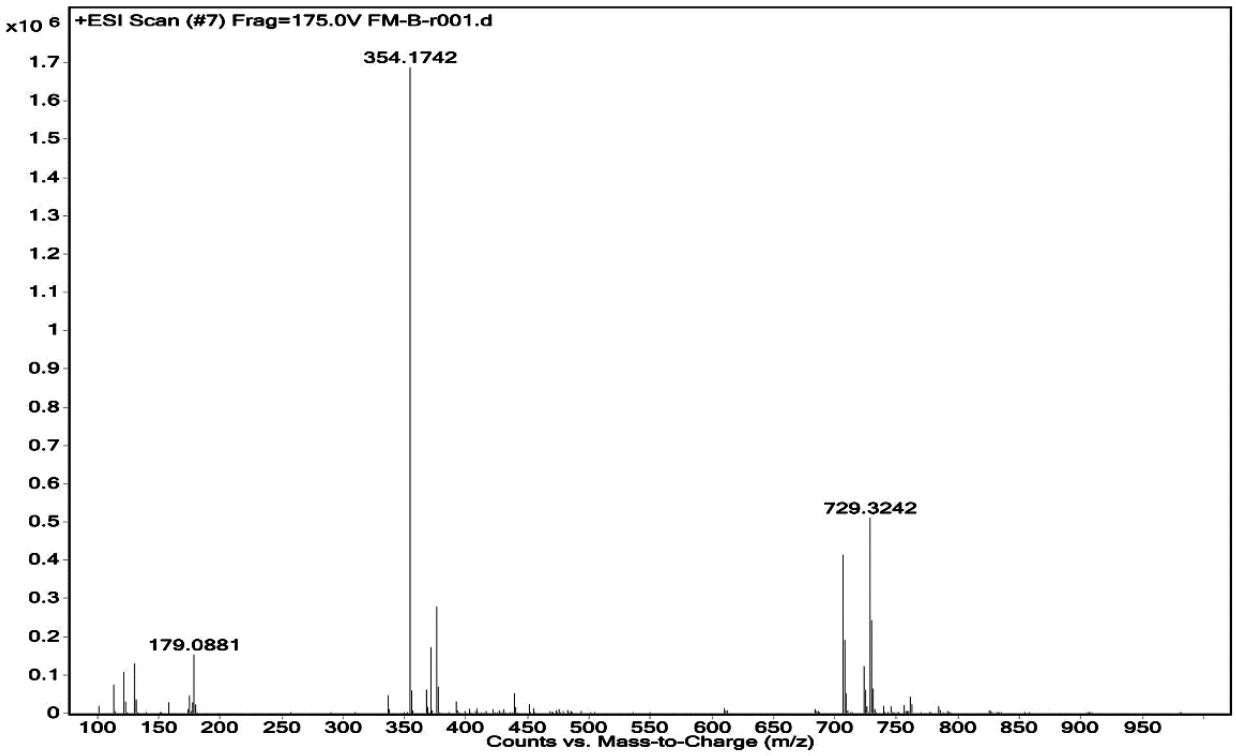

Figure A6. ESI-MS (m/z) of Fmoc-$\gamma^{3,3}$-OH. Calc. $(M+H)^+$ for $C_{21}H_{23}NO_4$ = 354.4155 Da; Obs. $(M+H)^+$ = 354.1742 Da, $(2M+Na)^+$ = 729.3242 Da.

TH-3141_166122021

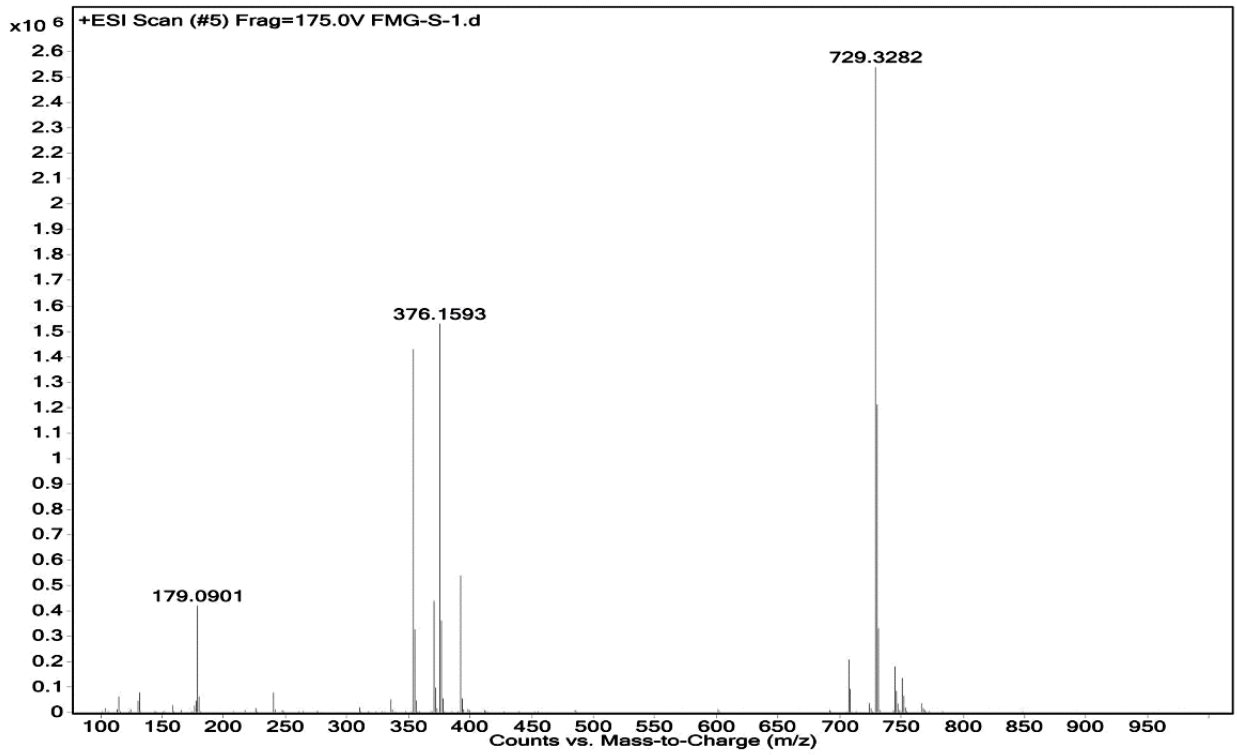

Figure A7. ESI-MS (m/z) of Fmoc-$\gamma^{4,4}$-OH. Calc. $(M+H)^+$ for $C_{21}H_{23}NO_4$ = 354.4155 Da; Obs. $(M+Na)^+$ = 376.1593 Da, $(2M+Na)^+$ = 729.3282 Da.

TH-3141_166122021

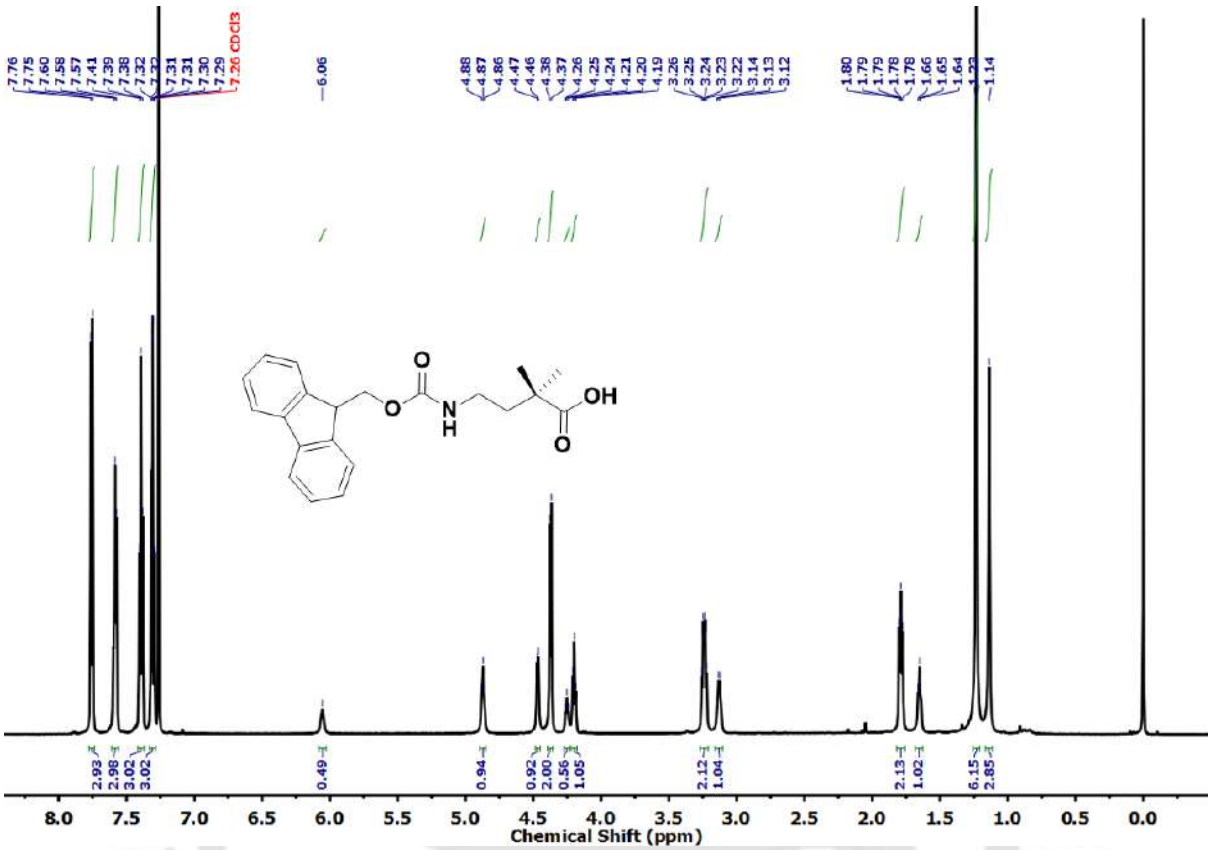

Figure A8. 600 MHz ^{1}H NMR spectrum of Fmoc-$\gamma^{2,2}$-OH in $CDCl_3$ at 10 mM concentration (298 K).

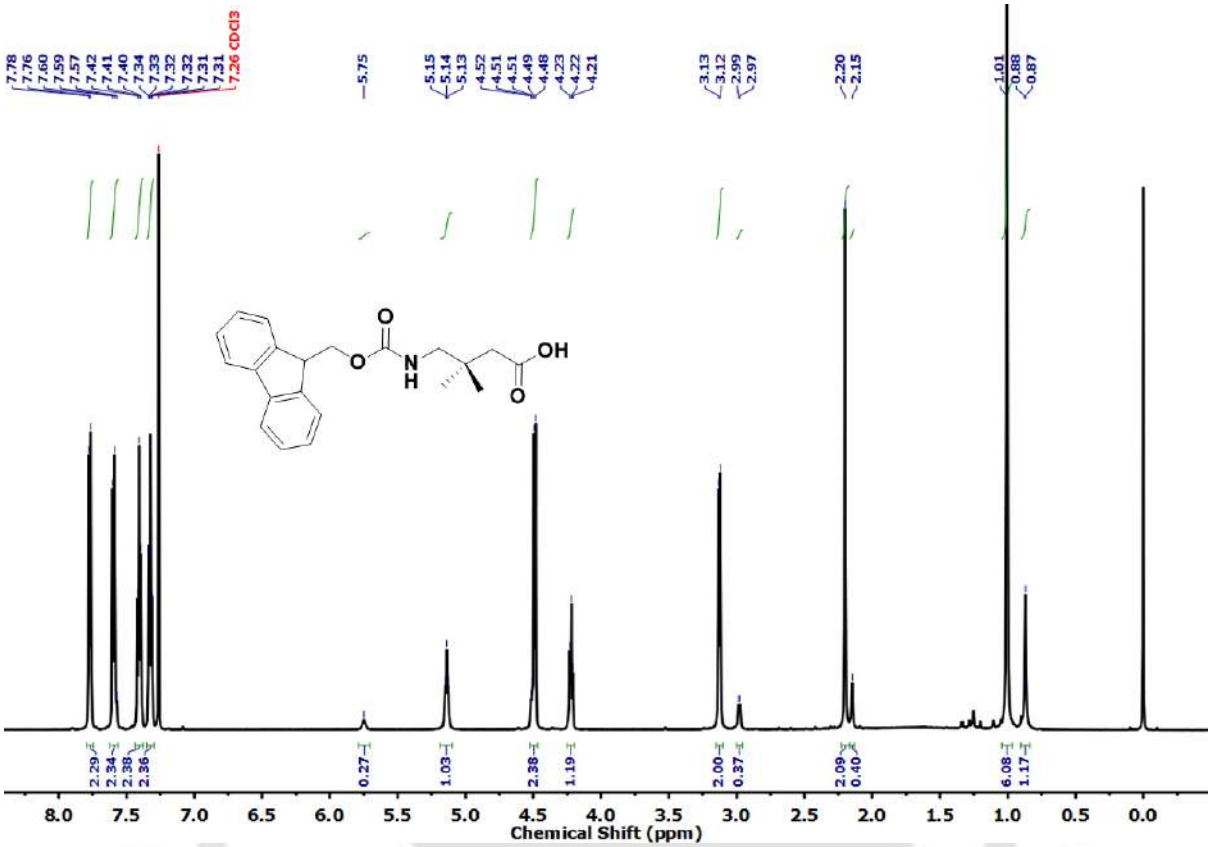

.

Figure A9. 600 MHz ^{1}H NMR spectrum of Fmoc-$\gamma^{3,3}$-OH in $CDCl_3$ at 10 mM concentration (298 K).

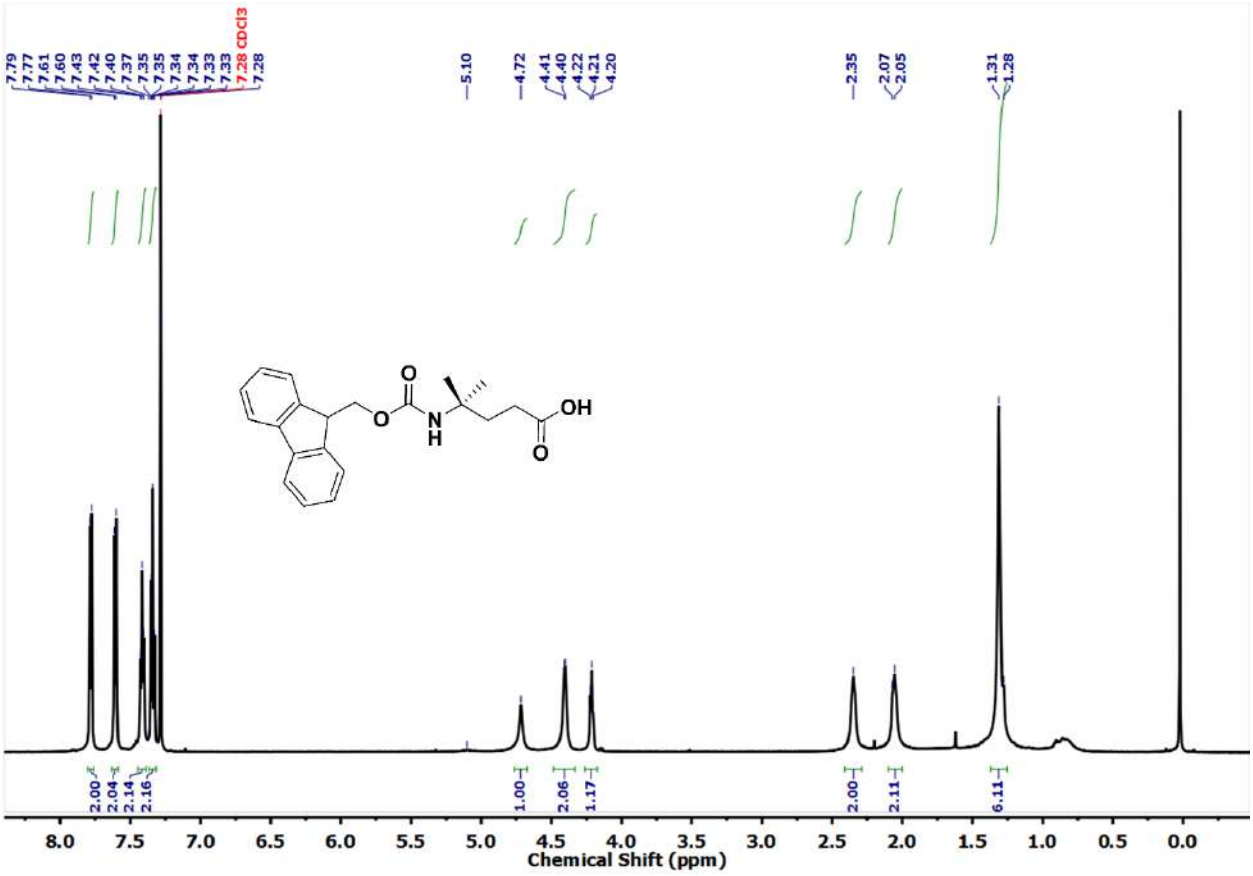

Figure A10. 600 MHz ^{1}H NMR spectrum of Fmoc-$\gamma^{4,4}$-OH in $CDCl_3$ at 10 mM concentration (298 K).

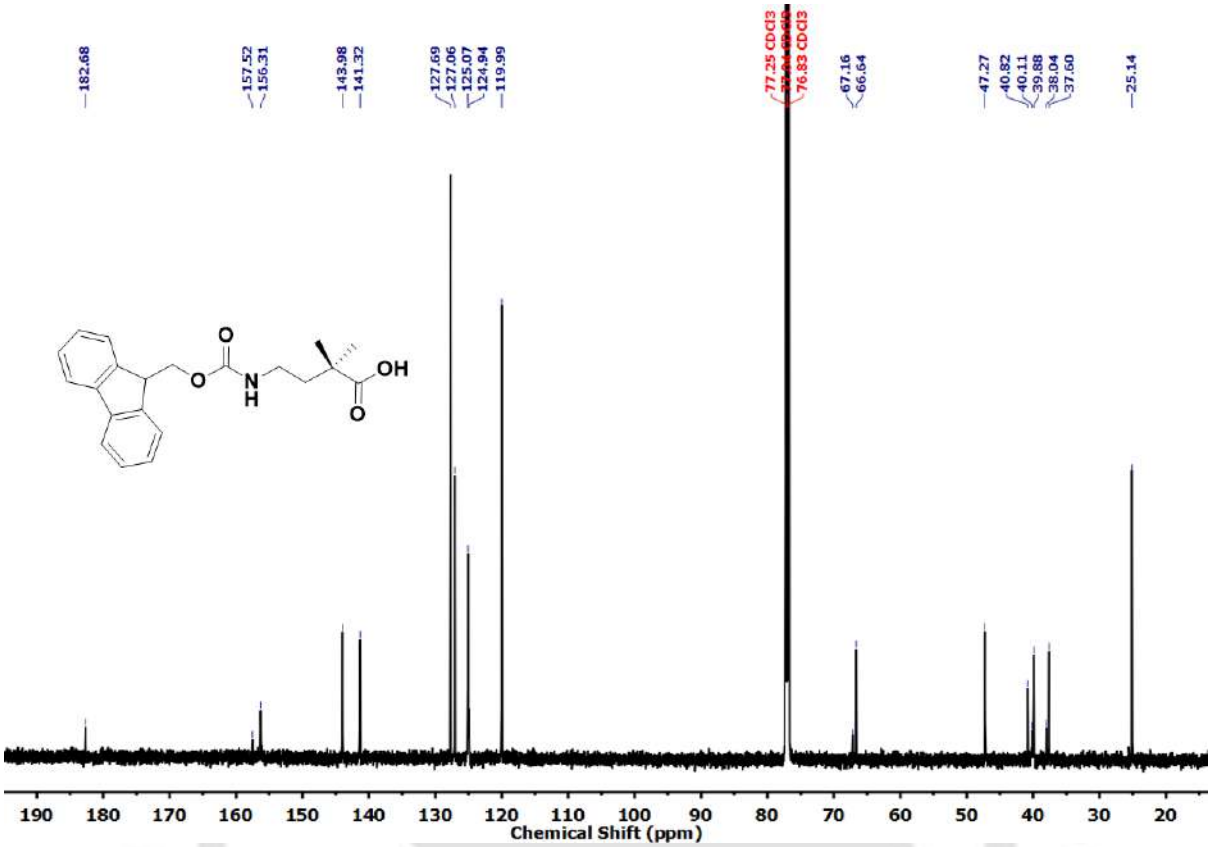

Figure A11. 150 MHz ^{13}C NMR spectrum of Fmoc-$\gamma^{2,2}$-OH in $CDCl_3$ at 10 mM concentration (298 K).

TH-3141_166122021

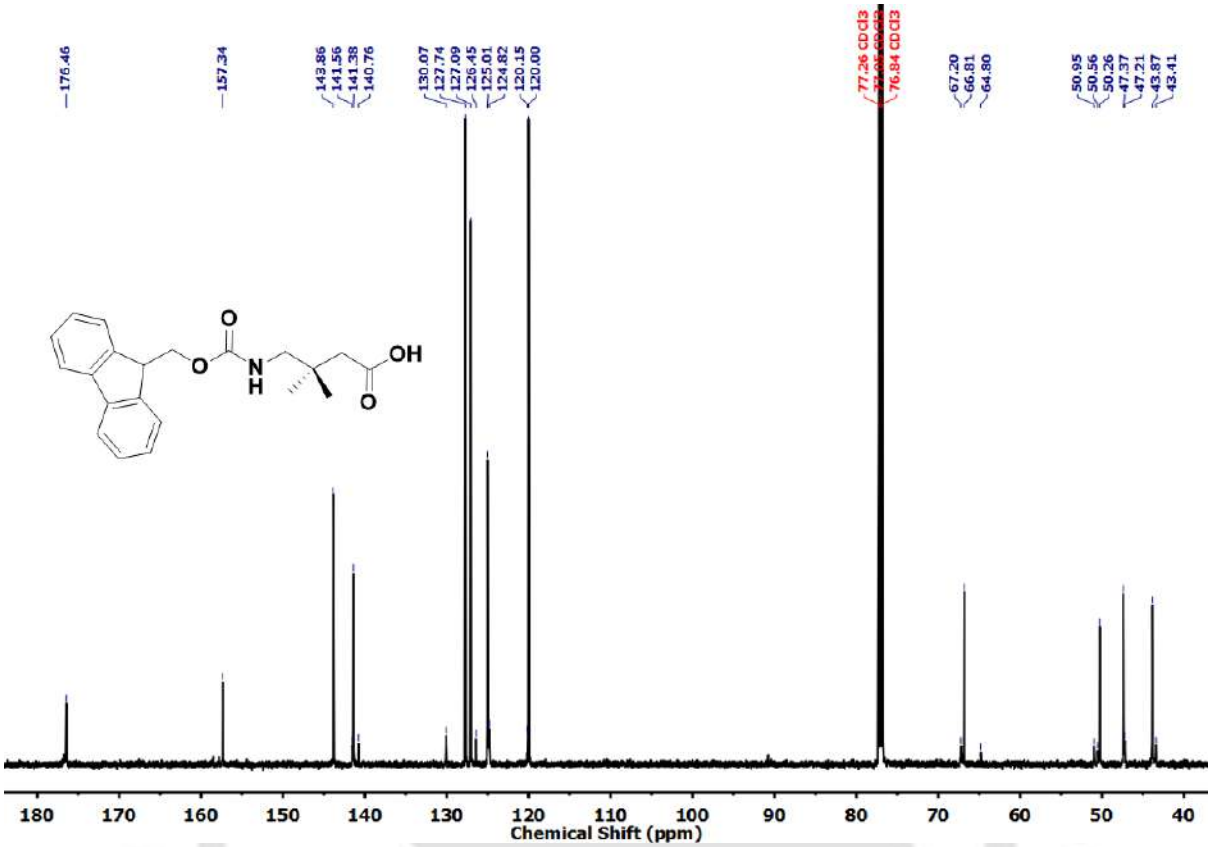

Figure A12. 150 MHz ^{13}C NMR spectrum of Fmoc-$\gamma^{3,3}$-OH in $CDCl_3$ at 10 mM concentration (298 K).

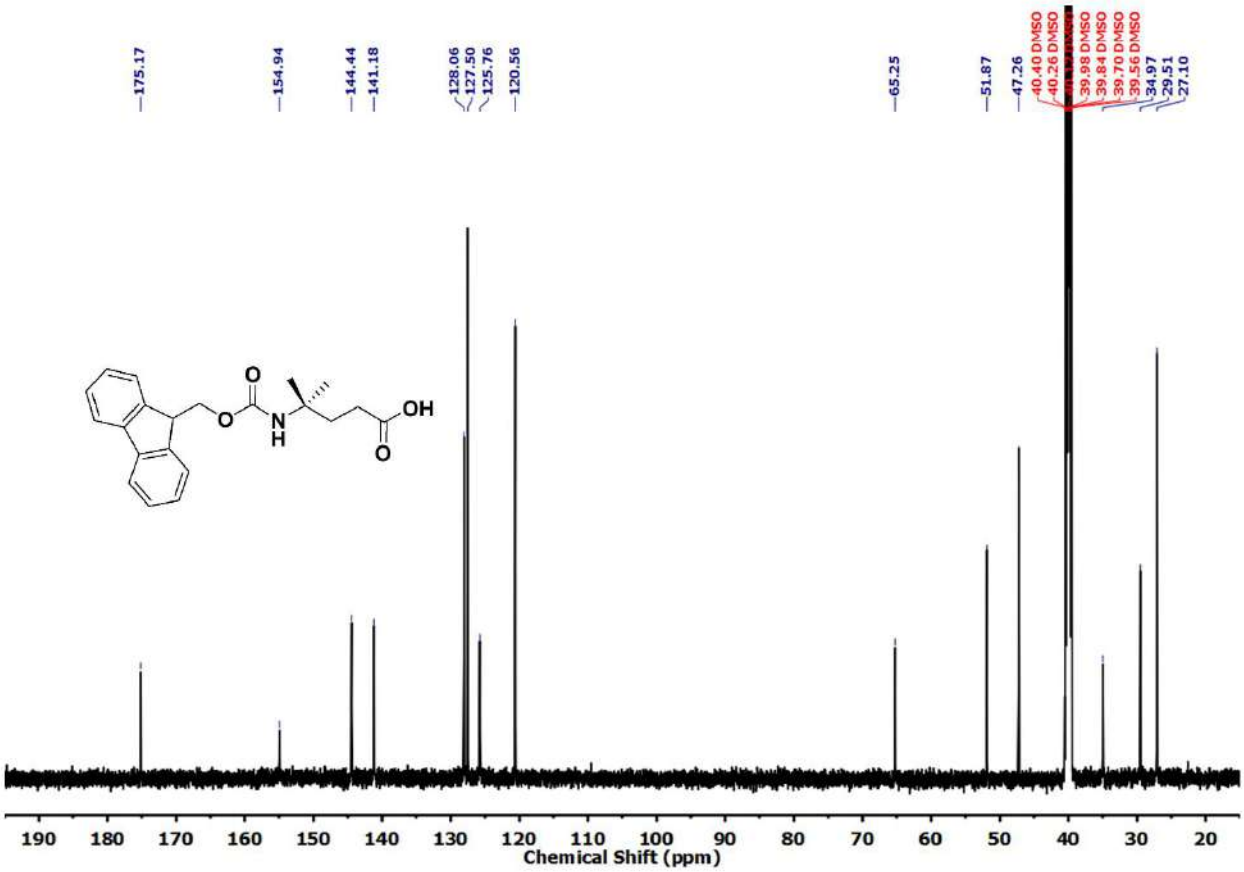

Figure A13. 150 MHz ^{13}C NMR spectrum of Fmoc-$\gamma^{4,4}$-OH in DMSO-d_6 at 10 mM concentration (298 K).

TH-3141_166122021

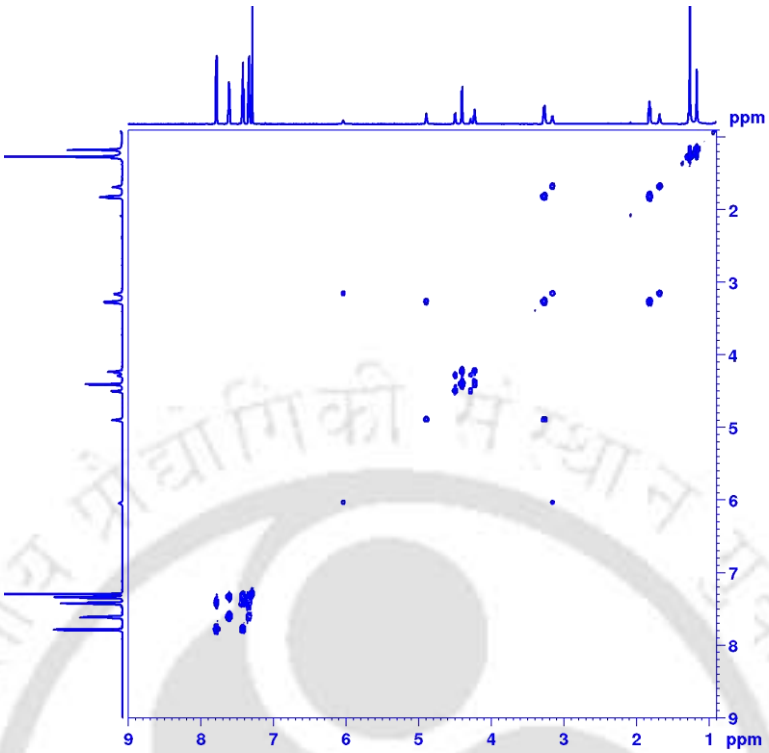

Figure A14. 600 MHz COSY spectrum of Fmoc-$\gamma^{2,2}$-OH in $CDCl_3$ at 10 mM concentration (298 K).

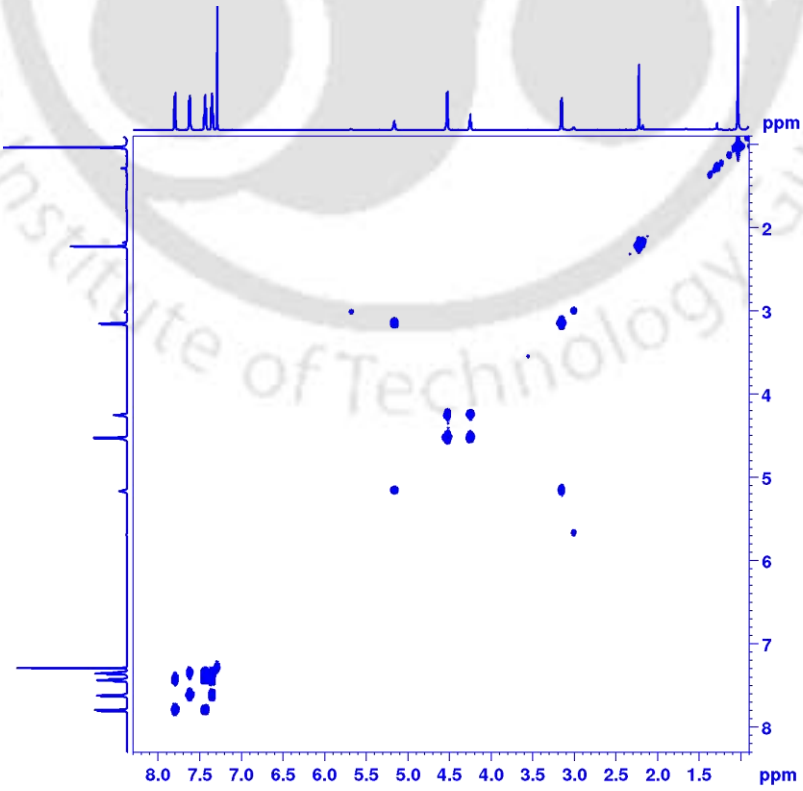

TH-3141_166122021

Figure A15. 600 MHz COSY spectrum of Fmoc-$\gamma^{3,3}$-OH in $CDCl_3$ at 10 mM concentration (298 K).

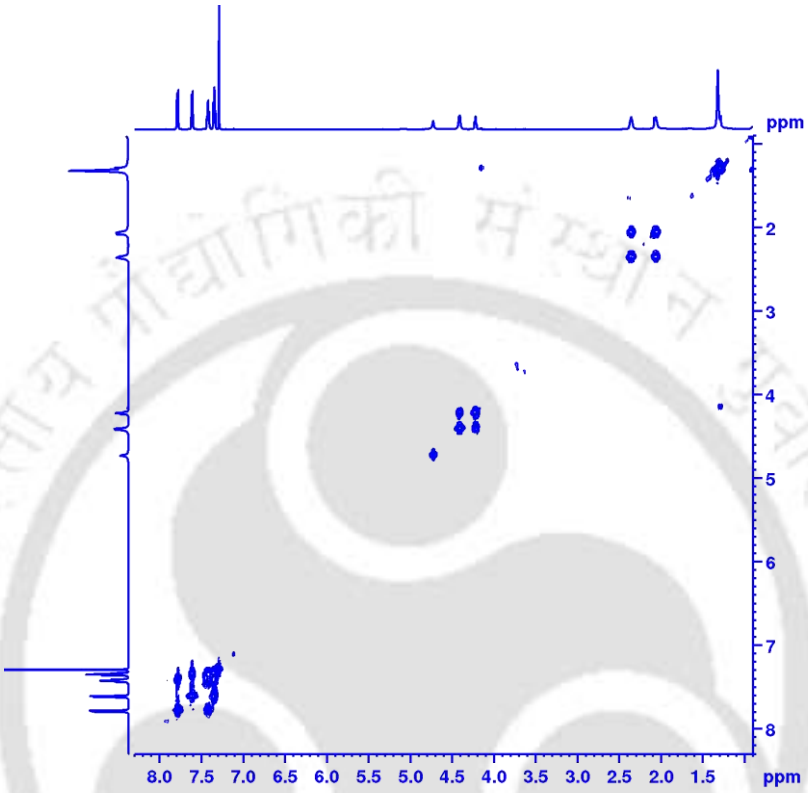

Figure A16. 600 MHz COSY spectrum of Fmoc-$\gamma^{4,4}$-OH in $CDCl_3$ at 10 mM concentration (298 K).

TH-3141_166122021

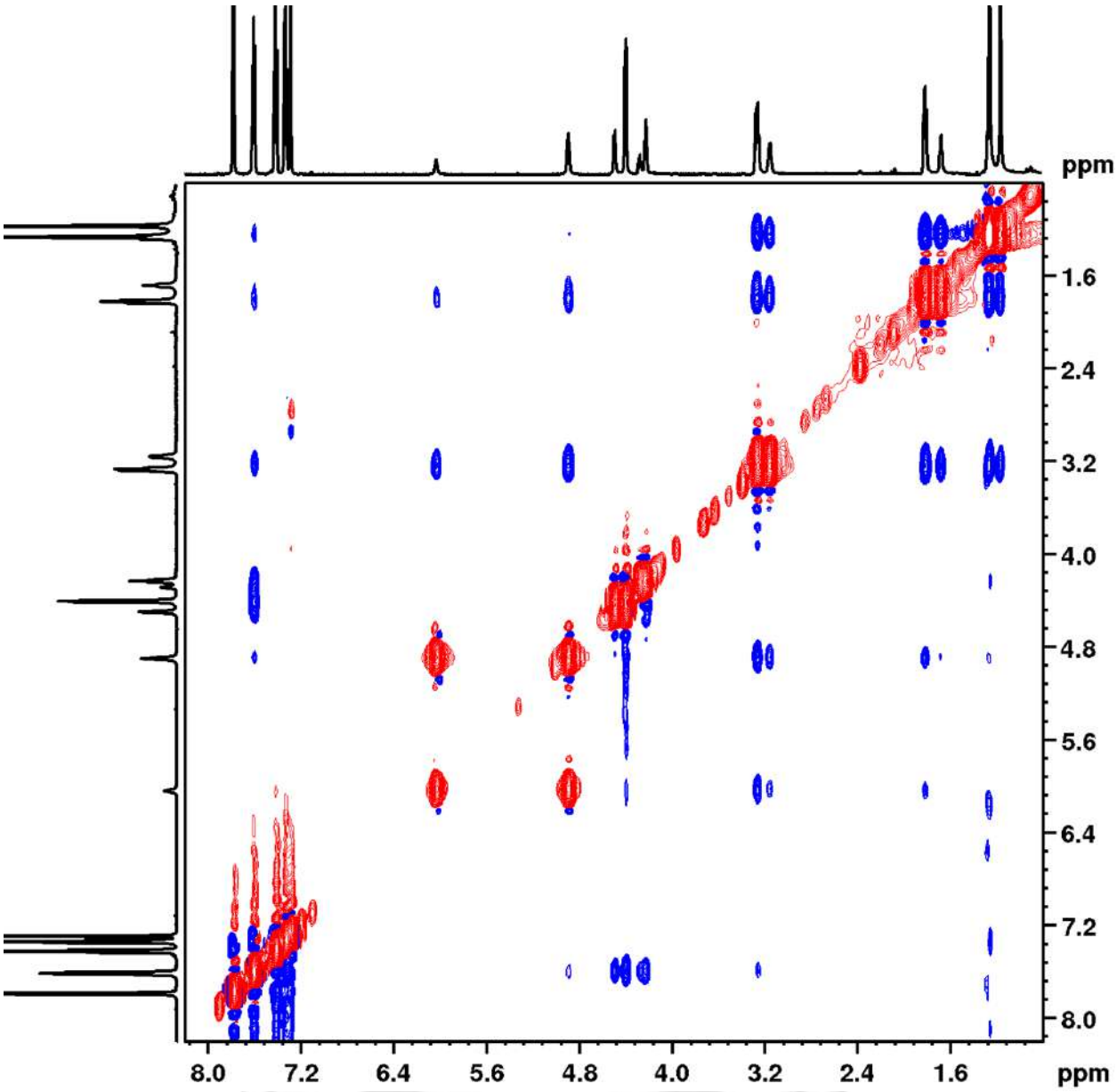

Figure A17. 600 MHz NOSEY spectra of Fmoc-$\gamma^{2,2}$-OH in $CDCl_3$ at 10 mM concentration (298 K)

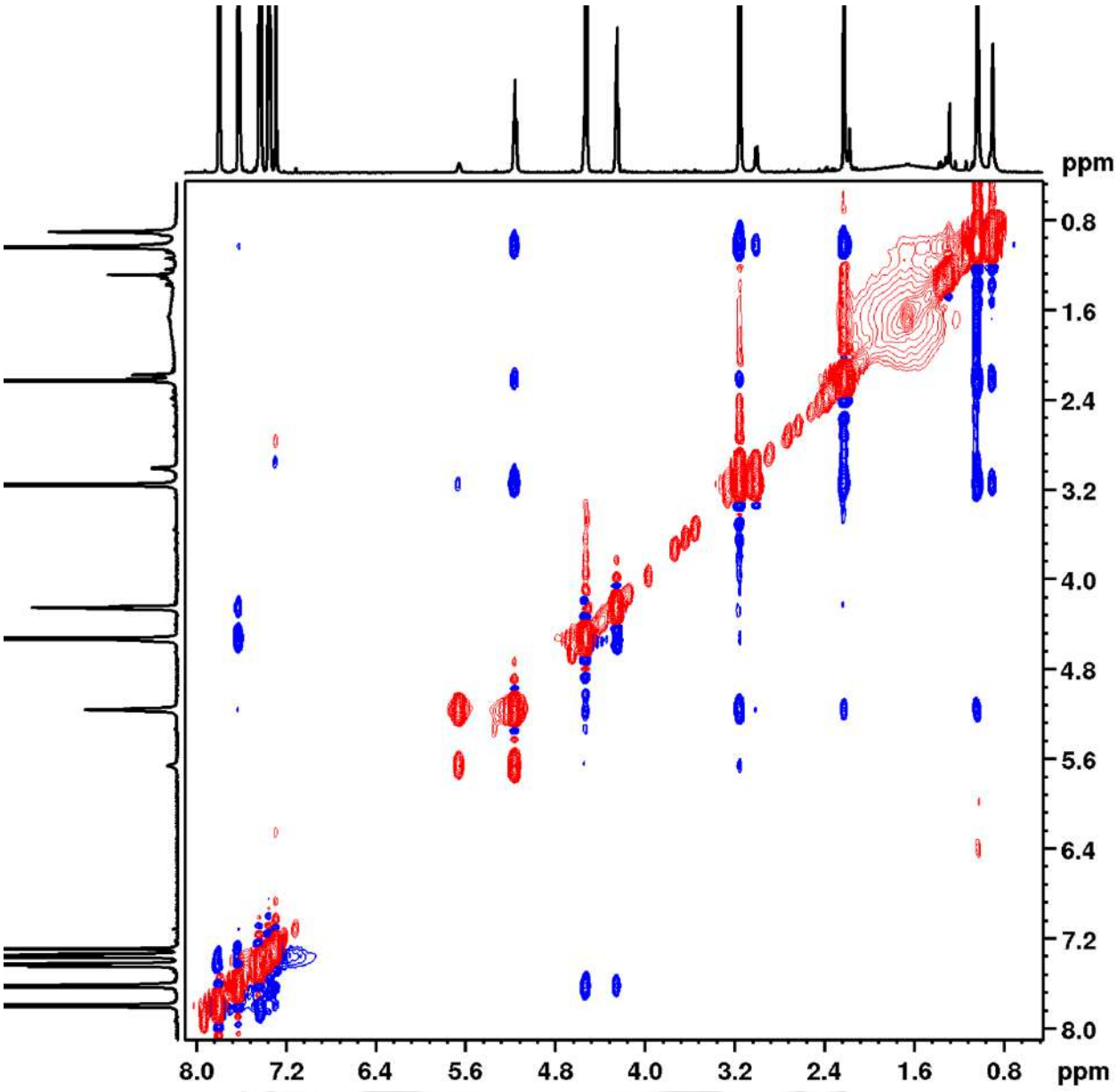

Figure A18. 600 MHz NOSEY spectrum of Fmoc-$\gamma^{3,3}$-OH in $CDCl_3$ at 10 mM concentration (298 K).

TH-3141_166122021

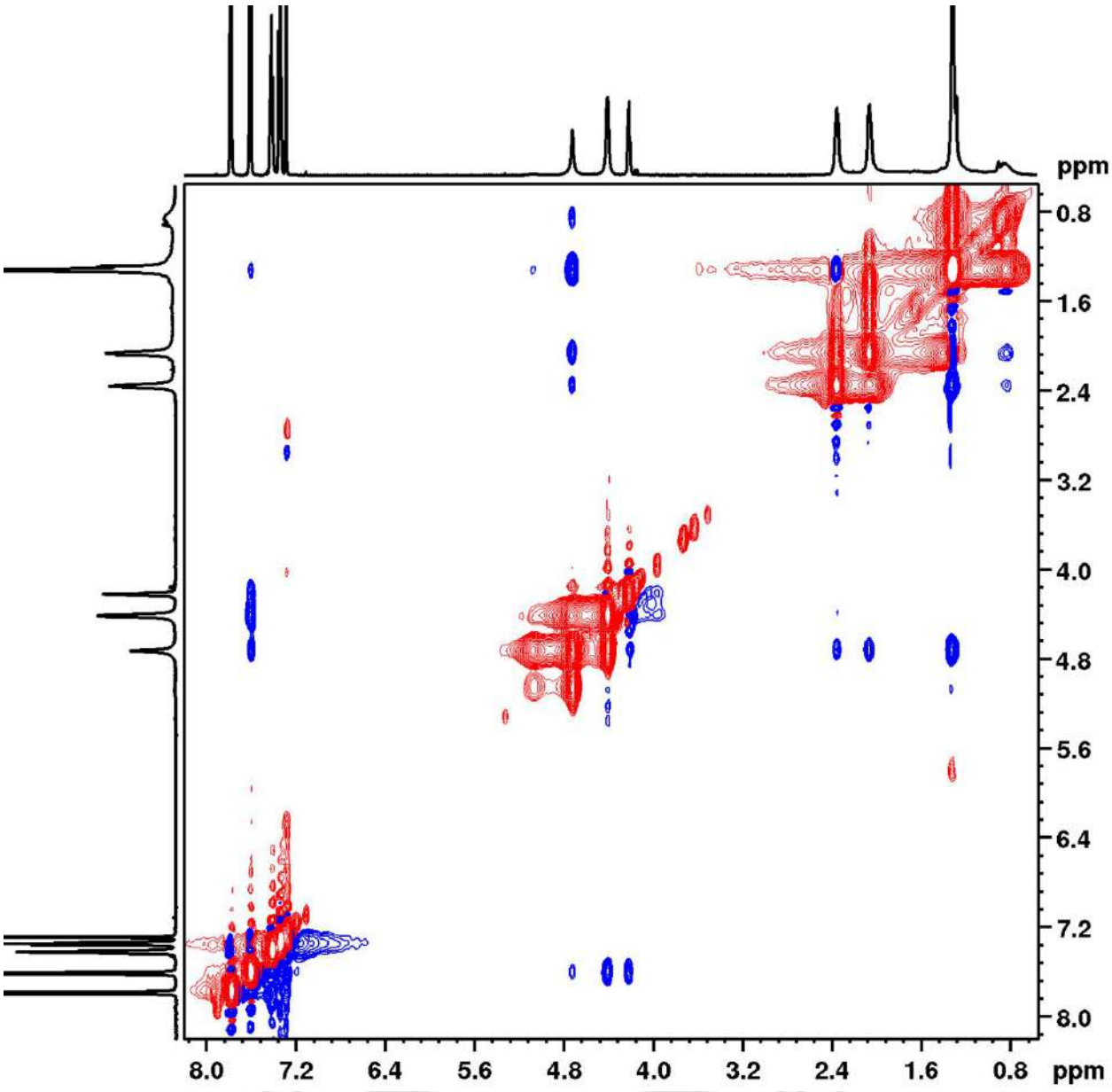

Figure A19. 600 MHz NOSEY spectrum of Fmoc-$\gamma^{4,4}$-OH in $CDCl_3$ at 10 mM concentration (298 K)

.

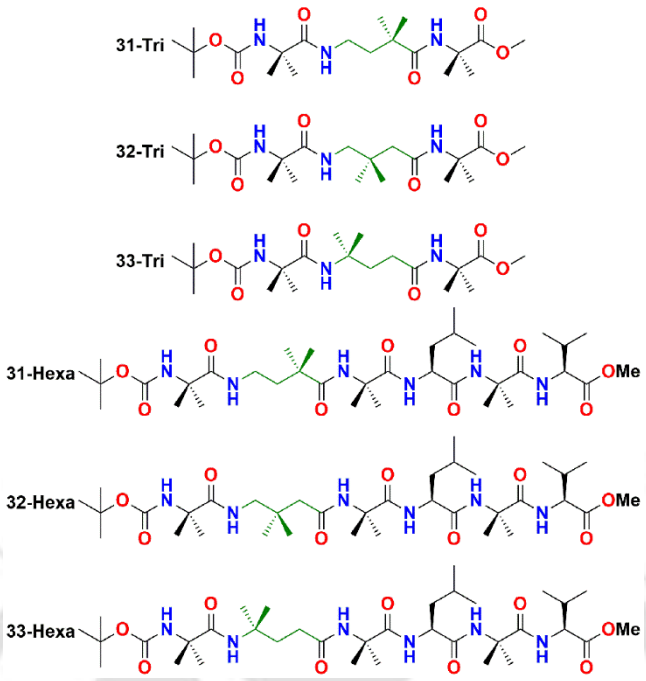

Figure A20. Chemical structures of the peptides (**31-33)-Tri** and **(31-33)-Hexa**.

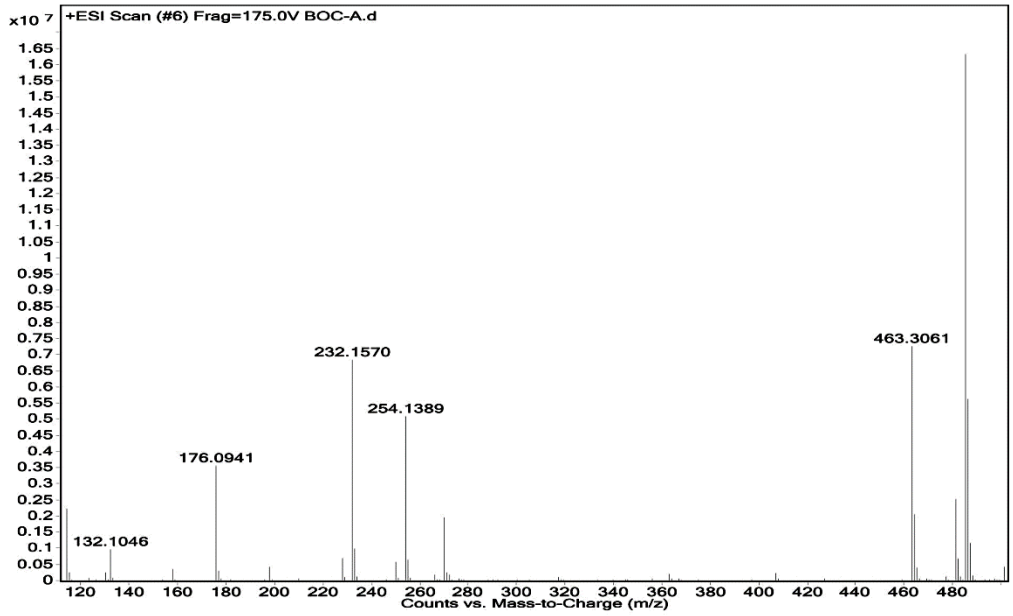

Figure A21. ESI-MS (m/z) of Boc-$\gamma^{2,2}$-OH: Calc. for $(M+H)^+$ $C_{11}H_{21}NO_4$ = 232.1504 Da; Obs. = 232.1570 Da, $(M+Na)^+$ = 254.1389, $(2M+H)^+$ = 463.6031 Da.

TH-3141_166122021

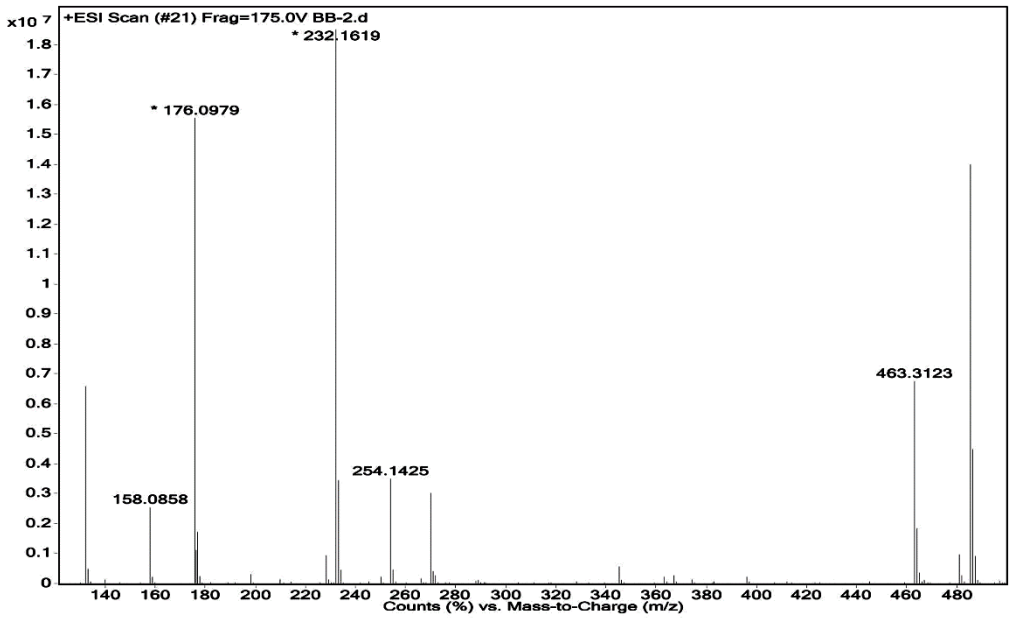

Figure A22. ESI-MS (m/z) of Boc-$\gamma^{3,3}$-OH: ESI-MS (m/z) of **Boc-$\gamma^{3,3}$-OH**: Calc. for $(M+H)^+$ $C_{11}H_{21}NO_4$ = 232.1504 Da; Obs. = 232.1619 Da, $(M+Na)^+$ = 254.1425, $(2M+H)^+$ = 463.3123 Da.

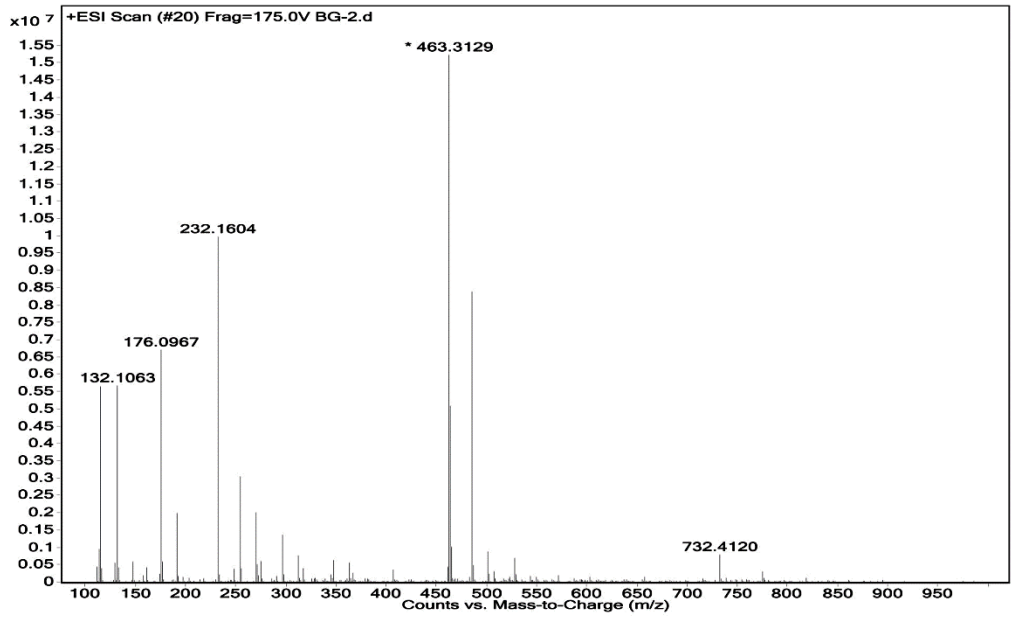

Figure A23. ESI-MS (m/z) of Boc-$\gamma^{4,4}$-OH. ESI-MS (m/z) of **Boc-$\gamma^{4,4}$-OH**: Calc. for $(M+H)^+$ $C_{11}H_{21}NO_4$ = 232.1504 Da; Obs. = 232.1604 Da, $(2M+H)^+$ = 463.3129 Da.

TH-3141_166122021

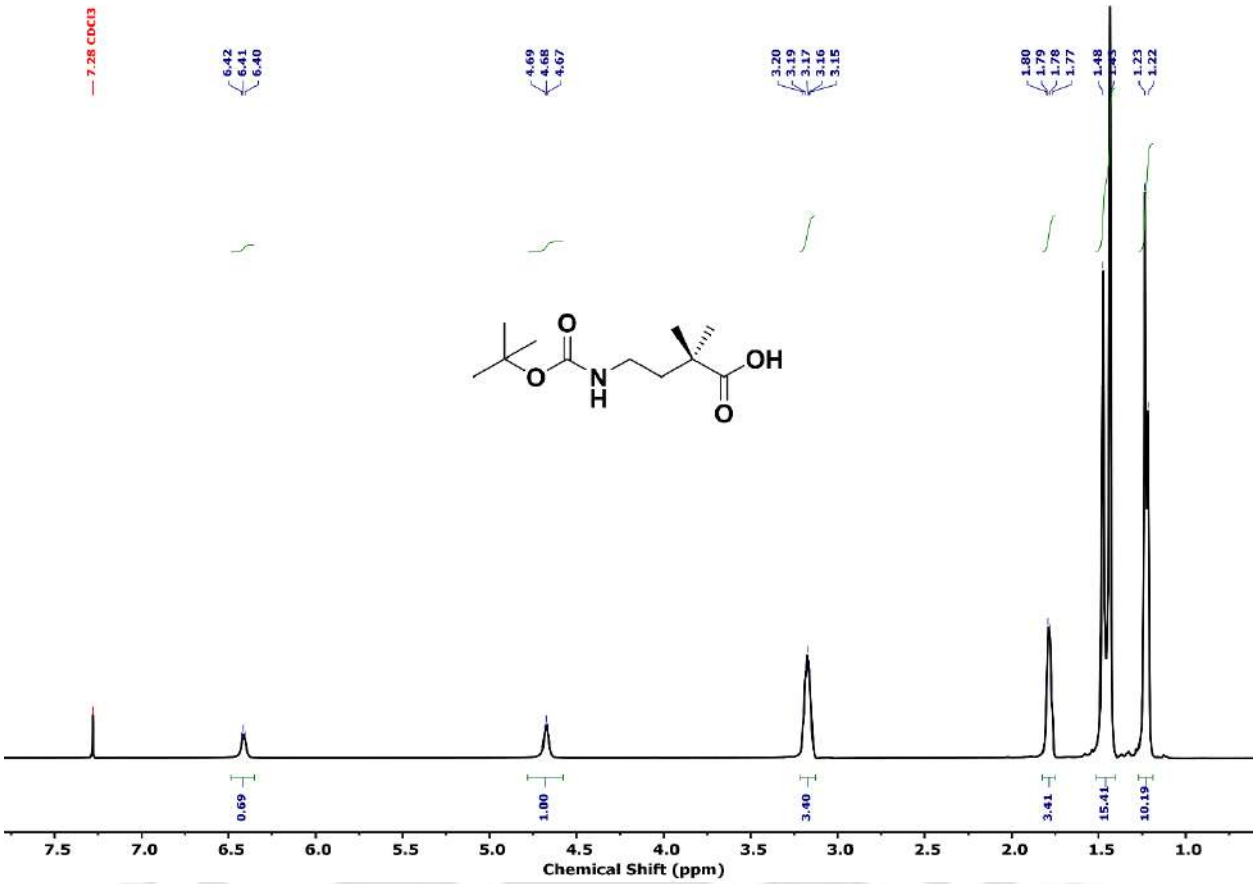

Figure A24. 600 MHz ^{1}H NMR spectrum of Boc-$\gamma^{2,2}$-OH in $CDCl_3$ at 10 mM concentration (298 K).

TH-3141_166122021

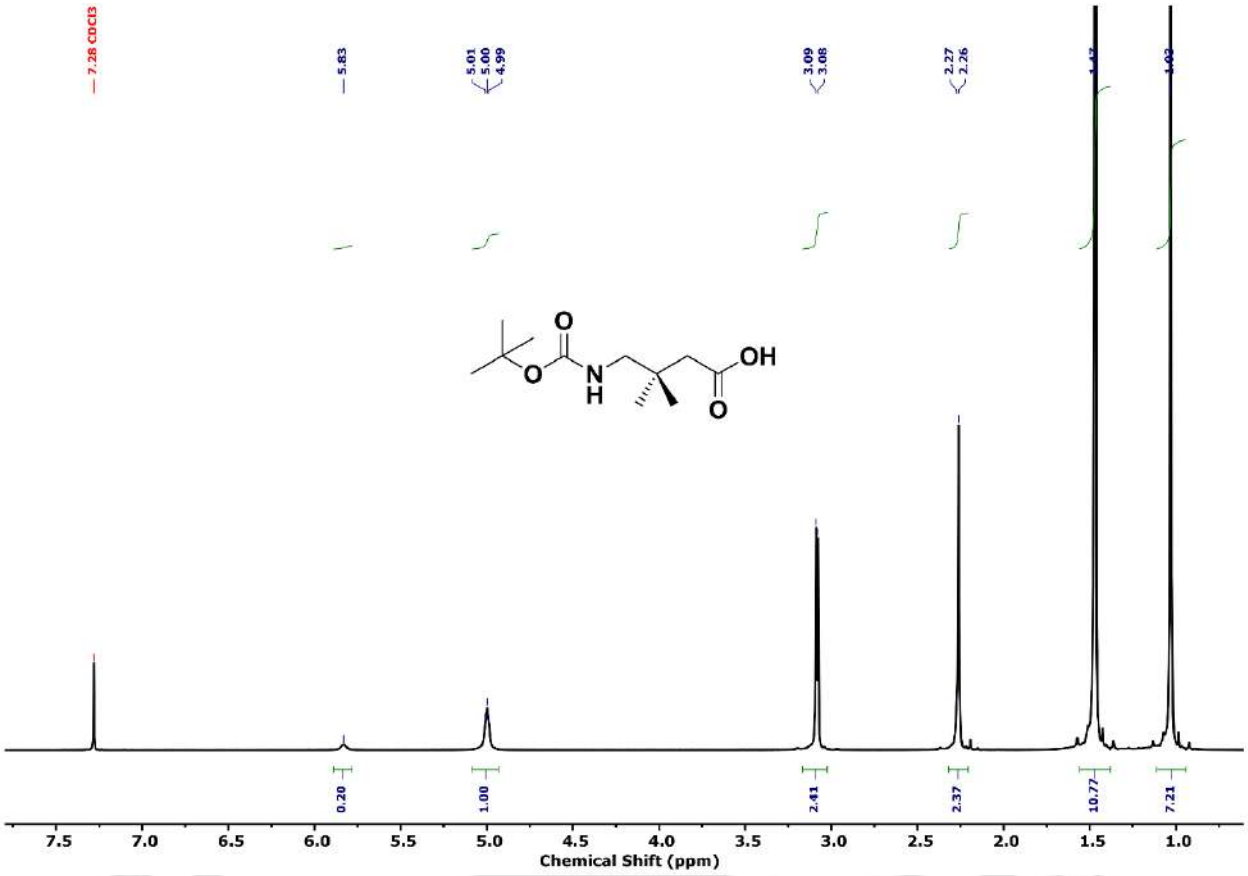

Figure A25. 600 MHz ^{1}H NMR spectrum of Boc-$\gamma^{3,3}$-OH in $CDCl_3$ at 10 mM concentration (298 K).

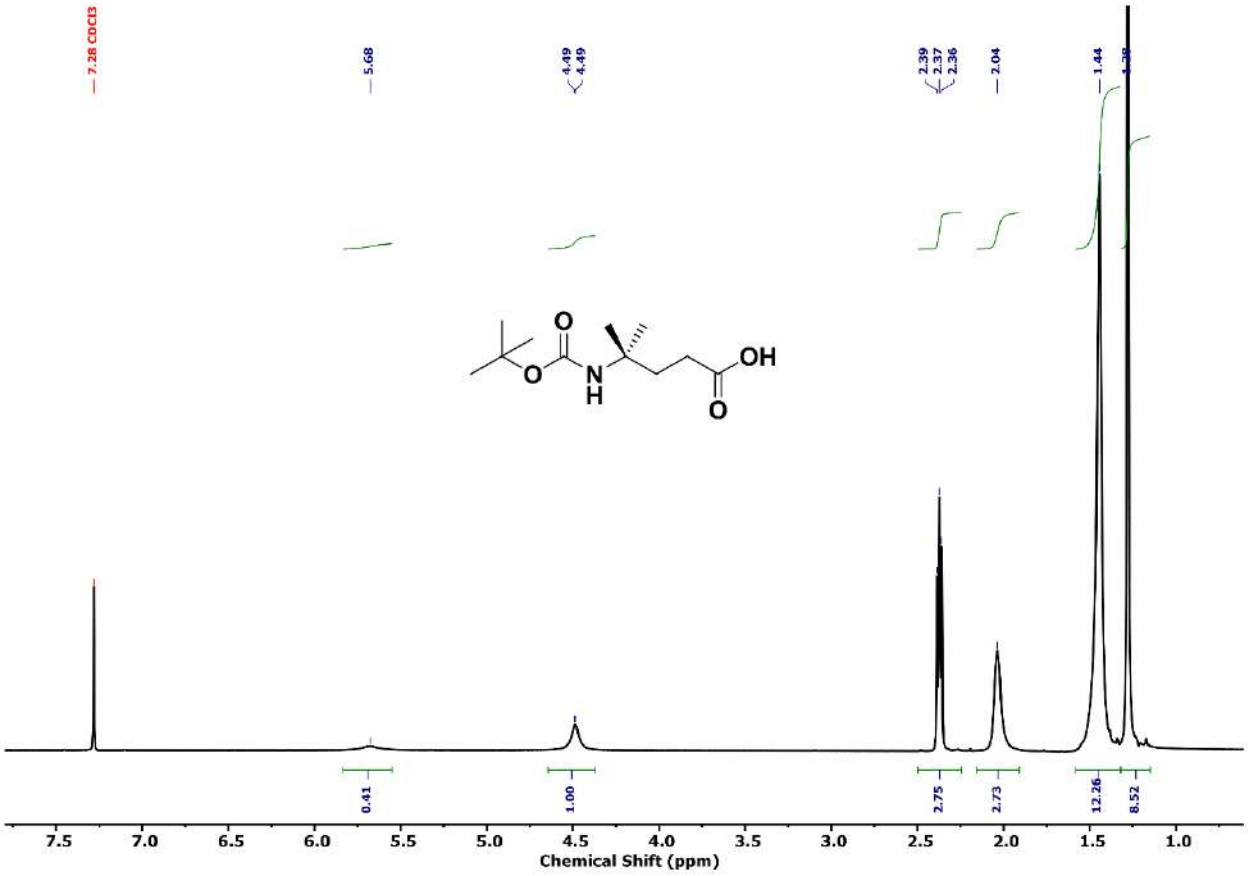

Figure A26. 600 MHz ^{1}H NMR spectrum of Boc-$\gamma^{4,4}$-OH in $CDCl_3$ at 10 mM concentration (298 K).

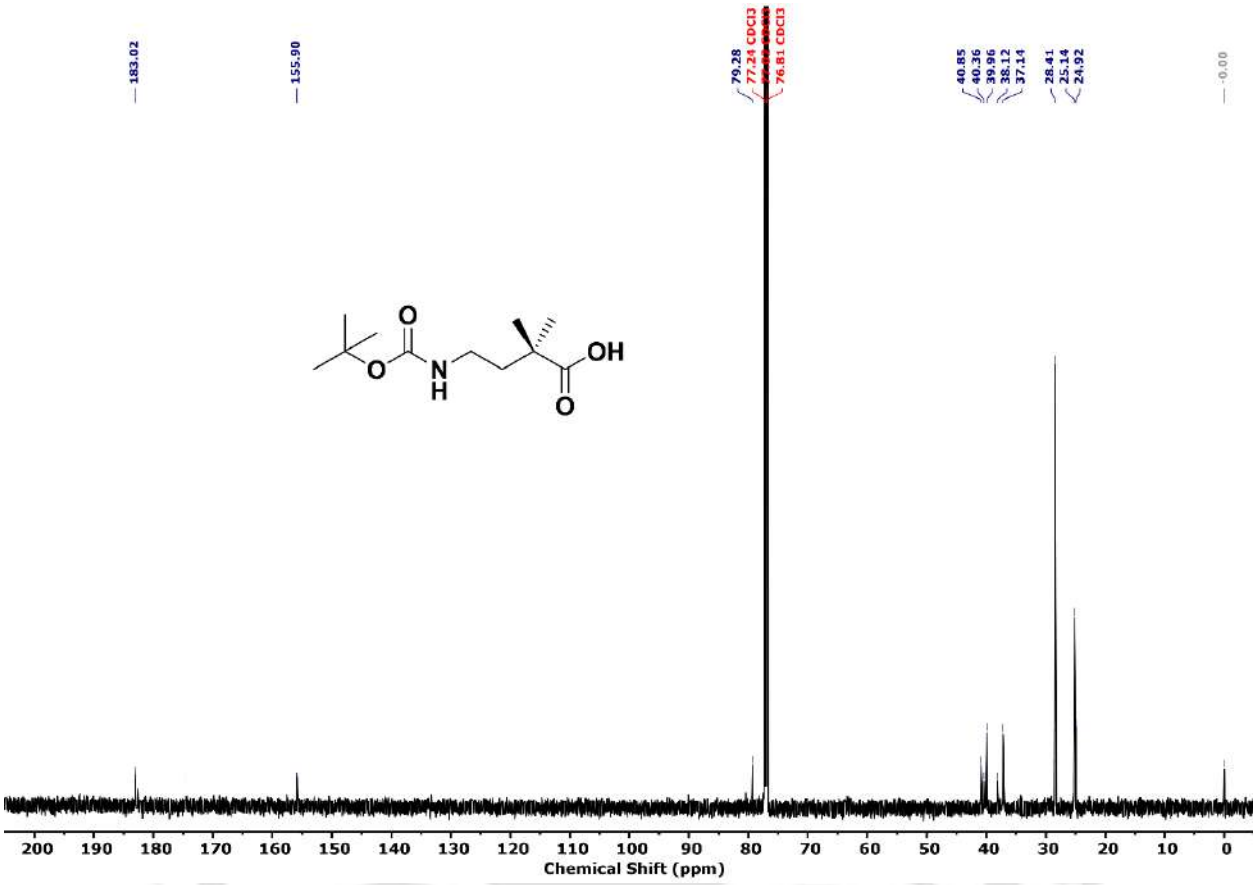

Figure A27. 150 MHz ^{13}C NMR spectrum of Boc-$\gamma^{2,2}$-OH in $CDCl_3$ at 10 mM concentration (298 K).

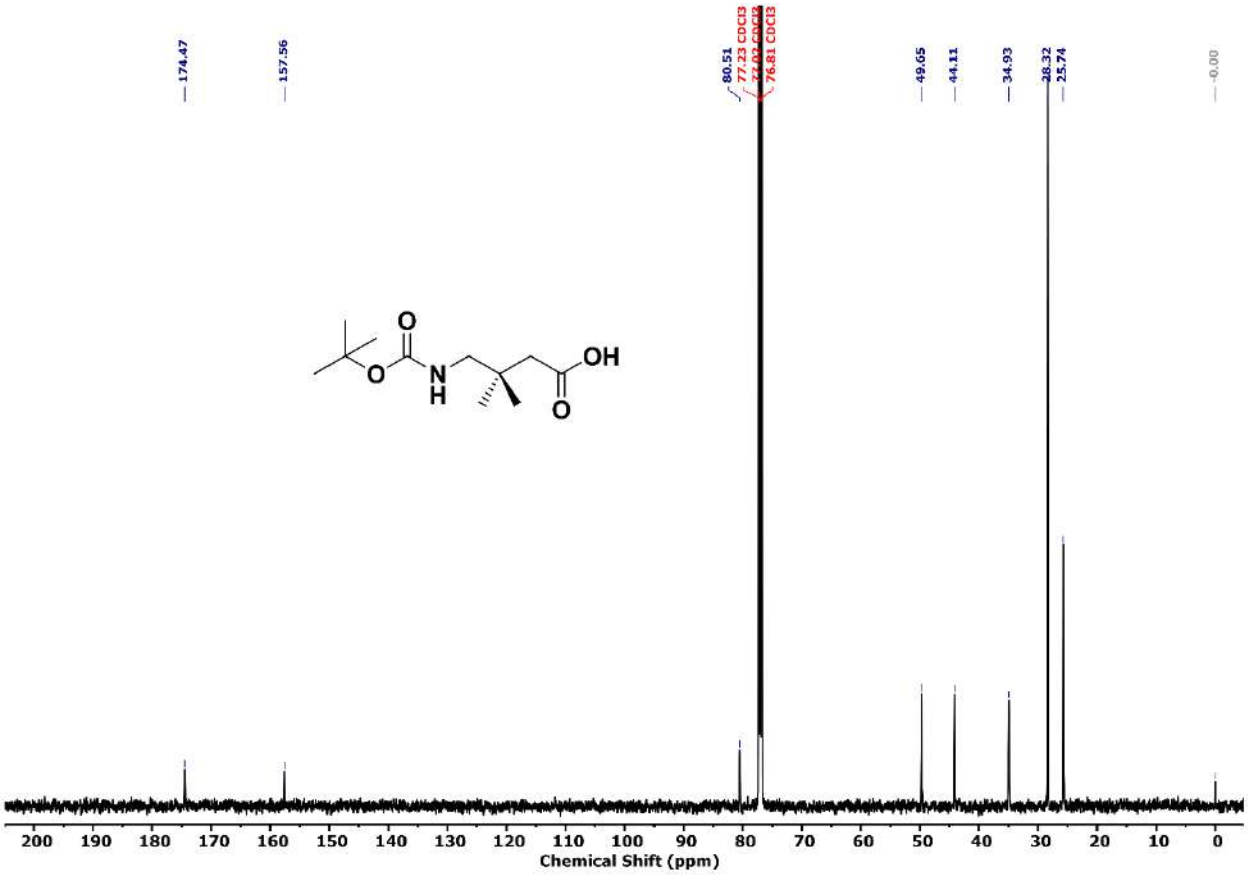

Figure A28. 150 MHz ^{13}C NMR spectrum of Boc-$\gamma^{3,3}$-OH in $CDCl_3$ at 10 mM concentration (298 K).

TH-3141_166122021

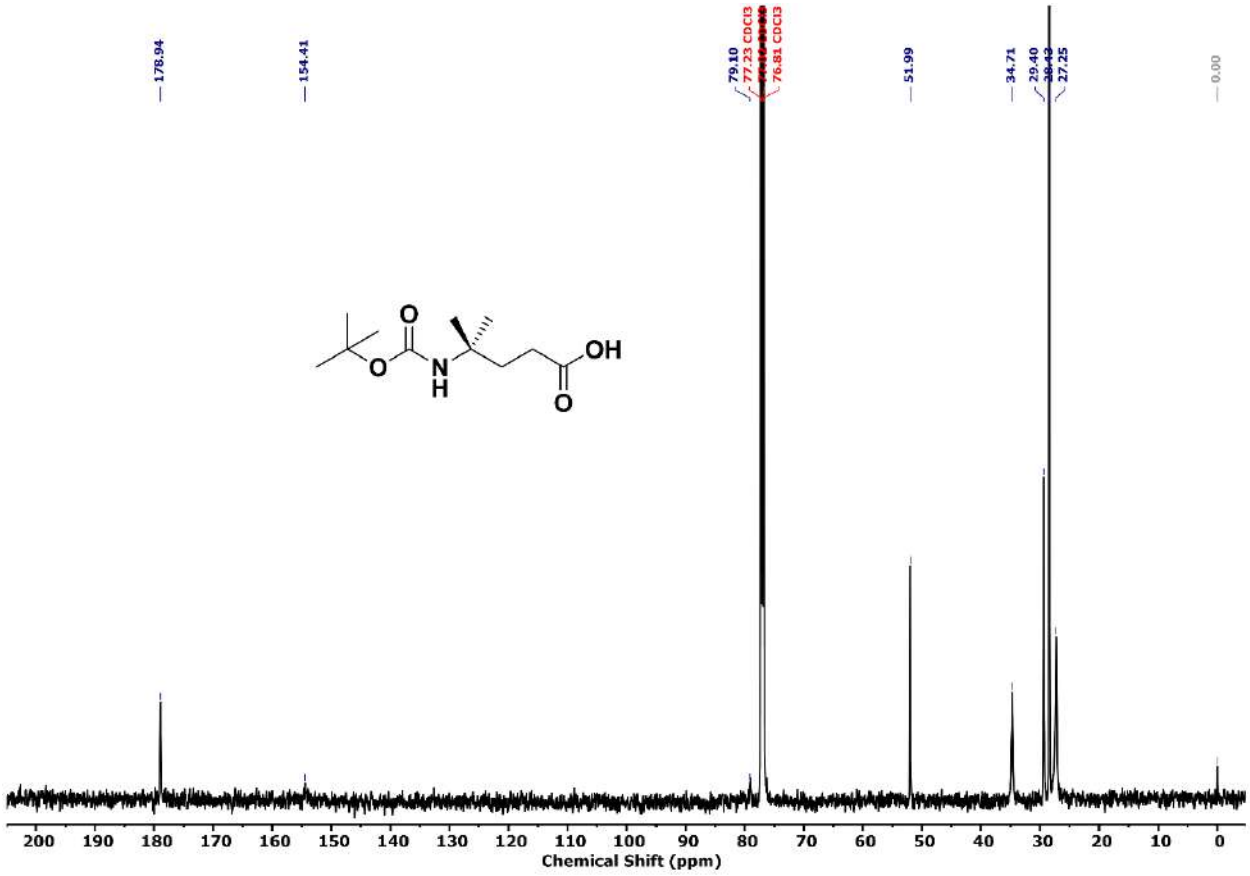

Figure A29. 150 MHz ^{13}C NMR spectrum of Boc-$\gamma^{4,4}$-OH in $CDCl_3$ at 10 mM concentration (298 K).

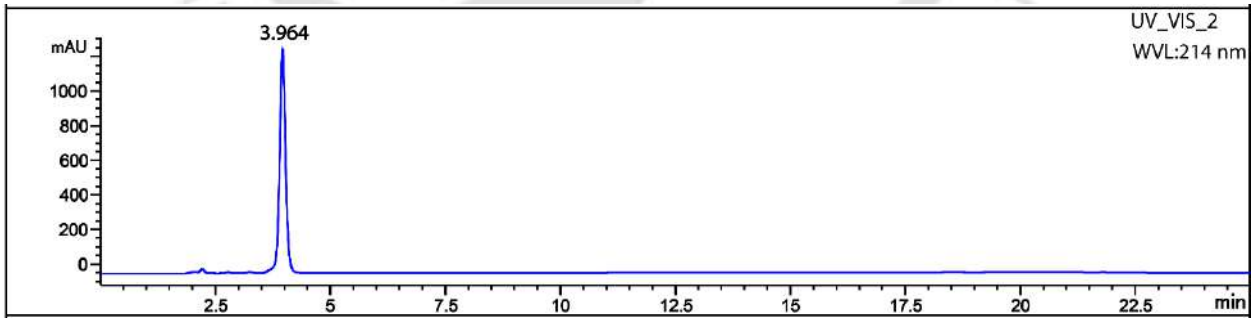

Figure A30. Analytical HPLC trace of **31-Tri** in ACN/H_2O.

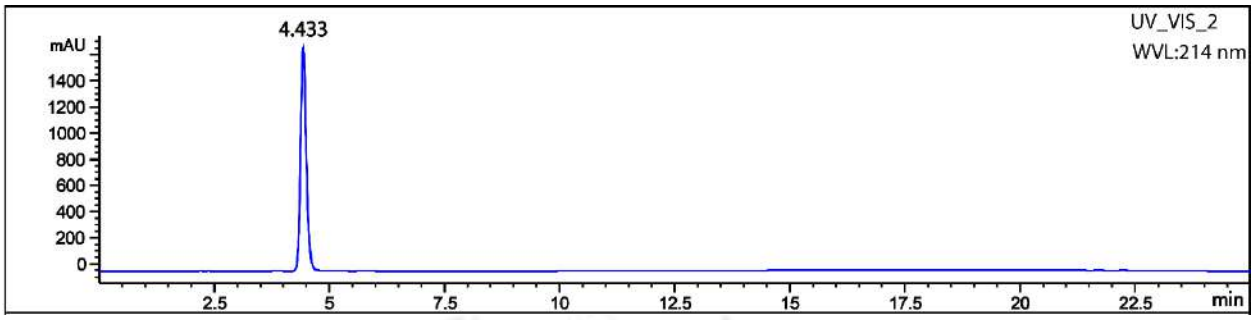

Figure A31. Analytical HPLC trace of **32-Tri** in ACN/H_2O.

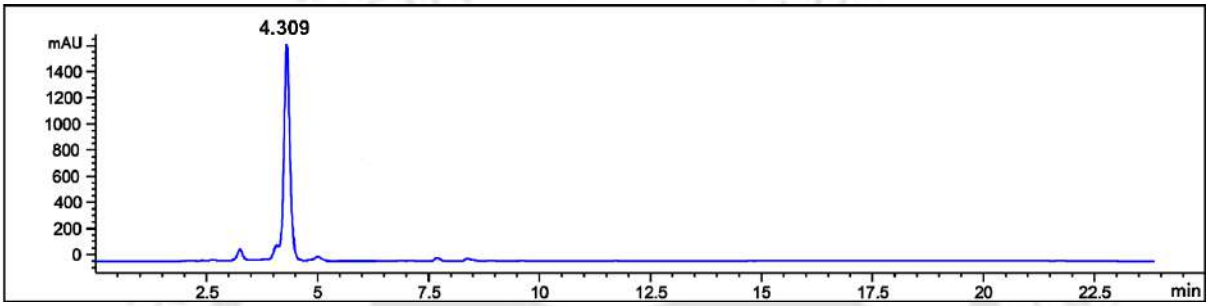

Figure A32. Analytical HPLC trace of **33-Tri** in ACN/H_2O.

TH-3141_166122021

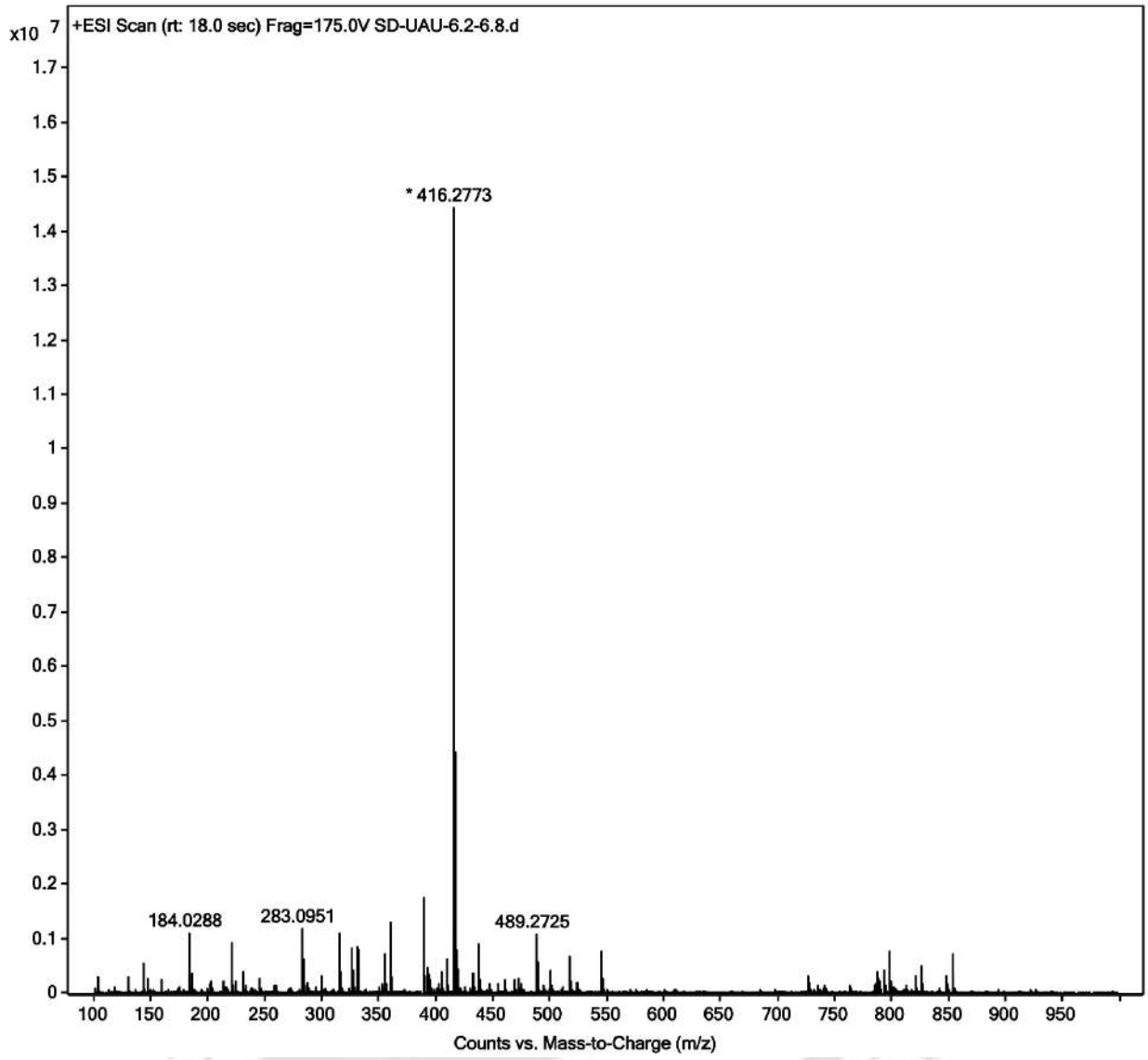

Figure A33. ESI-MS (m/z) of **31-Tri**. Calc. for $(M+H)^+$ $C_{20}H_{37}N_3O_6$ = 416.2716 Da; Obs. = 416.2773 Da.

TH-3141_166122021

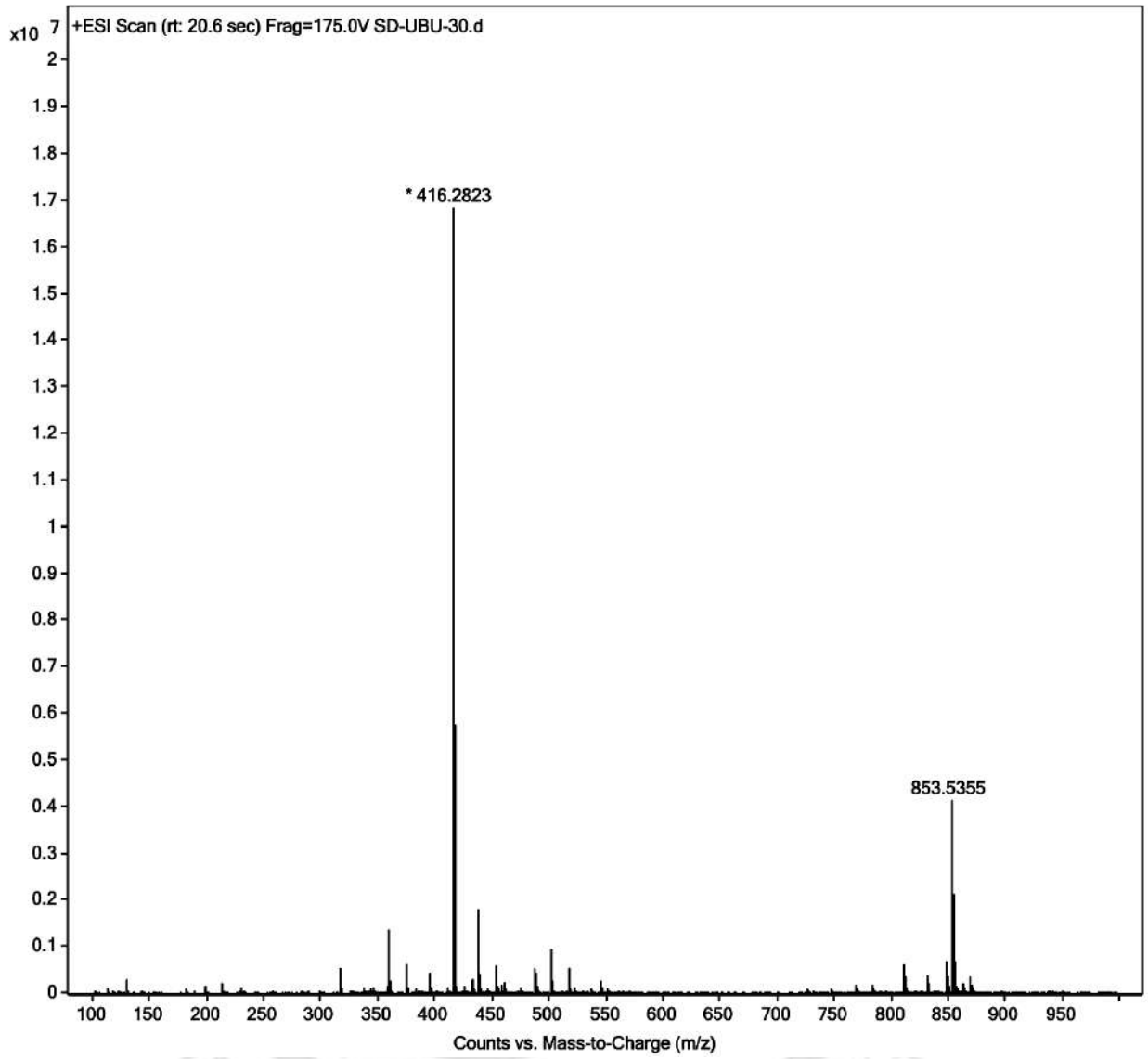

Figure A34. ESI-MS (m/z) of **32-Tri**. Calc. for $(M+H)^+$ $C_{20}H_{37}N_3O_6$ = 416.2716 Da; Obs. = 416.2823 Da, $(2M+Na)^+$ = 853.5355.

TH-3141_166122021

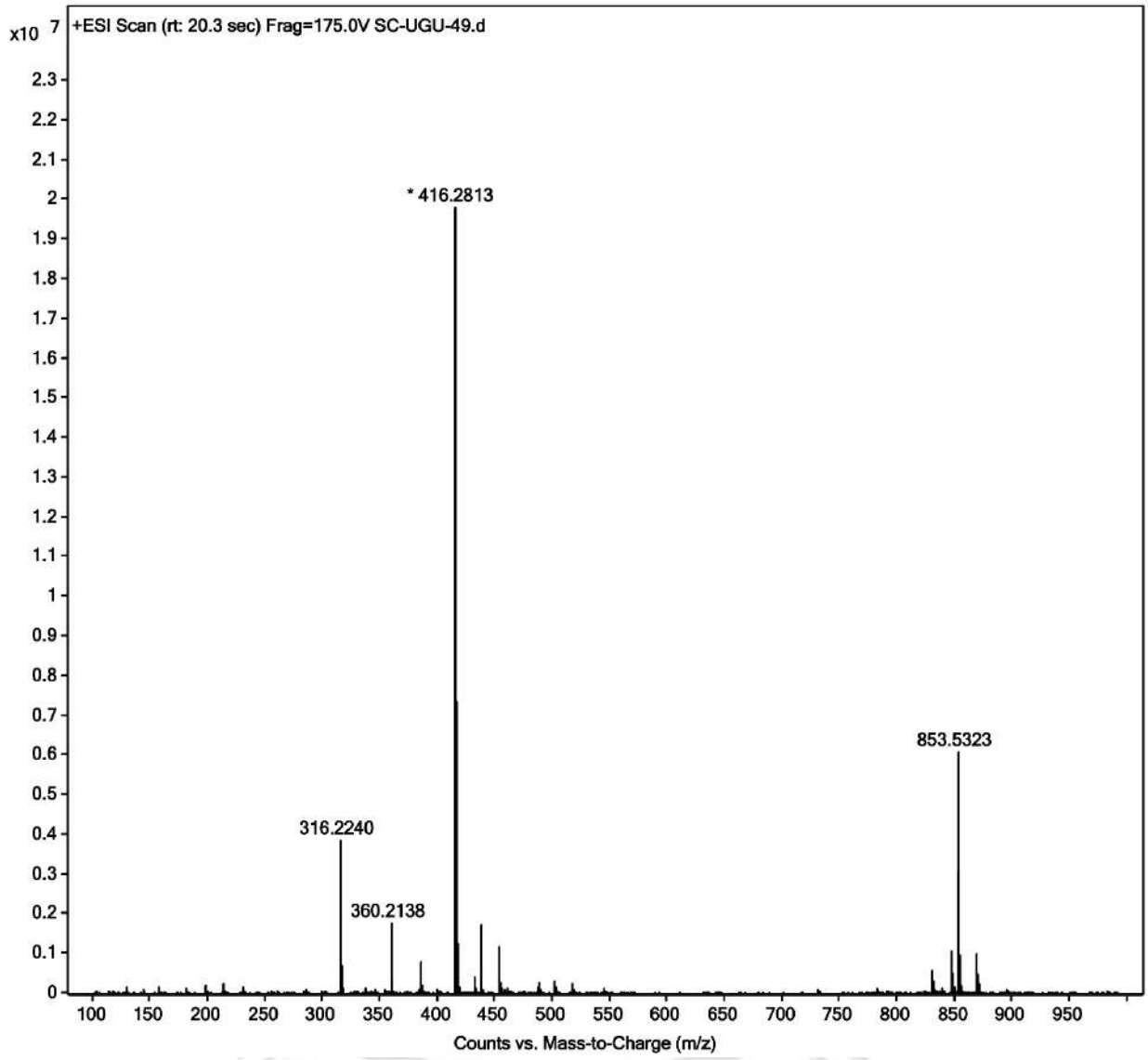

Figure A35. ESI-MS (m/z) of **33-Tri**. Calc. for $(M+H)^+$ $C_{20}H_{37}N_3O_6$ = 416.2716 Da; Obs. = 416.2813 Da, $(2M+Na)^+$ = 853.5323.

TH-3141_166122021

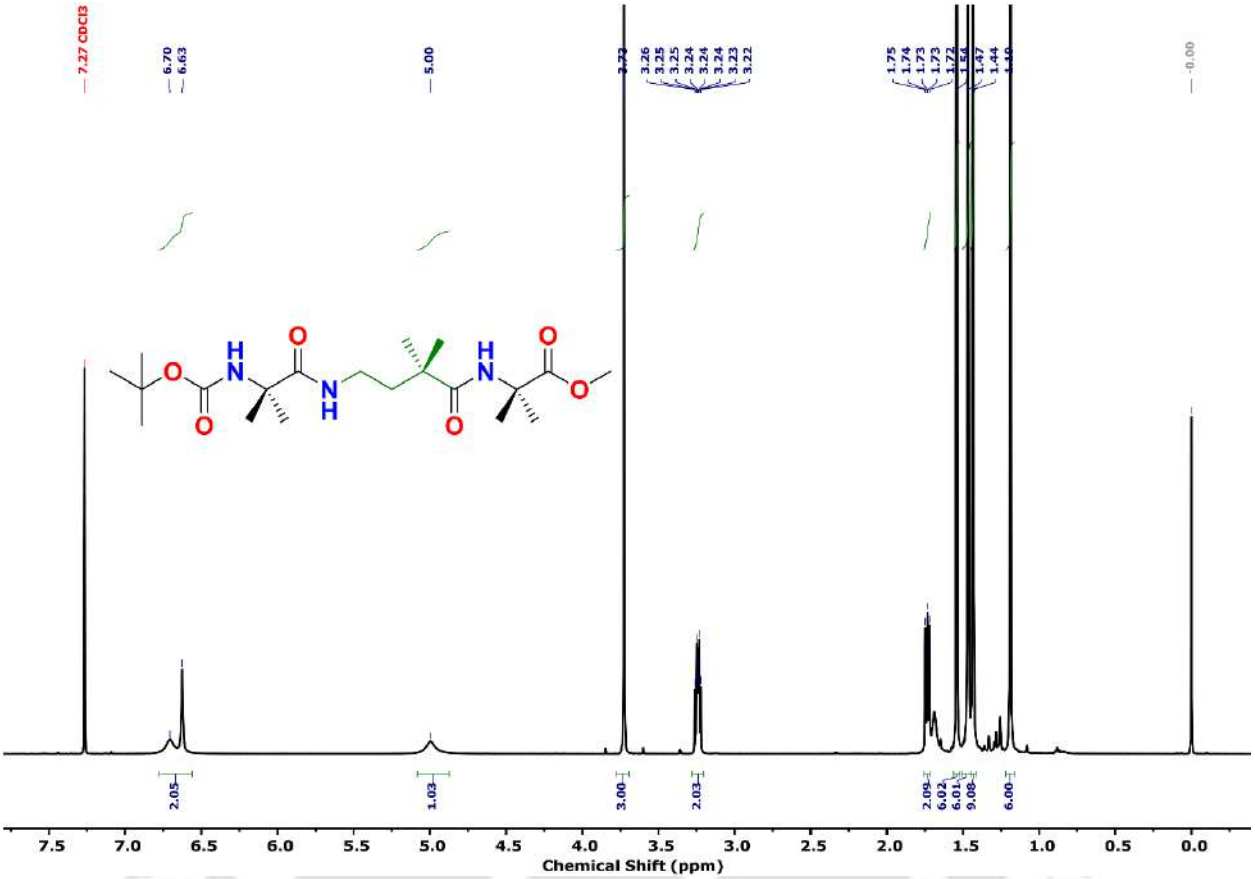

Figure A36. 600 MHz ^{1}H NMR spectra of **31-Tri** in $CDCl_3$ at 5 mM concentration (298 K).

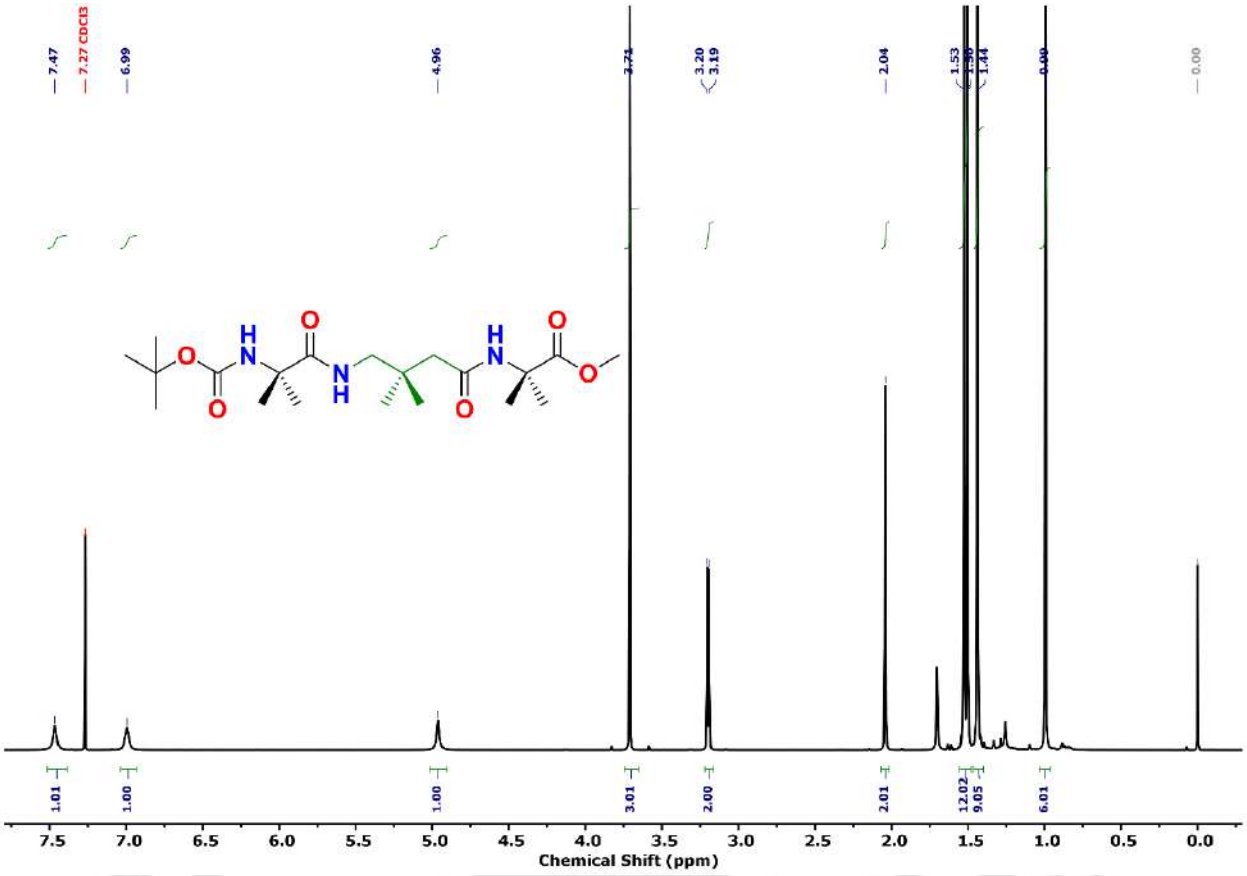

Figure A37. 600 MHz ^{1}H NMR spectra of **32-Tri** in $CDCl_3$ at 5 mM concentration (298 K).

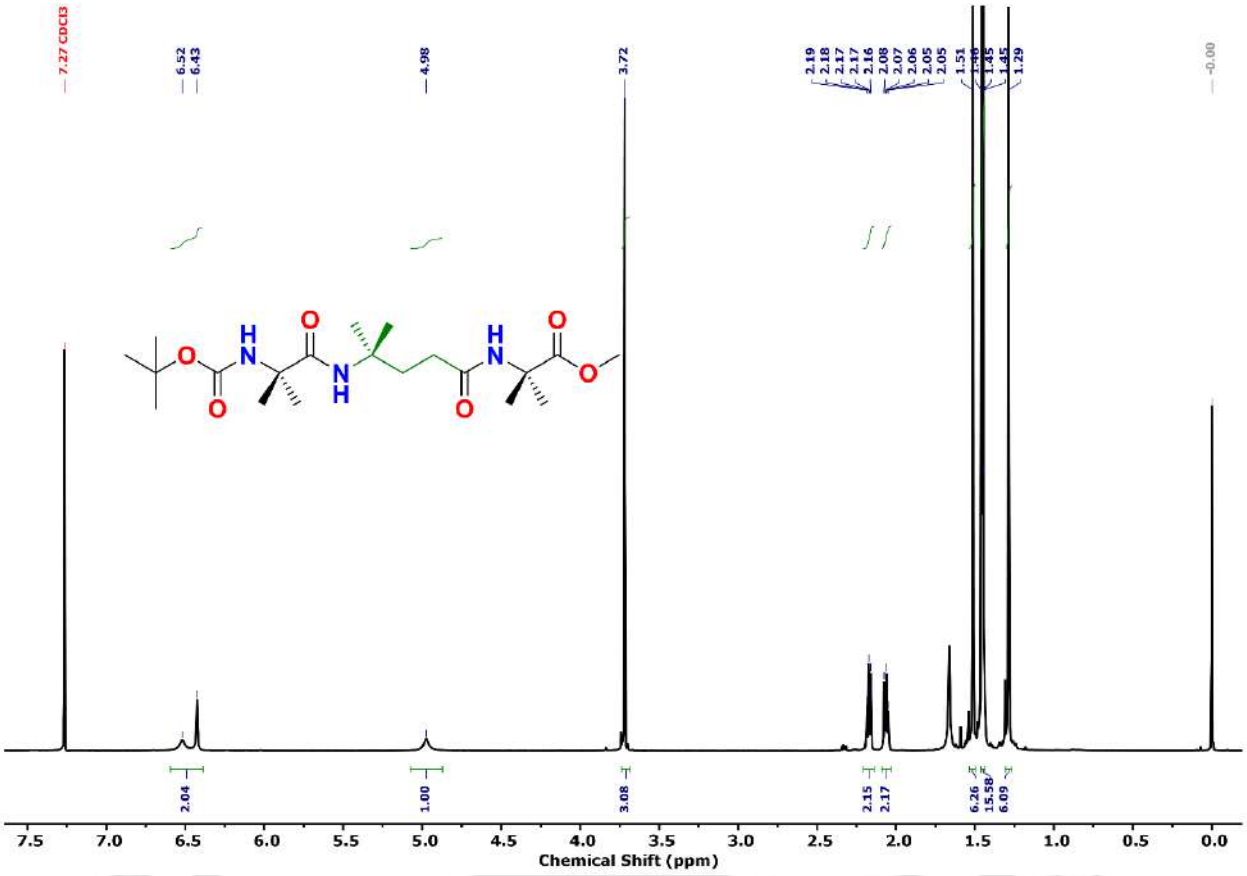

Figure A38. 600 MHz ^{1}H NMR spectra of **33-Tri** in $CDCl_3$ at 5 mM concentration (298 K).

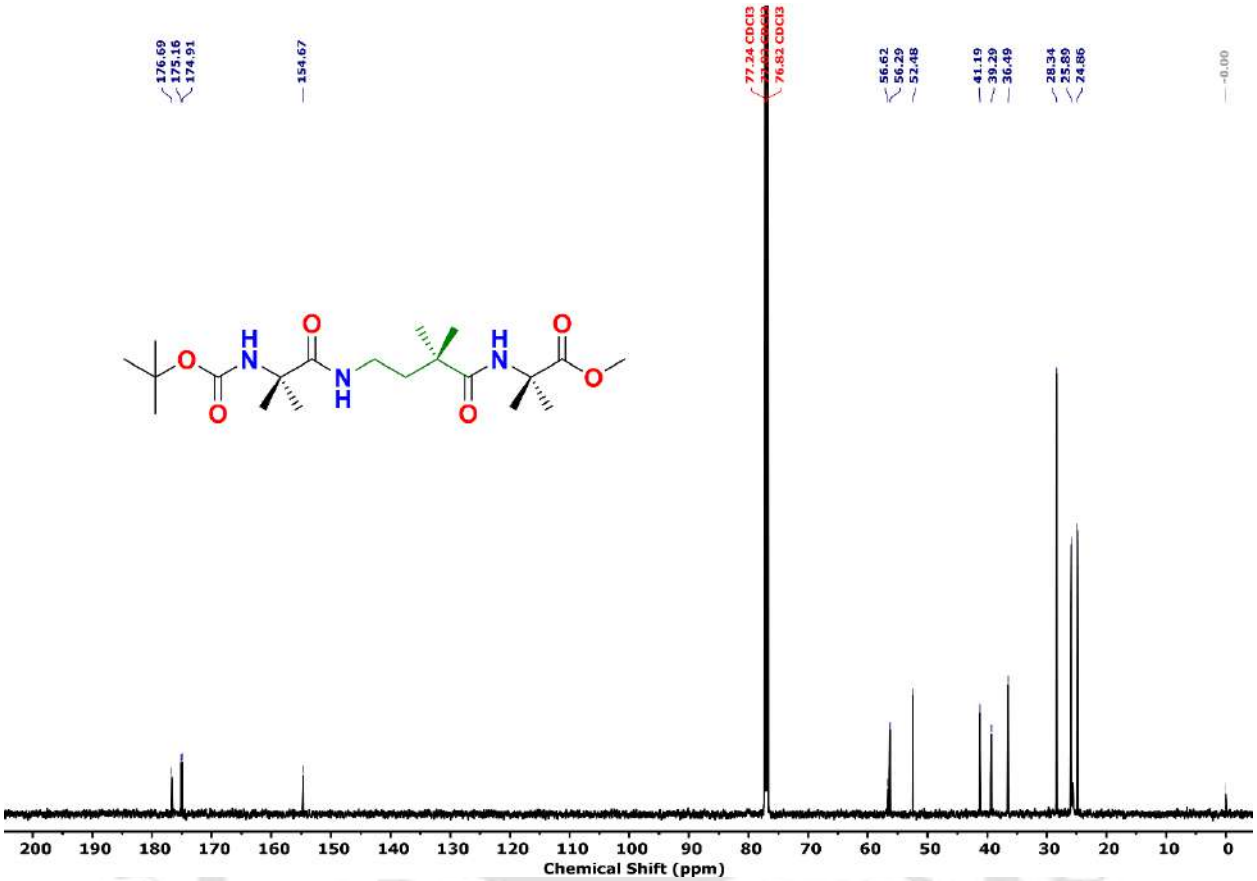

Figure A39. 150 MHz ^{13}C NMR spectrum of **31-Tri** in $CDCl_3$ at 5 mM concentration (298 K).

TH-3141_166122021

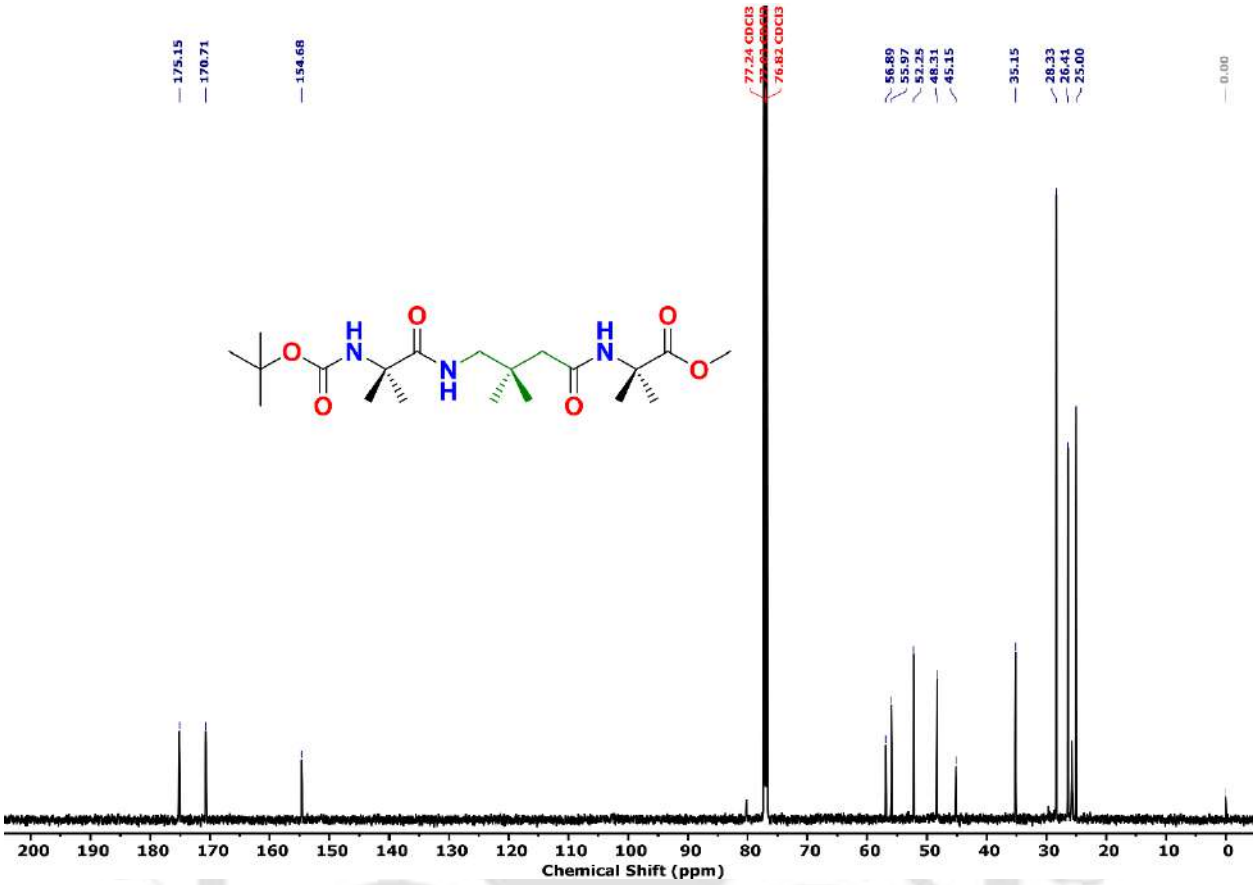

Figure A40. 150 MHz ^{13}C NMR spectrum of **32-Tri** in $CDCl_3$ at 5 mM concentration (298 K).

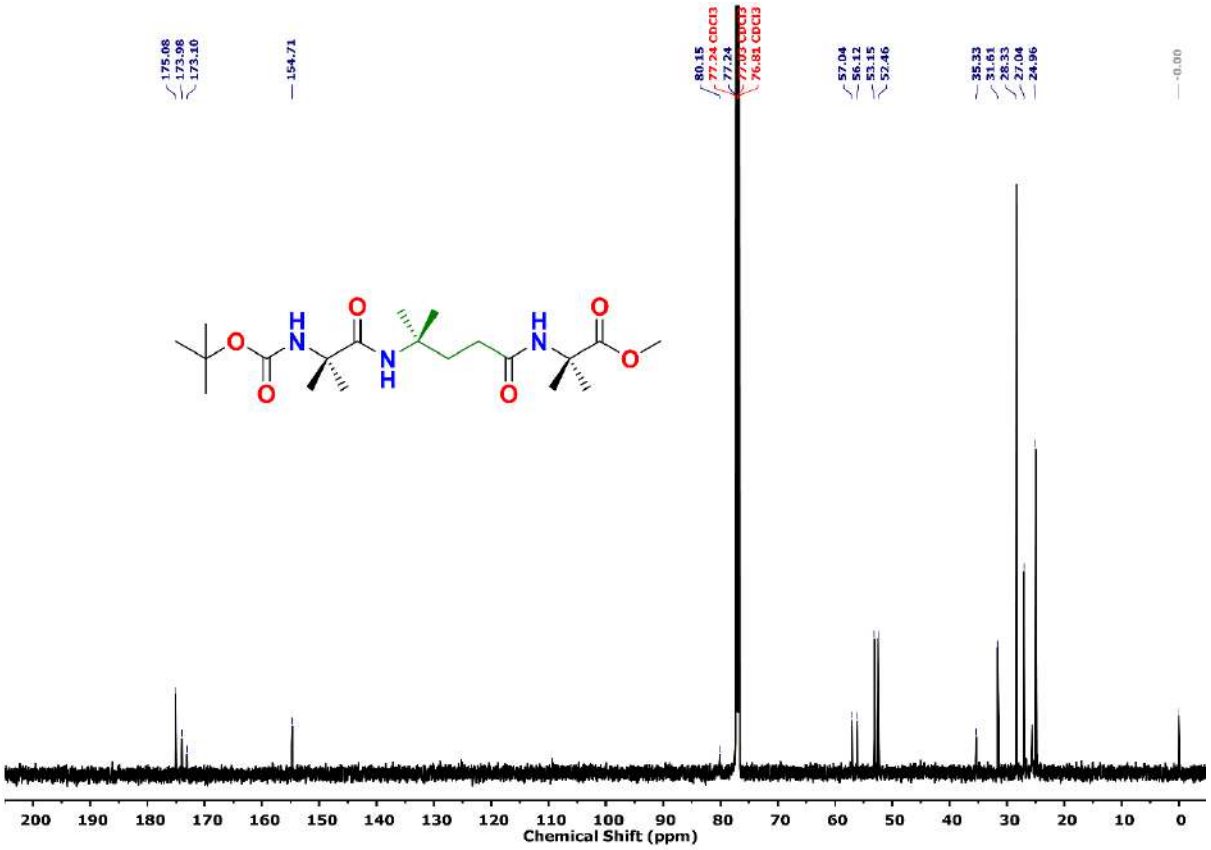

Figure A41. 150 MHz ^{13}C NMR spectrum of **33-Tri** in $CDCl_3$ at 5 mM concentration (298 K).

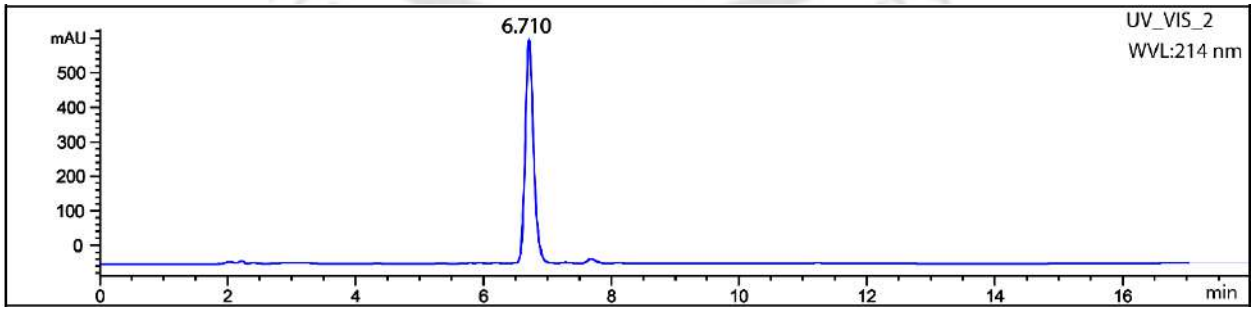

Figure A42. Analytical HPLC trace of **31-Hexa** in ACN/H_2O.

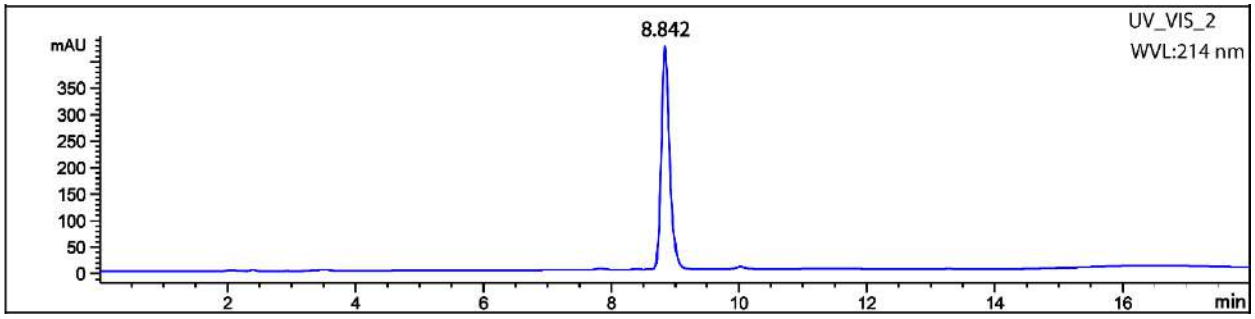

Figure A43. Analytical HPLC trace of **32-Hexa** in ACN/H_2O.

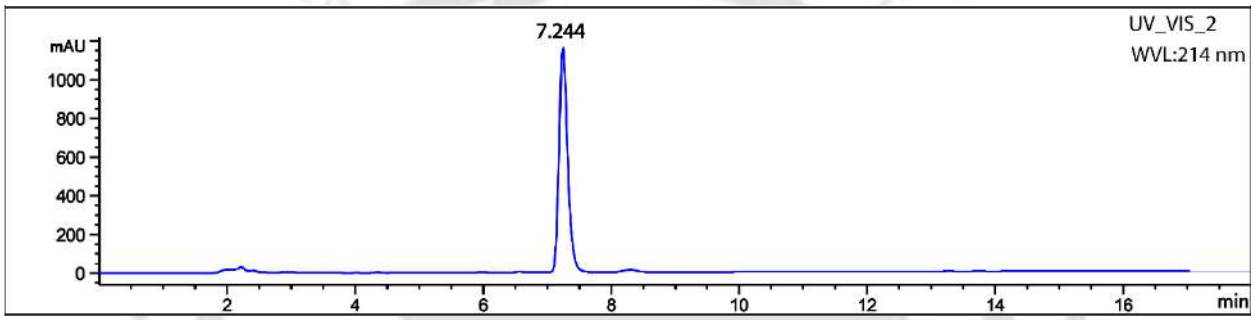

Figure A44. Analytical HPLC trace of **33-Hexa** in ACN/H_2O.

TH-3141_166122021

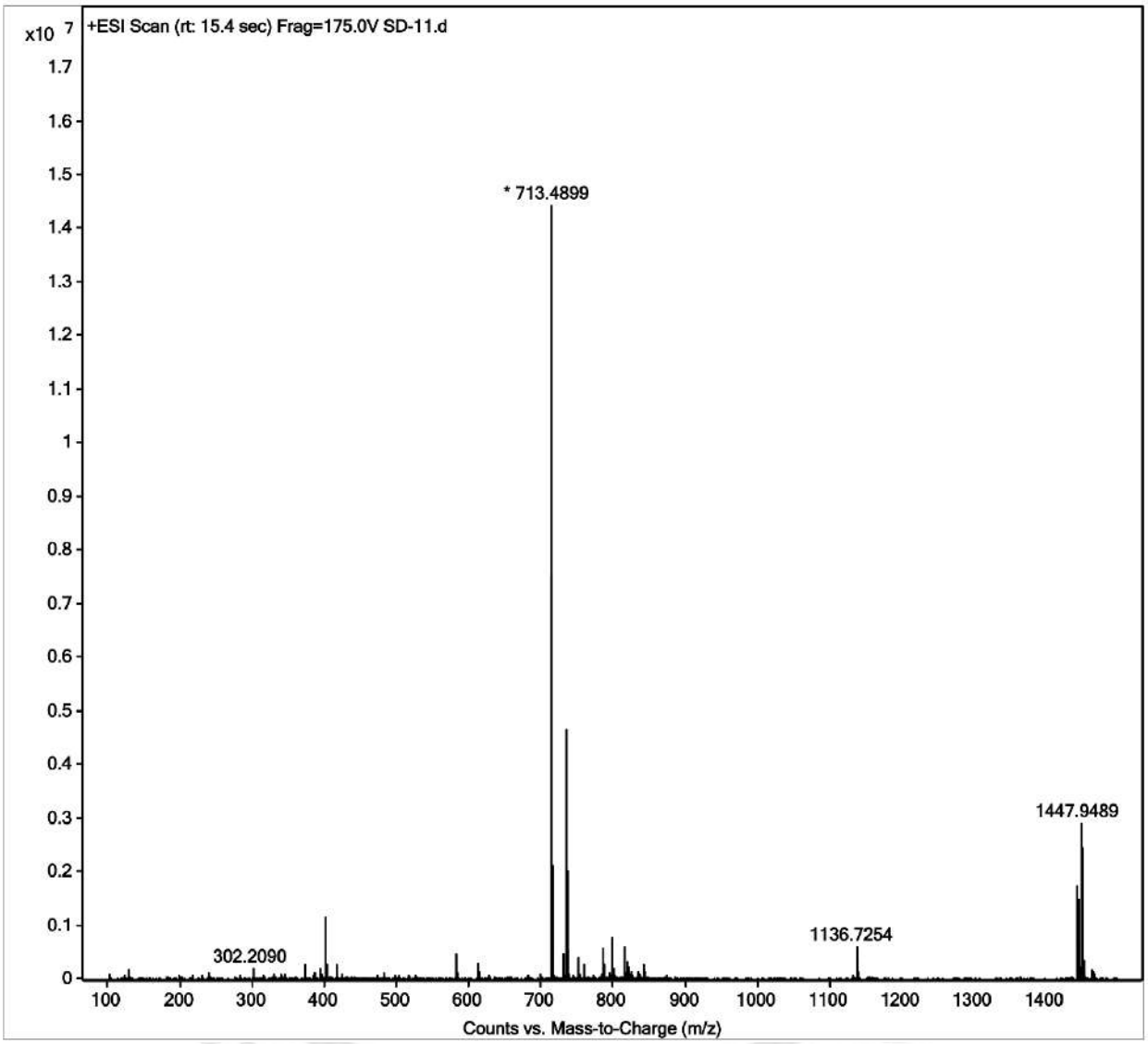

Figure A45. ESI-MS (m/z) of **31-Hexa**. Calc. for $(M+H)^+$ $C_{35}H_{64}N_6O_9$ = 713.4768 Da; Obs. = 713.4899 Da, $(2M+Na)^+$ = 1447.9489 Da.

TH-3141_166122021

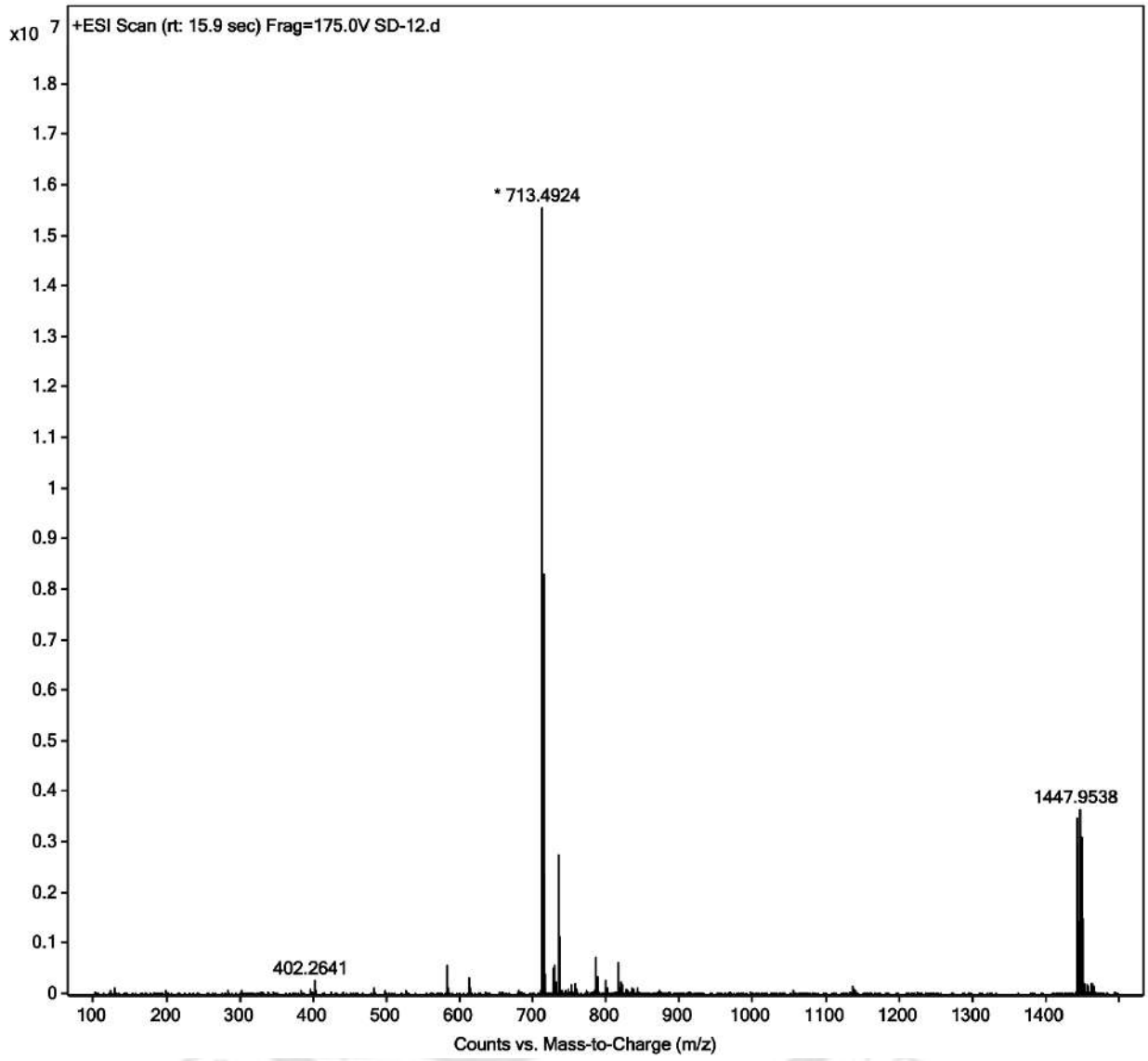

Figure A46. ESI-MS (m/z) of **32-Hexa**. Calc. for $(M+H)^+$ $C_{35}H_{64}N_6O_9$ = 713.4768 Da; Obs. = 713.4924 Da, $(2M+Na)^+$ = 1447.5938 Da.

TH-3141_166122021

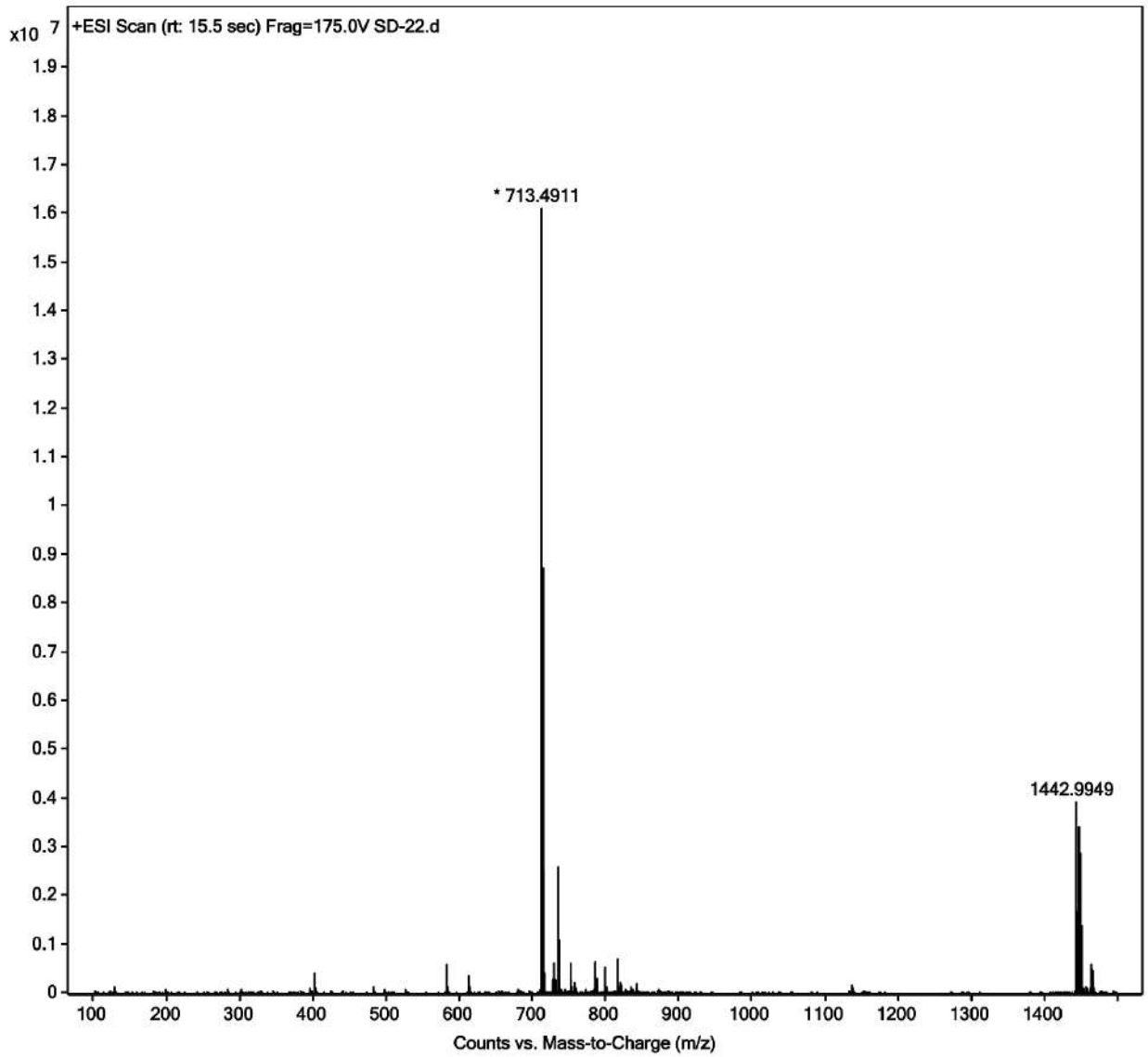

Figure A47. ESI-MS (m/z) of **33-Hexa**. Calc. for $(M+H)^+$ $C_{35}H_{64}N_6O_9$ = 713.4768 Da; Obs. = 713.4911 Da, $(2M+NH_4)^+$ = 1442.9949 Da.

TH-3141_166122021

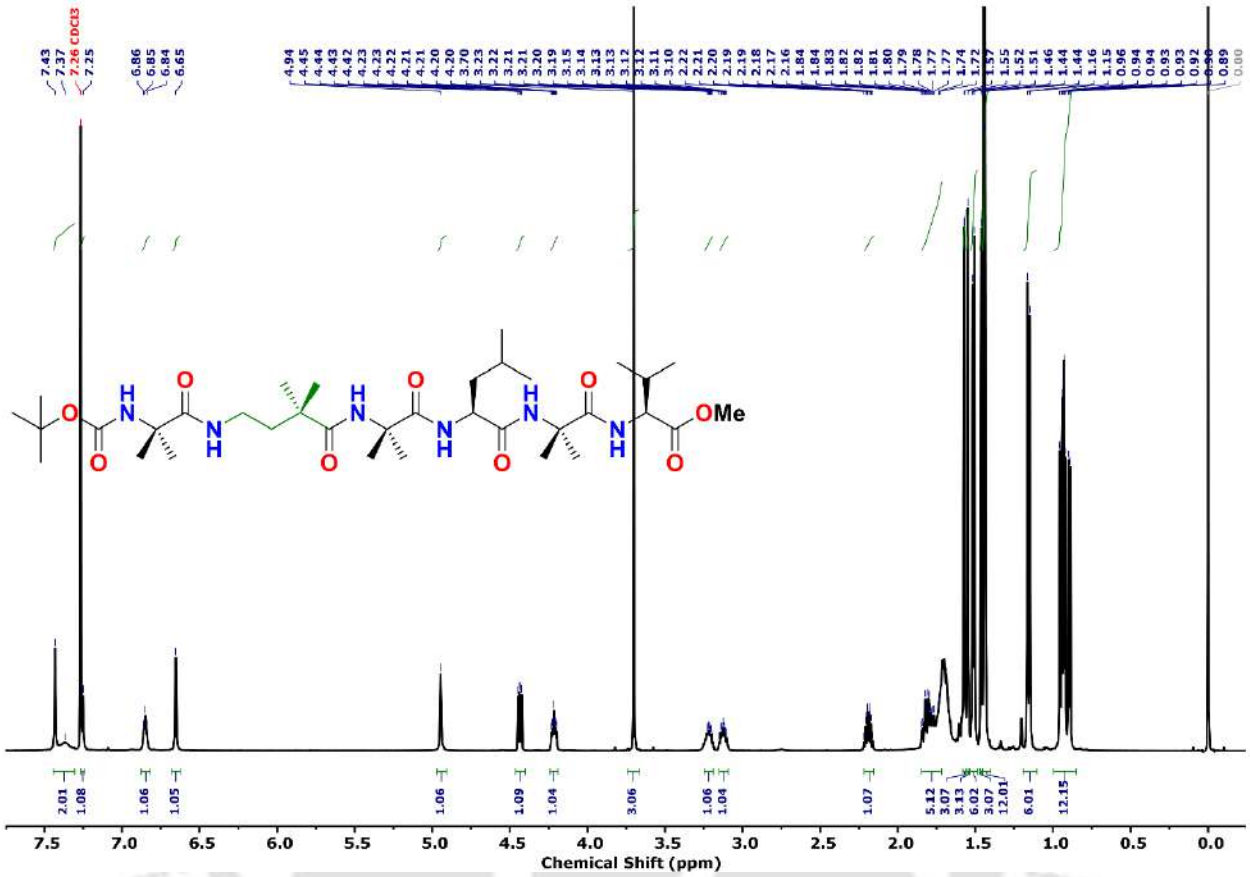

Figure A48. 600 MHz ^{1}H NMR spectra of **31-Hexa** in $CDCl_3$ at 5 mM concentration (298 K).

TH-3141_166122021

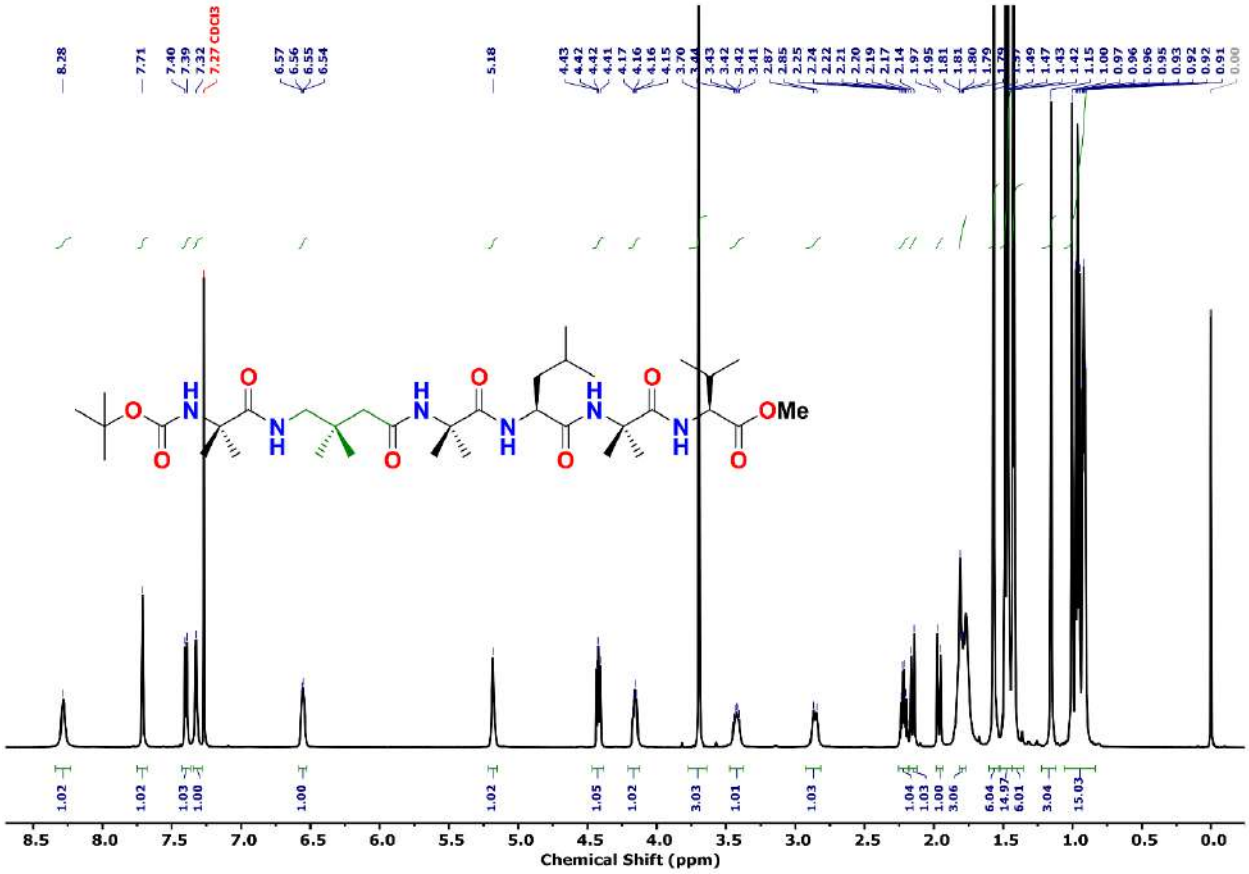

Figure A49. 600 MHz ^{1}H NMR spectra of **32-Hexa** in $CDCl_3$ at 5 mM concentration (298 K).

TH-3141_166122021

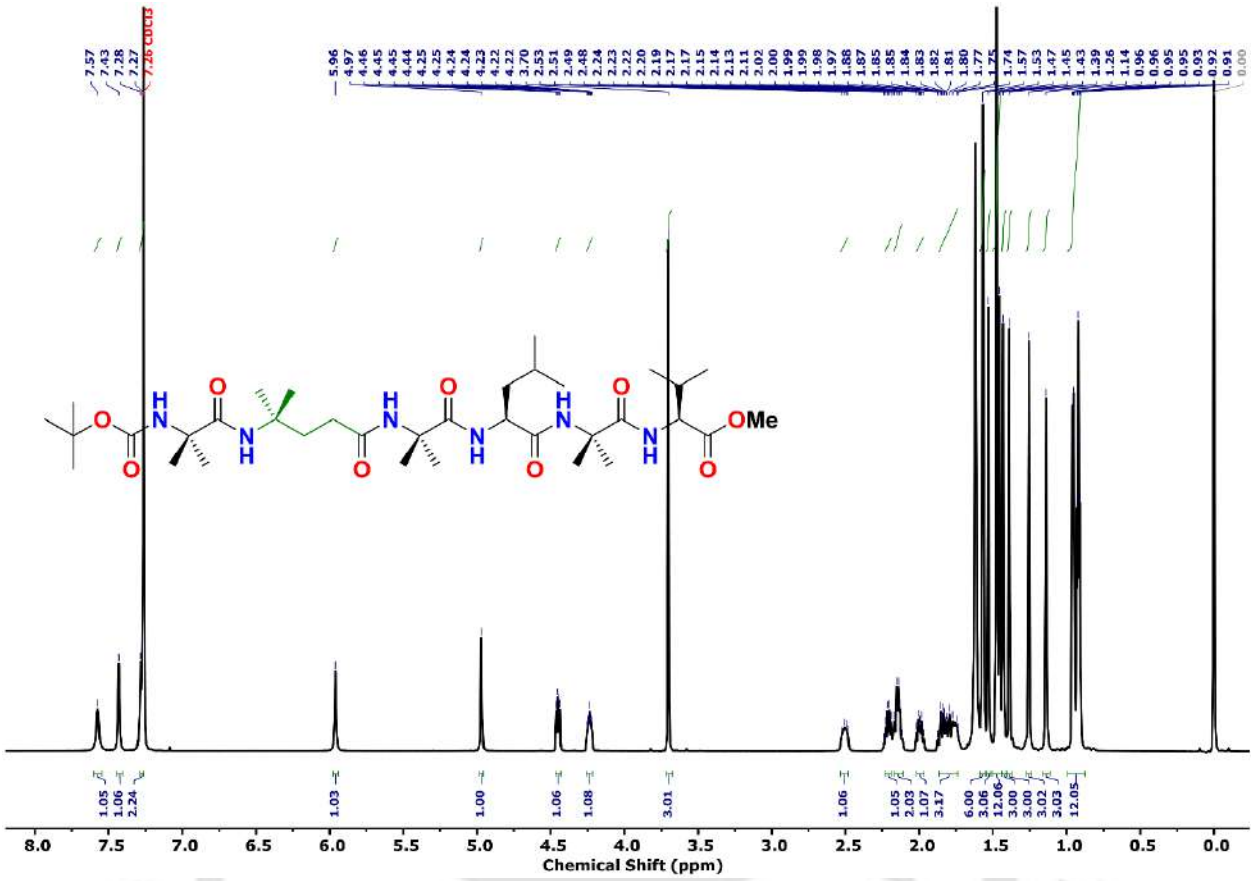

Figure A50. 600 MHz ^{1}H NMR spectra of **33-Hexa** in $CDCl_3$ at 5 mM concentration (298 K).

TH-3141_166122021

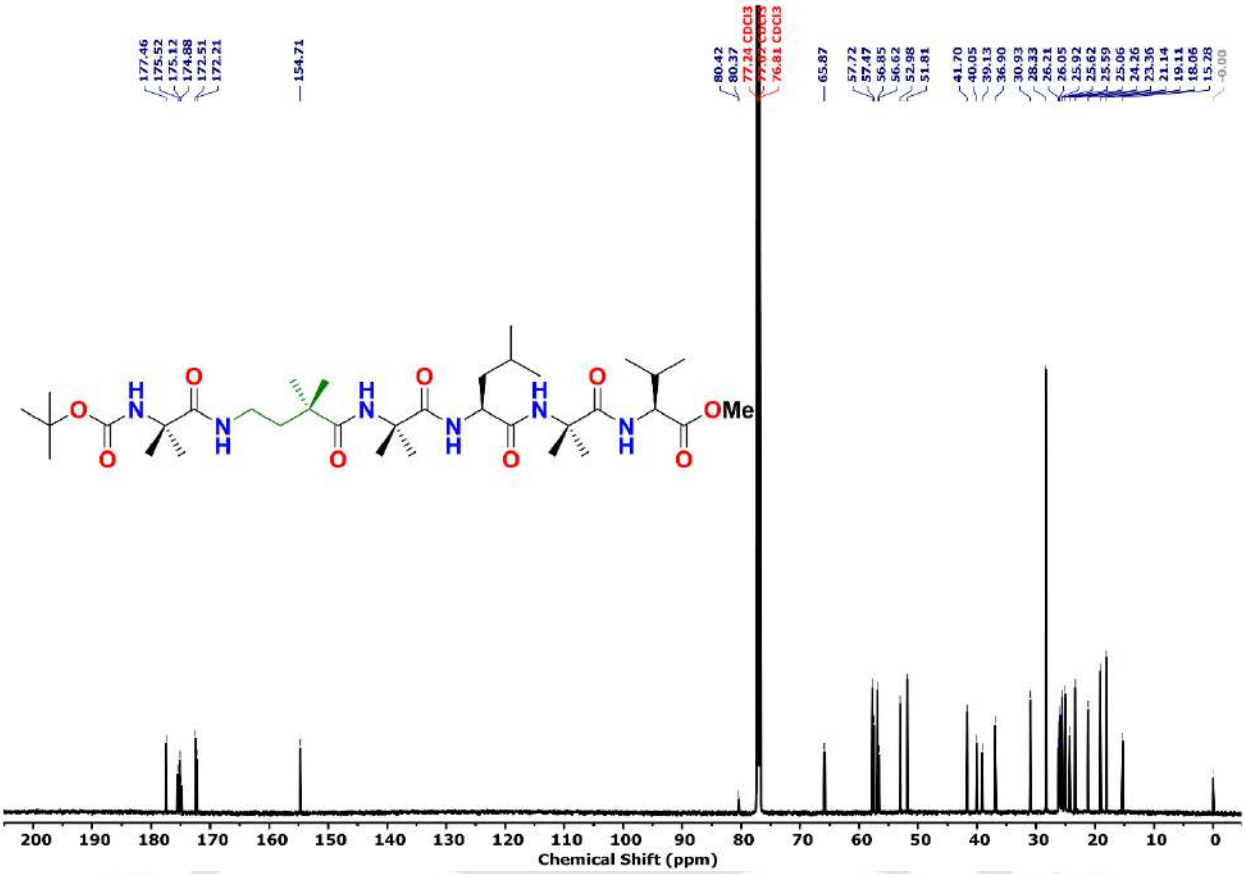

Figure A51. 150 MHz ^{1}H NMR spectra of **31-Hexa** in $CDCl_3$ at 5 mM concentration (298 K).

TH-3141_166122021

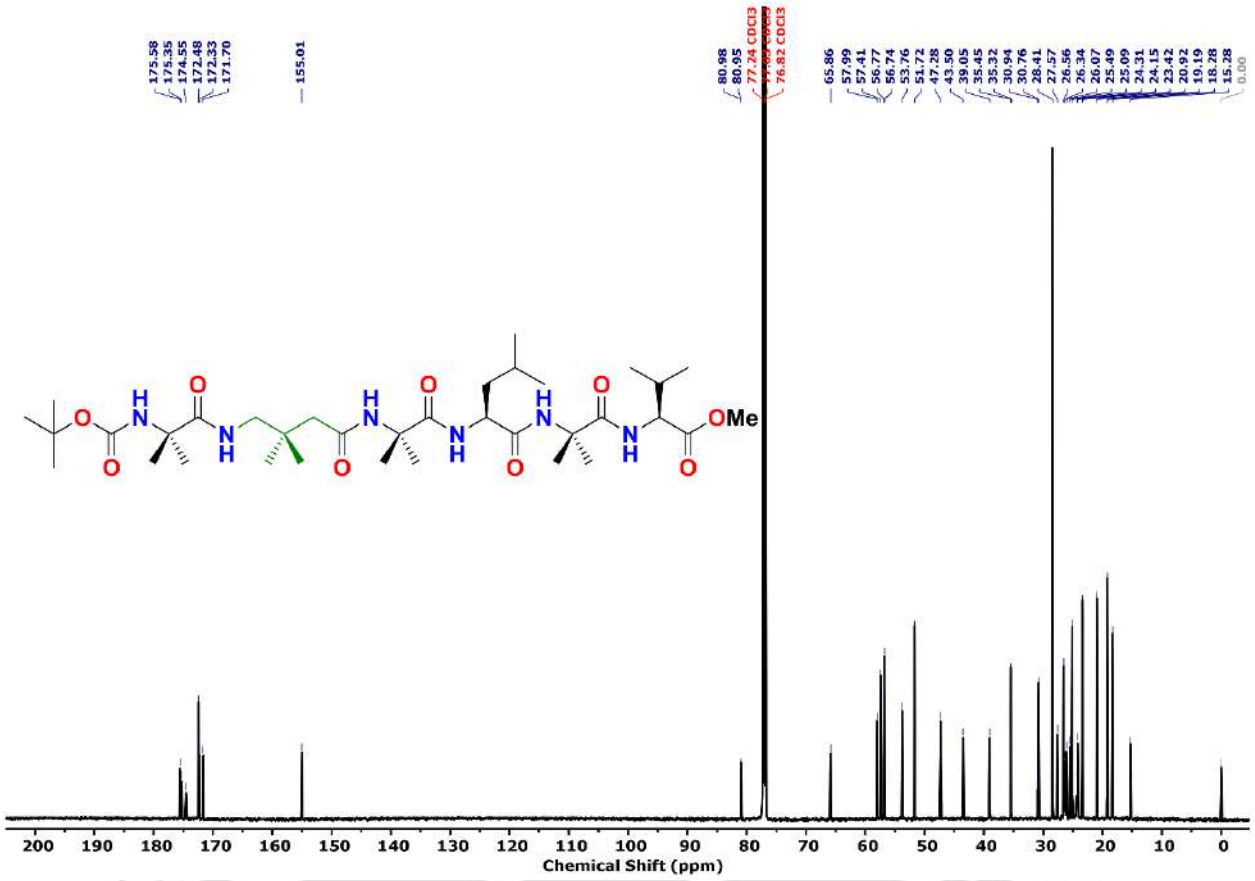

Figure A52. 150 MHz ^{1}H NMR spectra of **32-Hexa** in $CDCl_3$ at 5 mM concentration (298 K).

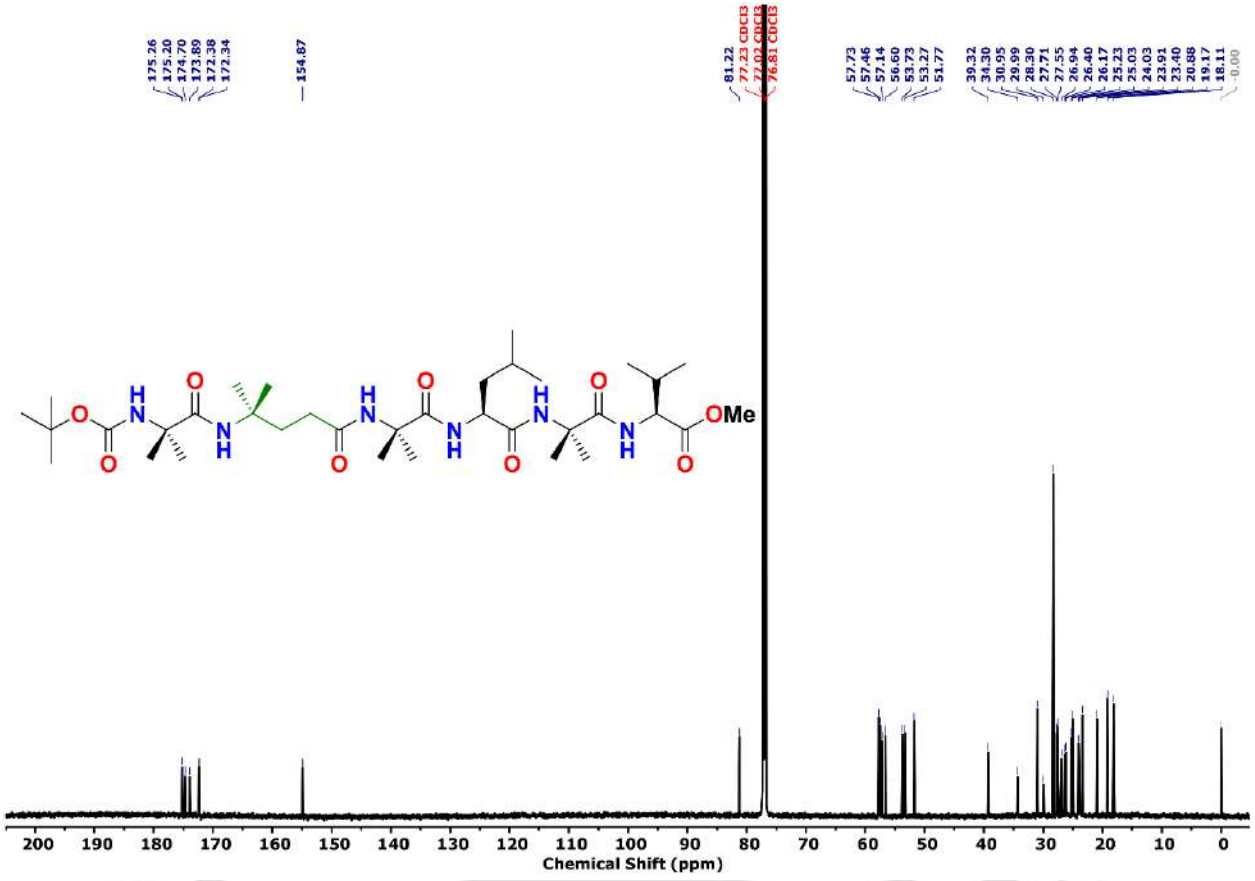

Figure A53. 150 MHz ^{1}H NMR spectra of **33-Hexa** in $CDCl_3$ at 5 mM concentration (298 K).

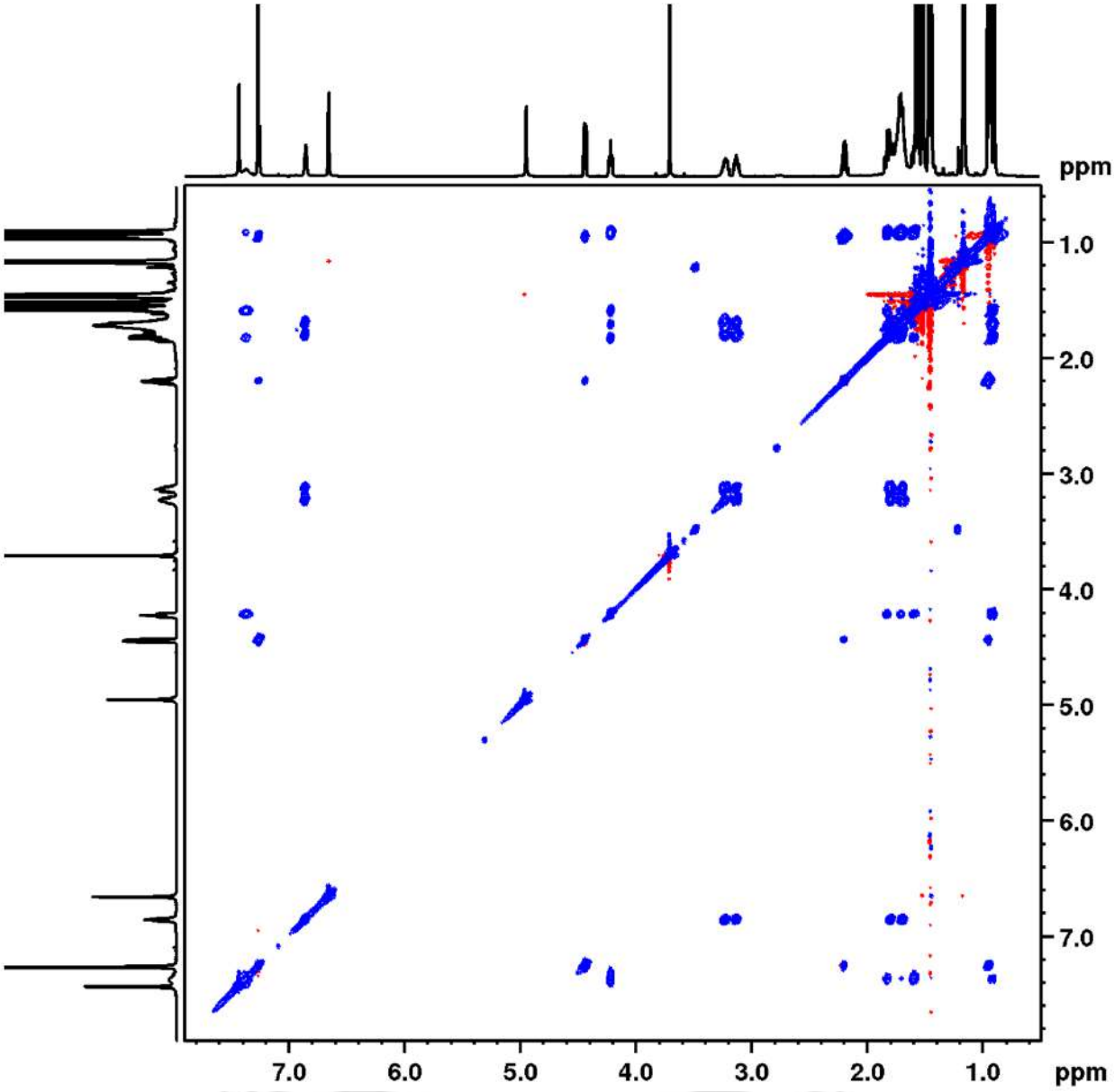

Figure A54. 600 MHz TOCSY spectra of peptide **31-Hexa** at 5 mM concentration in $CDCl_3$ at 298 K.

TH-3141_166122021

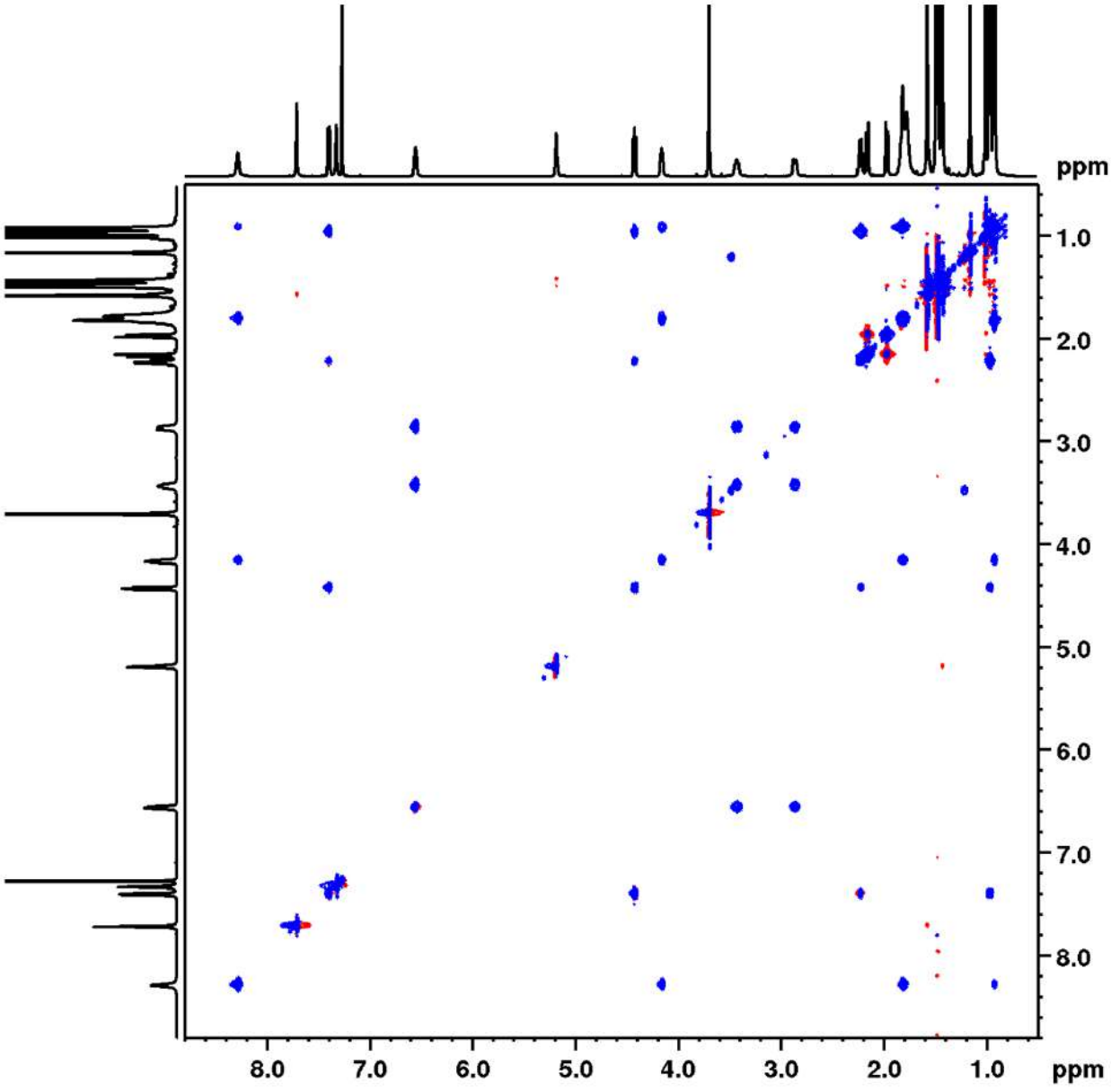

Figure A55. 600 MHz TOCSY spectra of peptide **32-Hexa** at 5 mM concentration in $CDCl_3$ at 298 K.

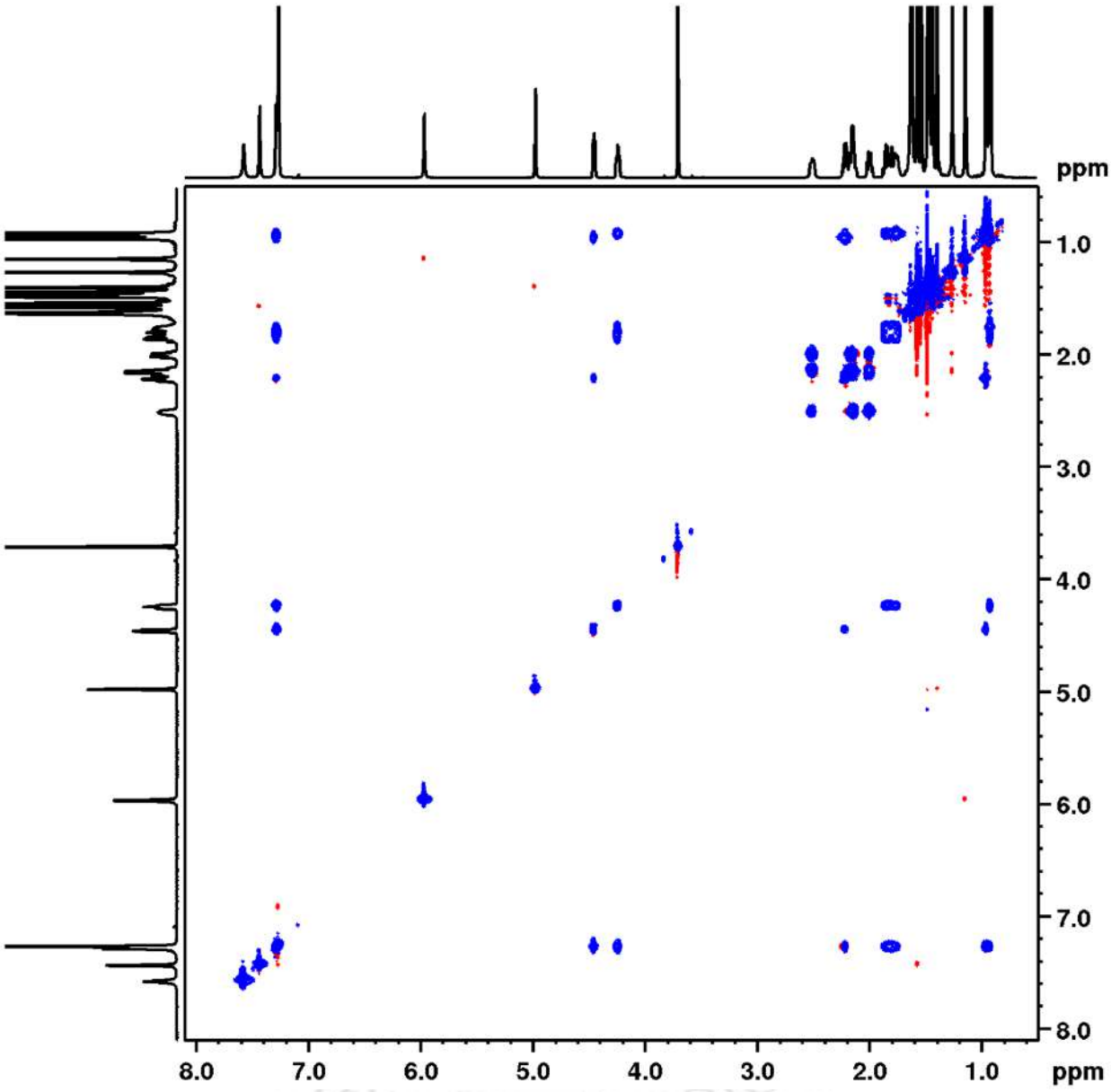

Figure A56. 600 MHz TOCSY spectra of peptide **33-Hexa** at 5 mM concentration in $CDCl_3$ at 298 K.

TH-3141_166122021

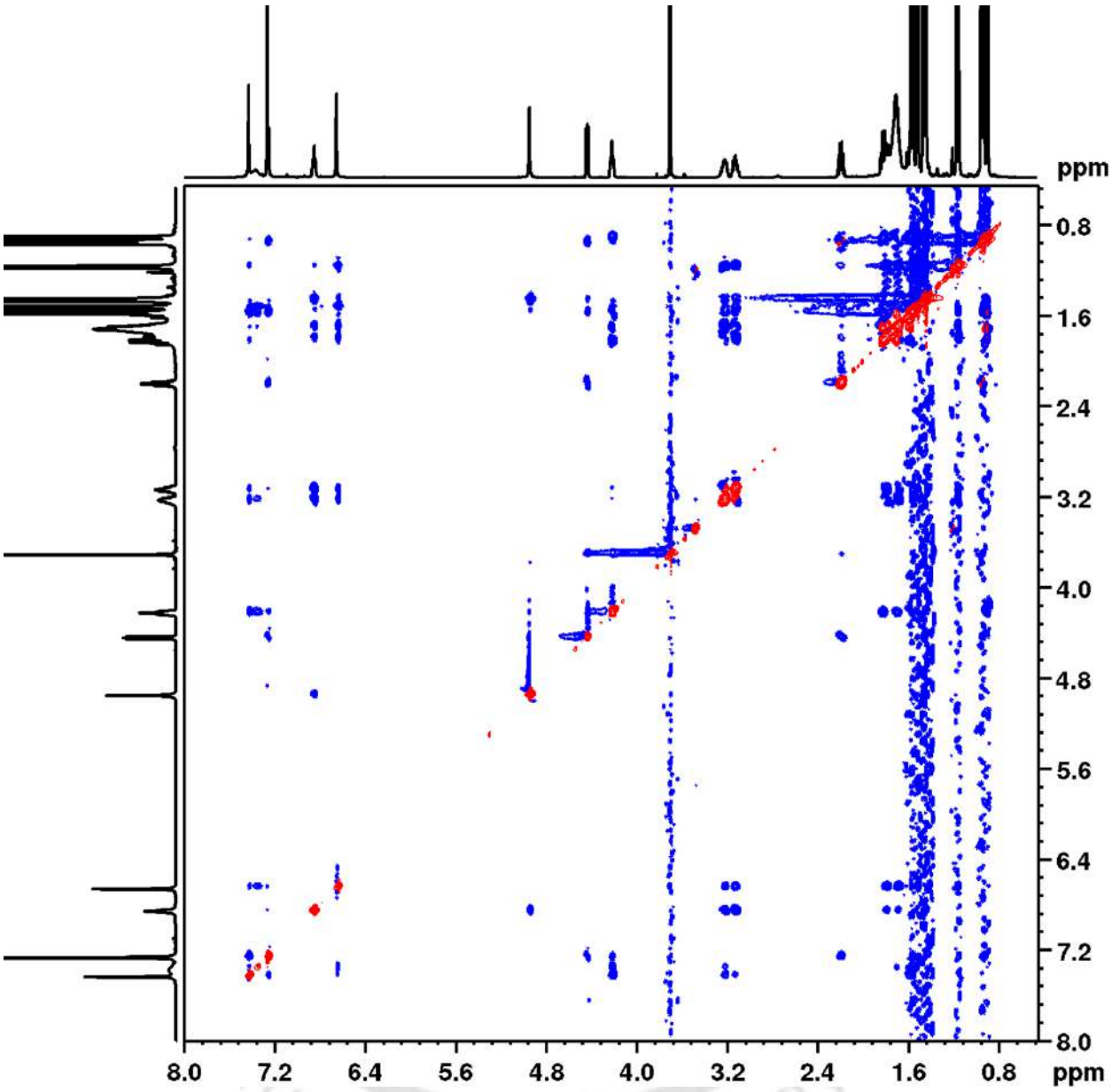

Figure A57. 600 MHz ROESY spectra of peptide **31-Hexa** at 5 mM concentration in $CDCl_3$ at 298 K.

TH-3141_166122021

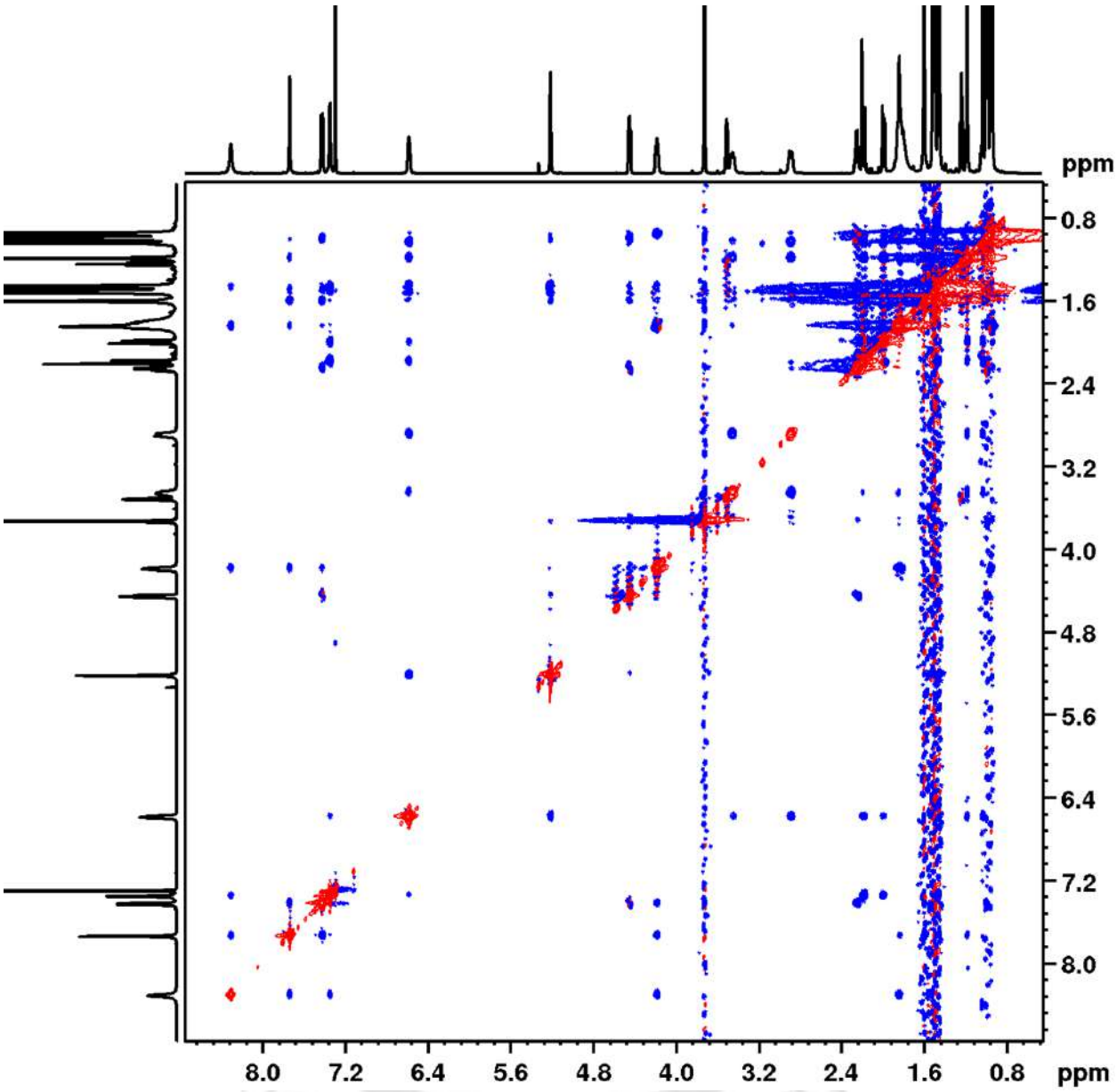

Figure A58. 600 MHz ROESY spectra of peptide **32-Hexa** at 5 mM concentration in $CDCl_3$ at 298 K.

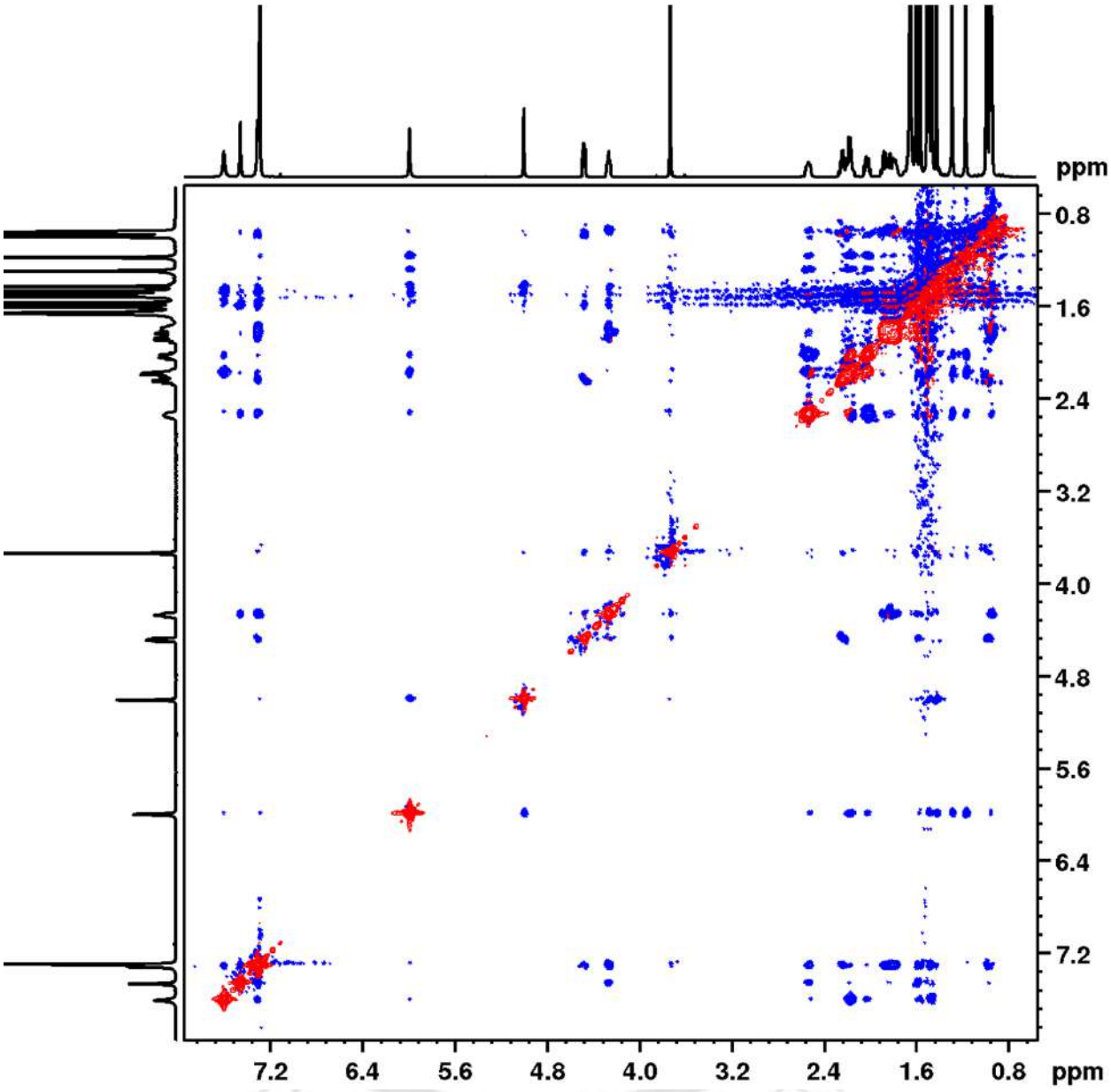

Figure A59. 600 MHz ROESY spectra of peptide **33-Hexa** at 5 mM concentration in $CDCl_3$ at 298 K.

TH-3141_166122021

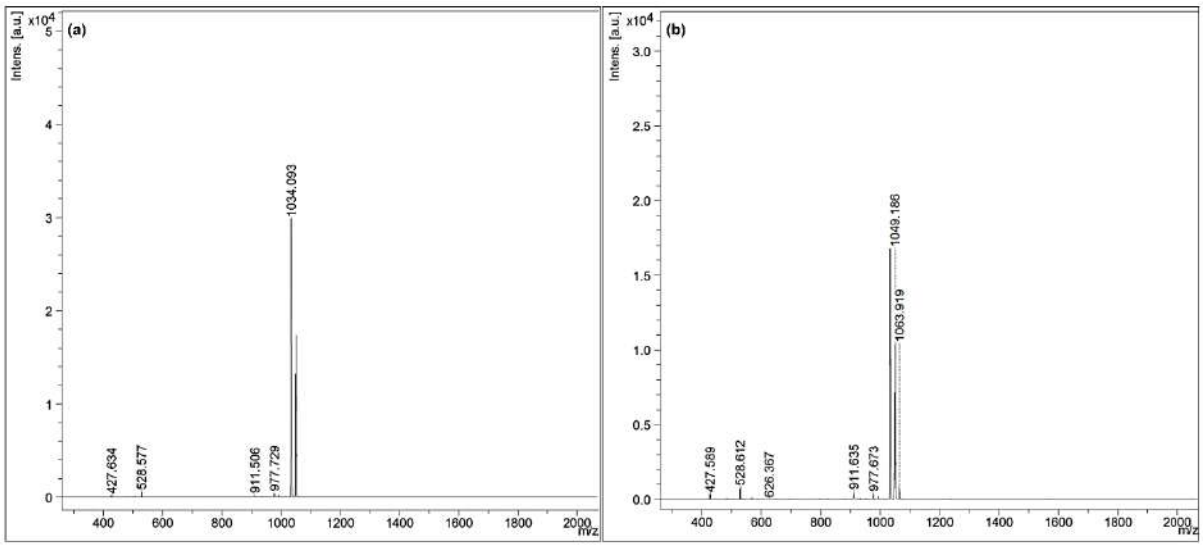

Figure A60. MALDI-TOF of **31-Nona**, analytical HPLC peak at (a) 9.7 min [Calc. $(M+Na+2H)^+$ for $C_{50}H_{91}N_9O_{12}$ = 1034.6841 Da, Obs. = 1034.093 Da] and (b) 10.3 min [Calc. $(M+K)^+$ for $C_{50}H_{91}N_9O_{12}$ = 1048.6424 Da, Obs. = 1049.186 Da].

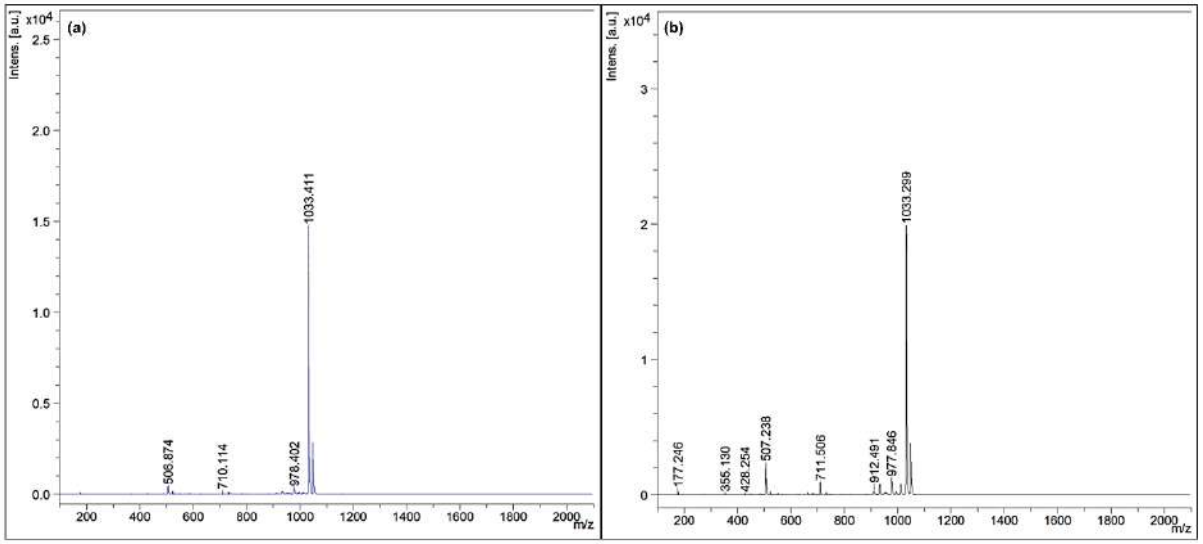

Figure A61. MALDI-TOF of **32-Nona**, analytical HPLC peak at (a) 11.3 min [Calc. $(M+Na+H)^+$ for $C_{50}H_{91}N_9O_{12}$ = 1033.6763 Da, Obs. = 1033.411 Da] and (b) 12.7 min [Calc. $(M+Na+H)^+$ for $C_{50}H_{91}N_9O_{12}$ = 1033.6763 Da, Obs. = 1033.299 Da].

TH-3141_166122021

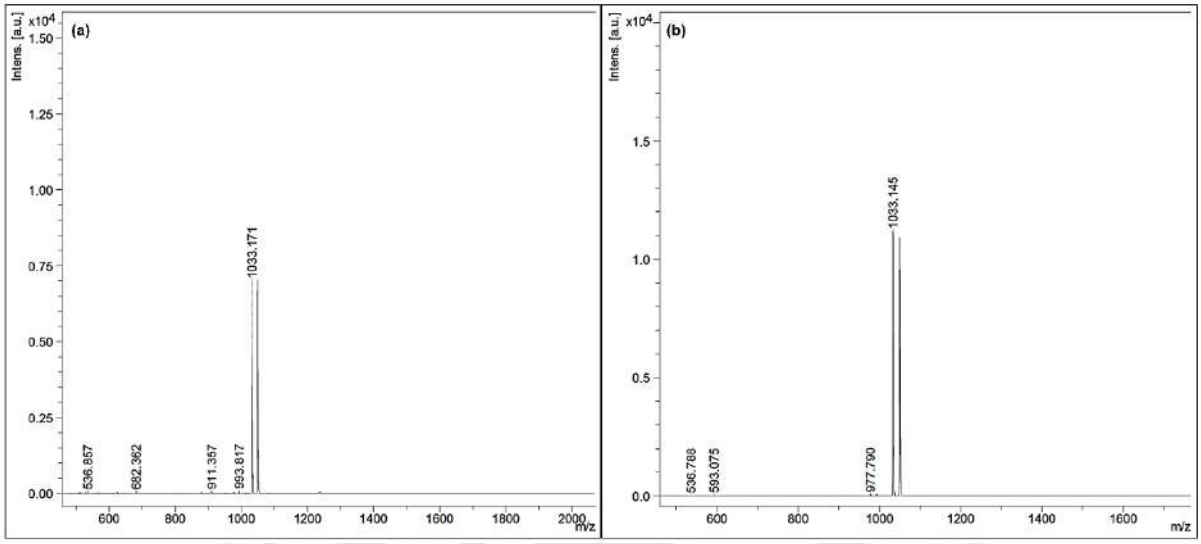

Figure A62. MALDI-TOF of **33-Nona**, analytical HPLC peak at (a) 10.9 min [Calc. $(M+Na+H)^+$ for $C_{50}H_{91}N_9O_{12}$ = 1033.6763 Da, Obs. = 1033.171 Da] and (b) 12.4 min [Calc. $(M+Na+H)^+$ for $C_{50}H_{91}N_9O_{12}$ = 1033.6763 Da, Obs. = 1033.145 Da].

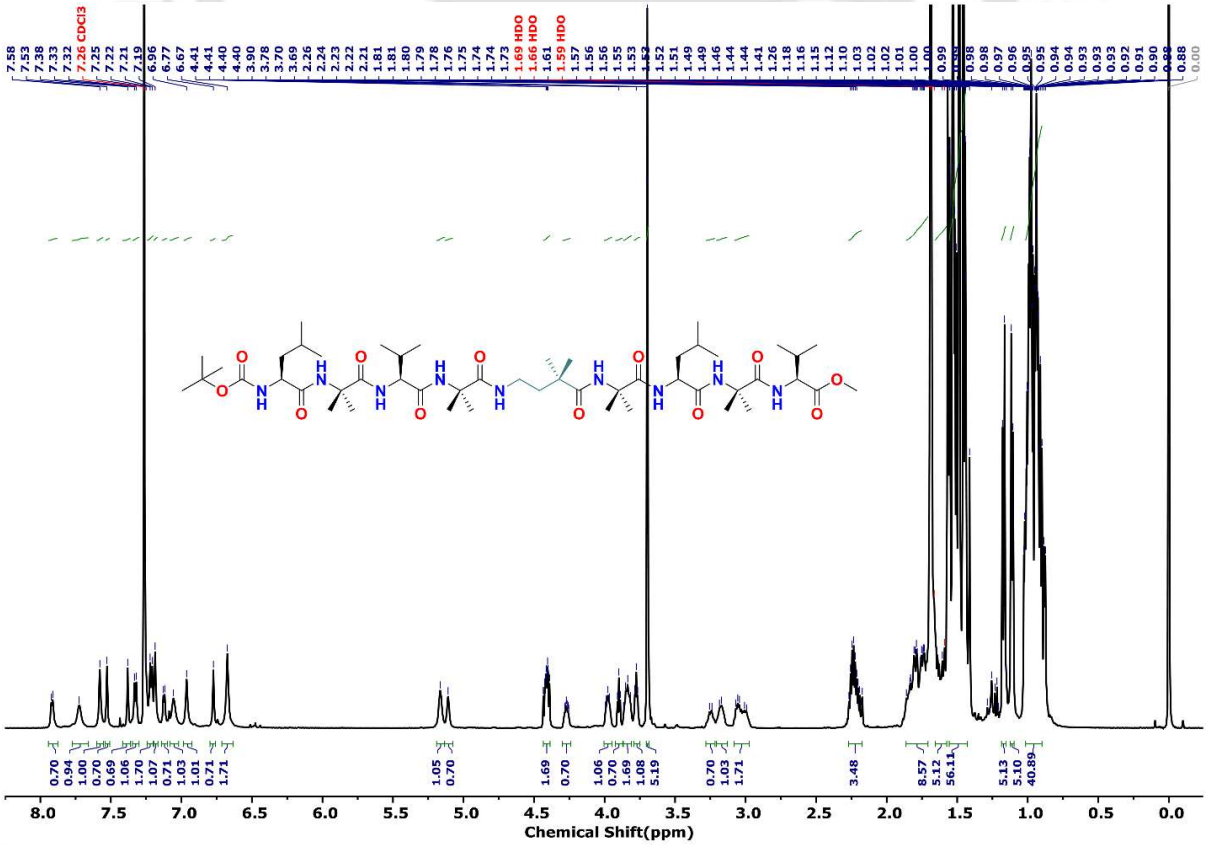

Figure A63. 600 MHz ^{1}H NMR spectra of **31-Nona** in $CDCl_3$ at 5 mM concentration (298 K).

TH-3141_166122021

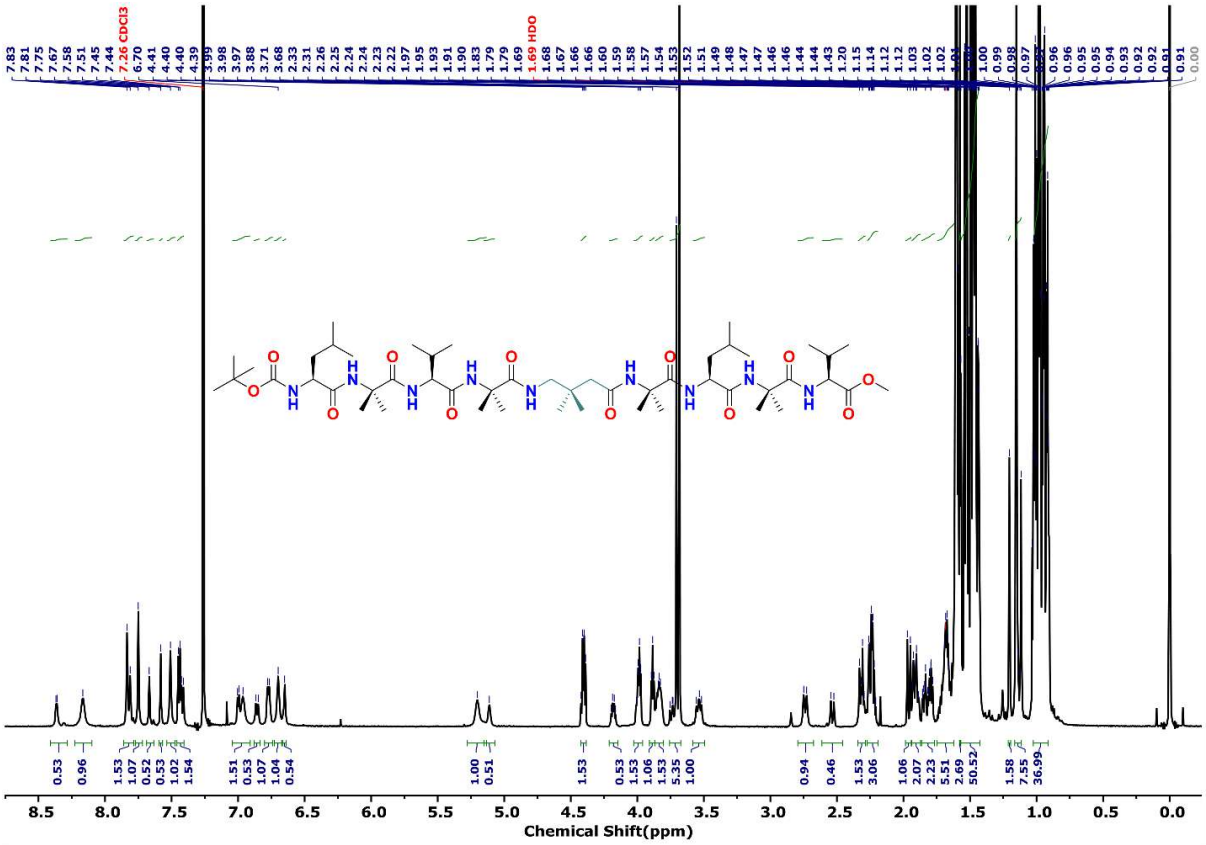

Figure A64. 600 MHz ^{1}H NMR spectra of **32-Nona** in $CDCl_3$ at 5 mM concentration (298 K).

TH-3141_166122021

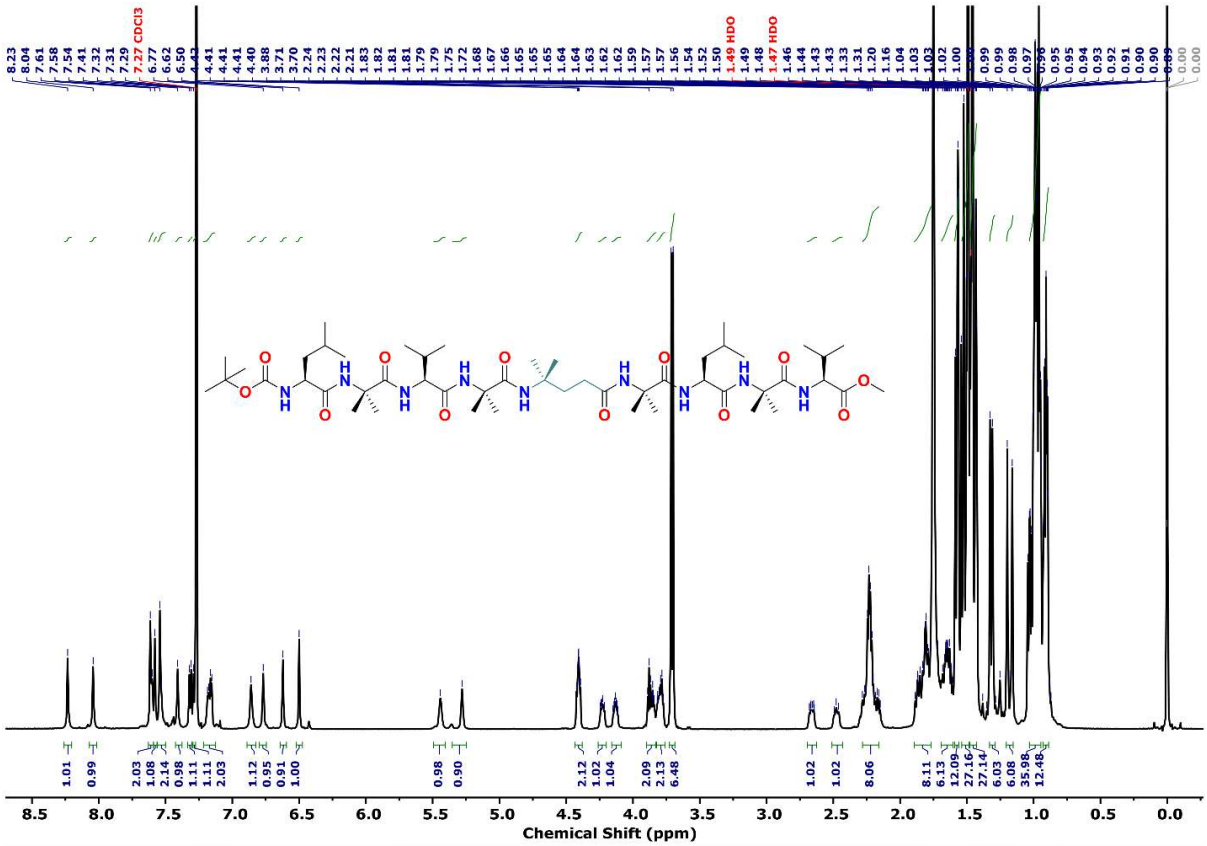

Figure A65. 600 MHz ^{1}H NMR spectra of **33-Nona** in $CDCl_3$ at 5 mM concentration (298 K).

TH-3141_166122021

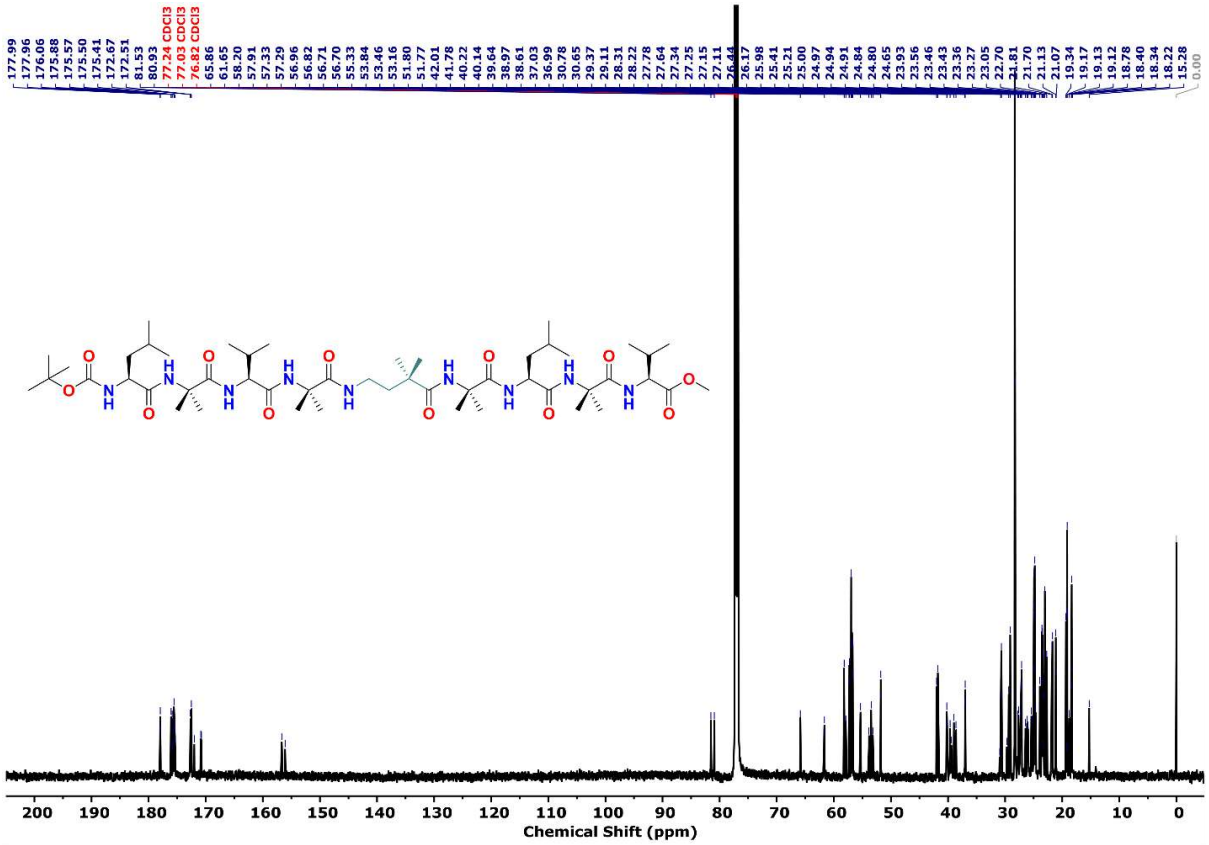

Figure A66. 150 MHz ^{13}C NMR spectra of **31-Nona** in $CDCl_3$ at 5 mM concentration (298 K).

TH-3141_166122021

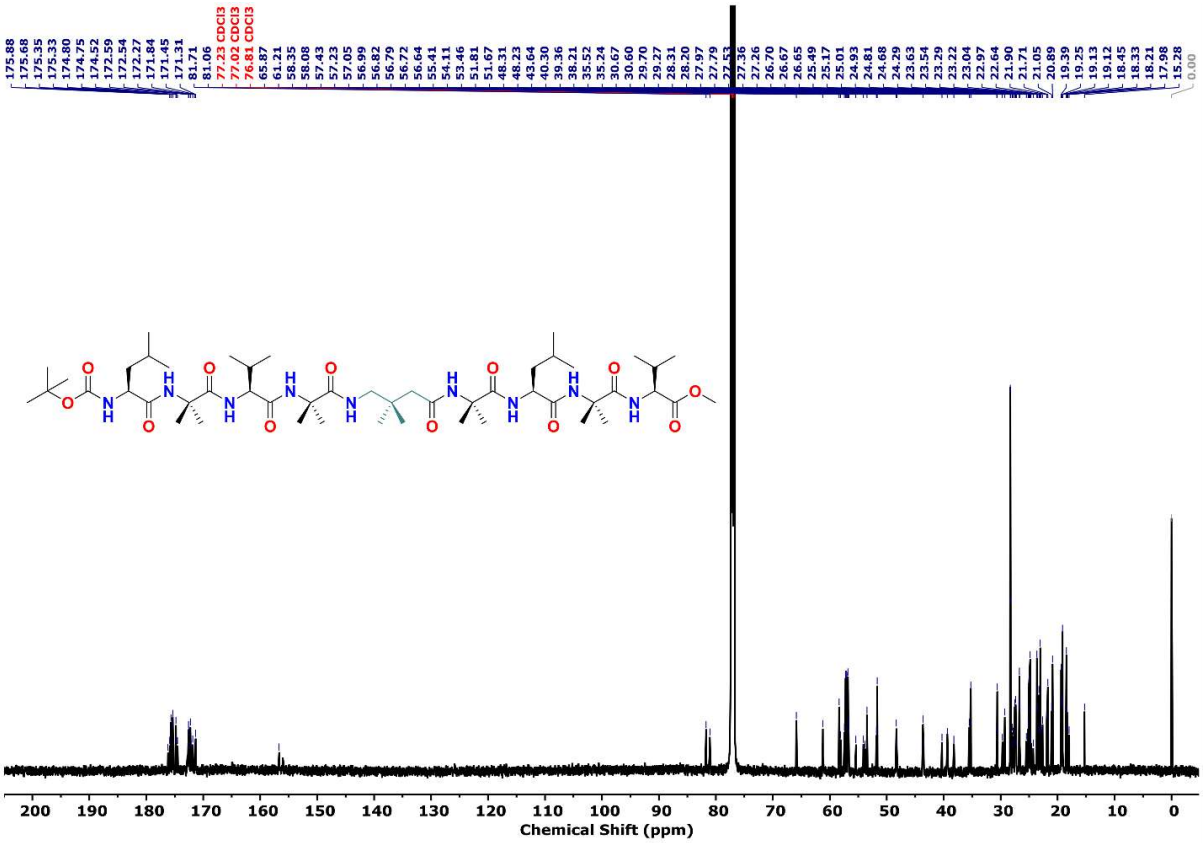

Figure A67. 150 MHz ^{13}C NMR spectra of **32-Nona** in $CDCl_3$ at 5 mM concentration (298 K).

TH-3141_166122021

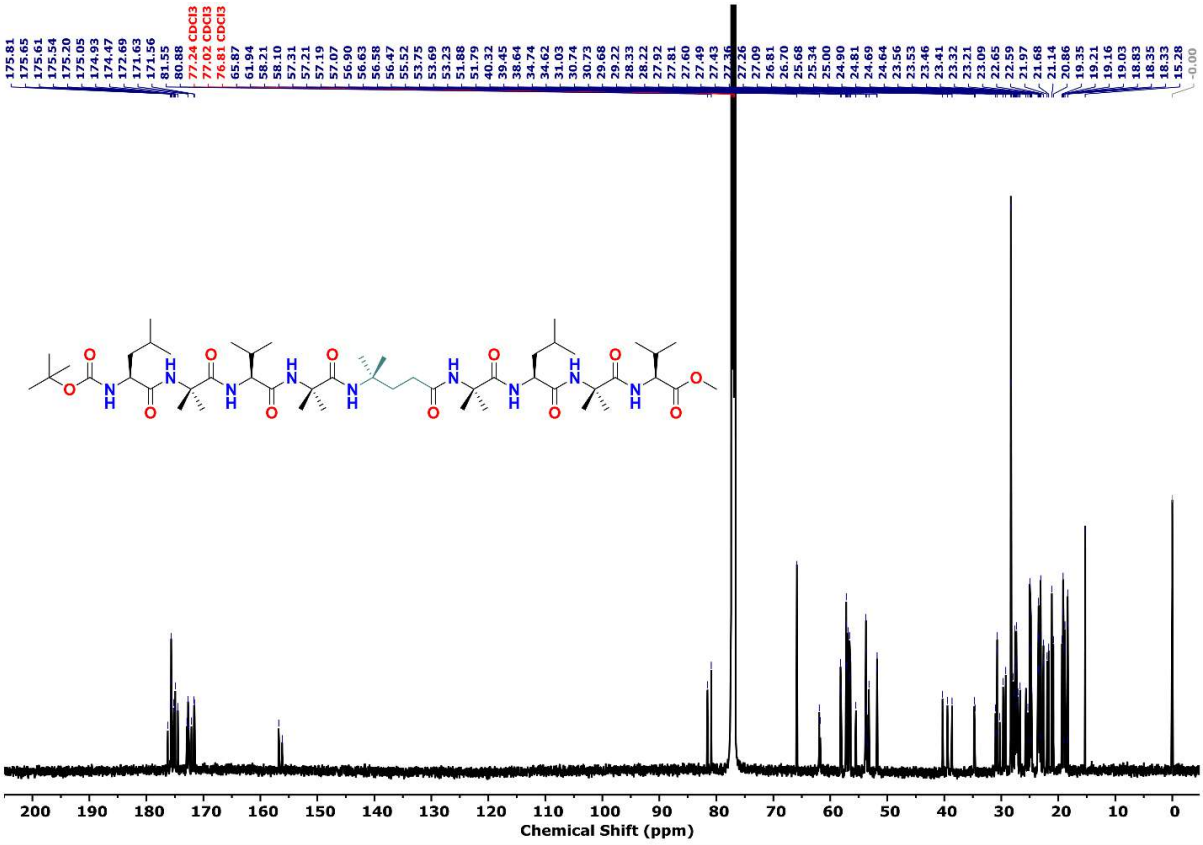

Figure A68. 150 MHz ^{13}C NMR spectra of **33-Nona** in $CDCl_3$ at 5 mM concentration (298 K).

TH-3141_166122021

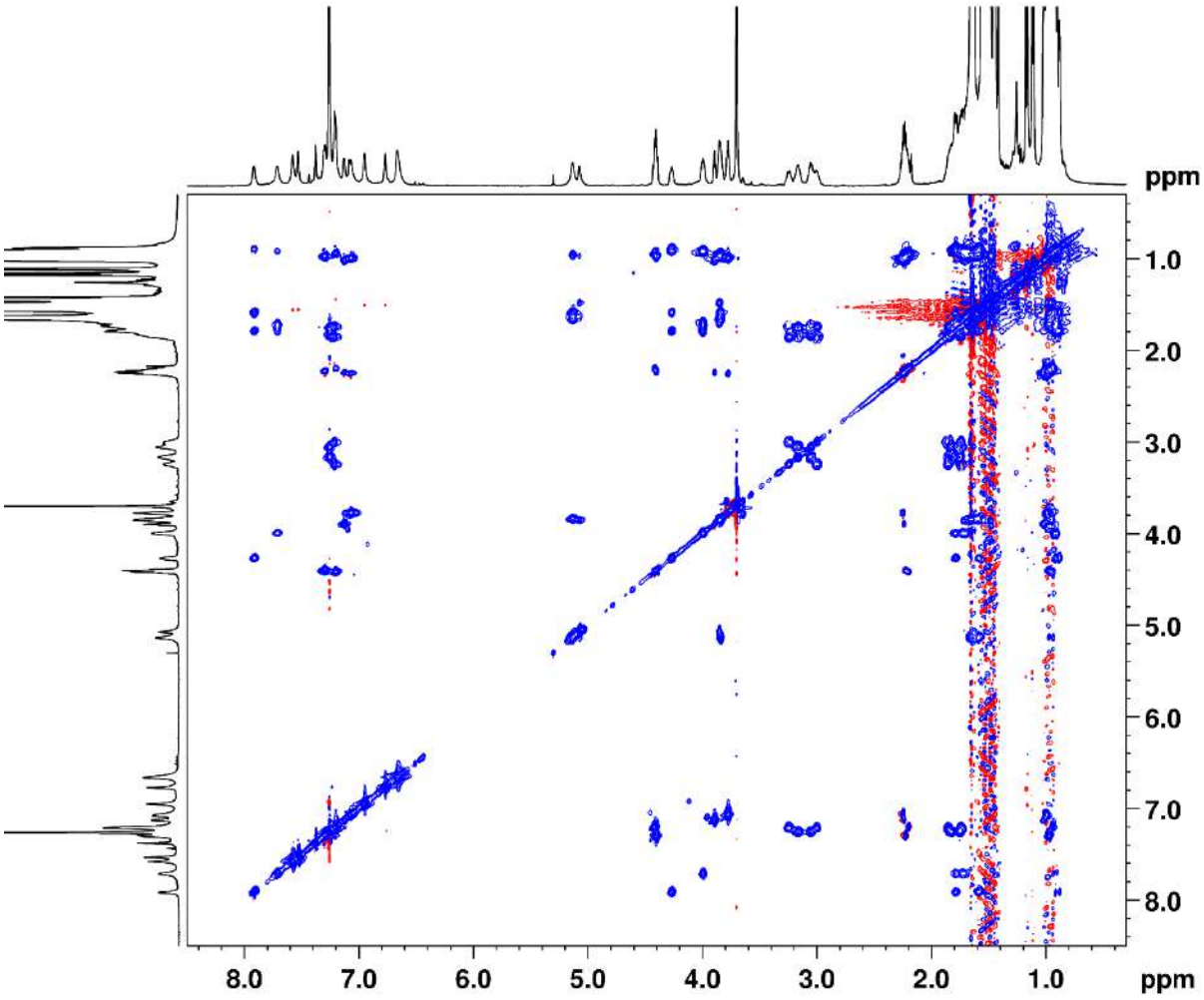

Figure A69. 600 MHz TOCSY spectra of peptide **31-Nona** at 5 mM concentration in $CDCl_3$ at 298 K.

TH-3141_166122021

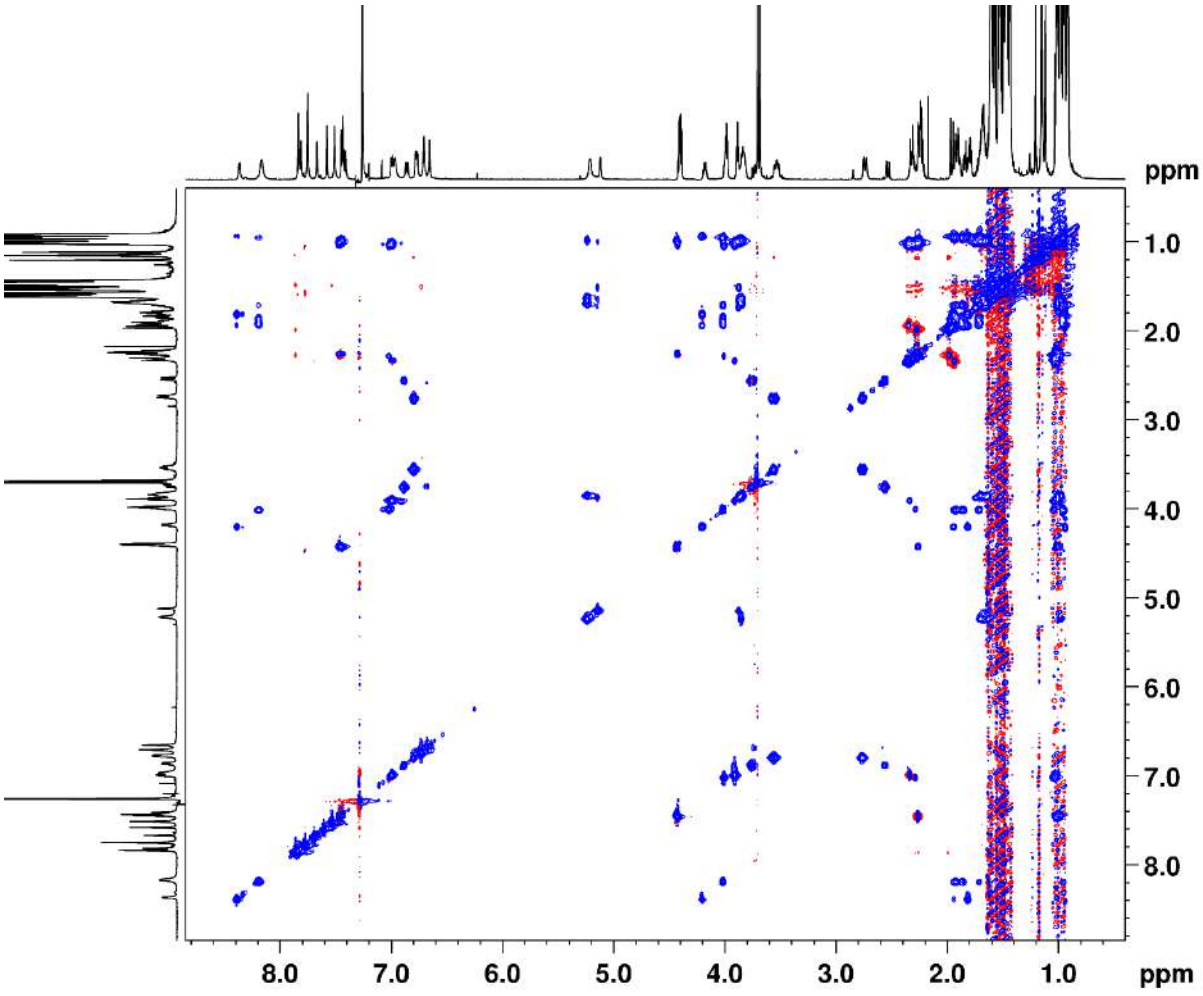

Figure A70. 600 MHz TOCSY spectra of peptide **32-Nona** at 5 mM concentration in $CDCl_3$ at 298 K.

TH-3141_166122021

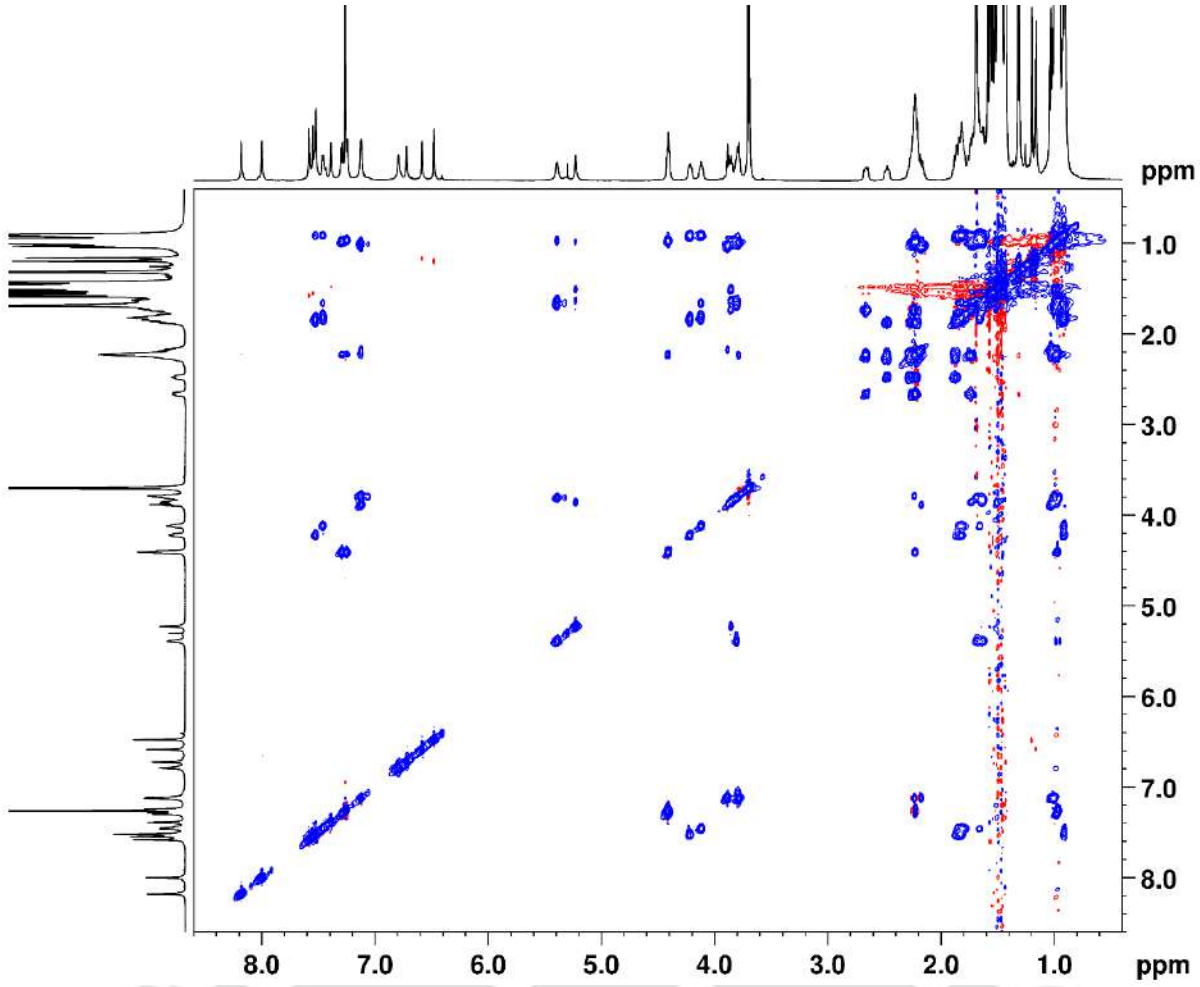

Figure A71. 600 MHz TOCSY spectra of peptide **33-Nona** at 5 mM concentration in $CDCl_3$ at 298 K.

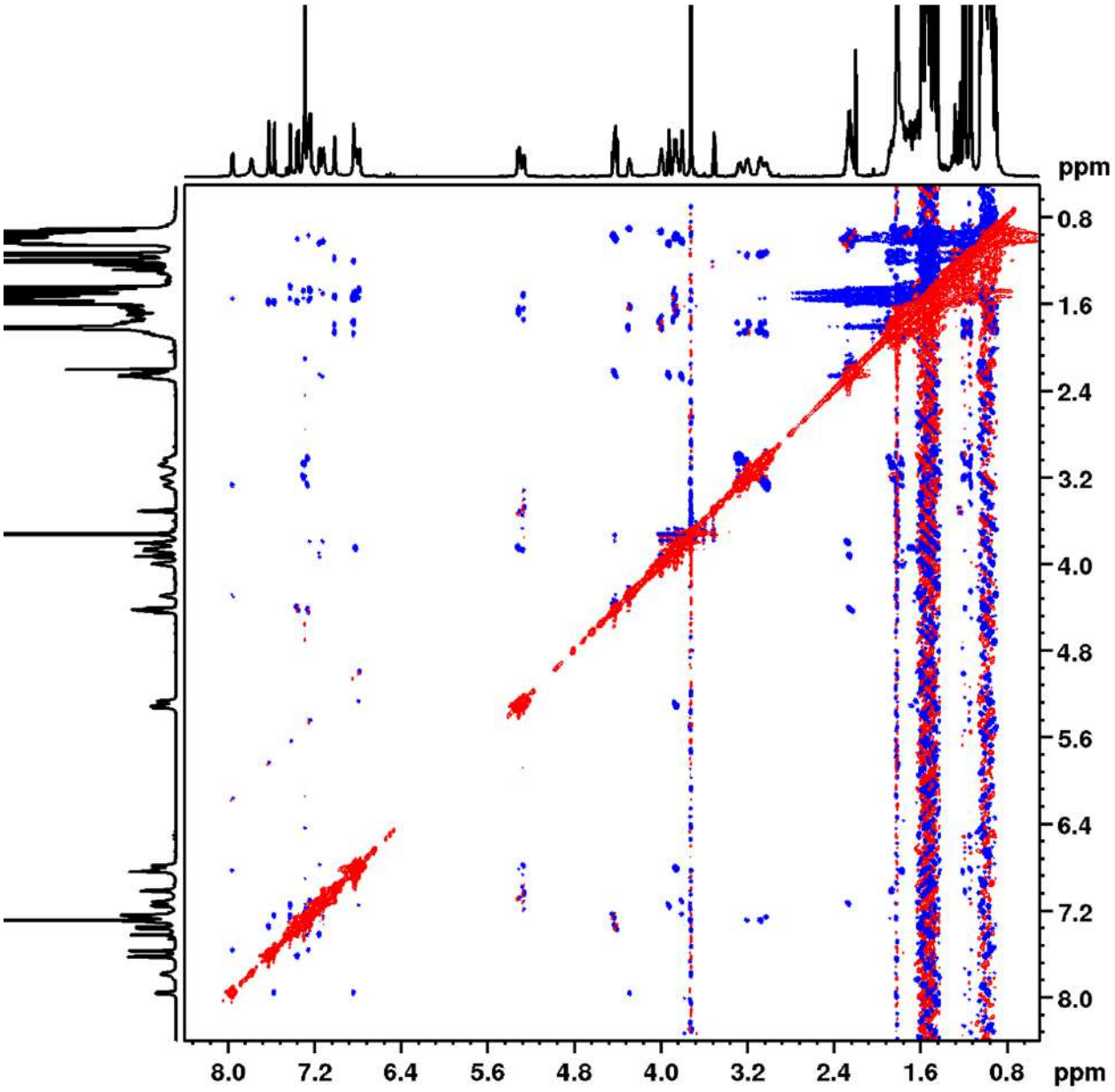

Figure A72. 600 MHz ROESY spectra of peptide **31-Nona** at 5 mM concentration in $CDCl_3$ at 298 K.

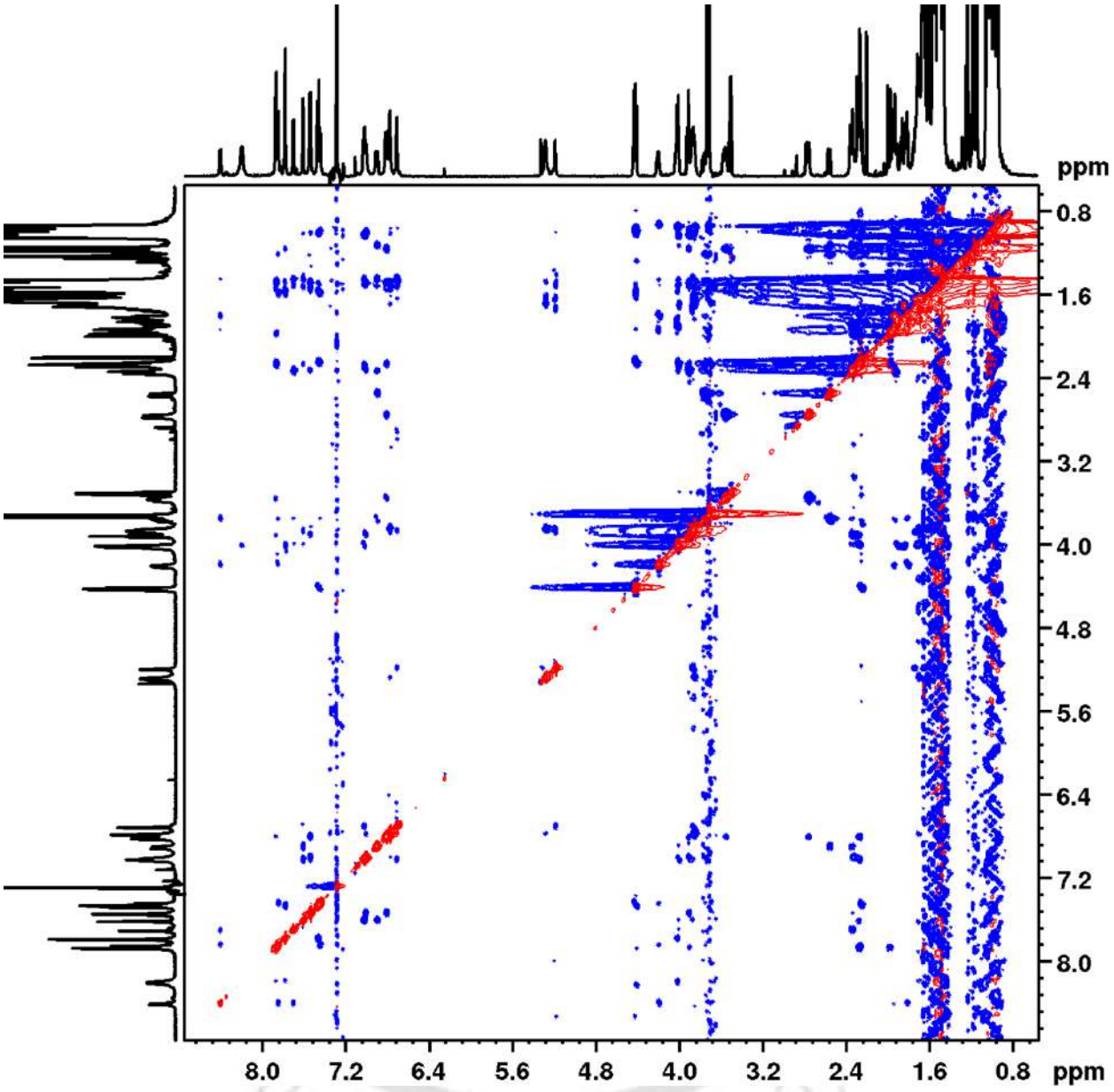

Figure A73. 600 MHz ROESY spectra of peptide **32-Nona** at 5 mM concentration in $CDCl_3$ at 298 K.

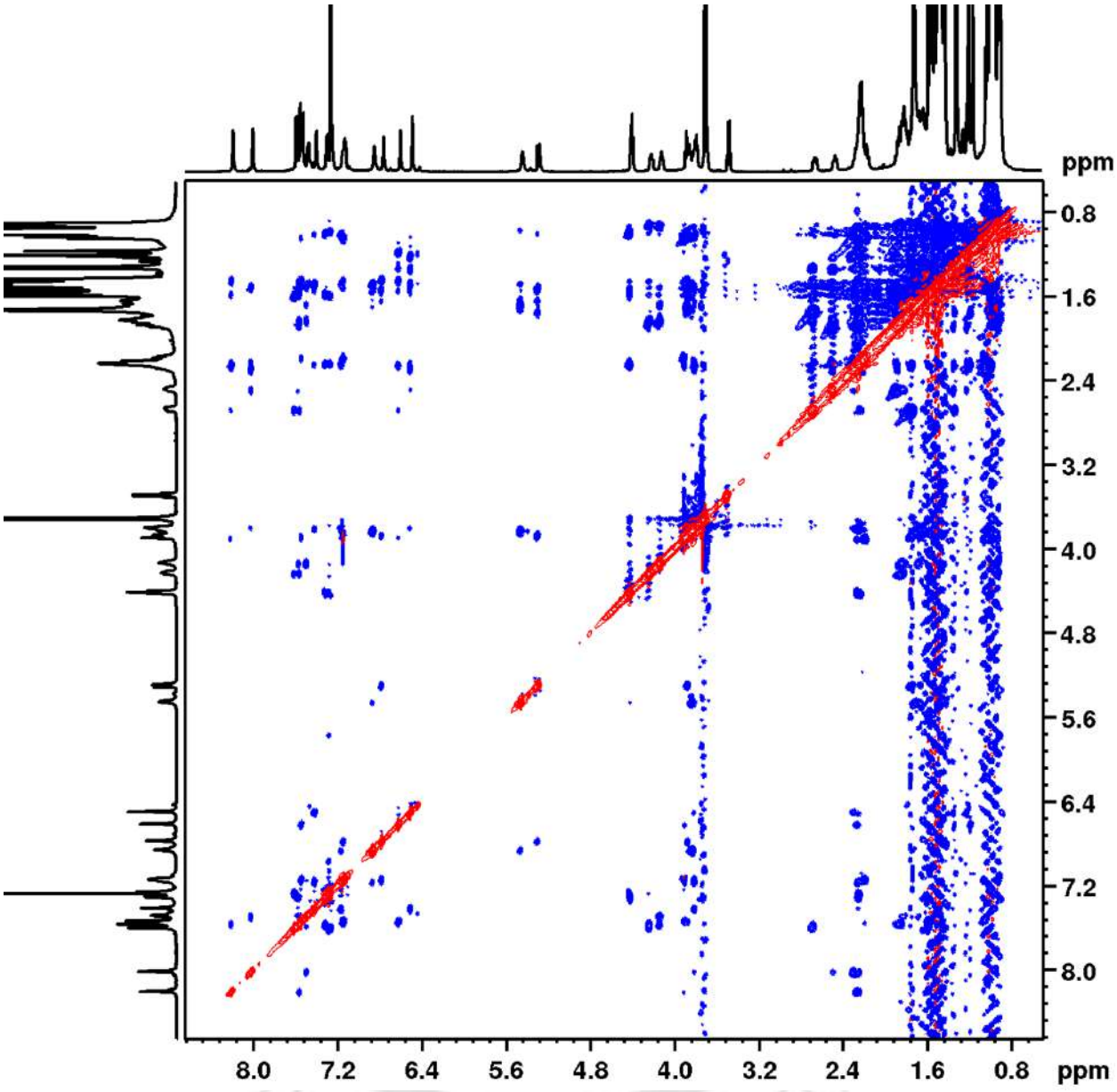

Figure A74. 600 MHz ROESY spectra of peptide **33-Nona** at 5 mM concentration in $CDCl_3$ at 298 K.

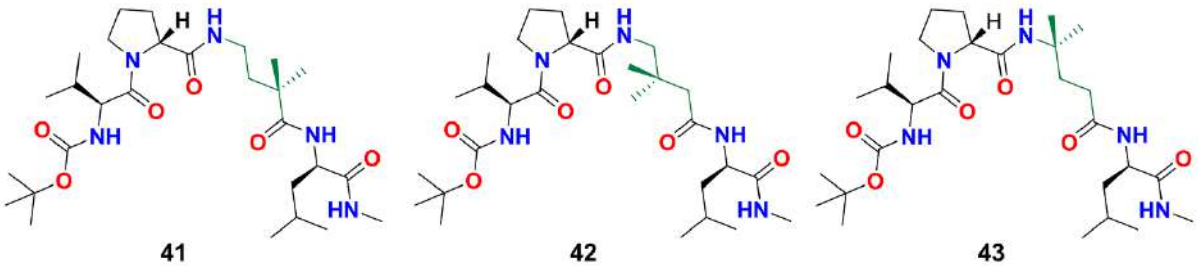

Figure A75. Chemical structures of the peptides **41-43**.

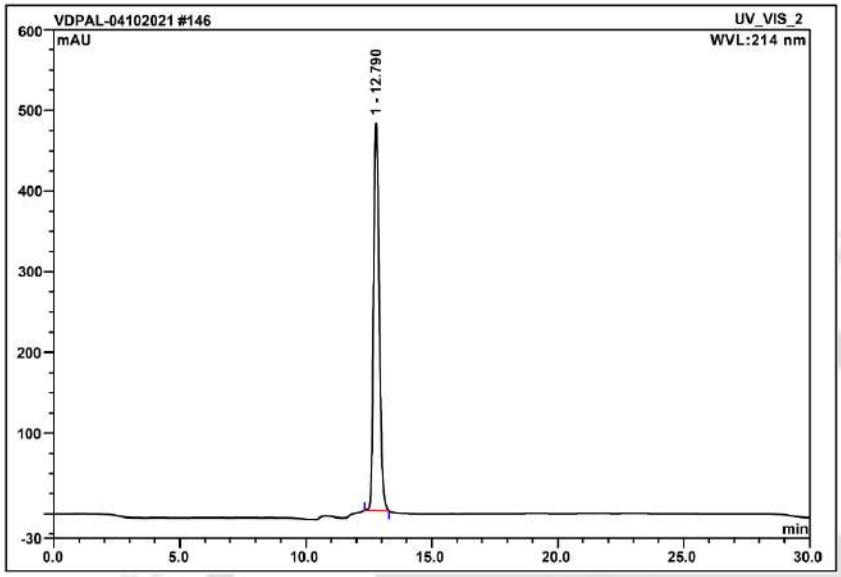

Figure A76. Analytical HPLC trace of **41** in MeOH/H_2O.

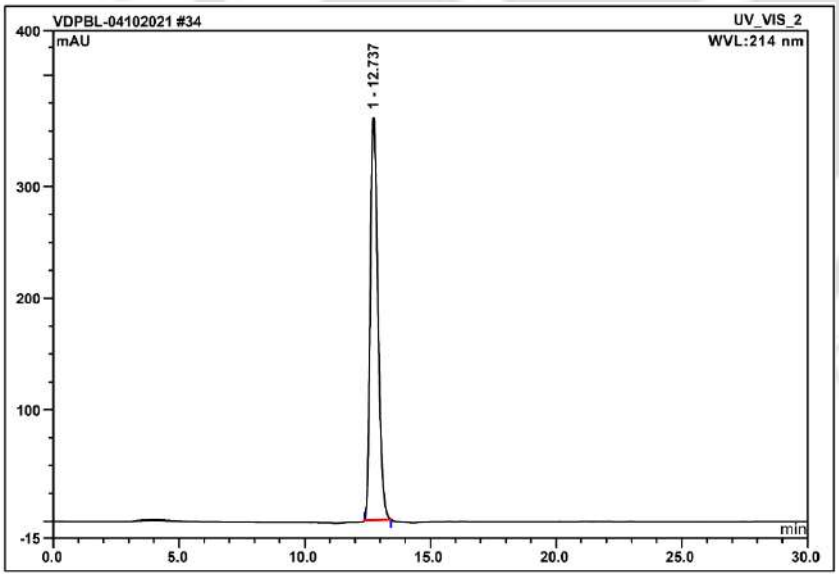

Figure A77. Analytical HPLC trace of **42** in MeOH/H_2O.

TH-3141_166122021

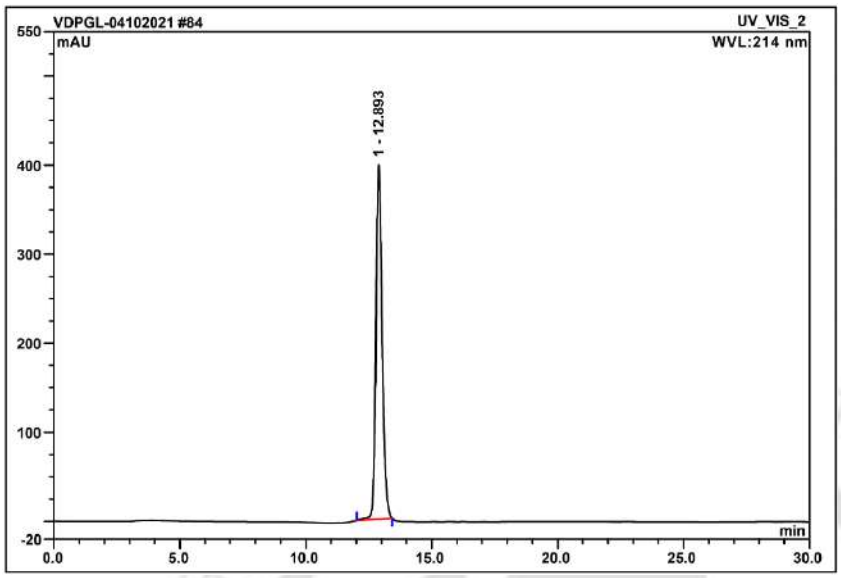

Figure A78. Analytical HPLC trace of **43** in MeOH/H_2O.

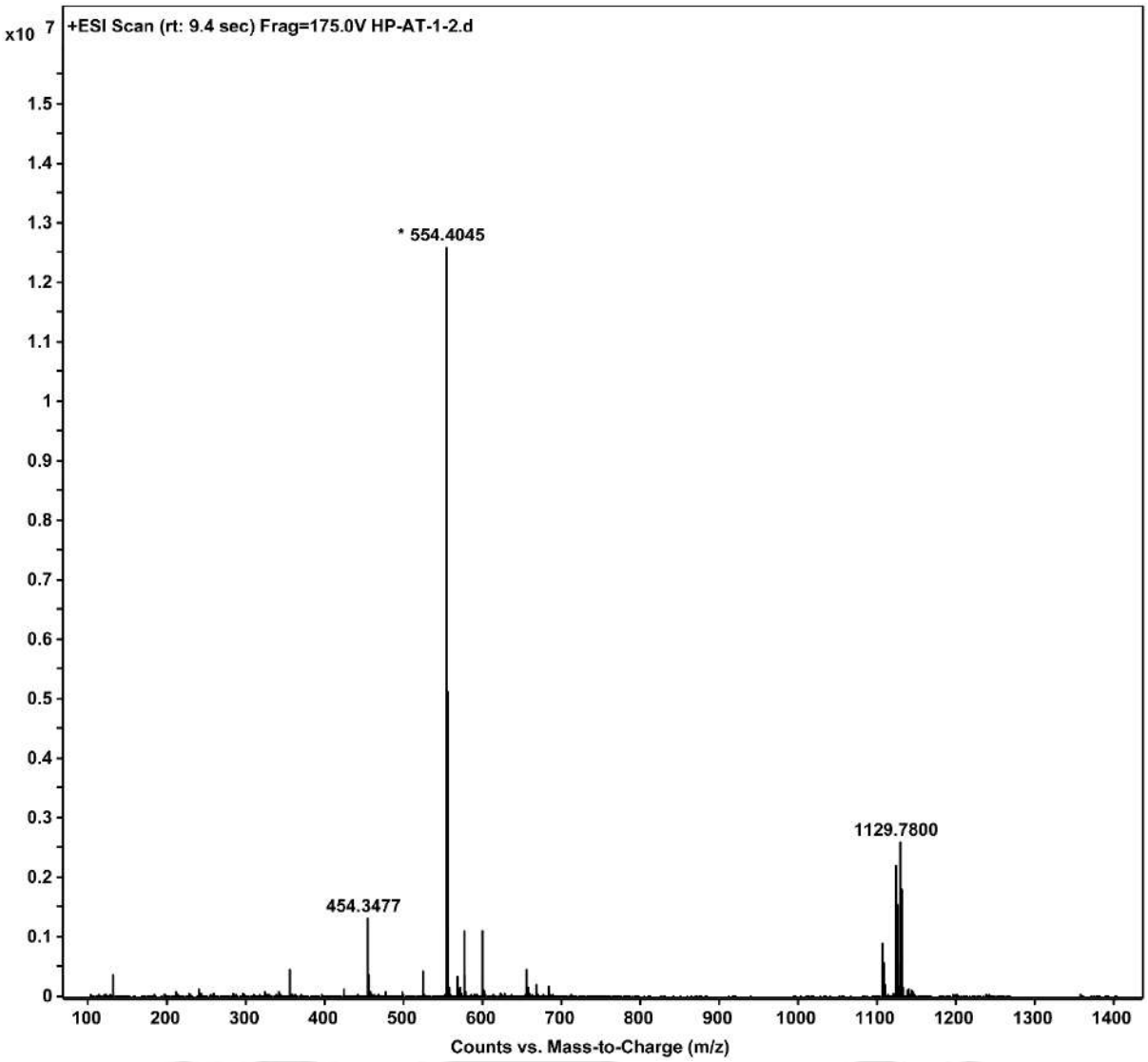

Figure A79. ESI-MS (m/z) of **41**. Calc. for $(M+H)^+$ $C_{28}H_{51}N_5O_6$ = 554.3878 Da; Obs. = 554.4045 Da, $(2M+Na)^+$ = 1129.7800 Da.

TH-3141_166122021

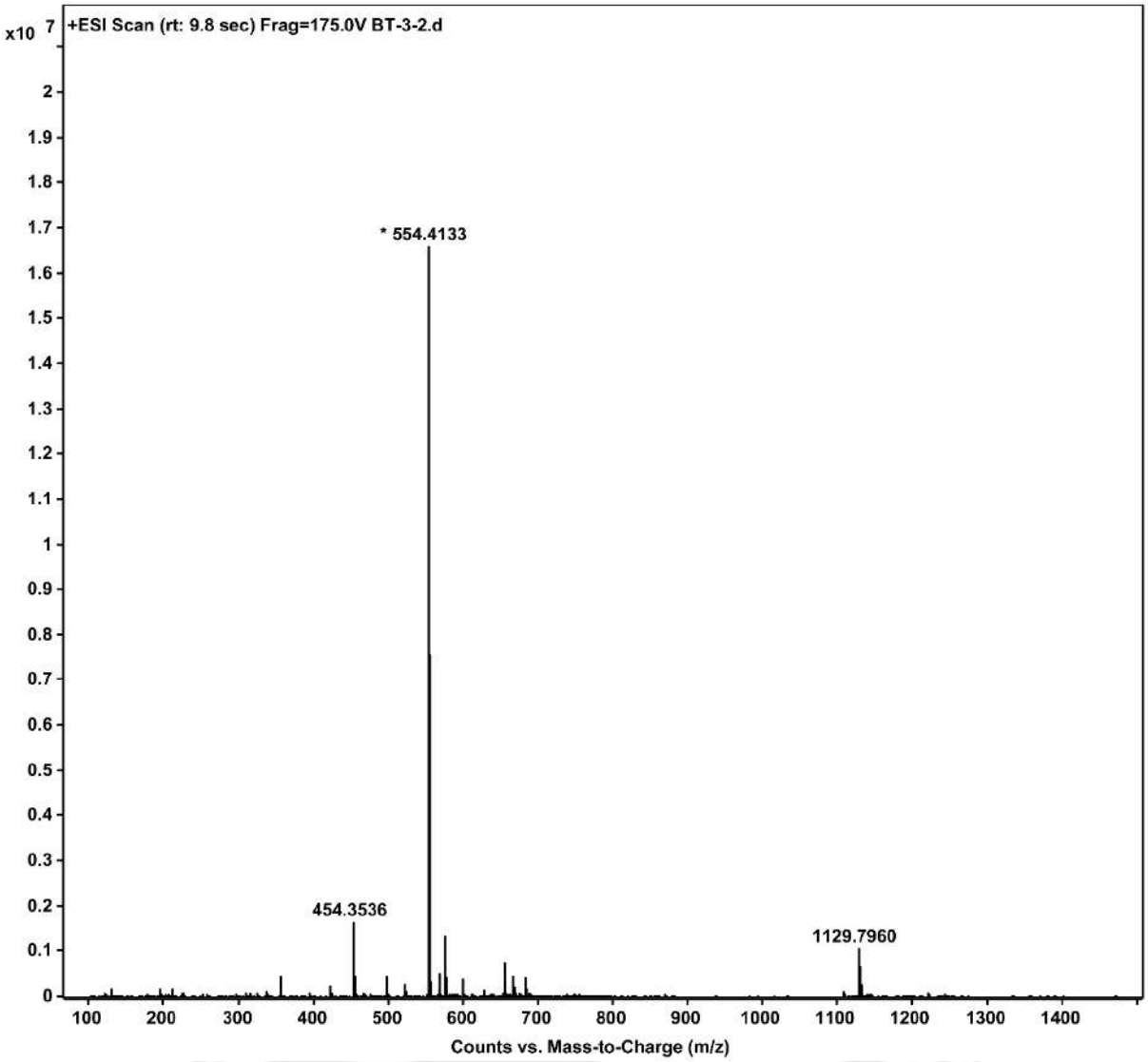

Figure A80. ESI-MS (m/z) of **42**. Calc. for $(M+H)^+$ $C_{28}H_{51}N_5O_6$ = 554.3878 Da; Obs. = 554.4133 Da, $(2M+Na)^+$ = 1129.7960 Da.

TH-3141_166122021

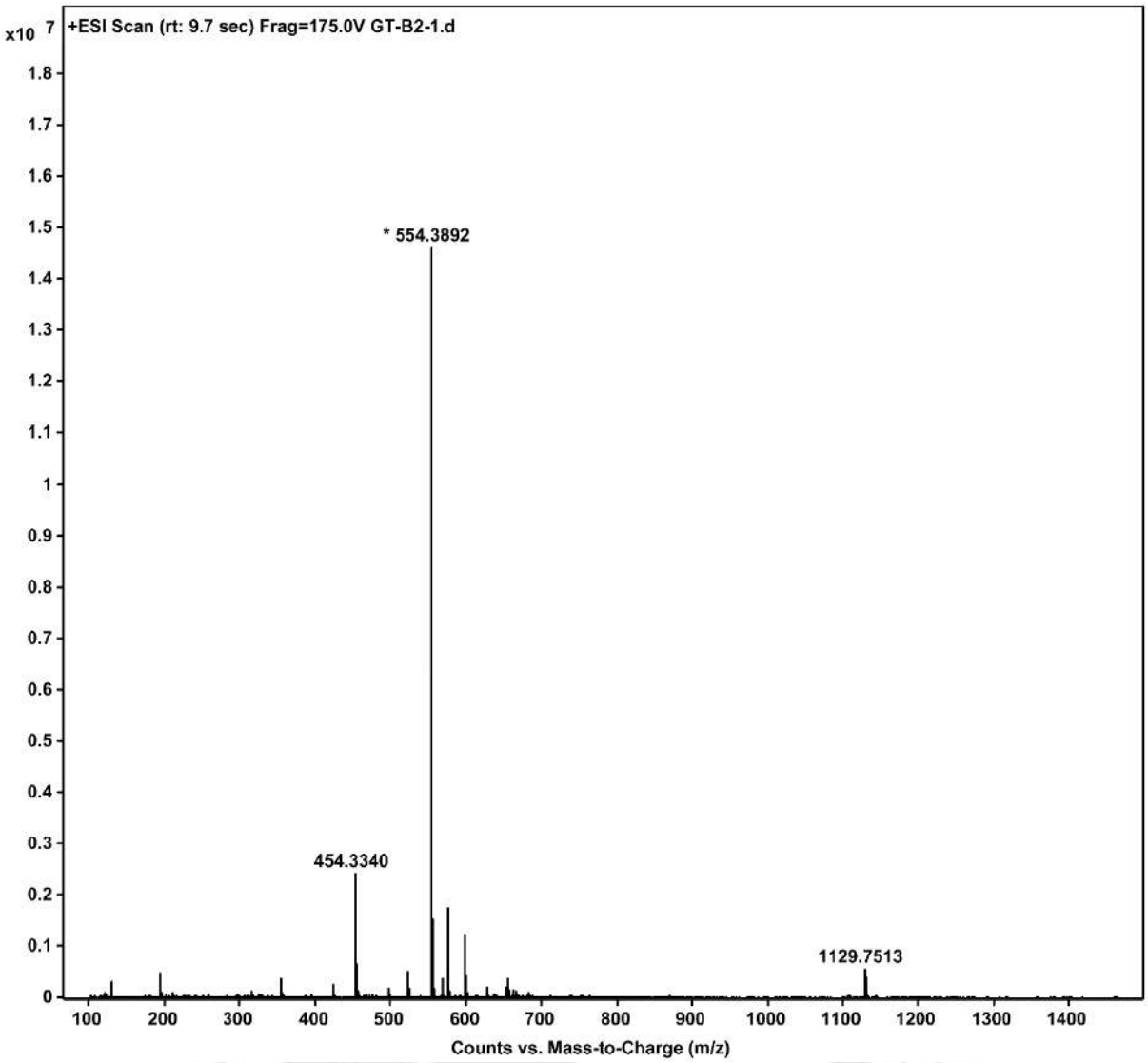

Figure A81. ESI-MS (m/z) of **43**. Calc. for $(M+H)^+$ $C_{28}H_{51}N_5O_6$ = 554.3878 Da; Obs. = 554.3892 Da, $(2M+Na)^+$ = 1129.7513 Da.

TH-3141_166122021

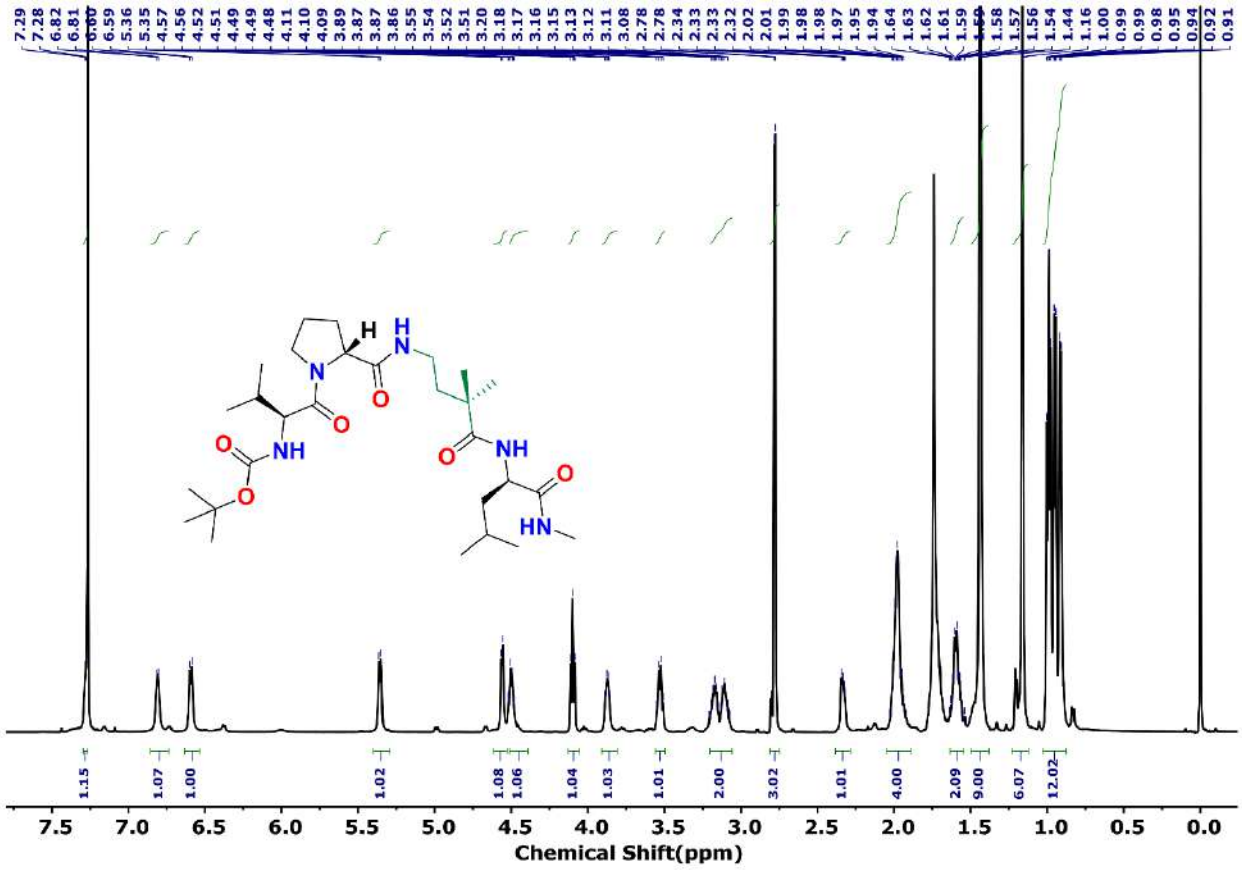

Figure A82. 600 MHz ^{1}H NMR spectra of **41** in $CDCl_3$ at 7 mM concentration (298 K).

TH-3141_166122021

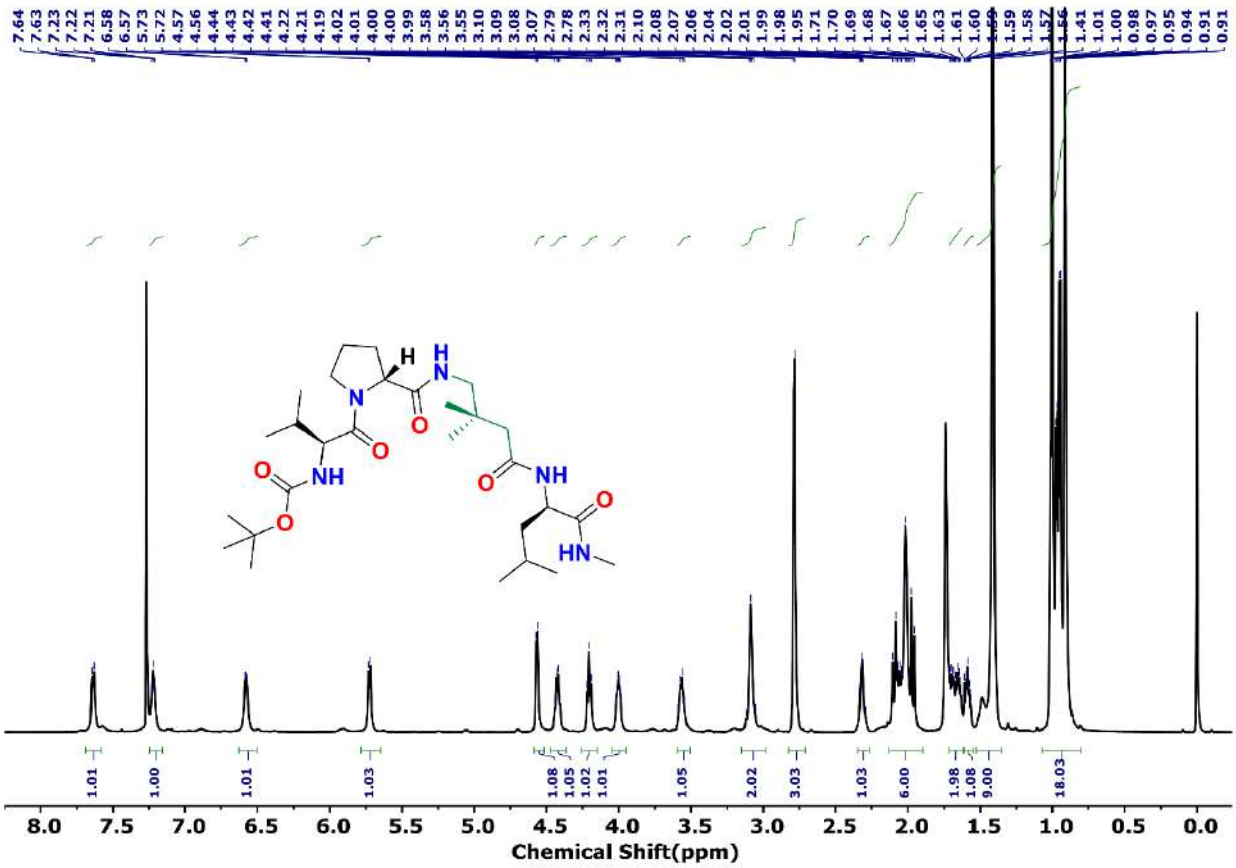

Figure A83. 600 MHz ^{1}H NMR spectra of **42** in $CDCl_3$ at 7 mM concentration (298 K).

TH-3141_166122021

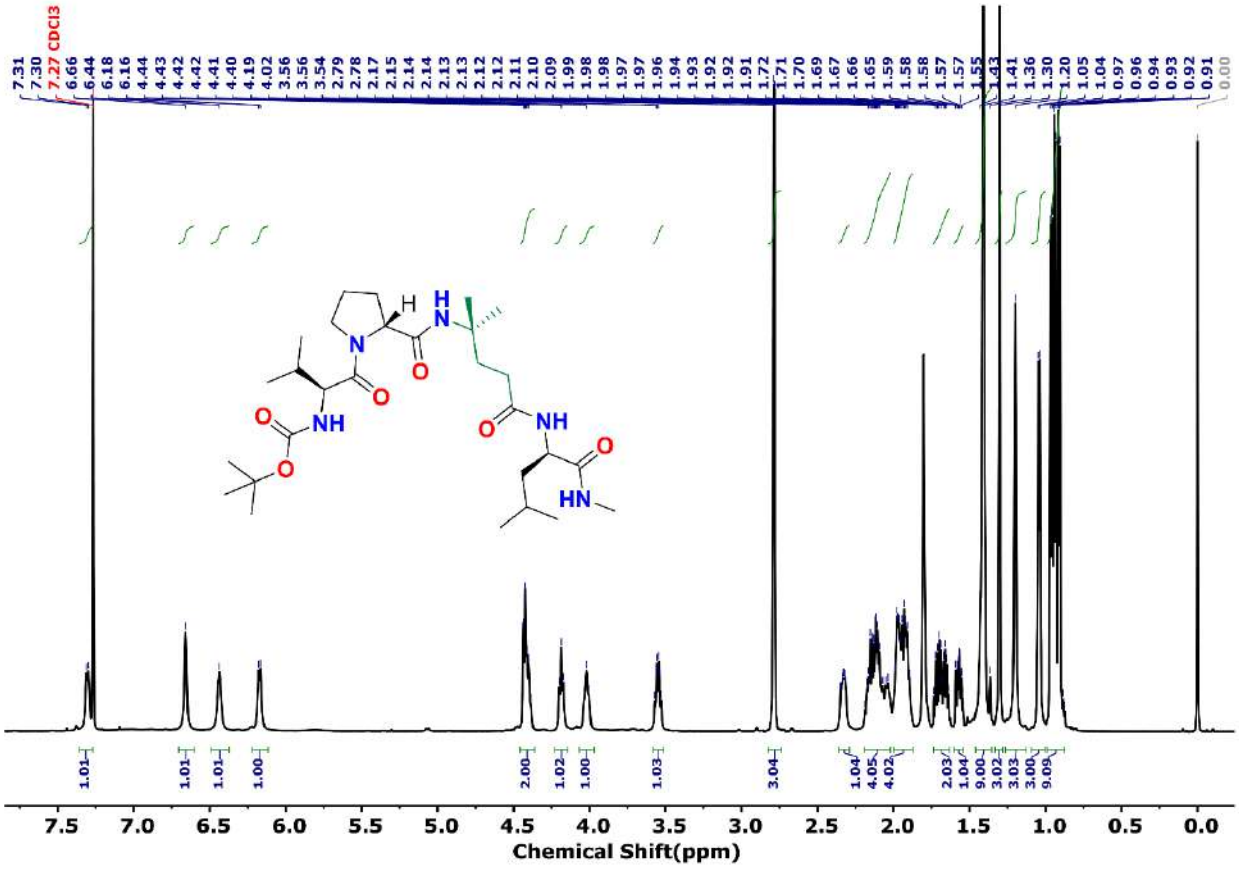

Figure A84. 600 MHz ^{1}H NMR spectra of **43** in $CDCl_3$ at 7 mM concentration (298 K).

TH-3141_166122021

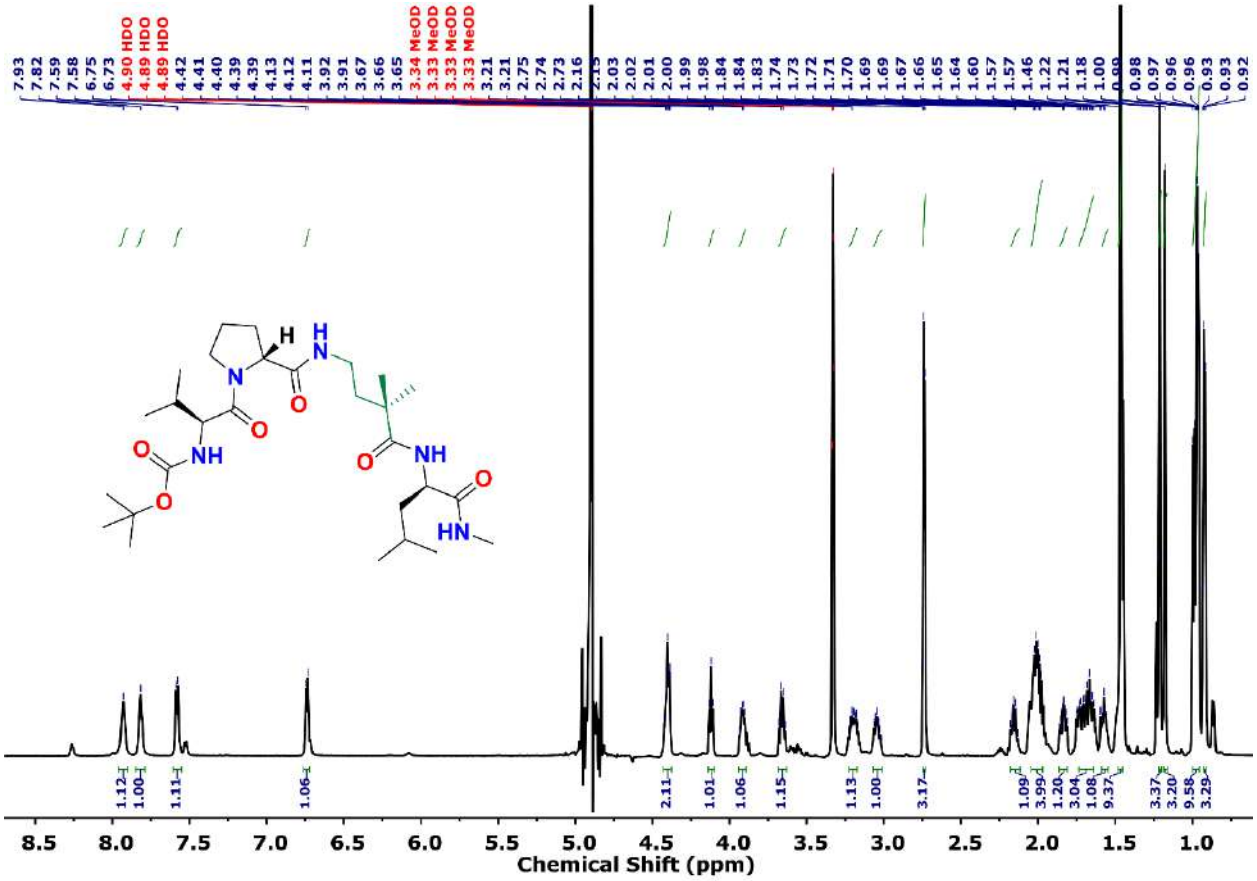

Figure A85. 600 MHz ^{1}H NMR spectra of **41** in CD_3OH at 7 mM concentration (298 K).

TH-3141_166122021

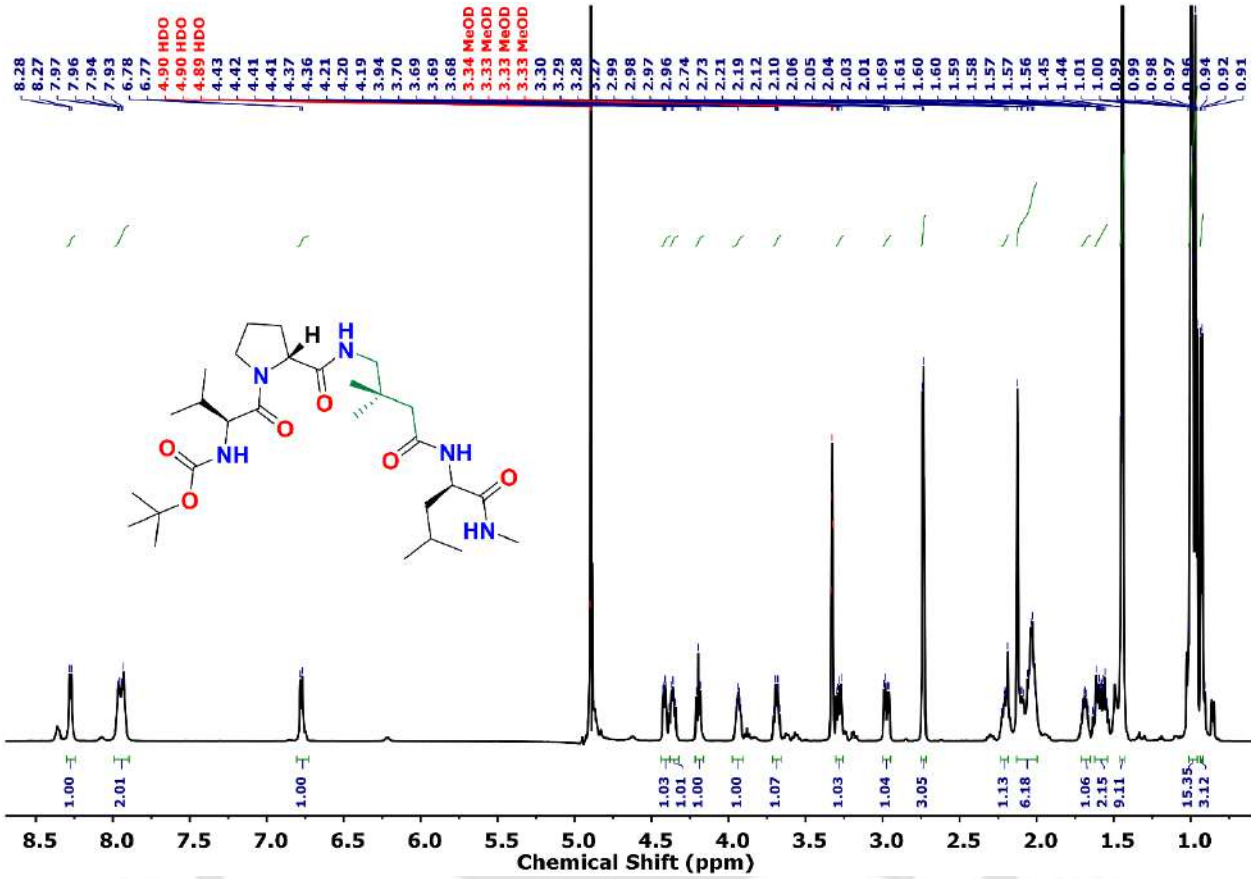

Figure A86. 600 MHz ^{1}H NMR spectra of **42** in CD_3OH at 7 mM concentration (298 K).

TH-3141_166122021

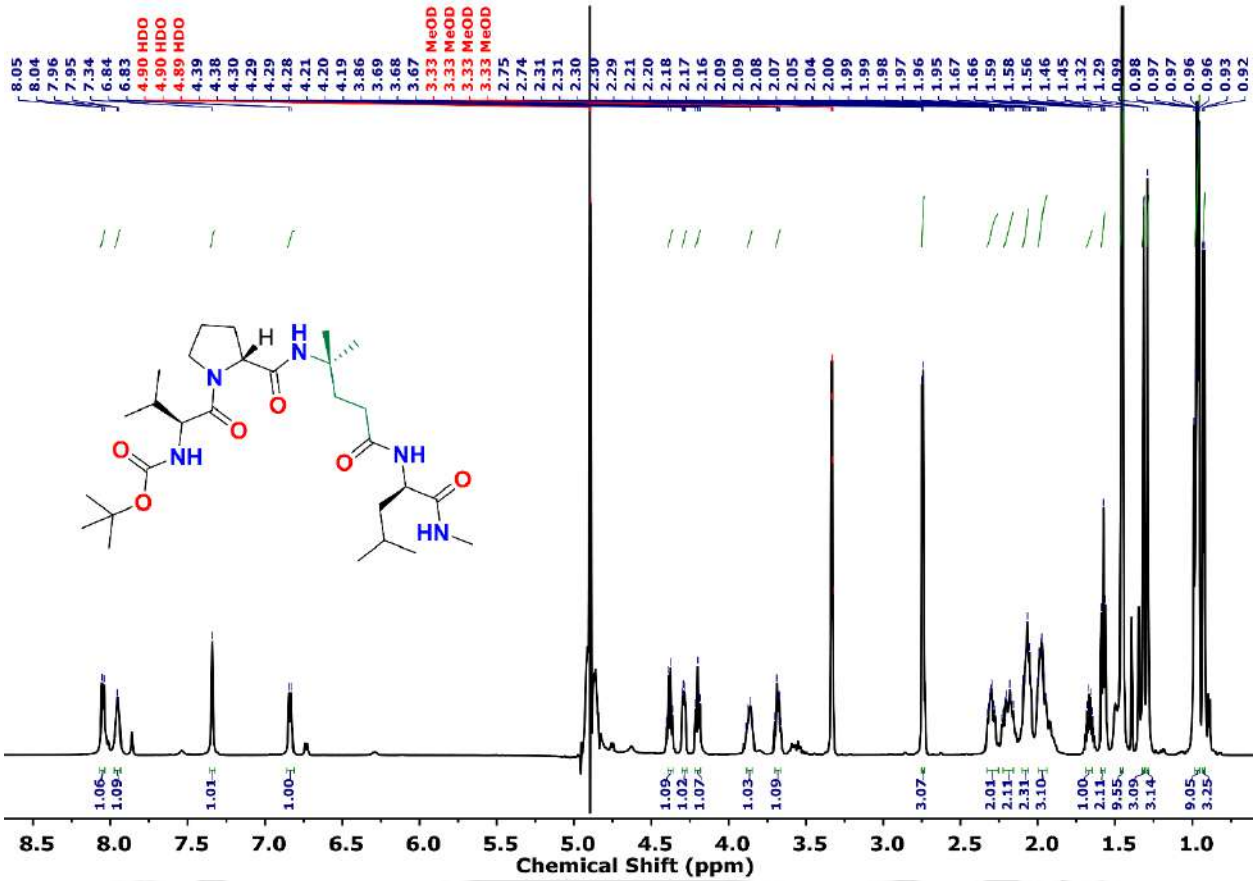

Figure A87. 600 MHz ^{1}H NMR spectra of **43** in CD_3OH at 7 mM concentration (298 K).

TH-3141_166122021

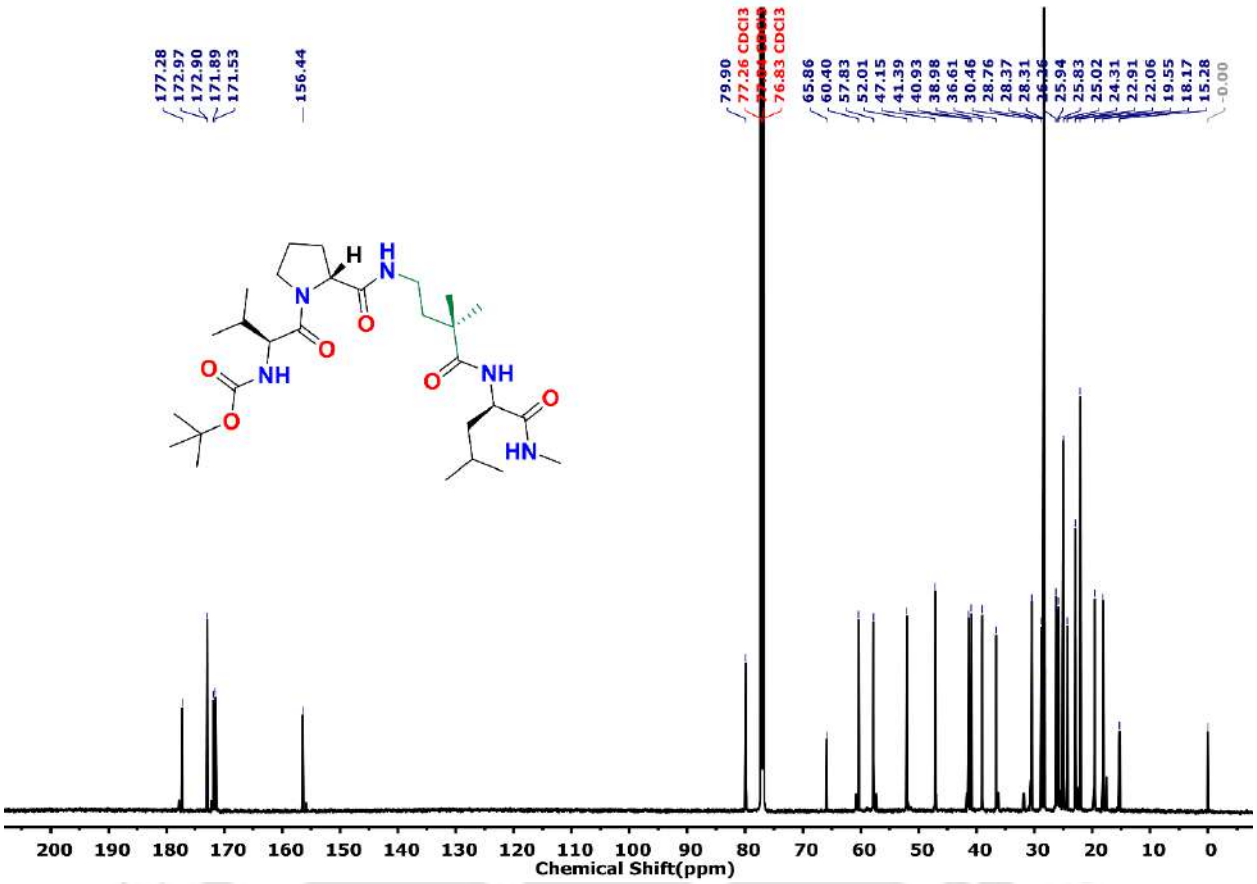

Figure A88. 150 MHz ^{13}C NMR spectra of **41** in $CDCl_3$ at 7 mM concentration (298 K).

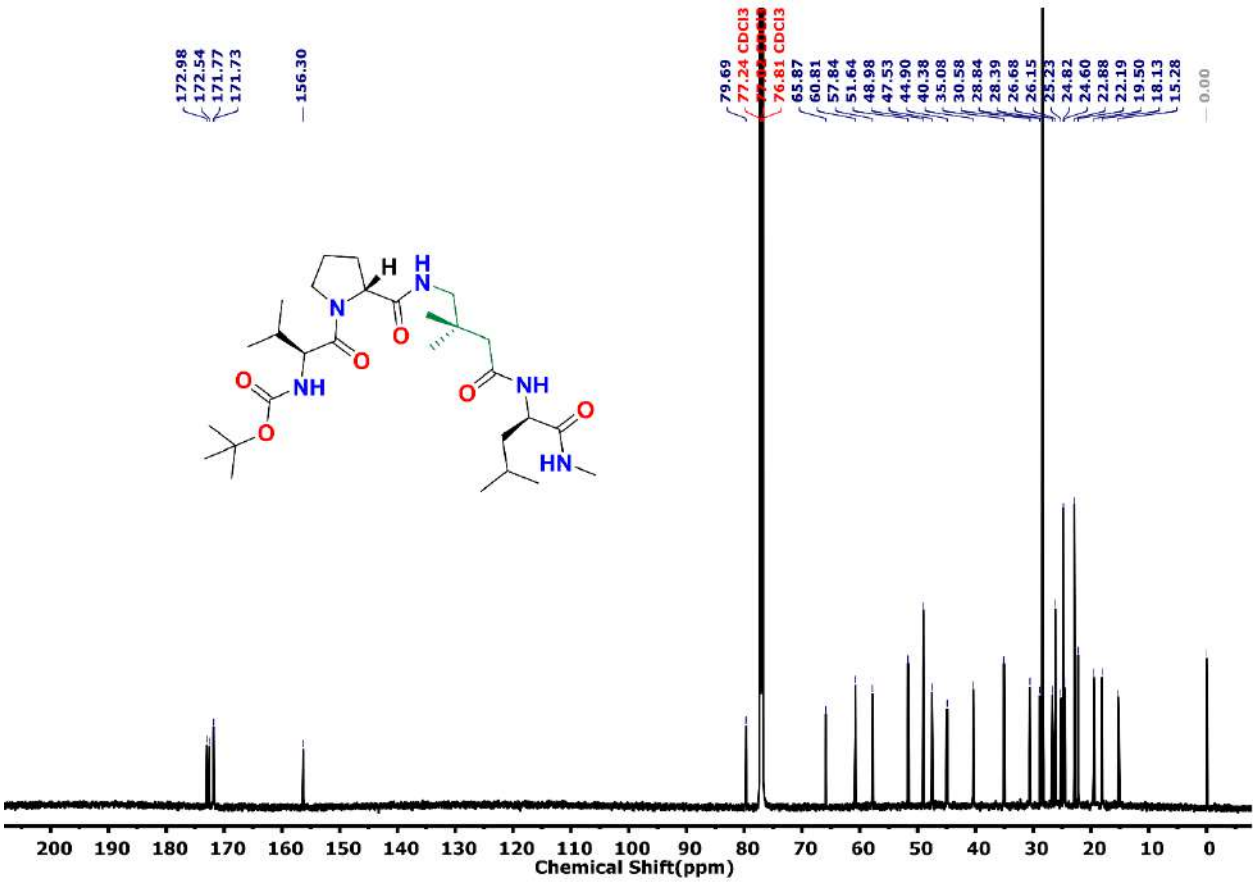

Figure A89. 150 MHz ^{13}C NMR spectra of **42** in $CDCl_3$ at 7 mM concentration (298 K).

TH-3141_166122021

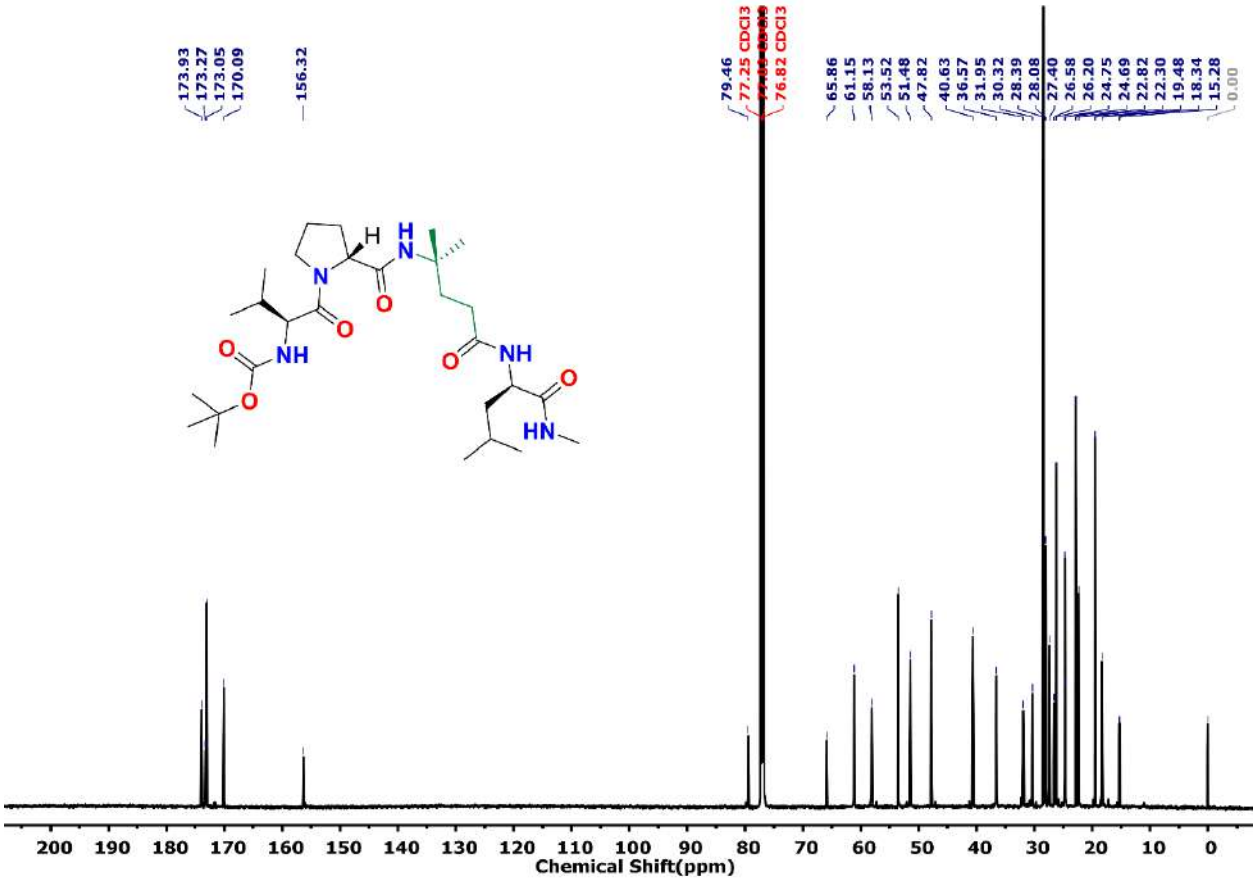

Figure A90. 150 MHz ^{13}C NMR spectra of **43** in $CDCl_3$ at 7 mM concentration (298 K).

TH-3141_166122021

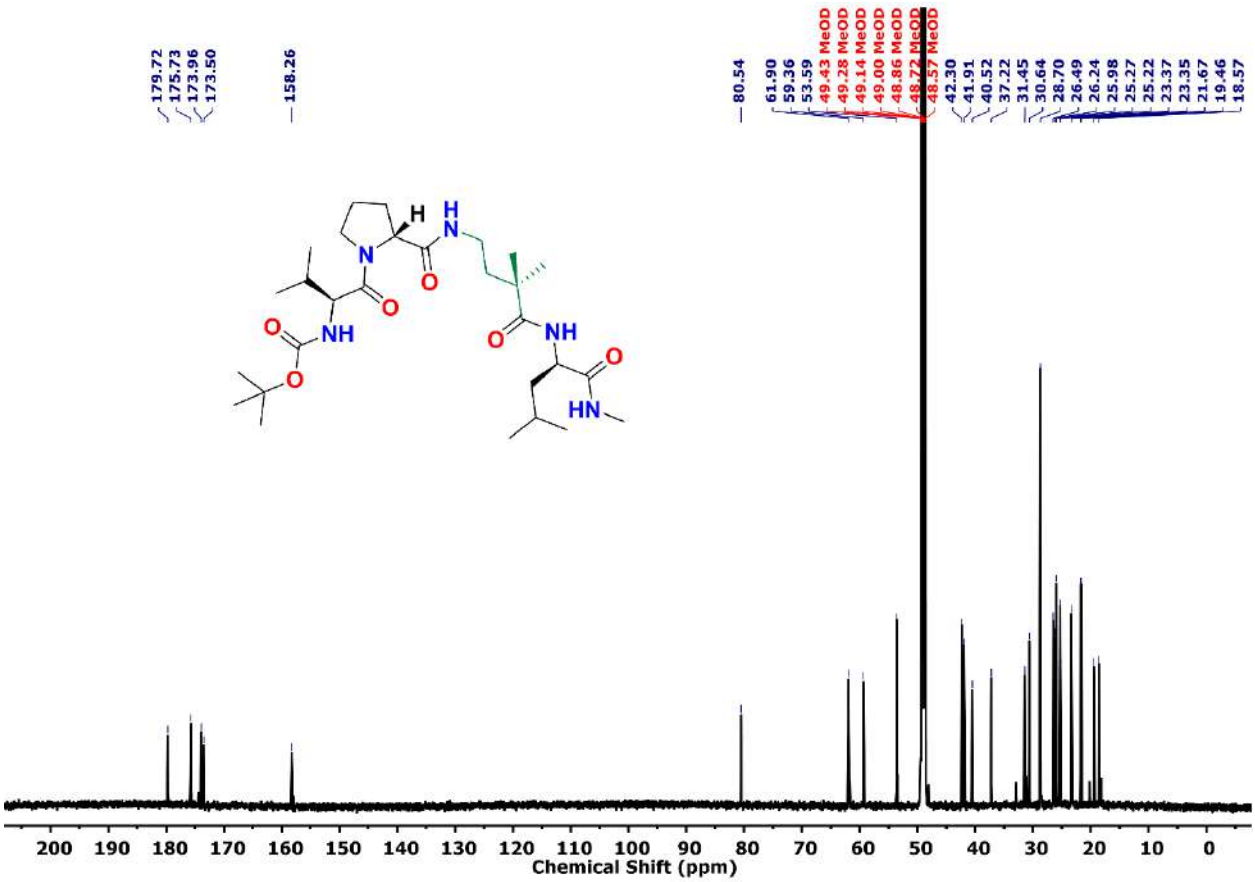

Figure A91. 150 MHz ^{13}C NMR spectra of **41** in CD_3OH at 7 mM concentration (298 K).

TH-3141_166122021

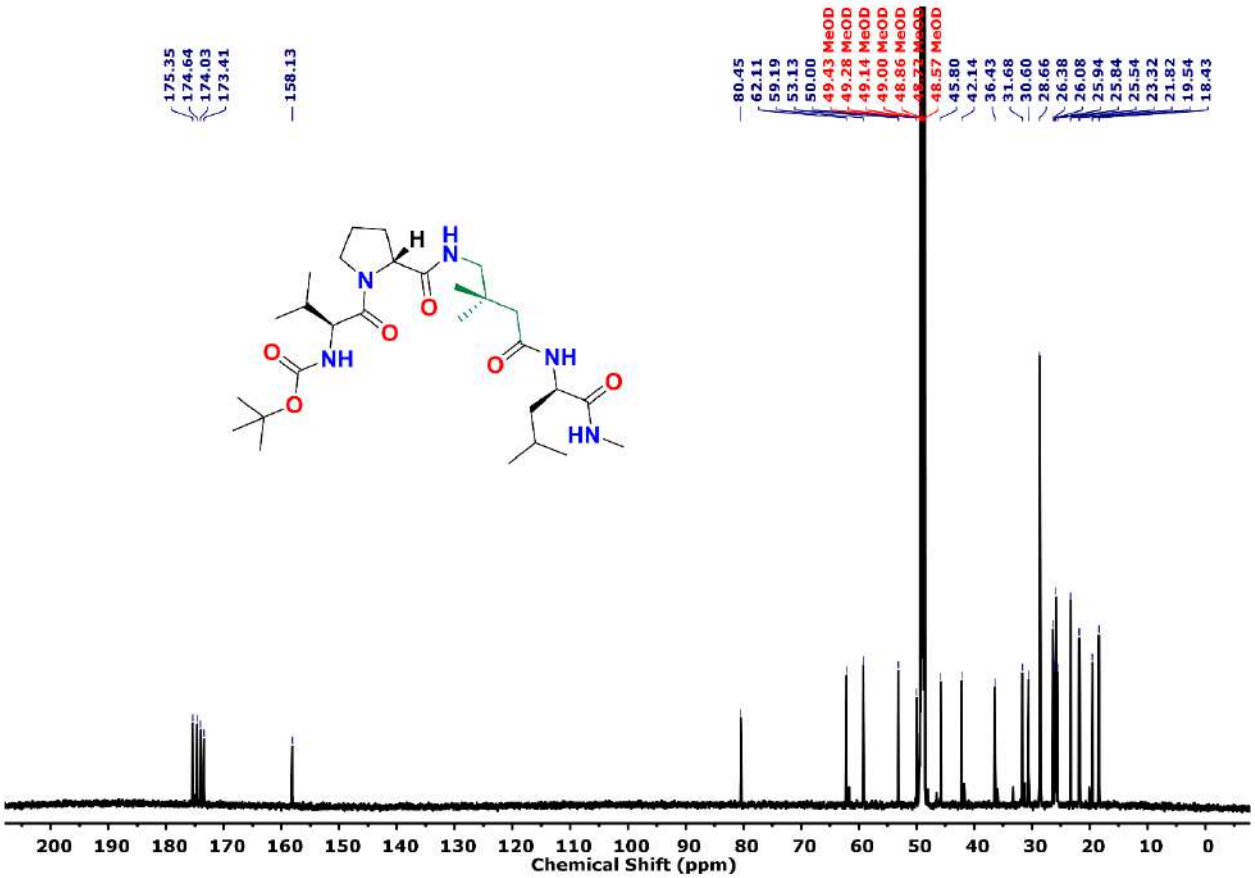

Figure A92. 150 MHz ^{13}C NMR spectra of **42** in CD_3OH at 7 mM concentration (298 K).

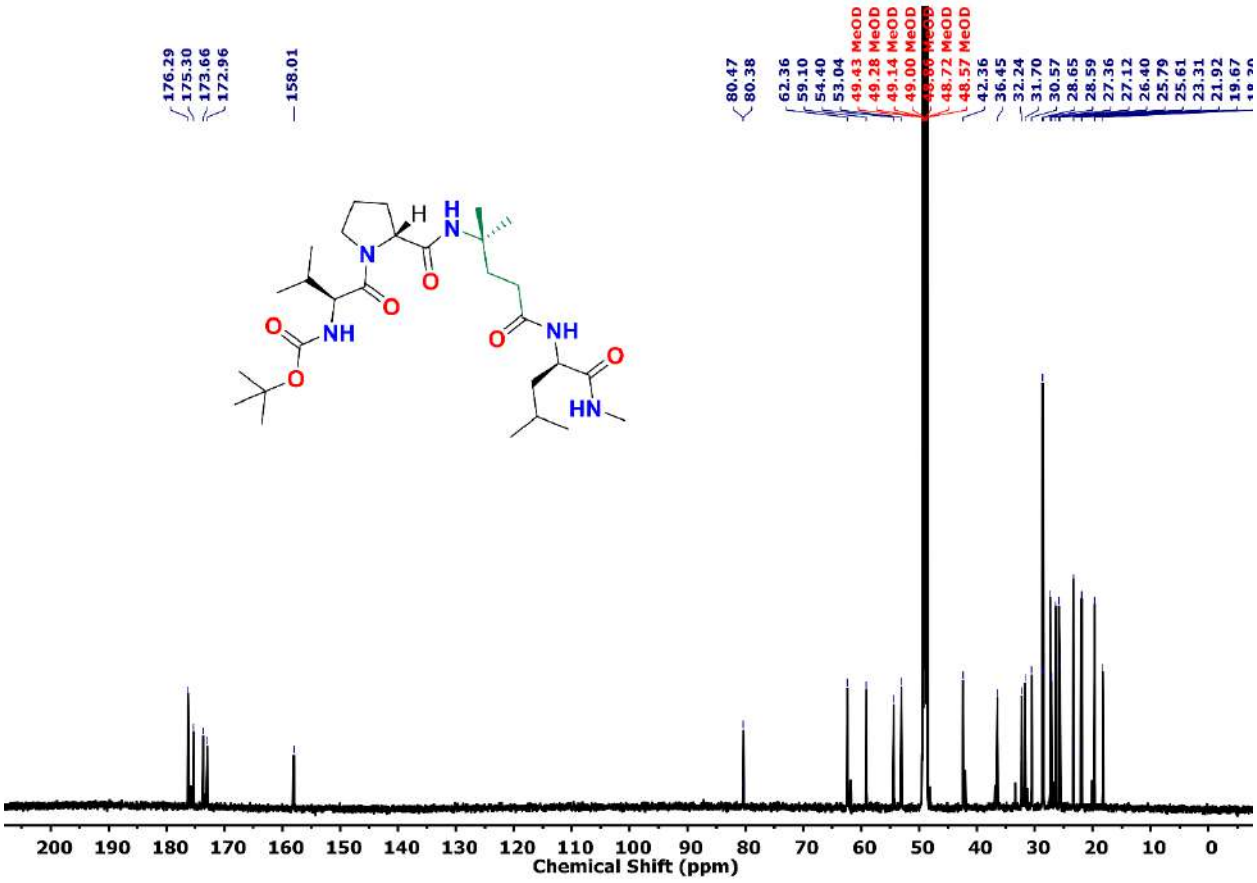

Figure A93. 150 MHz ^{13}C NMR spectra of **43** in CD_3OH at 7 mM concentration (298 K).

TH-3141_166122021

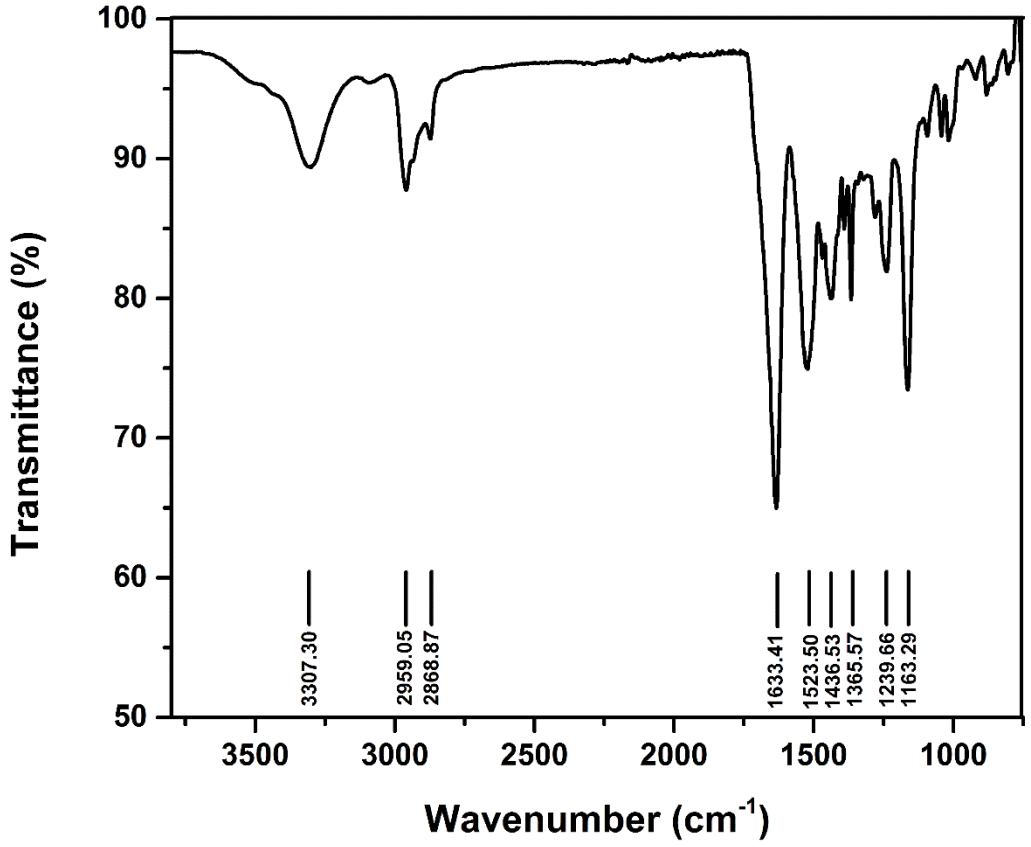

Figure A94. FT-IR spectra of **41** recorded in solid state at 298 K.

TH-3141_166122021

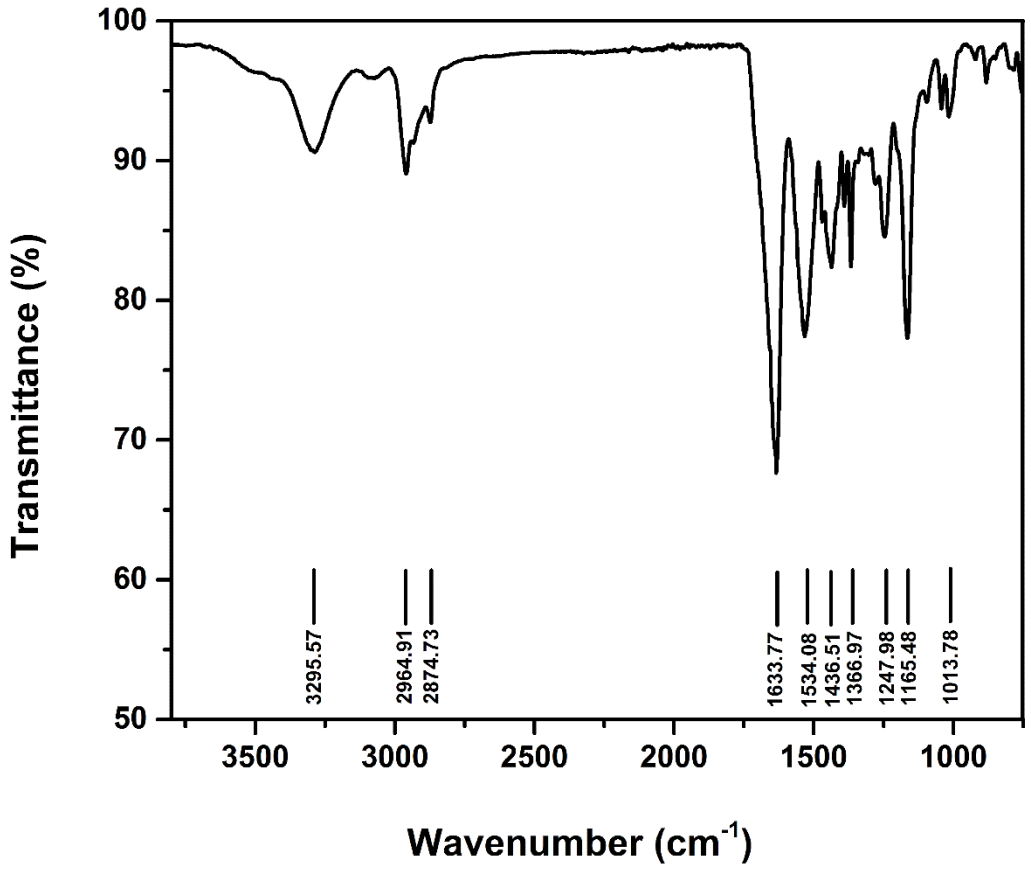

Figure 95. FT-IR spectra of **42** recorded in solid state at 298 K.

TH-3141_166122021

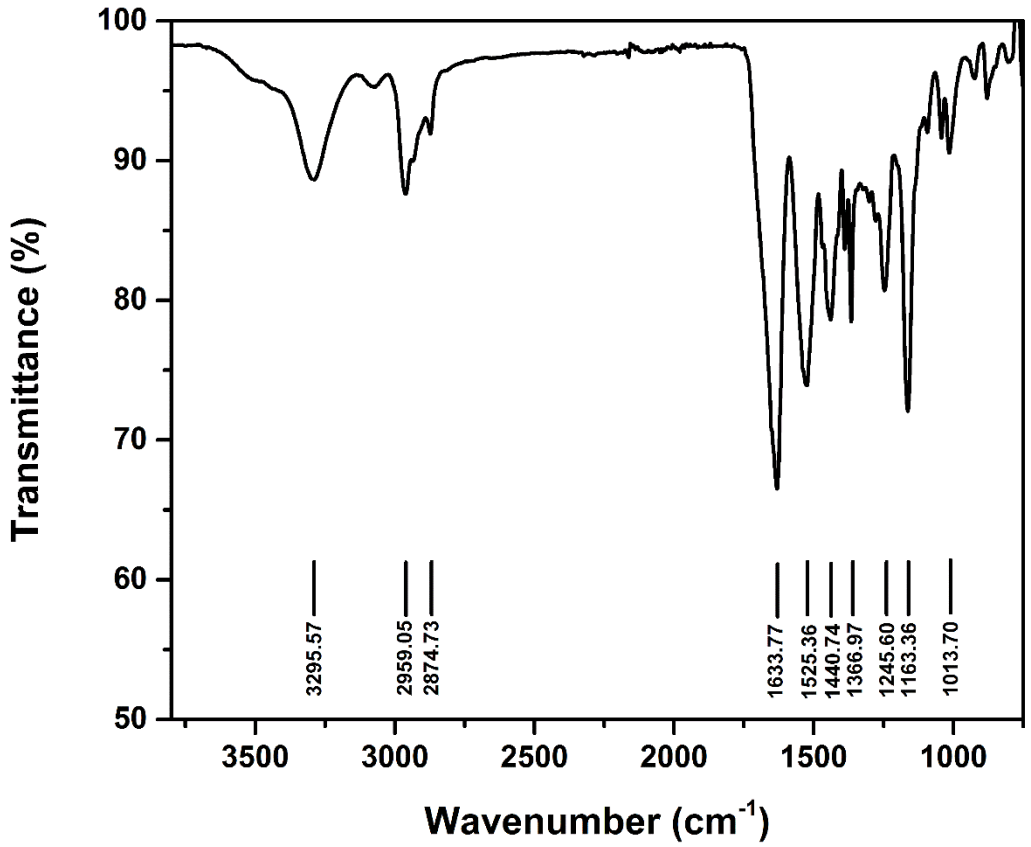

Figure A96. FT-IR spectra of **43** recorded in solid state at 298 K.

TH-3141_166122021

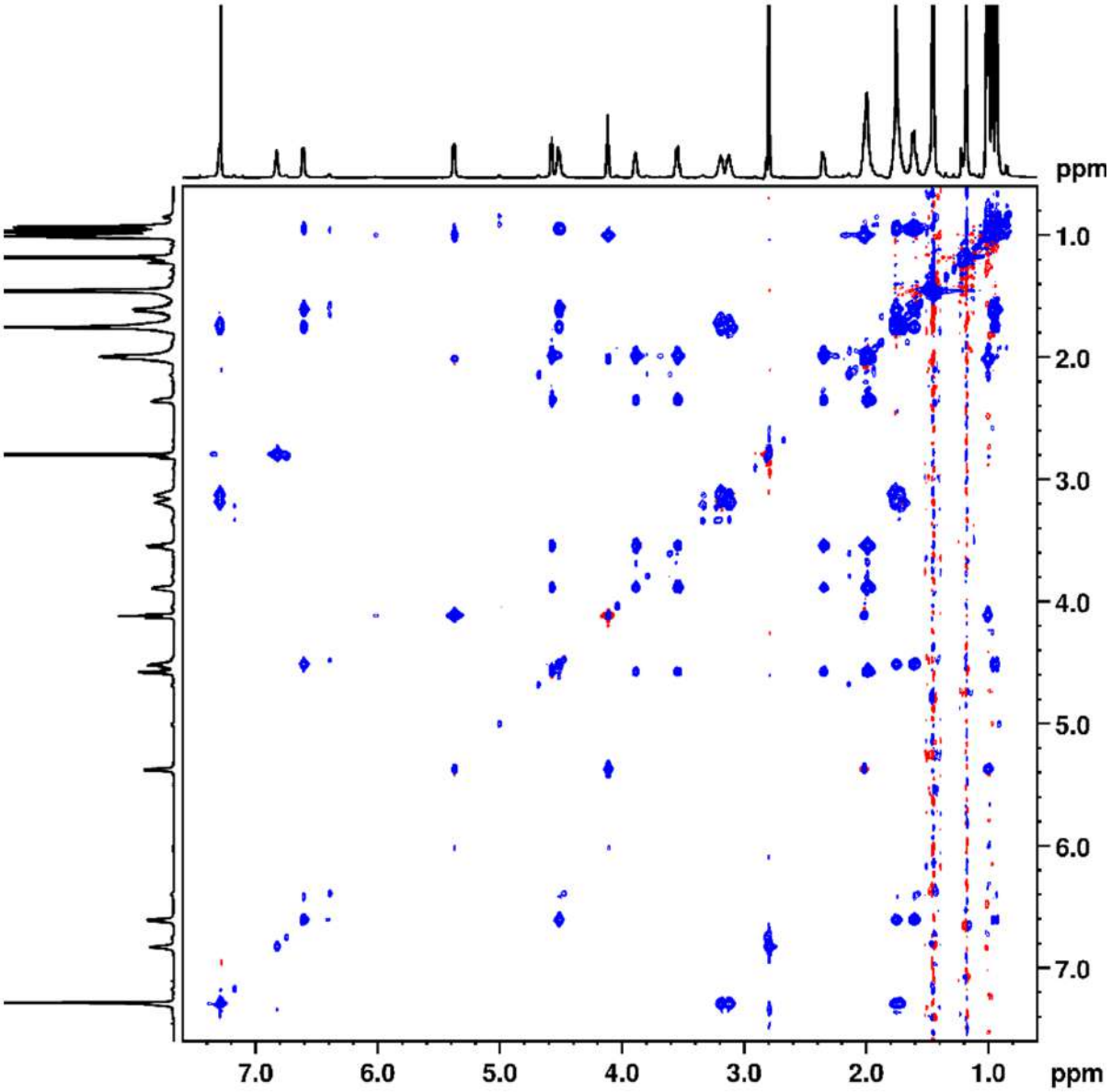

Figure A97. 600 MHz TOCSY spectra of peptide **41** at 7mM conc. in $CDCl_3$ at 298 K.

Institute of Technology

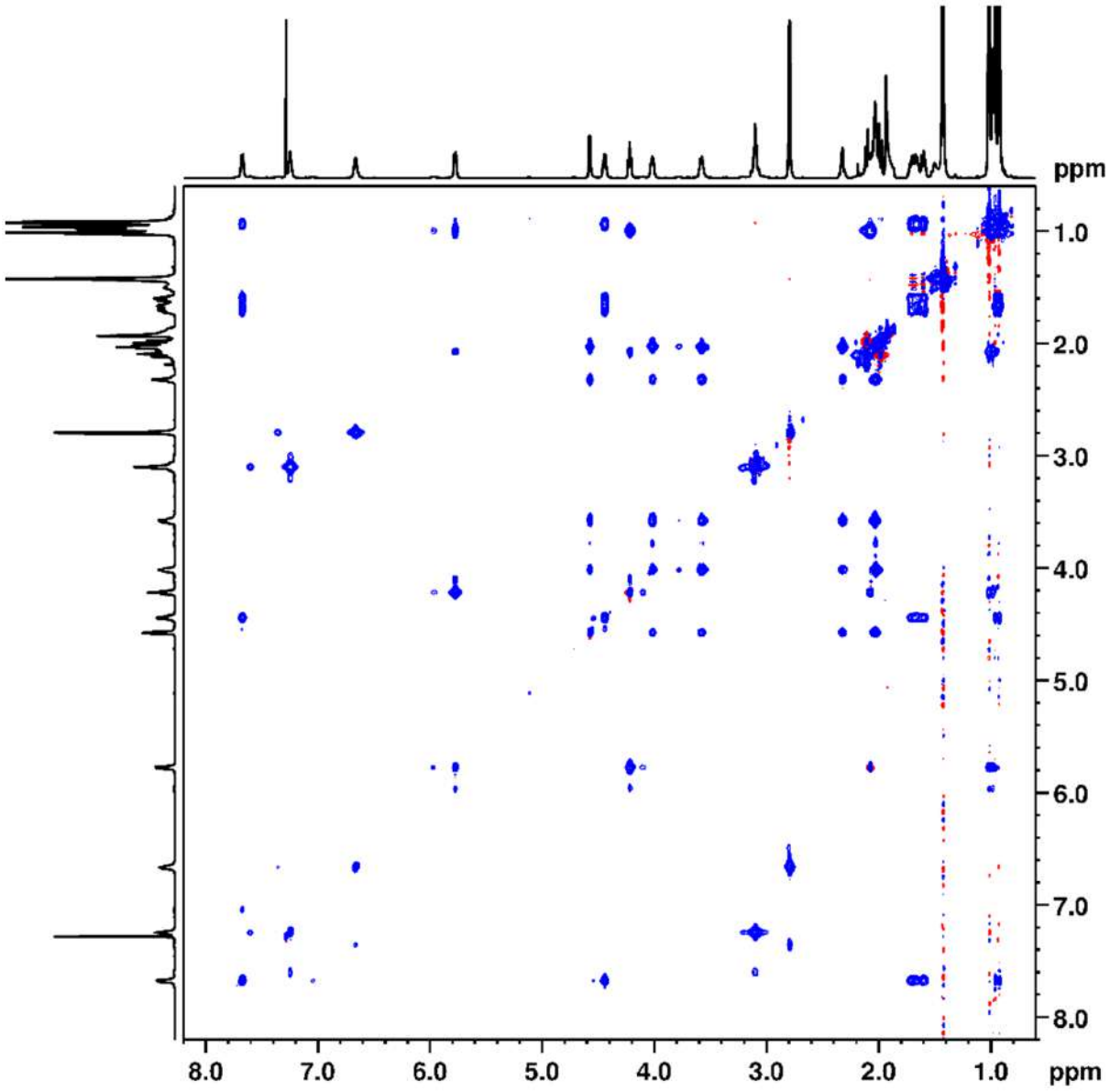

Figure A98. 600 MHz TOCSY spectra of peptide **42** at 7mM conc. in $CDCl_3$ at 298 K.

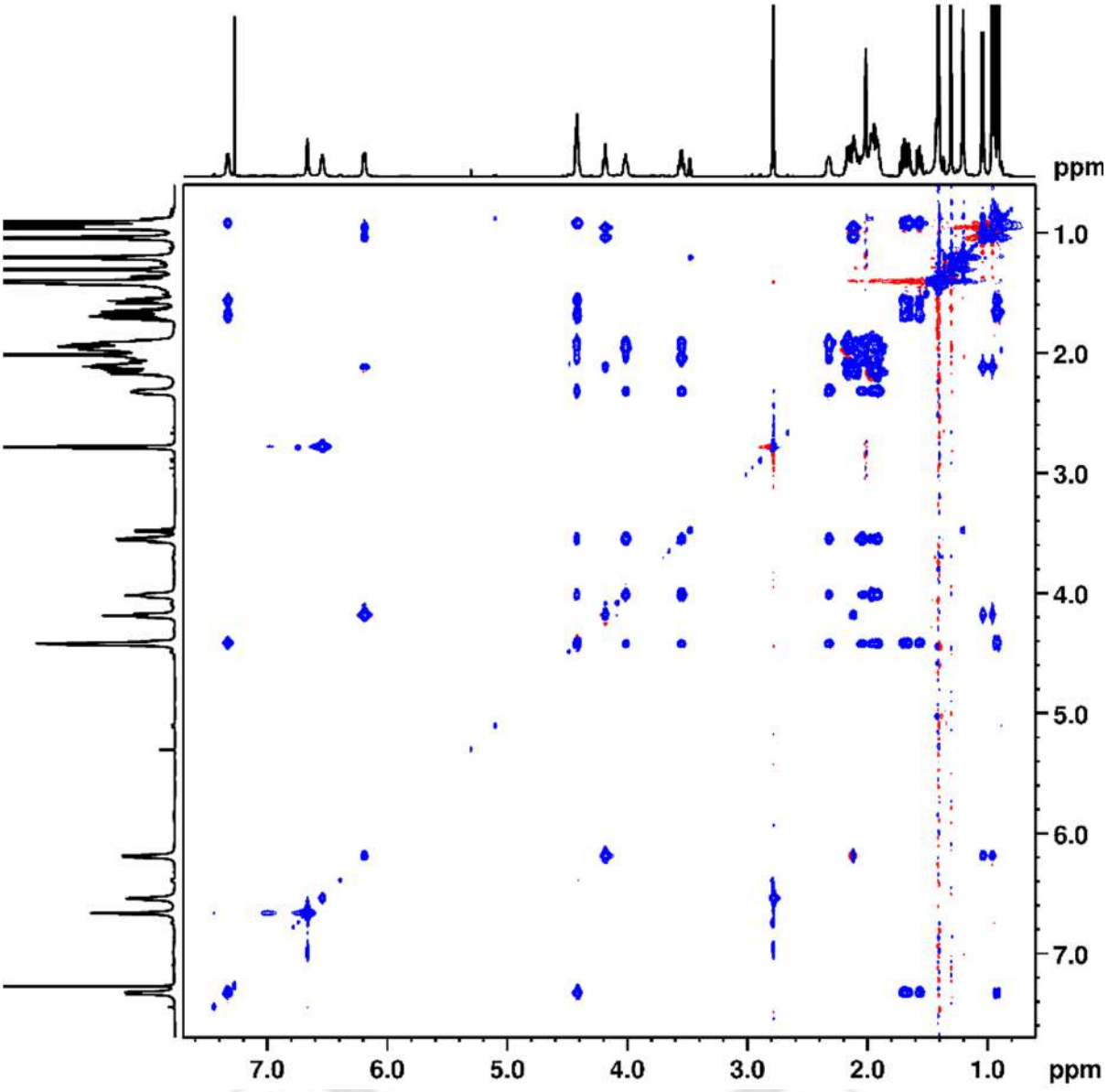

Figure A99. 600 MHz TOCSY spectra of peptide **43** at 7mM conc. in $CDCl_3$ at 298 K.

TH-3141_166122021

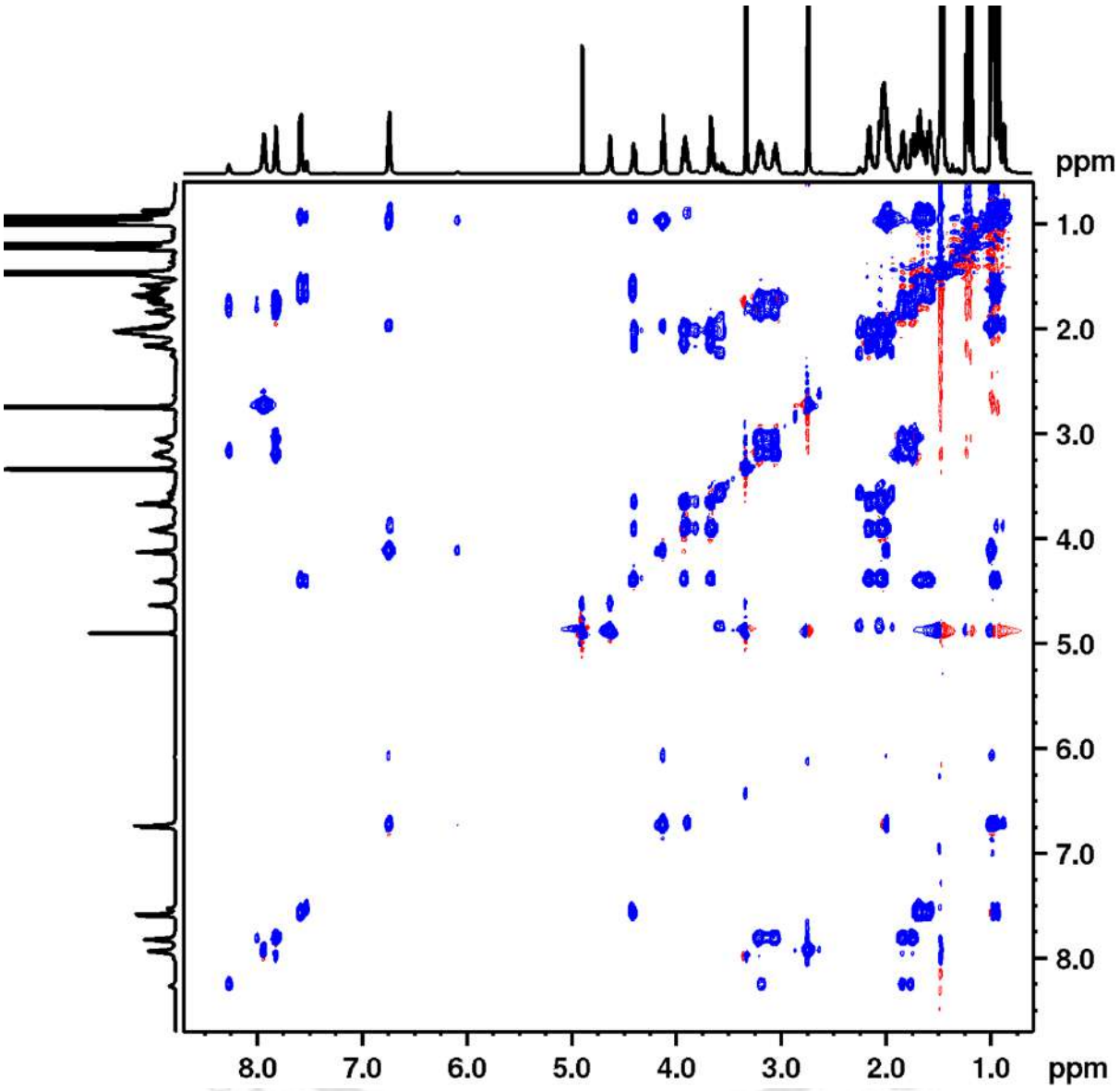

Figure A100. 600 MHz TOCSY spectra of peptide **41** at 7mM conc. in CD_3OH at 298 K.

TH-3141_166122021

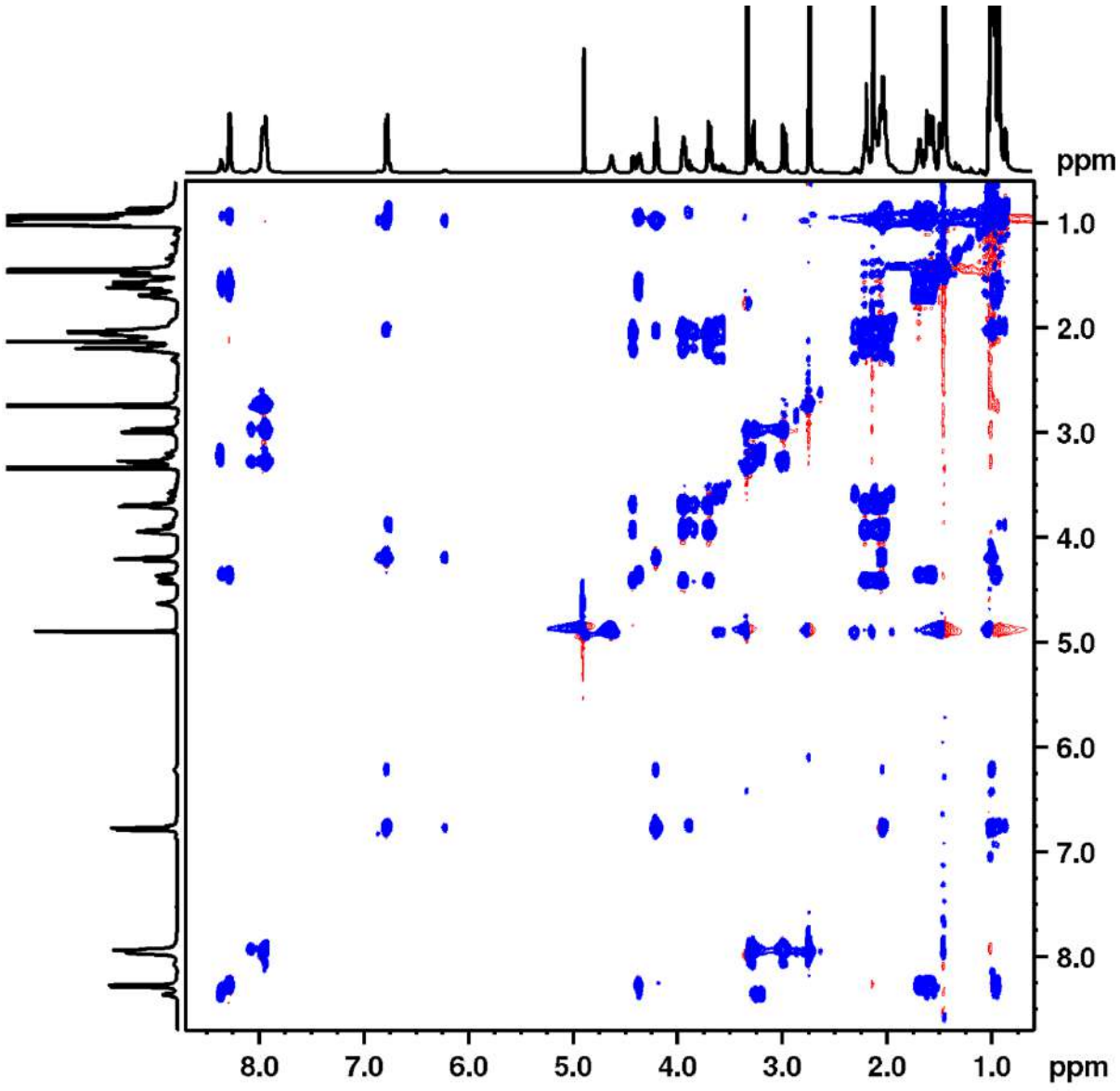

Figure A101. 600 MHz TOCSY spectra of peptide **42** at 7mM conc. in CD_3OH at 298 K.

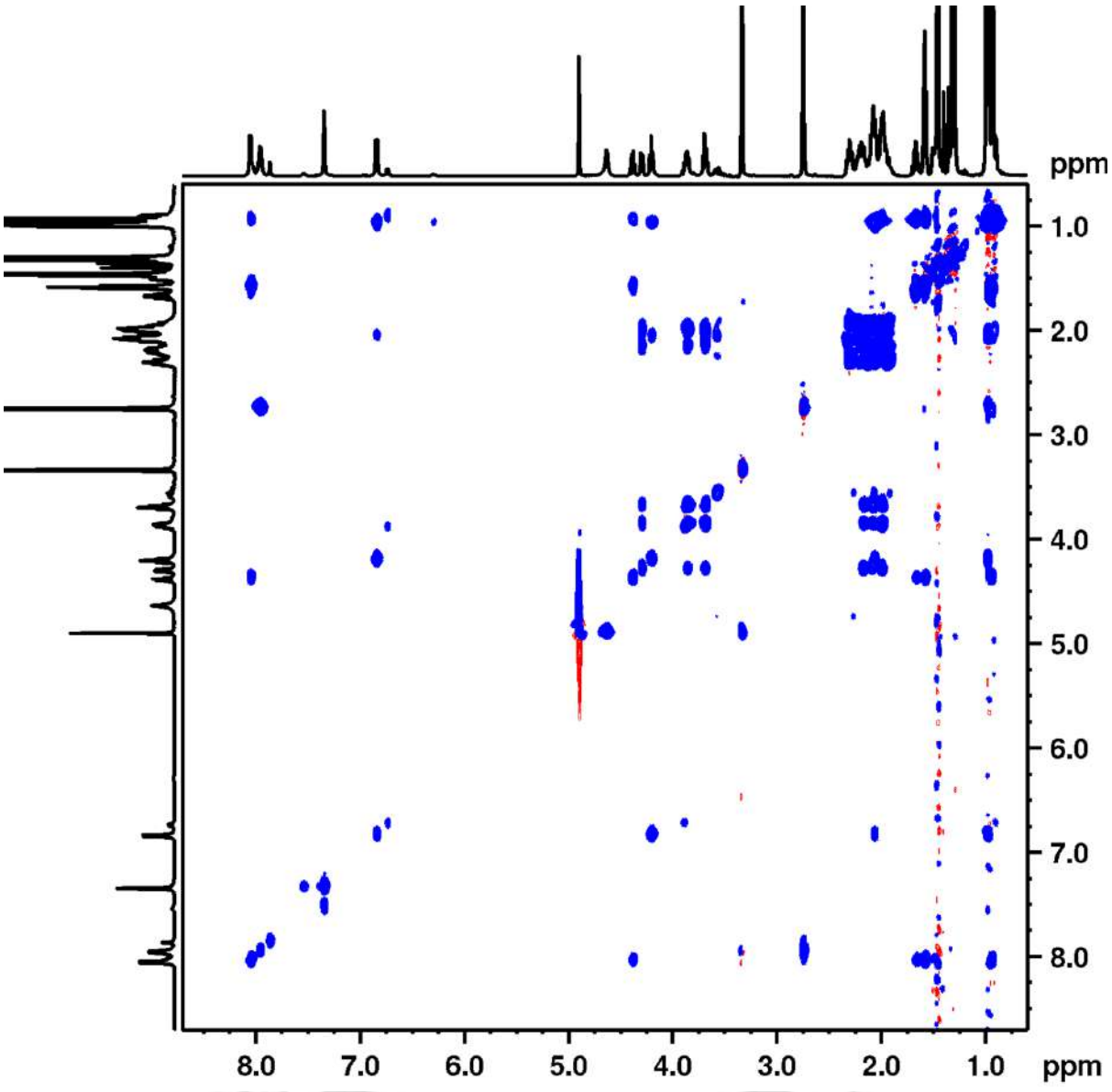

Figure A102. 600 MHz TOCSY spectra of peptide **43** at 7mM conc. in CD_3OH at 298 K.

TH-3141_166122021

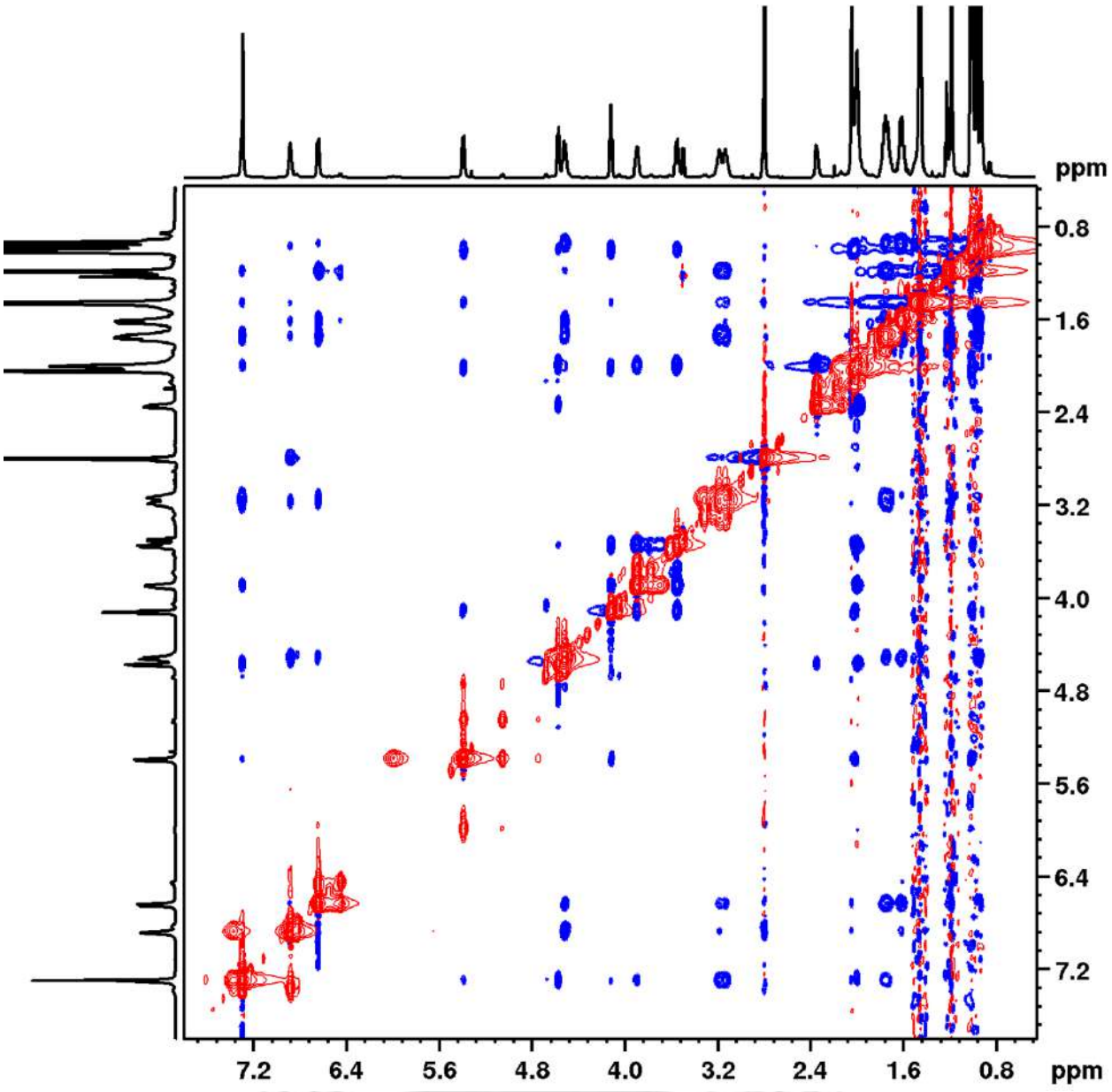

Figure A103. 600 MHz NOESY spectra of peptide **41** at 7mM conc. in $CDCl_3$ at 298 K.

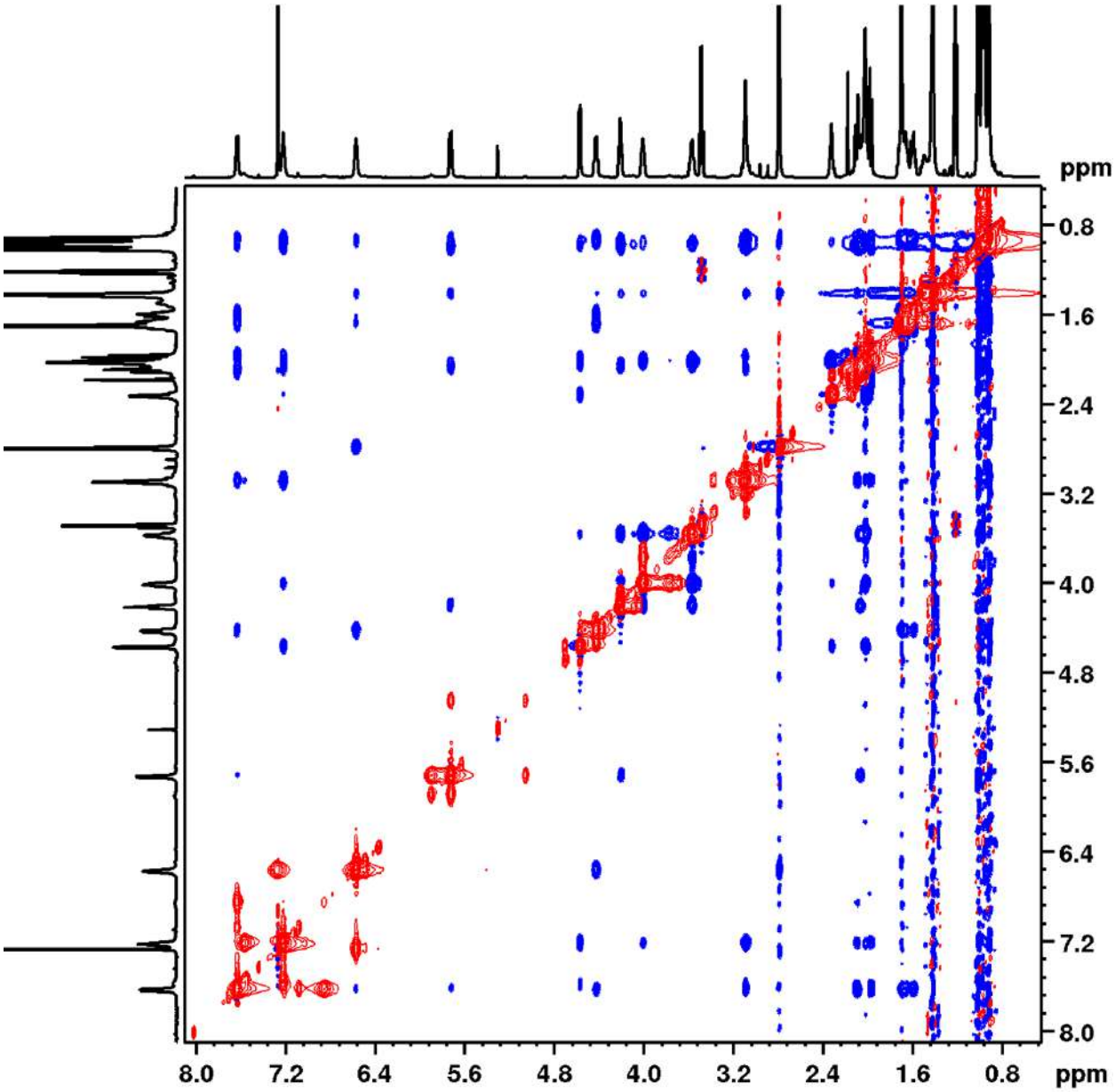

Figure A104. 600 MHz NOESY spectra of peptide **42** at 7mM conc. in $CDCl_3$ at 298 K.

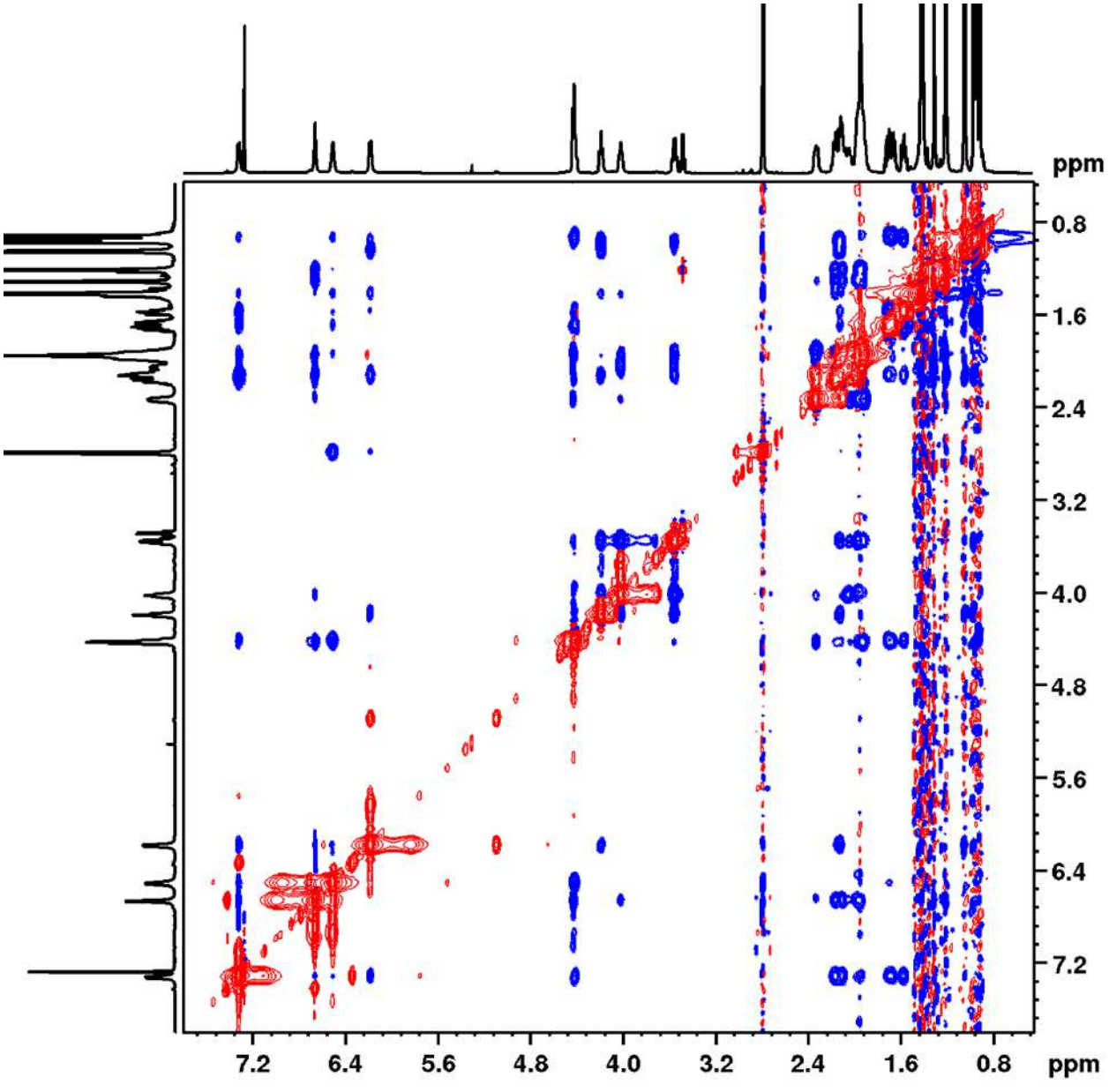

Figure A105. 600 MHz NOESY spectra of peptide **43** at 7mM conc. in $CDCl_3$ at 298 K.

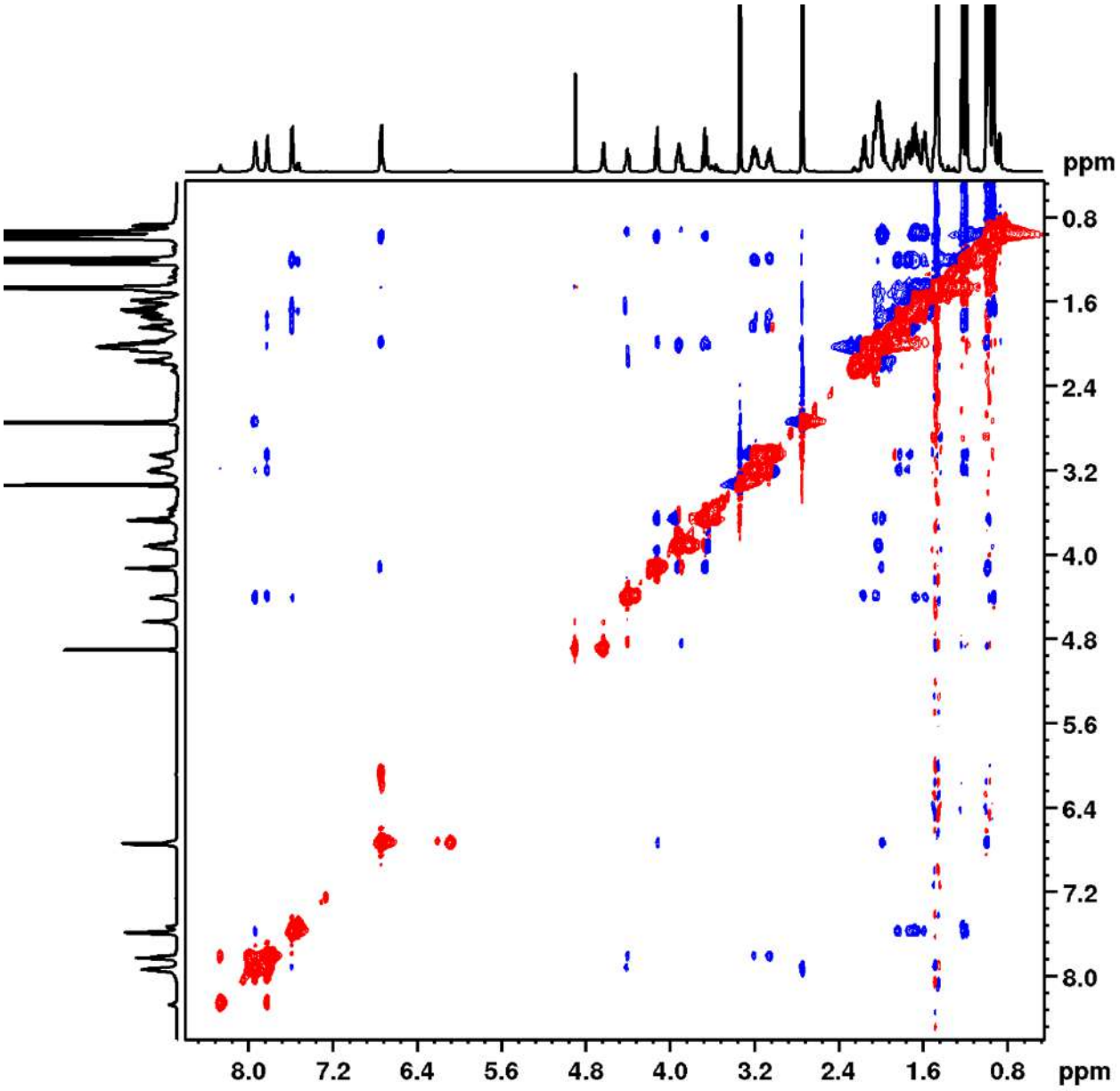

Figure A106. 600 MHz NOESY spectra of peptide **41** at 7mM conc. in CD_3OH at 298 K.

TH-3141_166122021

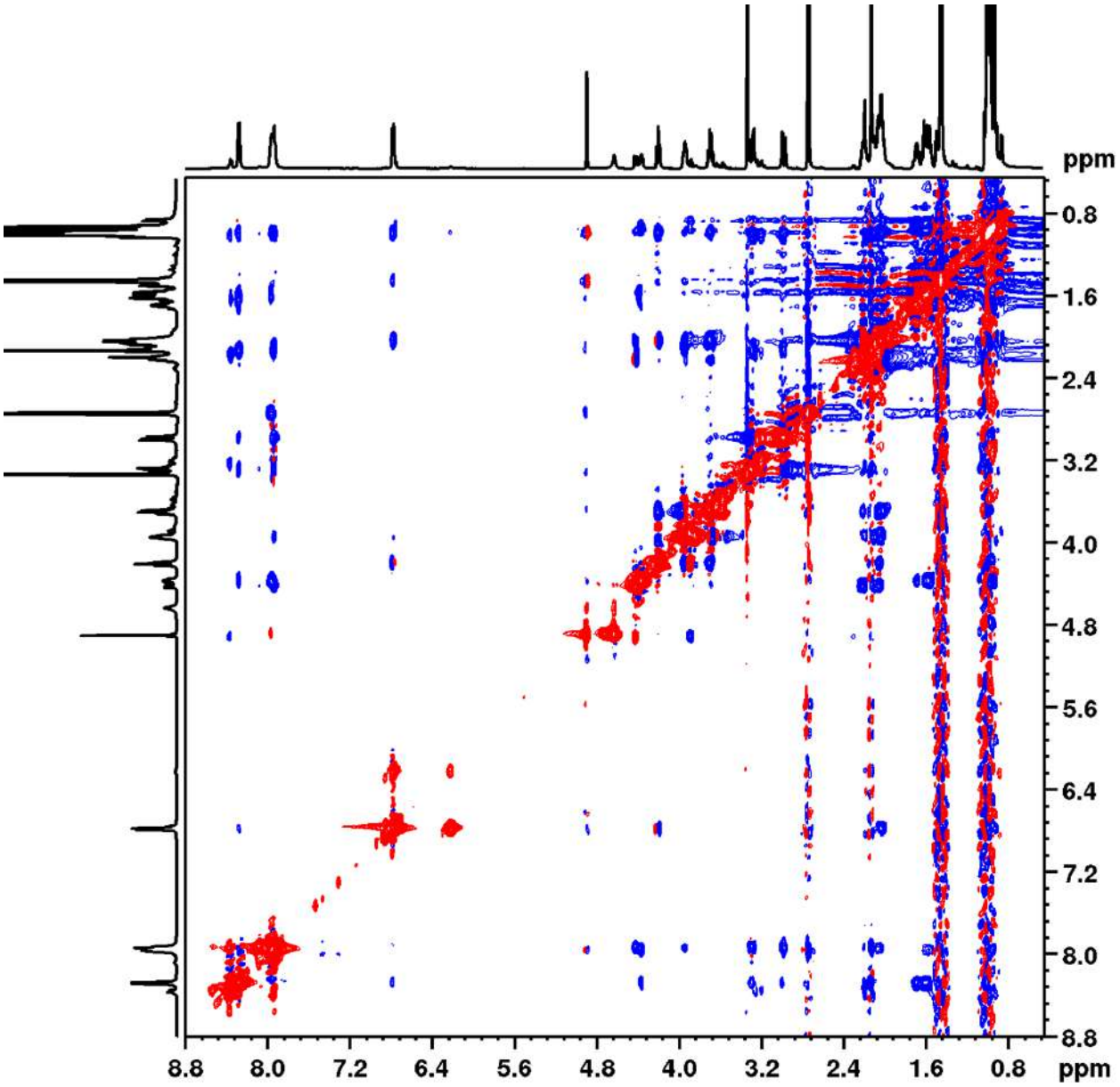

Figure A107. 600 MHz NOESY spectra of peptide **42** at 7mM conc. in CD_3OH at 298 K.

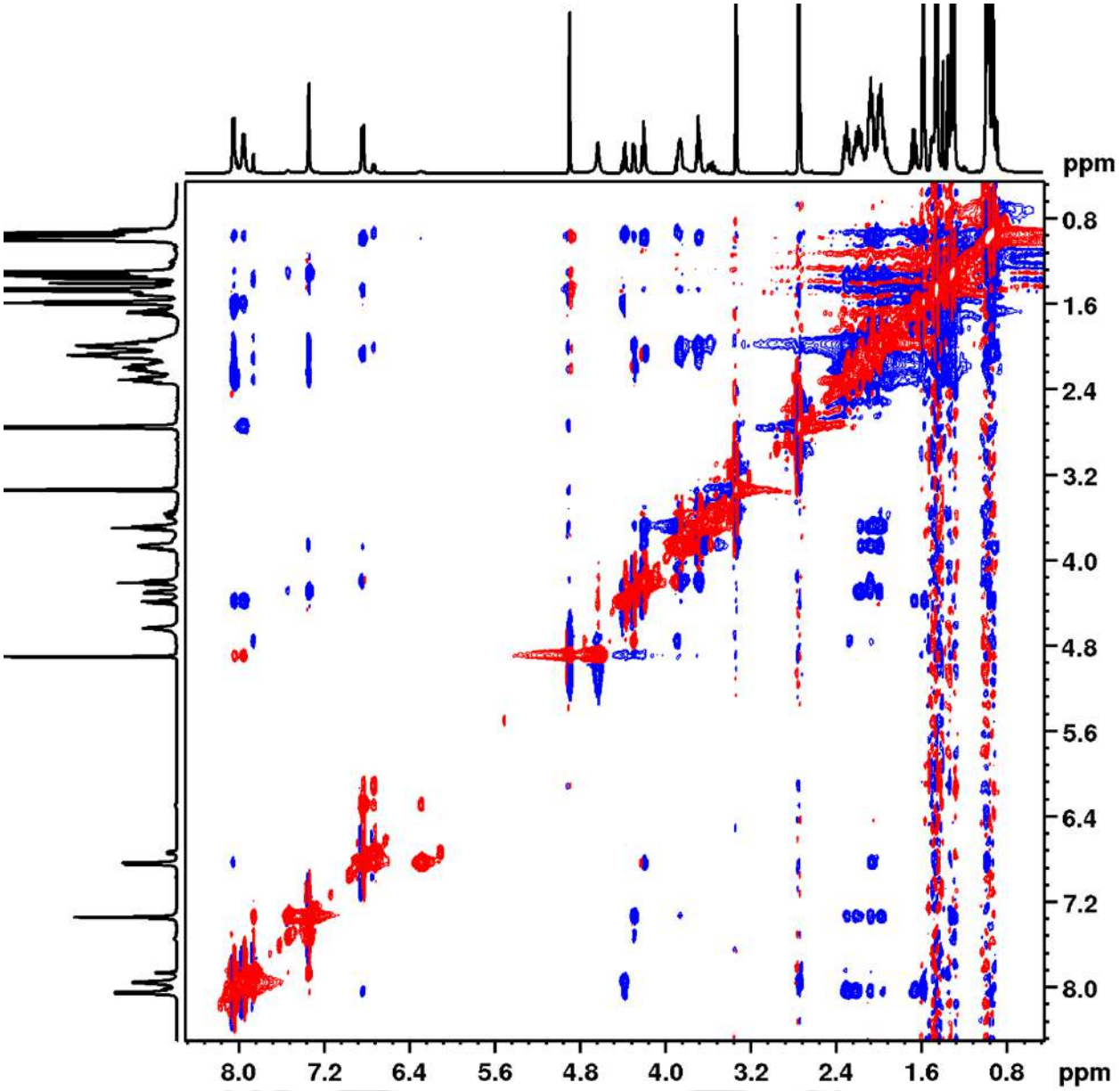

Figure A108. 600 MHz NOESY spectra of peptide **43** at 7mM conc. in CD_3OH at 298 K.

TH-3141_166122021

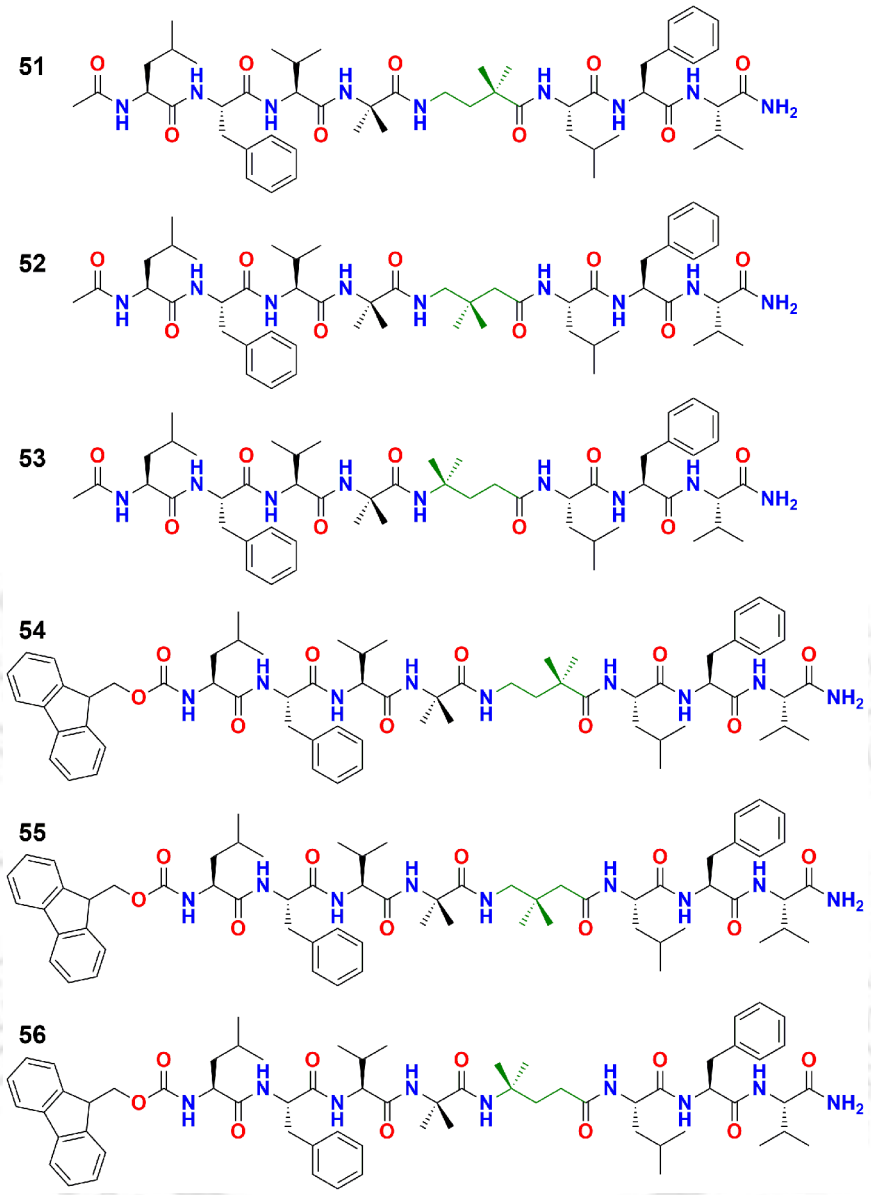

Figure A109. Chemical structures of the peptides **51-56**.

TH-3141_166122021

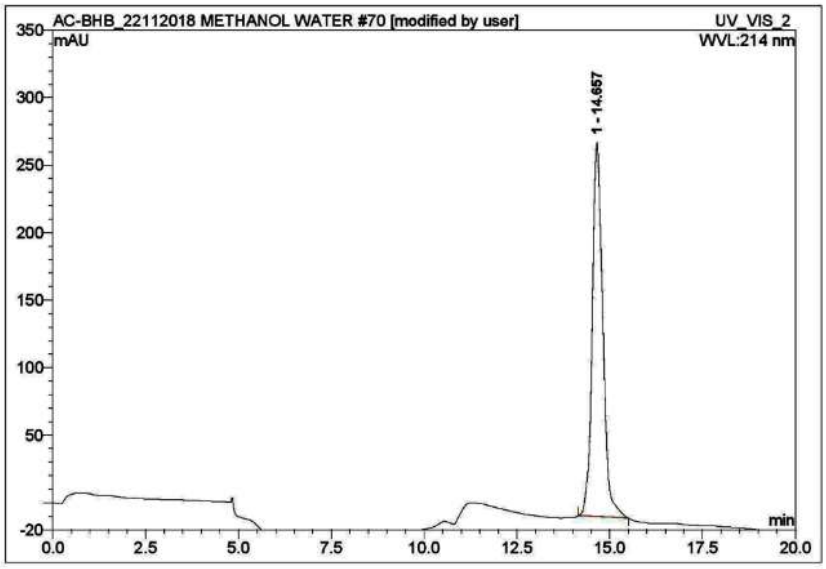

Figure A110. Analytical HPLC trace of **51** in MeOH/H_2O.

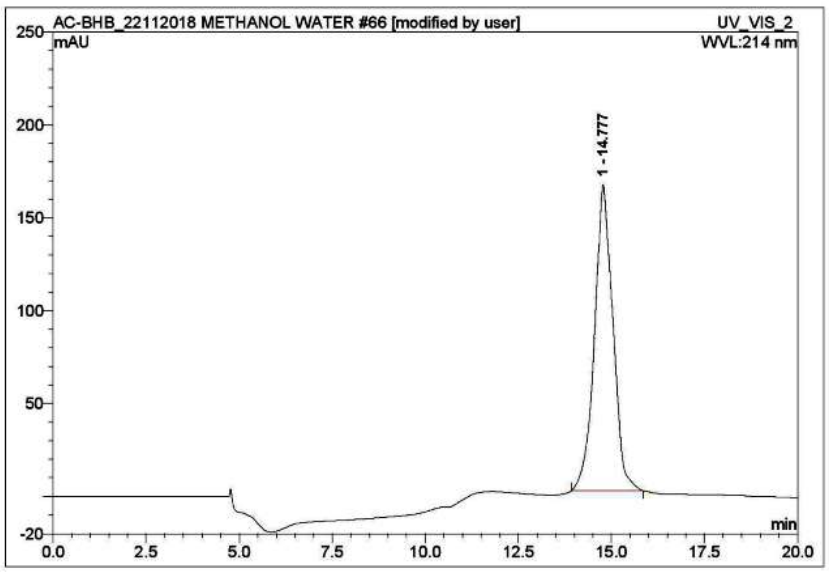

Figure A111. Analytical HPLC trace of **52** in MeOH/H_2O.

TH-3141_166122021

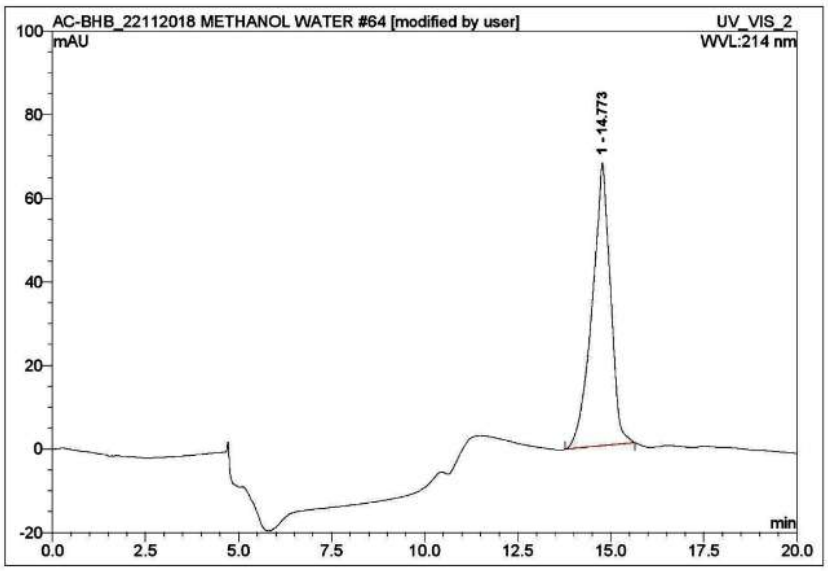

Figure A112. Analytical HPLC trace of **53** in MeOH/H_2O.

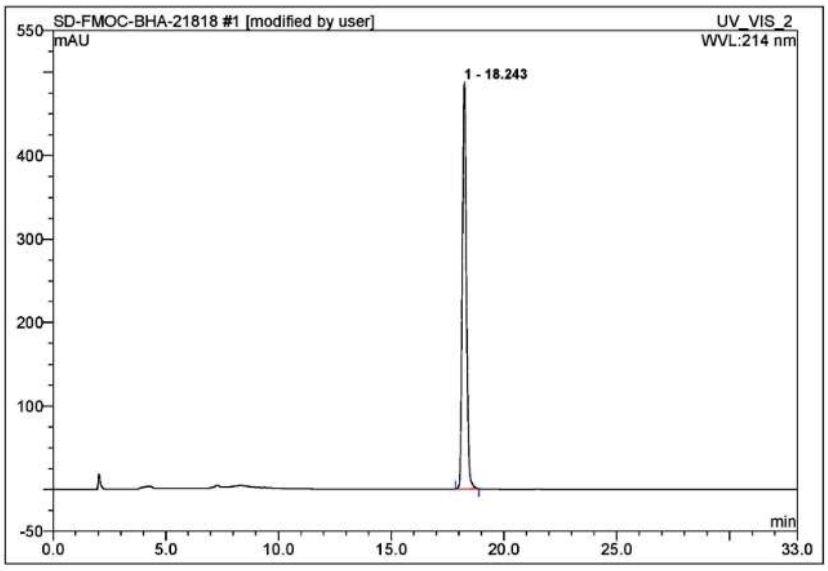

Figure A113. Analytical HPLC trace of **54** in MeOH/H_2O.

TH-3141_166122021

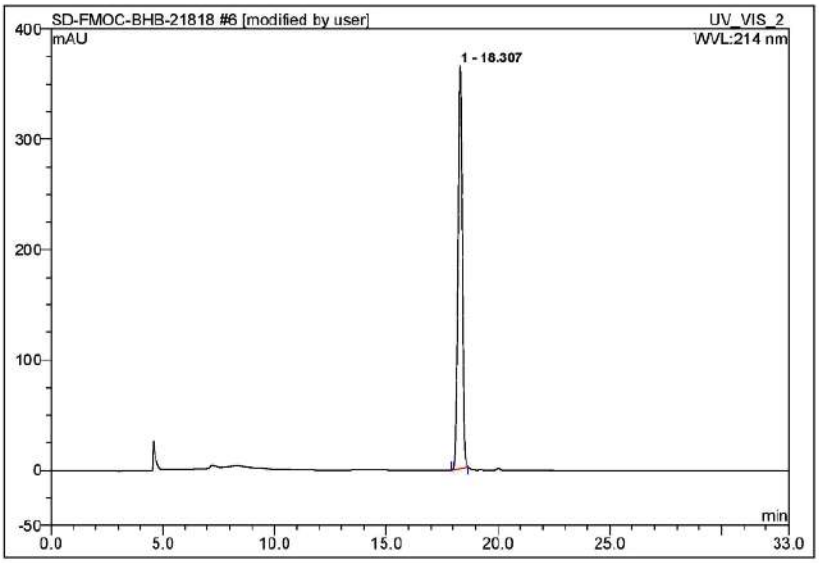

Figure A114. Analytical HPLC trace of **55** in MeOH/H_2O.

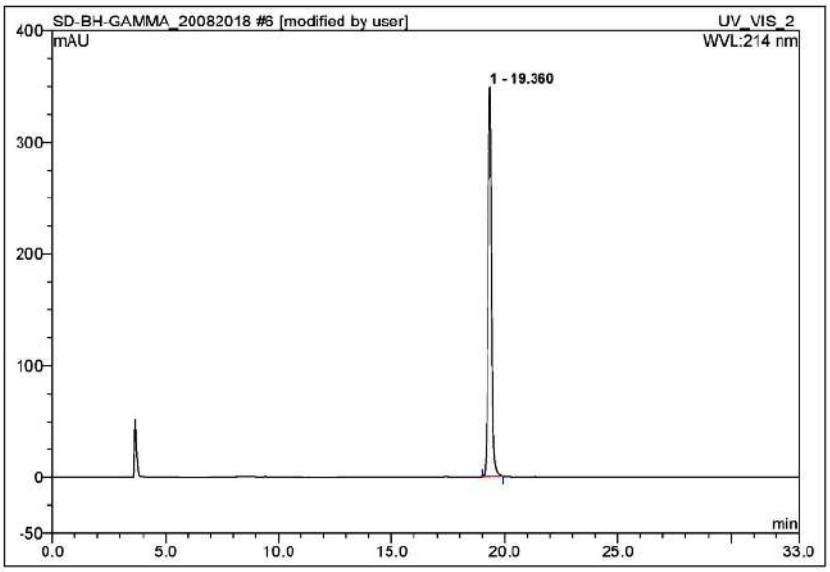

Figure A115. Analytical HPLC trace of **56** in MeOH/H_2O.

TH-3141_166122021

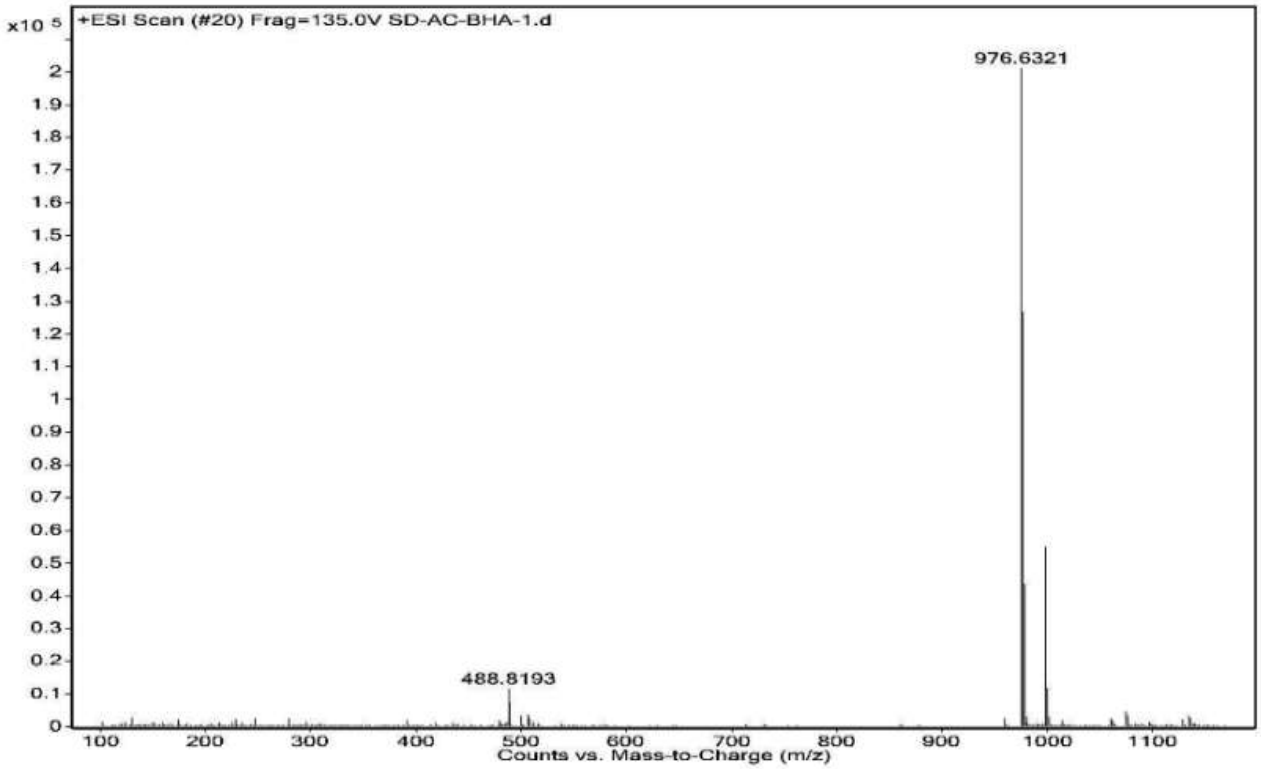

Figure A116. ESI-MS (m/z) of **51**. Calc. $(M+H)^+$ for $C_{52}H_{81}N_9O_9$ = 976.6191 Da; Obs. $(M+H)^+$ = 976.6321 Da.

TH-3141_166122021

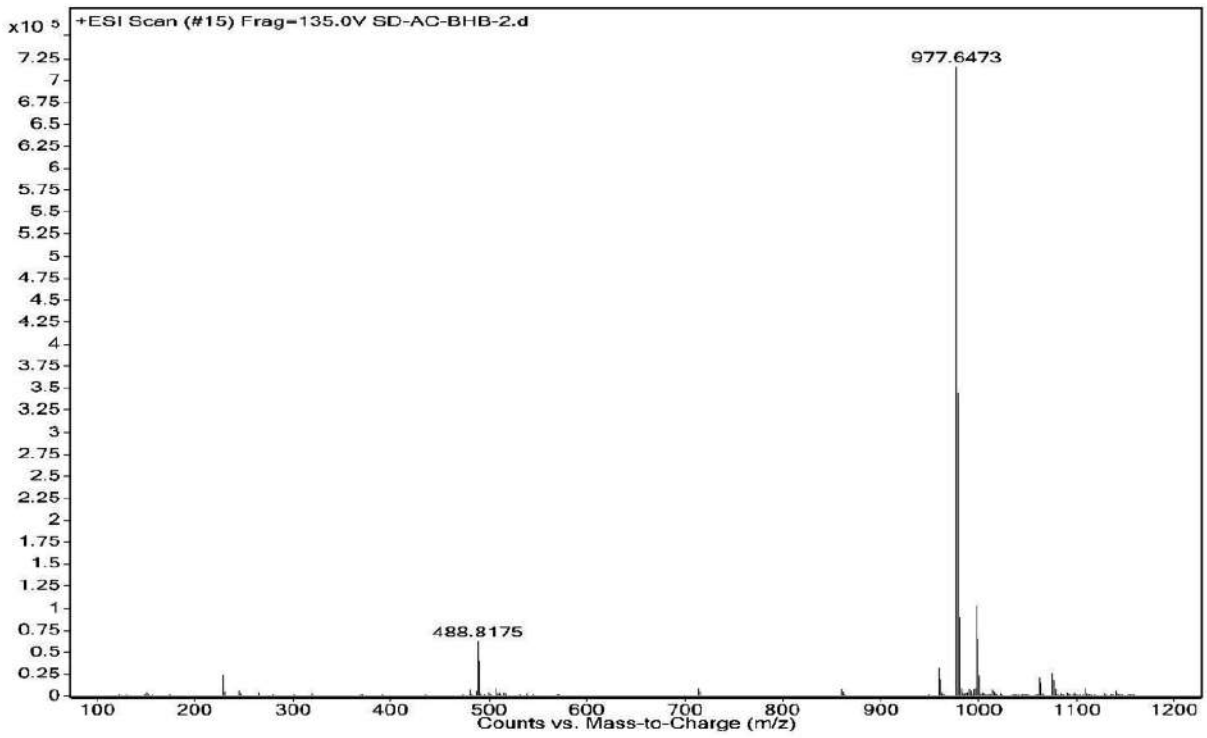

Figure A117. ESI-MS (m/z) of **52**. Calc. $(M+H)^+$ for $C_{52}H_{81}N_9O_9$ = 976.6191 Da; Obs. $(M+2H)^+$ = 977.6473 Da.

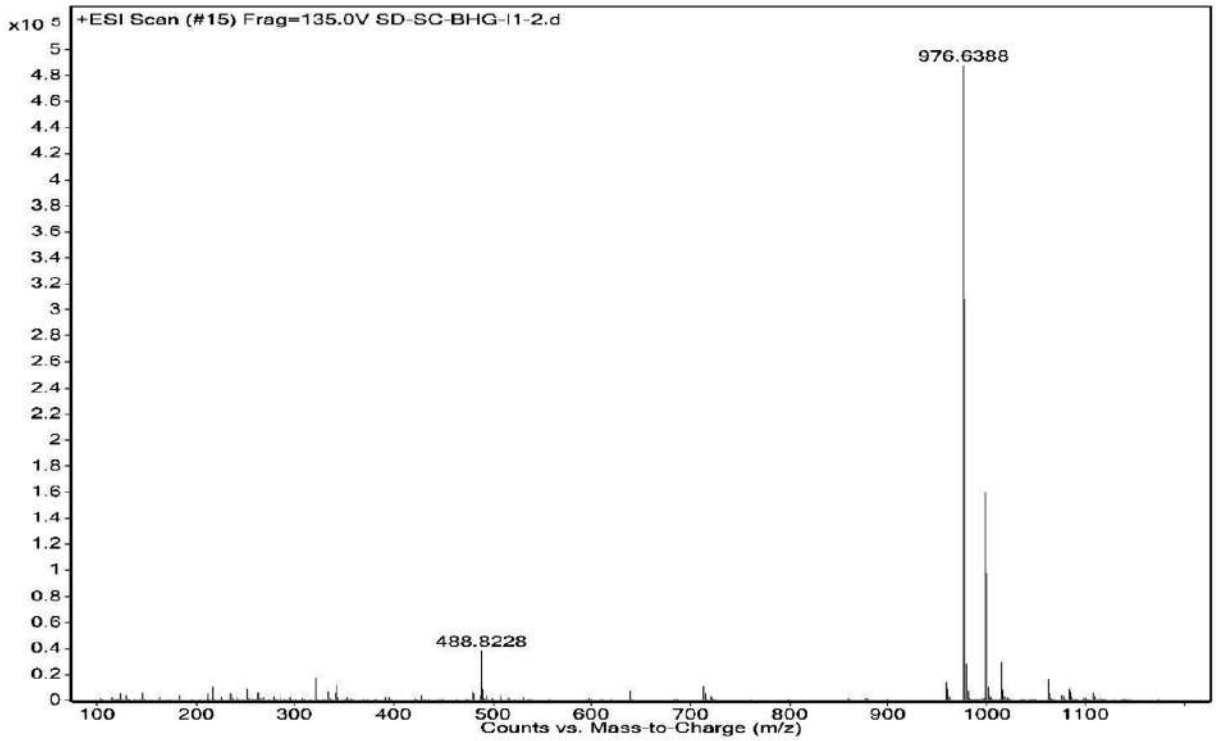

Figure A118. ESI-MS (m/z) of **53**. Calc. $(M+H)^+$ for $C_{52}H_{81}N_9O_9$ = 976.6191 Da; Obs. $(M+H)^+$ = 976.6388 Da.

TH-3141_166122021

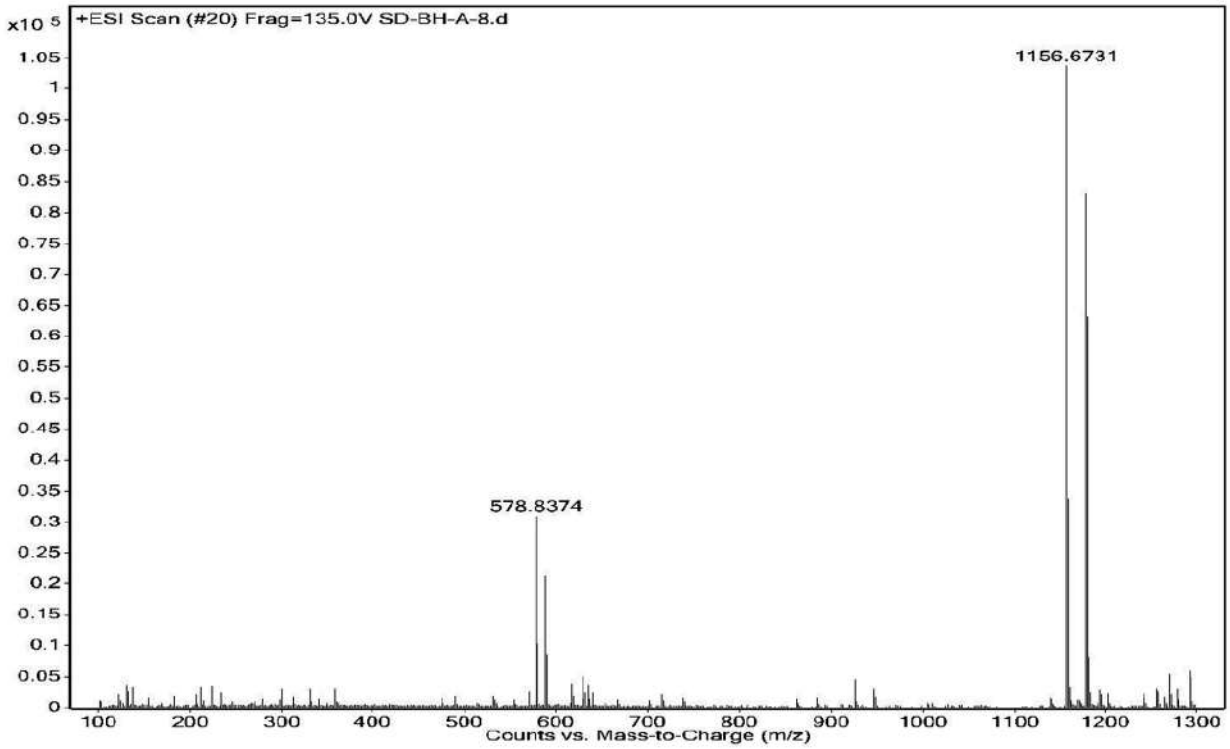

Figure A119. ESI-MS (m/z) of **54**. Calc. M^+ for $C_{65}H_{89}N_9O_{10}$ = 1156.4435 Da; Obs. M^+ = 1156.6731 Da.

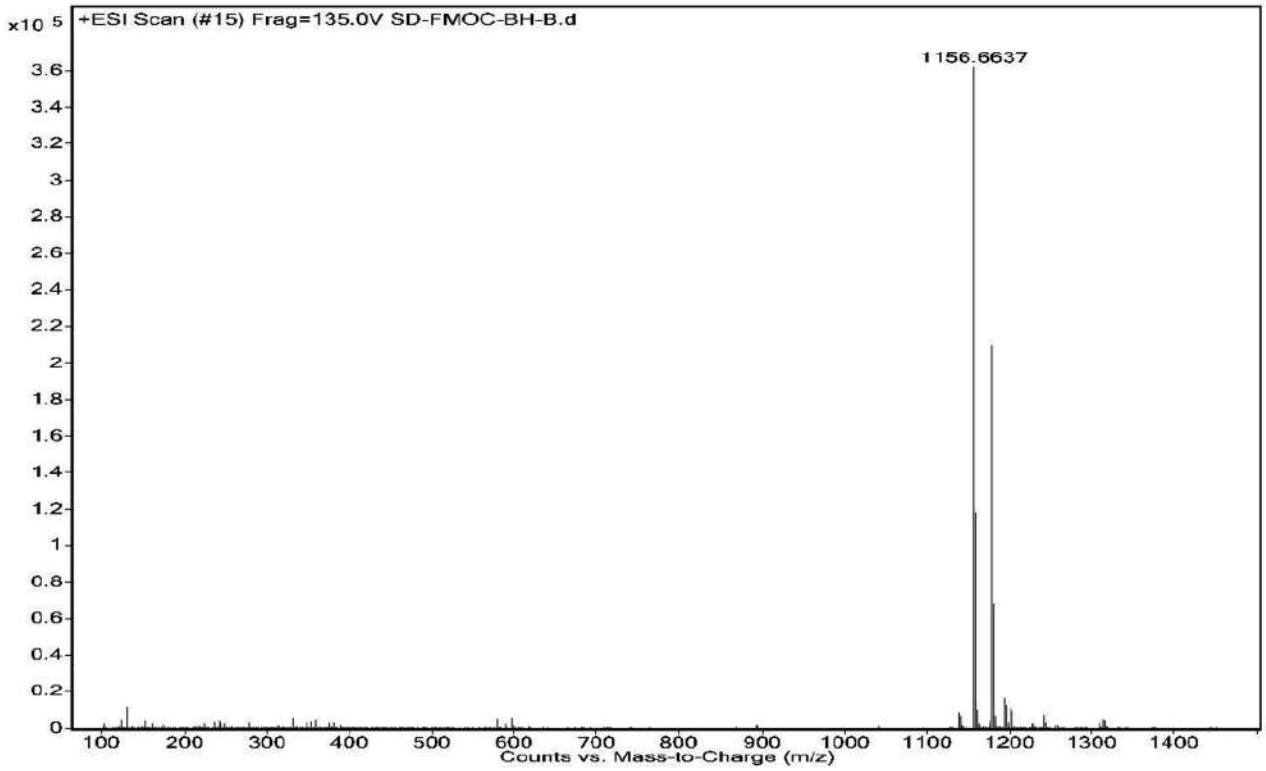

Figure A120. ESI-MS (m/z) of **55**. Calc. M^+ for $C_{65}H_{89}N_9O_{10}$ = 1156.4435 Da; Obs. M^+ = 1156.6637 Da.

TH-3141_166122021

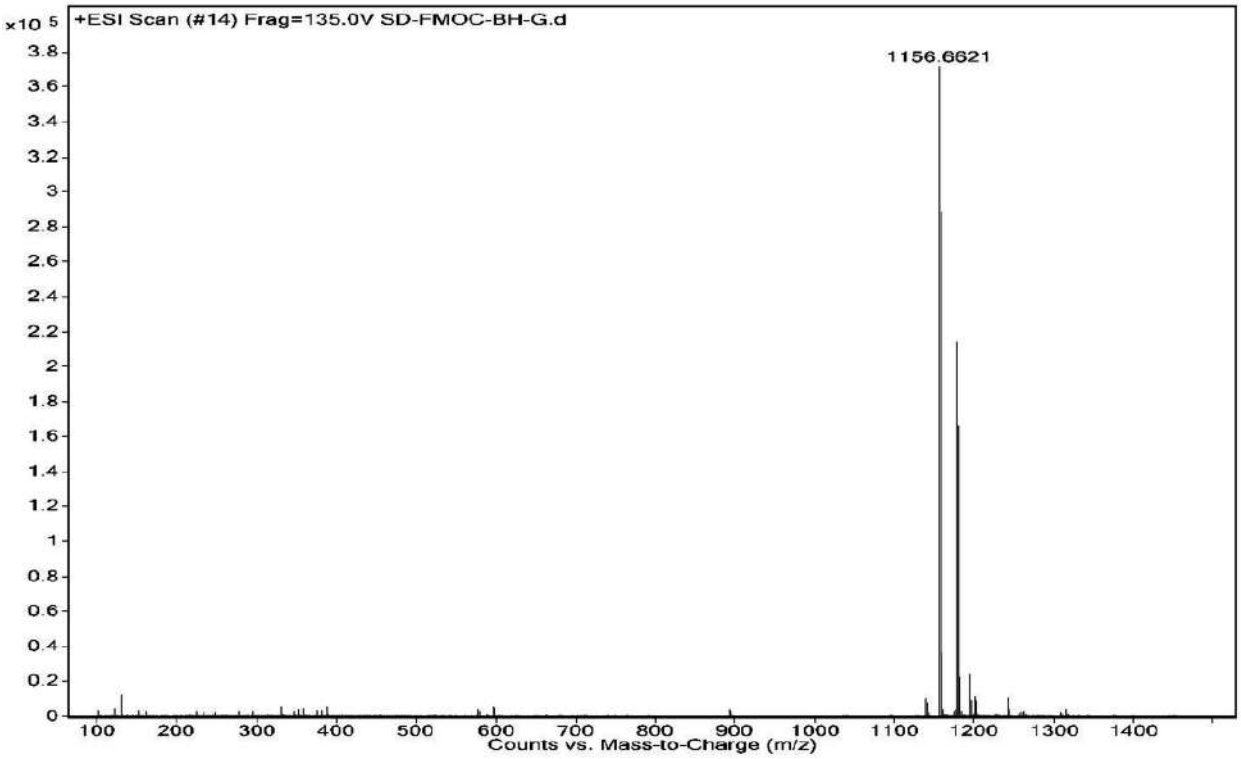

Figure A121. ESI-MS (m/z) of **56**. Calc. M^+ for $C_{65}H_{89}N_9O_{10}$ = 1156.4435 Da; Obs. M^+ = 1156.6621 Da.

TH-3141_166122021

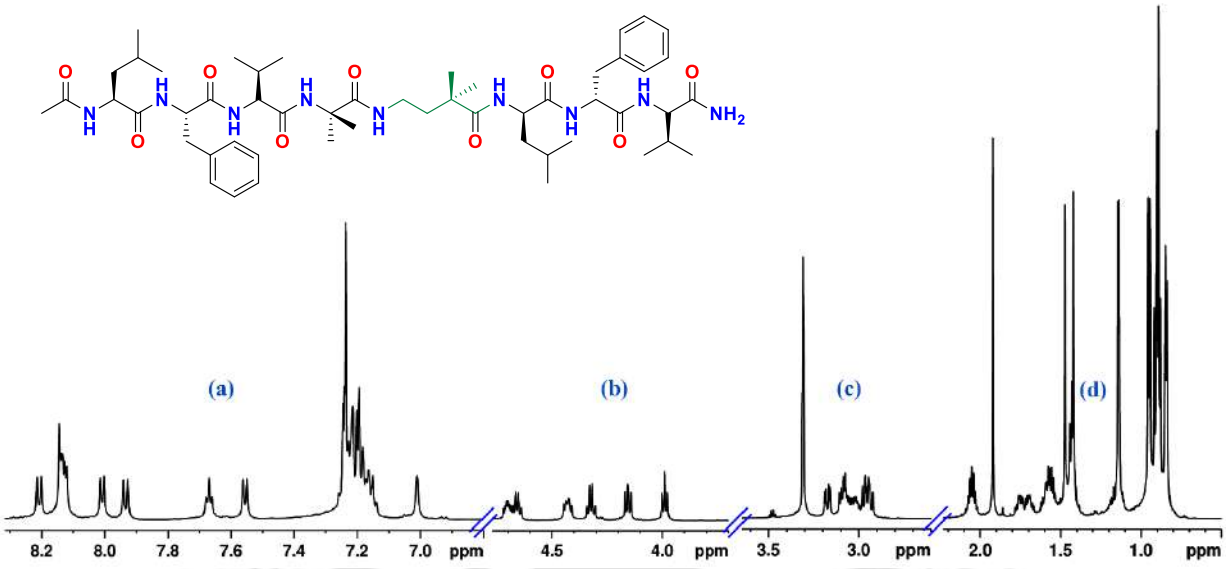

Figure A122. 600 MHz ^{1}H NMR spectra of **51** in CD_3OH. Different regions are (a) Amide, Aromatic and C-ter NH_2 (b) $C^{\alpha}H$ protons (b) $C^{\beta}H$ and $C^{\gamma}H$ of Phe & $\gamma^{2,2}5$ (d) All other aliphatic protons.

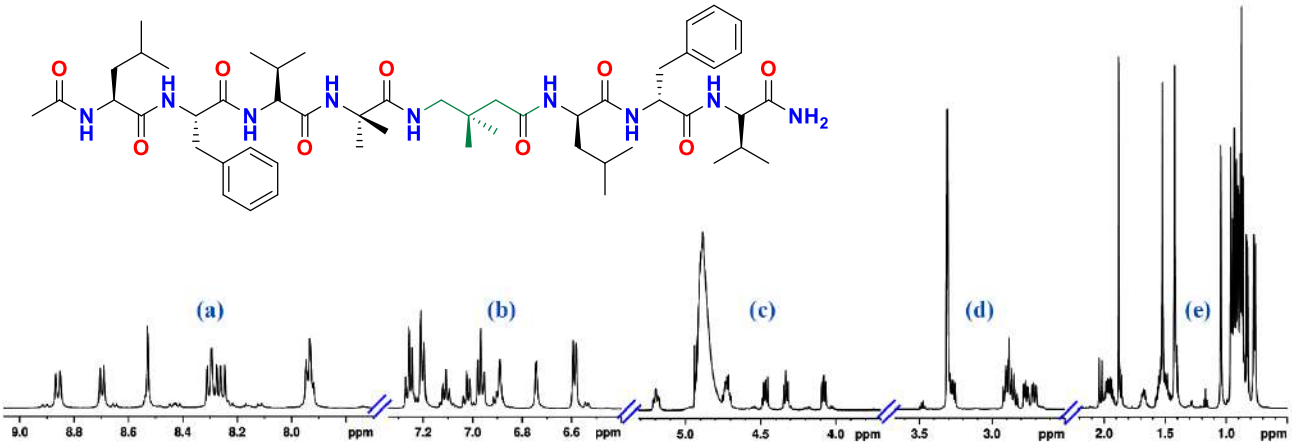

Figure A123. 600 MHz ^{1}H NMR spectra **52** in CD_3OH. Different regions are (a) Amide protons (b) Aromatic and C-ter NH_2 protons (c) Residual water and $C^{\alpha}H$ protons (d) $C^{\beta}H$ and $C^{\gamma}H/C^{\alpha}H$ protons of Phe & $\gamma^{3,3}5$ (e) All other aliphatic protons.

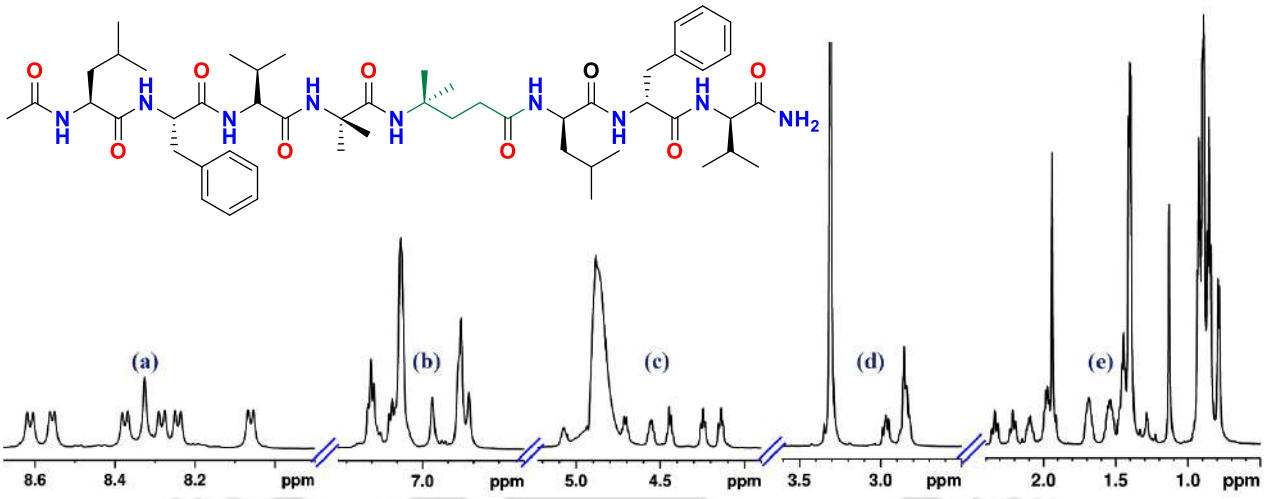

Figure A124. 600 MHz ^{1}H NMR spectra of **53** in CD_3OH. Different regions are (a) Amide protons, (b) Aromatic and C-ter NH_2 protons (c) Residual water and $C^{\alpha}H$ protons (d) $C^{\beta}H$ protons of Phe, (e) All other aliphatic protons.

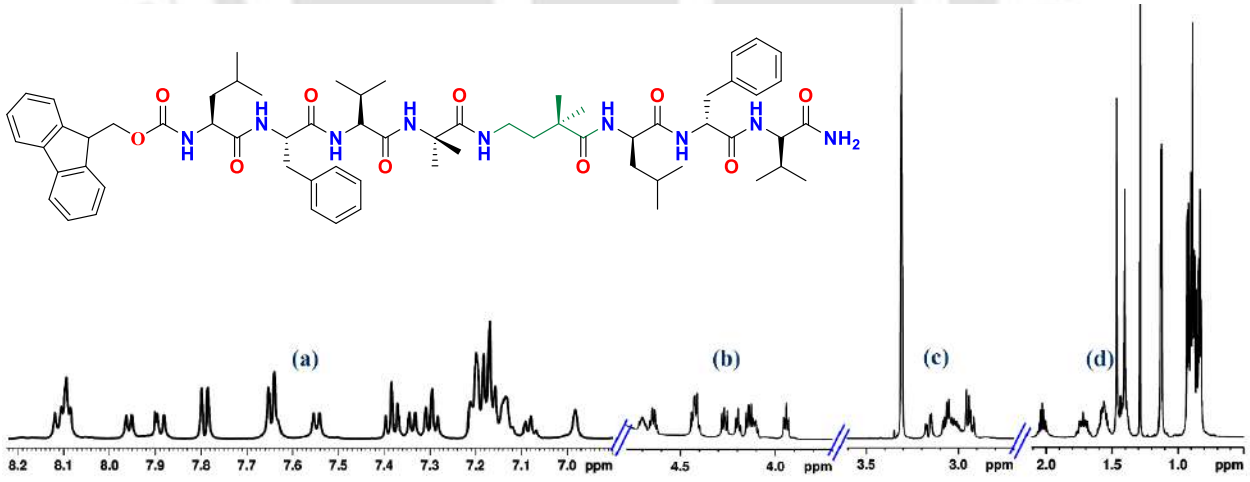

Figure A125. 600 MHz ^{1}H NMR spectra of **54** in CD_3OH. Different regions are: (a) Amide, Fmoc/Phe Aromatic and C-ter NH_2 protons, (b) $C^{\alpha}H$ and Fmoc aliphatic protons (c) $C^{\beta}H$ protons of Phe, (d) All other aliphatic protons.

TH-3141_166122021

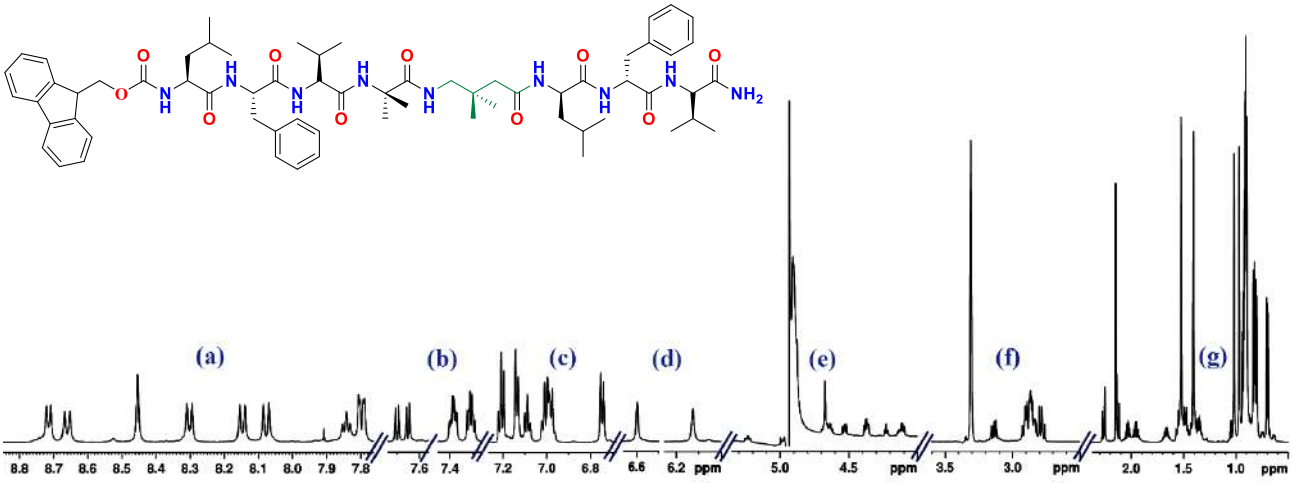

Figure A126. 600 MHz ^{1}H NMR spectra of **55** in CD_3OH. Different regions are (a) amide protons, (b) Fmoc aromatic protons, (c) Phe aromatic, (d) C-ter NH_2 (e) Residual water, $C^{\alpha}H$ and Fmoc aliphatic protons (f) $C^{\beta}H$ and $C^{\gamma}H/C^{\alpha}H$ protons of Phe&$\gamma^{3,3}5$ (g) All other aliphatic protons.

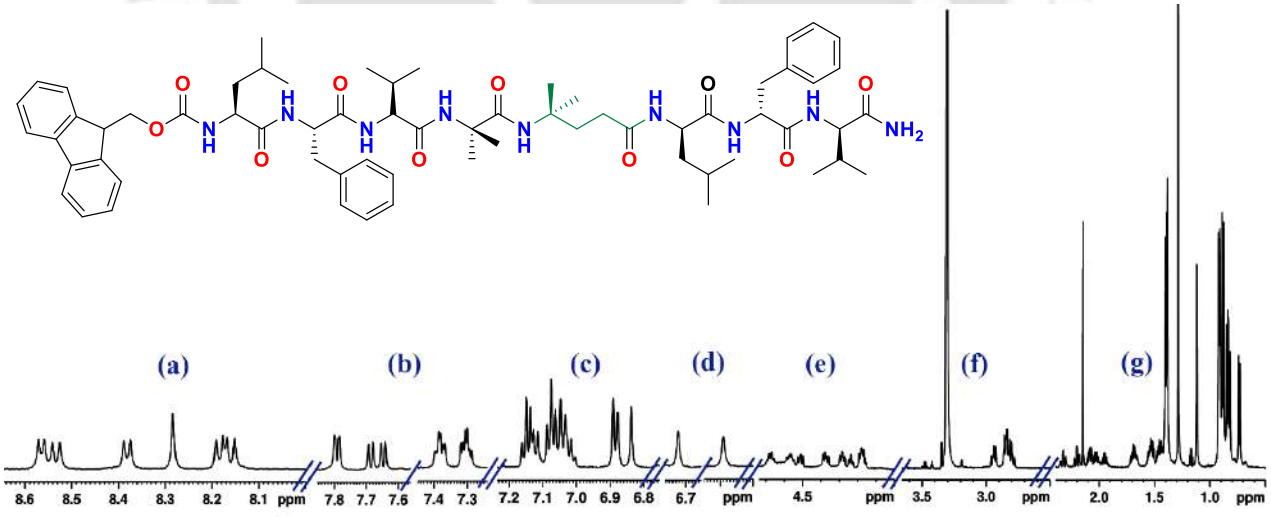

Figure A127. 600 MHz ^{1}H NMR spectra of **56** in CD_3OH. Different regions are (a) Amide protons (b) Fmoc aromatic (c) Phe aromatic (d) C-ter NH_2 (e) $C^{\alpha}H$ and Fmoc aliphatic Protons (f) $C^{\beta}H$ Protons of Phe (g) All other aliphatic protons.

TH-3141_166122021

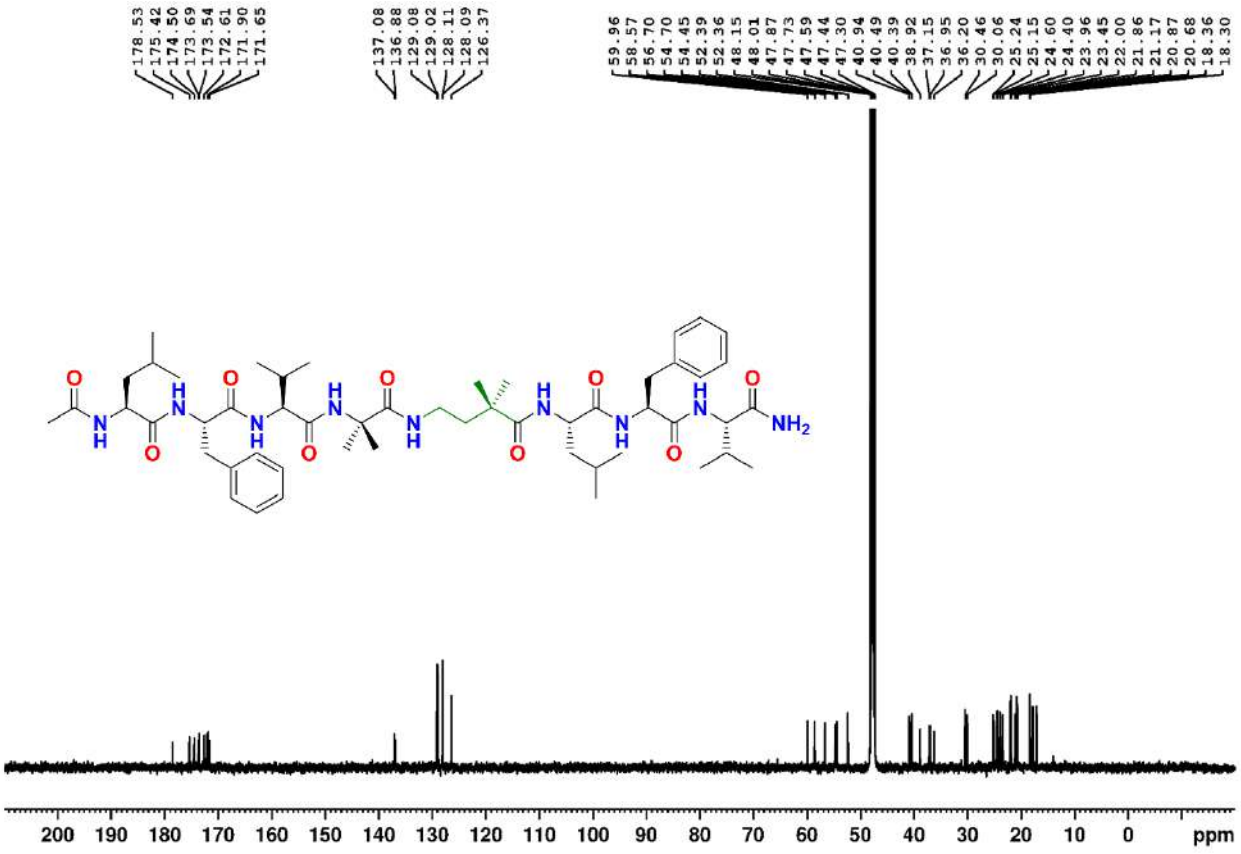

Figure A128. 150 MHz ^{13}C NMR spectra of **51** in CD_3OH at 5 mM concentration (298 K).

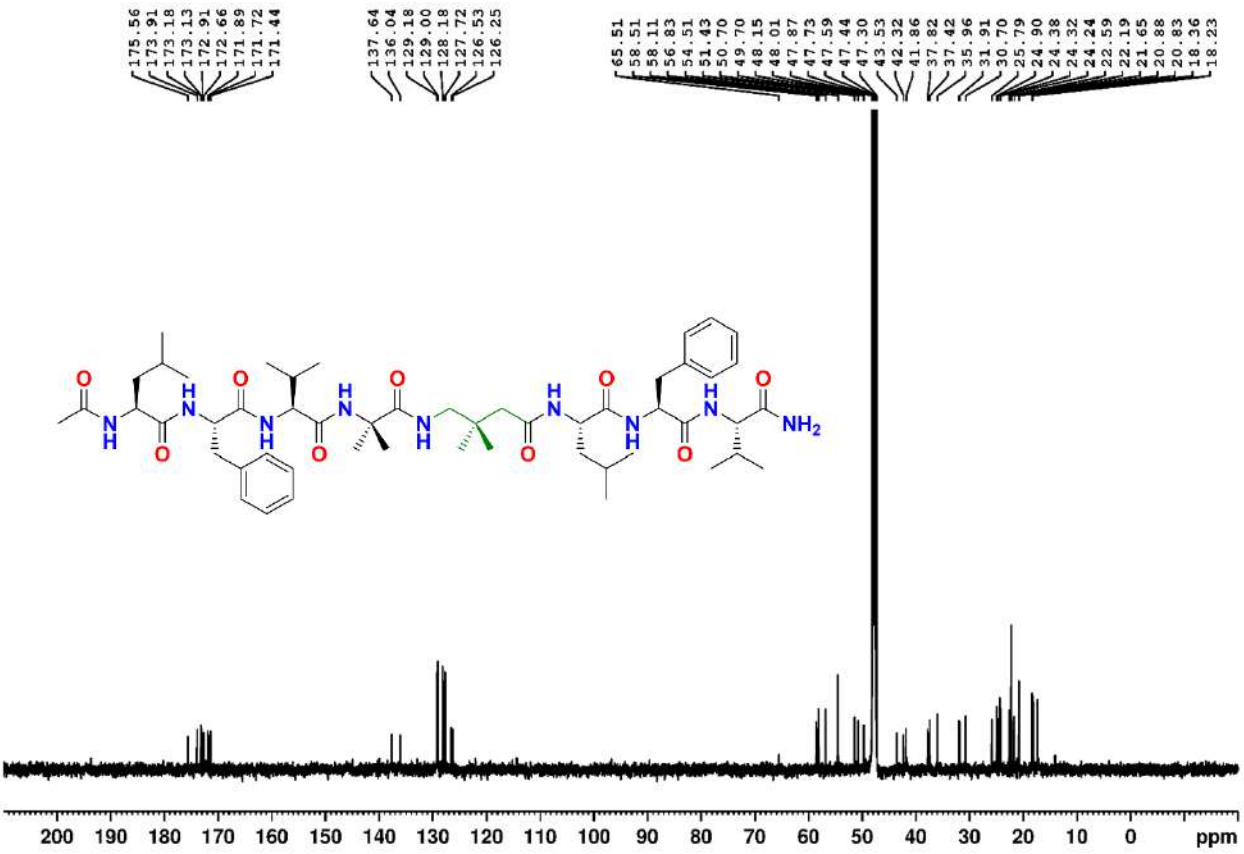

Figure A129. 150 MHz ^{13}C NMR spectra of **52** in CD_3OH at 5 mM concentration (298 K).

TH-3141_166122021

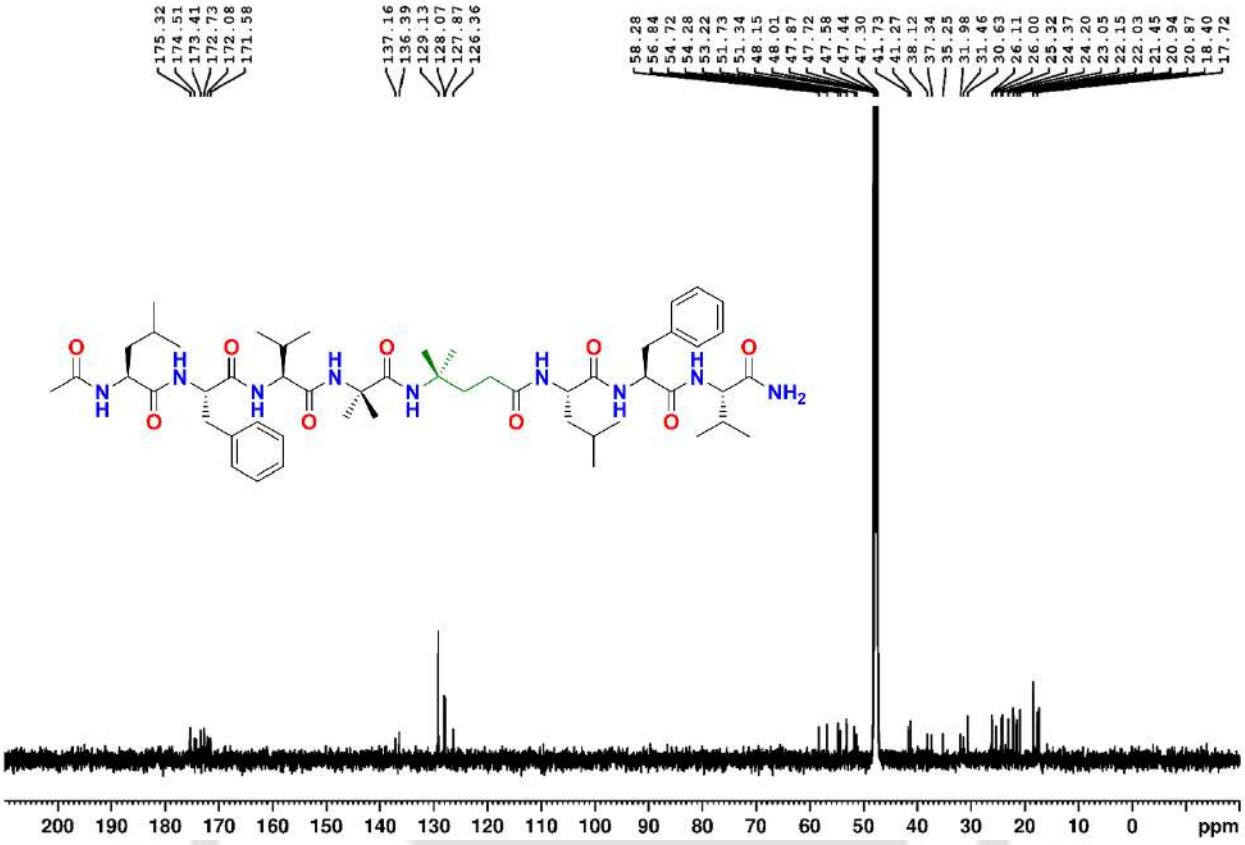

Figure A130. 150 MHz ^{13}C NMR spectra of **53** in CD_3OH at 5 mM concentration (298 K).

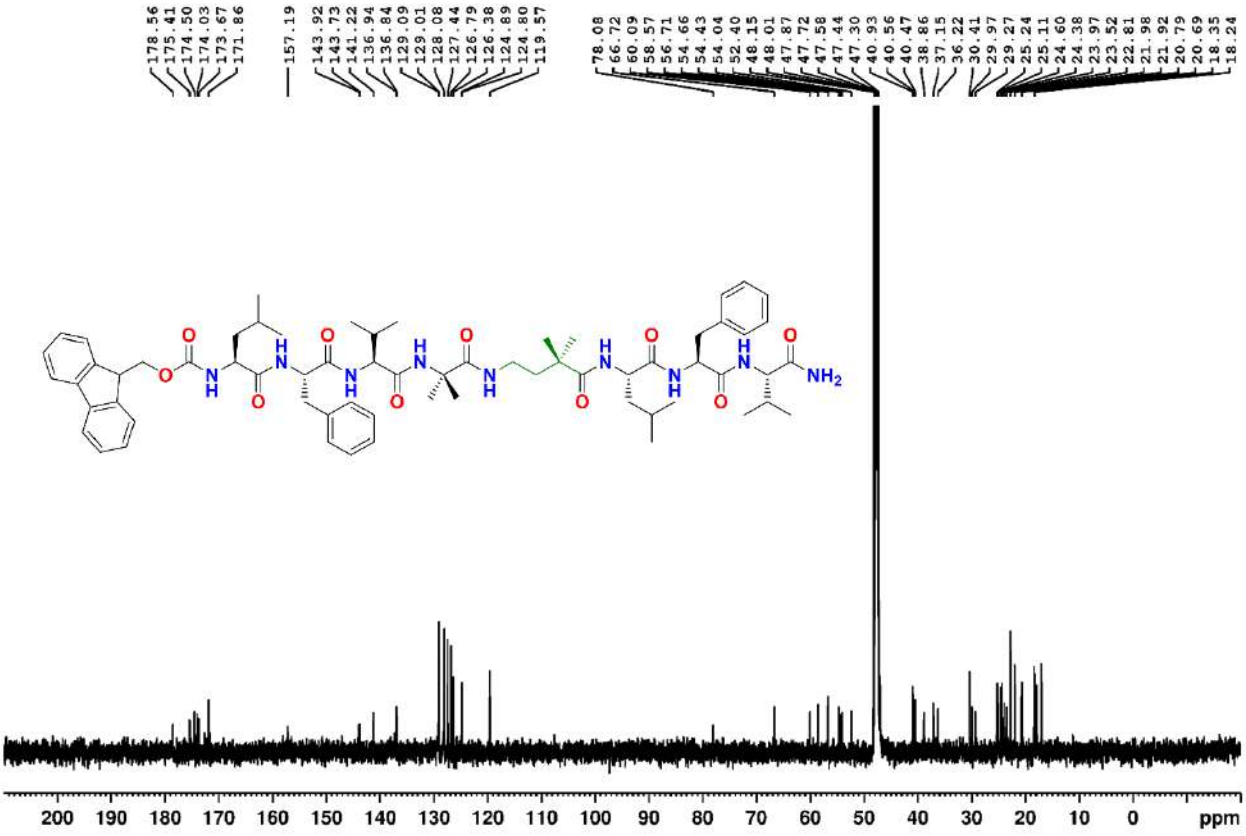

Figure A131. 150 MHz ^{13}C NMR spectra of **54** in CD_3OH at 5 mM concentration (298 K).

TH-3141_166122021

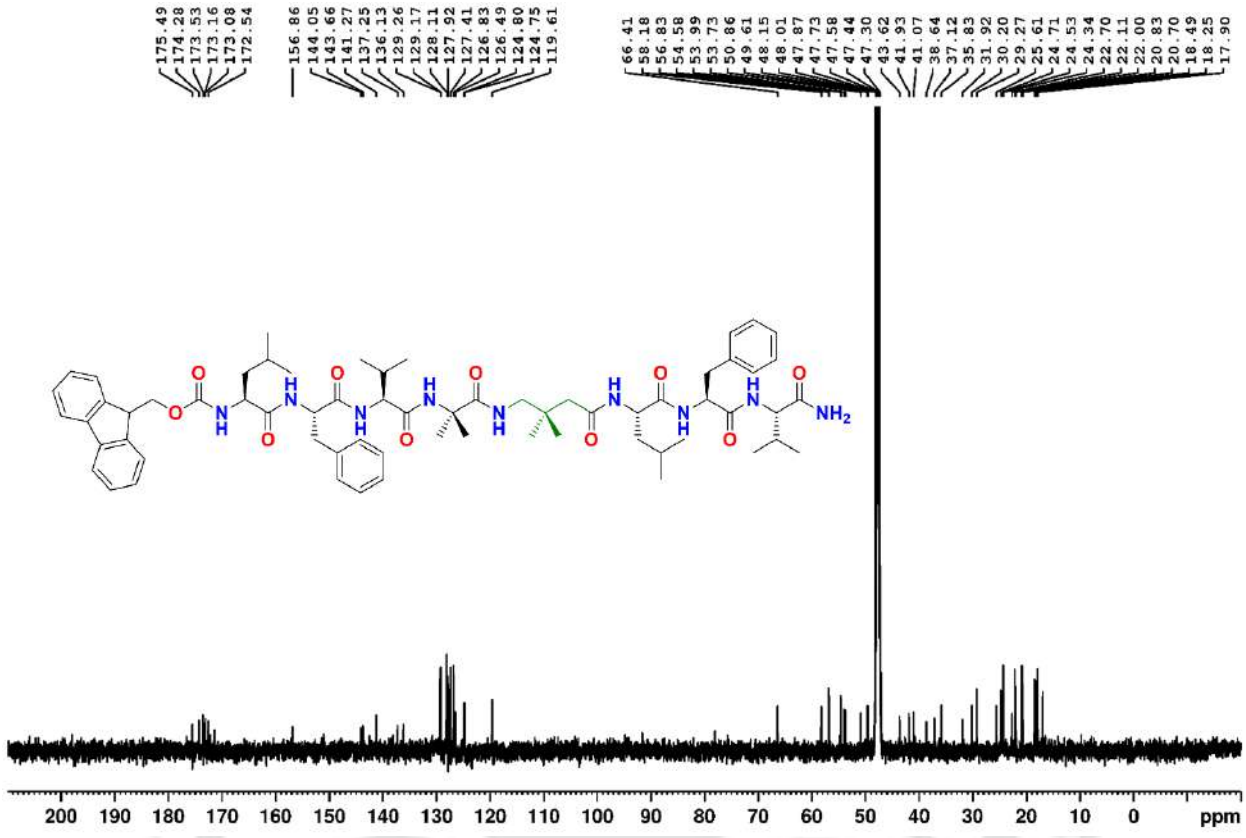

Figure A132. 150 MHz ^{13}C NMR spectra of **55** in CD_3OH at 5 mM concentration (298 K).

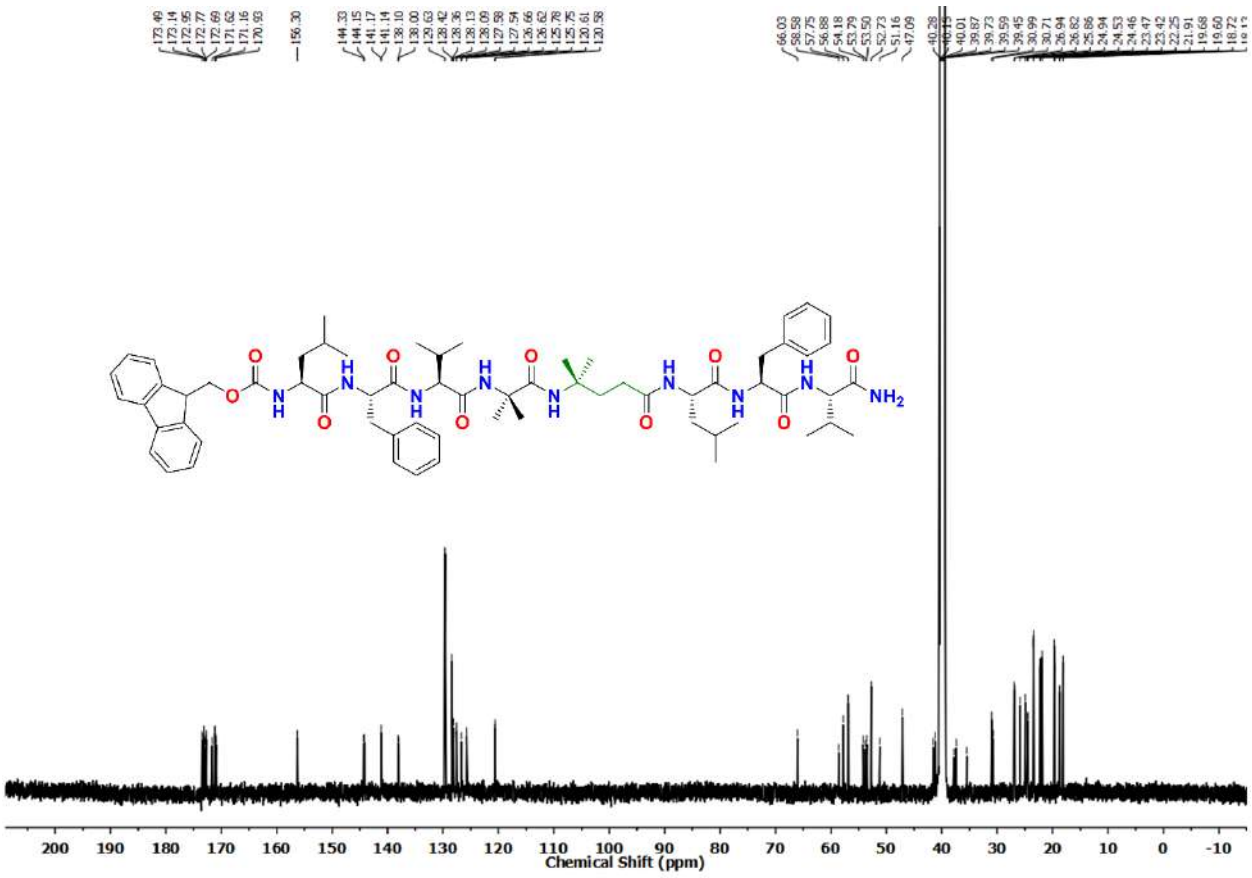

Figure A133. 150 MHz ^{13}C NMR spectra of **56** in DMSO-d_6 at 5 mM concentration (298 K).

TH-3141_166122021

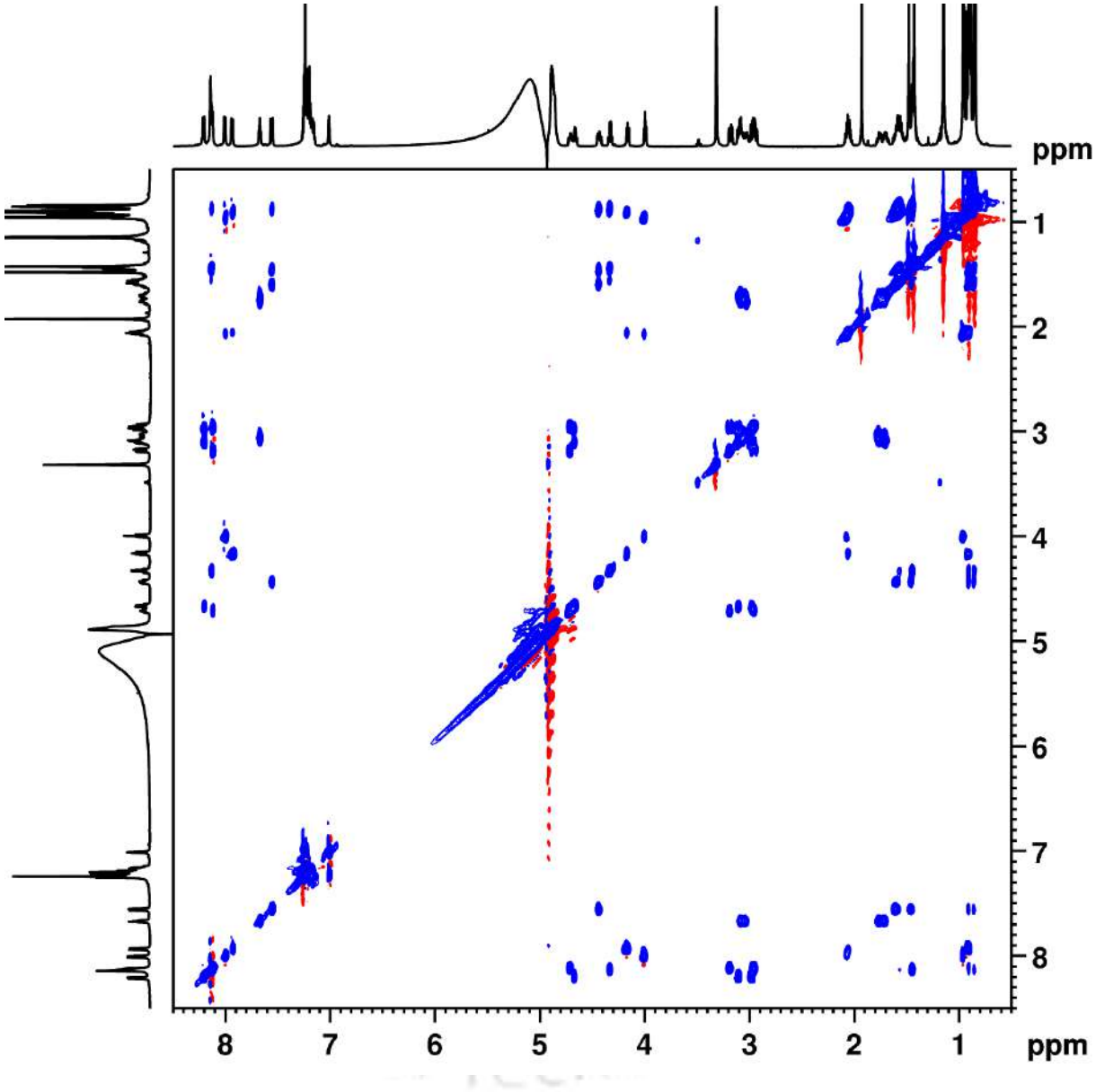

Figure A134. 600 MHz TOCSY spectra of peptide **51** at 5 mM conc. in CD_3OH at 298 K.

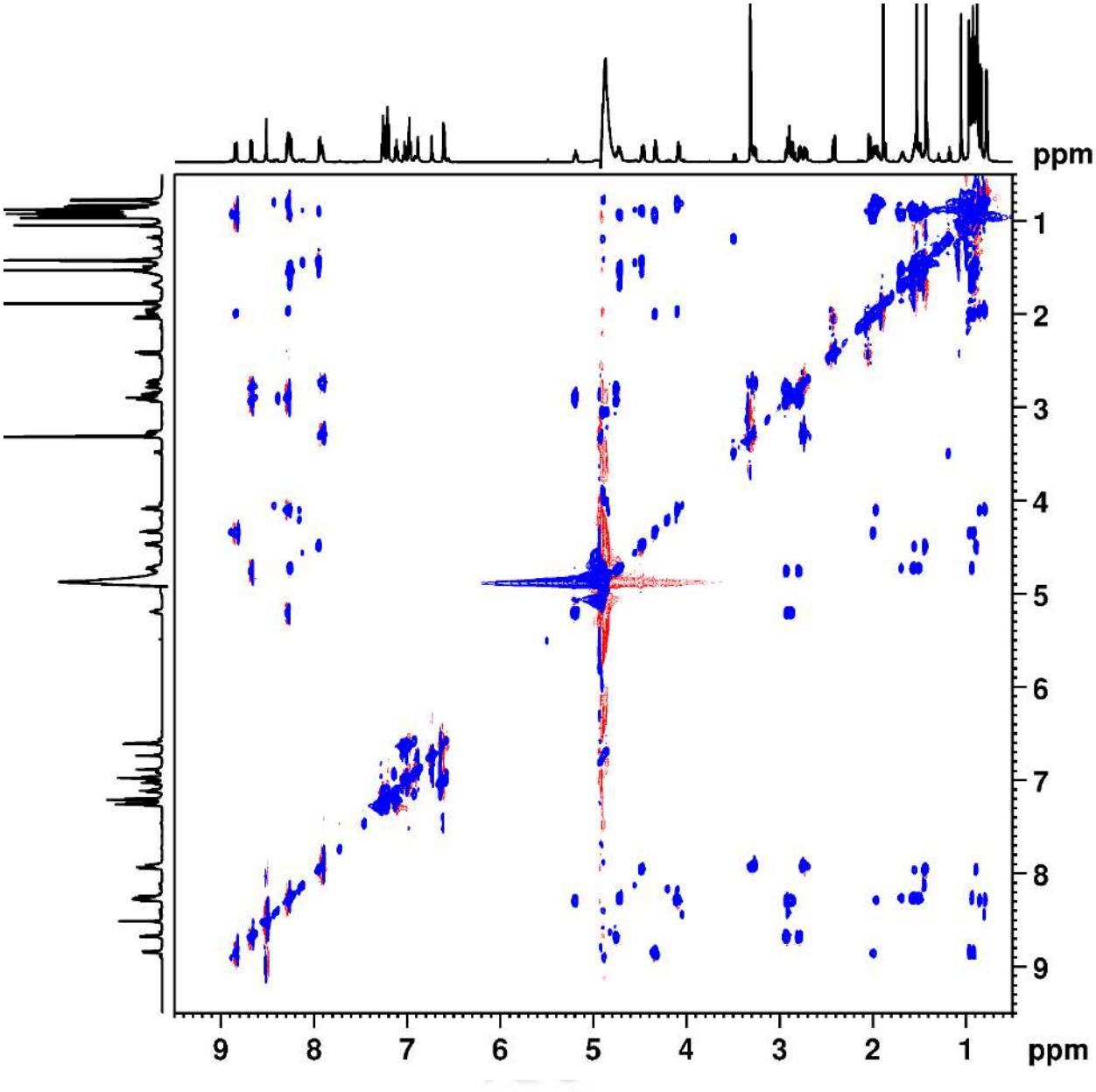

Figure A135. 600 MHz TOCSY spectra of peptide **52** at 5 mM conc. in CD_3OH at 298 K.

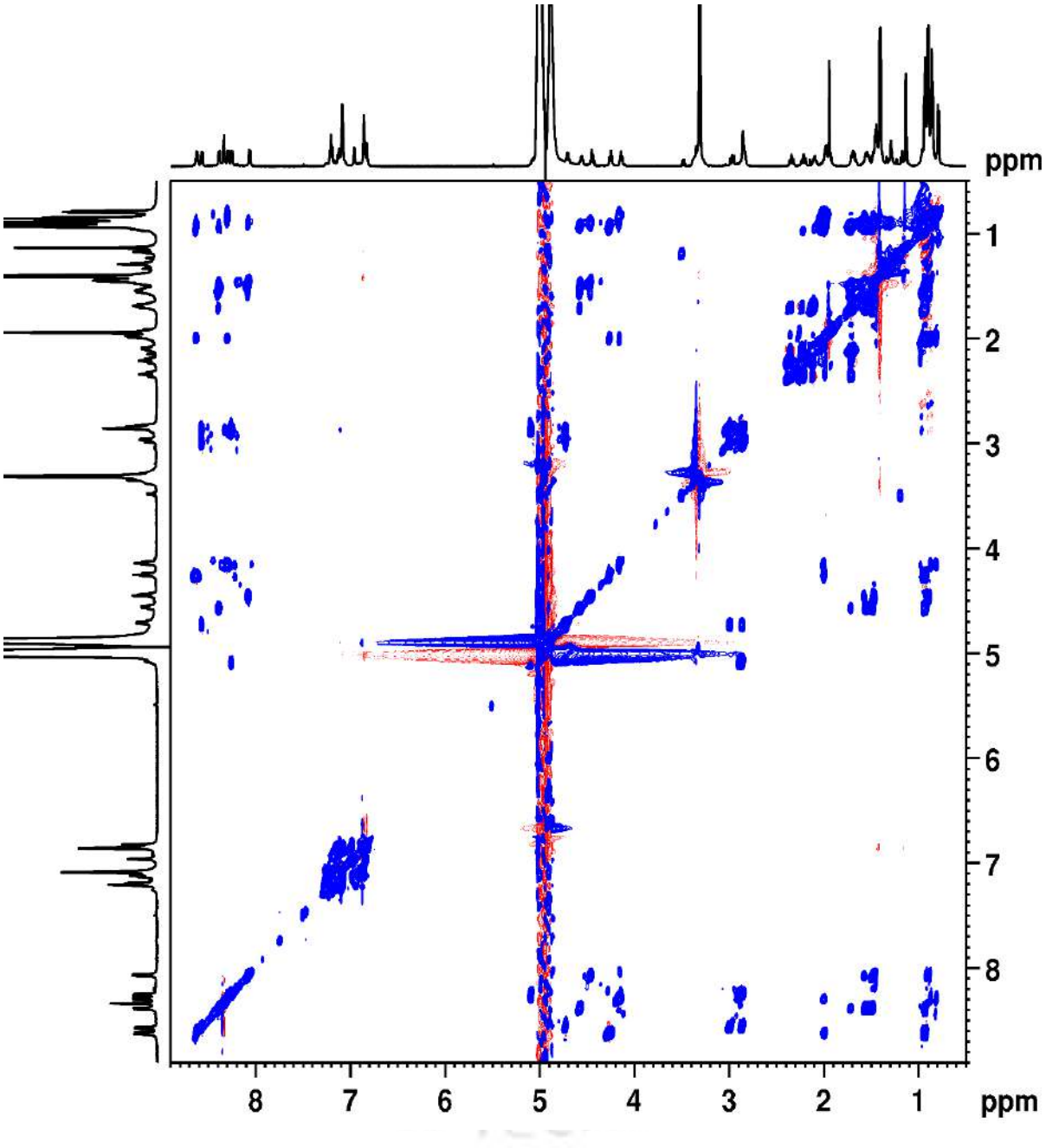

Figure A136. 600 MHz TOCSY spectra of peptide **53** at 4 mM conc. in CD_3OH at 298 K.

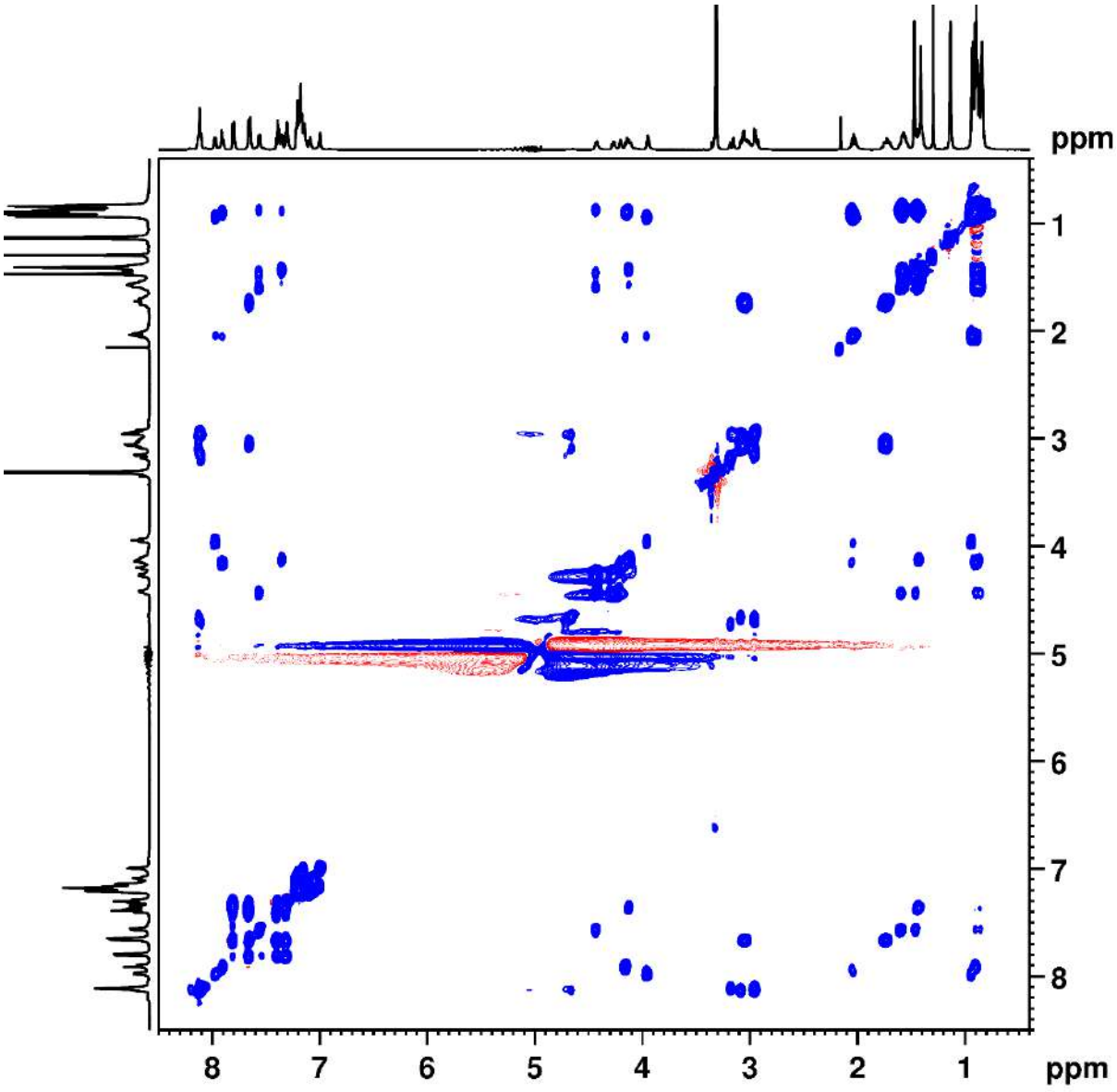

Figure A137. 600 MHz TOCSY spectra of peptide **54** at 5 mM conc. in CD_3OH at 298 K.

TH-3141_166122021

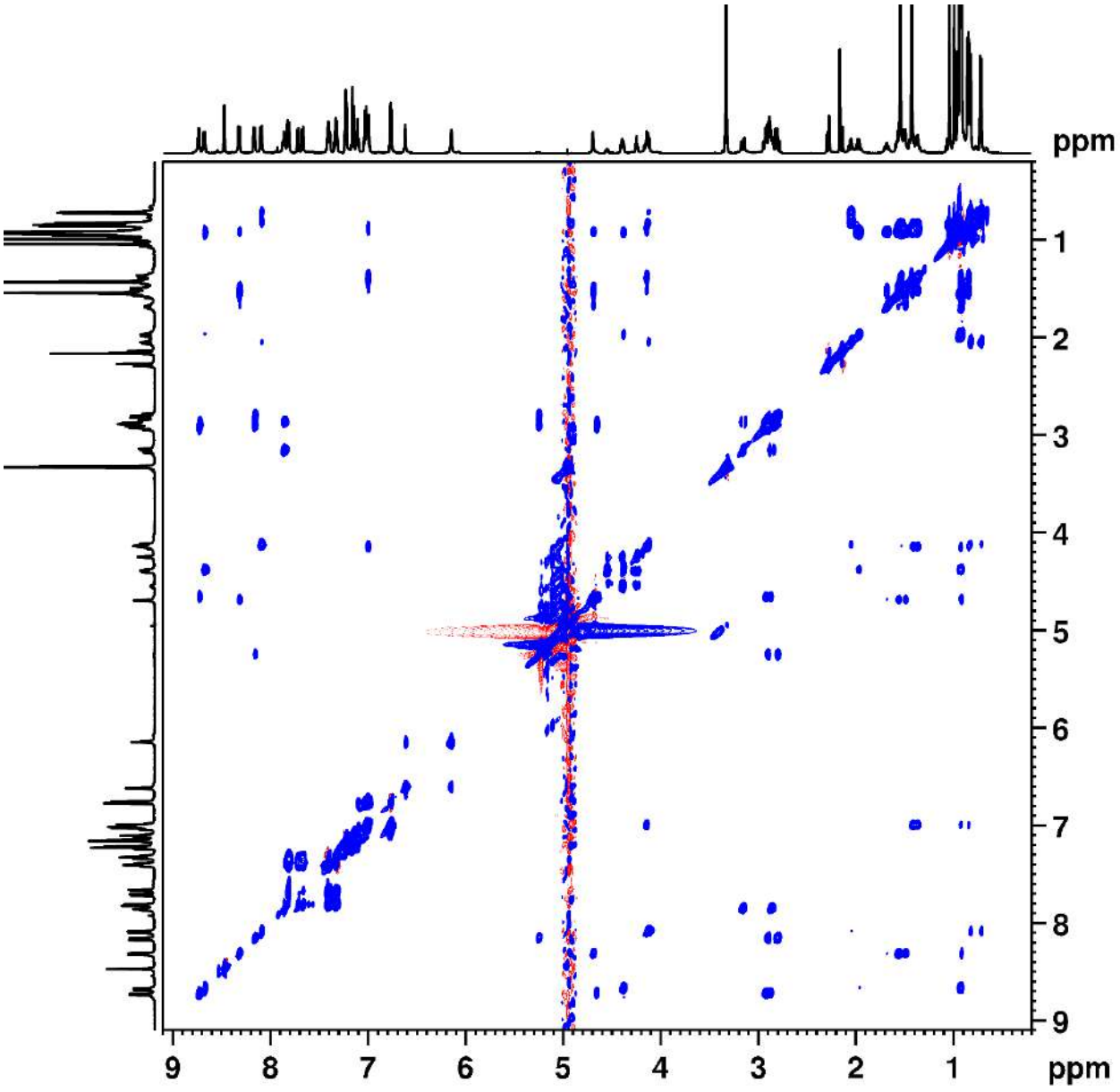

Figure A138. 600 MHz TOCSY spectra of peptide **55** at 5 mM conc. in CD_3OH at 298 K.

TH-3141_166122021

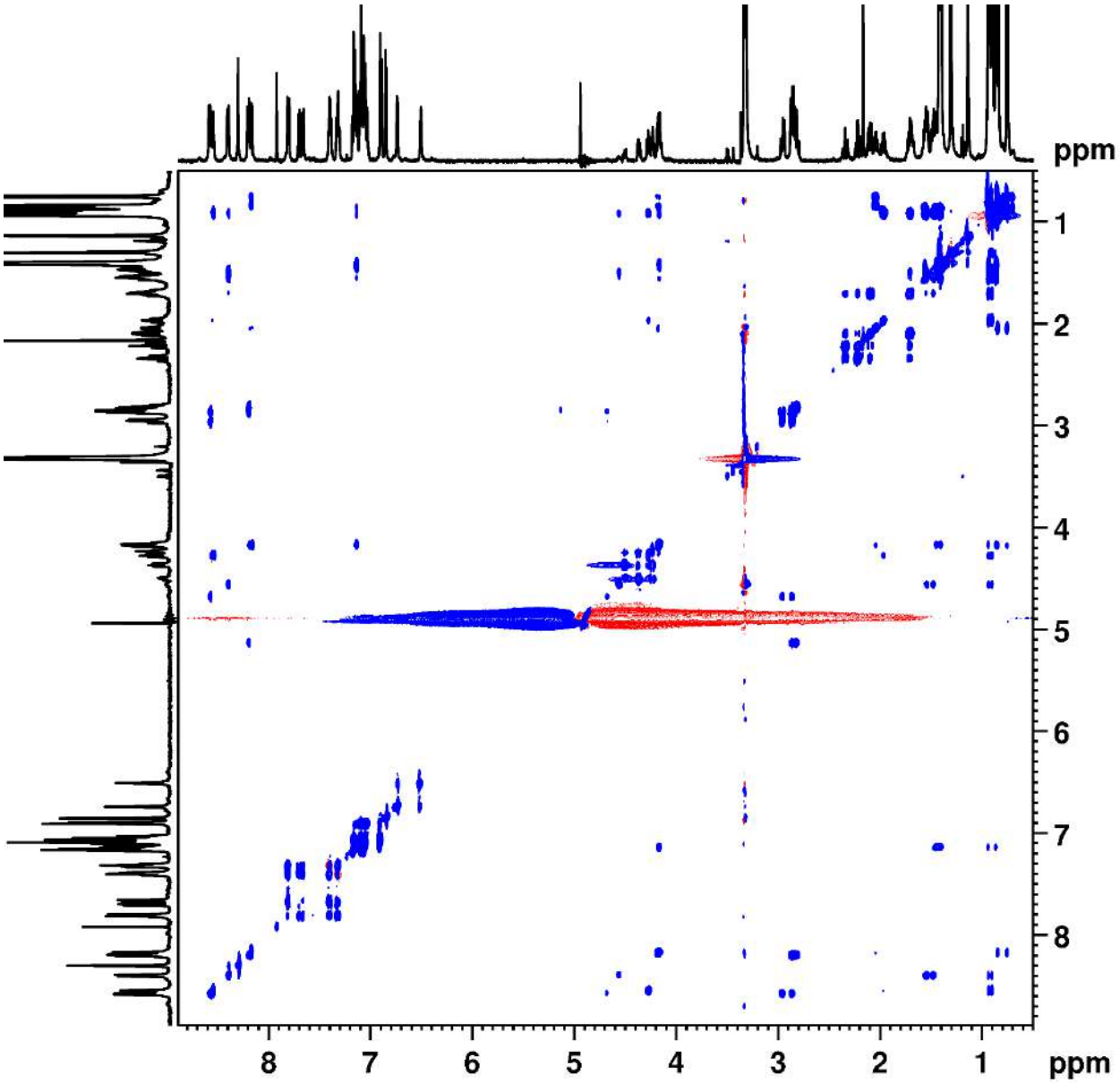

Figure 139. 600 MHz TOCSY spectra of peptide **56** at 2 mM conc. in CD_3OH at 298 K.

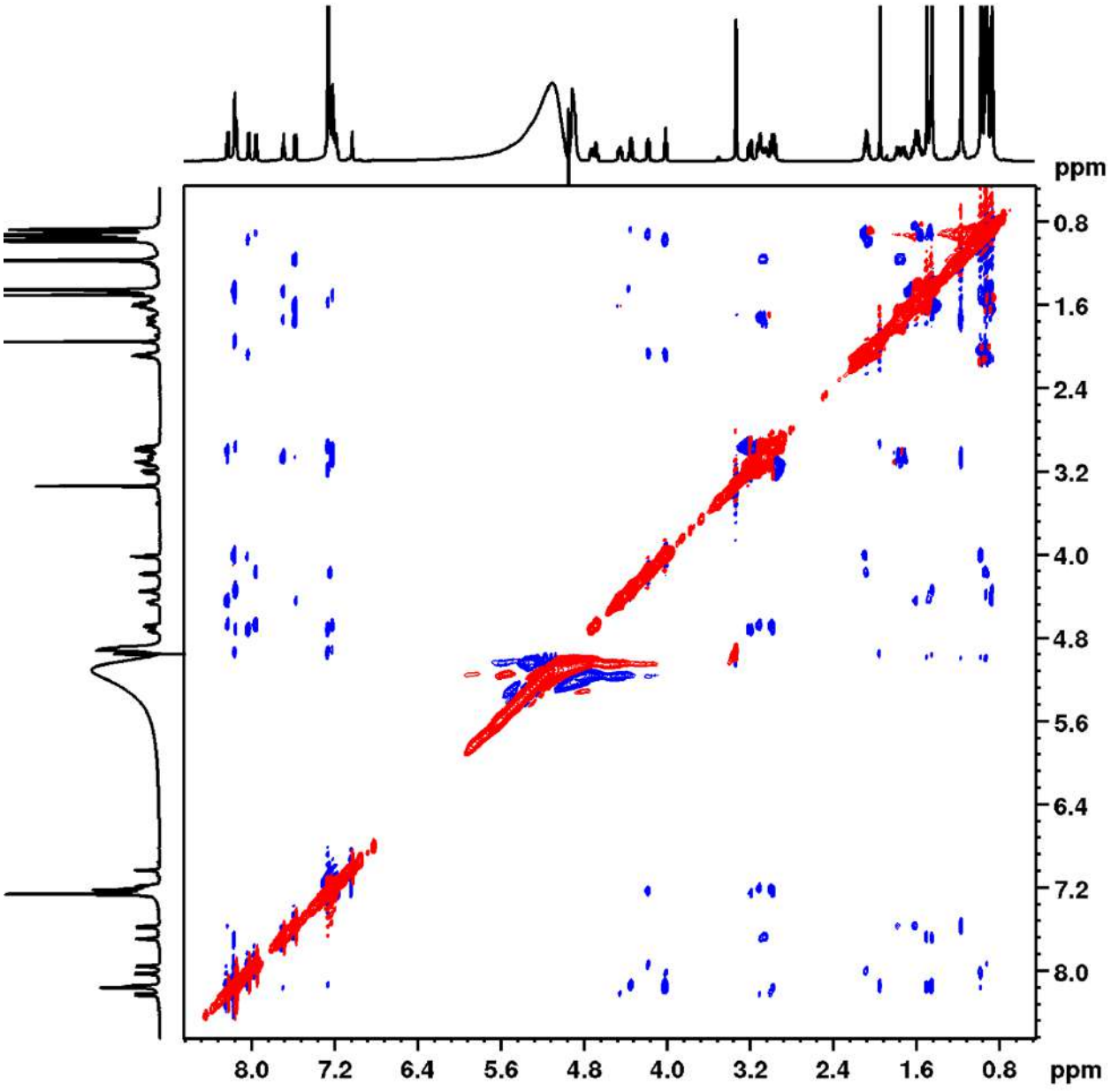

Figure A140. 600 MHz ROESY spectra of peptide **51** at 5 mM conc. in CD_3OH at 298 K.

TH-3141_166122021

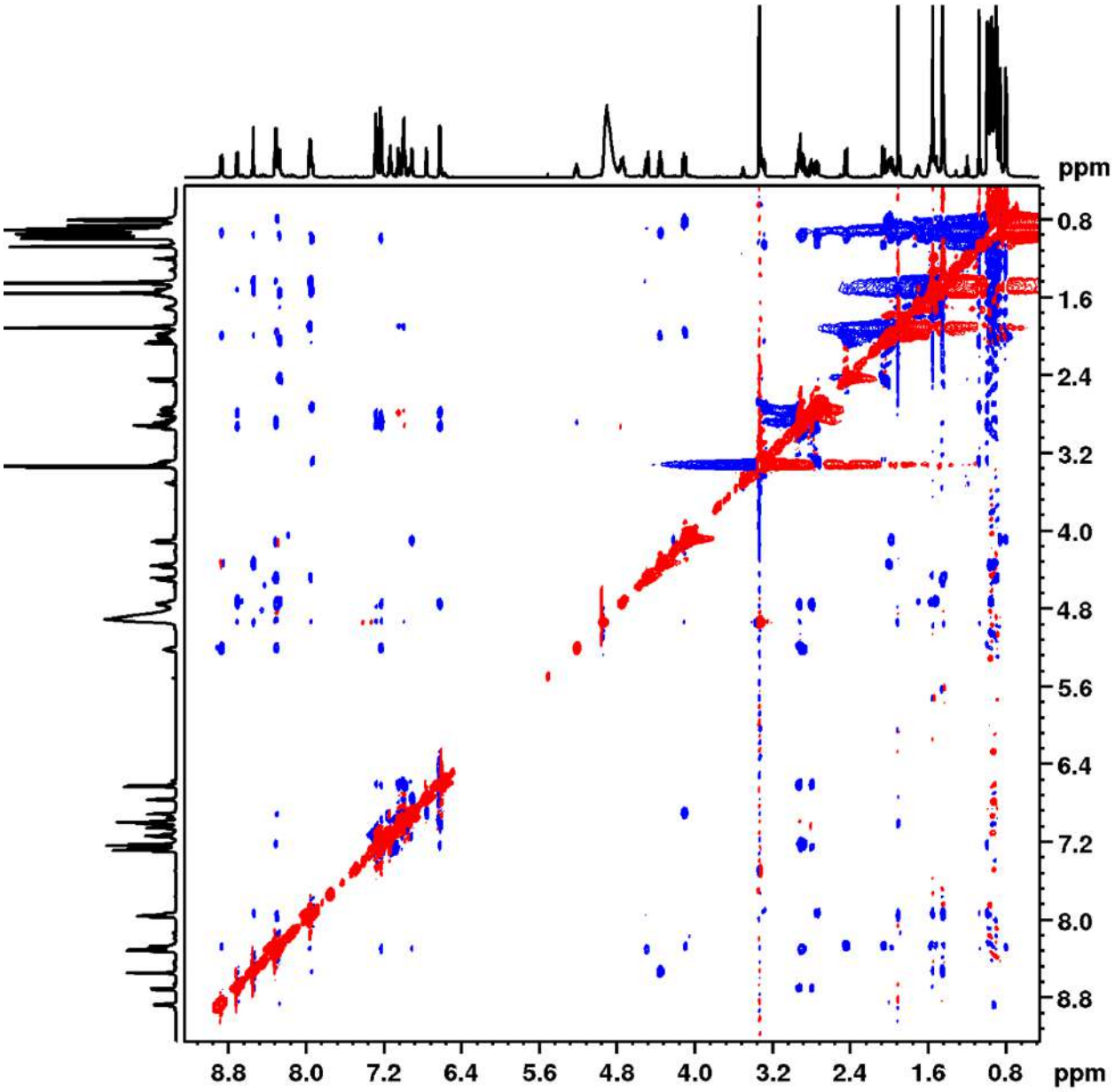

Figure A141. 600 MHz ROESY spectra of peptide **52** at 5 mM conc. in CD_3OH at 298 K.

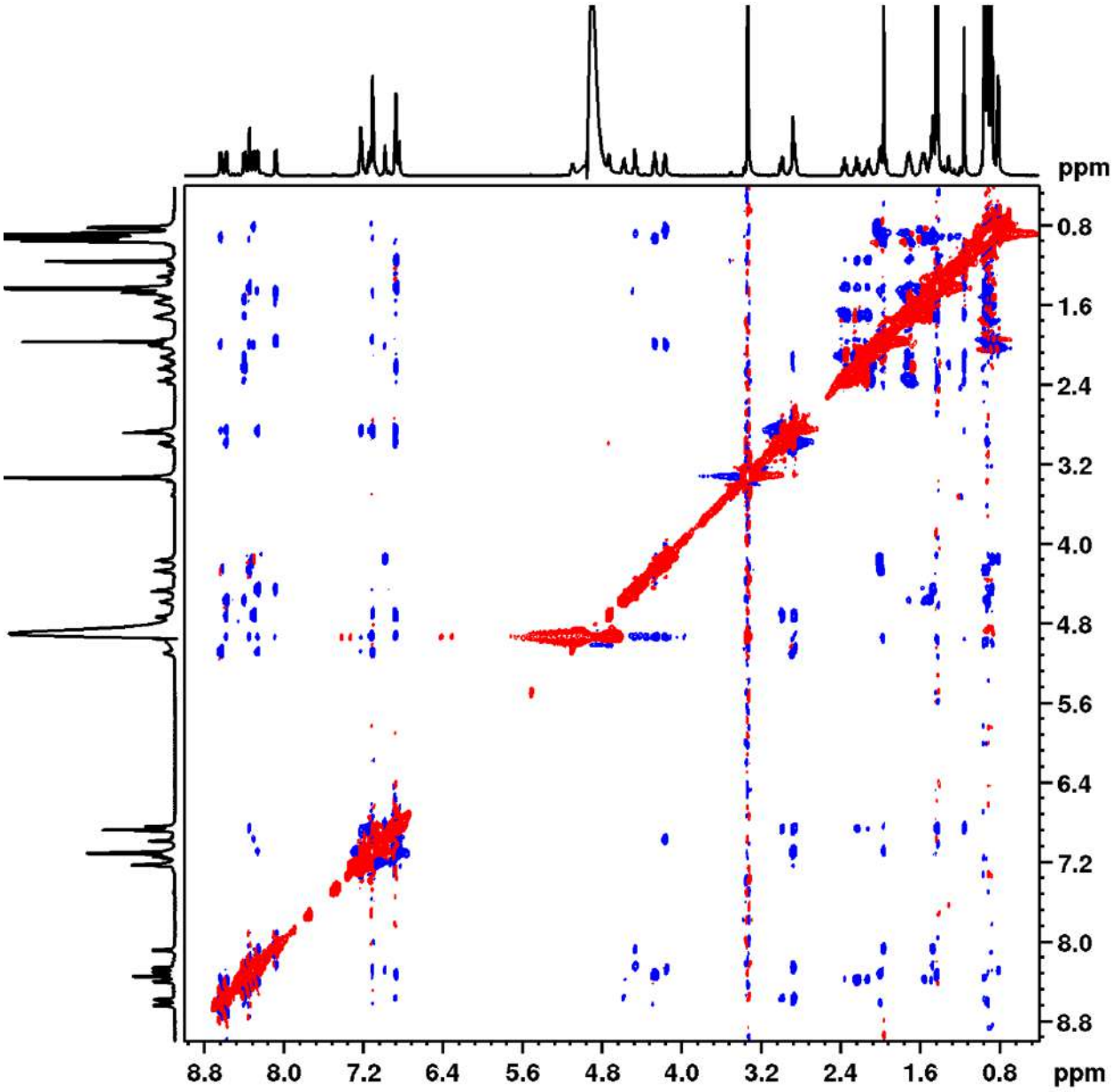

Figure A142. 600 MHz ROESY spectra of peptide **53** at 4 mM conc. in CD_3OH at 298 K.

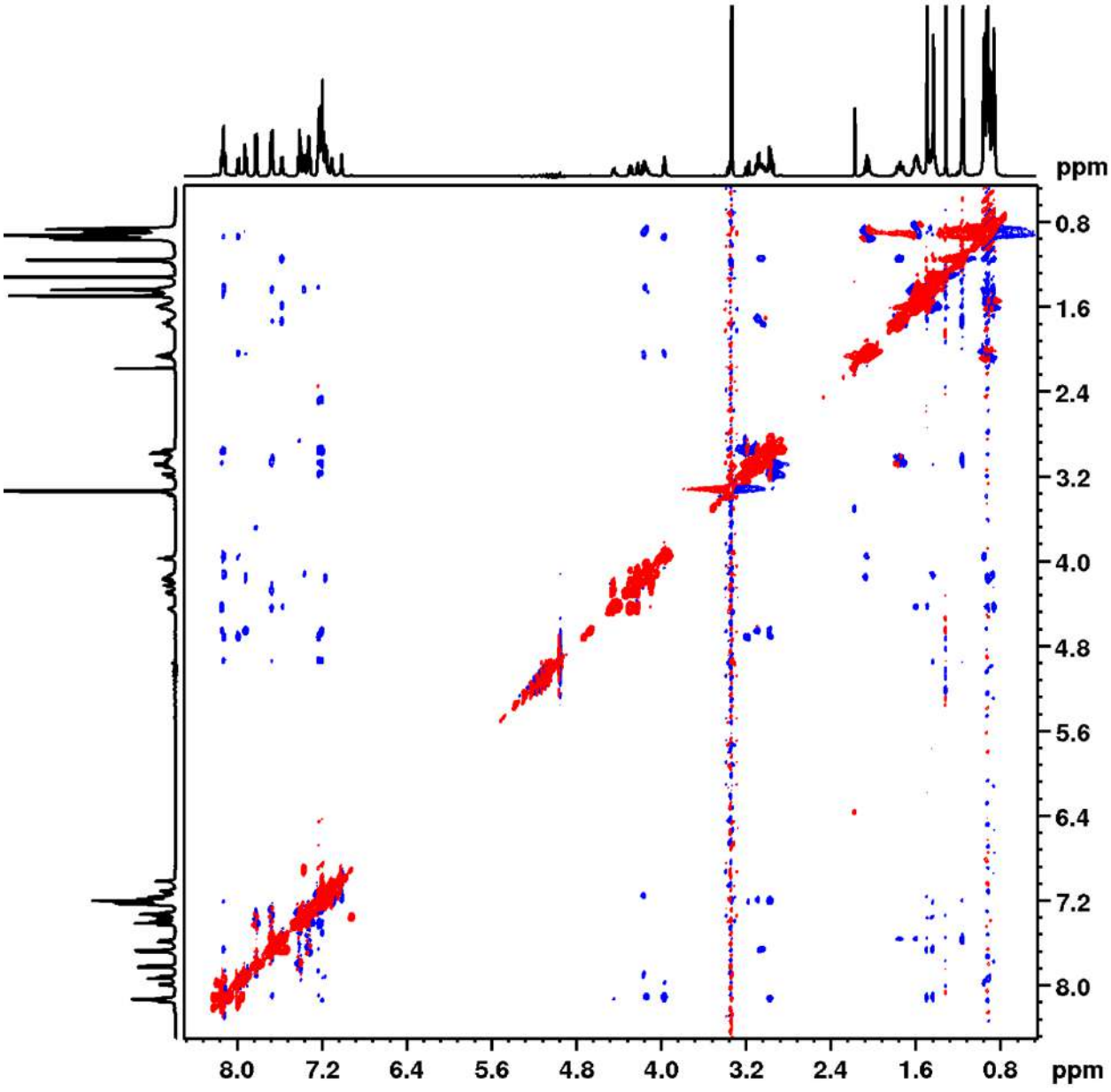

Figure A143. 600 MHz ROESY spectra of peptide **54** at 5 mM conc. in CD_3OH at 298 K.

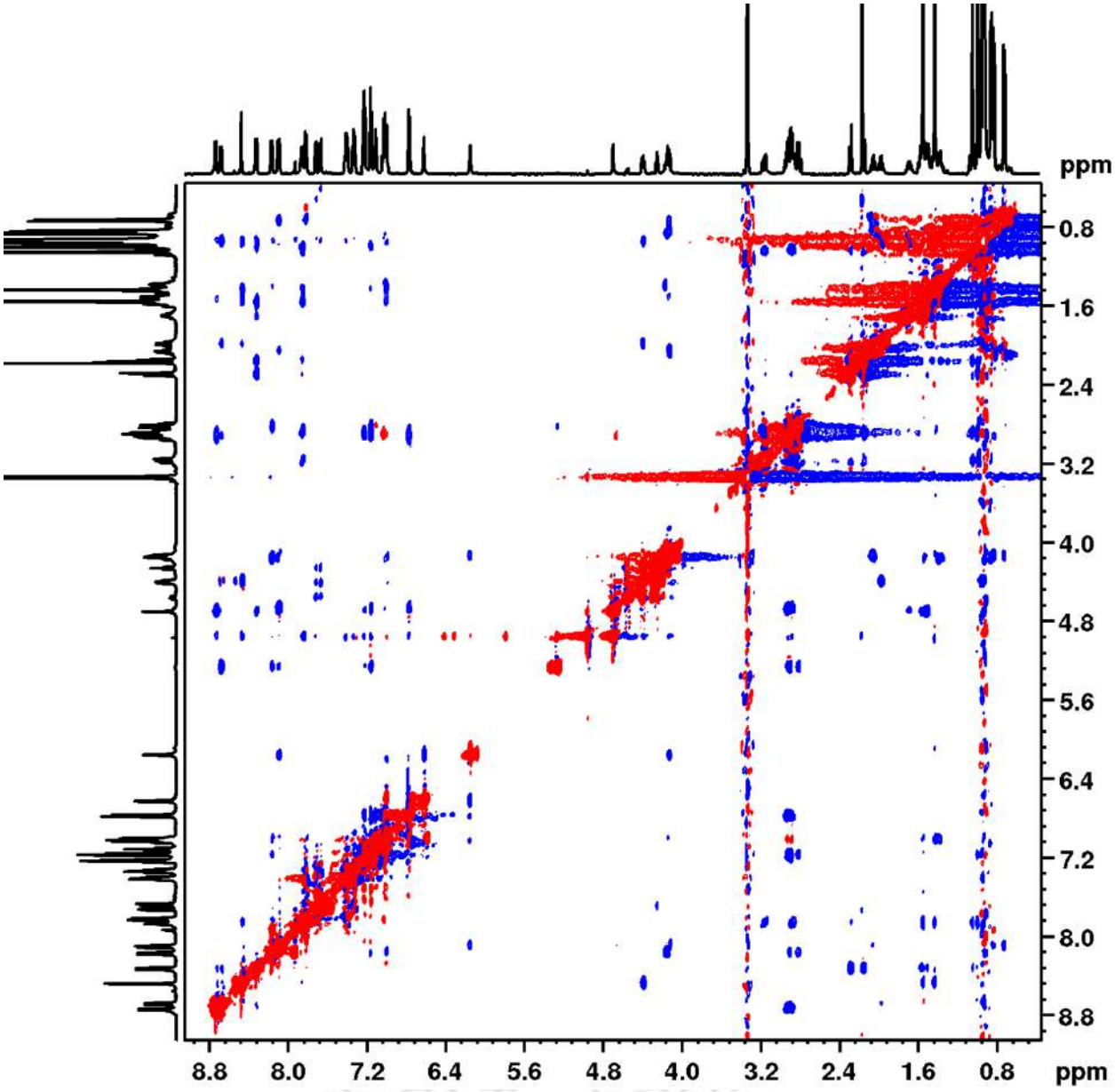

Figure A144. 600 MHz ROESY spectra of peptide **55** at 5 mM conc. in CD_3OH at 298 K.

TH-3141_166122021

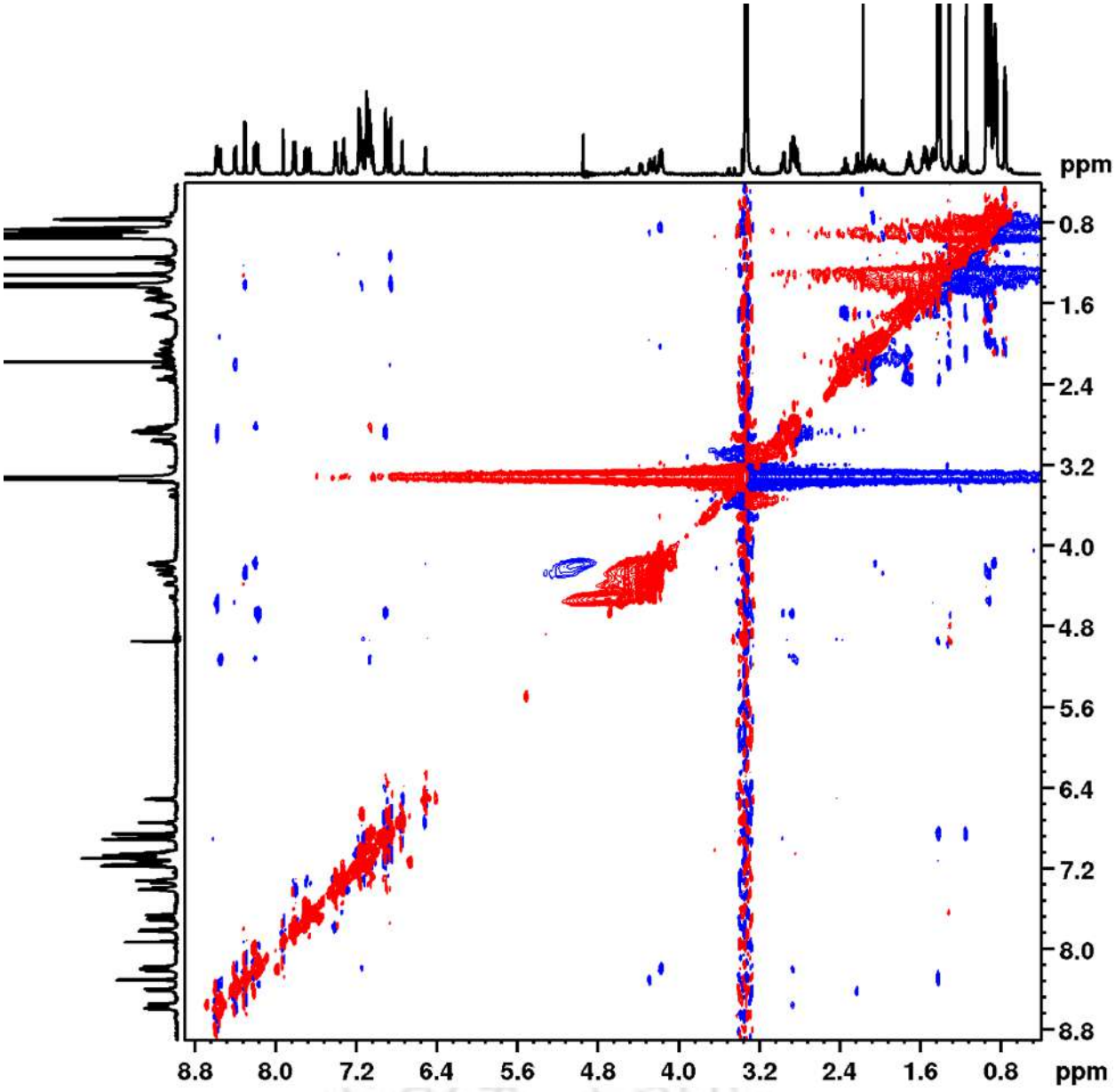

Figure A145. 600 MHz ROESY spectra of peptide **56** at 2 mM conc. in CD_3OH at 298 K.

TH-3141_166122021

Appendix B

B1. Materials Purchased:

All amino acids used in solution phase synthesis (except three unnatural γ amino acids), EDC.HCl, DMAP, DIC, DMF, DCM Piperidine, DIPEA, acetic anhydride were purchased from Spectrochem. All Fmoc protected amino acids, HOBt, PyBOP, Fmoc-OSu were purchased from GL Biochem.Ltd (Shanghai, China). Dioxane, Trifluoroacetic acid (TFA), HPLC graded acetonitrile and methanol were obtained from Merck. Di-tert-butyl dicarbonate (Boc), thionyl chloride ($SOCl_2$), calcium hydride, lithium hydroxide (LiOH) and other chemicals were purchased from Sigma-Aldrich. Methanol and dichloromethane were dried using magnesium turnings and calcium hydride (CaH_2), respectively. All reagents for peptide synthesis were used as received without further purification.

B2. Instruments Used for Various Studies:

1. HPLC: Thermo Scientific Dionex Ultimate 3000

2. ESI-MS: Agilent-Q-TOF 6500 instrument in electrospray ionization positive mode

3. MALDI-TOF: Bruker Daltonics Autoflex Speed analysis instrument

4. NMR: 400, 500, 600 MHz Bruker NMR spectrometer

5. SC-XRD: Oxford Supernova E, CCD diffractometer using Mo X-ray source (λ = 0.71073 Å).

6. FT-IR: Spectrum Two Perkin Elmer FT-IR spectrometer

7. FESEM: FESEM Sigma 300 microscope, FESEM Sigma Zeiss Gemini microscope

8. FETEM: JEOL JEM (Model 2100F) at an operating voltage of 200 KV

9. PXRD: Bruker D2 Phaser X Ray diffractometer (Cu-Kα radiation, λ = 1.5406 Å)

10. Fluorescence: Fluoromax-4 spectrophotometer

TH-3141_166122021

11. DLS: Zetasizer Nano ZS90 from Malvern using a 632.8 nm He−Ne laser

12. CD: Jasco J-1500 spectropolarimet

भारतीय प्रौद्योगिकी संस्थान गुवाहाटी
Indian Institute of Technology Guwahati

TH-3141_166122021

List of Publications

From the thesis:

(1) **Debnath, S.**; Ghosh, S.; Pandit, G.; Satpati, P.; Chatterjee, S. Effect of Differential Geminal Substitution of γ Amino Acid Residues at the (i+ 2) Position of αγ Turn Segments on the Conformation of Template β-Hairpin Peptides. *J. Org. Chem.* **2021**, *86*, 11310-11323.

(2) **Debnath, S.**; Ghosh, S.; Kumar, D.; Vasudev, P. G.; Satpati, P.; Chatterjee, S. Effect of Differential Backbone Di-substitution of Gamma Amino Acid Residues on the Conformation and Assembly of their Fmoc Derivatives in Solid and Solution States. *Chem. - Asian J.* **2022**, *17*, e202200356.

(3) **Debnath, S.**, S. R, Vignesh., Satpati, P., Chatterjee, S. Effect of Variable Position of Geminal Substitution of Gamma Amino Acid Residues on their Ability to form Isolated non-helical C_{12} β-turn Mimics Across ^{D}Pro-$\gamma^{x,x}$ Segments. *ChemistrySelect* **2023,** Just accepted.

(4) **Debnath, S.**, Kumar, D.; Vasudev, P. G.; Chatterjee, S. Enhanced C_{12} helical propensity of $\gamma^{3,3}$ and $\gamma^{4,4}$ amino acid residues compared to $\gamma^{2,2}$ amino acid residues. *ChemistrySelect* **2023**, Just accepted.

(5) **Debnath, S.**, S. R, Vignesh., Kumar, D., Das, B., Vasudev, P. G., Satpati, P., Chatterjee, S. Ambidexterity and Left-handedness Induced by Single Geminally Dimethyl Substituted Gamma Amino Acid Residues in all Alpha Chiral Helical Peptides. Manuscript under revision, **2023**.

Other projects:

(1) Chetia, M.; **Debnath, S.**; Chowdhury, S.; Chatterjee, S. Self-assembly and multifunctionality of peptide organogels: oil spill recovery, dye absorption and synthesis of conducting biomaterials. *RSC Adv.* **2020**, *10*, 5220-5233.

TH-3141_166122021

(2) Pandit, G.; Biswas, K.; Ghosh, S.; **Debnath, S**.; Bidkar, A. P.; Satpati, P.; Bhunia, A.; Chatterjee, S. Rationally designed antimicrobial peptides: Insight into the mechanism of eleven residue peptides against microbial infections. *Biochim. Biophys. Acta, Biomembr.* **2020**, *1862*, 183177-183192.

(3) Ghosh, S.; Pandit, G.; **Debnath, S**.; Chatterjee, S.; Satpati, P. Effect of monovalent salt concentration and peptide secondary structure in peptide-micelle binding. *RSC Adv.* **2021**, *11*, 36836-36849.

(4) Pandit, G.; Sarkar, T.; **Debnath, S**.; Satpati, P.; Chatterjee, S. Delineating the Mechanism of Action of a Protease Resistant and Salt Tolerant Synthetic Antimicrobial Peptide against Pseudomonas aeruginosa. *ACS Omega* **2022**, *7*, 15951-15968.

TH-3141_166122021

भारतीय प्रौद्योगिकी संस्थान गुवाहाटी
Indian Institute of Technology Guwahati